NASA TECHNICAL TRANSLATION

NASA TT F-787

NASA TT F-787

NON-EQUILIBRIUM PHYSICO-CHEMICAL PROCESSES IN AERODYNAMICS

V. P. Agafonov, V. K. Vertushkin, A. A. Gladkov, and O. Yu. Polyanskiy

"Mashinostroyeniye" Press
Moscow, 1972

NATIONAL AERONAUTICS AND SPACE ADMINISTRATION • WASHINGTON, D. C. • MARCH 1976

1. Report No.	2. Government Accession No.	
NASA TT F-787		

4. Title and Subtitle	5. Report Date
NON-EQUILIBRIUM PHYSICO-CHEMICAL PROCESSES IN AERODYNAMICS	March 1976
	6. Performing Organization Code
7. Author(s)	8. Performing Organization Report No.
V.P. Agafonov, V.K. Vertushkin, A.A. Gladkov, O. Yu. Polyanskiy	10. Work Unit No.
9. Performing Organization Name and Address	11. Contract or Grant No.
SCITRAN Box 5456 Santa Barbara, CA 93108	NASw-2483
	13. Type of Report and Period Covered
12. Sponsoring Agency Name and Address	Translation
National Aeronautics and Space Administration Washington, D.C. 20546	14. Sponsoring Agency Code

15. Supplementary Notes

Translation of: "Neravnovesnyye fiziko-khimicheskiye protsessy v aerodinamkie","Mashinostroyeniye" Press, Moscow, 1972, pp. 1 - 344

16. Abstract

The monograph is devoted to the present-day state of a new branch of aerodynamics, which is acquiring great practical importance in connection with the development of aerospace technology. A systematic analysis is given of the physico-chemical processes in high-temperature gas flows and their effect on gas dynamic parameters.

17. Key Words (Selected by Author(s))	18. Distribution Statement
	Unclassified - Unlimited Subject Category 02

19. Security Classif. (of this report)	20. Security Classif. (of this page)	21. No. of Pages	22. Price*
Unclassified	Unclassified	491	$11-50

ANNOTATION

The monograph is devoted to the present-day state of a new branch of aerodynamics, which is acquiring great practical importance in connection with the development of aerospace technology. A systematic analysis is given of the physico-chemical processes in high-temperature gas flows and their effect on gas dynamic parameters.

Information is given on the chemico-physical, thermodynamic, and kinematic properties of gases (primarily air). The fundamental equations are formulated, and the general properties of non-equilibrium flows are described.

One-dimensional flows, the structure of a shock wave in a gas mixture, and the properties of nonequilibrium flows in a stream filament are discussed. A description is given of the method of calculation and the similitude conditions for flows in nozzles. The basic determining parameters and correlation relations are introduced.

An analysis is given of the problems of external gas dynamics of nonviscous nonequilibrium flows, of the flow around blunt and sharp bodies, corresponding to the similitude laws. Within the framework of the boundary layer theory, a discussion is given of viscous nonequilibrium flows, including the effect of chemical reactions on the surface, the flow in the neighborhood of a critical point of a blunt body (including the effect of low gas density), the flow around a flat plate and a cone, as well as the

characteristic features of nonequilibrium wake flows.

The effect of radiation from a gas flowing around blunt bodies, the effect of nonequilibrium physico-chemical processes in gases on aerodynamic and thermal characteristics of hypersonic aircraft, and on the state of the flow in nozzles of gas dynamic plants, etc., are described. The radiation thermal flows are determined.

The book is designed for aeromechanical engineers acquainted with the fundamentals of hypersonic gas dynamics, and it may also be useful to upper-division and graduate students in those fields.

178 illustrations, 16 tables, 573 bibliographical entries.

Reviewer; Doctor of Physico-Mathematical Sciences, I. P. Ginzburg

PREFACE

If in the first half of the 20th century, the gas dynamics /3* of an ideal gas anticipated the demands of aircraft technology, beginning with the second half of the century, the development of missile and space technology has taken gas dynamics into the little known area of high temperatures and low densities. Under these circumstances, it was impossible to consider the gas ideal, with constant heat capacities.

Moreover, it became necessary to consider the finite rate of the physico-chemical processes in a gas (excitation of vibrations, dissociation, ionization, radiation), i.e., the nonequilibrium of the flow. Thus, nonequilibrium flows ceased to be something that only physicists would deal with. Today these questions are of great interest to a wide range of engineers working in the area of applied aerodynamics.

At hypersonic speeds of flight, corresponding to M = 10 and above, the real properties of a gas, in particular the nonequilibrium processes, have an effect on the characteristics of the flow field around aircraft. The real properties of a gas and nonequilibrium of the flow result in a substantial change in the amount of thermal flow to the walls of rocket nozzles and to the external surface of aircraft. They may have a great influence on the thrust of ram jet engines and even affect the aerodynamic characteristics of the aircraft. In particular, the nonequilibrium of a flow may influence the moment and center

*Numbers in the margin indicate pagination in foreign text.

of pressure, which in the final analysis should result, for example, in a substantial variation of the touchdown location of a descending vehicle.

There has been particular interest, shown recently in the study of nonequilibrium wake flows, in the problem of detecting objects entering the atmosphere at a hypersonic speed, and communication with them. It may be noted that it is very difficult and often practically impossible to simulate the real properties of the air and nonequilibrium processes in existing hypersonic experimental units. All this illustrates directly how important and necessary it is to study nonequilibrium flows theoretically.

In the monographs devoted to the aerodynamics of hypersonic flows, we do not find a description of the physico-chemical processes in a real gas, or their effect on the aerodynamic and thermal characteristics of flows, that would be sufficient for practical use. On the other hand, in the literature on the kinetics of physico-chemical processes we do not find any articles in which those questions are considered in terms of their application to aerodynamics.

The present book aims to fill this gap. It generalizes the rich factual material that has appeared in recent years in domestic and foreign literature. The basic goal of the book is to give the reader a general understanding of the problem of flows of nonequilibrium and radiating gas, to acquaint him with the basic features of such flows and the difficulties accompanying their investigation, as well as to equip him with a sufficient amount of factual data to enable him to obtain the

correct concept of the numerical effect of nonequilibrium processes*.

The book does not pretend to be an exhaustive exposition of all problems involved in the physics and aerodynamics of nonequilibrium flows. It does not discuss, for example, the questions related to plasma flows in the absence of thermodynamic equilibrium, nonequilibrium processes of turbulent transfer, processes of combustion in filaments, etc.. Each of these questions is a separate problem going beyond the scope of the present book and far from an exhaustive solution.

Chapters 1, 2 and Sections 1-5; 3.1 of Chapter 3 were written by A. A. Gladkov; Sections 6 and 7 of 3.1, 3.2 of Chapter 3, Chapter 4, by O. Yu. Polyanskiy; Chapter 5, by V. P. Agafonov; Chapter 6, by V. K. Vertushkin. The authors wish to thank to V. N. Zhigulev, V. V. Sychev, V. Ya. Neyland, and V. S. Galkin for useful discussions and valuable comments regarding individual questions. The authors are also grateful to I. P. Ginzburg who took it upon himself to review the book. The authors are particularly grateful to Academician A. A. Dorodnitsyn who sponsored the idea of writing such a book.

* The book was written mainly during 1967-1968, which determined the literature used. When preparing the manuscript for print, we have considered the most important papers that have been published after 1968.

REFERENCES

1. Bazarov, I. P. Termodinamika (Thermodynamics). Moscow, Fizmatgiz, 1961.

2. Blokhintsev, D. I. Osnovy kvantovoy mekhaniki (Fundamentals of Quantum Mechanics). Moscow. "Vysshaya Shkola", 1963.

3. Volkenshteyn, N. V. Stroyeniye i fizicheskiye svoystva molekul (Structure and Physical Properties of Molecules). Izdatel'stvo AN SSSR, 1955.

4. Godnev, I. N. Vychisleniye termodinamicheskikh funktsiy po molekularnym dannym (Computation of Thermodynamic Functions from Molecular Data). Moscow, Gostekhizdat, 1956.

5. Kondrat'yev, V. N. Kinetika khimicheskikh gazovykh reaktsiy (Kinetics of Chemical Gas Reactions). Izdatel'stvo AN SSSR, 1958.

6. Kondrat'yev, V. N. Struktura atomov i molekul (Structure of Atoms and Molecules). Izdatel'stvo AN SSSR, 1946.

7. Landau, L. D. and Ye. M. Lifshitz. Statisticheskaya Fizika (Statistical Physics). Moscow, "Nauka" Press, 1964.

8. Ter Haar, D. and G. Vergelant. Elementarnaya Termodinamika (Elementary Thermodynamics). Moscow "Mir" Publishers, 1968.

SYMBOL LIST

a - speed of sound

a_j, b_j - stoichiometric coefficients

$B = \frac{\sigma}{\pi} T^4$ - averaged Planck function

B_ν - Planck function

$c = 3 \cdot 10^{10}$ cm/sec - speed of light

$c_f = \frac{2\tau_w}{\rho_s u_s^2}$ - friction coefficient

$c_h = \frac{-q_w}{\rho_s u_s c_p (H_r - h_w)}$ - heat transfer coefficient

c_{pi} - specific heat capacity of active degrees at constant pressure

$\bar{c}_p = \sum_i c_{pi} a_i$ - average value of c_p

c_V - specific heat capacity at constant volume

c_{VK} - specific heat capacity of vibrational degrees of freedom

$c_x = \frac{2X}{\rho_\infty V_\infty^2 F}$ - drag coefficient

$c_y = \frac{2Y}{\rho_\infty V_\infty^2 F}$ - lift coefficient

D - dissociation energy

D_i^T - thermal diffusion coefficient of i-th component

D_{ij} - binary diffusion coefficient

d - characteristic relaxation length

E_a - activation energy

E, E_ν - total and spectral radiation strength, respectively

E - internal energy

e - specific internal energy

$E_n(x)$ - integral, exponential function

e_K - energy of vibrational degrees of freedom

f - frequency of gas molecule collisions

$f(\eta)$ - dimensionless stream function

F_ν - spectral flux of radiant energy

$g=\frac{H}{H_\delta}$ - total dimensionless enthalpy

g_n - static weight

$h=\sum a_i h_i$ - specific gas enthalpy (mixture)

$h=6{,}62\cdot10^{-34}$ J·sec - Planck constant

$h_i=\int_0^T c_{pi}dT+h_i^\circ$ - specific enthalpy of mixture i-th component

h° - heat of formation of component i

$H=h+u^2/2$ - gas braking enthalpy (mixture)

H - flight altitude

I - ionization potential

I - total radiation strength

I_ν - spectral strength of radiation

$\vec{J}_k$ - diffusion flux

$\vec{J}_e$ - flux of energy

$\vec{J}_q$ - heat flux

J_k - reaction rate

k, k_ν - volumetric coefficient of radiation absorption by gas

$k=1.38\cdot10^{-23}$J/K - Boltzmann constant

k_f, k_r - rate constant of forward and reverse reactions

k_w - surface catalycity coefficient

K_p, K_c - equilibrium constant

$Kn_r=\frac{1}{kL}$ - Knudsen radiation number

L - characteristic body length

$Le_i = \frac{\rho D_i \bar{c}_p}{\lambda} = \frac{Pr}{Sc_i}$ - Lewis-Semenov number of the i-th component

m_i - i-th component particle mass

M - M number

M_i - molecular weight of i-th component

$\bar{M}$ - average molecular weight

n_e - density (concentration) of electrons

n_i - number of i-th component particles per unit volume

$N_0 = 6.02 \cdot 10^{26}$ l/kmole - Avogadro number

Nu - Nusselt number

p - pressure

p_i - partial pressure of i-th component

$Pr = \frac{\bar{c}_p \mu}{\lambda}$ - Prandtl number

q - thermal flux (scalar)

q_i - parameter characterizing arbitrary nonequilibrium process (vibrational energy, degree of dissociation, concentration of i-th component, etc.)

Q - dimensionless value of thermal flux

R - universal gas constant

$R_M = \frac{R}{M_M}$ - gas constant of molecular component

R_b - radius of body curvature

$Re_x = \frac{\rho_\delta u_\delta x}{\mu_\delta}$ - Reynolds number calculated with flow parameters at outer boundary of viscous layer

$Re_s = \frac{\rho_\infty V_\infty R_b}{\mu(T_1)}$ - Reynolds number calculated from parameters behind normal shock wave

S - specific entropy

$Sc_i = \frac{\mu_l}{\rho D_i}$ - Schmidt number of i-th component

t - time

T - temperature

T_K - temperature of vibrational degrees of freedom

T_v - characteristic vibration temperature

T_d - characteristic dissociation temperature

u, v, w - velocity components

$\vec{v}$ - velocity vector

V - specific volume

V_∞ - body flight velocity

$\hat{v}$ - diffusion rate

$W = \frac{h - \bar{c}_p T}{\bar{c}_p T}$ - energy parameter

X - body drag

x, y, z - coordinates

$[X_i]$ - mole-volume concentration of i-th component

Y - body lifting force

$z_l = \frac{a_l}{a_\delta}$ - reduced mass concentration

Z_i - statistical sum

$a_l = \frac{\rho_l}{\rho}$ - mass concentration of atoms

α - degree of dissociation

β - degree of ionization

β_i - velocity gradient at critical point

γ_w - recombination efficiency on surface

δ - width of boundary layer

Δ - width of shock layer

ε - turbulent viscosity coefficient

ε - degree of blackness

ξ_{gi} - Damkeler number of gas phase

ξ_w - Damkeler number of reactions on surface

η - similarity coordinate in boundary layer

θ - temperature ratio

ϑ - half-angle of opening (wedge or cone)

$x = c_p/c_V$ - ratio of specific heat capacities of gas

x_e - effective value

λ - gas thermal conductivity coefficient (mixture)

λ - radiation wavelength

μ - gas viscosity coefficient (mixture)

μ - reduced mass of colliding particles

ν - radiation frequency

ρ - density

τ_1 - relaxation time

τ_w - friction stress

ψ - stream function

ω - parameter (characterizing optical thickness)

$\omega_0 = \int_0^x k_0 dx$ - optical thickness

Ω - solid angle

$\Omega_i^{(l,s)*}$ - reduced collision integral

SUBSCRIPTS

A - atom

M - molecule

d - dissociation

e - equilibrium value

f - braking value

i - component i

vib - vibrational degrees of freedom

0 - value at x=0

r - value at reduction temperature

w - value at body surface (at y=0 or η=0)

δ - value on outer boundary of viscous layer

∞ - unperturbed (advancing) flow

* - in critical cross section of nozzle

1 - conditions behind shock wave

SUPERSCRIPTS

j=0 - corresponds to plane flow

j=1 - corresponds to axisymmetric flow

TABLE OF CONTENTS

CHAPTER 1
PHYSICO-CHEMICAL PROCESSES IN GASES

The molecular structure of gases is not ordinarily considered /10 in gas dynamics. The gas is analyzed, not as a collection of particles, but as a continuous medium. The quantities that are related to molecular properties such as heat capacity, transfer coefficients, and the like enter the equations of gas dynamics as certain coefficients that can be determined by using the theory of molecular structure or not.

If we do not consider rarefied gases (or, which is the same thing, regions with dimensions comparable to the free path of the molecules), then one can disregard the motion of the molecules and remain within the limits of the traditional analysis accepted in gas dynamics, where gases are considered as continuous media. However, even in such an approach, in those cases when internal changes may take place in a gas, one has to take the existence of the particles of the gas into account and consider their internal structure and interactions. In particular, such are the conditions in a gas heated to high temperatures. Below we shall discuss the problems closely related to chemical kinetics, and we shall not deal with the problems of physical kinetics. Therefore, we should start the discussion with a brief survey of thermodynamics, molecular structure, and chemical kinetics of gases.

1.1 Equilibrium and nonequilibrium states

A collection of isolated material objects is called a system. It is assumed that heat transfer and diffusion of components may take place between parts of the system. The state of the system will be given by specifying independent macroscopic parameters that characterize it.

If all parameters of a system are constant in time and there are no steady flows of mass, momentum, and energy, due to external causes, the state is a state of (thermodynamic) equilibrium. /11

A thermodynamic system is defined as a system in the state of thermodynamic equilibrium. In thermodynamics, it is postulated that an isolated system which is under definite and constant external conditions will sooner or later reach a state of thermodynamic equilibrium and cannot leave it spontaneously. The external conditions include the volume occupied by the system, external force fields acting on it, and the temperature of the surrounding bodies.

The process involving the transition of a system to a state of equilibrium is called relaxation, and all states that differ from the state of equilibrium are called the nonequilibrium states. The process which goes through a series of nonequilibrium states is called a nonequilibrium process.

A transition to a state of equilibrium in the absence of external fields is characterized by the establishment of a homogeneous state in the entire system, establishment of constant composition. If chemical reactions or other internal processes are possible in a system, then the transition will include the cessation of all macroscopic processes and exchange of energy, momentum, particles between various parts of the system. Briefly, this can be expressed by saying that in a state of thermodynamic equilibrium all internal parameters of a system are functions of the external parameters and the temperature of the system. The constancy of the macroscopic parameters in the state of equilibrium does not exclude microprocesses in the system, but each of the microprocesses is balanced by a reverse process so that dynamic equilibrium is preserved.

The concept of temperature as a quantity uniquely related to the energy of a system may, strictly speaking, be introduced only for equilibrium systems. If a system is not thermally insulated, then the temperature in the state of equilibrium is equal to the temperature of the surrounding medium, and the energy of the system is determined by specifying the temperature of the surrounding bodies. If the system is thermally insulated, then there is no exchange of energy with the surrounding medium, the energy of the system remains constant, and the temperature is determined by a given energy of the system.

Often it is useful to use the concept of quasi-equilibrium systems, i.e., systems in which an exchange with the surrounding medium occurs much more slowly than the internal processes in the system. The state of quasi-equilibrium systems corresponds with great accuracy to a state of equilibrium. However, the temperature of a quasi-equilibrium system in general is not equal to the temperature of the surrounding medium, and is determined by the energy of the system.

Due to the exchange of energy with the surrounding medium, the state of equilibrium of a system changes. However, since the internal relaxation processes occur at a high rate, the system always remains in a state close to a state of equilibrium. Such a concept is very convenient, since it permits us to use a strictly defined state of equilibrium of a system in the calculation of exchange processes that shift the equilibrium.

In the cases of nonequilibrium states, the external parameters and the energy of a system do not uniquely determine the state of a system, and we need much more detailed information to describe the system. Thus if chemical reactions may occur in a gas volume element, then different compositions of the gas will correspond to the same external conditions. However, in a state of equilibrium the composition of a gas is completely determined by the external conditions and the temperature of the gas, since in the general case they determine an equilibrium state of the system. /12

The introduction of quasi-equilibrium systems is physically justified, even in a discussion of relaxation in gases. In the general case, the gas molecules have a number of degrees of freedom: translational, rotational, vibrational, to which one formally adds chemical processes: ionization, electron excitation. The relaxation processes corresponding to different degrees of freedom in general occur at different rates.

The translational and rotational degrees of freedom are called active, since the equilibrium with respect to these degrees is established faster than with respect to the other ones. The remaining degrees of freedom are called inertial or internal. Decomposition into quasi-equilibrium subsystems depends on the conditions. The role of quasi-equilibrium systems may be played by a part of the entire set of degrees of freedom of a gas or the individual degrees of freedom. Such a combination of individual degrees of freedom into quasi-equilibrium blocks in many cases leads to a substantial simplification of problems.

We shall primarily be interested in processes involving the establishment of local equilibrium of a separated mass of gas in time. The establishment of equilibrium, associated with the transfer processes will, as usual in the theory of continuous media, be accounted for by the introduction of suitable coefficients in the discussion of the boundary layer in Chapter 5.

1.2 States of equilibrium

Let us proceed to a more detailed discussion of the internal degrees of freedom of a gas, and let us obtain an expression for the heat capacity of a gas at high temperatures. The heat capacity of a gas at constant volume is defined as the derivative of the internal energy of a system with respect to the temperature.

The internal energy of a gas is composed of energies corresponding to different degrees of freedom: translational motion, rotation, vibrations of molecules, and electron excitation:

$$\varepsilon = \varepsilon_{transl} + \varepsilon_{rot} + \varepsilon_{vibr} + \varepsilon_{el} \tag{1.1}$$

All degrees of freedom with the exception of the translational motion are quantized. This means that the energies of the internal degrees of freedom of the particles making up a system may occupy only certain discrete levels ε_j $(j=0, 1, 2...)$. The energy /13
of a particle may change only by a value equal to the difference between the levels, and an increase in the energy of the system corresponds to an increase in the number of particles at higher energy levels. The difference in energy between two energy levels is called a quantum of energy. If the energy of a system is large as compared with the quantum of energy, then the distribution of energy among the levels may be considered to be continuous and the quantum effects may be neglected.

The probable number of particles, n_j, with energy ε_j in a state of equilibrium at temperature T is given by the Boltzmann distribution where $k=1{,}38\cdot10^{-23}$ J/K is the Boltzmann constant;

$$n_j = n_0 \frac{g_j}{g_0} \exp[-(\varepsilon_j - \varepsilon_0)/kT], \tag{1.2}$$

g_j is the number of different states of the same energy (the degeneracy number or the statistical weight of the state); n_0 is the number of particles in the ground state (j = 0).

The sum over all states

$$Z = \sum_j g_j \exp(-\varepsilon_j/kT) \tag{1.3}$$

is called the statistical sum and plays an important role in statistical thermodynamics, since various thermodynamic functions, characterizing a system, can be expressed in terms of it. Evidently, the total number of particles in the system will be

$$n=\sum_j n_j=\frac{n_0}{g_0}\exp(\varepsilon_0/kT)\sum_j g_j\exp(-\varepsilon_j/kT)=\frac{n_0 Z}{g_0}\exp(\varepsilon_0/kT). \tag{1.4}$$

The energy of particles in a state j is $\varepsilon_j n_j$, and the total energy of the system is

$$E=\sum_j \varepsilon_j n_j=\frac{n_0}{Z g_0}\sum_j g_j\varepsilon_j\exp(-\varepsilon_j/kT)=$$

$$=\frac{n_0}{Z_0}kT\frac{dZ}{dT}=RT^2\frac{d\ln Z}{dT}. \tag{1.5}$$

The heat capacity of the system at constant volume is

$$c_V=\frac{dE}{dT}=RT\frac{d}{dT}\left(T^2\frac{d\ln Z}{dT}\right). \tag{1.6}$$

The entropy is given by

$$S-S_0=R\left[\frac{d}{dT}(T\ln Z)-\ln Z_0\right].$$

/14

According to the third law of thermodynamics (Nernst's theorem), the entropy vanishes at absolute zero. This makes it possible to determine the absolute entropy.

For continuous distributions, the summation is replaced by integration, and the statistical sum becomes the statistical integral.

To calculate the energy of quantized degrees of freedom we must know the corresponding energy levels. Therefore it is necessary to know the internal structure of the molecules.

The atoms in a molecule may be located along a straight line, in which case the molecule is called linear, or they may be located arbitrarily, in a plane or in space. Linear molecules differ from other multiatomic molecules in that they only have two rotational degrees of freedom corresponding to a rotation relative to two mutually perpendicular directions, perpendicular to the line on which the atoms are located. If a molecule consists of N atoms which may be considered as material points, then the total number of the degrees of freedom is 3N. Among them, three are due to the translational motion of the molecule as a whole and two degrees of freedom in linear molecules and three in nonlinear molecules, due to rotational motion. Thus, linear molecules have 3N-5 vibrational degrees of freedom, and the nonlinear ones 3N-6.

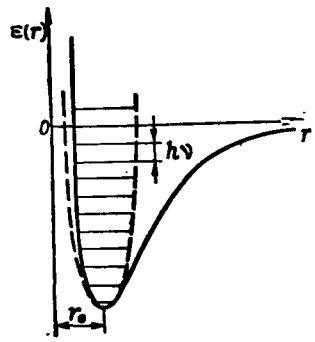

Figure 1.1 Potential of the interatomic interaction of a diatomic molecule (the dashed line - a parabola - represents the potential energy of a harmonic oscillator; the energy of the oscillator is counted from the minimum of the potential energy)

Vibrations

Forces acting between atoms and molecules attract atoms at large distances, and at small distances the forces of attraction change into sharply increasing forces of repulsion. The interatomic forces F are directly related to the potential energy of the interaction between atoms ε: $F=-\frac{d\varepsilon}{dr}$.

Therefore the function $\varepsilon(r)$ also determines the forces of interaction (Fig.1.1). There is a certain distance r_0 at which the forces of interaction between atoms vanish, and the corresponding position of the atoms is a position of equilibrium. /15

The values of r_0 for two-, three-atomic gases usually lie between 1 and 2 Å. The forces of interaction are difficult to calculate even for the simple case of a two-atomic molecule. Therefore one uses various empirical expressions that approximate the interaction potential. Since the oscillations of the atoms in a molecule occur about the position of equilibrium, the interaction potential is approximated primarily in that region.

One of the simpler types of approximation is the parabolic approximation of the potential (see Fig. 1.1). It gives good results for many problems in which one considers the neighborhood closest to the position of equilibrium. In addition, the parabolic approximation of potentials is convenient in many estimates since the solution of the problems of quantum mechanics for vibrations of atoms is particularly simple. When using the parabolic potential we deal with a harmonic oscillator. The energy levels of a harmonic oscillator are distributed uniformly and are given by

$$\varepsilon_v=h\nu\left(v+\frac{1}{2}\right);\ v=0,\ 1,\ 2,\ldots \tag{1.7}$$

Here ν— is the fundamental frequency of the oscillator characteristic for molecules of a given substance (Table 1); $h=6{,}62\cdot10^{-34}$ J · c is Planck's constant; v is the vibrational quantum number.

TABLE I

CHARACTERISTIC VIBRATIONAL TEMPERATURE [1]

Gas	H_2	I_2	O_2	N_2	CO	Cl_2	CO_2	N_2O
$T_v=\frac{h\nu}{k}$	5958	305	2228	3336	3080	797	959	847

Remark The values of T_v for CO_2 amd N_2O given in the table correspond to the frequency of two bending vibrations of a molecule. In addition to these values it is also possible to have the values of 1920 and 3380 for CO_2, 1850 and 3200 for N_2O.

It will be noted that the minimum of energy of vibrations is not zero. It has a certain definite value: $\varepsilon_0=\frac{h\nu}{2}$ (see Fig. 1.1). The mean vibrational energy of a harmonic oscillator is determined by summing over all levels:

$$\frac{E}{n}=\frac{\sum_{v=0}^{\infty}\varepsilon_v n_v}{\sum_{n=0}^{\infty}n_v} \qquad (1.8)$$ /16

and the population of a level is given by the Boltzmann distribution

$$n_v=n_0\exp(-vh\nu/kT). \qquad (1.9)$$

Substituting the expression for n_v in Eq. (1.8) and assuming that the energy of the ground state is zero, we get

$$E=\sum_{v=0}^{\infty}vh\nu\exp(-vh\nu/kT)=\frac{h\nu}{\exp\frac{T_v}{T}-1}. \qquad (1.10)$$

This is Planck's formula which is used also in theory of radiation. The statistical sum for the harmonic oscillator is

$$Z_{vib} = \sum_{0}^{\infty} \exp[-h\nu(v+1/2)/kT] = \frac{\exp(-h\nu/2kT)}{1-\exp(-h\nu/kT)}. \qquad (1.11)$$

The simplicity of the model of the harmonic oscillator is also the reason for its shortcomings. As shown by theory, in the model of the harmonic oscillator the transitions are possible only between neighboring levels (single quantum transitions). In real molecules multiquantum transitions are also possible although less likely.

In addition, the levels of the harmonic oscillator continue up to infinite energy. If the energy of the oscillator is low, this does not have a great importance since the population of the higher levels decreases very rapidly and has hardly any effect on the statistical sum. However, in a real molecule there exists an upper level for the energy of the interatomic bond (Fig. 1.2), corresponding to the dissociation of the molecule (the dissociation energy D).

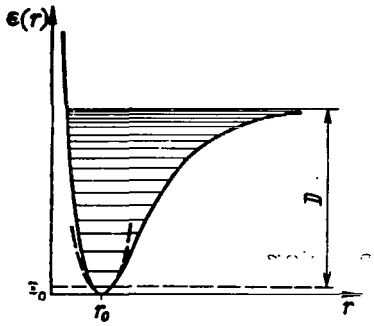

Figure 1.2 Morse potential (horizontal lines correspond to the energy levels of an anharmonic oscillator, the dashed line to the energy of the harmonic oscillator)

In order to take account of the finiteness of the upper energy level, one sometimes uses a model involving a harmonic oscillator with a cutoff, which assumes that the summation in Eq. (1.10) goes up to a certain finite $\tilde{v}$. In this case, the energy of the oscillator

is given by

$$E=\frac{h\nu}{\exp(h\nu/kT)-1}-\frac{\tilde{v}h\nu}{\exp(\tilde{v}h\nu/kT)-1}. \qquad (1.12)$$

/17

For $\tilde{v}$, we substitute the level number corresponding to the dissociation energy or the one closest to it. Usually, the number is on the order of a few tens.

The following Morse potential is closer to reality (see Fig. 1.2):

$$\varepsilon(r)=D[1-e^{-a(r-r_e)}]^2. \qquad (1.13)$$

The solution of the quantum-mechanical problem is also possible for this potential. The energy of the levels is given by

$$\varepsilon_v=\left(v+\frac{1}{2}h\nu\right)-\frac{h^2\nu^2}{4D}\left(v+\frac{1}{2}\right)^2. \qquad (1.14)$$

The energy levels are not spaced equally. They become closer as the level numbers increase.

However, in the model with the Morse potential we can no longer speak of harmonic vibrations, since for levels with a large number the anharmonicity of vibrations is important, and only for the lower levels are corrections for anharmonicity small. Multiquantum transitions are possible in this model. The Morse potential reproduces well the qualitative features of the actual potential. However, it is not easy to determine the constants that best approximate the real variation of the potential for specific substances. The number of levels for the Morse potential can be estimated by neglecting 1/2 as compared with v in Eq. (1.14). Then

$$v_{max}\approx\frac{2D}{h\nu}. \qquad (1.15)$$

For nitrogen, the number of levels is approximately equal to 70; for oxygen—50; and hydrogen—close to 13.

The calculation of even the harmonic vibrations of multiatomic molecules presents much greater problems [2] than for two-atomic ones. Usually, in the calculation for multiatomic molecules one determines the normal vibrations* and to each one of them there corresponds a harmonic oscillator with its fundamental frequency (see Table 1). Thus the problem reduced to a set of simpler problems.

Rotation

Considering the simplest case of the rotation of two-atomic molecules, we can represent them in the form of rigid dumbbells. Theory gives the following expression for the quantum levels of such a rigid rotator:

/18

$$\varepsilon_j = \frac{\hbar^2}{8\pi^2 J} j(j+1), \tag{1.16}$$

where $J=\mu r_0^2$; r_0 is the distance between atoms A and B, and μ is the reduced mass of a molecule, as given by the expression

$$\mu = \frac{m_A m_B}{m_A + m_B}, \tag{1.17}$$

where m is the atomic mass.

The weight of the state j is 2j + 1. The energy quantum in the ground state is $\Delta\varepsilon = \frac{\hbar^2}{8\pi^2 J}$. We can associate the characteristic temperature $T_r = \frac{\Delta\varepsilon}{k}$ with this value.

Using the characteristic values of the reduced mass and the interatomic distance, we get $T_r = 2—3$ K , for O_2, N_2 and $T_r = 85$ K

* In the general case, the vibrational motion of each of n degrees of freedom of a linear conservative system is anharmonic, since it represents a superposition of n vibrations with different frequencies. From them, one can obtain n linearly-independent combinations of vibrations, each of which corresponds to the vibration of a system at a definite frequency, i.e., to a harmonic vibration. These harmonic vibrations are called normal.

for H_2. Consequently, already at temperatures on the order of several hundred degrees $\left(\frac{T_r}{T} \approx 0{,}01\right)$, we can neglect the quantum character of rotation. This estimate is valid for molecules of a majority of substances considered in aerodynamics. Only for hydrogen (small moment of J) at temperatures on the order of 100 °K and below is it necessary to consider quantum effects of the rotational degrees of freedom.

The statistical sum of a linear rigid rotator is given by,

$$Z_r = \frac{8\pi^2 JkT}{\sigma h^2} \quad (T_r \ll T). \tag{1.18}$$

Here σ is a symmetry factor equal to unity for two-atomic molecules, consisting of different atoms (for example, NO), n = 2 for two-atomic molecules consisting of identical atoms.

In the general case of a multiatomic molecule, the expression for the statistical sum retains the form (1.18); the symmetry factor is defined as the number of interchanges of identical atoms in a molecule increased by 1, which is equivalent to the rotation of a molecule as a whole.

For nonlinear molecules

$$Z_r = \frac{8\pi^2}{\sigma}\left(\frac{2\pi JkT}{h^2}\right)^{3/2}, \tag{1.19}$$

where J represents the geometric mean of the three principal moments of inertia of a nonlinear molecule: $J = (J_1 J_2 J_3)^{1/3}$. The rigid rotator model is strictly speaking invalid when considering the rotational degrees of freedom, since there is always interaction between the rotational motion and vibrational motion, particularly at a higher amplitude of the vibrations of molecules. /19 However, this effect is usually neglected in simple calculations if the frequencies of rotation and vibrations have values of different orders of magnitude. In exact calculations, one also considers the effect of the anharmonicity and the interaction

between rotation and vibrations.

Translational motion

The distribution of molecules over velocities v in translational motion obeys the Maxwell distribution law

$$dn(v) = N\sqrt{\frac{2m^3}{\pi kT}}\, e^{-\frac{mv^2}{kT}} v^2 dv, \qquad (1.20)$$

where m is the mass of a molecule; N is the total number of the molecules.

The corresponding statistical sum is

$$Z = \frac{1}{h^3}(2\pi mkT)^{3/2}V, \qquad (1.21)$$

where V is the volume occupied by the gas.

The number of collisions per unit time of a molecule of gas A with molecules B is

$$f = 2d^2 n_B \left(\frac{2\pi kT}{m_B}\right)^{1/2},$$

where $d = \frac{1}{2}(d_A + d_B)$ is the sum of the radii of the molecules A and B; n_B is the number of molecules of gas B per unit volume.

Excitation of electrons

The quantum levels of electrons in molecules and atoms for a majority of substances differ even more than the vibrational levels of the molecules, and even at temperatures on the order of 10,000°K are greater than kT for many gases. For example, $\varepsilon_1 - \varepsilon_0 = 6.1$ eV for N_2; $\varepsilon_1 - \varepsilon_0 = 2.37$ eV for N; $\varepsilon_1 - \varepsilon_0 = 1.96$ eV for O; $\varepsilon_1 - \varepsilon_0 = 0.98$ eV for O_2; $\varepsilon_2 - \varepsilon_0 = 1.62$ eV for O_2; $\varepsilon_1 - \varepsilon_0 = 5.29$ eV for NO. Therefore, at temperatures up to 10^4°K, the molecules are mainly in the ground electronic state and the statistical sum to a first approximation consists only of one term, $g_0 e^{-\frac{\varepsilon_0}{kT}}$. The statistical

weights of the ground states will have the following values: $g_0 = 1$ for N_2; $g_0 = 4$ for N; $g_0 = 9$ for O; $g_0=3$, $g_1=2$, $g_2=3$ for O_2; $g_0 = 4$ for NO. Strictly speaking, atomic oxygen has two more levels with $\varepsilon_1-\varepsilon_0=0{,}0197$ and 0.0282 eV, and NO — a level with $\varepsilon_1-\varepsilon_0=0{,}0153$ eV. However, at temperatures on the order of several thousand degrees, these levels may be included in the ground state by changing its weight correspondingly. When calculating the statistical sums by means of computers, one takes a larger number of terms, but the contribution of the higher-order terms is small. / 20

Heat capacity of gases

Now we shall show how the heat capacity of a gas, whose composition does not change with a changing temperature, can be obtained in terms of the statistical sums of various degrees of freedom of a gas. Since the thermodynamic functions of a gas can be expressed in terms of the statistical sums, this will at the same time illustrate the computation of the former.

The classical theory of heat capacity of gases assumes that the energy of molecules is equally distributed among all degrees of freedom and equal to kT/2 per degree of freedom, except for the vibrational degrees, each one of which contributes the energy kT. Hence the heat capacity of a gas volume containing n molecules can be expressed as

$$c_V=\left(\frac{1}{2}i+i'\right)kn,$$

where i' is the number of the vibrational, and i is the number of all other, degrees of freedom of the molecule.

If only the translational and rotational degrees of freedom are excited, then the heat capacity of a gas composed of linear molecules will be

$$c_V=\frac{5}{2}kn, \qquad (1.22)$$

and of nonlinear molecules

$$c_V=\left(\frac{3}{2}+\frac{3}{2}\right)kn=3kn. \tag{1.23}$$

When the vibrational degrees of freedom are excited according to classical theory, one adds the expression i'kn to the above expressions.

Classical theory turns out to be valid only within certain limits, and only a statistical theory gives results that are applicable within a wide range of gas parameters [see Eq. (1.6)]. For a system having a number of degrees of freedom, in the absence of their interaction, the total statistical sum Z represents a product of the statistical sums corresponding to the individual degrees of freedom.

$$Z=Z_t Z_r Z_{vib} Z_{el}. \tag{1.24}$$

The statistical sum for a gas consisting of molecules of several types, equals the product of statistical sums for each type, Z_i, divided by the factorial of the number of molecules $N_i!$ of a given type in the system; Z_i is given by Eq. (1.24).

Since the heat capacity at constant volume is given by the logarithm of the statistical sum [see Eq. (1.6)], then each of the factors in the statistical sum makes its contribution to the heat capacity independently of the others. Consequently, the heat capacity changes depending on the temperature as different degrees of freedom become excited: for the air at room temperature it is determined only by the translational and rotational parts, defined by the classical formulas, and with increasing temperature up to several hundred degrees the vibrational degrees of freedom become excited. Here for a harmonic oscillator the heat capacity is

/21

$$c_{V_{vib}}=k\frac{(T_v/T)^2\exp(T_v/T)}{[\exp(T_v/T)-1]^2}. \tag{1.25}$$

The plot of the vibrational heat capacity versus T/T_V is shown in Fig. 1.3. With increasing T/T_V, the heat capacity approaches its classical value, equal to k. However, even at $kT \approx h\nu$ it differs very little from the limiting value for $T/T_v = 1$, $\frac{c_V}{k} = 0{,}92$).

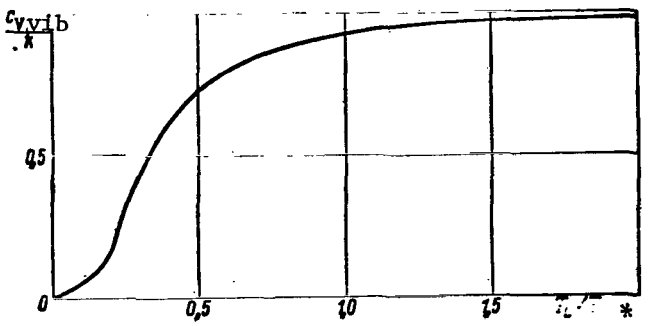

Figure 1.3 Heat capacity of a single vibrational degree of freedom versus temperature T/T_V

As shown in Table 1, the characteristic vibrational temperatures are very high, and under these conditions chemical reactions play a significant role. Therefore, / 22 the vibrational heat capacity of a gas does not reach its classical value.

1.3 Basic concepts and definitions of chemical kinetics

Homogeneous reactions

In chemical kinetics, we write reactions in the following form

$$A + B \underset{k_r}{\overset{k_f}{\rightleftarrows}} C + D, \qquad (1.26)$$

where k_f and k_r are the rate constants of the forward and reverse reactions; A,B,C,D are the substrates and products of the reaction.

Depending on the conditions, either the forward or reverse reaction may be dominant, but to some extent the process always goes in both directions.

Reactions are called monomolecular if one molecule participates in an elementary reaction; bimolecular - if two molecules are substrates, etc.. It is clear that the molecularity of the forward and reverse reactions may be different. For example, in

*Translator's note: Illegible in original foreign text.

the reaction $A \rightleftarrows B+C$ the forward reaction is monomolecular, and the reverse one - bimolecular.

In general, the reaction equation may be written in the form

$$\sum_{j=1}^{n} a_j X_j \rightleftarrows \sum_{j=1}^{n} b_j X_j, \tag{1.27}$$

where the sum is over all components participating in the reaction. The coefficients a_j and b_j (stoichiometric coefficients of the reaction) enter simultaneously in the equation, since the same substance may be among the substrates or products. If a substance appears (or disappears) in the course of a reaction, then on the other side of the equation the corresponding coefficient is zero.

A change per unit time in the amount of a substance determines the rate of the reaction. The reaction rate depends on the concentration of the components and can be expressed differently depending on the way in which the concentration is expressed.

The concentration of a substance i may be expressed in terms of the number of its molecules per unit volume, n_i, for example [$1/cm^3$]. The molar volume concentration is defined as the number of moles of a substance per unit volume [$mole/cm^3$]:

$$[X_i] = \frac{n_i}{N_0}, \tag{1.28}$$

where $N_0 = 6{,}02 \cdot 10^{23}$ is the Avogadro number. / 23

The molar mass concentration c_i is defined as the number of moles of a substance per unit mass [mole/g]:

$$c_i = \frac{[X_i]}{\rho}.$$

As the relative concentrations, we use the following:

1. Molar fraction

$$\xi_i = \frac{n_i}{\sum_i n_i}, \tag{1.29}$$

2. Mass fraction (relative density)

$$\alpha_i = \frac{m_i n_i}{\Sigma m_i n_i} = \frac{\rho_i}{\rho} = \frac{M_i n_i}{\Sigma M_i n_i}, \tag{1.30}$$

where m_i is the mass of a molecule of a substance; M_i is the molecular weight of the substance.

3. The degree of dissociation α is the ratio of the number of dissociated molecules to their total number before dissociation at constant mass of the gas.

4. The ratio of the number of molecules of a substance per unit volume to the equivalent number of molecules (the number of molecules obtained when recalculating the initial number of molecules n_∞ in proportion to the density):

$$\gamma_i = \frac{n_i}{n_э}; \quad n_э = n_\infty \left(\frac{\rho}{\rho_\infty}\right). \tag{1.31}$$

A reaction rate is most simply expressed in terms of the molar volume concentrations: according to the law of mass action, the rate of change of a component X_k in a constant volume in a direct reaction, expressed in terms of molar volume concentrations, will be

$$\frac{d[X_k]}{dt} = k_f (b_k - a_k) \prod_{j=1}^{n} [X_j]^{a_j} \tag{1.32}$$

and in a reverse reaction

$$\frac{d[X_k]}{dt} = k_r (a_k - b_k) \prod_{j=1}^{n} [X_j]^{b_j}, \tag{1.33}$$

where k_f, k_r are reaction rate constants (the subscript f here refers to the forward reaction; r — to the reverse one).

It will be noted that dividing Equation (1.32) by $b_k - a_k$, one obtains quantities which are identical for all components participating in the reaction. The expression $\frac{1}{b_k - a_k}\frac{d[X_k]}{dt} = k_f \prod_{j=1}^{n} [X_j]^{a_j}$ / 24 represents the rate of the forward reaction. Similarly, one obtains the rate of the reverse reaction.

It is easy to also write the rate of a reaction in terms of the number of molecules per unit volume, using (1.28). The dimensionality of the rate constant depends on the units in terms of which the concentration is expressed. In the case of concentrations expressed in mole/cm^3 the dimension of the rate constant for the reaction (1.32) is $[\text{mole}]^{1-s}\ [\text{cm}^3]^{s-1}\ [\text{s}]^{-1}$ where $s = \sum_{j=1}^{n} a_j$, and in the case of the concentration expressed in terms of the number of molecules per unit volume whose dimension will be $[\text{cm}^3]^{s-1}\ [\text{s}]^{-1}$.

The value of s determines the order of a reaction. If s = 1,2,3, etc., then the reaction is called a reaction of first, second, third order, respectively. The order of a reaction can be established experimentally by using Eq. (1.32). Then the value of s is considered an unknown. For complicated reactions by proceeding in several stages the order of a reaction may not coincide with its molecularity and may even be fractional. Evidently in such cases the equation of a reaction of the form (1.27), relating only the initial and final products (the gross reaction), does not reflect the complexity of the process.

The reaction rate constant does not depend on the concentration of substances and pressure, but it depends on the temperature. According to the Arrhenius law, the rate constant can be expressed as

$$k = B(T)e^{-\frac{E_a}{RT}}, \qquad (1.34)$$

where E_a is the activation energy; $B(T)$ is a factor multiplying the exponential (the classical Arrhenius law is obtained if B is independent of the temperature).

The exponent in the Arrhenius law yields a very sharp temperature dependence of the reaction: at temperatures much less than E_a/R, the rate constant is very small, and generally the reaction occurs only at temperatures on the order of E_a/R.

It is possible to interpret the Arrhenius law on the basis of the kinetic theory of gases [3]*. However, a theoretical determination of the reaction rate constants is so far impossible, and /25
theory at best gives only the order of magnitude of the constants, or makes it possible to make a reasonable extrapolation of the available data**. Therefore, the rate constants are found experimentally.

The sequence of elementary reactions, occurring in a system, is called the reaction mechanism. A reaction mechanism may involve a lot of branching (branched reactions) and include the set of reactions that do not enter the equation of the gross reaction, connecting the initial and final reaction products. The intermediate processes may determine the reaction rate, and therefore from the form of the gross reaction it not always possible to draw conclusions about the order of a reaction, its pressure dependence, etc. In particular, for example, in a monomolecular reaction there may participate inert atoms that do not change during the reaction, and the reaction will actually be bimolecular.

$$O_2 + M \rightarrow 2O + M.$$

---

* A reaction between molecules occurs only when the energy of colliding molecules exceeds a certain threshold E_a. The exponent in Eq. (1.34) corresponds to the temperature dependence of the number of molecules with energy greater than E_a.

** See, for example, [4,5].

In this example, the reverse reaction occurs through three collisions. A detailed explanation of the reaction mechanism is a very complex problem that has been completely solved only in very rare cases. The reaction mechanism may depend greatly on the temperature: as a result of the strong dependence of the reaction rate on the temperature, with a change in the temperature reactions that hardly occur at other temperatures may assume great importance. However, in many applications it is enough to know the equation of the gross reaction and the corresponding reaction rate coefficients.

It is clear that the total change in the amount of the substance during a reaction is determined both by the forward and reverse reactions:

$$\frac{d[X_k]}{dt}=k_f(b_k-a_k)\prod_{j=1}^{n}[[X_j]^{a_j}+k_r(a_k-b_k)\prod_{j=1}^{n}[X_j]^{b_j}. \tag{1.35}$$

The reaction rate can be written as

$$J_k=k_f\prod_{j=1}^{n}[X_j]^{a_j}-k_r\prod_{j=1}^{n}[X_j]^{b_j}. \tag{1.36}$$

In the initial stages, when only the initial substances exist in the system, the reaction goes primarily in the forward direction. As the final products accumulate, the reaction rate slows down, and in the state of equilibrium the rate of the forward reaction is equal to the rate of the reverse reaction (for any k):

$$\frac{d[X_k]}{dt}=0. \tag{1.37}$$

/ 26

Eqs. (1.36) and (1.37) imply that in the state of equilibrium the ratio of concentrations is constant. This quantity is called the equilibrium constant

$$K_c=\frac{k_f}{k_r}=\frac{\sum_{j=1}^{n}[X_j]^{b_j}}{\sum_{j=1}^{n}[X_j]^{a_j}}. \tag{1.38}$$

The temperature dependence of the equilibrium constant can be expressed in the form

$$K_c = F(T)e^{-\frac{\Delta E}{RT}}. \qquad (1.39)$$

This dependence is also very sharp, since it is mainly determined by the exponent $\exp(-\Delta E/RT)$. However, in contrast with the Arrhenius law the exponent involves the binding energy ΔE rather than the activation energy E_a. It is easy to see from Eq. (1.38) that the binding energy is equal to the difference between the activation energies of the forward and reverse reactions.

One can introduce the equilibrium constant that connects the partial pressures of the components if one uses the Clapeyron equation $p_j = [X_j]RT$:

$$K_p = \frac{\prod_j^n p_j^{b_j}}{\prod_j^n p_j^{a_j}} K_c (RT)^{\sum (b_j - a_j)}. \qquad (1.40)$$

This quantity also depends on the temperature and the molecular constants.

If one introduces the statistical sums Z_{cj}, in each of which the energy is measured from the lowest state, the equilibrium constant can be written as

$$K_c = \frac{\prod_{j-1}^n Z_{cj}^{b_j}}{\prod_{j-1}^n Z_{cj}^{a_j}} e^{-\frac{\Delta E}{RT}}, \qquad (1.41)$$

and, consequently, it can be calculated using the methods of statistical mechanics. The exponential multiplier in this formula is the quotient of the statistical sums of the ground electron states.

The equilibrium constant can be used to determine the rate constants of the forward or reverse reactions, if the rate constant / 27 of the reaction going in the opposite direction is known. The

present state of theory and experimental techniques is such that in many cases this method is more reliable than a direct determination of both reaction rate constants. However, it should be kept in mind that a determination of reaction rate constants assumes that the reacting system is homogeneous and that there is a thermodynamic equilibrium in vibrational, rotational, and translational degrees of freedom. This imposes certain restrictions on the use of reaction rate constants and on the possibility of their extrapolation to unusual conditions.

It will be noted that for reactions going through triple collisions the activation energy is negligible, and therefore the rate constant for the reverse reaction, as shown in experiments, may be written in the form

$$k_r(T)=B(T)\approx\frac{1}{T^n}. \tag{1.42}$$

Thus, the rate constant for the forward reaction can be expressed in terms of the equilibrium constant

$$k_f=B(T)F(T)e^{-\frac{\Delta E}{RT}}, \tag{1.43}$$

and the activation energy is equal to the binding energy, in this case the dissociation energy.

By using the equilibrium constant, Eq. (1.35) will be written in one of the following forms

$$\frac{d[X_k]}{dt}=(b_k-a_k)k_r\left[K_c\prod_{j=1}^{n}[X_j]^{a_j}-\prod_{j=1}^{n}[X_j]^{b_j}\right]; \tag{1.44}$$

$$\frac{d[X_k]}{dt}=(b_k-a_k)k_f\left[\prod_{j=1}^{n}[X_j]^{a_j}-\frac{1}{K_c}\prod_{j=1}^{n}[X_j]^{b_j}\right]. \tag{1.45}$$

The dependence of the reaction rate on the density ρ can be conveniently studied by going over to the relative density (1.30). In terms of the new variables, Eq. (1.35) will be

written as

$$\frac{1}{M_k}\frac{da_k}{dt}=\left(\frac{\rho}{N_0}\right)^{\sum_{j=1}^{n}a_j-1}k_f(b_k-a_k)\prod_{j=1}^{n}\left(\frac{a_j}{M_j}\right)^{a_j}+$$

$$+\left(\frac{\rho}{N_0}\right)^{\sum_{j=1}^{n}b_j-1}k_r(a_k-b_k)\prod_{j=1}^{n}\left(\frac{a_j}{M_j}\right)^{b_j}. \qquad (1.46)$$ / 28

(It is clear that M_j and N_0 may be introduced in the definition of the reaction rate constant. Hence we obtain a rule for the conversion of the constants.)

Eq. (1.46) implies that the greater the stoichiometric coefficients on one of the sides of the reaction equation, the stronger the dependence of the reaction rate on the density. In particular, for binary reactions

$$2A \underset{k_r}{\overset{k_f}{\rightleftarrows}} A_2, \qquad (1.47)$$

in which the rate of change of the substance is written in terms of the molar volume concentrations as

$$\frac{1}{2}\frac{d[A]}{dt}=-k_f\{[A]^2-K_c^{-1}[A_2]\}, \qquad (1.48)$$

we get

$$\frac{1}{2}\frac{da_A}{dt}=-k_{f_a}\{\rho a_A^2-K_c^{-1}a_{A_2}\}. \qquad (1.49)$$

This implies that the rate of a monomolecular reaction does not depend on the density. The rate of a binary reaction is proportional to the density. Similarly, the rate of a reaction going through triple collisions is proportional to the square of the density, etc.. If in the equation for the binary reaction we make a change of variables $\tau=\rho t$, we obtain a similitude law for a binary reaction: if the density is multiplied by a certain factor, the corresponding times become reduced by the same factor. This "binary similitude law" is used in the aerodynamics of non-equilibrium processes, and it takes different forms depending on

the specific problem. A similar law for triple collisions is given by $\tau=\rho^2 t$, etc..

In addition, there are a number of other general laws for chemical reactions.

1. In each reaction, the number of atoms of an element remains constant (law of the conservation of mass).

2. Dalton's law $p=\sum_i p_i$. In particular, this law assumes a particularly simple form when using relative densities and molar fractions,

$$\sum_{i=1}^{n} \alpha_i = 1; \quad \sum_{i=1}^{n} \xi_i = 1. \tag{1.50}$$

3. The law of conservation of energy. Since the formation and breakdown of substances leads to a change in the energy contained in a substance in the form of the binding energy, chemical reactions are usually accompanied by thermal effects. If, for example, the formation of substance A is accompanied by an absorption of energy h_A per mole, then the formation of a substance / 29
in the amount ΔA leads to an absorption of energy $h_A \Delta[A]$. The total thermal effect of a reaction is determined by summing similar expressions over all components.

Heterogenous reactions

In addition to homogeneous reactions, i.e., reactions occurring in one phase, in aerodynamics we may also deal with heterogeneous reactions, i.e., reactions between different phases. In particular, such processes occur in the theory of the boundary layer, where reactions are possible between a gas and a solid or liquid material of the wall around which the gas flow occurs. In a simplified formulation of the problem, the reactions occurring at a solid surface may formally be written in the form

$$A + \text{surface} \underset{k_{wr}}{\overset{k_{wf}}{\rightleftharpoons}} B + \text{surface} \tag{1.51}$$

If the surface substance affects the reactions, it may either participate directly in the reaction or serve as a catalyst for reactions in the gas phase. Formally the rate of a reaction on the surface is written in the same way as for reactions in the gas phase

$$\frac{d[A]}{dt} = -k_{wf}[A]^{n_1} + k_{wr}[B]^{n_2}, \tag{1.52}$$

where n_1 and n_2 are the orders of the forward and reverse reactions, and the reaction rate is per unit surface area.

Reaction rate constants depend on the surface material, gas component, and the surface temperature. Tables of k_w for different materials are given in Section 5.1.

By analogy with the preceding, one can also introduce the equilibrium constant

$$K_c = \frac{k_{wr}}{k_{wf}} = \frac{[A]_p^{n_1}}{[B]_p^{n_2}} \tag{1.53}$$

and the reaction rate can be written in the form

$$\frac{d[A]}{dt} = -k_{wf}\left\{[A]^{n_1} - \frac{[A]_p^{n_1}}{[A_2]_p^{n_2}}[A_2]^{n_2}\right\}. \tag{1.54}$$

In particular, with a catalytic recombination of dissociated atoms on the surface according to the reaction of the form (1.47), the reactions are usually of first order:

$$\frac{d[A]}{dt} = -k_{wf}\left\{[A] - \frac{[A]_p}{[A_2]_p}[A_2]\right\}. \tag{1.55}$$

The equilibrium constant $\frac{[A]_p}{[A_2]_p}$ for atoms of oxygen and nitrogen, recombining on the surface, whose temperature is below 2,000°K, is very small. Therefore, we can neglect the second / 30 term of Eq. (1.55) in engineering applications. Otherwise, the

second term is also small in a majority of other catalytic reactions occurring in industry.

Therefore, in a majority of cases

$$\frac{d[A]}{dt} = -k_{wf}[A]^n. \qquad (1.56)$$

In those cases when the surface material itself participates in the reaction, a detailed analysis of the processes occurring on the surface is a very complex problem due to the change of the surface properties.

1.4 Nonequilibrium processes in a high temperature gas

Let us consider in more detail the physico-chemical processes in gases at high temperatures.

Three processes associated with a change in the internal degrees of freedom are characteristic of a high-temperature gas: excitation of the vibrational degrees of freedom of multi-atomic molecules, dissociation, and ionization, and they manifest themselves precisely in this order as the temperature increases. The characteristic temperatures of the corresponding processes for components of the air are: for vibrations $(2—3)\cdot 10^3$ K, for dissociation $(6—10)\cdot 10^4$ K, and for ionization, $(1—5)\cdot 10^5$ K. Similar relations among the characteristic temperatures hold also for other gases. Our attention below will be focused mainly on high-temperature processes in the air and in its components. From the point of view of aerodynamics, we are also interested in processes occurring in mixtures containing CO_2 and CO.

Vibrational relaxation

The relaxation of the energy of vibrational degrees of freedom reduces to an exchange of the energies of the vibrational degrees of freedom with other degrees of freedom of molecules and to its redistribution among the vibrational degrees of freedom.

Most often one considers the exchange between the energies of the vibrational degrees of freedom and the active degrees. In pure form, this process is of importance under conditions when the vibrational degrees may contain substantial amounts of energy.

The rate of the energy exchange process affects both the amount of energy stored in the vibrational degrees of freedom and the instantaneous value of the kinetic temperature of a gas. In addition, the excitation of vibrational degrees of freedom is / 31 associated with dissociation, since the excited gas molecules undergo dissociation.

Exchange of vibrational energy

A molecule can change its vibrational energy only in a collision with other particles. Two extreme types of collisions of molecules in a gas are possible from the point of view of a change of the vibrational state of a molecule: inelastic, in which there is an exchange between the vibrational energy and the active degrees of freedom, and elastic when there is an exchange of energy among the vibrational degrees of freedom alone (resonant transitions).

Obviously, intermediate cases of the simultaneous exchange of the vibrational energy of one molecule with the kinetic and vibrational energies of another molecule are also possible. The rate of energy exchange in these processes is proportional to the frequency of collisions and the probability of transition of a molecule from one level to another. At temperatures less than the characteristic temperature, the probability of the exchange of vibrational energy in the process of elastic collisions of the molecules of a pure two-atomic gas is higher by several orders than in the case of inelastic collisions, and therefore the relaxation process in pure two-atomic gases consists actually of two processes: fast and slow.

The fast process, characterized by the short time of relaxation, leads to the establishment of an equilibrium distribution of the vibrational energy among molecules, and maintains it subsequently. However, the vibrational temperature T_{vib}, which can be introduced for such an equilibrium system, is not equal to the kinetic temperature and only the slow process occurring simultaneously through inelastic collisions leads to the equalization of temperatures. It is clear that, if a two-atomic gas constitutes an admixture to a one-atomic gas, then the fast process is absent, since one can neglect the collisions of two-atomic molecules among themselves.

The probability of transitions of vibrational quanta depends on the character of molecular collisions. In many cases, the collision process may be considered to be close to adiabatic, i.e., close to a process for which in the case of vibrations a large number of molecular vibrations occurs during the collision time τ_c. If $\tau_c = a/v$, is an estimate of the collision time, where a is the radius of the intermolecular interaction, and $v = \sqrt{\frac{2kT}{\mu}}$ is the mean velocity of the molecules, we shall obtain the adiabaticity condition in the form $\frac{a}{v}\nu \gg 1$. The physical meaning of this parameter is that, during a relatively slow adiabatic collision, the impact of the oncoming molecule is averaged over all atoms of the molecule, and the energy is transferred to the molecule as a whole, and during a fast non-adiabatic collision the interaction involves mainly one of the atoms in the molecule, which receives the entire energy transferred during the collision. The character of the collision changes the temperature dependence of the probability of a quantum transition. The parameter $\tau_c v$ determines the conditions under which one can expect the appearance of the nonadiabaticity of a collision. This is possible for heavy molecules, excited molecules, and with high molecular speeds.

/ 32

A majority of gases that will be considered below undergo adiabatic collisions in the range of conditions characteristic of aerodynamic studies. The nonadiabaticity of a collision may be manifested, for example, in mixtures of I_2 with He at temperatures less than 1000°K. At temperatures corresponding to the maximum population of the lower levels, mainly single quantum transitions to neighboring levels are important, and the probability of multiquantum transitions turns out to be much lower. This permits us to use the harmonic oscillator model with good accuracy, and a majority of the calculations of the probability of transition are made under this assumption.

Calculation of vibrational relaxation

Most frequently, the equation of relaxation of vibrational energy e_{vib} is taken in the simple form

$$\frac{de_{vib}}{dt} = \frac{e_{vib}(T) - e_{vib}}{\tau_v}, \tag{1.57}$$

where $e_{vib}(T)$ is the vibrational energy corresponding to the thermodynamic equilibrium with translational degrees of freedom; τ if the time of relaxation.

If $e_{vib}(T)$ is considered constant and the initial value of the vibrational energy is set equal to e_{vib0}, then the solution of Eq. (1.57) is

$$e_{vib}(T) - e_{vib} = [e_{vib}(T) - e_{vib\,0}]\, e^{-\frac{t}{\tau_v}}$$

and, consequently, the time of relaxation is equal to the time during which the initial difference between $e_{vib}(T)$ and e_{vib} changes by a factor of e.

The derivation of Eq. (1.57), starting with the classic work of Landau and Teller [6], was considered by many workers (see, for example, survey of literature in [7]) under various

assumptions about the physical model of the process of relaxation. It was shown theoretically that an equation in the form of (1.57) / 33 may be obtained for the process of relaxation of pure two-atomic gases or a mixture of a small quantity of a two-atomic gas with a one-atomic gas. However, in both cases the model of the harmonic oscillator must be laid as a basis. Theory (see [7]) gives the following expression for the time of relaxation

$$\tau_v = \left[f P_{10} \left(1 - e^{-\frac{T_v}{T}} \right) \right]^{-1}, \qquad (1.58)$$

where f is the number of collisions of a molecule per second.

P_{10} is the probability of the molecule transition during a collision from the first vibrational level to the gound level.

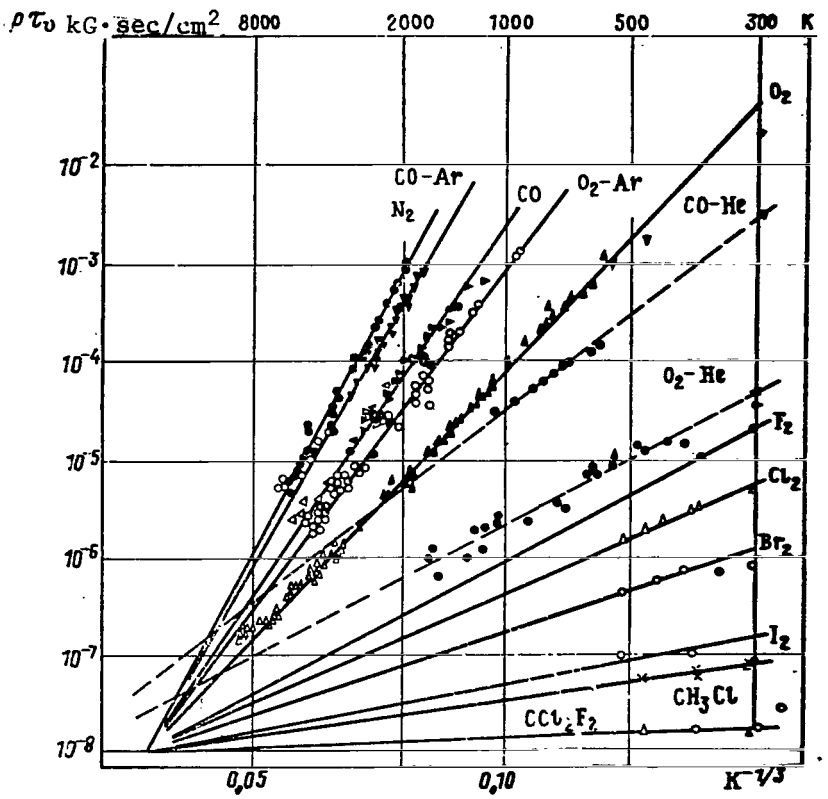

Figure 1.4 Time of relaxation of vibrational degrees of freedom of gases (Millikan and White's study of the experimental results obtained by different authors)

Since the theoretical dependence of P_{10} on the temperature in an adiabatic collision has the form $\ln P_{10} \sim T^{-1/3}$, then also the time of relaxation depends on the temperature mainly as $\exp -T^{-1/3}$, and the direct proportionality of the density of the number of collisions per unit time determines the direct proportionality between τ_v and the pressure. / 34

If the anharmonicity of vibrations plays an important role or the model of a harmonic oscillator with a cutoff is used (see Eq. (1.12)), then Eq. (1.57) turns out to be invalid and a more detailed study of the process of relaxation based on kinetic equations must be used. Therefore, Eq. (1.57) may be viewed as an approximate equation which describes the process better, the lower the temperature as compared with its characteristic value. The calculation of the transition probability presents a number of difficulties (see, for example, [8,9]), and a comparison of the theoretical results for P_{10} with experimental data shows the possibility of a discrepancy by an order of magnitude [10]. As far as the temperature dependence is concerned, the agreement with experiment is not bad (Fig. 1.4).

If the transition probabilities are known, then the relaxation process may be considered, using the kinetic equations, as describing the time dependence of the population of different levels of a quantum oscillator (see, for example, [11,12]). Such an approach is widely used in theoretical calculations of relaxation and has made it possible to obtain a number of interesting results, partially presented later.

Recently, general theoretical studies have appeared which make it possible to obtain the relaxation equations under very general assumptions starting with the Boltzmann equation [13-17]. Such an approach turned out to be productive in the study of vibrational relaxation. Thus, in [18], based on [13], the time of relaxation for N_2 and O_2 was obtained using a computer for

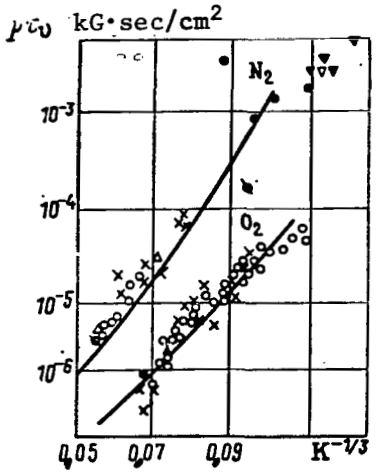

Figure 1.5. Comparison of theoretical time of relaxation with experimental data obtained by various workers (curve—theoretical data; points—experiment)

possible large differences between the temperatures of the vibrational and translational degrees of freedom. A comparison of theoretical results for the model of a harmonic oscillator with a cutoff with the results of experiments done by various workers is shown in Fig. 1.5.

Experimental data

/ 35

The time of vibrational relaxation at high temperature is mainly determined experimentally in shock tubes. Camac [19] who studied the relaxation of O_2 in a mixture of oxygen with argon in the temperature range 1200-7000°K gives the following expression for the time of relaxation.

$$\frac{1}{\tau_v} = nC_1T^{1/6}\left[1-\exp\left(-\frac{2228}{T}\right)\right]\exp\left[-(C/T)^{1/3}\right], \qquad (1.59)$$

where n is the number of molecules in 1 cm^3; $C = 1{,}04(\pm 30\%)\cdot 10^7$ K. The constant C_1 depends on the type of colliding molecules; for argon $C_1 = 1{,}2\cdot 10^{-7}$, for O_2 the constant is $C_1 = 6\cdot 10^{-7}\ \frac{\text{см}^3}{\text{sec}\cdot T^{1/6}\ \text{part}}$.

The times of relaxation, obtained according to Blackman's date [20] for oxygen and nitrogen are

$$\tau_v \cdot p = 1{,}6\cdot 10^{-9}\exp\left(\frac{10\,144}{T^{1/3}}\right)\ \text{kG·sec/cm}^2; \qquad (1.60)$$

$$\tau_v \cdot p = 1{,}1 \cdot 10^{-11} T^{1/2} \exp\left(\frac{154}{T^{1/3}}\right) \text{ kG} \cdot \text{sec}/\text{cm}^2 . \qquad (1.61)$$

The rate of vibrational relaxation of nitrogen oxide was studied by Robben and Rae. Robben [21] in the temperature range 400-1500°K has not found any effect of argon admixture on the relaxation process up to 99% argon content. Rae's experiments [22] encompassed the temperature range from 1500 to 7000°K. He found that the effectiveness of the NO-NO-collisions is approximately 50 times higher than that of the NO-Ar collisions. His results are in better agreement with theory than Robben's. However, it must be kept in mind that the relaxation of nitrogen oxide is anomalous, and does not fit into the general scheme (see [7]).

The most comprehensive data on the times of vibrational relaxation for various gases are given in a paper by Millikan and White [23]. These workers reduced the well-known results to a particularly simple form: in semilogarithmic coordinates $p\tau_v$, and $T^{-1/3}$, they constructed the straight lines that give the corresponding relations for oxygen and nitrogen, and then through the point of intersection of the straight lines ($(p\tau_v = 10^{-8}$ kG·sec/cm^2, $(T\,\text{K})^{-1/3} = 0{,}03$) they have plotted straight lines that best fit the experimental data for a large number of other gases (see Fig. 1.4).

It turned out that this type of simplication is possible in many other cases. It was assumed that the vibrational system allows only one type of collision between a two-atomic oscillator and another molecule. One also excludes the case of resonance, as for example for the N_2+CO [24], system [24], even though, as we can see from Figure 1.4, such an approach may also be used in the case of multiatomic gases. In addition, when one of the /36 particles is very light—for example, a helium atom— the experimental points do not fit a universal relation.

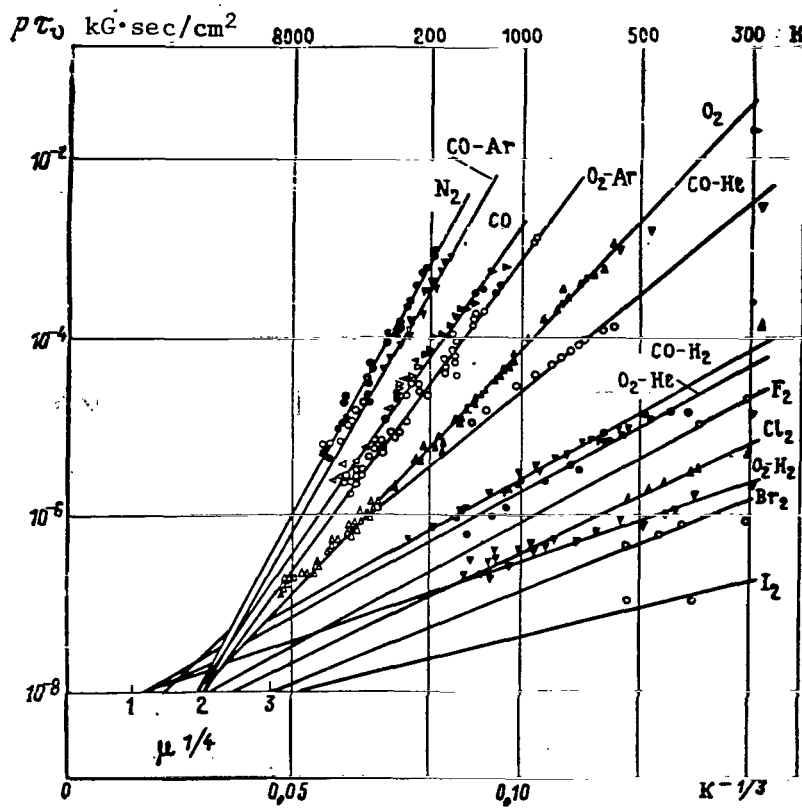

Figure 1.6. Relaxation times for vibrational degrees of freedom of gases (taking into account molecular masses)

This approach permits us to present in a general form, valid in the temperature range from 500 to 8000°K, numerous relations for the relaxation time that have been proposed earlier. This is also convenient for extrapolation in cases when the experiment gives only a few points.

The plot shown in Fig. 1.6 [23] may be more widely applicable. The plot also includes collisions with a light component. Here the straight lines do not pass through a single point any more but instead they depend on the parameter μ [μ is the reduced mass, see Eq. (1.17)], selected as a result of many tests. / 37

The relation illustrated in Fig. 1.6 has the form

$$p\tau_v = \exp[A(T^{-1/3} - 0{,}015\mu^{1/4}) - 18{,}42]. \qquad (1.62)$$

The values of A are given in Table 2 and in Figs. 1.7 and 1.8.

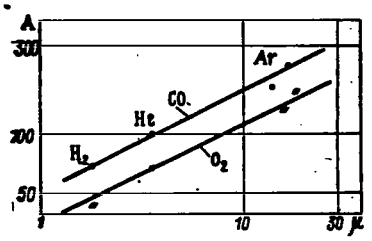

Figure 1.7. Plot of the coefficient A versus reduced mass μ for CO and O_2 (molecules colliding with CO or O_2 are shown around the corresponding points)

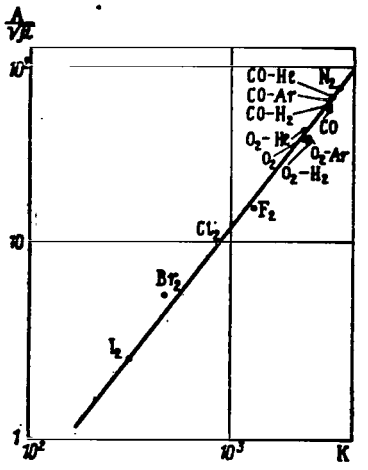

Figure 1.8. Plot of the coefficient $A\mu^{-1/4}$ versus the characteristic temperature $T_v = h\nu/k$.

TABLE 2

VALUES CHARACTERIZING THE VIBRATIONAL RELAXATION OF VARIOUS GASES*

Gases	N_2	CO—Ar	CO	CO—He	CO—H_2	O_2—Ar	O_2	O_2—He	O_2—H_2	F_2	Cl_2	Br_2	I_2
μ	14	16,5	14	3,5	1,75	17,8	16	3,56	1,88	19	35,5	79,9	126
T_v K	3395	3080	3080	3080	3080	2239	2239	2239	2239	1284	812	465	310
A	220	213	175	99	68	165	129	67	42	65	58	48	29

* Commas represent decimal points.

Using the Landau-Teller theory [6] which gives the principal term which is retained in more detailed analysis [9,10], one can obtain the relation between A and the reduced mass μ and the characteristic temperature T_v (see Fig. 1.8):

$$\lg p\tau_v = 5\cdot 10^{-4}\mu^{1/2}T_v^{4/3}(T^{-1/3} - 0{,}015\mu^{1/4}) - 8{,}00. \qquad (1.63)$$

The accuracy of this formula is illustrated in Table 3 [23]. / 38
On the average, the deviation is less than 50%, which is quite acceptable if one considers that the formula encompasses the following ranges $1{,}75 < \mu < 127$; $310\,\text{K} < T_v < 3395\,\text{K}$; $280\,\text{K} < T < 8000\,\text{K}$.
Of course, one must keep in mind that the relation is not satisfied, where dissociation becomes important. However, in general, Eq. (1.63) increases slightly the time of relaxation for collisions with a two-atomic molecule, and lowers it for collisions with atoms.

TABLE 3

COMPARISON OF EXPERIMENTAL AND THEORETICAL VALUES OF THE TIME OF RELAXATION*

Gases	T K	τ_v exp.	τ_v theor.
N_2	5000	6,6·10−6	6,5·10−6
	2000	7,4·10−4	6,4·10−4
CO	5000	1,9·10−6	3·10−6
	2000	6,8·10−5	1·10−5
O_2	5000	4,0·10−7	4,4·10−7
	2000	6,0·10−6	7,8·10−6
	1000	1,0·10−4	1,2·10−4
	500	2,5·10−3	4,0·10−3
O_2—Ar	2000	3,0·10−5	1·10−5
	1000	2,9·10−4	1,9·10−4
Cl_2	300	6,8·10−6	3,6·10−6
Br_2	300	9·10−7	5·10−7
I_2	400	1·10−7	1·10−7

* Commas represent decimal points.

Vibrational relaxation of a mixture of gases

If a two-atomic gas constitutes a small fraction in a mixture of one-atomic gases, then using the condition $\frac{f_{iA}}{f}=\xi_i$, where f_{iA} is the number of collisions of a two-atomic molecule A per second with molecules of a one-atomic gas i; f is the total number of collisions per second, and ξ_i is the molar fraction of molecules i, one can obtain the time of relaxation of a mixture from the relation

$$\frac{1}{\tau_v}=\sum_i \xi_i/\tau_{Ai}. \qquad (1.64)$$

Here τ_{Ai} is the time of relaxation of a two-atomic gas, obtained when all molecules of one-atomic gases are replaced with molecules i. For a binary mixture of a one-atomic gas A with a two-atomic gas BC, the expression for the time of relaxation is

$$\frac{1}{\tau_v}=\frac{1-\xi_A}{\tau_{BC-BC}}+\frac{\xi_A}{\tau_{A-BC}}. \qquad (1.65)$$

The relaxation of a mixture of two-atomic gases is greatly complicated as a result of the possible processes of vibrational energy exchange among components of the mixture [25]. Thus, in a binary mixture of two-atomic gases A and B three relaxation times are possible: two correspond to the relaxation of pure gases (τ_A and τ_B, and the third τ_{AB} corresponds to an exchange of vibrational energy among the components. /39

If the exchange may be neglected $(\tau_{AB}\gg\tau_A, \tau_B)$, then the relaxation of each component is independent, and when calculating the rate of relaxation for each component one does not have to take into account the internal degrees of freedom of the second component. If the exchange cannot be neglected, then various cases, determined by the relative values of $\tau_A, \tau_B, \tau_{AB}$, are possible. Thus, for $\tau_{AB}\ll\tau_A\ll\tau_B$ there is first a redistribution of the original vibrational energy among components of the mixture, and after a time τ_{AB} from the beginning of the process, it may be considered an equilibrium process. After

that the energy of translational motion will become converted to the vibrational energy of component A, since $\tau_A \ll \tau_B$.

The exchange of vibrational energy results in a transfer of vibrational energy from component A to component B, and since $\tau_A \gg \tau_{AB}$ the distribution of energy between A and B will be an equilibrium distribution. As a result, the relaxation of gas A occurs more slowly, and that of gas B speeds up and the process is characterized by a single time of relaxation, intermediate between τ_A and τ_B.

If $\tau_A \ll \tau_{AB} \ll \tau_B$, then initially an equilibrium energy distribution is established in gas A, and then the vibrational energy is removed from the equilibrium distribution of component A to component B.

As a result, the time of relaxation of gas B becomes less than τ_B. The time of relaxation of the mixture is determined by τ_{AB}.

In either case, the time of relaxation depends on the relative concentration of the components of the mixture.

The systems where an exchange of vibrational energy among components is important also include the practically important mixtures N_2—O_2, O_2—H_2, CO—O_2 in addition to N_2—CO . As shown in [26], the gas N_2 at temperatures below 3000°K in mixtures N_2—O_2 is excited much faster than in the case of a pure gas, but still slower than O_2 in the same mixtures. The process cannot be explained as a transfer of energy from the translational degrees of freedom in collisions of N_2 and O_2. The transfer of vibrational energy from O_2 to N_2 only slightly extends the time of relaxation of O_2. At the same time, the time of relaxation for N_2 decreases, for example, by an order of magnitude at the temperature 1600°K.

With an increase in the temperature, the effect of resonance exchange becomes smaller.

Relaxation of multiatomic gases

Comparison of the times of relaxation

In multiatomic gases, the vibrational relaxation is even more complicated than in two-atomic gases as a result of the presence of a large number of natural forms of molecular vibrations. In some cases, one can draw an analogy with the Millikan-White generalization [27]. One can make two extreme assumptions that simplify the discussion of relaxation: either all forms of vibrations are equivalent in the transfer of energy from translational degrees of freedom to vibrational ones (parallel excitation), or at first one of those forms is excited, and then there is an exchange of energy among the vibrational degrees of freedom (sequential excitation). In the first case, one writes and solves relaxation equations like the Landau-Teller equation for each form of vibrations, as, for example, in [28]. However, in general this area has been hardly touched.

From a comparison of the times of relaxation for different gases, one can draw the following general conclusions [1]:

1. Two-atomic molecules have the longest times of relaxation.

2. At a given temperature and pressure, the time of relaxation is in general longer for molecules with a large binding energy.

3. Three-atomic linear molecules have longer times of relaxation than the nonlinear three- or multiatomic ones.

4. Admixtures of other gases may have an extremely large influence on the time of relaxation. For example, the time of relaxation may be sharply reduced by water vapor.

Chemical Reactions

Kinetics of reactions in the air

The dissociation of molecules into atoms followed by the interaction of the atoms among themselves and with the nondissociated molecules is a characteristic feature of the behavior of multiatomic gases at high temperatures. In a gas mixture—for example, in the air—the reaction scheme at high temperatures is very complicated and usually includes a large number of reactions part of which are important in a certain temperature range and unimportant in another, where other reactions may play the principal role. The discovery of a reaction mechanism, playing an important role under given conditions, is the most important problem of the chemistry of a high-temperature gas.

For the air in the temperature range from 2000 to 10,000°K, the following scheme consisting of five reactions is considered basic

(1) $O_2+M+5{,}1\ \text{eV} \underset{k_r}{\overset{k_f}{\rightleftarrows}} 2O+M;$ (1.66)

(2) $N_2+M+9{,}8\ \text{eV} \rightleftarrows 2N+M;$ (1.67)

(3) $NO+M+6{,}5\ \text{eV} \rightleftarrows N+O+M;$ (1.68)

/ 41

(4) $N+O_2+1{,}4\ \text{eV} \rightleftarrows NO+O;$ (1.69)

(5) $O+N_2+3{,}3\ \text{eV} \rightleftarrows NO+N.$ (1.70)

(Here M is a third molecule.)

To this scheme we add still another reaction

(6) $N_2+O_2+1{,}9\ \text{eV} \rightleftarrows 2NO.$ (1.71)

The scheme includes three dissociation reactions (1,2,3) and two exchange reactions (4,5). The calculations originally made without considering reactions (4,5) have led to significant errors. Reaction (6) was considered in the calculations made after 1962, since in the studies published in [29,30] it was found that its rate is sufficiently high and the reaction may be included in the system of equations. With the reaction rates found, the reaction in question has an effect on the initial formation of NO behind a shock wave, even its effect on the thermo— and gas-dynamic parameters of the flow is small.

However, recent studies [31] of the rate constant of the forward reaction (6) give values 10 times lower than those obtained in [29], and a conclusion was drawn that the reaction may be neglected. [31] emphasizes that the NO balance is primarily influenced by the reaction

$$2NO \rightleftarrows N_2O + O.$$

In these calculations, the final results about the effect of reaction(6) were used only recently.

This reaction scheme was intensely studied by various workers, and the reaction rate constants continue to be found with increasingly greater precision. From time to time, papers appear in which the aerodynamic problems similarly formulated are solved again by using new data on chemical kinetics or by considering new processes which have not received enough attention before. As will be shown below, thus far there are no firmly established expressions for reaction rate constants. However, the results already available are in many cases sufficient not only in approximate calculations but also when one wants to obtain fairly reliable values of various quantities.

The values of the equilibrium constants are much more reliable, and can be considered to be established with a high

degree of accuracy. For the reactions given before, the constants are listed in Table 4 [22] (see also [32]).

The existing rate constants for reactions in the air are studied in detail in [7,22]. As compared with the first calculations made by Duff and Davidson [33] and S. A. Losev (see [7]) using a full system of reactions in the air, the reaction constants have changed a great deal. We shall show the variations of the rate constants using an example of oxygen dissociation.

TABLE 4

EQUILIBRIUM CONSTANTS $K_c = \frac{k_f}{k_r}$ FOR REACTIONS OF AIR COMPONENTS* / 42

Reaction	mole/cm^3
(1) $O_2 + M \rightleftarrows 2O + M$	$\frac{1{,}2 \cdot 10^3}{T^{1/2}} \exp\left(-\frac{59\,000}{T}\right)$
(2) $N_2 + M \rightleftarrows 2N + M$	$18 \exp\left(-\frac{112\,450}{T}\right)$
(3) $NO + M \rightleftarrows N + O + M$	$4{,}0 \exp\left(-\frac{75\,000}{T}\right)$
(4) $N + O_2 \rightleftarrows NO + O$	$4{,}2 \exp\left(\frac{16\,010}{T}\right)$
(5) $O + N_2 \rightleftarrows NO + O$	$4{,}5 \exp\left(-\frac{37\,500}{T}\right)$
(6) $N_2 + O_2 \rightleftarrows 2NO$	$19 \exp\left(-\frac{21\,490}{T}\right)$

* Commas represent decimal points.

Earlier, papers often used the rate constant for oxygen dissociation obtained by Mathews [34]:

$$k_f = 1{,}1 \cdot 10^{25} T^{-2{,}5} \exp\left(-\frac{59\,300}{T}\right) \frac{\text{cm}^3}{\text{mole} \cdot \text{sec}}. \qquad (1.72)$$

The same constant was also recommended in [7] for the temperatures 2400-7000°K on the basis of results obtained by S. A. Losev and N. A. Generalov.

The rate constants for reactions (1,3) occurring in collisions with molecules that do not change during the reaction depend on the type of colliding molecules. Rink, Knight, and Duff [35] give the following values for recombination constants for oxygen, determined in the temperature range 3000-6000°K

$$4{,}7\cdot 10^{17}T^{-1};\quad 1{,}6\cdot 10^{18}T^{-1};\quad 4{,}8\cdot 10^{18}T^{-1}\ \frac{\text{cm}^6}{\text{mole}^2\cdot\text{sec}}. \tag{1.73}$$

The authors have received these values for the cases when the other participants of the collision are Xe, O_2, O, respectively. It is noted that the experiment gives a deviation of the degree of the pre-exponential dependence on the temperature from -1/2 to -2. The minus one power in the above expressions was selected arbitrarily. Camac and Vaughan [36] give the following constant for the dissociation of oxygen in argon

$$k_f = 3{,}6\cdot 10^{18}T^{-1}\exp\left(-\frac{59\,800}{T}\right)\frac{\text{cm}^3}{\text{mole}\cdot\text{sec}}. \tag{1.74}$$

Rae [22] gives the relation $k_{fO}=25\,k_{fAr}$ and $k_{fN_2}\approx\frac{1}{4}k_{fO_2}$. The last relation coincides approximately with the one recommended in [7]. The other reactions have been studied to an even lesser degree. / 43

The existing lack of agreement on the reaction rate constants results in a situation where different workers use different values for these constants. Therefore, in the appraisal of the results of calculations one must consider the possible effect of the constants, and when comparing the results of different calculations one will have to give a summary of the reaction rate constants used. In any case one must consider the fact that the numerical factor in front of the rate constants of even relatively thoroughly studied reactions may be improved within an order of magnitude, and — what is even more important— one can improve the temperature dependence of the pre-exponential factor, giving the extrapolation of the constant to the region of higher temperatures.

We shall only give a summary of the reaction rate constants published relatively recently. Apparently, the most complete summary of the reaction rate constants for the air is given in a paper by Lin and Teare [37] (Table 5).

TABLE 5

SUMMARY OF REACTION RATE CONSTANTS FOR AIR*

Reaction	M	$k_f(cm^3)^{s-1}\,sec^{-1}$
(1) $O_2 + M \rightleftarrows O + O + M$	O	$6{,}2\cdot10^{-28}\,T^{-3/2}$
	O_2	$2{,}2\cdot10^{-28}\,T^{-3/2}$
	N_2	$1{,}7\cdot10^{-32}\,T^{-1/2}$
(2) $N_2 + M \rightleftarrows N + N + M$	N, NO	$8{,}3\cdot10^{-33}\,T^{-1/2}$
	N	$6{,}5\cdot10^{-27}\,T^{-3/2}$
	N_2	$7{,}6\cdot10^{-32}\,T^{-1/2}$
(3) $NO + M \rightleftarrows N + O + M$	O_2, O, NO	$3{,}0\cdot10^{-32}\,T^{-1/2}$
	NO	$5{,}5\cdot10^{-27}\,T^{-3/2}$
(4) $O + N_2 \rightleftarrows NO + N$	O, N, O_2, N_2	$2{,}8\cdot10^{-28}\,T^{-3/2}$
	—	$2{,}7\cdot10^{-11}$
(5) $N + O_2 \rightleftarrows NO + O$	—	$2{,}2\cdot10^{-14}\,T\exp\left(-\frac{3560}{T}\right)$
(6) $N_2 + O_2 \rightleftarrows NO + NO$	—	$0{,}4\,T^{-5/2}\exp\left(-\frac{43\,000}{T}\right)$

/ 44

* Commas represent decimal points

These constants differ from the constants used in the earlier papers by the same workers (see, for example, [38]); the constants also do not coincide with those recommended by the Soviet workers for the range from 2000 to 6000 - 8000°K (Table 6) [7].

Finally, Martin [39], basing himself on Bortner, gives a summary of constants which also gives an estimate of their accuracy (discrepancy in the powers of the pre-exponential factor) (Table 7).

TABLE 6

SUMMARY OF REACTION RATE CONSTANTS FOR AIR*

Reaction	M	k_f cm^3/mole·sec
(1) $O_2 + M \rightarrow O + O + M$	O_2	$5{,}2 \cdot 10^{10} T^{1/2} (D/RT)^3 \exp(-D/RT)$
$D = 118$ k cal/mole	N_2	$2{,}5 \cdot 10^{11} T^{1/2} (D/RT)^{3/2} \exp(-D/RT)$
	O	$6{,}25 \cdot 10^{12} T^{1/2} (D/RT)^{3/2} \exp(-D/RT)$
	N, NO	$k_{1f}^{O_2}$
	Ar	$4{,}2 \cdot 10^{11} T^{1/2} D/RT \exp(-D/RT)$
(2) $N_2 + M \rightarrow N + N + M$	N_2	$4{,}25 \cdot 10^{11} T^{1/2} (D/RT)^{2,2} \exp(-D/RT)$
$D = 225$ k cal/mole	N	$1{,}85 \cdot 10^{12} T^{1/2} (D/RT)^{1,5} \exp(-D/RT)$
	O_2, O, NO	$k_{2f}^{N_2}$
	Ar	$6{,}8 \cdot 10^{11} T^{1/2} (D/RT)^{1,5} \exp(-D/RT)$
(3) $NO + M \rightarrow N + O + M$	O_2, N_2, Ar	$7 \cdot 10^{10} T^{1/2} (D/RT)^2 \exp(-D/RT)$
$D = 150$ k cal/mole	NO, O, N	$20\ k_{3f}^{Ar}$
(4) $O + N_2 \rightarrow NO + N$	—	$7 \cdot 10^{13} \exp(-75\,500/RT)$
(5) $N + O_2 \rightarrow NO + O$	—	$1{,}3 \cdot 10^{10} \exp(-7100/RT)$
(6) $N_2 + O_2 \rightarrow NO + NO$	—	$9{,}1 \cdot 10^{24} T^{-5/2} \exp(-128\,500/RT)$

$R = 1{,}987$ k·cal/mole K

* Commas represent decimal points

Here for k_f and k_r the expression $AT^b e^{-E/RT}$ was used. The value of A is given in $(cm^3/mole)^{s-1} \cdot sec^{-1}$, where s is the molecularity of the reaction.

We shall also note [40] which gives the dissociation rate constant for N_2, given by $\frac{d[N]}{dt} = 2k_d [N_2][M]$, as equal to $4{,}8 \cdot 10^7 \cdot 10^{17} T^{-1/2} e^{-E/RT}$; $4{,}3 \cdot 10^{22}\ T^{-3,2} \times e^{-E/RT}$; $1{,}9 \cdot 10^{17} T^{-1/2} e^{-E/RT}$ cm^3/mole, respectively, where M represents N_2, N, and Ar. The constant E/R is equal to 133,200°K.

TABLE 7

SUMMARY OF REACTION RATE CONSTANTS FOR THE AIR *

Reaction	M	Forward reaction			Reverse reaction		
		A	b	E/R in K	A	b	E/R in K
	N_2, O_2	$2{,}3\cdot10^{18\pm1}$			$1{,}9\cdot10^{16\pm0{,}3}$		
(1) $O_2+M\rightleftarrows O+O+M$	O	$8{,}5\cdot10^{18\pm1}$	−1	59400	$7{,}1\cdot10^{16\pm0{,}4}$	−1/2	0
	M	$3\cdot10^{18\pm1}$			$2{,}5\cdot10^{15\pm1}$		
	N_2	$3{,}8\cdot10^{19\pm0{,}4}$			$2{,}5\cdot10^{18\pm0{,}4}$		
(2) $N_2+M\rightleftarrows N+N+M$	N	$1{,}3\cdot10^{20\pm0{,}5}$	−1	113200	$7\cdot10^{18\pm0{,}5}$	−1	0
	M	$1{,}9\cdot10^{19\pm1}$			$1\cdot10^{18\pm1}$		
(3) $NO+M\rightleftarrows N+O+M$	M	$2{,}4\cdot10^{17\pm1}$	−1/2	75500	$3{,}2\cdot10^{18\pm1}$	−1	0
(4) $O+N_2\rightleftarrows N+NO$		$6{,}8\cdot10^{13\pm0{,}3}$	0	37750	$1{,}5\cdot10^{13\pm0{,}3}$	0	0
(5) $O+NO\rightleftarrows N+O_2$		$4{,}3\cdot10^{7\pm0{,}3}$	3/2	19100	$1{,}8\cdot10^{8\pm0{,}3}$	3/2	3300
(6) $N_2+O_2\rightleftarrows 2NO$		$2\cdot10^{14}$	0	61600	$1\cdot10^{13}$	0	1500

/ 45

* Commas represent decimal points

Kinetics of reactions in mixtures containing CO_2

In addition to reactions among components of the earth's atmosphere, the reactions between gases contained in the Venusian atmosphere— N_2, CO_2, O_2 —are also interesting. The reaction mechanism in this case becomes even more complicated. A summary of reactions which are considered to be principal in such a system is given in Table 8 [41].

Reactions (1) and (2) in this table represent the reactions of dissociation of the basic components and yield CO and oxygen and nitrogen atoms. The oxygen atoms react with N_2 and CO_2 [reactions (3) and (15)], where the latter together with reaction (16) of the dissociation of O_2 forms a chain equivalent to the dissociation of CO_2. Carbon monoxide CO dissociates as a result

of reaction (4). The rate of reactions involving CO depends very strongly on the presence of even small quantities of water, H, and OH. Therefore, reaction (6) together with reaction (17) forms a chain equivalent to the dissociation of CO_2, but in many cases going much more rapidly. It should be noted that the reactions with H_2O, O, H form a very complicated system which is reflected in a very simplified way by reaction (5) that leads to the formation of hydrogen.

In many cases, one must consider radiation and include a reaction of type (18) in the system. Reactions (7-14) are included to study the processes of ionization.

The rate constants for dissociation of O_2 were considered earlier. The remaining reactions have been studied less. The rate constant for dissociation of CO was obtained as an estimate based on an analogy with other dissociation reactions. The rate constant for reaction (18) is also an estimate whose accuracy is half an order. /46

A more detailed analysis of the system of reactions in mixtures containing CO_2 has shown [5] that one can limit himself to the reactions given in Table 9. /47

These reaction rate constants have been obtained using experimentally found values [42-44] (see also [45, 46, 47]).

Relation between the dissociation rate constant and the excitation of vibrations

The rate of dissociation, as usually defined in chemical kinetics, assumes the existence of equilibrium between translational and vibrational degrees of freedom. With rapidly occurring processes, there may not be equilibrium among vibrational degrees of freedom, and the distribution of the vibrational degrees will be of the Boltzmann type, but will differ from the

TABLE 8

REACTION RATE CONSTANTS IN THE MIXTURE OF CO_2 AND N_2 *

Reaction	$k_f \frac{cm^3}{sec}$	k_r
(1) $CO_2 + M \rightleftarrows CO + O + M$	$1 \cdot 10^{-8} e^{-36,400/T}$	$1 \cdot 10^{-36}$
(2) $N_2 + M \rightleftarrows N + N + M$	$5,17 \cdot 10^{-6} T^{-1/2} e^{-113,000/T}$	$3,37 \cdot 10^{-31} T^{-1/2}$
(3) $O + N_2 \rightleftarrows N + NO$	$1,17 \cdot 10^{-12} T^{1/2} e^{-38,500/T}$	$2,22 \cdot 10^{-13} T^{1/2}$
(4) $CO + M \rightleftarrows C + O + M$	$1.10^{-8} e^{-125,000/T}$	$1 \cdot 10^{-35}$
(5) $H_2O + M \rightleftarrows H + OH + M$	$1 \cdot 10^{-11} e^{-50,300/T}$	$1 \cdot 10^{31}$
(6) $CO_2 + H \rightleftarrows CO + OH$	$5 \cdot 10^{-12} e^{-16,780/T}$	$3,83 \cdot 10^{-14} e^{-5,190/T}$
(7) $N_2 + M \rightleftarrows N_2^+ + e + M$	$2 \cdot 10^{-20} T^{3/2} \left(1 + 2 \times \times 105 \frac{n_e}{n}\right) e^{-181,000/T}$	$5 \cdot 10^{-26}$
(8) $N + M \rightleftarrows N^+ + e + M$	$2 \cdot 10^{-20} T^{3/2} \left(1 + 2 \times \times 105 \frac{n_e}{n}\right) e^{-158,000/T}$	$1 \cdot 10^{-27}$
(9) $CO_2 + M \rightleftarrows CO_2^+ + e + M$	$2 \cdot 10^{-20} T^{3/2} \left(1 + 2 \times \times 105 \frac{n_e}{n}\right) e^{-160,000/T}$	$5 \cdot 10^{-26}$
(10) $CO + M \rightleftarrows CO^+ + e + M$	$2 \cdot 10^{-20} T^{3/2} \left(1 + 2 \times \times 105 \frac{n_e}{n}\right) e^{-169,500/T}$	$5 \cdot 10^{-26}$
(11) $O + M \rightleftarrows O^+ + e + M$	$2 \cdot 10^{-20} T^{3/2} \left(1 + 2 \times \times 105 \frac{n_e}{n}\right) e^{-140,000/T}$	$1 \cdot 10^{-27}$
(12) $N + O \rightleftarrows NO^+ + e$	$1,2 \cdot 10^{-12} e^{-32,000/T}$	$1 \cdot 10^{-8}$
(13) $N + N \rightleftarrows N_2^+ + e$	$1,87 \cdot 10^{-14} T e^{-67,700/T}$	$1 \cdot 10^{-5} T^{-1/2}$
(14) $O + O \rightleftarrows O_2^+ + e$	$2,79 \cdot 10^{-15} T^{0,65} e^{-80,800/T}$	$9 \cdot 10^{-5} T^{-1}$
(15) $O + CO_2 \rightleftarrows CO + O_2$	$1 \cdot 10^{-12} e^{-29,500/T}$	$1 \cdot 10^{-15} e^{-25,000/T}$
(16) $O_2 + M \rightleftarrows O + O + M$	$9,18 \cdot 10^{-7} T^{-1/2} e^{-59,800/T}$	$6,09 \cdot 10^{-32} T^{-1/2}$
(17) $OH + M \rightleftarrows O + H + M$	$1 \cdot 10^{-8} e^{-50,000/T}$	$1 \cdot 10^{-32}$
(18) $CO + N \rightleftarrows CN + O$	$4 \cdot 10^{-12} T^{1/2} e^{-46,000/T}$	$2 \cdot 10^{-13} T^{1/2} e^{-5,300/T}$

* Commas represent decimal points

TABLE 9 *

/ 47

Reaction	k_j cm^3/mole·sec
(1) $CO_2 + M \rightleftarrows CO + O + M$	$1{,}2 \cdot 10^{11} T^{1/2} \exp\left(-\frac{34\,360}{T}\right)$
(2) $N_2 + M \rightleftarrows 2N + M$	$8{,}6 \cdot 10^{19} T^{-1} \exp\left(-\frac{113\,350}{T}\right)$
(3) $NO + M \rightleftarrows N + O + M$	$2{,}9 \cdot 10^{19} T^{-1} \exp\left(-\frac{75\,500}{T}\right)$
(4) $CO + M \rightleftarrows C + O + M$	$8{,}5 \cdot 10^{19} T^{-1} \exp\left(-\frac{128\,960}{T}\right)$
(5) $CN + M \rightleftarrows C + N + M$	$5{,}2 \cdot 10^{19} T^{-1} \exp\left(-\frac{94\,140}{T}\right)$
(6) $N_2 + O \rightleftarrows NO + N$	$7{,}0 \cdot 10^{13} \exp\left(-\frac{38\,000}{T}\right)$
(7) $N_2 + C \rightleftarrows CN + N$	$2 \cdot 10^{10\pm1} T \exp\left(-\frac{31\,500}{T}\right)$
(8) $CO + N \rightleftarrows CN + O$	$2 \cdot 10^{10\pm1} T \exp\left(-\frac{45\,800}{T}\right)$
(9) $CO + NO \rightleftarrows CO_2 + N$	$1 \cdot 10^{3\pm2} T^2 \exp\left(-\frac{20\,980}{T}\right)$

* Commas represent decimal points

equilibrium distribution for the given temperature. In particular, in normal shock waves at high temperatures the times of vibrational relaxation and dissociation become comparable, and these processes occur simultaneously. Since the excited molecules mainly dissociate, the rate of dissociation will also change [48-51].

It is known [52] that, in the case of a harmonic oscillator with an infinite number of levels, the distribution of the vibrational levels approaches the equilibrium distribution, going through a sequence of Boltzmann distributions corresponding to the instantaneous vibrational temperature. As shown by approximate calculations, in the case of an oscillator with a cutoff, the distribution differs from the Boltzmann distribution.

/ 48

According to current ideas, the molecules dissociate when their vibrational energy exceeds the binding energy (energy of dissociation). The more a molecule is excited, and consequently the higher the vibrational levels are excited, the less energy must be transmitted to the molecule in order for it to dissociate, and the more effective are the collisions of molecules with a smaller relative energy of translational motion.

There are two methods of regarding dissociation: in the first method, one assumes that molecules may dissociate from any level if only the energy transmitted during a collision is sufficient for dissociation. In the second, the dissociation may occur primarily from the highest levels. It is taken for granted that in both methods an important role is played by the excitation of the intermediate levels, and consequently, by the entire process of the establishment of the vibrational equilibrium. Cases are possible [53] when the stage determining the rate of excitation of the upper vibrational levels is in the form of the excitation of certain intermediate levels, above and below which the process of energy exchange occurs much more intensely. In particular, the existence of such intermediate levels with a slower exchange may lead to a certain overpopulation of the upper vibrational levels in the processes of expansion of a two-atomic gas and to a corresponding slowing down of gas recombination [54,55].

The model that takes into account the coupling of dissociation to vibration and considered in [56] is called the CVD model (coupled-vibration-dissociation). However, [56] has not taken account of the reverse effect of dissociation on the energy of vibrations. This was included later in papers by Treanor and Marrone who have analyzed the process in more detail (CVDV model). They have studied both possible approaches to the problem of dissociation [57,58,59] of two-atomic molecules.

Since these effects were used in the calculation of relaxation, we shall state their results. The calculations use a model of a harmonic oscillator with a cutoff. The distribution of the vibrational energy is assumed to be of the Boltzmann type, except that it corresponds to the time dependent vibrational temperature, rather than the temperature of the vibrational degrees of freedom.

The mean vibration energy of molecules has the following time dependence

$$\frac{dE_{\text{vib}}}{dt} = \frac{E_{\text{vib}}(T) - E_{\text{vib}}}{\tau_v} - \frac{\overline{E}(T, T_{\text{vib}}) - E_{\text{vib}}}{[X_2]} \left(\frac{d[X_2]}{dt}\right)_f + \frac{\overline{E}(T, T) - E_{\text{vib}}}{[X_2]} \left(\frac{d[X_2]}{dt}\right)_r, \quad (1.75)$$

where T is the temperature of the translational degrees of freedom;

T_{vib} -is the vibrational temperature: / 49

$E(T, T_{\text{vib}})$ -is the mean energy lost by the vibrational degrees of freedom during one act of dissociation;

$\overline{E}(T, T)$ -is the mean energy obtained by the vibrational degrees of freedom during one act of recombination;

$[X_2]$ -is the concentration of the X_2 molecules.

The subscript f refers to the dissociation process, r to the recombination process. The terms $\frac{E_{\text{vib}}}{[X_2]}\left(\frac{d[X_2]}{dt}\right)_f - \frac{E_{\text{vib}}}{[X_2]}\left(\frac{dX_2}{dt}\right)_r$ express the variation of the mean vibrational energy as a result of a change in the number of excited molecules during dissociation and recombination. It will be noted that in the second and third term we used the product of two mean quantities even though it was necessary to use the mean of the product [60].

In the state of equilibrium $\frac{d[X_2]}{dt} = 0$.

Let us consider the case when dissociation is possible from any level. The probability of dissociation from level v is given by

$$p_v = CN_v f_v, \quad (1.76)$$

where N_v is the population of level with energy E_v;

f_v is the number of collisions with the relative collision

energy greater than $D-E_v$;

C is the normalization factor $\left(\sum_v p_v = 1\right)$.

In the case when the translational and vibrational degrees of freedom obey the Boltzmann distribution

$$N_v = \frac{1}{Z(T_{\text{vib}})} \exp(-E_v/kT_{\text{vib}}); \tag{1.77}$$

$$f_v = \exp[-(D-E_v/kT)], \tag{1.78}$$

where $Z(T_{\text{vib}})$ is the partition function for temperature T_{vib}:

$$Z(T_{\text{vib}}) = \sum_v \exp(-E_v/kT_{\text{vib}}). \tag{1.79}$$

Substituting (1.77) and (1.78) in (1.76), we get

$$p_v = \frac{1}{Z(T_m)} \exp(-E_v/kT_m), \tag{1.80}$$

where

$$\frac{1}{T_m} = \frac{1}{T_{\text{vib}}} - \frac{1}{T}.$$

The vibrational energy lost during one act of dissociation is E_j. Consequently, the mean energy lost per act is

$$E = \sum_v E_v p_v = \frac{1}{Z(T_m)} \sum E_v \exp(-E_v/kT_m) = -kT_m^2 \frac{\partial}{\partial T_m} \ln Z(T_m). \tag{1.81}$$

Hence

$$\bar{E}(T, T_{\text{vib}}) = \bar{E}(T_m) \quad \text{and} \quad \bar{E}(T, T) = \bar{E}(\infty). \tag{1.82}$$

/50

To calculate $\bar{E}$ in explicit form, we must select an oscillator model. For a linear oscillator, cut off at energy D, we get

$$Z = \sum_{v=0}^{\tilde{v}} \exp\left(-\frac{vh\nu}{kT}\right) = \frac{1-\exp\left(-\frac{\tilde{v}h\nu}{kT}\right)}{1-\exp\left(\frac{h\nu}{kT}\right)}, \tag{1.83}$$

where $\tilde{v}$ is the smallest integer closest to $\frac{D}{h\nu}$, and

$$\bar{E}(T_m) = \frac{h\nu}{\exp(h\nu/kT_m)-1} - \frac{\tilde{v}h\nu}{\exp(\tilde{v}h\nu/kT_m)-1}. \tag{1.84}$$

As $\frac{1}{T_m} \to \infty$

$$\bar{E}(T_r, T_r) = \lim_{T_m \to \infty} \bar{E}(T_m) = \frac{1}{2} h\nu(\tilde{v}-1). \tag{1.85}$$

Collecting all the terms, we can write the relaxation equation in its final form:

$$\frac{dE_{\text{vib}}}{dt} = \frac{E_\infty - E_{\text{vib}}}{\tau_v}\left[\frac{h\nu}{\exp(h\nu/kT_m)-1} - \frac{\tilde{v}h\nu}{\exp\left(\frac{\tilde{v}h\nu}{kT_m}\right)-1} - E_{\text{vib}}\right]_f \times$$
$$\frac{1}{[X_2]}\frac{d[X_2]}{dt} + \left[\frac{1}{2}(\tilde{v}-1)h\nu - E_{\text{vib}}\right]_r \frac{1}{[X_2]}\frac{d[X_2]}{dt}. \qquad (1.86)$$

The temperature dependence of $\bar{E}$ is shown in Fig. 1.9.

When dissociation occurs primarily from the upper levels, the line of reasoning remains similar, except that the probability of dissociation from level v is written as

$$p_v = CF(v)N_v f_v, \qquad (1.87)$$

where F(v) is the probability of transition from level v to the continuous spectrum.

For F(v), we take the expression

$$F(v) = \exp[-(D - E_v)/kU], \qquad (1.88)$$

where U is a parameter, with the dimension of temperature, whose values are selected by means of a comparison with experiment. The formally negative value (-U) may be viewed as the "vibrational temperature" at which molecules recombine.

Again, in view of Eqs. (1.77), (1.78), (1.88), we obtain the following expression for the probability

$$p_v = \frac{1}{Z(T_F)}\exp(-E_v/kT_F), \qquad (1.89)$$

/ 51

where

$$\frac{1}{T_F} = \frac{1}{T_{\text{vib}}} - \frac{1}{T} - \frac{1}{U},$$

and for the energy

$$\bar{E}(T, T_{\text{vib}}) = \sum_v E_v p_v = \frac{1}{Z(T_F)}\sum_v E_v \exp(-E_v/kT_F) = E_{\text{vib}}(T_F); \qquad (1.90)$$

$$\bar{E}(T, T) = \frac{1}{Z(-U)}\sum_v E_v \exp(E_v/kU) = E_{\text{vib}}(-U). \qquad (1.91)$$

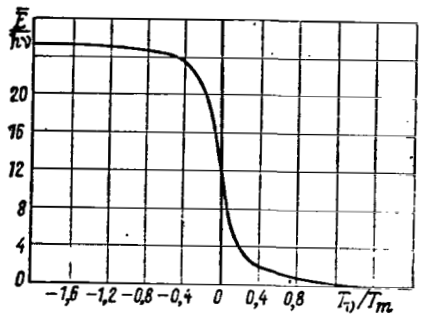

Figure 1.9. Variation of the term accounting for the relation between dissociation and vibrational degrees of freedom depending on the temperature T_m for O_2 (N=27)

Considering dissociation of a molecule X_2 from a vibrational level v as a result of collisions with a molecule A, we obtain from the definition of p_v

$$\left(\frac{d[X_2]}{dt}\right)_f = k_{fv}[X_{2v}][A] = p_v k_f [X_2][A] \qquad (1.92)$$

and consequently,

$$k_{fv} = k_f p_v \frac{[X_2]}{[X_{2v}]}. \qquad (1.93)$$

Since k_{fv} does not depend on the number of molecules on the level v (it is independent of T_{vib}), then k_{fv} may be written as

$$k_{fv} = k_{f\,eq}\, p_{v\,eq}\, \frac{Z(T)}{\exp(-E_v/kT)} = k_f p_v \frac{Z(T_{vib})}{\exp(-E_v/kT_{vib})} \qquad (1.94)$$

and consequently,

$$\frac{k_f}{k_{f\,eq}} = \frac{Z(T)\, p_{v\,eq}\, \exp(-E_v/kT_{vib})}{Z(T_{vib})\, p_v \exp(-E_v/kT)} = \frac{Z(T)\, Z(T_F)}{Z(T_{vib})\, Z(-U)}. \qquad (1.95)$$

For $U=\infty$ we obtain expressions for the equilibrium dissociation from any level. The method of the calculation of k_f in the CVD method is the same as in the CVDV method. One only changes the relaxation equation for E_{vib}, and consequently also the time dependence of T_{vib}.

It is clear that, if we consider the incomplete excitation of the vibrational levels, this will reduce the rate of dissociation.

Fig. 1.10 [58] shows the variation of the dissociation rate constant, calculated using the vibrational temperature obtained by setting to zero the first two terms on the right-hand side

of Eq. (1.75). The plot was based on experimental data for oxygen obtained from [19,36] and extrapolated by means of Eq. (1.95) to the domain of higher temperatures. As shown in calculations, the temperature dependence of the dissociation constant is stronger in the case when dissociation occurs primarily from upper levels (approximately $\sim T^{-3,5}$ as compared with $\sim T^{-1}$ in the case of equiprobable dissociation). Such a strong temperature dependence of dissociation from upper levels is not confirmed experimentally, and apparently indicates that the calculations used too high a rate for upper levels (approximately equal to 300:1). However, there are no experiments as yet which would provide a basis for a reliable choice.

The corrections obtained cannot be used at temperatures above 10,000°K.

To estimate the effect of the fact that the distribution of the vibrational levels differs from the Boltzmann distribution, a calculation was made of the relaxation in the shock wave of a gas composed of fictitious molecules (harmonic oscillators), having 18 levels of vibrational energy. The time of relaxation, energy, and rate of dissociation were the same as for oxygen. (For hydrogen such calculations were made by Pritchard [61]). These calculations may be interpreted as a relaxation in a gas during a sharp increase in temperature and pressure after the equilibrium in translational and rotational degrees of freedom has become established. The distance of a gas element from the front of a shock wave corresponds to the development of a process in time. The probability of a transition from level v to level v - 1 is taken in the form $k_{v,\,v-1} = vk_{10}$, where $k_{10} = \frac{1}{\tau}\frac{1}{1-e^{-h\nu/kT}}$. The population of a level, n_v, is taken in the form $\frac{n_v}{n_0} = \exp[-E_v/\theta_v]$, where θ_v is the "population factor" for level v; in the Boltzmann distribution all θ_v are identical and equal to the vibrational temperature.

/ 52

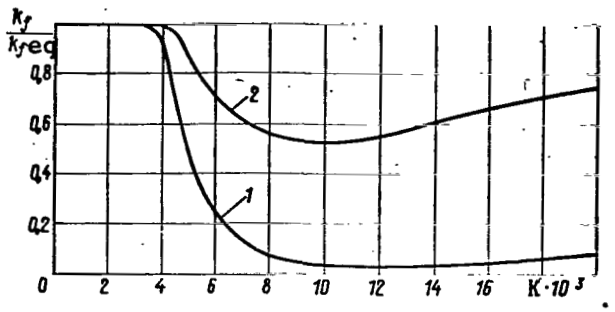

Figure 1.10. Effect of the nonequilibrium of vibrations on the dissociation rate constant:

1 - primary dissociation;
2 - equilibrium dissociation

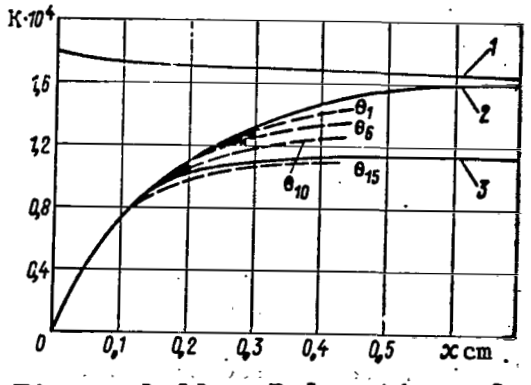

Figure 1.11. Relaxation of vibrations for dissociation primarily from upper levels as a function of the distance behind the shock wave for P_1=0.263 mm Hg; u_∞=4410 m/sec (gas composed of molecules having 18 vibrational energy levels, constitutes 4% admixture to argon):

1 - temperature of translational degrees of freedom;
2 - model without dissociation;
3 - model taking into account dissociation with vibrational degrees of freedom

The results of calculations for a strong shock wave propagating at the speed $u_\infty(T_\tau \sim 17000$ K) are shown in Fig. 1.11 [58]. If there is no dissociation, all θ_v are identical, and relaxation goes through a sequence of Boltzmann distributions (curve 2).

Calculations including dissociation were made for both equiprobable dissociation from any level and dissociation primarily from upper levels.

In the latter case, the rate of recombination to a level v was taken in the form

$$k_{rv} = k_r \frac{e^{v\hbar\nu/kU}}{\sum_{v=1}^{17} e^{v\hbar\nu/kU}}, \qquad (1.96)$$

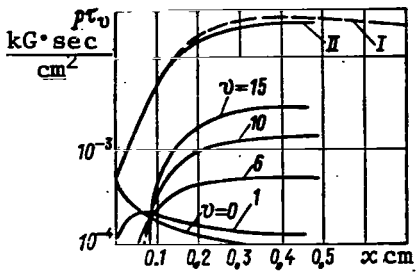

Figure 1.12. Rate of dissociation from different levels of vibrational energy as a function of the distance behind a shock wave for p_1=0.263 mm Hg; u_∞=4410 m/sec (gas composed of molecules having 18 levels is a 4% admixture to a argon):
1 - model accounting for relation of dissociation to vibrational degrees of freedom;
2 - total rate of dissociation

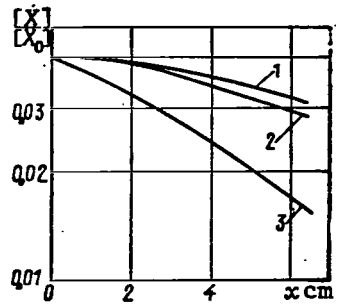

Figure 1.13. Concentration of molecules behind a shock wave (ratio of moles to initial mole) as a function of the distance behind the shock wave for P_1=0.263 mm Hg; u_∞= 4410 m/sec:
1 - dominant dissociation (gas consisting of molecules with 18 levels);
2 - model considering the relation of dissociation to vibrational degrees of freedom (dominant dissociation);
3 - model considering the relation between dissociation and the vibrational degrees of freedom - equiprobable dissociation (96% Ar+4% gas consisting of molecules with 18 levels).

where [36] $k_r = 3\cdot 10^{15} T^{-1.2} \frac{cm^6}{mole^2 \cdot sec}$ and $U = \frac{1}{6}\frac{D}{k}$.
(D is the dissociation energy of oxygen).

Such a rate function corresponds to the case when the constants for the upper levels are approximately 300 times greater than that for the ground level. For an equiprobable dissociation $U=\infty$ and all k_{rv} are identical. /53

Fig. 1.11 [58] shows the variation of population factors in the case of dissociation from upper levels. It is interesting that the curve for the Boltzmann distribution (solid line 3) enters the region θ_v for the upper levels. /54

Similar calculations for an equiprobable dissociation gave an even greater discrepancy in population, but the vibrational temperature obtained for the Boltzmann distribution, is close to θ_{v-v}. The calculations for weaker shock waves ($T_\infty = 6000°$) gave similar results.

Since the vibrational temperature changes similarly to θ_v for those levels from which most of the dissociation occurs, the rate of dissociation calculated using the vibrational temperature of the Boltzmann distribution is very close to the total rate of dissociation from 18 levels (see Fig. 1.12). The total effect on the concentration is shown in Fig. 1.13 [58] in comparison with the calculations based on the Boltzmann distribution. The agreement must be considered good, and this justifies the use of the Boltzmann distribution in calculations involving vibrational relaxation.

It is interesting to note in Fig. 1.13 the appearance of a time lag (induction period) for a model with dissociation primarily from the upper levels. The appearance is related to the fact that the upper levels must be sufficiently populated before noticeable dissociation begins. The induction period was measured by Ray [62]. However, even for this quantity there are not enough experimental data.

Ionization

In gases at high temperatures, two ionization processes are possible (ionization by radiation is not considered): ionization due to an impact and ionization accompanied by chemical reactions.

Collisions of molecules having a large relative energy may be

accompanied by a change of their electronic state: electrons, absorbing energy, are capable of making a transition to a higher energy level. This process is called the electron excitation.

If the energy transmitted to an electron is sufficiently high, the electron may completely separate from a molecule. In this case, we have impact ionization. Partners in collisions may include both neutral molecules and electrons and ions

$$A+A\rightarrow A+A^{+}+e; \tag{1.97}$$

$$A+e\rightarrow A^{+}+2e; \tag{1.98}$$

$$A+A^{+}\rightarrow 2A^{+}+e. \tag{1.99}$$

The energy necessary for ionization is called the ionization potential I (Table 10) [63]. Depending on the number of ionized electrons, one speaks of the first, second, etc. ionization potential. The ionization energy increases for each successive ionized electron.

TABLE 10

Substance	H_2	He	N	N_2	O	O_2	NO	Ar	Ne	Hg
I	15.4	24.5	14.6	15.6	13.6	12.1	9.3	15.8	21.5	10.4

Remarks. 1 eV = $1.6\cdot10^{-19}$ J = $3.82\cdot10^{-20}$ cal = 11,600°K

Sometimes collisions lead not only to removal of an electron, but also to a combination of molecules or to an exchange of the composite parts of the molecules. Such, for example, are the ionic reactions of the type* /55

$$A+B\rightarrow AB^{+}+e; \tag{1.100}$$

$$A+B^{-}\rightarrow AB+e. \tag{1.101}$$

* A reaction of the type (1.100) going in the forward direction is called a reaction of associated ionization, and in the reverse direction - a dissociative recombination.

These processes occur, in general, with less energy than impact ionization, since the required energy is less than the energy of formation of the final composite molecule by one order of magnitude. Therefore, it plays an important role at relatively low temperatures.

It is clear that the total electric charge of a gas volume does not change as a result of the internal processes occurring in it (law of the conservation of charge).

In addition to the processes of ionization in gases, it is also possible to have processes of charge redistribution

$$A^+ + B \rightarrow A + B^+ \tag{1.102}$$

and electron sticking

$$A + e \rightarrow A^-, \tag{1.103}$$

which also change the concentration of ionic components. Even though the charge in this case does not change, the total rate of ionization may, due to the fact that the rate of reactions with the participation of different ionic components is different. As a result, the total number of ions may change.

Ionic reactions in a system composed of several components may be very diverse, and in order for them to be taken into account it is necessary to have a detailed knowledge of the reaction mechanism with all the difficulties resulting from it. The ionization mechanisms are in general understood even less than the dissociation processes. The equilibrium concentration of electrons and ion components, ionized m and m + 1 times, is given by the Saha equation

$$\frac{n_{m+1}n_e}{n_m} = 2\frac{Z_{m+1}}{Z_m}\left(\frac{2\pi m_e kT}{h^2}\right)^{3/2} e^{-\frac{I_{m+1}}{kT}}, \tag{1.104}$$

which may be obtained as a law of mass action for the equilibrium concentration of substances in the reacion $A_m \rightleftarrows A_{m+1} + e$. Accordingly, in the expressions for Z_m, Z_{m+1} the energy is measured

from the ground state, and the partition function of a free electron is equal to twice the partition function of its translational motion.

The difference between the ground energies of ions is equal to the ionization potential. The right-hand side of Eq. (1.104) represents the equilibrium constant $K_{m+1}(T)$ of the ionization reaction. As the relative concentration, one introduces the degree of ionization, β_e, equal to the number of free electrons per initial molecule $\beta=\frac{N_e}{N}$, and the ion concentration, $\beta_m=\frac{N_m}{N}=\frac{n_iV}{N}=\frac{n_i}{N\rho}$ (N_1 is the number of molecules of type i per unit mass of the gas). / 56

Passing in Eq. (1.104) to relative concentrations, we get

$$\frac{\beta_{m+1}\beta_e}{\beta_m}=\frac{1}{\rho N}K_{m+1}(T), \tag{1.105}$$

In particular, for the first ionization $\beta_1=\beta_e=\beta$, and

$$\frac{\beta^2}{1-\beta}=2\frac{Z_1}{Z_0}\frac{1}{\rho N}\left(\frac{2\pi m_e kT}{h^2}\right)^{3/2}e^{-\frac{I}{kT}}. \tag{1.106}$$

Ionization in inert gases

Ionization is most simply studied in inert gases, since in them the ionization process is manifested in the purest form without complications due to any prior processes involving excitation of vibrations and dissociation [64].

For example, when equilibrium is established in argon it is possible for impact ionization, mentioned above, to occur. The electron-atom collisions yield maximum effects. However, in order for the process to be important, a certain definite electron concentration must be achieved. Therefore, in the initial stages an important role is played by other processes, in particular by the atom-atom collisions.

A study of ionization in argon under the conditions of a sharp temperature rise [65] has led to the conclusion that the process may be subdivided into three successive stages. In the

initial stage I, the principal role is played by an ionization process due to atom-atom collisions. The process occurs in two steps

atom excitation $$A+A\rightarrow A^*+A \quad (1.107)$$

and its ionization $$A^*+A\rightarrow A^+ + e + A, \quad (1.108)$$

where the excitation is the step that determines the rate of the process. Such a two-step occurrence of the process turns out to be more effective than direct ionization of the atom.

The electrons produced possess a relatively low energy, and it is only after a certain number of collisions with heavy molecules that they acquire enough energy for ionization of atoms. When the number of such electrons is sufficient, the principal stage II begins in which ionization occurs through electron-atom collisions (1.98) [66]. However, also in this stage one considers a two-step process along with direct ionization. / 57

The rate of ionization in the principal ionization zone is completely determined by the local concentration of ions and electron temperature. The velocity distribution of electrons in a gas may be considered Maxwellian, except with the temperature which is different from the atom temperature. This is related to the fact that the exchange of electron energies occurs faster than the energy exchange between electrons and atoms (the numbers of collisions are different by approximately a factor of 10^5), and the ionized electrons are not in equilibrium with heavy molecules.

In order to define the electron temperature, one uses the equation representing the balance between the rate of energy loss by the electrons as a result of ionizing collisions

and the rate of energy increase as a result of elastic collisions with hotter atoms and ions. The temperature corresponding to a translational motion of atoms and ions is uniquely determined by the local ion concentration and the energy equation. Since the energy losses in each ionization act are large, and the elastic exchange of energy with heavy molecules occurs slowly, the electron temperature turns out to be less than the temperature of the heavy molecules.

During an exchange with heavy molecules, the elastic collisions with ions become more effective than the collisions with atoms even for a low (on the order of 10^{-3}) degree of ionization. Therefore, with an increase in the degree of ionization, we have a rapid increase in the electron temperature and an increase in the rate of ionization. As a result, it turns out that the electron density increases monotonically approximately exponentially until the rate of recombination limits the growth of concentration. Then Stage III begins in which recombination is dominant.

Ionization in the air

When the temperature increases sharply to very large values ($kT \gg D$) the ionization in the air should apparently resemble ionization in argon. However, in the temperature range $kT < D$ the phenomena occur in a much more complex fashion. An analysis of the processes in this range becomes simplified due to the fact that usually the degree of ionization of a gas is low, and the processes of ionization do not strongly affect the chemical processes and the energy balance. This makes it possible to separate the chemical processes from ionization, to consider the temperature, density, and chemical composition independently of the ionization, and then to obtain the ion concentration using the instantaneous characteristics of the mixture that have already been computed. For shock waves in the air,

the upper limit at which such a separation of processes is still possible lies in the range of shock wave speeds which are somewhat greater than 9 km/sec, where the degree of ionization reaches nearly 1%.

A full list of ionization reactions in the air is given in [37] which discusses several dozen ionic processes (see also [67-69]. It is not particularly difficult to consider all these reactions. However, to get an approximate idea of the rates of ionization reactions, we must solve the problem of determining which of these processes is of greatest importance from the point of view of ionization. /58

For the air under the conditions of shock waves moving at the speed up to 9 km/sec, the following reaction represents a process in the above category

$$N+O+2{,}8\ \text{eV} \rightleftarrows NO^{+}+e \tag{1.109}$$

and at higher temperatures the reaction

$$N+N+5{,}8\ \text{eV} \rightleftarrows N_2^{+}+e. \tag{1.110}$$

is in that category.

All other possible ionization reactions occur with a greater energy loss. Finally, at high temperatures the ionization by electron impact yields a comparable reaction rate.

The constants for these reactions, as given by different workers, also differ widely. Thus, [37] gives the following constants for the reaction (1.109).

$$\left.\begin{aligned} k_f &= 5\cdot 10^{-11} T^{-1,2} \exp\left(-\frac{32\,500}{T}\right)\frac{\text{cm}^3}{\text{sec}};\\ K_c &= (1{,}4\cdot 10^{-8} T + 1{,}2\cdot 10^{-12} T^2 + 1{,}4\cdot 10^{-16} T^3)\exp\left(-\frac{32\,500}{T}\right). \end{aligned}\right\} \tag{1.11}$$

Ray [22] also gives the values for these constants

$$\left.\begin{aligned} k_f &= 6{,}4\cdot 10^{9} T^{1,2} \exp\left(-\frac{32\,645}{T}\right)\frac{\text{cm}^3}{\text{mole}\cdot\text{sec}};\\ K_c &= 3{,}6\cdot 10^{-10} T^{3/2} \exp\left(-\frac{32\,500}{T}\right). \end{aligned}\right\} \tag{1.12}$$

Martin [39] gives the following values for the constants (see Table 8):

$$\left.\begin{aligned} k_f &= 1{,}3\cdot 10^8 T \exp\left(-\frac{31\,900}{T}\right)\frac{\text{cm}^3}{\text{mole}\cdot\text{sec}} \\ k_r &= 2\cdot 10^{19} T^{-1}\,\frac{\text{cm}^3}{\text{mole}\cdot\text{sec}}. \end{aligned}\right\} \qquad (1.13)$$

The experiments made recently have shown that Eq. (1.111) gives a value for the recombination rate which is 2-3 times too low [70]. A better agreement with experiment is obtained by using a relation deduced theoretically in [71]:

$$\left.\begin{aligned} k_r &= 4{,}8\cdot 10^{-8}(kT)^{-1/2}[1-\exp(-0{,}27/kT)]\,\frac{\text{cm}^3}{\text{sec}}; \\ K_c &= 1{,}4\cdot 10^{-4} kT\,[1-\exp(-0{,}27/kT)]^{-1}\exp(-2{,}8/kT), \end{aligned}\right\} \qquad (1.14)$$

where kT is expressed in eV. /59

In addition to the fact that the lack of precision in our knowledge of the rate constants for the reaction (1.109) affects our knowledge of the electron concentration, we must keep in mind that — since the latter is determined by the concentration of N, O, and NO — the concentration is affected by all constants of the system of chemical reaction in the air (1.166)—(1.171) . Consequently, the accuracy of the electron concentration calculations is lower than the accuracy of the calculations for the neutral components of the air.

The ionization of gas mixtures other than the air has been studied even less. Some data on the reactions and ionization constants of CO and CO_2 may be found in Table 8.

REFERENCES

1. Griffith, V. Ts. Times of Relaxation of Vibrational Degrees of Freedom. In the Collection: Osnovnyye rezul'taty eksperimentov na udarnykh trubakh (Basic Results of Shock Tube Experiments), Moscow, State Publishing House for Atomic Science and Technology, 1963.

2. Vol'kenshteyn, N. V., M. A. Yel'yashevich and B. I. Stepanov. Kolebaniya molekul (Molecular Vibrations), Moscow-Leningrad, Gostekhizdat, Vol. 1, 1949.

3. Fowler, R. and E. Guggenheim. Statistical Thermodynamics Moscow, Foreign Literature Press (IL), 1949.

4. Hansen, C. Estimates for Collision — Induced Dissociation Rates — AIAA J. Vol. 3, No. 1, 1965.

5. McKenzie, R. L. The Qualitative Behavior and Effects in Gas Mixture of CO_2 and N_2 — AIAA Technical Papers, Stepping Stones to Mars. Meeting Baltimore, Maryland, 1966.

6. Landau, L. and E. Teller. The Theory of Sound Dispersion. Physikalische Zeitschrift der Sowjetunion, Vol. 10, No. 1, 1936, pp. 34-43.

7. Stupochenko, Ye. V., S. A. Losev, and A. I. Osipov. Relaksatsionnyye protsessy v udarnykh volnakh (Relaxation processes in shock waves). Moscow, "Nauka" Publishing House, 1965.

8. Schwartz, R. N., Z. I. Slavskiy and K. F. Gertsfel'd. Calculation of the Vibrational Relaxation Times in Gases. In the Collection: Gazodinamika i teploobmen pri nalichii khimicheskikh reaktsiy (Gas dynamics and heat transfer in the presence of chemical reactions), Moscow, IL, 1962.

9. Schwartz, R. N. and K. F. Gertsfel'd. Vibrational relaxation time in gases, ibid.

10. Herzfeld, K. F. Relaxation Phenomena in Gases. In the Collection: High Speed Aerodynamics and Jet Propulsion. Thermodynamics and Physics of Matter. N. Jersey, Vol. 1, 1955.

11. Leskov, L. V. and F. A. Savin. Relaxation of nonequilibrium gas systems. Uspekhi Fizicheskikh Nauk (UFN), Vol. 72, No. 4, 1960.

12. Losev, S. A., A. I. Osipov. Study of Nonequilibrium Phenomena in Shock Waves. UFN, Vol. 74, No. 3, 1961.

13. Zhigulev, V. N. Equations of Physical Hydrodynamics. Inzhenernyy Zhurnal (Inzh.Zh.), Vol. 3, No. 1, 1963.

14. Vallander, S. V., and Ye. A. Nadgnibeda. General Formulation of Problems Related to the Description of Relaxation Processes in Gases with Internal Degrees of Freedom. Vestnik Leningradskogo Universiteta (Vestn. Len. U.), No. 13, 1963.

15. Kogan, M. N. Dinamika razrezhennogo gaza. Kineticheskaya teoriya. (Dynamics of a Rarefied Gas. Kinetic Theory). Moscow, "Nauka" Press, 1967.

16. Nagnibeda, Ye. A. Solution of Equations of a Nonequilibrium Gas. Vestn. Len. U., No. 7, 1969.

17. Nagnibeda, Ye. A. Solution of Relaxation Equations for a Mixture of Gases with Nonequilibrium Chemical Reactions. Vestn. Len. U., No. 7, 1970. / 60

18. Yegorov, B. V. Relaxation Equation for Vibrational Degrees of Freedom of a Diatomic Gas. Izvestiya Akademii Nauk SSSR (Izv. AN SSSR), Mekhanika, No. 3, 1965.

19. Camac, M. O_2 Vibration Relaxation in Oxygen-Argon Mixtures. J. Chem. Phys., Vol. 34, II, No. 2, 1961.

20. Blackman, V. Vibrational Relaxation in Oxygen and Nitrogen. In the Collection: Gazodinamika i teploobmen pri nalichii khimicheskikh reaktsii (Gas Dynamics and Heat Transfer in the Presence of Chemical Reactions). Moscow, IL, 1962.

21. Robben, F. Vibrational Relaxation of Nitric Oxide. J. Chem. Phys., Vol. 31, VIII, No. 2, 1959.

22. Ray, K. Chemical Kinetics of High-Temperature Air. In the Collection: Issledovaniye giperzvukovykh techeniy. (Investigation of Hypersonic Flows). Moscow, "Mir" Press, 1964.

23. Millikan, R. C. and D. R. White. Systematics of Vibrational Relaxation. J. Chem. Phys., Vol. 39, X, No. 12, 1963.

24. Millikan, R. C. and D. R. White. Vibrational Energy Exchange Between N_2 and CO. The Vibrational Relaxation of Nitrogen. J. Chem. Phys., Vol. 39, VII, No. 1, 1963.

25. Osipov, A. I. Relaxation of Vibrational Energy in a Binary Mixture of Diatomic Gases. Zhurnal Prikladnoy Matematiki i Teoreticheskoy Fiziki (ZhPMTF), No. 1, 1964.

26. White, D. R. and R. C. Millikan. Vibrational Relaxation in Air. AIAA J., Vol. 2, No. 10, 1964.

27. Boade, R. R. Effect of Collision Partners on Vibrational Relaxation. J. Chem. Phys. Vol. 43, IV, No. 8, 1965.

28. Blythe, Y. A. Non-Equilibrium Flow of a Polyatomic Gas Through a Normal Shock Wave. ARC Current Pap. No. 645, 1963.

29. Freedman, E. and J. W. Daiber. Decomposition Rate of Nitric Oxide Between 3000° and 4300°K. J. Chem. Phys., Vol. 34, IV, No. 4, 1961.

30. Wray, K. L. and I. D. Teare. Shock-Tube Study of the Kinetics of Nitric Oxide at High Temperatures. J. Chem. Phys., Vol. 36, V, No. 10, 1962.

31. Camac, M. and R. M. Feinberg. Formation of NO in Shock-Heated Air. Eleventh Symposium on Combustion Held at Univ. of California, Berkeley, Cal. Aug. 14-20, 1966. The Comb. Inst. Pittsburg, Pennsylvania, 1967.

32. Termodinamicheskiye svoytsva individual'nykh veshchestv (Thermodynamic Properties of Individual Substances), Edited by Glushko, V. P., Izd. AN SSSR, 1962.

33. Duff, R. E. and W. Davidson. Calculation of Reaction Profiles Behind Steady State Shock Waves. P II Dissociation of Air. J. Chem. Phys., Vol. 31, X, No. 4, 1959.

34. Matthews, D. L. Interferometric Measurement in the Shock-Tube of the Dissociation Rate of Oxygen. Phys. of Fluids, Vol. 2, III-IV, No. 2, 1959.

35. Rink, I. P., H. T. Knight, and R. E. Duff. Shock-Tube Determination of Dissociation Rates of Oxygen. J. Chem. Phys., Vol. 34, VI, No. 6, 1961.

36. Camac, M. and A. Vaughan. O_2 Dissociation Rates in O_2-Ar Mixtures. J. Chem. Phys., Vol. 34, II, No. 2, 1961.

37. Lin, S. Ch., and J. D. Teare. Rate of Ionization behind Shock Waves in Air. P. II. Theoretical Interpretations. Phys. of Fluids, Vol. 6, III, No. 3, 1963.

38. Lin, S. Ch. and J. D. Teare. A Streamtube Approximation for Calculation of Reaction Rates in the Inviscid Flow Field of Hypersonic Objects. In the Collection: Ballistic Missile and Aerospace Technology. Vol. 4, Re-Entry Proc. of the Sixth Symposium Held in Los Angeles, Cal. in Aug. 1961. N.Y. - London, 1961.

39. Martin, J., Atmospheric Entry. Moscow, "Mir" Press, 1969.

40. Byron, S. Shock-Tube Measurement of the Rate of Dissociation of Nitrogen. J. Chem. Phys. Vol. 44, II, No. 4, 1966.

41. Bortner, M. H. Chemical Kinetics of Planetary Entry. In the Collection of: Symposium on Dynamics of Manned Lifting Planetary Entry. N.Y. - London, 1963.

42. Davies, W. O. Carbon Dioxide Dissociation at 6000° to 11000°K. J. Chem. Phys., Vol. 43, X, No. 8, 1965. / 61

43. Davies, W. O. Carbon Dioxide Dissociation at 3500°K to 6000°K. J. Chem. Phys., Vol. 41, IX, No. 6, 1964.

44. Brabbs, T. A., F. E. Belles and S. A. Zlatarich. Shock-Tube Study of Carbon Dioxide Dissociation Rate. J. Chem. Phys., Vol. 38, IV, No. 8, 1963.

45. Losev, S. A. et al. Investigation of the Dissociation of the Molecules of Carbon Monoxide at High Temperatures. Doklady Akademii Nauk (DAN), Vol. 15, No. 4, 1963.

46. Losev, S. A. and L. B. Terebenina. Kinetics of Dissociation of Carbon Dioxide Molecules Behind the Front of a Shock Wave. ZhPMTF, No. 4, 1966.

47. Bazhenova, T. V. et al. Udarnyye volny v real'nykh gazakh (Shock Waves in Real Gases), Moscow, "Nauka" Publishing House, 1967.

48. Nikitin, Ye. Ye. and N. D. Sokolov. Relationship Between Rate Constants of Thermal Dissociation of Diatomic Molecules in the Presence and Absence of Equilibrium. DAN, Vol. 15, No. 4, 1963.

49. Nikitin. Modern Theories of Thermal Dissociation and Isomerization of Molecules in a Gas Phase. Moscow, "Nauka" Publishing House, 1964.

50. Kuznetsov, N. M. Relationship Between Vibrational Relaxation and Dissociation of Diatomic Molecules. DAN, Vol. 164, No. 5, 1965.

51. Lunikin, Yu. P. and F. D. Popov. Effect of Vibrational and Dissociative Relaxation on Supersonic Flow Around Blunt Bodies. Zhurnal Teoreticheskoy Fiziki (ZhTF), No. 4, 1966.

52. Montroll, F. W. and K. Shuler. Studies in Nonequilibrium Rate Processes. P. I. The Relaxation of a System of Harmonic Oscillators. J. Chem. Pys. Vol. 26, III, No. 3, 1957.

53. Nikitin, Ye. Ye. Mechanism of Intermolecular Energy Exchange in Dissociation of a Diatomic Gas. DAN, Vol. 132, No. 2, 1960.

54. Rush, D. G. and H. O. Pritchard. Vibrational Disequilibrium in Chemical Reactions. Eleventh Symp. on Combustion Held at the Univ. of California. Aug. 14-20, 1966, Pittsburg, Pennsylvania, 1967.

55. Bray, K. N. C. and N. H. Pratt. Conditions for Significant Gasdynamically Induced Vibration-Recombination Coupling. Ibid.

56. Hammerling, P., J. D. Teare and B. Kivel. Theory of Radiation from Luminous Shock Waves in Nitrogen. Phys. of Fluids, Vol. 2, VII-VIII, No. 4, 1959.

57. Marrone, P. V. and C. E. Treanor. Chemical Relaxation with Preferential Dissociation from Exited Vibrational Levels. Phys. of Fluids, Vol. 6, X, No. 10, 1963.

58. Treanor, C. E. and P. V. Marrone. Vibration and Dissociation Coupling Behind Strong Shock Waves. In the collection: Symposium on Dynamics of Manned Lifting Planetary Entry. N. Y. - London, 1963.

59. Treanor, C. E. and P. V. Marrone. Effect of Dissociation on the Rate of Vibrational Relaxation. Phys. of Fluids, Vol. 5, IX, No. 9, 1962.

60. Heims, S. P. Moment Equations for Vibrational Relaxation Coupling with Dissociation. J. Chem. Phys. Vol. 38, II, No. 3, 1963.

61. Pritchard, H. O. The Kinetics of Dissociation of a Diatomic Gas. J. Phys. Chemistry, Vol. 65, III, No. 3, 1961

62. Wray, K. L. Shock-Tube Study of the Coupling of the O_2-Ar Rates of Dissociation and Vibrational Relaxation. J. Chem. Phys., Vol. 37, IX, No. 6, 1962.

63. Zel'dovich, Ya. B. and Yu. P. Rayzer. Fizika udarnykh voln i vysokotemperaturnykh gidrodinamicheskikh yavlenii. (Physics of Shock Waves and High-Temperature Hydrodynamic Phenomena), Moscow, Physics and Mathematics Press (Fizmatgiz), 1963.

64. Blackman, V. G. and Niblitt. Ionization processes in shock tubes. In the Collection: Osnovnyye rezul'taty eksperimentov na udarnykh trubakh (Basic Results of Shock Tube Experiments). Moscow, Gos. Izd. Lit. po atomnoy nauke i tekhnike. 1963.

65. Wong, H. and D. Bershader. Thermal Equilibration behind an Ionizing Shock. J. Fluid Mech. Vol. 26, No. 3, 1966.

66. Pechek, Kh. Ye. and S. Bayron. Approach to Equilibrium Ionization Behind a Strong Shock Wave in Argon. In the Collection: Na poroge v kosmos (At the threshold of Space), Moscow, 1960 /62

67. Danilov, A.D. and G. S. Ivanov-Kholodnyy. Ionic-Molecular Reactions and Dissociative Recombination, UFN, Vol. 85, No. 2, 1965.

68. Danilov, A.D. Khimia ioniosphery (Chemistry of the Ionosphere). Gidrometeoizdat, 1967.

69. Witten, R. K. and I. J. Poppov. Physics of the Lower Ionosphere. Moscow, "Mir" Press, 1968.

70. Frohn, A. and C. De Boer. Ion Density Profiles Behind Shock Waves in Air. AIAA J. Vol. 5, No. 2, 1967

71. Hansen, C. F. Temperature Dependence of the NO^{+}+e Dissociative-Recombination Rate Coefficients. Phys. of Fluids, Vol. 11, IV, No. 4, 1968.

CHAPTER 2

GENERAL PROPERTIES OF NONEQUILIBRIUM FLOWS

2.1 Equations of state and motion of a relaxing gas

The equations of motion of a compressible gas are based not only on the laws of mechanics, but also on thermodynamic relations. Therefore, the first problem will be to determine the necessary thermodynamic properties of a relaxing gas. The thermal equation of state of a pure gas may in general be written as

$$p = Z(p, T)\frac{\rho RT}{M}, \qquad (2.1)$$

where $Z(p, T)$ is the compressibility factor.

Let us limit ourselves to the range of densities, where one can neglect the Van der Waals corrections. Under these conditions which are usual in classical gas dynamics, the compressibility factor for a gas whose composition does not change is equal to unity.

Thermal and caloric equations of state of a gas mixture

The thermal equation of state of a single-component gas is expressed in the form of the Clapeyron law

$$p_i = \frac{R}{M_i}\rho T = \frac{R}{M_i V}T = n_i kT, \qquad (2.2)$$

where $R = 1{,}987$ cal/mole · K $= 8{,}31 \cdot 10^3$ J/kcal · K $= 0{,}0821$ m^3 kg/kmole · K · cm^2 is the universal gas constant; n_i is the number of gas molecules per unit volume. Gases that obey Eq. (2.2) are called thermally ideal. Gas mixtures obey Dalton's law which expresses the total pressure of a mixture in terms of partial pressures of the components, $p_i = \sum_i p_i$. Using the Clapeyron equation (2.2)

for components, we obtain the thermal equation of state for a gas mixture under the assumption of thermodynamic equilibrium of translational degrees of freedom.

$$p=\sum_i p_i=\sum_i n_i kT=\sum_i \frac{R}{M_i}\rho_i T, \qquad (2.3)$$

/64

where T is the temperature of the translational degrees of freedom of the gas.

The density of a mixture is defined by

$$\rho=\sum_i \rho_i=\sum_i \frac{n_i M_i}{N_0}. \qquad (2.4)$$

Comparing this expression with Eqs. (2.2), (2.3), we define the effective molecular weight of the mixture

$$\overline{M}=\frac{\sum_i n_i M_i}{\sum_i n_i}. \qquad (2.5)$$

Now we can write the thermal equation of state in a form analogous to (2.2):

$$p=\frac{R}{\overline{M}}\rho T. \qquad (2.2')$$

If the composition of the gas does not change with pressure or temperature, then the gas mixture behaves like a thermally ideal gas. However, if the composition changes, then the analogy with Eq. (2.2) becomes formal. Therefore, it is more convenient to write Eq. (2.2') in a form analogous to Eq. (2.1) by introducing the molecular weight of the mixture, M_0, under the conditions of normal pressures and temperatures, when there is no gas dissociation

$$p=\frac{M_0}{\overline{M}}\frac{R}{M_0}\rho T. \qquad (2.1')$$

The ratio $\frac{M_0}{\overline{M}}=Z(p, T)$ is also called the compressibility factor or the pseudo-compressibility factor (Fig. 2.1).

Very simple relations are obtained for the dissociation of a diatomic gas consisting of identical atoms:

$$A_2 \rightleftarrows A+A.$$

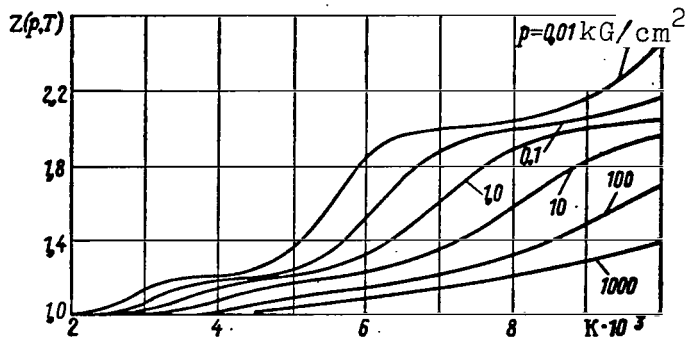

Figure 2.1. Compressibility factor for the air (based on tables from [2-4]).

If M_1 denotes the atomic component, then the molecular weight of the gas is $M_2=2M_1$. The mass concentration of the atomic component is

/ 65

$$\alpha_1=\frac{M_1n_1}{\sum_i M_in_i}=\frac{n_1}{n_1+2n_2}=\frac{\rho_1}{\rho}, \qquad (2.6)$$

and of the molecular component

$$\alpha_2=\frac{M_2n_2}{\sum_i M_in_i}=\frac{2n_2}{n_1+2n_2}.$$

It is clear that

$$\frac{1}{\overline{M}}=\sum_i\frac{\alpha_i}{M_i}=\frac{1}{M_1}\left(\alpha_1+\frac{\alpha_2}{2}\right).$$

Then the equation of state (2.2) with the use of the relation $\alpha_1+\alpha_2=1$ may be written in the form

$$p=\rho RT\left(\frac{\alpha_1}{M_1}+\frac{1-\alpha_1}{M_2}\right)=\rho(1+\alpha_1)\frac{RT}{M_2}. \qquad (2.7)$$

It is clear that the value of α_1 may vary between 0 and 1. Consequently, the compressibility factor which is equal to $1+\alpha_1$ for a diatomic gas according to Eq. (2.7) may vary from 1 to 2.

To determine the equilibrium state of a gas with a constant composition, it is sufficient to specify two parameters, for

example, the pressure and temperature. The third parameter is determined from the equation of state. If a gas changes its composition, then the equation of state is not sufficient, and it is necessary to use additional relations to determine the composition of the gas. The law of mass action gives such relations for equilibrium states.

In application to a diatomic gas, Eq. (1.38) gives

$$\frac{n_1^2}{n_2}=K_c(T).$$

/66

Using the expressions for mass concentrations, we get

$$n_1=\alpha_1(n_1+2n_2);\ n_2=\frac{1}{2}(1-\alpha_1)(n_1+2n_2) \tag{2.8}$$

and

$$\frac{\alpha_1^2}{1-\alpha_1}2(n_1+2n_2)=K_c(T);$$

since $m_1(n_1+2n_2)=\rho$, then

$$\frac{\alpha_1^2}{1-\alpha_1}=\frac{m_1}{2\rho}K_c(T). \tag{2.9}$$

Eqs. (2.7) and (2.9) determine completely the state of a gas, and here it is enough to just know the pressure and temperature. It is important that the system of algebraic equations obtained is nonlinear.

In addition to the thermal equation of state, relating the temperature, density, and pressure, a gas is characterized by the caloric equation of state. The caloric equation of state relates the internal energy of a gas to the thermodynamic state variables. Using the expressions for the energy of the individual degrees of freedom of a gas and knowing its composition, it is not difficult to obtain the caloric equation for a gas mixture. For example, for a dissociating diatomic gas, if e_1 is the energy of the atomic component, e_2 - the energy of the molecular component, then the energy per unit mass of a

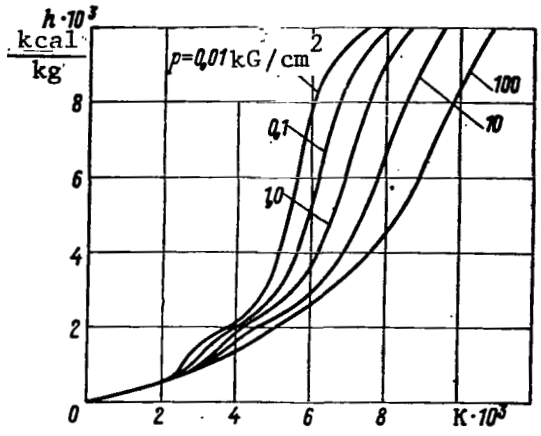

Figure 2.2. Specific enthalpy of the air (based on tables from [2-4])

gas will be

$$e=\alpha_1 e_1+(1-\alpha_1)e_2+\alpha_1\frac{R}{2m}\frac{D}{k}. \qquad (2.10)$$

For a gas mixture, one needs to sum the energies over all gas components. Thus, the thermodynamic functions of a dissociating /67 gas depend on its composition (Fig. 2.2).

Calculation of the equilibrium state of a gas mixture

To calculate the equilibrium composition of a gas mixture, one uses the law of mass action for each reaction in the system, the conservation of the number of atoms (equation of material balance) and Dalton's law. These relations are sufficient to determine the equilibrium composition of the gas.

Suppose that there are k components that may be involved in r reactions. Each component may consist of a different elements A_m. For example, the composition of a molecule k_i will be

$$\sum_m^a n_{im} A_m .$$

To characterize the composition, we shall use the molar fractions of the components, ξ_i . Dalton's law, expressed in terms of molar fractions, is

$$\sum_{i}^{k} \xi_i = 1. \tag{2.11}$$

The number of atoms of each element remains constant

$$\frac{\sum_{i=1}^{k} n_{im}\xi_i}{\sum_{i=1}^{k} n_{i1}\xi_i} = p_{m1};\ m = 1,\ldots a; \tag{2.12}$$

$p_{11}=1$ by definition.

Finally, for each of the r reactions written in the form

$$\sum_{i=1}^{k} (a_{si} - b_{si}) X_i = 0;\ s = 1,\ldots r$$

(a_{si}, b_{si} are the stoichiometric coefficients of reaction s), we have the law of mass action

$$\frac{K_{ps}}{p^{\nu_s}} = \sum_{i=1}^{k} \xi_i^{(a_{si}-b_{si})};\quad \nu_s = \sum_{i=1}^{k} (a_{si} - b_{si}). \tag{2.13}$$

Thus, altogether we have $a-1+1+r=a+r$ equations for the k unknowns ξ_i . However, not all of the r equations of the law of mass action are independent. For example, for a system of reactions in the air, relating five substances (O_2, O, N_2, N, NO) , consisting of atoms of two elements (O and N), the law of mass action gives five relations: /68

$$\frac{\xi_O^2}{\xi_{O_2}} = \frac{K_{p1}}{p};\quad \frac{\xi_N^2}{\xi_{N_2}} = \frac{K_{p2}}{p};\quad \frac{\xi_O \xi_N}{\xi_{NO}} = \frac{K_{p3}}{p};$$

$$\frac{\xi_N \xi_{O_2}}{\xi_{NO}\xi_O} = K_{p4};\quad \frac{\xi_O \xi_{N_2}}{\xi_{NO}\xi_N} = K_{p5}.$$

Upon dividing the third relation by the first, we obtain the fourth, and upon dividing the third by the second, we find the fifth. Thus, the law of mass action only gives three independent relations.

In general, the number of independent relations is k - a.

The total number of equations in the system is equal to the number of unknowns, and the system has a unique solution [1]. If the temperature and pressure are given, then the calculation reduces to solving the nonlinear system of equations (2.11), (2.12), (2.13). The accuracy of the calculation, in addition to other factors, depends on the accuracy with which the equilibrium constants are calculated. The calculation is a fairly complicated task, and computers are used to obtain reliable results. Such calculations were made for the air and carbon dioxide for a wide range of temperatures and pressures [2-8]. The results of the calculations are shown in the form of tables which in addition to the composition give the thermodynamic functions of gases. Tables in [2-4 and 6] present the greatest detail.

Tables in [6] differ from tables in [2-4] in that they cover a greater parameter range (temperatures from 200 to $3 \cdot 10^6$°K and densities from 10^{-6} to 30 times the normal density) and in that the independent variables selected are the temperature and density rather than the temperature and pressure.

The ionization is considered by analogy with dissociation. In addition, one also considers the condition of the conservation of charge in the system. The results of ionization calculations are also included in the table. Fig. 2.3 gives the results of calculating equilibrium composition of the air for various pressure values as a function of the temperature. These relations may simultaneously serve as an illustration of the role of different processes, depending on the variation of thermodynamic parameters.

Ideal dissociating gas

For an equilibrium dissociation of diatomic gases, Lighthill proposed a model in the form of a hypothetical gas [9] which provides a good approximation of the behavior and thermodynamics

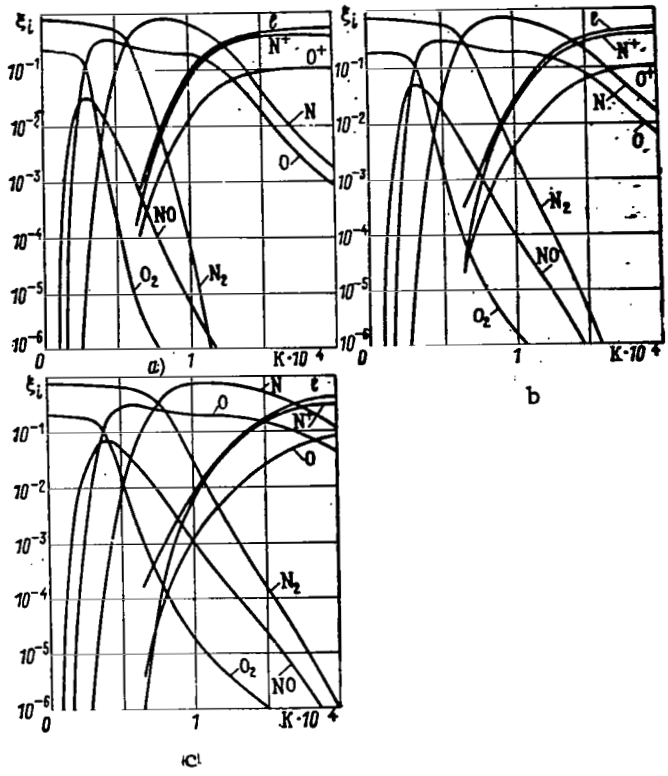

Figure 2.3. Equilibrium composition of the air (based on tables from [2-4]):
a - for p = 0.1 kG/cm^2;
b - for p = 1 kG/cm^2;
c - for p = 10 kG/cm^2.

of individual real gases. The model gas was called an "ideal dissociating gas". Its properties are described by only three constants, and this permits us to analyze the effect of dissociation in a single-generalized form. /69

Dissociation of a pure diatomic gas is described by the equation $A_2 \rightleftarrows 2A$, and obeys the law of mass action

$$\frac{n_A^2}{n_{A_2}} = \frac{Z_A^2}{Z_{A_2}} e^{-\frac{D}{kT}}.$$

Using the expressions for mass concentrations (2.6), density

$$\rho = m(n_A + 2n_{A_2}) \tag{2.14}$$

and partition functions Z (1.24), (1.21), (1.18), (1.11), where in the electron partition function we limit ourselves to the ground state, one can write the law of mass action in the form

$$\frac{\alpha_1^2}{1-\alpha_1} = \frac{n_A^2}{2n_{A_2}(n_A + 2n_{A_2})} = \frac{m}{2\rho}\frac{n_A^2}{n_{A_2}} = \tag{2.15}$$

$$= \frac{e^{-\frac{D}{kT}}}{\rho}\left[\frac{m}{2}\frac{(\pi mkT)^{3/2}}{h^2}\left(\frac{2T_r}{T}\right)\left(1-e^{-\frac{T_v}{T}}\right)\frac{Z_{эл\,A}}{Z_{эл\,A_2}}\right]. \qquad /70$$

The expression in brackets has a dimension of density, and it may be denoted by ρ_d .

$$\frac{\alpha_1^2}{1-\alpha_1} = \frac{\rho_d}{\rho} e^{-\frac{T_d}{T}}. \tag{2.16}$$

The quantities ρ_d and $T_d = \frac{D}{k}$ are called the characteristic density and temperature. The characteristic temperature is a constant for each real gas, and the characteristic density varies with temperature. However, in a wide temperature range from 1000 to 7000°K, the changes in ρ_d are small. In any case, they are much smaller than the change in the factor $e^{-\frac{T_d}{T}}$. For example, for O_2 the value of ρ_d changes from 123 to 170 g/cm^3, and for N_2— from 113 to 136 g/cm^3. Therefore, ρ_d may be conveniently considered as a constant and may be set, for example, for nitrogen to $\rho_d = 130$ g/cm^3 and for oxygen to $\rho_d = 150$ g/cm^3.

Using Eq. (2.16), it is easy to obtain the plots of equilibrium dissociation versus temperature for various values of density (Fig. 2.4). To fully describe the behavior of an ideal dissociating gas, we must obtain its equation of state and the expression for the internal energy. The equation of state has the form

$$p = kT(n_A + n_{A_2}) = \frac{kT}{2}(1+\alpha_1)(n_A + 2n_{A_2}) = \frac{k}{2m}\rho T(1+\alpha_1), \tag{2.17}$$

or, after introducing the characteristic pressure,

$$p_d=\frac{k}{2m}\rho_d T_d=\frac{D\rho_d}{2m}\ \frac{p}{p_d}=\frac{\rho}{\rho_d}\frac{T}{T_d}(1+\alpha_1). \qquad (2.18)$$

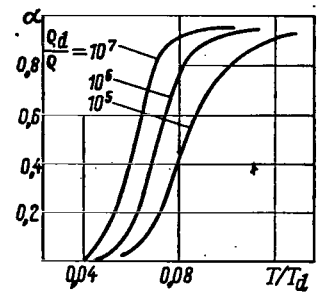

Figure 2.4 Variation of mass concentration of atoms of an ideally dissociating gas

/71

The internal energy is taken in the form

$$E=\frac{3}{2}kT(n_A+2n_{A_2})+\frac{1}{2}Dn_A \qquad (2.19)$$

under the assumption that the vibrational degrees of freedom of molecules are halfway excited. The 3/2 factor in front of n_A and $2n_{A_2}$ in the expression (2.19) of course differs from its exact value, which for O_2 and N_2 in the temperature range from 2000 to 7000°K varies from 1.31 to 1.72, (the factor multiplying n_A changes naturally very little). However, the assumption used is acceptable, since the error thus resulting is small as compared with the dissociation energy.

Passing to the specific energy per unit mass, we obtain

$$e=\frac{E}{\rho}=\frac{3k}{2m}T+\frac{D}{2m}\alpha_1 \qquad (2.20)$$

and upon introducing the characteristic energy $e_d=\frac{D}{2m}$, we finally find

$$\frac{e}{e_d}=3\frac{T}{T_d}+\alpha_1. \qquad (2.21)$$

Eqs. (2.16), (2.18), and (2.21) completely describe an ideal dissociating gas. Sometimes these relations are written taking

as the units of temperature, pressure, density, and energy the following characteristic parameters

$$\frac{\alpha_1^2}{1-\alpha_1}=\frac{1}{\rho}e^{-\frac{1}{T}};\quad p=\rho T(1+\alpha_1);\quad e=3T+\alpha_1.$$

The specific enthalpy, expressed in terms of these units, will be

$$h=e+\frac{p}{\rho}=(4+\alpha_1)T+\alpha_1, \tag{2.22}$$

and the specific entropy

$$S=3\ln T+\alpha_1(1-2\ln\alpha_1)-(1-\alpha_1)\ln(1-\alpha_1)-(1-\alpha_1)\ln\rho+\text{const}.$$

Approximate methods

The final result of an exact calculation of an equilibrium state is presented in the form of tables. In applied calculations, it is desirable to have simple methods of determining the equilibrium state of a gas mixture, perhaps with lower accuracy but at the same time with less labor and time. In addition, it is advisable to obtain simple relations for the thermodynamic properties of a gas, which could be used in analytic solutions.

/72

The simplest methods for approximating thermodynamic functions are based on the use of the effective adiabatic exponent. Here in relations between thermodynamic parameters, the adiabatic exponent is replaced by a certain constant, which may be formally viewed as an adiabatic exponent and actually corresponds to it for unexcited internal degrees of freedom of a gas. This quantity is defined in various ways, depending on the processes in which the gas participates, and the relations in which the quantity enters. Thus, Hayes and Probstein [10] give three different definitions of the effective adiabatic exponent. An example of one of them which is convenient in the study of shock waves is provided by

a quantity defined by the ratio

$$\varkappa_e = \frac{h}{e}. \qquad (2.23)$$

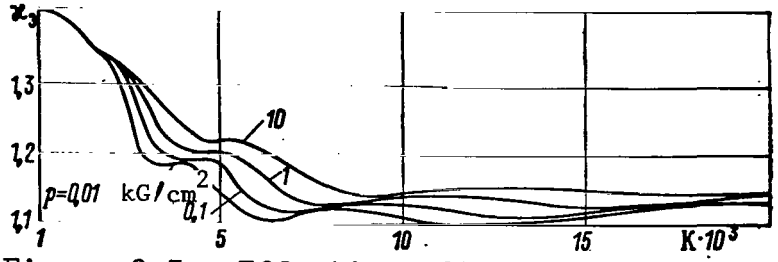

Figure 2.5. Effective adiabatic exponent κ_e as a function of the temperature and pressure (based on tables from [2-4])

This quantity is convenient, in particular, in those cases when p and ρ are used as thermodynamic parameters, since it enables us to represent enthalpy in the form $h = \frac{\varkappa_e}{\varkappa_e + 1}\frac{p}{\rho}$. κ_e depends on both pressure and temperature (Fig. 2.5), but if one considers a small range of gas parameters, then it may be viewed as a constant average quantity that corresponds to given conditions.

To obtain the approximate analytic expressions for the thermodynamic functions of the air, one generalizes the ideal dissociating gas to the case of a gas mixture [11] and ionization [12]. The partition functions of the form of (2.15) are replaced by approximate expressions. It is assumed that the vibrational degrees of freedom of molecules receive the energy 3/4 kT. If one neglects the presence of nitrogen oxide and argon in the air, then the equations of mass action can be solved for the degree of dissociation of oxygen and nitrogen. This makes it possible, by analogy with an ideal dissociating gas, to obtain simple, although somewhat involved, expressions for the thermodynamic functions of a gas in the variables ρ and T. The introduction of arbitrary constants makes it possible to obtain exact agreement at an arbitrary point between the approximate expressions and those in the tables. To obtain an explicit dependence on p and T, it is

/73

assumed that oxygen and nitrogen dissociate in sequence. In the discussion of ionization, the air is considered to be a single-component gas with the ionization energy equal to the ionization energy of a gram-mole of the air. A similar calculation was made for CO_2 [13]. A better approximation may be obtained by taking a larger number of terms in the partition functions [14].

More accurate expressions for the thermodynamic properties of pure components [15] and gas mixtures take into account the anharmonicity of vibrations, electronic excitation, simultaneous dissociation of various components, formation of nitrogen oxide, and a single ionization. For pure gases, these effects are accounted for by the introduction of the corresponding partition functions. The degrees of dissociation and ionization are expressed in terms of partition functions, and the thermodynamic functions— in terms of the degree of dissociation, pressure, and temperature. In this, one assumes that dissociation is completed before the onset of ionization. On the basis of the expressions obtained for gas components, one deduces the analytic expressions for the composition and thermodynamic functions of an arbitrary mixture of nitrogen, oxygen, and argon. The composition of a mixture is found by solving a relatively simple system of equations by the method of successive approximations. The thermodynamic functions are obtained in the form of algebraic expressions in the degree of dissociation, p, and T. Their calculation is distinguished by its simplicity from the calculation in [14]. The ionization of a mixture, as in [12], is considered for a single-component gas. At the same time, the calculation is quite laborious, and digital computers must be used. The computational error for a mixture does not exceed 1%. The time expended is much shorter than in "exact" calculations.

The availability of a standard program for calculations according to this and the previous method permits us to use them in numeric gas dynamic calculations.

Finally, in methods for the approximate calculation of an equilibrium state, one approximates the equilibrium state tables. The approximation may be accomplished by either selecting and approximating an analytic expression depending on the parameters selected for the problem [17,18,19] or by expanding the tabular values of thermodynamic functions in series in a certain system of functions.

To reduce the approximation error, it is more convenient not to use the thermodynamic functions themselves, but rather their ratios to expressions approximating the thermodynamic functions with lower accuracy. Such an approximation using Legendre polynomials, dependent on lg p and the temperature, was made for the functions $\frac{Z(p, T)}{Z(p, T)_M}$ and $\frac{h}{h_M}$ [20] of the air, where $Z(p, T)_M$ and h_M are taken from the approximate representation [12]. The relative approximation error of this type does not exceed fractions of 1%, even if one uses only six terms of a series in each of the variables. / 74

Nonequilibrium ideal dissociating gas

The model of an ideal dissociating gas may be generalized to the case of nonequilibrium dissociation [21]. Starting with the elementary concepts on the reaction rates Freeman suggested the following expression for the rate of dissociation of an ideal dissociating gas

$$r_d = C\rho(1-\alpha_1)T^{-s}e^{-\frac{D}{kT}}, \qquad (2.24)$$

where C and s are some constants.

The structure of the formula resembles the expression of the law of mass action if the expression for the reaction rate constant (1.46) is written explicitly. Since in the state of equilibrium we have (2.16), the rate of the reverse recombination reaction is

$$r_R = \frac{CT^{-s}}{\rho_d} \rho^2 \alpha_1^2. \tag{2.25}$$

The rate of the reverse reaction depends on the concentration of the atomic component, and just as in any reaction that goes through triple collisions, it is proportional to the square of the density.

From Eqs. (2.24) and (2.25) we obtain the following for the rate of dissociation

$$\frac{d\alpha_1}{dt} = C\rho T^{-s}\left[(1-\alpha_1)\, e^{-\frac{D}{kT}} - \frac{\rho}{\rho_d}\alpha_1^2\right]. \tag{2.26}$$

The entire kinetics of the nonequilibrium process is determined by the parameters C and s (in addition to the constants D and ρ_d, that characterize an ideal gas). Their values should be selected based on the reaction rates for real gases. It will be noted that $(C\rho T^{-s})^{-1}$ has the dimension of time and it may be viewed as the characteristic time of the process.

Equations of motion of a gas

The equations of gas dynamics taking into account the nonequilibrium processes can be written under the assumption that a local thermodynamic equilibrium exists for each degree of freedom. Thus, for each degree of freedom one can introduce /75
its temperature, energy, entropy, etc. The system of hydrodynamic, thermodynamic, and kinetic equations describes the motion of a gas and the process of the establishment of equilibrium between individual degrees of freedom. In those cases when there is no equilibrium for some degrees of freedom class

(for example, vibrational), the class is subdivided into subclasses. New degrees of freedom are introduced which satisfy the assumptions about the thermodynamic equilibrium, for example the relaxation between the levels. Thus, the principal formulation of the problem remains unchanged.

Let us make a short derivation of the gas dynamic equations of continuity, momentum, and energy for a relaxing gas, following basically the exposition in [22] (see also [23-26]).

It will be assumed that a gas consists of n components, participating in r transformations. The number of components includes the degrees of freedom that are in the state of quasi-equilibrium. Thus, one can introduce for each such degree of freedom the temperature, enthalpy, and other thermodynamic parameters. It will also be assumed that there are no mass forces. We recall that at each point of space occupied by a gas, the velocity $\vec{v}_k$ of component k may in general differ from the mean local velocity of the center of mass

$$\vec{v}=\sum_k^n \frac{\vec{v}_k\rho_k}{\rho}, \qquad \text{where} \qquad \rho=\sum_k^n \rho_k.$$

To deduce the equation of continuity we consider in the space an arbitrary stationary volume V bounded by a fixed surface S [22]. The rate of change of the mass of component k in the volume

$$\frac{d}{dt}\int_V \rho_k dV=\int_V \frac{\partial \rho_k}{\partial t} dV$$

is equal to the sum of the flux of the mass of component k entering volume V through the surface, and the rate of the formation of k due to processes inside V:

$$\int_V \frac{\partial \rho_k}{\partial t} dV=-\int_S \rho_k \vec{v}_k \vec{dS}+\sum_{j=1}\int_V \nu_{kj} J_j dV. \tag{2.27}$$

Here $\vec{dS}$ is the vector surface element whose positive direction is to the outside; $\nu_{kj}J_j$ is the rate of formation of

the component k per unit volume due to process j.

ν_{kj} is defined as the ratio of ρ_k and the accepted expression for J_j. Applying Gauss' Theorem to the surface integral in Eq. (2.27), we obtain the equation of continuity for component k in a differential form /76

$$\frac{\partial \rho_k}{\partial t} = -\operatorname{div} \rho_k \vec{v}_k + \sum_{j=1}^{n} \nu_{kj} J_j; \; k = 1, 2 \ldots n. \tag{2.28}$$

Since the total mass is conserved as a result of all internal processes, we obtain upon summing over k, the equation of continuity in the ordinary form

$$\frac{\partial \rho}{\partial t} = -\operatorname{div} \rho \vec{v}. \tag{2.29}$$

If one introduces the "diffusive flux" of substance k relative to the center of mass $\vec{J}_k = \rho_k (\vec{v}_k - \vec{v})$. Eq. (2.28) can be written in the final form

$$\frac{\partial \rho_k}{\partial t} = -\operatorname{div} \rho_k \vec{v} - \operatorname{div} \vec{J}_k + \sum_{j=1}^{r} \nu_{kj} J_j; \; k = 1, 2 \ldots n. \tag{2.30}$$

To deduce the momentum equations we apply d'Alembert's principle to the separated gas volume. The principle asserts that at each instant of motion all forces applied to the system, including the force of inertia, mutually balance each other

$$\int_V \vec{w} \rho dV = \int_S \vec{P}_n d\vec{S},$$

where $\vec{w}$ is the acceleration of a gas element, and P_n is the surface force vector directed along the outside normal. The equation can be transformed [23] to the form

$$\frac{d\vec{v}}{dt} = \frac{1}{\rho} \operatorname{div} P,$$

where the vector divergence of the tensor P is defined by

$$\operatorname{div} P = \frac{\partial \vec{P}_x}{\partial x} + \frac{\partial \vec{P}_y}{\partial y} + \frac{\partial \vec{P}_z}{\partial z}$$

and its i component is

$$(\operatorname{div} P)_i = \frac{\partial P_{xi}}{\partial x} + \frac{\partial P_{yi}}{\partial y} + \frac{\partial P_{zi}}{\partial z}.$$

Tensor P is considered symmetric $(P_{ij} = P_{ji})$. Decomposing tensor P in two parts: static pressure p multiplied by the unit tensor U, and the viscous stress tensor Π,

$$P = -pU + \Pi, \tag{2.31}$$

/77

we find the momentum equation in the vector form

$$\frac{d\vec{v}}{dt} = -\frac{1}{\rho}\operatorname{div} pU + \frac{1}{\rho}\operatorname{div}\Pi. \tag{2.32}$$

Thus the form of the momentum equation does not differ from the equations of a nonrelaxing gas.

To derive the energy equation consider a certain gas volume. The change of energy in the volume is determined by the energy flux through its surface

$$\frac{d}{dt}\int_V \rho\left(\frac{1}{2}\vec{v}^2 + e\right)dV = \int_V \frac{\partial}{\partial t}\left[\rho\left(\frac{1}{2}\vec{v}^2 + e\right)\right]dV = -\int_S \vec{J}_e d\vec{S},$$

where $\vec{J}_e$ is the energy flux through a unit area per unit time.

Applying Gauss' Theorem to the volume, we obtain the energy equation in differential form

$$\frac{\partial\rho\left(\frac{1}{2}\vec{v}^2 + e\right)}{\partial t} = -\operatorname{div}\vec{J}_e. \tag{2.33}$$

The energy flux consists of the convective term $\rho\left(\frac{1}{2}\vec{v}^2 + e\right)\vec{v}$, the mechanical work done to the system $P\vec{v}$, and the "heat flux" - the term $\vec{J}_q$, including all other energy forms

$$\frac{\partial\rho\left(\frac{1}{2}\vec{v}^2 + e\right)}{\partial t} = -\operatorname{div}\left[\rho\left(\frac{1}{2}\vec{v}^2 + e\right)\vec{v} - P\vec{v} + \vec{J}_q\right].$$

Here the i component of $\vec{Pv}$ is $\sum_k P_{ik} v_k$.

Using the representation (2.31) and introducing enthalpy $h = e + \frac{p}{\rho}$, we bring the energy equation to its final form

$$\frac{\partial \rho \left(\frac{1}{2}\vec{v}^2 + e\right)}{\partial t} = -\operatorname{div}\left[\rho\vec{v}\left(\frac{1}{2}\vec{v}^2 + h\right)\right] + \operatorname{div}(\Pi\cdot\vec{v}) - \operatorname{div}\vec{J}_q.$$

It will be noted that using the relation

$$\rho\frac{da}{dt} = \frac{\partial a\rho}{dt} + \operatorname{div} a\rho\vec{v},$$

which follows from Eq. (2.29), and the expression

$$\frac{da}{dt} = \frac{\partial a}{\partial t} + \vec{v}\operatorname{grad} a,$$

/78

we can write Eqs. (2.28) and (2.33) in the form

$$\frac{d\rho_k}{dt} + \rho_k \operatorname{div}\vec{v} = \sum_{j=1}^{r} \nu_{kj} J_j - \operatorname{div}\vec{J}_k \qquad (2.34)$$

and

$$\frac{d\left(\frac{1}{2}\vec{v}^2 + e\right)\rho}{dt} = -\operatorname{div} p\vec{v} + \operatorname{div}(\Pi\cdot\vec{v}) - \operatorname{div}\vec{J}_q. \qquad (2.35)$$

Eqs.(2.34), (2.32), and (2.35) form the system of gas dynamic equations.

The specific form of ν_{kj}, J_j, $\vec{J}_k$, Π, $\vec{J}_q$ depends on the formulation of the problem and on the processes considered. It is clear that the corresponding equations must be added to the system of the gas dynamic equations.

Below the diffusion, viscosity, and heat conduction processes will only be considered in Chapter 5 which is devoted to the boundary layer, and the energy flow from the outside in the form of radiation only in Chapter 6. In the absence of these processes the equations of motion simplify and assume the

following form

$$\frac{d\rho_k}{dt}+\rho_k \operatorname{div}\vec{v}=\sum_j^r \nu_{kj}J_j;\quad k=1,\ 2\ldots n; \tag{2.36a}$$

$$\left.\begin{aligned}\frac{du}{dt}&=-\frac{1}{\rho}\frac{\partial p}{\partial x};\\ \frac{dv}{dt}&=-\frac{1}{\rho}\frac{\partial p}{\partial y};\\ \frac{dw}{dt}&=-\frac{1}{\rho}\frac{\partial p}{\partial z};\end{aligned}\right\} \tag{2.36b}$$

$$\frac{\partial\rho\left(e+\frac{u^2+v^2+w^2}{2}\right)}{dt}=-\operatorname{div}\left[\vec{\rho v}\left(\frac{u^2+v^2+w^2}{2}+h\right)\right], \tag{2.36c}$$

where u, v, w are the components of the velocity $\vec{v}$.

To the gas dynamic equations we must add the equations that describe the internal processes and thermodynamic properties of a gas.

In the following two chapters we shall only consider the chemical reactions and the excitation of the vibrational degrees of freedom of a gas.

To set up the equations of chemical kinetics we must first of all know the mechanism of chemical reactions. After a certain mechanism is established one writes down the expressions for the rates of formation of the components $\nu_{kj}J_j$ in each of r reactions. For example, if the continuity equation is taken in the form (2.36a) and the molar-volume concentrations are used for reaction rates, then

$$\nu_{kj}=M_k(b_k-a_k);\quad J_j=k_f\prod_{l=1}^{n}[X_l]^{a_l}-k_r\prod_{l=1}^{n}[X_l]^{b_l}, \tag{2.37}$$

/ 79

where a_k, b_k, k_f, k_r depend on $j\ (j=1\ldots r)$.

One can write the continuity equations by also using other expressions for the concentration

$$\left.\begin{aligned}
&[X_i]=\frac{\rho_i}{M_i}=\frac{n_i}{N_0}=\xi_i\frac{\Sigma n_i}{N_0}=\gamma_i\frac{n_\infty}{N_0}\frac{\rho}{\rho_\infty};\\
&c_i=\frac{[X_i]}{\rho}=\frac{1}{M_i}\frac{\rho_i}{\rho};\\
&\alpha_i=\frac{\rho_i}{\rho}=c_iM_i=\frac{[X_i]M_i}{\rho};\\
&\xi_i=\frac{[X_i]}{\sum\limits_i[X_i]}=\frac{c_i}{\sum c_i}=\frac{\alpha_i}{M_i}\Big/\sum_i\frac{\alpha_i}{M_i}=\frac{n_i}{\sum n_i}=\frac{\gamma_i}{\sum\gamma_i};\\
&\gamma_i=\frac{n_i}{n_\infty}\frac{\rho_\infty}{\rho}=\xi_i\frac{\overline{M}_\infty}{\overline{M}};\\
&n_i=N_0[X_i]=\gamma_i\rho\frac{n_\infty}{\rho_\infty}.
\end{aligned}\right\}\qquad(2.38)$$

Then the left-hand side of Eq. (2.36a) may be put in one of the following forms

$$\frac{d\rho_k}{dt}+\rho_k\operatorname{div}\vec{v}=M_k\left(\frac{d[X_k]}{dt}+[X_k]\operatorname{div}v\right)=$$
$$\frac{M_k}{N_0}\left(\frac{dn_k}{dt}+n_k\operatorname{div}\vec{v}\right)=n\left(\frac{d\xi_k}{dt}-\frac{\xi_k}{\overline{M}}\sum_k M_k\frac{d\xi_k}{dt}\right)=$$
$$=M_k\rho\frac{dc_k}{dt}=\rho\frac{d\alpha_k}{dt}=\rho\left(\frac{M_k}{\overline{M}_\infty}\right)\frac{d\gamma_k}{dt},$$

where $n=\sum\limits_k n_k$; $\overline{M}=\dfrac{\sum\limits_k M_k n_k}{n}$; however, the right-hand side will involve an expression for the reaction rate (2.37), transformed to the corresponding variables. It will be noted that the concentrations c_k, α_k, γ_k ,divided by the density, permit us to simplify the equations.

To relate ρ_i, p, T, h, $\overline{M}$ to the concentrations and to each other, one uses the thermodynamic relations: /80

$$p=\sum_i p_i=\sum_i\frac{\rho_iRT}{M_i}=RT\sum_i[X_i]=\rho RT\sum_i c_i=$$
$$\rho RT\sum_i\frac{\alpha_i}{M_i}=\frac{\rho RT}{\sum\limits_i M_i\xi_i}=\frac{\rho RT}{\overline{M}_\infty}\sum_i\gamma_i;\qquad(2.39a)$$

$$h=\sum_i h_i\alpha_i=\sum_i\tilde{h}_ic_i=\frac{\sum\limits_i\tilde{h}\xi_i}{\sum\limits_i M_i\xi_i}=\sum_i\frac{\tilde{h}_i[X_i]}{\rho}=$$
$$\frac{1}{M_\infty}\sum h_iM_i\gamma_i,\qquad(2.39b)$$

where

$$h_i = c_v T + \frac{p_i}{\rho_i} + e_{ki} + h_i^\circ = c_p T + e_{ki} + h_i^\circ; \tag{2.40}$$

h_i° is the specific enthalpy of formation.

$$\left.\begin{aligned} \tilde{h}_i &= h_i M_i = \tilde{c}_{pi} T + \tilde{e}_{ki} + \tilde{h}_i^\circ; \\ \tilde{h}_i^\circ &= h_i^\circ M_i;\ \ \tilde{e}_{ki} = e_{ki} M_i;\ \ \tilde{c}_{pi} = \frac{\varkappa_i R}{\varkappa_i - 1}. \end{aligned}\right\} \tag{2.41}$$

Here c_v refers to the heat capacity at constant volume of a gas with unexcited vibrational degrees of freedom. For the relaxation of the vibrational degrees of freedom of energy e_{vib} one must use the corresponding relaxation equations (see Eq. (1.75)). For example, in the simplest case the relaxation equation may be obtained by analogy with Eq. (2.30). Using the expression for the specific energy, divided by the density, we obtain the relaxation equation in the simple form

$$\frac{de_{vib}}{dt} = \frac{e_\kappa(T) - e_\kappa}{\tau_v}. \tag{2.42}$$

Finally, one can use the following relations that may be viewed as Dalton's law:

$$\left.\begin{aligned} &\rho = \sum_i M_i [X_i] = \frac{1}{N_0} \sum_i M_i n_i; \\ &\sum_i \alpha_i = 1;\ \ \sum_i \xi_i = 1;\ \ \sum_i \gamma_i = \frac{\overline{M}_\infty}{\overline{M}}, \end{aligned}\right\} \tag{2.43}$$

as well as the relations giving the molecular weight:

$$\overline{M} = \frac{\sum_i M_i [X_i]}{\sum_i [X_i]} = \frac{\sum_i n_i M_i}{\sum_i n_i} = \frac{\sum_i \gamma_i M_i}{\sum_i \gamma_i} = \frac{\sum_i M_i c_i}{\sum_i c_i} = \sum_i \xi_i M_i. \tag{2.44}$$

The last group of relations expresses the equations of material balance (2.12)

/81

$$\frac{\sum_i n_{im} \xi_i}{\sum_i n_{ii} \xi_i} = p_{mi};\ \ m = 1, \ldots a. \tag{2.45}$$

All these relations in general overdetermine the system and in specific cases only some of them are used in solving a problem. Thus, with the concentration variables chosen the total number of equations of chemical kinetics, equations of material balance, ane the necessary equations from the group of (2.43), (2.44)

must equal the number of components in the system.

The present system of differential equations is close in form to the system of equations for a gas that does not undergo any transformations. Therefore the transition to various coordinate systems is possible by means of the transformations obtained for classical gas dynamics (see for example [23]). Here for illustration we shall write the equations in the natural coordinates for the two-dimensional case. It will be noted that in steady state motion

$$\frac{da}{dt}=\vec{v}\,\mathrm{grad}\,a$$

and Eqs. (2.36a), (2.36c) may be written as

$$\left.\begin{aligned}&\mathrm{div}\,\rho_k\vec{v}=\sum_j^n \nu_{kj}J_j;\\&\vec{v}\,\mathrm{grad}\left(\frac{1}{2}\vec{v}^2+h\right)=0.\end{aligned}\right\} \qquad (2.46)$$

In the natural coordinates s, n, where s is the coordinate along a streamline and n is perpendicular to it, the equations of adiabatic flow taking into account chemical reactions and relaxation assume the following forms [27].

The equation of continuity

$$\frac{1}{\rho}\frac{\partial\rho}{\partial s}+\frac{1}{u}\frac{\partial u}{\partial s}+\frac{\partial\vartheta}{\partial n}+j\frac{\sin\vartheta}{y}=0. \qquad (2.47)$$

Here ρ is the density; u is the stream velocity; ϑ is the angle that the streamline makes with the x axis; y is the coordinate perpendicular to the x axis; j = 0 for the two-dimensional flow and j = 1 for axisymmetric flow.

The momentum equations are

$$\rho u\frac{\partial u}{\partial s}=-\frac{\partial p}{\partial s}; \qquad (2.48)$$

$$\rho u^2\frac{\partial\vartheta}{\partial s}=-\frac{\partial p}{\partial n}. \qquad (2.49)$$

The energy equation is

$$\frac{\partial h}{\partial s}+u\frac{\partial u}{\partial s}=0. \qquad (2.50)$$ /82

The equation of state for each component (2.39a) and for a mixture is

$$p=R\rho T\sum_k\frac{\alpha_k}{M_k}.$$

The equation of continuity for each component is

$$\rho u\frac{\partial\alpha_k}{\partial s}=\sum_{j=1}^{r}\nu_{jk}J_j. \qquad (2.51)$$

To the system we may add the relation $\sum_k\alpha_k=1$ and the equation of material balance. For example, for the air (21% O_2 and 79% N_2 by volume)

$$\frac{\frac{1}{16}\alpha_O+\frac{1}{16}\alpha_{O_2}+\frac{1}{30}\alpha_{NO}}{\frac{1}{14}\alpha_N+\frac{1}{14}\alpha_{N_2}+\frac{1}{30}\alpha_{NO}}=\frac{21}{79}.$$

Finally, to the system we must add the caloric equation of state (2.40) and the equations of vibrational relaxation (2.42), ionization, and conservation of charge (if these processes are considered).

2.2 General properties of the flow of a relaxing gas

Relative values of the characteristic times for various processes

Each of the relaxation processes, described by the equations of the form (1.35), (1.57), occurs at a certain characteristic rate which depends on the physical conditions in which the process takes place (temperature, pressure, and concentration of components). This rate may be compared with the characteristic relaxation time τ. If the relaxation times for various processes

differ widely, then one can distinguish regions in which certain processes are dominant, and others occur much slower. The slow processes are said to be "frozen". The opposite case involves processes for which the relaxation times are very short so that local equilibrium is established almost instantaneously. Such processes are called equilibrium processes.

The subdivision into regions of flow according to the equilibrium and frozen processes is convenient in approximate calculations and is widely used in practice. As a criterion for considering or neglecting the relaxation processes we use the ratio of the characteristic time that a gas particle spends in a given flow region, $t = L/v$, where L is the characteristic length, and v is the characteristic flow speed, to the characteristic time of the relaxation process.*

The smaller the ratio, the greater the accuracy with which the process may be considered frozen; conversely, the larger the ratio, the closer is the flow to an equilibrium flow.

Thus, the effect of relaxation processes depends not only on the thermodynamic parameters of the flow, such as the density, temperature, gas composition, but also on the dimensions of the flow region L and the flow speed v.

Speed of sound

To the two limiting cases of the flow of a relaxing gas there correspond two speeds of sound: "frozen" one, a_f, and "equilibrium" one, a_e. The first corresponds to the propagation of sound, which is not accompanied by any changes in the energy of the internal degrees of freedom of the molecules. Such, for

* Karman [28] calls this ratio the first characteristic number.

example, is the propagation in a gas of a vibrational process at a very high frequency when the internal degrees of freedom do not have enough time to exchange energy with the active degrees during the vibration period T (the ratio $\frac{\tau}{T} \gg 1$). Conversely if the disturbances propagate at a low frequency $\left(\frac{\tau}{T} \ll 1\right)$ the exchange of energy of internal degrees of freedom follows the change in the external conditions and the process occurs quasi-statically and reversibly.

The frozen speed of sound is defined as $\left(\frac{\partial p}{\partial \rho}\right)_{s,q}$, where the derivative is taken at constant gas composition and constant entropy. The equilibrium speed of sound is defined as $a_e^2 = \left(\frac{\partial p}{\partial \rho}\right)_{s,q_e}$, where the derivative is taken at constant entropy and equilibrium composition of the gas. These relations may be written in terms of the derivatives of frozen h or, respectively, of the equilibrium $\bar{h}$ entropy of the gas with respect to the density and pressure

$$a_f^2 = -\frac{h_\rho}{h_p - 1/\rho}; \tag{2.52}$$

$$a_e^2 = -\frac{\bar{h}_\rho}{\bar{h}_p - 1/\rho}. \tag{2.53}$$

For example, for an ideal dissociating gas the frozen speed / 84
of sound is defined as

$$a_f^2 = \frac{4+\alpha_1}{3}(1+\alpha_1)RT, \tag{2.54}$$

and the equilibrium speed of sound as

$$a_e^2 = \frac{\alpha_1(1-\alpha_1^2)\left(1+2\frac{T}{D}\right)+(8+3\alpha_1-\alpha_1^3)\left(\frac{T}{D}\right)^2}{\alpha_1(1-\alpha_1)+3(2-\alpha_1)\left(\frac{T}{D}\right)^2} RT. \tag{2.55}$$

Fig. 2.6 shows the plot of the ratio $(a_f/a_e)^2$ for an ideal dissociating gas modeling oxygen [29].

In general the speed of sound in a relaxing gas depends on the frequency and varies between the equilibrium and frozen

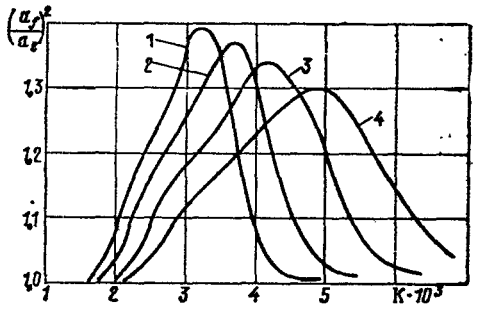

Figure 2.6. Ratio of the speeds of sound versus the temperature for "oxygen-like" ideal dissociating gas:
1 - for p = 0.01 kG/cm^2;
2 - for p = 0.1 kG/cm^2;
3 - for p = 1 kG/cm^2;
4 - for p = 10 kG/cm^2

speeds of sound. Thus, the dispersion of sound occurs in a relaxing gas. In addition, the sound signal propagates with damping that also depends on the frequency. Also: the frozen speed of sound is greater than its equilibrium value [30]. In magnitude these two speeds do not differ very much, however, the difference is of great theoretical importance.

The perturbations introduced in the flow first always propagate at the frozen speed of sound since for an exchange of the energy of internal degrees of freedom to occur it is necessary to wait a certain time on the order of the relaxation time. During that time the speed of the propagation of disturbances gradually changes and in the limit becomes equal to the equilibrium speed of sound. This leads to interesting and fairly complicated phenomena that occur due to the propagation of disturbances introduced in a moving gas [31,32].

The lesser the role of the internal degrees of freedom of the molecules, the smaller will be the difference between the frozen and the equilibrium speeds of sound. If the effect of the internal degrees is completely nonexistent, the difference between the two speeds of sound vanishes. Thus we arrive at a single speed of sound that plays such an important role in classical gas dynamics. /85

Variation of entropy

The equations of motion of a relaxing gas were obtained under the assumption that the gas may be represented by a set of subsystems in a state close to equilibrium. For equilibrium systems it is not difficult to obtain the expression for the entropy, and the variations of the entropy for each of the subsystems may be written simply as $dS_i = \frac{dQ_i}{T_i}$, where dQ_i is the amount of heat received by the subsystem.

If relaxation processes occur in a nonequilibrium system, then the entropy of the system increases, even if the system does not exchange energy with the external medium.

This will be shown using an example of a system consisting of two quasi-equilibrium subsystems. Suppose that the temperature of one of the subsystems is T_1, and of the second T_2. If the first subsystem releases heat in the amount dQ, and the other acquires this amount of heat, then the change in the entropy of the system will be

$$dS = \frac{dQ}{T_2} - \frac{dQ}{T_1} = dQ\left(\frac{1}{T_2} - \frac{1}{T_1}\right). \qquad (2.56)$$

Since $T_1 > T_2$, the value of dS will be positive. The relaxation processes result in a dissipation of mechanical energy also in the general case. At the same time, one can see that the entropy of the individual subsystems may either increase or decrease in the process of relaxation. If the translational degrees of freedom of a gas are taken as one of the subsystems, and one of the internal degrees of freedom is taken as the other, then during the excitation of the internal degrees of freedom the entropy corresponding to the translational degrees of freedom will decrease. If, in addition, afterwards the internal degree of freedom of a gas element becomes frozen, then the entropy of the translational degrees of freedom remains reduced in its entire subsequent motion. This phenomenon may lead to an

occurrence of relaxation entropy layers.

The change in the total entropy of a gas may be compared with the value of the entropy itself.* If these changes are relatively small, then they can be neglected and the entropy of the flow may be considered constant [33].

The variations of entropy, due to an exchange of energy with the internal degrees of freedom, are absent in the two limiting cases of flow: equilibrium and frozen. In the first case the temperatures of the equilibrium subsystems are always equal and the expression in (2.56) is zero. In the second case the internal degrees of freedom are completely excluded from the exchange. /86

Energy parameter

The ratio of the energy Q, participating in the exchange (in particular, of the heat of reaction), to the enthalpy of the gas, h, is still another parameter that characterizes flows with an exchange of the energies of internal degrees of freedom. In foreign literature [28] this parameter is referred to as the so-called second characteristic number, equal to $\frac{Q}{c_p T}\frac{L}{u\tau}$. Depending on the problem at hand the energy parameter may be constructed using either the total entropy or the local value of entropy, or the entropy of the active degrees of freedom.

If the ratio Q/h is low, then one can neglect the variation in the energy of the active degrees of freedom due to nonequilibrium processes. Then one can exclude the effect of the inertial degrees of freedom on the active ones and the relaxation of the inertial degrees of freedom may be viewed

* We recall that according to Nernst's theorem one is able to determine the absolute value of the entropy.

in a given field of the thermo-gas dynamic parameters determined by the active degrees of freedom.

2.3 Equations of motion in the characteristic form

To calculate the flows in a supersonic region one often uses the method of characteristics, which may be applied to the flows of a relaxing gas [27, 34, 35]. We shall limit ourselves to considering the equations of the characteristics only in the two-dimensional axisymmetric cases * in application to Eqs. (2.47) — (2.51).

Using Eqs. (2.48), (2.50), and (2.39a), one can rewrite Eq. (2.47) in the form

$$\frac{1}{\rho u^2}\frac{\partial p}{\partial s}(M^2-1)+\frac{\partial \vartheta}{\partial n}+j\frac{\sin\vartheta}{y}=\overline{M}\sum_i\left(1-\frac{h}{T\overline{c}_p}\right)\frac{\partial c_i}{\partial s}, \qquad (2.57)$$

where $\overline{c}_p=\sum_i c_i c_{pi}$. $M=u/a_f$ is the frozen Mach number;

$$a_f^2=\left(\frac{\partial p}{\partial \rho}\right)_{c_i,S}=\frac{p}{\rho}\frac{\overline{c}_p}{\overline{c}_p-R}. \qquad (2.58)$$

Eqs. (2.57) and (2.58) form a system of quasilinear partial differential equations with respect to p and ϑ . To them /87 one must add Eqs. (2.51) and the algebraic relations for h, ρ, and other variables. For $u>a_f$ the system is hyperbolic and its characteristic directions are given by

$$\operatorname{tg}\mu=\frac{\partial n}{\partial s}=\pm\frac{1}{\sqrt{M^2-1}}. \qquad (2.59)$$

The characteristic equations have the form (see also [34]):

$$\left.\begin{aligned}\frac{\partial \vartheta}{\partial s_1}+\frac{(M^2-1)^{1/2}}{\rho u^2}\frac{\partial p}{\partial s_1}+\sin\mu\left[\frac{j\sin\vartheta}{y}-\sum_i\left(\overline{M}-\frac{\rho R}{p}\frac{h_i}{\overline{c}_p}\right)\frac{\partial c_i}{\partial s}\right]=0;\\ -\frac{\partial \vartheta}{\partial s_2}+\frac{(M^2-1)^{1/2}}{\rho u^2}\frac{\partial p}{\partial s_2}+\sin\mu\left[\frac{j\sin\vartheta}{y}-\sum_i\left(\overline{M}-\frac{\rho R}{p}\frac{h_i}{\overline{c}_p}\right)\frac{\partial c_i}{\partial s}\right]=0.\end{aligned}\right\} \qquad (2.60)$$

They involve derivatives with respect to just one variable: s_1 or s_2. In this respect Eqs. (2.48) and (2.51), which are also characteristic (the characteristics are streamlines), are

* For equilibrium flows the method of characteristics is presented, for example, in the book by J. D. Hayes and R. F. Probstein [10], p. 330.

analogous to them.

The variation of concentration may also be calculated along streamlines in accordance with the relaxation equations (2.51).

In the x, y coordinates the streamlines are defined by

$$\frac{dy}{dx} = \operatorname{tg} \theta \tag{2.61}$$

and the Mach lines

$$\frac{dy}{dx} = \operatorname{tg} (\theta \pm \mu). \tag{2.62}$$

To these equations, we must add the equations describing the composition and thermodynamics of a gas.

2.4 Linearization of the equation

Sometimes one can consider the linearized system of equations, which often gives useful information on nonequilibrium gas flows, without applying complicated computational methods [36—41,26].

We shall show how one can obtain a linearized system of equations from the general equations of motion of a gas with internal degrees of freedom. As a basis, we shall take System (2.36) and add the equation for an arbitrary relaxing parameter q that characterizes the internal degree of freedom

$$\frac{dq}{dt} = \frac{L(\rho, p, q)}{\theta}, \tag{2.63}$$

where θ is a quantity that characterizes the reaction time. The smaller θ, the faster will be the reaction.

If a gas is in equilibrium, dq/dt is zero, and Eq. (2.63) determines the state of equilibrium, then

$$L(\rho, p, \bar{q}) = 0, \tag{2.64}$$

whence

$$\bar{q} = \bar{q}(p, \rho). \tag{2.65}$$

If $\theta = 0$, then Eq. (2.63) implies $L(p, \rho, q) = 0$ and the gas is in local equilibrium. This is the case of the equilibrium flow.

If $\theta \to \infty$, the equation passes into $\bar{q} = \text{const}$; the flow is frozen.

We shall assume that the linearization is done relative to / 88
the main flow $u = u_\infty,\ v = w = 0,\ p = p_\infty,\ h = h_\infty,\ q = \bar{q}_\infty$. The perturbations of the main flow will be denoted by using a bar above the symbols. Substituting the linearized variables in the system, we obtain a system of equations for the perturbations

$$\rho_\infty \left(\frac{\partial u'}{\partial x} + \frac{\partial v'}{\partial y} + \frac{\partial w'}{\partial z} \right) + u_\infty \frac{\partial p'}{\partial x} = 0; \tag{2.66}$$

$$\left.\begin{aligned} \rho_\infty u_\infty \frac{\partial u'}{\partial x} + \frac{\partial p'}{\partial x} &= 0; \\ \rho_\infty u_\infty \frac{\partial v'}{\partial x} + \frac{\partial p'}{\partial y} &= 0; \\ \rho_\infty u_\infty \frac{\partial w'}{\partial x} + \frac{\partial p'}{\partial z} &= 0; \end{aligned}\right\} \tag{2.67}$$

$$u_\infty \frac{\partial u'}{\partial x} + \frac{\partial h'}{\partial x} = 0; \tag{2.68}$$

$$u_\infty \frac{\partial q'}{\partial x} = \frac{1}{\theta_\infty} \left(L_{p_\infty} p' + L_{\rho_\infty} \rho' + L_{q_\infty} q' \right); \tag{2.69}$$

$$dh' = h_{p_\infty} dp' + h_{\rho_\infty} \rho' + h_{q_\infty} q', \tag{2.70}$$

where the indices denote derivatives with respect to the corresponding variables.

Now let us introduce $\bar{q}'$, that corresponds to local equilibrium

$$L_{p_\infty} p' + L_{\rho_\infty} \rho' + L_{q_\infty} \bar{q}' = 0. \tag{2.71}$$

With the aid of this equation, we can write the relaxation equation (2.63) in the form

$$u_\infty \frac{\partial q'}{\partial x} = \frac{\bar{q}' - q'}{\tau_\infty}, \tag{2.72}$$

where $\tau_\infty = -\frac{\theta}{L_{q_\infty}}$ is the relaxation time of a nonequilibrium process.

If several reactions are possible in a system, then the system may also be brought to the equations of the form similar to (2.72) [42-44]. The equation of the vibrational relaxation can be written directly in the form (2.72).

$\bar{q}$ can be determined from Eq. (2.65), whose differential form is

$$d\bar{q}' = \bar{q}_{p_\infty} dp' + \bar{q}_{\rho_\infty} d\rho'. \tag{2.73}$$

Eqs. (2.66 - 2.70), (2.72), (2.73) form a complete system of equations in eight unknowns. The system may be reduced to a single equation. After some transformations, using the expressions for the equilibrium and frozen speeds of sound, and the corresponding numbers $M_{e\infty} = \frac{u_\infty}{a_{e\infty}}$, $M_{f\infty} = \frac{u_\infty}{a_{f\infty}}$, we obtain the equation

$$K \frac{\partial}{\partial x}\left[\left(1 - M_{f\infty}^2\right)\frac{\partial u'}{\partial x} + \frac{\partial v'}{\partial y} + \frac{\partial w'}{\partial z}\right] + \left[\left(1 - M_{e\infty}^2\right)\frac{\partial u'}{\partial x} + \frac{\partial v'}{\partial y} + \frac{\partial w'}{\partial z}\right] = 0, \tag{2.74}$$

where

$$K = \frac{h_{p\infty} u_\infty \tau_\infty}{h_{p\infty} + h_{q\infty}\bar{q}_{p\infty}}.$$

/ 89

Applying the rot operator to the linearized momentum equation

$$\rho_\infty u_\infty \frac{\partial \bar{u}'}{\partial x} + \operatorname{grad} p' = 0;$$

we obtain $\frac{\partial}{\partial x}(\operatorname{rot} \bar{u}') = 0$. Inasmuch as $\frac{d}{dt} = u_\infty \frac{\partial}{\partial x}$, the vorticity of a liquid element remains constant. This is an important property of linearized flows. If in an unperturbed flow there is no vorticity, the latter will also be absent in the entire flow. Consequently, one can introduce a perturbation potential φ, so that $u = \frac{\partial \varphi}{\partial x}$, $v = \frac{\partial \varphi}{\partial y}$, $w = \frac{\partial \varphi}{\partial z}$.

Now Eq. (2.74) becomes an equation for the potential

$$K \frac{\partial}{\partial x}\left[\left(1 - M_{f\infty}^2\right)\frac{\partial^2 \varphi}{\partial x^2} + \frac{\partial^2 \varphi}{\partial y^2} + \frac{\partial^2 \varphi}{\partial z^2}\right] + \left[\left(1 - M_{e\infty}^2\right)\frac{\partial^2 \varphi}{\partial x^2} + \frac{\partial^2 \varphi}{\partial y^2} + \frac{\partial^2 \varphi}{\partial z^2}\right] = 0. \tag{2.75}$$

Eq. (2.75) becomes the Prandtl-Glauert equation for the equilibrium flow at K = 0, i.e. at $\tau_\infty = 0$. In the second limiting case, when K = ∞ the equation also changes into the Prandtl-Glauert equation in which one uses the frozen speed of sound.

For intermediate values of K, the characteristics of the equation are determined by terms involving derivatives of third

order. In particular, for two-dimensional flows $\left(\frac{\partial^2\varphi}{\partial x^2}=0\right)$ the characteristics are given by the equations y = const and $\frac{dy}{dx}=\pm\frac{1}{\sqrt{M_{f\infty}^2-1}}$. Correspondingly, Eq. (2.62) is either of elliptic or hyperbolic type, depending on whether $M_{f\infty}$ is smaller or greater than 1. The type of equation is preserved for all K that differ from zero. However, for K = 0 it is possible for the type of the equation to change, since in this case the equation may be of the elliptic or hyperbolic type depending on the ratio of $M_{e\infty}$ to unity. Cases are possible when one of the terms $M_{e\infty}, M_{f\infty}$ is greater than unity, and the other smaller. In these cases, the type of the equation changes discontinuously at k = 0.

REFERENCES

/90

1. Zel'dovich, Ya. B. A Proof of the Uniqueness of the Solution of Equations for the Law of Mass Action, Zhurnal Fizicheskoy Khimii, Vol. 11, No. 5, 1938.

2. Predvotitelev, A. S., Ye. V. Stupochenko, A. S. Pleshanov, Ye. V. Samuylov and I. B. Rozhdestvenskiy. Tables of Thermodynamic Air Functions (for Temperatures from 200 to 6,000 °K and Pressures from 0.001 to 1000 Atmospheres), Izd. AN SSSR, 1961.

3. Predvotitelev, A. S., Ye. V. Stupochenko, Ye. V. Samuylov, I. P. Stakhanov, A. S. Pleshanov and I. B. Rozhdestvenskiy. Tables of Thermodynamic Air Functions (for Temperatures from 6000 to 12000°K and Pressures from 0.001 to 1000 Atmospheres), Izd. AN SSSR, 1957.

4. Predvotitelev, A. S.,Ye. V. Stupochenko, A. S. Pleshanov, Ye. V. Samuylov and I. B. Rozhdestvenskiy. Tables of Thermodynamic Air Functions (for Temperatures from 12000 to 20000°K and Pressures from 0.001 to 1000 Atmospheres), Izd. AN SSSR, 1959.

5. Pleshanov, A. S., and S. G. Zaytsev. Composition, Thermodynamic and Gas-dynamic Properties of Carbon Dioxide for Temperatures from 1000 to 12000°K and Pressures from 10^{-2} to 10^{3} atm. In the Collection: Fizicheskaya gasodinamika, teploobmen i termodinamika gazov vysokikh temperatur (Physical Gas Dynamics, Heat Exchange, and Thermo-

dynamics of High-Temperature Gases), Izd. AN SSSR, 1962.

6. Kuznetsov, N. M., Termodinamicheskie funktsii i udarnyye adiabaty vozdukha pri vysokikh temperaturakh (Thermodynamic functions and Shock Air Adiabates at High Temperatures), Moscow, "Mashinostroyeniye", 1965.

7. Selivanov, V. V. and I. Ya. Shlyapintokh. Thermodynamic Properties of the Air in Thermal Ionization and a Shock Wave. Zhurnal Fizicheskoy Khimii, Vol. 32, No. 3, 1958.

8. Hilsenrath, J. and C. Beckett. Thermodynamic Properties of Argon Free Air. Nat. Bur. of Stds. Rept. No. 3991.

9. Lighthill, M. J. Dynamics of a Dissociating Gas P. I. Equilibrium Flow. J. Fluid Mech. Vol. 2, 1957, p. 1.

10. Hayes, U. D. and R. F. Probstein. Theory of Hypersonic Flows. Moscow, IL, 1962.

11. Mikhaylov, V. V. Analytic Representation of the Thermodynamic Functions of Dissociating Air. Inzhenernyi Sbornik, Vol. 28 1960.

12. Mikhaylov, V.V. Approximate Analytic Representation of Thermodynamic Functions of the Air. Inzh. Sb., Vol. 31, 1961.

13. Mikhaylov, V. V. Approximation of the Enthalpy and the Equation of State of Carbon Dioxide. Inzh. Zhurnal. Vol. 2, No. 2, 1962.

14. Hansen, F. Approximation for the Thermodynamic and Transport Properties of High Temperature Air. NASA Techn. Rep. R—50, 1959.

15. Sevast'yanov, R. M. Thermodynamic Functions of High-temperature Gases. Inzh. Zhurnal, Vol. 3, No. 3, 1963.

16. Sevast'yanov, N. M. and M. D. Zdunkevich. Thermodynamic Functions of a Gas Mixture at High Temperatures. Inzh. Zhurnal. Vol. 4, No. 4, 1964.

17. Kvashinia, S. S. and V. P. Korobeynikov. A Solution of Certain Problems on the Motion of the Air Considering Dissociation and Ionization. Izvestiya AN SSSR, "Mekhanika i Mashinostroyeniye". No. 2, 1960.

18. Vertushkin, V. K. Approximation of Thermodynamic Functions of the Air. Inzh. Zhurnal, Vol. 2, No. 4, 1964.

19. Krayko, A. I. Analytic Representation of the Thermodynamic Functions of the Air. Inzh. Zhurnal, Vol. 4, No. 3, 1964.

20. Naumova, I. I. Approximation of Thermodynamic Properties of the Air. Zhurnal vychislitel'noy matematiki i matematicheskoy fiziki. Vol. 1, No. 2, 1961. /91

21. Freeman, N. C. Nonequilibrium Flow of an Ideal Dissociating Gas. J. Fluid Mech. No. 4, 1958.

22. De Groot, S. and P. Mazur. Nonequilibrium Thermodynamics. 1964.

23. Kochin, N.Ye., I. A. Kibel', and N. V. Roze. Teoreticheskaya gidromekhanika (Theoretical Hydromechanics), Vol. 1, Vol. 2 Leningrad-Moscow, GITTL, 1948.

24. Wood, V. V. and J. G. Kirkwood. Hydrodynamics of a Reacting and Relaxing Medium. In the Collection: Gas Dynamics and Heat Exchange in the Presence of Chemical Reactions, Moscow, IL, 1962.

25. Gubanov, A. I. and Yu. P. Lun'kin. Equations of Kinetics of Dissociation of a Gas Considering Diffusion. Zhurnal Teoreticheskoy Fiziki, Vol. 27, No. 11, 1957.

26. Stupochenko, Ye. V. and I. P. Stakhanov. Equations of Relaxation Hydrodynamics. Doklady Akademii Nauk, Vol. 134, No. 4. 1960.

27. Spurk, I. H., N. Gerber and R. Sedney. Characteristic Calculation of Flow Field with Chemical Reactions. AIAA J. Vol. 4, No. 1, 1966.

28. Karman, Th. Dimensionless Variables in Aerodynamic Fringe Areas. Z. f. Flugwissenschaften Vols. 1-2, 1956.

29. Clark, J. and M. MacChesny. Dynamics of Real Gases. 1967.

30. Landau, L. D. and Ye. M. Lifshitz. Mechanics of Continuous Media. 1953.

31. Stakhanov, I. P. and Ye. V. Stupochenko. Structure of Mach Lines in Relaxing Media. Doklady Akademii Nauk, Vol. 134, No. 5, 1960.

32. Stakhanov, I. P. and Ye. V. Stupochenko. Certain Problems of the Hydrodynamics of Relaxing Media. ZhPMTF, No. 2, 1963.

33. Eschenroeder, A. Q. Entropy Changes in Nonequilibrium Flows. Phys. of Fluids, X, No. 10, 1963.

34. Belotserkovskiy, O. M. and V. K. Dushin. Supersonic Flow Over Blunt Bodies of a Nonequilibrium Gas. Zhurnal Vychislitel'noy matematiki i matematicheskoy fiziki. Vol. 4, No. 1, 1964.

35. Katskova, O. M. and A. N. Krayko. Raschet ploskikh i osesimmetrichnykh sverkhzvukovykh techeniy pri nalichii neobratimykh protsessov. (Calculation of Flat and Axisymmetric Supersonic Flows in the Presence of Irreversible Processes.) VTs An SSSr, 1964.

36. Clarke, J. T. The Linearized Flow of a Dissociating Gas. J. Fluid Mech. Vol. 7, No. 4, 1960.

37. Vincenti, W. G. Non-Equilibrium Flow Over a Wavy Wall. J. Fluid Mech., Vol. 6, No. 4, 1959.

38. Moore, F. K. and W. E. Gibson. Propagation of Weak Disturbances in a Gas Subject to Relaxation Effects. JASS, No. 2, 1960.

39. Clarke, J. F. Relaxation Effects on the Flow Over Slender Bodies. J. Fluid Mech. Vol. 11, No. 4, 1961.

40. Ryhming, I. L. On Slender Airfoil Theory for Nonequilibrium Flow. JAS, No. 9, 1962.

41. Khodyko, Yu. V. Flow of a Relaxing Gas over a Slender Cone of Revolution. Doklady AN Byelorussian SSR, Vol. 8, No. 8, 1964.

42. Pavlova, L. M. Nonequilibrium Flows of a Dissociating Gas Close to Equilibrium. Izvestiya AN SSSR, "Mekhanika i Mashinostroyeniye", No. 3, 1961.

43. Tkalenko, R. A. Supersonic Nonequilibrium Gas Flow over Slender Bodies of Revolution, ZhPMTF, No. 2, 1964.

44. Krayko, A. N. A Study of Weakly Perturbed Supersonic Flows for an Arbitrary Number of Nonequilibrium Processes. Prikladnaya matematika i mekhanika, Vol. 30, No. 4, 1966.

CHAPTER 3

NONEQUILIBRIUM ONE-DIMENSIONAL FLOWS

3.1 Normal shock wave

One-dimensional flows are the simplest case for which one can / 92
study and estimate the effect of nonequilibrium processes. A great role in the study of the relaxation processes and their effect on the flow characteristics is played by the calculations of normal shock waves. This is explained, on one hand, by the fact that to obtain experimental data on reaction rates at high temperatures we use shock tubes, and therefore the calculations of shock waves are of direct interest in the estimation and verification of the role of various reactions from the point of view of the comparison of computational results and experiment. On the other hand, in the case of flows over blunt bodies the relaxation phenomena are manifested primarily when a gas flows through a front shock wave and the calculations of normal shock waves may give important information on the role of relaxation.

The results obtained for normal shock waves may be generalized directly to oblique shock waves. (For this, one resolves the velocity of the flow incident on an oblique shock wave into components that are normal and tangential to the wave. The normal component changes during the transition through the wave, as in a normal shock wave, and the tangential component remains unchanged).

A shock wave is characterized by a sharp variation of the state of thermodynamic equilibrium of a gas. When a moving gas element passes through a shock wave, as a result of molecular collisions the energy of translational motion is transformed

into thermal energy, and after relaxation takes place, the gas achieves a new state of equilibrium. When the wave has high intensity, the heating of the gas may be sufficient for the relaxation processes to begin. This is associated with a change of the energy of the inert degrees of freedom of the gas.

The relaxation processes determine the structure of a shock /93
wave, i.e., the transitional zone between two equilibrium states. The rate of relaxation of different degrees of freedom is diverse since the rate of energy exchange in collisions for different processes differs by a large factor. Thus, to establish equilibrium in translational and rotational degrees, one needs from 3 to 5 molecular collisions. To establish equilibrium in vibrational degrees of freedom, one needs on the order of 1,000 collisions, and to establish chemical and ionic equilibrium the number of the required collisions is many times greater. The difference between the rates at which equilibrium is established in different processes results in a situation where a quasi-equilibrium state is rapidly established in certain degrees of freedom, and then the much slower process occurs of the transition to full thermodynamic equilibrium.

Thus, in the case of a complete spatial separation of different processes the structure of a shock wave is as follows. In the narrow front whose extension is on the order of several free paths, the equilibrium is established in the translational and rotational degrees of freedom. A sharp discontinuity in the temperature, pressure, and density exists. Then the vibrational degrees of freedom become excited, and, as a result, there is a drop in the temperature. In the relaxation process, the degrees of freedom that were excited earlier remain in quasi-equilibrium, but their temperatures change and become closer as a full thermodynamic equilibrium is approached. The establishment of full equilibrium occurs asymptotically, and the width of the shock wave

is determined by the distance at which deviations from the state of final equilibrium reach a certain small fraction of their equilibrium values.

The feasibility of separating the excitation processes for different degrees of freedom vanishes as the temperature behind a shock wave increases, since at high temperatures the characteristic times for different processes become comparable. Estimates show that the feasibility of process separation is retained until the flow incident on the shock wave in the air reaches approximately the speed of 7 km/sec (it is also possible to use one of the methods in which dissociation is coupled to vibrations). However, experiments were performed [1] that show that, when the M number in front of a shock wave in oxygen ranges from 10 to 14, vibrations interact strongly with the excitation of the translational and rotational degrees of freedom, and for M>14, dissociations also participate in the coupling.

We are particularly interested in the structure of the discontinuity, which is determined by the relaxation of the internal degrees of freedom of a gas, and a great deal of attention is given to the vibration and chemical nonequilibrium processes. Thus, the distances are measured from a somewhat indeterminate front of the discontinuity in the translational temperatures. / 94
This, however, does not introduce substantial errors, since the basic processes that are of interest occur at distances of many tens and hundreds of free paths. In such a formulation, one neglects diffusion, viscosity, and heat conductivity, since these processes are associated with large gradients of hydrodynamic quantities, existing mainly in the discontinuity of translational temperatures.

Approximate calculation of the structure of shock waves

The flow in a shock wave is described by the equation of continuity, momentum and energy

$$\rho_1 u_1 = \rho_\infty u_\infty; \tag{3.1}$$

$$p_1 + \rho_1 u_1^2 = p_\infty + \rho_\infty u_\infty^2; \tag{3.2}$$

$$h_1 + \frac{u_1^2}{2} = h_\infty + \frac{u_\infty^2}{2}. \tag{3.3}$$

To these equations, one should add the thermodynamic relations, generally written considering the internal changes in a gas.

Here the velocity of the flow is relative to a system associated with the front of a shock wave; u, p, ρ, h are the speed, pressure, density, and specific enthalpy of a gas. The subscript "1" denotes the state behind the shock wave, and the subscript "∞" denotes the equilibrium state in front of a shock wave.

If there is no relaxation, then for an ideal gas $h = \frac{\varkappa}{\varkappa - 1}\frac{p}{\rho}$ and one can express the flow parameters behind a shock wave in terms of the parameters in front of the shock wave, the M_∞ number of the shock wave $\left(M_\infty = \frac{u_\infty}{a_\infty}\right)$ and the adiabatic exponent κ:

$$u_1 = u_\infty\left(1 - \frac{2}{\varkappa + 1}\frac{M_\infty^2 - 1}{M_\infty^2}\right); \tag{3.4}$$

$$\rho_1 = \rho_\infty \frac{(\varkappa + 1) M_\infty^2}{(\varkappa - 1) M_\infty^2 + 2}; \tag{3.5}$$

$$p_1 = p_\infty\left(\frac{2\varkappa}{\varkappa + 1} M_\infty^2 - \frac{\varkappa - 1}{\varkappa + 1}\right). \tag{3.6}$$

In particular, if $M_\infty \gg 1$, then Eqs. (3.4—3.6) become:

$$u_1 = u_\infty \frac{\varkappa - 1}{\varkappa + 1}; \tag{3.7}$$

$$\rho_1 = \rho_\infty \frac{\varkappa+1}{\varkappa-1}; \tag{3.8}$$

$$p_1 = p_\infty \frac{2\varkappa}{\varkappa+1} M_\infty^2. \tag{3.9}$$ /95

Clearly, as M_∞ increases the values of u_1 and ρ_1 approach certain limits, and p_1 (and T_1) increase without limit (strong shock wave).

The limit in case of a strong wave is obtained from Eqs. (3.1—3.3) when one may neglect the pressure and enthalpy in front of a shock wave as compared with $\rho_\infty u_\infty^2$ and $\frac{u_\infty^2}{2}$.

The state of a gas may be conveniently represented in the p, $V = \frac{1}{\rho}$ coordinates: pressure, specific volume. Passing in Eqs. (3.1—3.3) to the specific volume, we obtain the relations

$$\frac{V_\infty}{V_1} = \frac{u_\infty}{u_1}; \tag{3.10}$$

$$u_\infty^2 = V_\infty^2 \frac{p_1 - p_\infty}{V_\infty - V_1}; \tag{3.11}$$

$$u_1^2 = V_1^2 \frac{p_1 - p_\infty}{V_\infty - V_1}, \tag{3.12}$$

which follow from the mechanical conservation laws alone, and

$$h_1 - h_\infty = \frac{1}{2}(p_1 - p_\infty)(V_\infty + V_1). \tag{3.13}$$

The latter relation is called the shock adiabate. Since the state in front of a shock wave is assumed to be known, Eq. (3.11) in the p, V plane results in a straight line that passes through the point p_∞, V_∞ (Fig. 3.1).

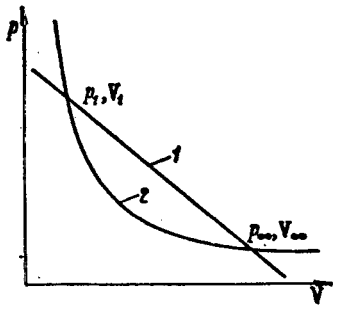

Figure 3.1 Representation of states in a shock wave in the p,V plane:
1 - straight line (3.11);
2 - shock adiabate

Using the caloric equation of state, the enthalpy of thermodynamically equilibrium states may be represented in the form of a function of p, V, and the shock adiabate may also be represented in the p,V plane. In contrast with the straight line described by Eq. (3.11), representing the entire sequence of states of a gas element in a shock wave, the shock adiabate represents only the equilibrium states. The final equilibrium state of a gas is determined by the point of intersection of a shock adiabate and the straight line (3.11) (see Fig. 3.1). In the p,V plane, the transition from the initial to the final state corresponds to the transition from point p_∞, V_∞ to point p_1, V_1 along the straight line (3.11). / 96

For an ideal gas, it is easy to obtain the equation of a shock adiabate in explicit form. Substituting the expression for the enthalpy of an ideal gas $h=c_pT=\frac{\varkappa}{\varkappa-1}pV$ in Eq. (3.13)

$$\frac{V_1}{V_\infty}=\frac{(\varkappa-1)p_1+(\varkappa+1)p_\infty}{(\varkappa+1)p_1+(\varkappa-1)p_\infty}. \qquad (3.14)$$

As the intensity of a shock wave increases, the ratio of specific volumes approaches a constant [see also (3.8)].

$$\left(\frac{V_1}{V_\infty}\right)_r=\frac{\varkappa-1}{\varkappa+1}. \qquad (3.15)$$

and, consequently, the shock adiabate in the p,V plane is bounded on the left by an asymptote which depends on the adiabatic exponent of the gas, κ. In particular, for a monoatomic gas $\varkappa=\frac{5}{3}$ we obtain $\left(\frac{V_1}{V_\infty}\right)_r=\frac{1}{4}$; for a diatomic gas $\varkappa=\frac{7}{5}$ we get $\left(\frac{V_1}{V_\infty}\right)_r=\frac{1}{6}$, and in general for $\varkappa\to1$ we get $\left(\frac{V_1}{V_\infty}\right)_r\to0$.

Taking a derivative with respect to κ of (3.14) one can show that at constant κ and unchanged initial state in front of the wave the shock adiabate, corresponding to larger κ, lies entirely for $V<V_\infty$ to the right of the shock adiabate corresponding to the smaller κ.

Neglecting the significant changes in the density in a shock wave, the pressure and enthalpy at large compressions depend relatively little on the compression. Using Eqs. (3.1) - (3.3), we can obtain

$$p_1=\rho_\infty u_\infty^2\left(1-\frac{V_1}{V_\infty}\right); \tag{3.16}$$

$$h_1=\frac{1}{2}u_\infty^2\left[1-\left(\frac{V_1}{V_\infty}\right)^2\right]. \tag{3.17}$$

For example, if the gas is diatomic, then

$$(p_1)_r=\rho_\infty u_\infty^2\left(1-\frac{1}{6}\right);\quad (h_1)_r=\frac{u_\infty^2}{2}\left(1-\frac{1}{36}\right), \qquad /97$$

and if the gas is monoatomic

$$(p_1)_r=\frac{\rho_\infty u_\infty^2}{2}(1-1/4);\quad (h_1)_r=\frac{u_\infty^2}{2}(1-1/16).$$

In those cases when the energy of the internal degrees changes, and the gas undergoes physico-chemical changes, it is not possible to represent the equation of a shock adiabate in explicit form relative to p and V. The curve representing the shock adiabate, in those cases will have a more complicated form as compared with the one shown in Fig. 3.1.

However, one can obtain a qualitative idea of the changes in a shock wave on the basis of fairly simple concepts. Let us imagine that the region of relaxation behind a shock wave is subdivided into a number of zones corresponding to different relaxation processes, and at the end of each zone a thermodynamic

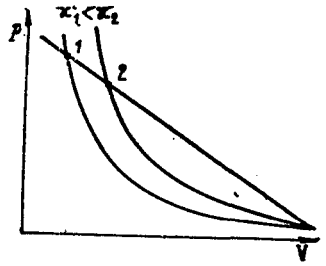

Figure 3.2 Variation of the state in a shock wave with relaxation for $\varkappa_1<\varkappa_2$.

equilibrium is successively established in each of the processes, at the same time as the processes that are still unexcited remain frozen [2,3]. Thus, after the excitation of the translational and rotational degrees of freedom the gas behaves as a monoatomic gas. Then upon the excitation of the vibrational degrees of freedom it behaves like a multiatomic gas. Then, after complete dissociation (and ionization), it behaves like a monoatomic gas again. This suggests that the state of a gas after passing each of the zones may be found on shock adiabates corresponding to different κ. In particular, this at once implies that the degree of compression increases when the vibrational degrees of freedom behind a shock wave become excited, and the degree of compression may decrease during dissociation.

Suppose that an equilibrium state to which there corresponds a certain κ is established after a certain process. This state is represented by a point of intersection of a straight line 1 (Fig. 3.2) by a shock adiabate constructed for this value of $\varkappa_1$. If in the process of relaxation that follows this state κ increases, then the point representing the successive state of equilibrium moves along the straight line 1-2 to the right and below the shock adiabate corresponding to the new value of $\varkappa_2$. (see Figure 3.2). If κ decreases, then the image point moves to the left and upward. Strictly speaking, in this case it is necessary to consider the variation of the energy of internal degrees of freedom of a gas, and more precisely the changes of states may be associated with $\varkappa_e$ [4] , determined by the relation (2.23).

Eq. (3.14) may in general be written in the form /98

$$\frac{V_1}{V_\infty}=\frac{\frac{p_1}{\rho_1}}{h_1+e_1-(h_\infty+e_\infty)+\frac{p_\infty}{\rho_\infty}}, \tag{3.18}$$

which for strong shock waves assumes the form

$$\frac{V_1}{V_\infty}=\frac{p_1/\rho_1}{h_1+e_1}=\frac{h_1-e_1}{h_1+e_1}=\frac{\varkappa_e-1}{\varkappa_e+1}. \tag{3.19}$$

The shock adiabate corresponding to the state of equilibrium behind the shock wave may be calculated directly by using the values of $\varkappa_e$ taken from the tables of equilibrium states of the gas (analogous to those given in Fig. 2.4). However, the calculation of pressure and temperature, on which $\varkappa_e$ depends must be made using the equations of the conservation, the caloric and thermal equations of state, and the law of mass action. Introduction of $\varkappa_e$ allows a simplification of the calculation by the method of successive approximations but in general $\varkappa_e$ does not have to be introduced.

In explicit form the system for calculating a shock adiabate for strong shock waves in a diatomic gas without considering ionization has the following form [4]:

$$\frac{p_1}{p_\infty}=\frac{2\varkappa_\infty M_\infty^2}{\varkappa_e+1}; \tag{3.20}$$

$$\frac{\rho_1}{\rho_\infty}=\frac{\varkappa_e+1}{\varkappa_e-1}; \tag{3.21}$$

$$\frac{T_1}{T_\infty}=\frac{p_1}{p_\infty}\frac{\rho_\infty}{\rho_1}\frac{1}{1+\alpha}; \tag{3.22}$$

$$\varkappa_e=\frac{h}{h+(1+\alpha)RT}; \tag{3.23}$$

$$h=(1-\alpha)h_{A_2}+\alpha(D+2h_{A_1}); \tag{3.24}$$

$$\frac{4\alpha^2}{1-\alpha}=\frac{K_c(T)}{p}. \tag{3.25}$$

When ionization (which is assumed to start after dissociation comes to a full stop) is considered in the system of equations, one changes the last four equations

$$\frac{T_1}{T_\infty}=\frac{p_1}{p_\infty}\frac{\rho_\infty}{\rho_1}\frac{1}{2(1+\beta)}; \tag{3.26}$$

$$\varkappa_e=\frac{h}{h-2(1+\beta)RT}; \quad h=(D+2h_A)[(1-\beta)+\beta I]; \tag{3.27}$$

$$\frac{\beta^2 p}{1-\beta}=2\frac{g_1}{g_0}\left(\frac{2\pi m_e}{h^2}\right)^{3/2}(kT)^{5/2}e^{-\frac{I}{kT}}. \tag{3.28}$$ / 99

The Sach equation (3.28) is written for the case of a single ionization.

A similar study can also be made for each of the zones of partial establishment of equilibrium. In this case, introduction of $\varkappa_e$ permits a considerable simplification of the problem since one does not have to use tables for each state of partial equilibrium. Eqs. (3.20)-(3.28) are also valid in this case.

Equilibrium shock adiabates for bromium and oxygen, obtained by the method of successive approximations [4], are shown in Figs. 3.3 and 3.4. The variation of pressure, density, and temperature versus M_∞ is shown in Figs. 3.5-3.7.

An analysis of the equations and theoretical results leads to the following conclusions. When vibrations are excited (increase of c_p, $\alpha=\beta=0$) $\varkappa_e$ decreases with increasing temperature behind a shock wave, and consequently, the compression increases. This decrease in $\varkappa_e$ does not depend on pressure. As dissociation begins for small α when the separation of the shock wave into quasi-equilibrium zones is only possible, the contribution of dissociation depends on the value of the ratio $\frac{\alpha D}{(1-\alpha)h_{A_2}}$. As long as this value is much less than unity $\varkappa_e$ decreases with an increase of temperature (Eqs. (3.23), (3.24)). The pressure dependence is determined by Eq. (3.25) which shows that with a

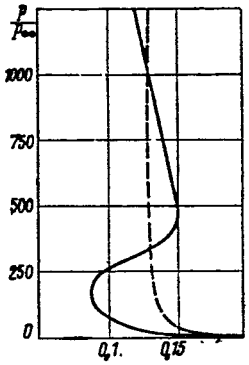

Figure 3.3. Shock adiabate for bromium for $T_\infty = 293$ K, $p_\infty = 0{,}2276$ kG/cm^2 in relation to ρ_∞/ρ (dashed line corresponds to an ideal gas)

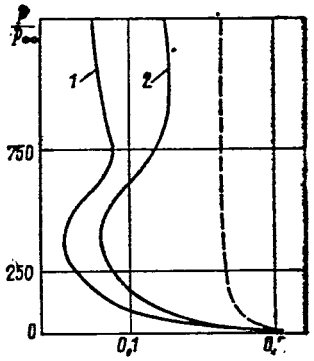

Figure 3.4. Shock adiabate for oxygen for $T_\infty = 293$ K in relation to ρ_∞/ρ (dashed line corresponds to an ideal gas):

1 - for $p_\infty = 0{,}2276 \cdot 10^{-4}$ kG/cm^2;
2 - for $p_\infty = 0{,}2276$ kG/cm^2

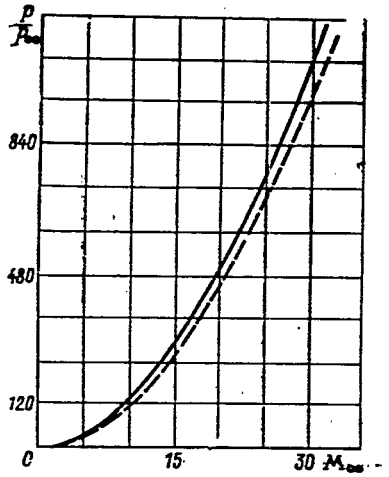

Figure 3.5. Dependence of equilibrium pressure in a shock wave on M_∞ for $T_\infty = 293$ K (dashed line corresponds to an ideal gas with a constant value of $\varkappa$).

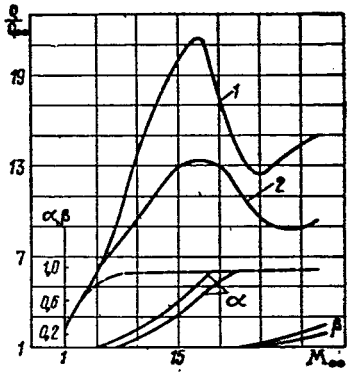

Figure 3.6. Dependence of equilibrium density in a shock wave, degree of dissociation, and ionization on M_∞ for $T_\infty = 293$ K (dashed line corresponds to an ideal gas with a constant value of $\varkappa$):

1 - for $p_\infty = 0{,}2276 \cdot 10^{-4}$; kG/cm^2
2 - for $p_\infty = 0{,}2276$ kG/cm^2

decrease of pressure behind a shock wave, identical degrees of dissociation are obtained at lower temperatures (see Fig. 3.6). /100
When the degree of dissociation is high, the contribution of the dissociation energy becomes considerable, the value of $\varkappa_0$ increases, and the amount of compression decreases.

The maximum compression will be much greater than in the case of an ideal gas and may, for example, equal 20. The effect of ionization on compression is similar to the effect of dissociation, and in general the appearance of additional heat capacity in a gas results in a decrease of $\varkappa_0$. For large initial ionization $\varkappa_0$ increases, with the origin of the second ionization it decreases again, etc.. As a result a shock adiabate assumes a wavy character (see Fig. 3.3). A more detailed analysis shows that the parameters in a shock wave may change nonmonotonically when passing from zone to zone (see also [5,6]). In practical calculations of equilibrium states behind shock waves in a gas mixture, in addition to the method of successive approximations [4,7], methods were proposed that use tables of equilibrium states [8, 9, 10]. Finally, there are tables of gas parameters behind a normal shock / 101
wave that are based on tables of parameters for equilibrium states [11, 12, 13].

Calculation of the Structure of Shock Waves in Air

To study nonequilibrium flows in normal shock waves it is necessary to solve the system of differential equations that describes the chemical kinetics of the gas. If in calculations one does not use digital computers, then only estimates are possible, which in certain cases permit the obtaining of fairly accurate results [14]. However, the choice of the simplifying assumptions, necessary for a solution, and especially an estimate of the conditions of the validity of the solutions obtained are complicated and should be based on a clear understanding of the role of

different kinetic prccesses and the ability to distinguish dominant reactions.

The development of computers had the result that the calculation of a normal shock wave became a theoretically simple problem. The basic condition of obtaining correct results is to know the kinetics of the processes. Such calculations were made in both this country (for example, [15,16]) and abroad (for example, [17,18]). The basic features of the air flows in shock waves are well known. At the present time we can only speak of increasing the accuracy of calculations as the new data on reaction rate constants appear, and of studies of more subtle effects in shock waves, such as, for example, the variation of electron concentration. Also in the case when computers are used, there still remains the difficulty of distinguishing the dominant processes since when too many processes are considered, the calculations become laborious. However, even here computers may be useful since they make it possible to make calculations that permit one to estimate the effect of individual processes.

Lin and Teare's calculation remains as one of the most complete calculations of the structure of shock waves in air [18]. The calculation was made for chemical reactions according to the scheme (1.66)-(1.71) which considers a large number of different ionization reactions. The reaction rates for a majority of ionization reactions are known only superficially. The calculation estimates their relative importance. /102

The gas dynamics equations of flow in a shock wave have the form

$$\left.\begin{aligned} &\rho_1 u_1 = \rho_\infty u_\infty; \\ &p_1 + \rho_1 u_1^2 = p_\infty + \rho u_\infty^2; \\ &e_1 + \frac{p_1}{\rho_1} + \frac{u_1^2}{2} = e_\infty + \frac{p_\infty}{\rho_\infty} + \frac{u_\infty^2}{2}. \end{aligned}\right\} \qquad (3.29)$$

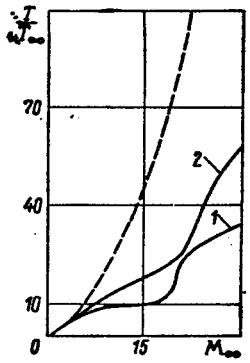

Figure 3.7. Dependence of the equilibrium temperature in a shock wave on M_∞ for T_∞ =293 K (dashed line corresponds to an ideal gas with a constant *) :
1 - for $p_\infty = 0{,}2276 \times 10^{-4}$ kG/cm^2.
2 - for $p_\infty = 0{,}2276$ kG/cm^2.

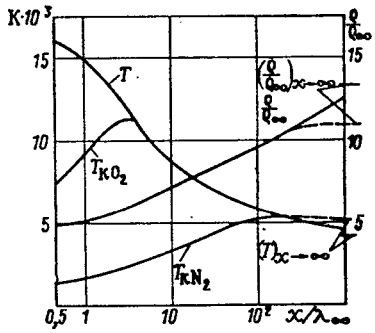

Figure 3.8. Typical distribution of temperature and density behind a shock wave in air for u_∞= 6.9 km/sec, calculated considering the connection between the vibrational excitation and chemical reactions (solid line for p_∞ = 0.02 mm Hg, dashed line for p_∞ = 2 mm Hg)*

γ (1.31) is convenient to use as the concentration of components. The thermodynamic relations are written as

$$p=\frac{\rho RT\sum_l \gamma_l}{\overline{M}_\infty};\quad e=\frac{1}{\overline{M}_\infty}\sum_l e_l M_l \gamma_l, \tag{3.30}$$

where e_l depends on the translational and vibrational temperatures of the components, and $\overline{M}_\infty$ is the molecular weight of the gas in front of the shock wave.

Dalton's law implies that

$$\sum_l \gamma_l M_l = \overline{M}_\infty = 28{,}98. \tag{3.31}$$

* x/λ_∞ is the ratio of the distance behind a translational-rotational discontinuity to the mean free path of molecules in front of the discontinuity.

Finally the equation for the conservation of mass under the assumption that the air consists by volume of 79% nitrogen and 21% oxygen yields

$$\frac{\gamma_O + 2\gamma_{O_2} + \gamma_{NO}}{\gamma_N + 2\gamma_{N_2} + \gamma_{NO}} = \frac{21}{79}. \tag{3.32}$$

The connection with the relaxation of vibrational excitation was considered using the CVD method (see p. 48), i.e., the dissociation rate constant was taken in the form

$$k = \eta(k)_{eq}$$

where

$$\eta = \frac{1}{\tilde{v}} \frac{1 - \exp\left[\tilde{v}\left(\frac{T_v}{T_{vib}} - \frac{T_v}{T}\right)\right]\left[\exp\left(\frac{T_v}{T_{vib}}\right) - 1\right]}{\left[\exp\left(\frac{T_v}{T_{vib}} - \frac{T_v}{T}\right) - 1\right]\left[\exp\left(\frac{T_v}{T}\right) - 1\right]},$$

and the vibrational temperature T_{vib} is related to the translational relaxation by the equation

$$\frac{de_{kl}}{dt} = \frac{e(T)_l - e_{kl}}{\tau_{vl}}, \tag{3.33}$$

where

$$e_{kl} = \frac{h\nu}{\exp\frac{T_v}{T_{vib}} - 1} \gamma_l \frac{n_\infty}{\rho_\infty}.$$

/103

In this case, the vibrational relaxation of O_2 and N_2 was considered, and it was assumed that the vibrational temperature of NO is in equilibrium with the translational temperature, since NO is formed from particles with sufficient energy.

The equations of chemical kinetics are written for each component, for example,

$$\frac{d\gamma_{O_2}}{dt} = -\left(\sum_l k_{f1}^l \gamma_l + k_{f5}\gamma_N + k_{f6}\gamma_{N_2}\right)\gamma_{O_2}\frac{\rho_1}{\rho_\infty} n_\infty + \\ + (k_{r5}\gamma_{NO}\gamma_O + k_{r6}\gamma_{NO}^2)\frac{\rho_1}{\rho_\infty} n_\infty + \sum_l k_{r1}^l \gamma_{O_2}^2 \gamma_l \left(\frac{\rho_1}{\rho_\infty}\right)^2 n_\infty^2. \tag{3.34}$$

However, in this form the system of equations turns out to be overdetermined, and one may either exclude Eqs. (3.31), (3.32) or

exclude one or two kinetic equations; to determine the sufficient concentrations of components one uses Eqs. (3.31), (3.32).

Subsequent calculations reduce to solving a system of differential equations of the form (3.33), (3.34) using the relations (3.29), (3.30), (3.31), (3.32) for the initial conditions $\gamma_{O_2}=0{,}21$; $\gamma_{N_2}=0{,}79$; $\gamma_N=\gamma_O=\gamma_{NO}=e_K=0$. This formulation of the problem is rather typical of shock wave calculations.

The calculations were made in the pressure range $0{,}02\leqslant p\leqslant 0{,}2$ mm Hg and speed range $4{,}5\leqslant u_\infty\leqslant 7$ km/sec. With the aid of a computer, one obtains the variation of the chemical composition of the gas with time or distance $x=\int_0^t u(t)\,dt$ from the shock front for the translational and rotational degrees of freedom.

Typical plots of gas dynamic parameters and the composition of the mixture are shown in Figs. (3.8) and (3.9), respectively. One should note the typical rapid variation of the concentration of O_2 and N_2 at the beginning of the process (within the distance of ten free paths from the wavefront, the degree of dissociation is 75 and 50%, respectively; this is associated with a temperature drop within the same length by a factor of 2) and a very slow approach to equilibrium values. Thus, for N_2 the concentrations and temperatures differ from their equilibrium values by 10% only at a distance of several hundred free paths.

First, dissociation of oxygen occurs. The dissociation of nitrogen is much slower and to a lesser extent, even at speeds /104
on the order of 7 km/sec. The fact that the maximum concentration of NO_2 exceeds the equilibrium value is of basic importance.

The fundamental reaction that starts the entire process behind the shock wave is in the form of the dissociation of O_2. Atomic nitrogen, particularly at moderate shock wave speeds, is formed as a result of the exchange reactions (1.69) - (1.70).

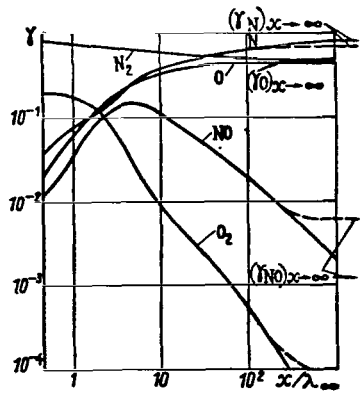

Figure 3.9. Typical distribution of neutral particles behind a shock wave in air for u_∞ = 6.9 km/sec (solid line for p_∞ = 0.02 mm Hg, dashed line for p_∞ = 2 mm Hg).

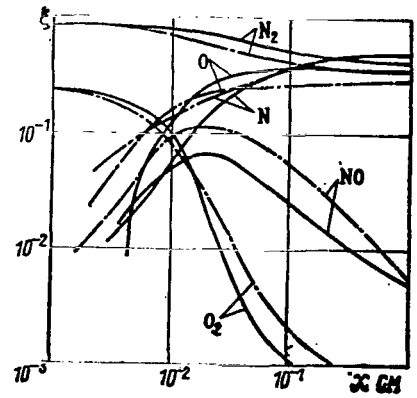

Figure 3.10. Molar fractions of air components depending on the distance behind a shock wave (dot-dash lines based on the solution [18] for u_∞ = 6.9 km/sec, solid lines based on the solution [19] for u_∞ = 6.55 km/sec)

These reactions along with (1.68) which runs in the opposite direction lead to a formation of NO. The equilibrium in exchange reactions is established faster than in the others. Reaction (1.68) reaches rapidly a state of quasi-equilibrium, and following a change in the temperature, it leads to a drop in the concentrations of NO. Thus one obtains a maximum of γ_{NO}. At higher concentrations of NO and O reaction (1.69) goes from right to left and also results in a drop of concentration of NO. The reactions that result in a formation of NO are bimolecular, and therefore the value of the maximum is practically independent of the pressure.

The fact that dissociation of nitrogen is practically absent in weak shock waves and that in strong ones it starts after dissociation of oxygen comes to an end was often used in calculations (for example, [14]).

The effect of a different choice of reaction rate constants /105
does not result in any significant changes of gas dynamic parameters and gas composition behind a shock wave, as one can see from Fig. (3.10) which shows the results of shock wave calculations using the constants proposed in 1961 [19] and in 1963 [18] (see also [15]). Comparison with experiment shows that theoretical results differ from experimental ones at high shock wave intensities. However, the difference is relatively small (2-5 times over the length of relaxation) and it decreases as the values of reaction rate constants are improved. In general, the accuracy of the existing calculations is satisfactory for main gas dynamic applications.

The law of binary similitude ρt = const is satisfied for the greater part of the shock wave. This is associated with the fact that the fundamental reactions (1.66) - (1.70) are binary and go in the forward direction. The reverse reactions, however, are ternary, and at gas densities that exist behind a shock wave they may be neglected in the main part of the shock wave with the exception of the region close to the state of equilibrium, where they play an important role.

In Figs. (3.8) and (3.9), the distance measured on the axis of abscissas is essentially divided by the density, since the free path is inversely proportional to the density. According to the binary law of similitude, the dependence on the initial gas pressure in front of a shock wave is manifested only at the end of the relaxation zone.

Calculation of the ionization of air in a shock wave

The accuracy of the electron concentration calculation is lower than for neutral components, since the theoretical rates of ionization reactions depend not only on the accuracy of the

ionization rate constants, but also on the accuracy with which the concentrations of the gas components that become ionized have been calculated. Therefore, the use of different sets of reaction rate constants has a particular effect on the electron concentrations.

The rate of ionization for different groups of processes is shown in Fig. 3.11 for three speeds of a shock wave. Curve 1 (atom-atom) refers to the ionization processes in collisions /106
N-O, O-O, N-N, and gives the sum of ionization due to these reactions. Curves 3 (molecule-molecule and atom-molecule) refer to the sum of reactions of the molecular components.

According to the computational results, the atom-atom reactions are the most important group of ionization processes, especially if the shock waves are relatively weak. The ionization processes by electron impact may be neglected at flow speeds relative to the wave of less than 5 km/sec, but they may become important at speeds greater than 10 km/sec.

The effect of pressure on ionization is hardly felt, since the binary collisions play the dominant role. The N-O (1.109) reaction is dominant among the atom-atom reactions in the range considered. However, as the wave reaches a speed of 9 km/sec, the effect of the N-N (1.110) reaction becomes just as important.

Normalized electron and ion densities are plotted in Fig. 3.12. The electron concentration increases monotonically until the atom-atom reaction starts to reduce it. At moderate shock wave speeds, the NO+ ions form the principal fraction of the ions, and at speeds over 9 km/sec the N+, O+ ions become dominant. The maximum of the electron concentration, manifested when flow speeds in front of a shock wave become from 5 to 9 km/sec, is important. At shock wave speeds of 2-4 km/sec, the electron concentration is rather small, and at speeds over 9.5 km/sec the maximum of the electron concentration vanishes.

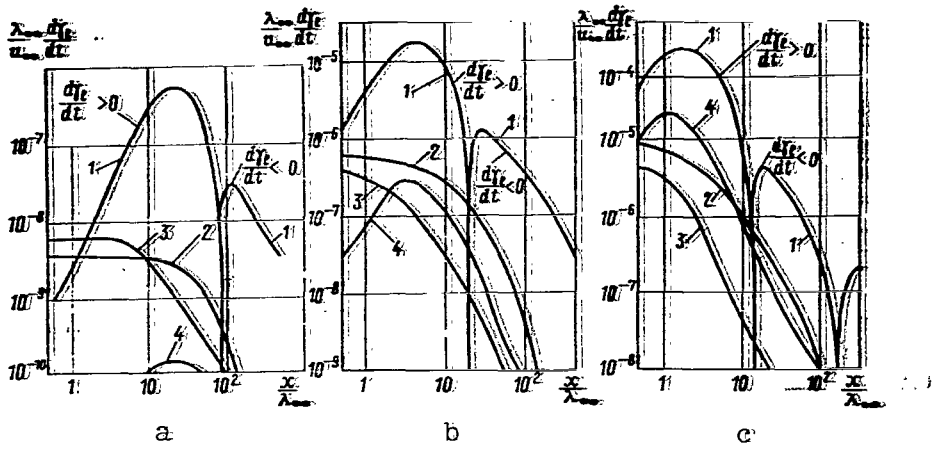

a b c

Figure 3.11. Specific rates of ionization in the air for different processes depending on the distance behind a shock wave for three values of the shock wave speed and pressure (p_∞ = 0.02 mm Hg): a – for u_∞ = 5 km/sec; b – for u_∞ = 6.9 km/sec; c – for u_∞ = 9 km/sec; 1 – atom-atom; 2 – photoionization; 3 – molecule-molecule; atom-molecule; 4 – electron impact

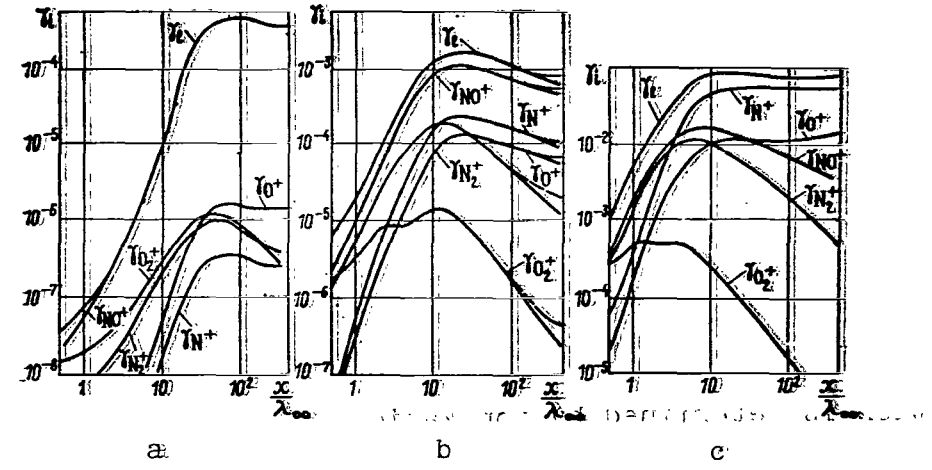

a b c

Figure 3.12. Distribution of free electrons and various positive ions for three different speeds of a shock wave in the air and different values of initial pressure: a – for u_∞ = 5 km/sec and p_∞ = 0.02 mm Hg; b – for u_∞ = 6.9 km/sec, p_∞ = 0.02 mm Hg (solid line) and p_∞ = 2 mm Hg (dashed line); c – for u_∞ = 9 km/sec and p_∞ = 2 mm Hg

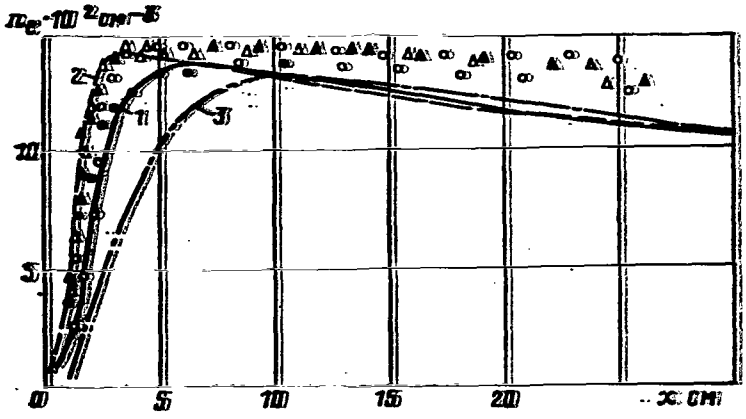

Figure 3.13. Comparison of theoretical and experimental values of the electron density distribution behind a shock wave in air for u_∞ = 6.9 km/sec, p_∞ = 0.02 mm Hg: theoretical curve 1 was obtained for the value of the reaction constant ((1.112)), curves 2 and 3 were obtained by increasing and decreasing it, respectively, by a factor of 3 at constant values of the rate constants for the remaining reactions; dots refer to experimental data, circles are for u_∞ = 6.95 km/sec, triangles for u_∞ = 6.85 km/sec.

Fig. 3.13 shows a comparison between theoretical results and experiment [20]. The curves obtained theoretically reproduce fairly well the shape of the forward front of ionization. However, behind the maximum the deviations are significant, which is apparently due to experimental errors. /108

When the flow speeds in front of the shock wave are greater than 10 km/sec the air ionization may be considered as ionization in atomic gases (see page 63). The width of the zone of dissociation under those conditions is very small, and the width of the zone of relaxation is determined by ionization processes. Calculations are difficult, because one has to consider a large number of chemical compounds forming behind the wave, as well as the large number of the excited states of atoms and molecules and radiation processes. Nevertheless, when processes are combined into quasi-equilibrium blocks, the required estimates can be made [21].

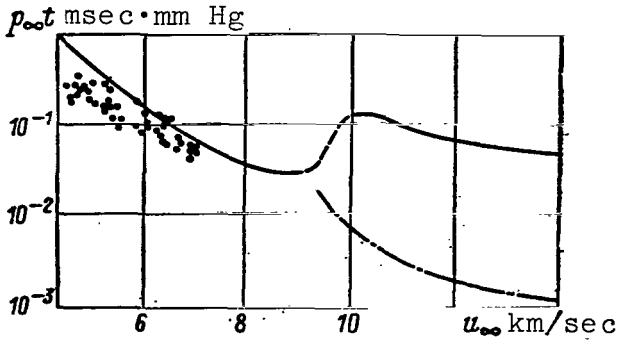

Figure 3.14. Dependence of the product of the relaxation time and the pressure before the front of the shock wave on the velocity of the shock wave (solid line - ionization relaxation for $u_\infty \leqslant 9$ km/sec from [18]; points - experimental results from [20]; dot-dash line - estimate of dissociation relaxation).

The reactions $N+O \rightleftarrows NO^+ + e$, $N+N \rightleftarrows N_2^+ + e$ give the main fraction of electrons in the initial stage. As the electrons accumulate, the role of the electron-atom collisions increases, and the rate of ionization is determined by the electron temperature (see also [22,23]). In contrast with the fact that the velocities before a shock wave — where extension of the zone of relaxation is determined by the kinetics of molecule dissociation — range up to 9 km/sec, at velocities above 10 km/sec there occur qualitative changes in the process, and the length of the relaxation zone is determined by the ionization processes. In addition, in the 9-10 km/sec velocity range, the time of relaxation increases discontinuously (Fig. 3.14). /109

The sharp widening of the relaxation zone is associated with the disappearance of the maximum of electron concentration. Calculations [24] show the following process development. Dissociation of O_2 and N_2 occurs behind a shock wave front, and the electron concentration increases due to the reactions (1.109) and (1.110). The charge redistribution process slows down the reverse processes by lowering the concentrations of NO+ and N_2+. This results in establishment of a local equilibrium of all ions. The

temperature drop behind a wave due to dissociation lowers the rate of formation of electrons according to the reactions (1.109), (1.110). Since the dissociation of nitrogen continues when the velocities of the flow before the wave are less than 9.5 km/sec, it results in the formation of an [e] maximum before the dissociation ends. At large flow velocities, the rate of reactions (1.109), (1.110) becomes less than the rate of dissociation of N_2. This results in a situation where nitrogen dissociates almost completely, and the energy contribution of ionization is still low. Therefore, with an increase in the velocity of the flow before a shock wave, the equilibrium temperature and the electron concentration behind it increase sharply. Near the front of the shock wave, the reactions (1.109) and (1.110) do not have enough time to produce an equilibrium concentration of electrons, and after reactions (1.109), (1.110) decelerate, the electron concentration slowly approaches its equilibrium value after dissociation had come to an end. The disappearance of the maximum results in a situation where a concentration of electrons is reached which is comparable with equilibrium after a long time, and it is only the latter that determines the extension of the relaxation zone.

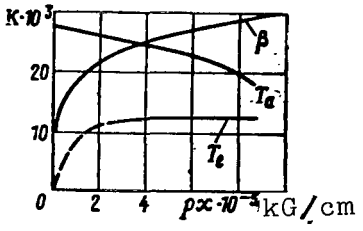

Figure 3.15 Profile of the parameters of a non-equilibrium gas behind a shock wave for u_∞ = 12 km/sec.

An analysis of ionization processes when the velocities before a shock wave are greater than 10 km/sec has shown that up to $\beta = 0{,}5\beta_{eq.}(p)$ the process also occurs according to a binary scheme, and for each velocity one can give a universal dependence on pressure (Fig. 3.15) [21].

Effect of the connection between dissociation and excitation of vibrations

Calculations showing the effect of the excitation of vibrational degrees of freedom on dissociation were made for a shock wave in nitrogen and oxygen [25,26]. In this case, the relaxation times obtained by Blackman (1.60), (1.61) were used, and the dissociation rate constants for oxygen (1.72). Dissociation of nitrogen was assumed to go through the reactions

$$N_2+N \underset{k_{r_3}}{\rightleftarrows} 2N+N; \quad N_2+N_2 \underset{k_{r_3}}{\rightleftarrows} 2N+N_2,$$

where

$$k_{r_3}=3{,}33\cdot 10^{21}T^{-\frac{3}{2}} \ \frac{\text{cm}^6}{\text{mole}^2\text{sec}};$$

$$k_{r_3}=3{,}33\cdot 10^{19}T^{-\frac{3}{2}} \ \frac{\text{cm}^6}{\text{mole}^2\text{sec}}.$$

/110

Computations show that, when the velocity of the shock wave corresponds to a 10-20% dissociation, the latter terms in Eq. (1.75) do not play any role. The vibrational temperatures in the CVD model may have a maximum exceeding the equilibrium temperature and even greater than the corresponding local value of the translational temperature. The vibrational temperature becomes equal to the translational temperature during the relaxation process and then follows it.

The CVDV model differs from the CVD model (Figs. 3.16, 3.17; equiprobable possibility of dissociation).

In the CVDV model, the time of relaxation of vibrations increases substantially, the time of the formation of atomic components increases and the vibrational temperature always is lower than the translational tempeature, even though in some cases it attains a maximum just as in the CVD model.

The formation of a "plateau" of vibrational temperature turns out to be characteristic. The vibrational temperature, after the

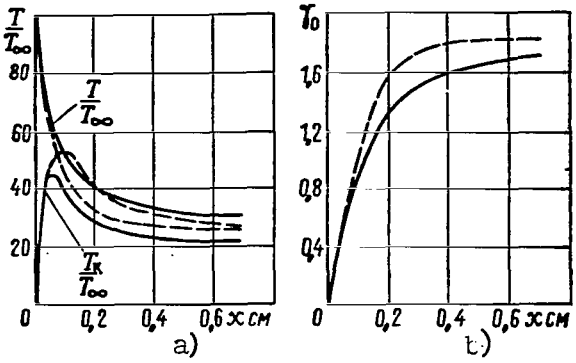

Figure 3.16. Relaxation behind a shock wave in oxygen (solid line - CVDV model, dashed line - CVD model): for u_∞ = 7 km/sec, $p_\infty = 2.23 \cdot 10^4$ kG/cm^2, T_∞ = 249 K. a - function $T/T_\infty(x)$; b - function $\gamma_0(x)$.

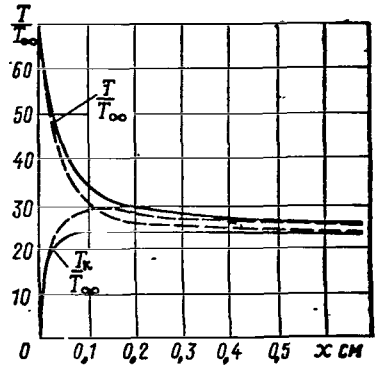

Figure 3.17. Distribution of temperature behind a shock wave in nitrogen (solid line - CVDV model, dashed line - CVD model): for u_∞ = 7 km/sec, p_∞ = 1 mm Hg, T_∞ = 285 K.

initial sharp changes, remains almost constant, slowly approaching the translational temperature when passing to an equilibrium stage. This is associated with the fact that the transition of energy from translational degrees of freedom to the vibrational ones is almost balanced by a removal of energy as a result of /111
dissociation. The experimental values of the rate of dissociation are determined precisely in that region of quasi-equilibrium. Therefore the dependence of the pre-exponential factor in Arrhenius' law on the temperature comes into play. When calculating relaxation behind shock waves with dominant dissociation from upper levels in the region of quasi-equilibrium we used the dissociation constants obtained by Camac and Vaughan [27], but without considering the dependence of the pre-exponential factor on the temperature

$$(k_f)_{eq} = 9 \cdot 10^{14} \exp \times$$
$$\times \left(-\frac{59\,300}{T}\right) \frac{\text{см}^3}{\text{mole sec}}.$$

By the same token the temperature dependence is introduced in the factor $\eta = k_f/(k_f)_{eq}$ which is taken as equal to unity at the

temperature 4,000°K. In the expression for the vibrational energy we considered cubic terms and took 34 levels for the harmonic oscillator.

In the calculation we studied the effect of various parameters but primarily U (see Eq. (1.88)), which was taken equal to $\frac{D}{6k}$, $\frac{D}{3k}$, $\frac{D}{k}$, $\frac{3D}{k}$, and ∞, where $\frac{D}{k}=T_d=59000°$ is the characteristic temperature of oxygen dissociation. The relaxation time τ_v was the second parameter whose effect was studied.

As already noted, Fig. 1.13 (curves 1,2) clearly shows the deceleration of dissociation, caused by the delaying effect of the excitation of the upper levels of the molecule - so-called time of incubation. By selecting values for τ_v and U one can obtain the dissociation constant and the time of incubation that closely correspond to experimental data. For this calculation the agreement was obtained for $U=\frac{D}{6k}$ and τ_v calculated using (1.58), and for $U=\frac{D}{3k}$ and τ_v equal to one-half the theoretical value. /112

The variation of the pre-exponential factor is shown in Fig. 3.18. This temperature dependence for models with dominant dissociation in the 4,000-8,000°K region is fairly sharp — on the order of $1/T^3$. For an equiprobable dissociation the temperature dependence is on the order of 1/T. Thus, it is possible to obtain a satisfactory agreement between this scheme and the experimental data.

Calculations of shock waves in the air considering vibrational relaxation of components are given in [28].

Shock waves in gases different from the air

In addition to the air the calculations of normal shock waves were also made for other gases [29]; the scheme for these calculations is basically similar to the one already presented.

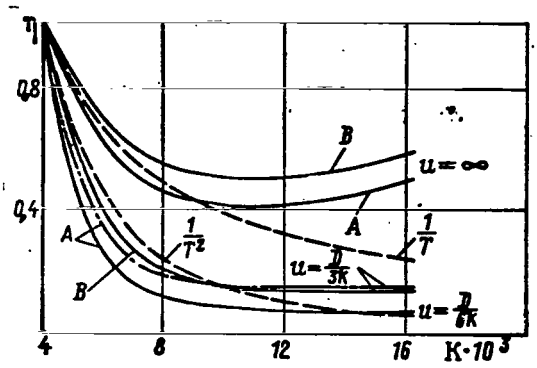

Figure 3.18. Effect of the non-equilibrium of vibrations on the dissociation rate constant:
A - for $\tau_v=\langle\tau_v\rangle$ theory
B - for $\tau_v=1/2\ \langle\tau_v\rangle$ theory

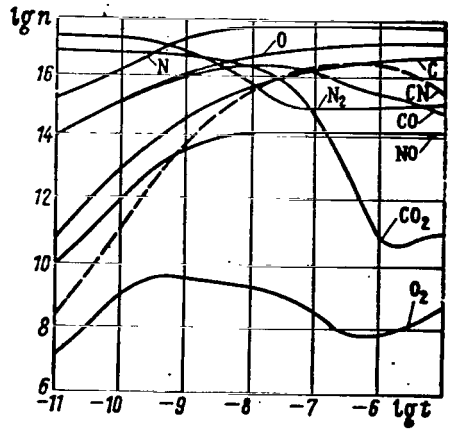

Figure 3.19. Dependence of the concentration (in cm^{-3}) of neutral components on time (in sec) spent in a shock wave for M_∞= 41.3 (0.74 N_2; 0.25 CO)

Calculations of the direct shock waves in a gas consisting of CO_2, N_2 and Ar were made using schemes and reaction constants from Table 8 for different compositions of the atmosphere(0.09 CO_2, 0.01 Ar, 0.9 N_2 and 0.74 N_2, 0.25 CO_2, 0.01 Ar) for different altitudes [30]. As an example we give Figs. 3.19 and 3.20. As in the air, the atoms form fairly fast behind a discontinuity; however, the remaining molecules also play a great role. At the beginning of the process the fundamental role is played by the ion N_2^+, then atomic ions dominate. The ion equilibrium is attained much later than the equilibrium of chemical composition. There are also differences depending on the initial composition of the gas - state behind a shock wave in gas mixtures with a high content of CO_2 approaches equilibrium slowly.

Direct dissociation [reactions (1), (2), Table 8] was the basic /113
mechanism of the decomposition of CO_2 and N_2. Reactions (3) and (15) become important in later stages of the process. The electrons form mainly due to associative ionization [reaction (13)]. The reaction in which CN forms (18) turns out to be very rapid, and

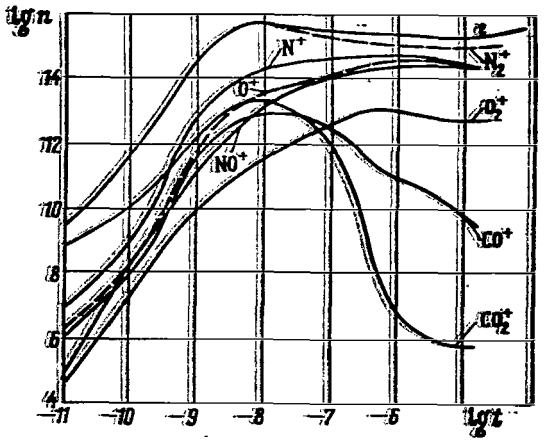

Figure 3.20. Dependence of concentration (in cm^{-3}) of electrons and ions on time (in sec) spent in a shock wave for $M_\infty = 41.3$ ($0.74\ N_2 + 0.25\ CO_2$)

consequently it affects all components participating in the reaction. However, it is considered that the rate of this reaction is somewhat indeterminate and the electron concentration is determined to within an order of magnitude.

Similar calculations using reaction rate constants from Table 9 [31] confirmed the presence of a maximum of the concentration of CO, O_2, NO and CN.

The concentration of CN, in particular, strongly depends on the initial CO_2 content in the mixture. The distribution of CN behind a shock wave is of particular interest in connection with its effect on gas radiation.

Reculiarities of the distribution of weak shock waves / 114

Above we have described the regularities in the structure of the relaxation zone, which are typical of strong shock waves and waves of moderate intensity. However, if the wave is weak, namely such that the speed of its propagation D is less than the frozen speed of sound a_f (such cases when $a_f > D > a_e$ are possible in a relaxing medium), then the gas flow in the wave will have a different character: a discontinuity is absent, where the profile is smooth, and the state of the gas in the wave changes continuously from the initial equilibrium state for $x = -\infty$ to the final $x = \infty$ [5, 7, 32–36]. (In foreign literature such a structure is usually referred to as a "shock wave with full dispersion").

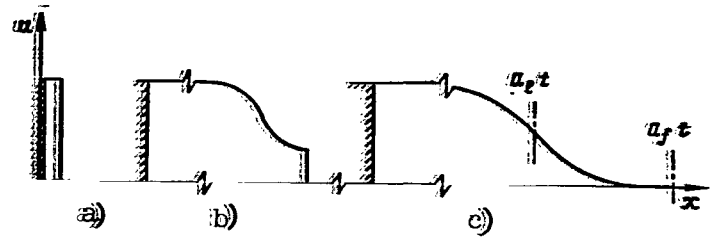

Figure 3.21. Velocity profile in a perturbation wave before a moving piston: a – for $t<\tau$; b – for $t\sim\tau$; c – for $t\gg\tau$.

A shock wave with a smooth profile represents essentially the limiting state which arises in front of a flat piston which is instantaneously brought into motion with a sufficiently small constant velocity. When this problem is studied in linear approximation [7, 37] one obtains the following picture:* a discontinuity of low intensity forming at $t = 0$ ($x = 0$) first propagates with the speed $D = a_f$, and its intensity decays as e^{-kx}, where $k \approx \frac{a_f - a_0}{a_f^2 \tau^+}$, and τ^+ has the same order of magnitude as the time of relaxation τ. The wave structure for $\bar{t} \ll 1$ ($\bar{t} = t/\tau$) is determined by the specific features of the propagation of the high-frequency disturbances (see Section 4.1). Wave profiles for $\bar{t} \ll 1$ and $\bar{t} \sim 1$ are shown schematically in Figs. 3.21, a and b. /115

For $\bar{t} \gg 1$ the wave of disturbance has a smooth profile (see Fig. 3.21, c). The region in which the speed changes from 0 to u_0, in the linear approximation has the characteristic width $l \approx a_f \tau^+ \sqrt{\frac{a_f^2 - a_0^2}{a_0^2} \frac{2x}{a_f \tau^+}}$, and the maximum values of the

* In the classical case when a medium is in the form of an ideal gas, in front of a piston that starts moving at a constant velocity u_0 there arises a shock wave that also moves at a constant velocity $D > a$, and is followed by a region of uniform flow. If, in addition, $u_0 \ll a$, then $D \approx a$ and the flow is approximately described by a solution of a linear (acoustic) equation.

derivatives of gas dynamic functions, for example $\frac{du}{dx}$, lie on the line $x=a_e t$. Since the width of the relaxation zone increases as $x^{1/2}$, the maximum values of the derivatives du/dx etc., approach 0 as $x^{-1/2}$ independently of the value of u_0. Thus, according to the linear theory with time the wave becomes "washed out", and it does not approach an asymptotic stationary state.

This result disagrees with the actual limiting state of a gas in the wave before a piston moving at a constant velocity. The reason for it is the fundamentally nonlinear character of flow in a compression wave (what is paradoxical is that the structure of flow becomes most complicated precisely in the limiting case when $u_0 \to 0$). We shall describe the structure of the limiting state on the basis of [33] and [125].

The solution will have a different character depending on the value of the parameter

$$s=\frac{u_0}{a_f-a_e}. \tag{3.35}$$

There is a certain piston velocity u_{0*}, equal in order of magnitude to a_f-a_e, for which the velocity of the wavefront becomes as $t\to\infty$ strictly equal to the frozen speed of sound, a_f. In a coordinate system moving at the speed a_f, to this case corresponds a steady flow with $M_f = 1$. The derivative du/dx at $x=a_f t$ (wavefront) is discontinuous; the function itself, however, is continuous (see Fig. 3.22, case $D/a_f=1$).

For $u_0>u_{0*}$ the wavefront represents a discontinuity moving at the speed $D>a_f$. The width of the relaxation zone in this case will be on the order of τD. For /116

$$0<u_0<u_{0*} \tag{3.36}$$

the wave has a smooth profile, and the velocity of its propagation D will vary in the range

$$a_e<D<a_f \tag{3.37}$$

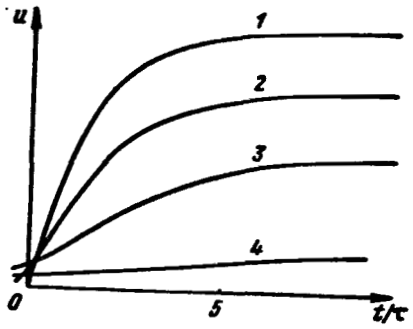

Figure 3.22. Velocity distribution in a wave with a smooth profile:
1 - for $\frac{D}{a_f}=1$;
2 - for $a_f-D<D-a_e$;
3 - for $a_f-D\sim D-a_e$;
4 - for $a_f-D>D-a_e$.

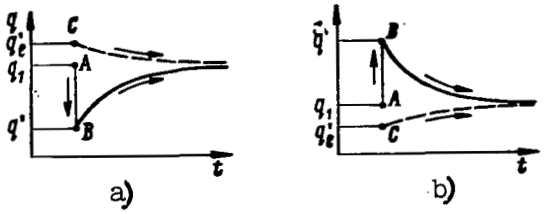

Figure 3.23. A scheme of the development of a relaxation process: a- for $u>a_f$; b - for $u<a_e$

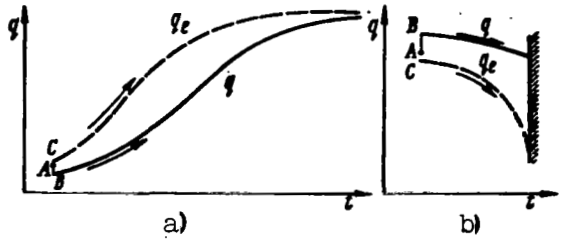

Figure 3.24. A scheme of the development of a relaxation process: a - for $e<e_e$; b - for $e>e_e$.

Here depending on the value of the parameter s the width of the relaxation zone, d, will have different values:

a) for $s\sim 1$ (i.e., for $u_0\sim a_f-a_e$).

$$d_1\sim a_f\tau; \tag{3.38}$$

b) for $s\ll 1$ (i.e., for $u_0\ll a_f-a_e$) the width of the relaxation zone increases in inverse proportion to s:

$$d\sim\frac{d_1}{s}=\frac{a_f\tau(a_f-a_e)}{u_0}. \tag{3.39}$$

This property of very weak compression waves with a smooth profile was first discovered by Ya. B. Zel'dovich [32].

Instability of the flows of a relaxing gas

A characteristic property of steady flows of a relaxing gas is their instability which is manifested when flow velocities u vary in the range $a_f > u > a_e$ [33,38]. Without giving the proof which can be found in these papers we shall give a qualitative description of the relaxation process occurring when the relaxation parameter q deviates from its equilibrium value q_e.

Let us consider a homogeneous equilibrium gas flow($q = q_e$), which moves with velocity u along the x axis.

Suppose that at $x = x_1$ (point A in Figs. 3.23 and 3.24) the value of q is given a small increment and it becomes equal to q' (point B). Here according to the law of the conservation of energy the local equilibrium value of q_e will change and will be equal to q_e' (point C). If then the velocity of the flow u is less than the equilibrium value or greater than the frozen velocity of sound ($u < a_e$ or $u > a_f$), then the relaxation process will develop /117 according to the scheme shown in Fig. 3.23, a and b (solid lines show the variation of q, dashed lines - variation of q_e). As a result the system will return to its initial equilibrium state.

For $a_f > u > a_e$ the behavior of the relaxation process will be completely different (see Fig. 3.24). In the case shown in Fig. 3.24, a, the system achieves a new equilibrium state that differs from the initial one. In this equilibrium state $u < a_e$. What is important is that in this case in the initial stage of the process the curves describing the variation of q and q_e move apart instead of coming closer.

In the case shown in Fig. 3.24, b, the velocity of the flow as a result of the relaxation process reaches the value of a_f but equilibrium will not be reached. Subsequent steady flow is impossible (when the gas flows with an addition of heat there develops a phenomenon of the type of "heat crisis").

3.2 Nonequilibrium flows in nozzles

Basic properties of steady nonequilibrium flows in a stream filament

The study of a nonequilibrium expansion of chemically reacting gas mixtures in a stream filament is of considerable interest in connection with the development of hypersonic aerodynamic tubes, gas-dynamic lasers, and jet engines designed for a flight at high supersonic velocities. Along with the purely practical side these problems also deserve attention from a theoretical point of view, since they permit us to study in the most simple form a number of features that are characteristic of any expanding flows of a relaxing gas.

Let us consider a steady state nonequilibrium gas flow in a stream filament of variable cross-section (quasi-one-dimensional flow in a nozzle)*. We shall assume that a thermodynamic equilibrium exists within each degree of freedom and the relaxation process ends by establishing an equilibrium between the active and internal degrees of freedom (see Section 1.1).

In the absence of viscosity, heat conductivity, and diffusion /118 the full system of equations describing a nonequilibrium flow of a multicomponent gas mixture in a stream filament consists of the equations of continuity, momentum, energy, thermal and caloric equations of state, and the equations of kinetics, and has the form

$$\rho u F = \text{const} \quad \text{or} \quad \frac{d\rho}{\rho} + \frac{du}{u} + \frac{dF}{F} = 0; \tag{3.40}$$

$$u du + \frac{dp}{\rho} = 0; \tag{3.41}$$

* Three-dimensional gas flows in nozzles are studied in [39-44].

$$\frac{u^2}{2}+h=H=\text{const} \quad \text{or} \quad udu+dh=0; \tag{3.42}$$

$$p=p(\rho, T, \langle q_i\rangle); \tag{3.43}$$

$$h=h(\rho, T, \langle q_i\rangle). \tag{3.44}$$

Here $\langle q_i\rangle$ denotes the set of all relaxation parameters $q_1, q_2, \ldots, q_N$ which describe a nonequilibrium state of the gas, for example, energy of vibrations, concentration of components, etc.. In contrast with equilibrium flows, where $q_i=C_i$ (C_i are constants), in nonequilibrium gas flows these parameters are not functions of the gas state alone but depend also on the kinetic properties of the medium (rate of the physico-chemical processes) and on the flow dynamics, for example, on $d\rho/dt$. The equations expressing the rate of change of the parameters q_i in a gas flow are called the kinetics equations or relaxation equations.* The basic form (2.36a) is rarely used directly. Other forms that follow from (2.36a) are used more often. Naturally, the relaxation equations assume different forms depending on which processes they characterize, how these processes are interrelated, and in terms of which variables the equations are written. **

If as the parameters q_i we choose the specific variables (per unit mass), for example the molar-mass concentrations or mass fractions, then in terms of these variables the relaxation equations may be written in a form which is simplest and

---

* In physical chemistry the equations of kinetics usually refer to the equations for the rates of flow of the physico-chemical processes in a system at constant volume.

** As the variables characterizing the composition of a mixture we can use the molar or mass fractions ξ_i and α_i, molar-volume, and molar-mass concentrations $[X_i]$ and c_i, etc. (See Sections 1.3 and 2.1).

most general for different processes

$$\frac{dq_l}{dt}=F_l(\rho, T, \langle q_k\rangle), \qquad (3.45)$$ / 119

where d/dt denotes the total time derivative (in the case of a steady quasi-one-dimensional flow d/dt = u d/dx). The specific form of the functions F_i for different physico-chemical processes is given in Chapter 1. In particular, for vibrational relaxation in a simple diatomic gas, Eq. (3.45) assumes the form (1.57) (model of a harmonic oscillator)

$$\frac{de_k}{dt}=\frac{e_{ke}-e_k}{\tau(T, p)}, \qquad (3.46)$$

and for an ideal dissociating gas - the form (2.26) or its equivalent

$$\frac{d\alpha}{dt}=\frac{C\rho^2T^{-s}}{\rho_D}\left[\frac{1-\alpha}{1-\alpha_e}\alpha_e^2-\alpha^2\right], \qquad (3.47)$$

where $\alpha_e(T, \rho)$ is the equilibrium value of the degree of dissociation (see Eq. (2.16)).

For a mixture of chemically reacting gases the relaxation equations can be written in terms of the variables α_i and c_i as

$$\frac{d\alpha_l}{dt}=\frac{J_lM_l}{\rho}, \quad \frac{dc_l}{dt}=\frac{J_l}{\rho}, \qquad (3.48)$$

where $J_l=J_l(\rho, T, \langle q_k\rangle)=\frac{d[X_l]}{(b_k-a_k)dt}$ is the rate of change of the i-th component, mole/cm^3 sec (see Eq. (1.36)).

The form of the functions J_i in terms of the variables T, $[X_k]$ and variables T, ρ, α_k for a single reaction is given in Chapter 1. For a system of m reactions with the participation of n components

$$\sum_{i=1}^{n}a_{ij}X_i \underset{k_{rj}}{\overset{k_{fj}}{\rightleftarrows}} \sum_{i=1}^{n}b_{ij}X_i; \quad j=1, 2, \ldots, m \qquad (3.49)$$

In terms of the variables c_i Eqs. (3.48) assume the following form (we sum the rates of change of the i-th component in all j reactions):

$$\frac{dc_l}{dt}=\frac{1}{\rho}\sum_{j=1}^{m}(b_{lj}-a_{lj})\left[k_{fj}\rho^{\tilde{a}_j}\prod_{l=1}^{n}c_l^{a_{lj}}-k_{rj}\rho^{\tilde{b}_j}\prod_{l=1}^{n}c_l^{b_{lj}}\right], \qquad (3.50)$$

where

$$\tilde{a}_j=\sum_{i=1}^{r_m}a_{ij},\quad \tilde{b}_j=\sum_{i=1}^{m}b_{ij}. \tag{3.51}$$

In the case of a mutual connection between the processes of the excitation of vibrations and chemical reactions the relaxation equations will have a more complicated form (see Chapter 1). /120

If we write the relaxation equations in terms of other variables (for example, in terms of $[X_i]$), then they will assume a different form

$$\frac{d[X_i]}{dt}-[X_i]\frac{d\rho}{dt}=I_i(T,[X_1],[X_2],\ldots,[X_n]).$$

Below we shall use the relaxation equation in the form (3.45), assuming that the corresponding variables are used as q_i. We shall also assume that the gas is a mixture of thermally ideal gases that obey Clapeyron's law. Eqs. (3.43) and (3.44) for the pressure and specific enthalpy can then be written as

$$p=\sum_i p_i=RT\sum_i[X_i]=\frac{\rho RT}{\sum_i M_i\xi_i}=\rho RT\sum_i\frac{a_i}{M_i}; \tag{3.52}$$

$$h=\sum_i a_ih_i=\sum_i\xi_iM_ih_i\Big/\sum_i\xi_iM_i; \tag{3.53}$$

$$h_i=c_{pi}T+e_{ai}+h_{io}. \tag{3.54}$$

Here c_p is the specific heat capacity of active degrees of freedom, and h_{io} is the specific enthalpy of formation.

The expressions for p and h with different ways of expressing the concentrations (in terms of $a_i, \xi_i, c_i, [X_i]$, etc.) are given in Section 2.1. A detailed summary of the formulas connecting a_i, ξ_i, etc. is also given therein.

Thus, the steady quasi-one-dimensional flows of a non-equilibrium gas are described by the system (3.40) – (3.45). The initial and boundary conditions will depend on the type of the problem. For a purely supersonic flow, there is of course a problem with initial conditions. For a gas flow in the Lavalle nozzle in the supersonic regime the conditions are given for the

precombustion chamber and for the critical section. The gas in the precombustion chamber is usually assumed to be in equilibrium. The condition in the critical section determines the maximum possible flow rate for which a supersonic flow can be realized.

The basic features of nonequilibrium flows are associated with the behavior of the parameters q_i along the nozzle. One can distinguish three basic types of nonequilibrium flows: flows close to equilibrium ($q_i \approx q_{ie}$) ; flows close to being frozen ($q_i \approx \text{const}$) and the intermediate types of flow. Of course, each specific case depending on the kinetic properties of the medium and the geometric characteristics of the nozzle (stream fillament) within the individual parts of a nozzle there may be realized the first, second, or all three types of flow.

Let us consider the particular features of nonequilibrium flows in a stream fillament using the simple example when the state of a gas is characterized by a single relaxation parameter q and Eq. (3.45) becomes // 121

$$\frac{dq}{dt} = F(p, T, q). \tag{3.55}$$

F in itself does not determine how the system will react to a deviation from equilibrium. Thus, for example, F = 0 in both a steady equilibrium gas and in the flow of a frozen gas. In the flow of an equilibrium gas with non-zero gradients of gas dynamic functions $F = dq_e/dt \neq 0$, even though the rate of the relaxation process is infinite. In view of this fact let us write Eq. (3.55) in the form in which the time of relaxation appears explicitly:

$$\frac{dq}{dt} = \frac{f(p, T, q)}{\tau(p, T, q)}, \tag{3.56}$$

where

$$\tau = -\left(\frac{\partial F}{\partial q}\right)^{-1}_{p,T} > 0 \tag{3.57}$$

$$f = -F \Big/ \left(\frac{\partial F}{\partial q}\right)_{p,T}. \tag{3.58}$$

τ, having the dimension of time, is essentially the time of relaxation: the characteristic time needed by a gas to reach equilibrium. For example, for a flow close to equilibrium the function F may be expanded in a Taylor's series

$$F=F(\rho, T, q_e(\rho, T))+\left(\frac{\partial F(\rho, T, q_e)}{\partial q}\right)_{\rho, T}(q-q_e)+\cdots$$

Considering that $F(\rho, T, q_e)=0$, Eq. (3.55) may be approximately written as

$$\frac{dq}{dt}=\frac{q_e-q}{\tau(\rho, T)}, \qquad (3.59)$$

where τ is determined by the ratio (3.57). In this form the physical meaning of τ as the characteristic time of the process for establishing equilibrium is obvious. (Here we shall not dwell on various individual special cases. Also we shall not discuss the fact that, when F is given not as a function of ρ and T, but as a function of another pair of thermodynamic parameters, for example ρ and p, then $\tau_1=-\left(\frac{\partial F}{\partial q}\right)^{-1}_{\rho, p}$ generally speaking may differ somewhat from τ given by (3.57). For more details, see [34]; below this is unimportant.) /122

Let us study the behavior of q(t) when a gas moves in a narrowing-widening stream filament (in a Lavalle nozzle), originating in the precombustion chamber where the gas is in equilibrium. Here, at least in the initial portion of the stream filament, the flow will be close to equilibrium (flow velocity is small), and Eq. (3.55) may be approximately written in the form (3.59) *. If q_e and τ are constant, then the solution of Eq. (3.59) will be in the form

$$q(t)=q_e+(q(0)-q_e)e^{-t/\tau}, \qquad (3.60)$$

* For certain processes, as for example for vibrational relaxation, this form is exact whether or not q and q_e are close to each other (see Chapter 1).

Hence it is clear that for $t/\tau \gg 1$, even if the initial state of the gas differs considerably from equilibrium, within a major portion of the interval of t, with the exception of the narrow region near t = 0 with the characteristic time scale $t_1 \sim \tau$ the flow will be close to equilibrium. In the other limiting case when $t/\tau \ll 1$ the flow will be close to a frozen one.

In real flows, both τ and q_e depend on T and p, and vary greatly along the nozzle. In addition, even though these types of flows may be realized in individual parts of the nozzle, also in those cases the general structure of the flow will be more complicated.

The variation of q(t) along a nozzle depends on the relative values of the three time scales τ, t_* and t_{char} that are associated with the thermo-kinetic properties of the gas and the gas-dynamic characteristics of the flow [$\tau(t)$ is the time of relaxation; t_{char} is the characteristic gas-dynamic time - time spent by a gas particle in a given part of the nozzle (for example, in the region of supersonic velocities or in the region, where $\tau \sim t_*$,etc.); $t_*(t)$ is the time scale characterizing the rate of change of q_e].

We take

$$t_* = \left| \frac{1}{q_e} \frac{dq_e}{dt} \right|^{-1}. \qquad (3.61)$$

With this definition, t_* is the time segment within which the equilibrium value of q_e changes by a value of its order of magnitude.

Sometimes the scale t_* is chosen on the basis of T(t) or h(t) [45,46], for example

$$t_{*T} = \left| \frac{1}{T} \frac{dT}{dt} \right|^{-1}.$$

It is not hard to estimate the order of magnitude of the change of t_{*T} along a nozzle, if one uses the ideal gas model with a constant heat capacity. /123

In this case

$$t_{*T} = \frac{r}{\sqrt{2H}} \left(\frac{\varkappa+1}{\varkappa-1}\right)^{3/2} \frac{\lambda^2-1}{\lambda^4} \left(\frac{d \ln F/F_*}{d(x/r)}\right)^{-1}, \qquad (3.62)$$

where r is the radius of the critical nozzle cross section, λ is the reduced velocity, equal to u/a*

Calculations show that the value of t_{*T} along a stream filament outside of the region $\lambda \ll 1$ does not change greatly. Thus, if the distribution of the cross-sectional area of the nozzle is

$$\bar{F} \equiv F/F_* = 1 + (x/l)^2; \quad l = r/\operatorname{tg}\vartheta \qquad (3.63)$$

(the nozzle is approximately conical with the vertex half-angle ϑ), then in the range from M = 1 to M = 3 the value of t_{*T} decreases approximately by a factor of 3.

When a gas moves in the nozzle, a sharp change occurs usually not only in the local values of $\tau(t)$ and $t_*(t)$, but in the ratios τ/t_*, τ/t_{char}, etc.. Usually this is caused by a very strong dependence of the time of relaxation τ on the temperature and pressure. Thus, for vibrations, dissociation, and a number of other processes, the value of τ, when a gas moves from the precombustion chamber to the area of moderate supersonic velocities changes by several orders, and the ratio τ/t_* changes from $\tau/t_* \ll 1$ to $\tau/t_* \gg 1$. Without giving a full classification of the types of nonequilibrium flows depending on the relative values of the scales τ, t_* and t_{char}, we shall only note the basic regimes.

If in the portion of the nozzle under consideration

$$\tau(t) \ll t_*(t) \qquad (3.64)$$

and if the initial state in that portion is close to equilibrium, then the flow will be close to equilibrium in the entire portion. If

$$t_{char} \ll \tau, \qquad (3.65)$$

then the flow will be close to a frozen one*. The region of a noticeable deviation from equilibrium is naturally characterized by the condition

$$\tau \sim t_*. \tag{3.66}$$

Usually in the initial portion of the subsonic section of the nozzle $\tau \ll t_*$ (or $\lambda \to 0$ $t_* \to \infty$) and the flow will be close to equilibrium. Later, as τ increases or t_* decreases, the values of τ and t_* become of the same order, which results in a noticeable deviation from equilibrium. The subsequent character of the variation of q is determined by the relative values of the scales τ and t_{char} in the region, where $\tau \sim t_*$ (the parameters in that region will be denoted by the subscript "p"). If $\tau_{interm} \sim (t_{char})_{interm}$ or $\tau_{interm} \gg (t_{char})_{interm}$, then the flow will freeze rapidly and q_f will be on the order of q_{interm} or even $q_f \approx q_{interm}$ (q_f is the frozen value of q). The freezing process develops in precisely /124 this fashion in many practically important cases (rapid freezing, localized in a narrow region between regions of near-equilibrium and near-frozen flows, see Section "Method of Instantaneous Freezing").

However, if $\tau_{interm} \ll (t_{char})_{interm}$, then before the flow freezes (if it freezes at all) the value of q will change considerably and cases are possible when $q_f \ll q_{interm}$.

Fig. 3.25 gives a schematic plot of q(t) which is typical of nonequilibrium flows in a nozzle. The same plot includes values of $\tilde{q}_e$ for an equilibrium flow ($\tau \equiv 0$) and q_e which are locally - equilibrium values of q corresponding to the local values of T and

* For certain combinations of the scales τ, t_* and t_{char} and the corresponding initial conditions, cases are possible when $q \approx q_e$ const, i.e., the flow is at the same time close to equilibrium and to a frozen flow.

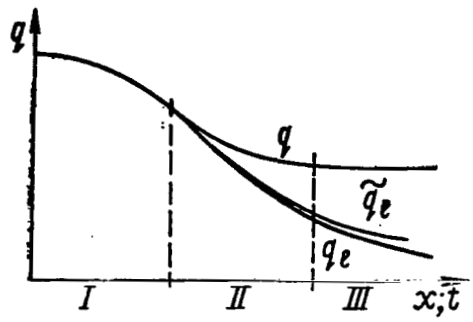

Figure 3.25. A scheme of the development of a relaxation process in a nozzle.

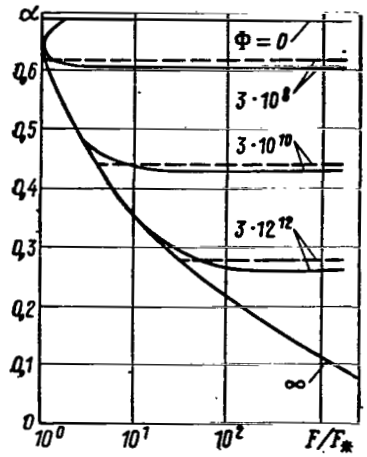

Figure 3.26. Degree of dissociation in a hypersonic nozzle (solid lines - exact solution; dashed line - approximate solution using the method of instantaneous freezing).

ρ in a nonequilibrium flow.

We set

$$\delta = q - q_e. \tag{3.67}$$

It is clear that, in order for the flow to be close to equilibrium, it is necessary that

$$\delta/q_e \ll 1$$

(More precisely, it is also necessary that

$$d\delta/dt \ll dq_e/dt).$$

Eqs. (3.59) and (3.67) imply

$$q = q_e - \tau\left(\frac{dq_e}{dt} + \frac{d\delta}{dt}\right).$$

Considering that in the region of a near-equilibrium flow the differences q—q_e and $q - \tilde{q}_e$ are of the same order, we obtain

$$\frac{q - \tilde{q}_e}{\tilde{q}_e} \sim \frac{q - q_e}{q_e} \approx \tau/t_*. \tag{3.68}$$

Thus, the condition (3.64) becomes necessary for the flow to be close to equilibrium.

For relaxation processes described by Eq. (3.59), it is easy to obtain a condition sufficient for the existence of a frozen

state. Eq. (3.59) for $q_e \ll q$ implies

/125

$$q(t) \approx q(t_1) \exp\left(-\int_{t_1}^{t} \frac{dt}{\tau(t)}\right). \qquad (3.69)$$

Consequently, for $t > t_1$ the flow will be close to a frozen one ($q \approx \text{const}$) if

$$\int_{t_1}^{t} \frac{dt}{\tau} \ll 1, \qquad (3.70)$$

which agrees with the condition (3.65).

The specific features of nonequilibrium flows in nozzles were studied in detail by Bray [47] using the example of an ideal dissociating Lighthill gas. Typical results of Bray's calculations are shown in Figs. 3.26-3.29. They were obtained for the following conditions in the precombustion chamber: $T_0/T_d = 0.1$ and $p_0/\rho_d e_d = 5 \cdot 10^{-6}$, which corresponds to $T_0 = 5900$ K and $p_0 = 115$ kG/m^2 for oxygen and $T_0 = 11300$ K and $p_0 = 215$ kG/cm^2 for nitrogen; in this case the initial degree of dissociation is 0.69.

The cross-sectional area of a nozzle was given by Eq. (3.63). All the results were obtained for s = 0 [s is the exponent in Eq. (3.47)]. For other values of s for which calculations were made ($-0.5 \leqslant s \leqslant 2.5$) the behavior of α, basically remains the same, and the following general law is confirmed: the stronger the dependence of the relaxation processes on T and ρ, the more rapid the freezing process and the more narrow the transition region between the equilibrium and frozen flows.

/126

Figs. 3.26-3.29 show the results for several values of a dimensionless parameter of the dissociation rate

$$\Phi = \frac{C T_0^{-s} \rho_d}{2\sqrt{\pi} \operatorname{tg}\vartheta} \sqrt{\frac{F_*}{R_{A_2} T_d}},$$

which includes both the physico-chemical properties of the gas and the geometrical characteristics of the nozzle. For usual hypersonic nozzles, the values of Φ range from $3 \cdot 10^8$ to $3 \cdot 10^{12}$. The plot $\alpha(F/F_*)$ shown in Fig. 3.26, is typical of flows of

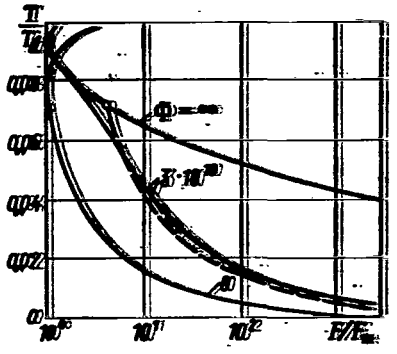

Figure 3.27 Reduced temperature in a hypersonic nozzle ((solid lines – exact solution; dashed line – approximate solution using the method of instantaneous freezing))

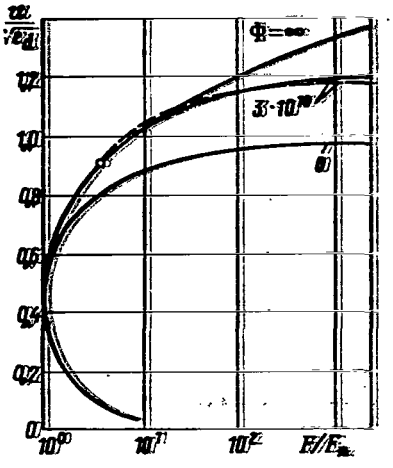

Figure 3.28. Reduced velocity ((solid lines – exact solution; dashed line – approximate solution using the method of instantaneous freezing)).

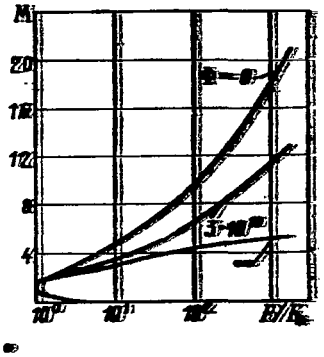

Figure 3.29. Variation of the M number in a hypersonic nozzle.

dissociating diatomic gases [48], as well as of flows with vibrational relaxation [49–51], [118] (in this case instead of α we use e_k)) and of flows of air with relatively low temperatures [52, 53]. The calculations made in [52] have shown that for air flows in axisymmetric nozzles with the diameter of the critical section of about 1 cm for $T_0 = 3000$—4000 and $p_0 = 1$—100 kG/cm^2, the freezing of the concentrations of various components occurs near the critical section and takes place fairly rapidly. For higher temperatures and pressures in the precombustion chamber, the variation of the concentrations becomes more complicated [54, 55].

Method of Instantaneous Freezing

In many cases, the variation of the ratio τ/t_* near the transition region by a factor of several dozen occurs within a small portion of the nozzle, which permits us to treat approximately the region of transition from an almost equilibrium flow to an almost frozen flow as a certain "surface of discontinuity" or a "freezing point" [46, 47]. Thus, one arrives at the following model of a nonequilibrium flow in a stream filament (nozzle): before a certain point, the freezing point, the flow is in equilibrium; at the freezing point all processes associated with the excitation (disactivation) of the internal degrees of freedom stop instantaneously, and the subsequent flow is frozen. //127

An approximate computational method based on this model came to be called the method of instantaneous freezing [46, 47]. If the process of transition from an equilibrium to a frozen state occurs sufficiently fast, the increase in entropy will be insignificant [56], and the method of instantaneous freezing should as a whole give fairly good results.

The most important point in the practical realization of the method is the choice of the freezing point which, of course, should lie in the intermediate flow region $\tau \sim t_*$. As a criterion to be used in the determination of the freezing point, one can use the following ratio, which can be deduced from Eqs. (3.66) and (3.69):

$$\left\| \frac{dq_e}{q_e dt} \right\| = \frac{1}{\tau(p_e, T_e)}. \qquad (3.71)$$

There are also other criteria for determining the freezing point, but a majority of them are essentially variants of the criterion (3.71). Bray [47] determines the position of the freezing point in the following way. The relaxation equation

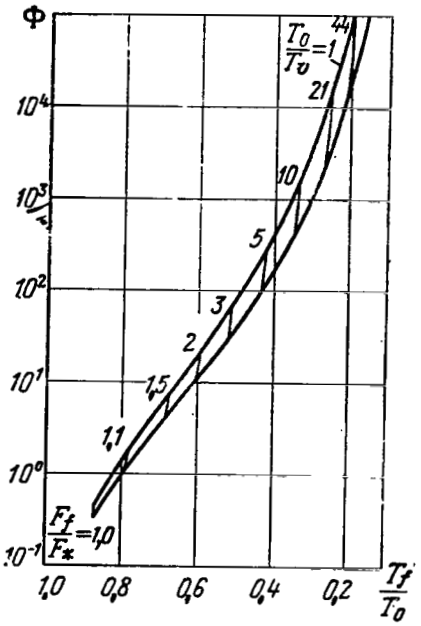

Figure 3.30. Criterion to be used in determining the freezing point of the vibrational degrees of freedom in a nozzle.

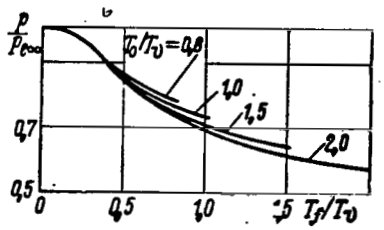

Figure 3.31. Effect of the freezing of the vibrational degrees of freedom on the asymptotic values of pressure in a nozzle for $\frac{T_0}{T_v}=1$ and 2.

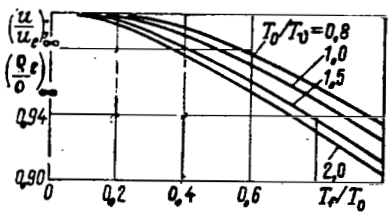

Figure 3.32. Effect of the freezing of vibrational degrees of freedom on the asymptotic values of the velocity and density in a nozzle.

for the degree of dissociation is written as

$$\frac{da}{dt}=r_D-r_R,$$

where r_D is the rate of dissociation, and r_R is the rate of recombination.

In the region of a near-equilibrium flow, the rates r_D and r_R are both large as compared with $\left|\frac{da}{dt}\right|$, i.e.,

$$-\frac{da}{dt}\ll r_D\sim r_R. \qquad (3.72)$$

/128

As the gas expands in the nozzle, r_D and r_R decreases due to the decrease in T and ρ. This is accompanied by a

progressive deviation of α from its equilibrium value α_e, where the decrease of r_D occurs particularly sharply due to the exponential dependence of r_D on T ($r_D \sim e^{-D_0/RT}$). In the region of an almost frozen flow, the rate of dissociation r_D becomes negligible as compared with r_R, and

$$-\frac{d\alpha}{dt} \approx r_R \gg r_D. \tag{3.72a}$$

Thus, as the state of the flow changes from an almost equilibrium flow to an almost frozen flow, r_D changes from a value much greater than $\left|\frac{d\alpha}{dt}\right|$ to a value much less than $\left|\frac{d\alpha}{dt}\right|$. Consequently, there should exist an intermediate region where $\left|\frac{d\alpha}{dt}\right|$ will be on the order of r_D. When the intermediate region is of small size, the values of α, ρ and T in it will not differ very much from the values of α_e, ρ_e and T_e in the equilibrium flow. Therefore, it is logical to define the freezing point as a point at which the following relation is satisfied

$$\left|\frac{d\alpha_e}{dt}\right| = \zeta r_D(\rho_e, T_e, \alpha_e),$$

where ζ is a constant on the order of unity which is usually taken as equal to unity. Thus, the freezing point is defined by Bray as a point at which

$$\left|\frac{d\alpha_e}{dt}\right| = r_D(\rho_e, T_e, \alpha_e). \tag{3.73}$$

The results of calculating the flow parameters using the method of instantaneous freezing and the criterion (3.73) are shown in Figs. 3.26-3.27 with dashed lines. Bray notes that a better agreement with the results of exact calculations may be obtained if $\zeta = 1.6$. However, the method itself gives no basis for an a priori selection of such a value of ζ. What is important is something else – namely, the fact that the results

only weakly depend on the choice of ζ .

Using the method of instantaneous freezing, one can calculate fairly simply the flow parameters for a gas with simple kinetics. For diatomic gases, for example, O_2, N_2, Cl_2 with a nonequilibrium excitation of the vibrational degrees of freedom Phinney [58] (see also [117, 118]) obtained approximate universal relations for the position of the freezing point and asymptotic ($M\to\infty$) values of the ratios of velocities $(u/u_e)_\infty$, densities $(\rho/\rho_e)_\infty$ pressures $(p/p_e)_\infty$, and temperatures $(T/T_e)_\infty$ in nonequilibrium / 129 and equilibrium flows (Figs. 3.30-3.32). Here u and u_e, p and p_e, etc., are taken for the same value of $\bar{F}$; the distribution of $\bar{F}$ is given by Eq. (3.63). For sufficiently large values of M, the ratios u/u_e, ρ/ρ_e ,etc. will be close to their limiting ($M=\infty$) values, and therefore the same plots may be used within a wider range of the M numbers.

Fig. 3.30 shows a plot* which can be used to determine the ratio of the temperature at the freezing point, T_f, to the temperature in the combustion chamber, T_0, as a function of T_0 and the dimensionless parameter Φ :

$$\Phi=\frac{r}{2\tau_0\,\mathrm{tg}\vartheta\sqrt{2RT_0/M}};\quad \tau_0=\tau(T_0,\ p_0). \tag{3.74}$$

Fig. 3.30 also shows the values of F_f/F_* at the freezing point. The possibility of using the method of instantaneous freezing in the calculation of multicomponent mixtures of gases with mutually interrelated reactions is not so evident, at least for the cases where not one, but several reactions are energetically and kinetically important. However, there have been attempts to extend the method of systems with a fairly complex kinetics [61-63].

---

* The plot is constructed on the basis of calculations by A. V. Chirikhin using the procedure of [58], see also [117].

Remarks on nonequilibrium flows with vibrational relaxation.

1. Similitude of flows in nozzles. If in Eqs. (3.40) - (3.44) and (3.46) describing the flow with a nonequilibrium excitation of vibrational degrees of freedom, we change to dimensionless variables / 130

$$\bar{x}=\frac{x}{l},\ \bar{F}=\frac{F}{F_*},\ \bar{p}=\frac{p}{p_0},\ \bar{\rho}=\frac{\rho}{\rho_0},\ \bar{T}=\frac{T}{T_0},$$

$$\bar{u}=\frac{u}{\sqrt{R_1T_0}},\ \bar{e}_k=\frac{e_k}{R_1T_0}\left(R_1=\frac{R}{M}\right)$$

and consider that

$$e_{ke}=R_1T/(\exp\theta/T-1),\ \tau p=B\exp AT^{-1/3}\ \text{ and }\ F=F(x)$$

($A, B, \theta, F(x)$ are given), then the system of equations becomes

$$\left.\begin{aligned}
&\bar{F}=f(\bar{x}),\ \frac{1}{\bar{\rho}}\frac{d\bar{\rho}}{d\bar{x}}+\frac{1}{\bar{u}}\frac{d\bar{u}}{d\bar{x}}+\frac{1}{\bar{F}}\frac{d\bar{F}}{d\bar{x}}=0,\\
&\bar{u}\frac{d\bar{u}}{d\bar{x}}+\frac{1}{\bar{\rho}}\frac{d\bar{p}}{d\bar{x}}=0;\\
&\frac{\bar{u}^2}{2}+\frac{\varkappa}{\varkappa-1}\bar{T}+\bar{e}_k=\text{const}=\frac{\varkappa}{\varkappa-1}+\bar{e}_{ke0},\ \bar{p}=\bar{\rho}\bar{T};\\
&\frac{d\bar{e}_k}{d\bar{x}}=\frac{(\bar{e}_{ke}-\bar{e}_k)\,\bar{p}}{\bar{u}\,\lambda\exp\left[N\left(\bar{T}^{-1/3}-1\right)\right]},
\end{aligned}\right\}\qquad(3.75)$$

where

$$\lambda=\frac{B\exp\left(AT_0^{-1/3}\right)\sqrt{R_1T_0}}{p_0l};\ N=AT_0^{-1/3}.$$

The conditions in the pre-combustion chamber will be

$$\bar{u}=0;\ \bar{\rho}=\bar{p}=\bar{T}=1;\ \bar{e}_{k0}=\bar{e}_{ke0}=\bar{\theta}/(\exp\bar{\theta}-1),\qquad\text{where}\qquad\bar{\theta}=\theta/T_0.$$

Hence it is clear that different flows will be similar for identical parameters $\lambda, N, \varkappa, \bar{\theta}$ and functions $\bar{F}(\bar{x})$. If one considers flows of the same gas at the same freezing temperature T_0, then the parameters $\varkappa$, N and $\bar{\theta}$ automatically coincide. /131

If in addition we limit our discussion to a family of nozzle contours (3.63) and as the characteristic dimension we take $l=r/\text{tg}\theta$, then the expression for $\bar{F}$ becomes $F=1+\bar{x}^2$, i.e. it will not involve any additional parameters. In this case,

the only similitude parameter will be λ (the ratio of the time of relaxation in the precombustion chamber to the characteristic time $l/\sqrt{R_1 T_0}$). Considering that T_0 and the gas composition are fixed, we conclude that the flows of the same gas in a nozzle (3.63) at the same temperature in the precombustion chamber T_0 will be identical if the combination $p_0 r/\mathrm{tg}\theta$, is identical, i.e. $p_0 r/\mathrm{tg}\theta$ is the similitude parameter (an example of the law of binary similitude).

2. Time of relaxation When calculating τ one must keep in mind that, when a gas expands in a nozzle, i.e., under the conditions when the energy is transmitted from the vibrational to the translational degrees of freedom, the time of relaxation may differ from its value behind shock waves when the energy is transmitted from the translational to vibrational degrees of freedom. This fact was established by Hurle, Russo, and Hall (see [59]), who found that the relaxation time of vibrations in an expanding nitrogen flow is approximately 70 times less than the time of relaxation in a shock wave (in the early papers the ratio of these times was found to be 1/15 [60]). To determine τ_{N_2} in a nozzle the study [59] proposes the formula

$$p\tau_{N_2}\ (\text{in the nozzle}) = 3\cdot 10^{-12}\exp(1817T^{-1/3})\ \frac{\text{kG}}{\text{cm}^2}\cdot\text{sec} \qquad (3.76)$$

One of the basic reasons underlying the difference between τ in the nozzle and τ in the shock wave is, according to many workers, the influence of the anharmonic vibrations (see, for example, [119], [120]). In this case Eq. (3.46) becomes generally inapplicable and should be replaced with a more complicated system of kinetic equations. A number of researchers also note the very strong effect of impurities [121]. At this point, these questions still cannot be considered to be solved.

3. Investigation of vibrational relaxation acquires great practical importance in connection with the development and creation of a gas-dynamic laser, one of those most important elements is a non-equilibrium flow of a special gas mixture, for example, a mixture of CO_2 and N_2 with an inverted population of the vibrational levels (see, for example, [121]).

Results of exact calculations and experimental data

In the case of flows of complex gas mixtures with mutually related reactions, reliable numerical results can only be obtained by making exact calculations. A majority of such flows /132
will not follow the simple picture that was described above. In particular, the transitional region may not be so narrow that one could speak of instantaneous freezing. In addition, there may not exist any clearly expressed regions with q_i = const. The interaction of relaxation processes (for example, vibrations and dissociation) complicates the character of flow even more.

Thus far, a large number of theoretical [52-55, 61-70] and experimental studies [41, 42, 69, 71-79] have been performed whose results give a more detailed picture of the development of nonequilibrium processes in the flows of air and other gas mixtures with a fairly complicated kinetics, and which also help in selecting a more accurate kinetic model of a gas and in explaining the effect of various factors. With a small exception, the theoretical and experimental results are in good mutual agreement.

Figures 3.33 - 3.36 give data for nitrogen and air. The experiments were made in a hypersonic nozzle, nearly conical with a 30° vertex angle and the diameter of the critical section equal to 25.4 and 12.7 mm; the M number at the exit from the nozzle was 10.

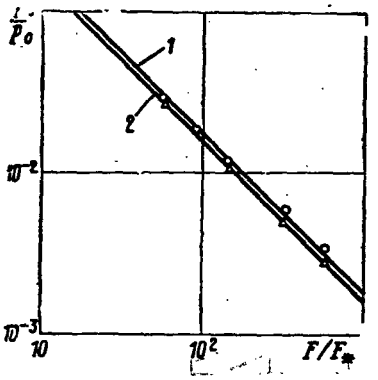

Figure 3.33. Ratio of total pressure behind a normal shock wave to total pressure in the precombustion chamber as a function of the geometric ratio of areas (for nitrogen):
1 - theoretical values for an equilibrium flow for p_0= 7 kG/cm^2 and T_0= 6000 K; theoretical values for an ideal gas for κ=1.4; experimental data are indicated with: triangles - for p_0=7 kG/cm^2 and T_0= 6000 K; circles - for p_0= 35 kG/cm^2 and T_0=4800 K.

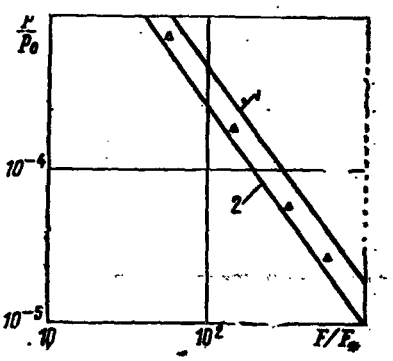

Figure 3.34. Ratio of static pressure to the pressure in the precombustion chamber for nitrogen for p_0=7 kG/cm^2,
1 - theoretical values for an equilibrium flow;
2 - theoretical values for an ideal gas for κ = 1.4; triangles indicate experimental data.

Figure 3.33 [71] shows a plot of the ratio of the total pressure behind a normal shock wave p_0', to the total pressure in the precombustion chamber (these data were used to determine the correction for the effect of the displacement thickness of the boundary layer and to calculate the effective ratio of the areas $(F/F_*)_{eff}$). Measurements of the pressure p_0' show that / 133
it is practically independent of the character of the flow: whether it is in equilibrium or frozen. In contrast with p_0' the static pressure depends substantially on nonequilibrium processes (see Figures 3.34 [71], 3.35 and 3.36 [72]).

Let us consider in more detail the development of nonequilibrium processes in an air flow at fairly high braking temperatures ($T_0 \sim$ 6000—8000 K) . If the concentration of nitrogen

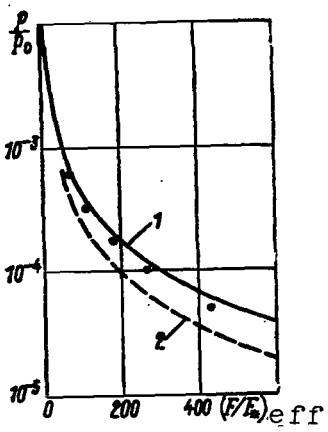

Figure 3.35. Ratio of static pressure to pressure in the precombustion chamber as a function of the effective ratio of nozzle areas for the air for p_0= 31 kG/cm^2, T_0= 4000 K, l= 2.7 cm (see Eq. (3.63)):
1 - theoretical values for equilibrium flow; 2 - theoretical values for an ideal gas for κ= 1.4; dots refer to experimental data.

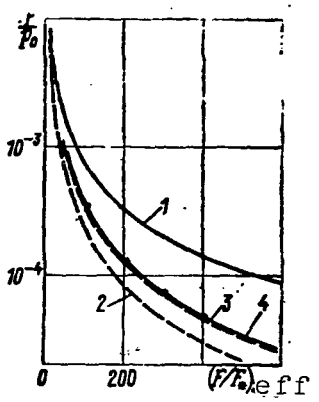

Figure 3.36. Ratio of static pressure in the flow to the pressure in the precombustion chamber as a function of the effective ratio of nozzle areas for the air for p_0= 17.5 kG/cm^2, T_0= 7000 K, l= 2.75 cm.
1 - theoretical values for equilibrium flows;
2 - theoretical values for a flow frozen with the values of the parameters equal to those in the precombustion chamber; 3 - theoretical values for l - 3 cm; 4 - theoretical values for l - 2 cm; dots refer to experimental data.

atoms depended only on the single dissociation-recombination reaction $N_2+M\rightleftarrows N+N+M$, then one might expect that the method of instantaneous freezing will give good results, since the recombination of N_2 would occur only in triple collisions whose number would fall off very rapidly with a decrease in density, / 134
and the rate of dissociation would become negligible because of the factors $e^{-D/RT}$. However, in reality due to bimolecular exchange reactions with the participation of nitrogen monoxide ($N+O_2\rightleftarrows NO+O$ and $O+N_2\rightleftarrows NO+N$) the rate at which nitrogen atoms "disappear" remains fairly high (these reactions have relatively low energies of activation) and nitrogen atoms hardly

become frozen (more precisely, the freezing does occur, but at such low temperatures that the frozen concentration of nitrogen will constitute a small fraction of the concentration of nitrogen in the precombustion chamber (see Fig. 3.37 [54]).

For oxygen, the picture will be different. In this case the rates of exchange reactions, which involve oxygen atoms, are low due to the high energy of activation, and these reactions cannot stop the process of oxygen freezing. The results given in Table 11 [54] give an idea of the effect of nonequilibrium processes in the air on the parameters of the flow in a hypersonic nozzle. (The shape of the nozzle is determined by Eq. (3.63) for l = 1 cm; it is assumed that the vibrational and electron degrees of freedom are in equilibrium with the translational and rotational degrees; ionization is not considered).

TABLE 11

RATIO OF GAS DYNAMIC PARAMETERS IN A NONEQUILIBRIUM FLOW OF AIR TO THE CORRESPONDING VALUES IN AN EQUILIBRIUM FLOW AT THE SECTION, WHERE $M_e = u_e/a_e = 20$ (l = 1 cm)*

T_0 K	6000		8000	
p_0 kG/cm^2	100	1000	100	1000
e_f/H	0,155	0,048	0,194	0,0813
$p\ p_e$	0,425	0,875	0,159	0,544
$T\ T_e$	0,359	0,855	0,121	0,497
ϱ/ϱ_e	1,095	1,014	1,110	1,045
u/u_e	0,913	0,987	0,901	0,957
M/M_e	1,455	1,06	2,301	1,305

*Commas represent decimal points

Detailed results of the calculations of the air flow in a hypersonic nozzle for different T_0 and p_0 are given in [55]. The shape of the nozzle was taken to be the same as in [54]. The kinetics of the reactions differed somewhat from the one used there. Figure 3.37, b and c [55] illustrate the development of

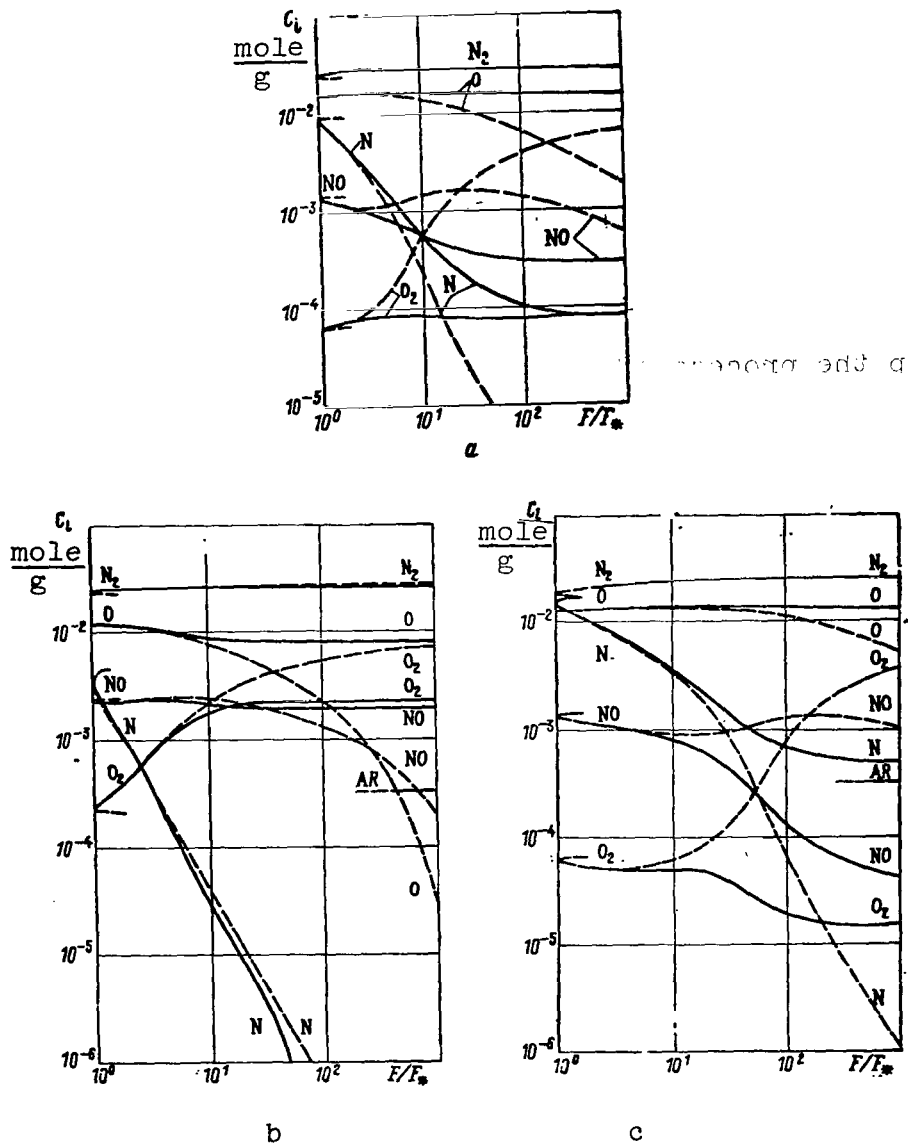

Figure 3.37. Distribution of the concentrations of components during expansion of air in a hypersonic nozzle l = 1 cm (solid lines - nonequilibrium flow; dashed lines - equilibrium flow): a - for T_0=8000 K, p_0= 100 kG/cm^2; b - for 8000 K, p_0=362 kG/cm^2, ρ_0/ρ_H = 10 (ρ_H is the density of the air under normal conditions); c - for T_0 = 10,000 K, p_0 = 528 kG/cm^2, ρ_0/ρ_H=10.

non-equilibrium processes in the flow of air through a nozzle, depending on the variation of conditions in the precombustion chamber.

The flow of ionized gas is one of the important cases when the method of instantaneous freezing may lead to considerable errors. Studies [80] and [81] show that in this case there is no clearly expressed region of frozen flow that would be characterized by constant electron concentration (Figure 3.38, [80]).

The electron concentration in the area right after the transition region decreases smoothly, and is sufficiently well described by the asymptotic solution in which one neglects the equilibrium concentration of electrons as compared with the non-equilibrium concentration. /136

Analytic solutions

In gas dynamics of nonequilibrium flows, the analytic solutions are very rare. They permit us to distinguish the basic determining parameters and on their basis to make a stricter classification of various types of flows.

Blythe [82, 83] considered the vibrations, dissociation, and ionization under conditions where the energy of these degrees of freedom is much less than enthalpy. This permitted him to separate to a first approximation the equations of gas dynamics and kinetics, and to construct a solution whose analysis has shown, in particular, that in this case the method of instantaneous freezing is not mathematically correct.

Cheng and Lee [84,85] made a detailed study of a flow with nonequilibrium dissociation under the condition that everywhere in the region, where the flow is close to equilibrium, the energy

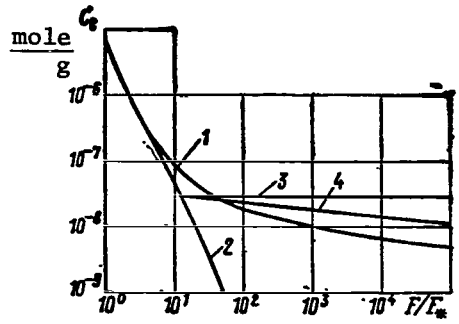

Figure 3.38. Electron concentration in air flow through a hypersonic nozzle at T_0 = 8000 K, p_0 = 1000 kG/cm^2:
1 = exact solution; 2 - solution for equilibrium flows; 3 - approximate solution by the method of instantaneous freezing; 4 - approximate solution by the method of instantaneous freezing in combination with an asymptotic solution in which one neglects the equilibrium electron concentration as compared with a nonequilibrium concentration.

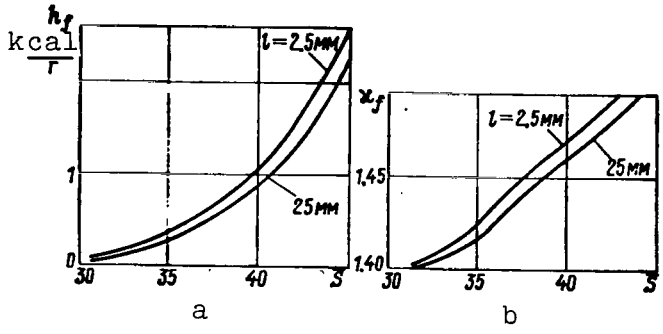

Figure 3.39. Dependence of frozen enthalpy (a) and frozen adiabatic exponent (b) for the air on reduced entropy.

parameter is of the order of unity ($\alpha D_0 \sim RT$) . In this case the kinetic processes exert a strong influence on the distribution of the gas dynamic parameters. It is shown that in this case the entire flow may be divided into the following four regions: 1) region of equilibrium, 2) region of beginning transition, 3) region of sharp transition, and 4) region of recombination.

It was established that the model of instantaneous freezing gives sufficiently accurate values for the speed, specific momentum, and frozen degree of dissociation α_∞. However, for the temperature the solution in the region of recombination will not be close to the exact solution (one has in mind the order of the relative error of the constructed solution), even though the discrepancy from the exact solution is numerically small.

The study [84] also gives the conditions for freezing, i.e., when $\alpha_{x\to\infty}=\alpha_{\infty}\neq 0$. It is established that in nozzles whose cross-sectional area varies as $F\sim x^k$, the freezing will occur / 137 for $k > 1/2$.

An analysis of the freezing of the electron concentration n_e for flows in an expanding stream filament for gases with different kinetics was made by A.V. Vasil'yeva and Yu. S. Sayasov [86]. On the basis of the asymptotic solutions obtained, they studied, in particular, the dependence of $n_{e\infty}$ on the concentration of a slightly ionized admixture x_A and showed that there is a certain critical value of x_A, starting at which the frozen concentration $n_{e\infty}$, is practically constant.

Similitude of flows in nozzles

If we bring Equations (3.40) - (3.45) to a dimensionless form and separate all determining dimensionless parameters, then for complex gas mixtures there will be so many of these parameters that their direct use will be of little practical value. Therefore, this method of separating dimensionless combinations (similitude parameters) which is traditional in classical gas dynamics, has not become very widespread as applied to non-equilibrium flows [91].

Much more productive is the approach associated with the search for the conditions of an approximate partial similitude and the construction of approximate correlation relations. The so-called "entropy correlation", proposed by Bray [87], has become most popular.

Using the example of an ideal dissociating gas, Bray has shown that within the framework of the method of instantaneous

freezing, the enthalpy h_f and the temperature T_f at the freezing point should depend only on the entropy S_0 and enthalpy H in the precombustion chamber and nozzle geometry. Furthermore, Bray has shown that the dependence of h_f and T_f on H will be very weak, and approximately we may assume that the enthalpy and temperature at the freezing point for a fixed nozzle are determined only by the value of the entropy in the precombustion chamber, i.e., that

$$h_f = h_f(S_0); \quad T_f = T_f(S_0). \tag{3.77}$$

Later it was shown [55] that this relation is also approximately satisfied for more complicated gas mixtures, for example by the air, not only for h_f and T_f, but also for frozen concentrations of individual components [88]. Auxiliary materials for calculating the nonequilibrium flows of the air on the basis of the entropy correlation are contained in [89] and [90].

Figures 3.39, a and b, give the values of h_f and κ_f for the air, constructed on the basis of results of [55, 88, 89]. Here $\bar{S} = S/R_\infty$, S is the specific entropy, R_∞ is the gas constant for non-dissociated air, $R_\infty = R/M_\infty$, where $M_\infty = 28.97$. The cross-sectional area of the nozzle was determined by (3.63). The values of $\bar{S}$ in Figures 3.39, a and b were determined on the basis of the tables by A.S. Predvotitelev, et al., [8] and [9]. These values of entropy differ from the values used when constructing the correlation relations in [55] and others.* /138

The relationship between the values of entropy in [8, 9] and [55, 88, 89] for the temperature and pressure ranges $T < 12000$ K

* Foreign authors normally use the tables by Hilsenrat, et al., and Gilmore.

and $10<p<1000$ kG/cm^2 can be approximately represented by

$$\bar{S}_{[8,\,9]} = 1.7 + \bar{S}_{[55,\,88,\,89]}. \qquad (3.78)$$

Figure 3.40 gives the values of $\bar{S}$ versus T and p, constructed on the basis of [8] and [9].

Basic determining parameters and approximate relations

For approximate estimates, it is advisable to use certain parameters (characteristic variables) which reflect the total effect of various physico-chemical processes and under certain conditions play the role of similitude parameters.

Along with the energy parameter W and the compressibility factor Z, which were introduced in Chapter 2, we define a parameter κ_* which relates pressure and density along a streamline in an adiabatic flow: /139

$$\varkappa_* \equiv \left(\frac{\partial \ln p}{\partial \ln \rho}\right)_\psi = \varkappa_f \left[1 + \frac{\sum_i \frac{\partial h}{\partial q_i}\left(\frac{\partial q_i}{\partial \rho}\right)_\psi}{\frac{\partial h}{\partial \rho}}\right]. \qquad (3.79)$$

Here κ_f is the adiabatic exponent calculated under the assumption of the local freezing of the physico-chemical processes ("frozen" adiabatic exponent); enthalpy h is assumed given as $h=h(p, \rho, q_1, q_2, \ldots, q_n)$. The partial derivatives are taken at constant remaining arguments; the subscript ψ means that the derivative is calculated along a streamline.

By virtue of the specific features of nonequilibrium flows in nozzles, i.e., the rapid freezing of the internal degrees of

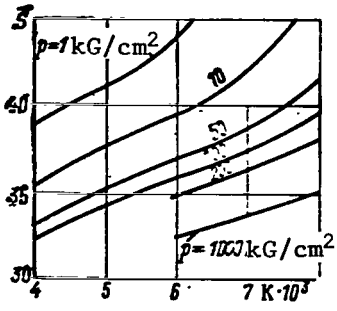

Figure 3.40. Reduced entropy versus temperature and pressure.

freedom, in practical calculations one does not deal with the complex expression (3.79), but with its asymptotic forms: with the isentropic exponent ("effective ratio of specific heat capacities") $\varkappa_e = \frac{\rho a^2}{p} = \left(\frac{\partial \ln p}{\partial \ln \rho}\right)_s$ (see [92]) in the region of an almost equilibrium flow and at constant value of the frozen adiabatic exponent in the region of a frozen flow.

The quantity κ_e can be determined using thermodynamic tables at each point of the flow field; one can also determine the constant averaged values of κ_e for a certain section of the nozzle. As the gas expands and T decreases, T κ_e will approach κ_∞ which is the value of the isentropic exponent of the gas under normal conditions (for diatomic gases, $\kappa_\infty = 1.4$). At temperatures $T \sim 6000—8000$ K , $\varkappa_e \approx 1{,}15—1{,}2$, and its average value within the nozzle section from the precombustion chamber to the section, where M = 10, may amount to 1.2-1.3.

The frozen adiabatic exponent is easily determined if we know the concentrations of the gas mixture components

$$\varkappa_f = \sum_i C_{pi}\xi_i \Big/ \sum_i C_{vi}\xi_i, \qquad (3.80)$$

where C_p and C_v are the molar heat capacities, and ξ_i are molar fractions.

For gas mixtures, consisting only of monoatomic and diatomic components

$$\varkappa_f = \frac{7 - 2\Sigma\xi_{A_l}}{5 - 2\Sigma\xi_{A_l}}, \qquad (3.80a)$$

where $\Sigma\xi_{A_l}$ is the sum of the molar fractions of all monoatomic components. /140

For example, for the air in the absence of ionization, $\Sigma\xi_{A_l} = \xi_N+\xi_O+\xi_{Ar}$. Let us estimate the temperature, pressure, and other gas dynamic parameters in a nonequilibrium (frozen) hypersonic flow (see [123]). We assume that we know the distribution of these parameters in the corresponding equilibrium flow, i.e., in the same nozzle and for the same deceleration parameters, as well as the frozen energy e_f and frozen adiabatic exponent κ_f (for the air, they can be approximately determined from Figures 3.39 and 3.40). A comparison of the parameters for the equilibrium and nonequilibrium flows will be made for the same section of the nozzle F (and not for the same M number).

For $M \gg 1$ we have

$$u \approx u_{\max} = \sqrt{2(H-h_f)} = u_{e\max}\sqrt{1-W_f} \approx u_0\left(1-\frac{W_f}{2}\right), \qquad (3.81)$$

where

$$u_{e\max} = \sqrt{2H},\ W_f = e_f/H. \qquad (3.82)$$

Furthermore, since the gas flow rate through a nozzle only weakly depends on nonequilibrium processes, from the condition that the flow rates in the equilibrium and nonequilibrium flows be equal, we get

$$\frac{\rho}{\rho_e} \approx \frac{u}{u_e} \approx \frac{1}{\sqrt{(1-W_f)}} \approx 1+\frac{W_f}{2}. \qquad (3.83)$$

(If the freezing occurs in the supersonic part of the nozzle, then the equality $\rho u = \rho_e u_e$ is satisfied exactly).

To determine T and p, we use the concept of instantaneous freezing, which is the same as assuming that the entropy is constant. Let "1" denote the flow parameters at the freezing point. Then in the region downstream of the section F_1

$$\frac{p(F)}{p_1}=\left(\frac{\rho(F)}{\rho_1}\right)^{\varkappa_f}. \tag{3.84}$$

Now if we let

$$\tilde{\varkappa}_e=\frac{\lg p_e(F)-\lg p_e(F_1)}{\lg \rho_e(F)-\lg \rho_e(F_1)},$$

where

$$p_e(F_1)=p_1,\ \rho_e(F_1)=\rho_1,$$

and we can write

$$\frac{p_e}{p_1}=\left(\frac{\rho_e}{\rho_1}\right)^{\tilde{\varkappa}_e}, \tag{3.84a}$$

where the subsdcript "e" refers to the parameters in the equilibrium flow.

From Equations (3.84) and (3.84a) we obtain

$$\frac{p(F)}{p_e(F)}=\left(\frac{\rho(F)}{\rho_e(F)}\right)^{\varkappa_f}\left(\frac{\rho_e(F)}{\rho_1}\right)^{\Delta\varkappa}\approx\left(1+\frac{\varkappa_f}{2}W_f\right)\left(\frac{\rho_e}{\rho_1}\right)^{\Delta\varkappa}, \tag{3.85}$$

/141

where

$$\Delta\varkappa=\varkappa_f-\tilde{\varkappa}_e. \tag{3.86}$$

If we assume that the section in which one compares the parameters of a nonequilibrium (frozen) and equilibrium flow is in the hypersonic part of the nozzle, where $M_e = M_\infty$ (M_∞— is the molecular weight of a given gas under normal conditions,) then from Clapeyron's equation, in view of Eq. (3.85), we get

$$\frac{T}{T_e}=\frac{M_1}{M_\infty}\frac{p}{p_e}\frac{\rho_e}{\rho}\approx Z_1^{-1}\left(1+\frac{\varkappa_f-1}{2}W_f\right)\left(\frac{\rho_e}{\rho_1}\right)^{\Delta\varkappa}. \tag{3.87}$$

where $Z_1 = M_\infty/M_1$ is the compressibility factor.

The ratio M/M_e can be determined from the relation

$$\frac{M}{M_e}=\frac{u}{u_e}\frac{a_e}{a}=\sqrt{\frac{u}{u_e}\frac{p_e}{p}\frac{\varkappa_\infty}{\varkappa_f}}\approx$$
$$\approx\sqrt{\frac{\varkappa_\infty}{\varkappa_f}}\left[1-\frac{W(\varkappa_f+1)}{4}\right]\left[\frac{\rho_1}{\rho_e}\right]^{\frac{\Delta\varkappa}{2}}, \qquad (3.88)$$

where κ_∞ is the value of κ_e for a given gas mixture under normal conditions (for diatomic gases $\kappa_\infty = 1.4$).

For example, for the air at $T_0 = 8000$ K, $p_0 = 100$ kg/cm^2, $M_e = 20$, $l=1$ cm [the shape of the nozzle is given by Equation (3.63)] and $M_1 = 3$ we have

$$W_f\approx 0{,}2;\ \varkappa_f\approx 1{,}46;\ \Delta\varkappa\approx 0{,}2;\ \varkappa_\infty=1{,}4;\ \rho/\rho_1\approx 10^{-5},$$

whence $p/p_e\approx 0{,}12;\ T/T_e\approx 0{,}09$ and $M/M_e\approx 2{,}7$.

On the basis of these relations, one can extrapolate the experimental and theoretical data. Thus, for example, if $p/pe)_2$ and $T/Te)_2$ are given for a certain section "2" in the hypersonic part of the nozzle, where the temperature T_e is relatively low and $\varkappa_e\approx\varkappa_\infty$, then for $F > F_2$ we have

$$\left.\begin{aligned}
&\frac{p(F)}{p_e(F)}=\left(\frac{p}{p_e}\right)_2\left(\frac{\rho(F)}{\rho_2}\right)^{\varkappa_f-\varkappa_\infty}\approx\left(\frac{p}{p_e}\right)_2\left(\frac{F_2}{F}\right)^{\varkappa_f-\varkappa_\infty};\\
&\frac{T}{T_e}=\left(\frac{T}{T_e}\right)_2\left(\frac{F_2}{F}\right)^{\varkappa_f-\varkappa_\infty};\\
&\frac{M}{M_e}=\left(\frac{M}{M_e}\right)_2\left(\frac{F}{F_2}\right)^{\frac{\varkappa_f-\varkappa_\infty}{2}}.
\end{aligned}\right\} \qquad (3.89)$$

These formulas indicate, in particular, that there is a qualitative difference between the asymptotic (for $F\to\infty$) behavior of p/pe, T/T_e and M/Me in the freezing of the vibrational degrees of freedom and the freezing of the recombination processes. /142

These estimates imply that in a hypersonic nozzle the nonequilibrium processes may have a substantial influence on the pressure, temperature, and the M number, and a fairly insignificant effect on the velocity and density. The velocity head and pressure of deceleration behind a normal shock wave also differ very little in the equilibrium and frozen flows:

$$\frac{p_0'}{p_{0e}'} \approx \frac{\rho u^2}{\rho_e u_e^2} \approx 1 - \frac{W_f}{2}. \qquad (3.90)$$

More accurate estimates are given in [1232 and [124].

Peculiarities of nonequilibrium flows near the critical section of the nozzle

The equilibrium flows and flows of ideal gases, due to their isentropicity, have a remarkable property: the transition from the subsonic to supersonic velocities occurs in the most narrow section of a stream filament. In fact, from Equations (3.40) and (3.41) it follows that

$$\frac{du}{u} = \frac{dF}{F} \Big/ \left(\frac{u^2}{dp/d\rho} - 1 \right),$$

where in the nozzle $du/dx \neq 0$, and by virtue of the isentropicity of the flow $(dp/d\rho)_s = a^2$. Therefore, dF/F = 0 for M = 1. This fact greatly simplifies the calculation of such flows in supersonic nozzles, since the flow rate is known beforehand, and all dimensionless gas-dynamic functions (p/p_0, T/T_0, ρ/ρ_0, M number, and others) depend on the ratio of the areas F/F_*, conditions in the precombustion chamber, and chemical nature of the gas, and are independent of the shape and size of the nozzle. In particular, for an ideal gas p/p_0, T/T_0, etc., depend only on F/F_* and κ.

Nonequilibrium flows do not possess this property. For them, the state of flow in the nozzle is determined not only by the thermodynamic properties of the gas and the ratio of the areas F/F_*, but also by the entire prehistory of the motion, associated with the behavior of $F(x)$, and the critical section does not coincide with the most narrow section of the nozzle. (Here the critical section is defined as the section where the M number, calculated using the frozen speed of sound, is equal to unity).

For simplicity and ease of visualization, let us first consider the characteristic features of nonequilibrium flows near the critical section of a nozzle using the example of a gas with nonequilibrium excitation of the vibrational degrees of freedom. In this case, the full system of equations, describing a one-dimensional flow, can be written as

$$\rho u F = \text{const}; \quad u du = -dp/\rho; \quad u^2/2 + c_p T + e_k = \text{const};$$
$$p = \rho R_1 T; \quad \left(R_1 = \frac{R}{M}\right); \quad \frac{de_k}{dx} = \frac{e_{ke} - e}{u\tau}. \qquad (3.91)$$

Certain qualitative features of nonequilibrium flows can be seen directly from the form of the equations. The difference from the section of an ideal gas is manifested only in the energy equation which has the form of the energy equation for an ideal gas with an addition of heat [93]: / 143

$$u du + c_p T = dQ. \qquad (3.92)$$

In such a treatment, the relaxation equation can be viewed as an equation giving the law of heat addition:

$$dQ = -de_k.$$

Eliminating p and ρ from (3.91), we obtain the ratio which is valid along the stream filament

$$-\frac{\varkappa M^2-1}{\varkappa M^2 R_1 T}de_k+\frac{1-M^2}{(\varkappa-1)M^2}\frac{dT}{T}=\frac{dF}{F} \qquad (3.93)$$

and

$$(M^2-1)\frac{du}{u}=\frac{dF}{F}+\frac{(\varkappa-1)de_k}{\varkappa R_1 T}, \qquad (3.93a)$$

where M has been calculated using the frozen speed of sound, $\varkappa=\varkappa_f=c_p/c_v$. It is clear that the equalities M = 1 and dF = 0 will be satisfied simultaneously only when $de_k=0$.

Considering that along a nozzle $de_k<0$, we may conclude that the critical section will be found in the expanding part of the nozzle, since for M - 1 we have $\frac{dF}{F}=-\frac{(\varkappa-1)de_k}{\varkappa R_1 T}>0$.

For flows close to equilibrium, Equations (3.92) and (3.93) may be conveniently put in a slightly different form

$$udu+c_{pe}dT=dQ_e;$$

$$\frac{\varkappa_e M_e^2-1}{\varkappa_e M_e^2 R_1 T}dQ_e+\frac{1-M_e^2}{(\varkappa_e-1)M_e^2}\frac{dT}{T}=\frac{dT}{F},$$

where

$$dQ_e=de_{ke}-de_k;\quad M_e=u/a_e;\quad \varkappa_e=\frac{c_{pe}}{c_{ve}}=\frac{c_p+c_{vk}}{c_u+c_{vk}}.$$

If the flow is in equilibrium, then $e_k=e_{ke}$ and dQ = 0, and M = 1 in the most narrow section of the nozzle. (In a nonequilibrium flow, the location of the section where M_e = 1 is determined by more subtle properties of the flow; for $dQ_e<0$ the section where M_e = 1 will be in the narrowing part of the nozzle.)

An equation similar to (3.93a) will not be hard to obtain even in a more general case. Assuming that the enthalpy h is given as a function of p, ρ and parameters q_i, we can write dh as $dh = h_p dp + h_\rho d\rho + \Sigma h_{q_i} dq_i$. Eliminating dp, dρ, and dh from this

equation and from the first two equations of System (3.91), and considering that $a_f^2 = -\frac{h_\rho}{h_p - 1/\rho}$ and $M = u/a_f$, we get /144

$$(M^2 - 1)\frac{du}{u} - \frac{dF}{F} + \frac{\sum_l h_{q_l} dq_l}{\rho h_\rho} = 0. \qquad (3.94)$$

At the critical section (M = 1), we must have

$$\frac{dF}{Fdx} = \frac{\sum_l h_{q_l} dq_l/dx}{\rho h_\rho}. \qquad (3.95)$$

The characteristic features of the transition through the speed of sound, and analysis of states close to equilibrium and frozen ones, and certain problems of the theory of the flow of a nonequilibrium gas considering friction and heat transfer, are discussed in [64, 94-97].

Comments on the methods of calculating nonequilibrium flows

In a nonequilibrium flow, we do not have a prior knowledge of either the position of the critical section, or the mass flow rate, and therefore the calculation of nonequilibrium flows involves certain difficulties. Figure 3.41 shows schematically the integral curves for Equations (3.40) - (3.45). Each curve corresponds to a certain value of the flow rate m. Curve 1, passing through a singularity B (saddle point), represents the desired solution ($m = m_1$). The integral curves, passing above and below point B, correspond to subsonic and supersonic flows in the entire nozzle. To the integral curves to the right and left of point B there correspond nonreal regimes of flow $m > m_1$. Thus, to solve the problem of a supersonic flow in a nozzle, we must basically find an integral curve 1 passing through

the two singular points A and B (at point A, the speed of flow is zero).

Given a gas flow rate m_1, the calculation of a nonequilibrium flow can be basically done in the following way: since in the initial part of the subsonic section of the nozzle the flow is arbitrarily close to equilibrium, then with the aid of the equations for an equilibrium flow one can deviate somewhat from point A and calculate all gas dynamic parameters at a certain section 1, where $M_{e1} \ll 1$. The values of these parameters are used as starting values for the subsequent numerical integration.

In reality, the flow rate m is not given, and therefore in the direct method when the shape of the nozzle is given and one finds the solution, the calculation of nonequilibrium flows proceeds using the trial and error method: one is given the flow rate m, and the equations are integrated for this m. In this case, generally speaking, Condition (3.95) will not be satisfied. This indicates that for a selected flow rate the flow through a given nozzle will either be impossible or will be entirely subsonic. We can achieve a situation where Condition (3.95) will be satisfied by selecting m by, for example, the trial and error method. /145

Usually the flow rate of a gas through a nozzle in a nonequilibrium flow is close to the flow rate m_e in an equilibrium flow, and therefore it is advisable to use m_e as the starting value of the flow rate when using the curve fitting method. After one passes the critical section, the calculation of the supersonic flow will not present serious difficulties.

In the case when the energy parameter is small, good results are obtained with the method of successive approximations in which one first calculates the gas dynamic parameters of the

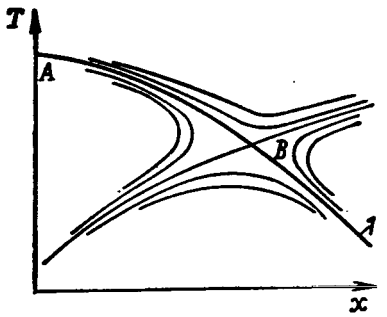

Figure 3.41. Integral curves for Eqs. (3.40) - (3.45)

corresponding frozen or equilibrium flow and on their basis one calculates q_e, τ and $q(x)$ to a first approximation. Then the values of p,ρ,T, q_e and τ are improved, and q is found to a second approximation, etc. To calculate the flows with nonequilibrium excitation of vibrations, it turns out that two approximation steps are sufficient [49-51]. In general, the smaller the energy parameter, the faster the convergence of the procedure.

In practice, nonequilibrium flows in a nozzle are often calculated using a reverse method in which one is given the flow rate and the distribution of any gas dynamic parameter along the nozzle, and then one determines the remaining parameters and the variation of the area, F(x). Even more often one uses a combined method of computation, where the subsonic region of flow is calculated using the reverse method, and the supersonic region — using the direct method.

If it is desirable that in the combined method the nozzle contour be close to the starting contour, then it is advisable to be given the distribution of the density or velocity as functions that are least sensitive to nonequilibrium processes, and to take these functions from the calculation of an equilibrium flow [54].

Pressure and temperature may also be used as the given functions. In the latter case, for some simple gas models the solution can be obtained analytically [97]. It is clear that the reverse method is preferable in those cases when general

properties of flows are being studied, and there is no need to consider the flow in a certain nozzle given beforehand. To overcome the difficulties involved in the calculation of nonequilibrium flows, it is convenient to use special techniques presented in [54] and [98].

Integration of equations, describing flows close to equilibrium

The inclusion of the kinetic equations in the system of equations of gas dynamics significantly complicates the calculations. Even greater difficulties arise in the case when the flow is close to thermodynamic equilibrium. And this does not occur as a result of any peculiarities of the flow field, but as a rule as a result of the properties of the computational schemes that are not adapted to the integration of equations of the kinetic equation type with small parameters in front of higher derivatives. When these equations are integrated by the usual Euler or Runge-Kutta methods, the necessity to stabilize the computation requires that such a small integration step be chosen that the calculation, even using today's fast computers, is still too laborious.

Let us consider some features of the integration of such equations using the example of the simplest kinetic equation

$$\frac{dq}{dt} = \frac{f(q, t)}{\tau}, \tag{3.96}$$

where

$$f(q, t) = q_e(t) - q, \ \tau = \text{const}. \tag{3.97}$$

/ 146

Let us determine the error in the calculation of q when using the simplest first-order difference scheme

$$q_{n+1} = q_n + \frac{f(q_n, t_n)}{\tau}\Delta; \ \ \Delta = t_{n+1} - t_n. \tag{3.98}$$

Let us assume that $q_e(t)$ in the initial data are known exactly, so that the entire computational error for q will be due to the error of the method. Letting $\tilde{q}(t)$ denote the exact solution of Eq. (3.96), from Eq. (3.98), we obtain

$$q_1 = q_0 + \frac{q_{e0} - \tilde{q}_0}{\tau}\Delta = \tilde{q}_1 + O(\Delta)^2;$$

$$q_2 = q_1 + \frac{q_{e1} - q_1}{\tau}\Delta = \tilde{q}_1 + O(\Delta^2) + \frac{q_{e1} - \tilde{q}_1 - O(\Delta^2)}{\tau}\Delta =$$

$$= \tilde{q}_2 + O\left[\Delta^2\left(1 + \frac{\Delta}{\tau}\right)\right].$$

i.e., the total error in the calculation of q_2 by Eq. (3.98) for $\Delta/\tau \gg 1$ will be on the order of $\Delta^2\frac{\Delta}{\tau}$. Similarly, one can calculate the error ε_3 for q_3, etc. For ε_k, for example, we obtain

$$\varepsilon_k = O\left(\Delta^2\left(\frac{\Delta}{\tau}\right)^{k-1}\right).$$

Therefore, for $\Delta/\tau \gg 1$ a small error in the determination of q in the preceding step (or preceding approximation if we deal with a more complex kinetic equation and calculate q_k by the method of successive approximations) leads to a large error in the calculation of q in the subsequent step (next approximation).

Thus, for $\Delta/\tau \gg 1$ we come across a catastrophic growth of the error, which makes the calculation according to a scheme like (3.98) practically impossible. Here the actual solution of the differential equation (3.96), the function q(t), may be very smooth, for example, almost linear, and the calculation of q(t), generally speaking, may be conducted using a very large step.

From all of the above, we can conclude that the scheme (3.98) is impractical for numerical integration of Equation (3.96) for very small τ.

For Eq. (3.96) one can easily find a scheme which is free from the deficiencies of Scheme (3.98). Let us consider

the scheme

$$q_{n+1} = q_n + f\frac{(q_{n+1},\ t_{n+1})}{\tau}\,\Delta, \tag{3.98a}$$

from which, in view of (3.97), we obtain

$$q_{n+1} = q_n + \frac{q_{e,\,n+1} - q_n}{(1+\Delta/\tau)}\cdot\frac{\Delta}{\tau}. \tag{3.99}$$

This scheme, just like Scheme (3.98), is a first-order scheme of approximation, but in contrast with Scheme (3.98) it does not require restrictions on the value of Δ/τ and permits us to conduct the computation for $\Delta/\tau \gg 1$.

In practice, one ordinarily uses difference equations of a higher order, and the function $f(q, t)$ in Eq. (3.96) is not solved for q.

If for the integration of Eq. (3.96) we use the second-order difference scheme /147

$$q_{n+1} = q_n + \frac{f_{n+1} + f_n}{2\tau}\,\Delta \tag{3.100}$$

and in each step we conduct the calculation using the method of successive approximations, then as one can easily see — for example, for the case (3.97) [39] — for the convergence of the iterative process it is necessary that the following condition be satisfied

$$\Delta < 2\tau. \tag{3.101}$$

Just as in the previous example, the transition to non-explicit schemes, one can construct various stable finite-difference schemes that do not require that the Condition (3.101) be satisfied. The techniques of constructing such schemes and an analysis of the solutions of equations of type (3.96), called "inelastic", can be found in the papers by O. N. Katskova, A. N. Krayko, P. I. Chushkin, N.S. Galyun, V.N. Kamzolov, and

Yu. G. Pirumov, V. P. Strulov, V. P. Shkadov, L. I. Turchak, V. K. Dushin, Curtis and Girschfelder, Trinor, et al. [39, 40, 44, 52, 64, 99-103].

On the basis of Schemes (3.98) and (3.98a), one can construct a whole class of finite-difference schemes depending on the parameter μ:

$$\frac{q_{n+1}-q_n}{\Delta}=\mu\frac{f_n}{\tau}+(1-\mu)\frac{f_{n+1}}{\tau};\quad 0<\mu\leq 1. \qquad (1.102)$$

For $\mu = 1$ we obtain Scheme (3.98); for $\mu = 0$ - Scheme (3.98a); for $\mu = 1/2$ - Scheme (3.100).

In the selection of the optimal finite-difference scheme, one has to consider at least two factors: decrease of the error in each step and making sure that the error is damped in the initial data. A compromise solution of this problem can lead to a selection of values of μ, different from zero to one-half $(0\leqslant\mu\leqslant 1/2)$. An analysis of various finite-difference schemes of the type of (3.102) from these positions is made in [52] and [100].

Another method, also permitting us to increase the integration step is the method of linearization relative to a known equilibrium solution [45, 54, 104] or the method of local linearization, developed by Moretti [105,106] in which the system of nonlinear equations of kinetics in the successive intervals is replaced by a system of linear equations which can be solved exactly. Other methods are known, in which it is possible to avoid the difficulties of integration of near-equilibrium flows [107].

All these methods are quite laborious, even though, just like the methods of constructing stable finite-difference schemes, they permit us to considerably increase the step of integration.

"Optimal" nozzle

As already noted, the freezing of internal degrees of freedom and the resulting binding of a large fraction of enthalpy in the form of chemical energy, not transformed into the energy of translational degrees of freedom, is accompanied by a considerable decrease (as compared with equilibrium flows) of the temperature and pressure, and a lesser decrease of the velocity and specific momentum. However, in a number of cases even a relatively small change in momentum may have a decisive influence on the total characteristics of the engine, in particular on its thrust. Such a situation will exist, for example, in the case of air-feed jet engines [108-110]. Figure 3.42 [108] shows a graph illustrating the character of the variation of thrust of a typical air-feed jet engine as a function of the M number for the flight (fuel-mixture of hydrogen and air, ratio - stoichiometric). When M is near 11, the thrust decreases to practically zero thanks to the freezing of the recombination processes. / 148

In this connection, the problem arises of optimum profiling of the nozzle, i.e. the construction of a nozzle contour for which thrust losses due to nonuniformity are reduced to a minimum.* Such a nozzle, as is clear from physical considerations, should remove the freezing point of the contents farther away and lower the value of the frozen energy. One should separately consider two sides of the problem: what can be obtained by the profiling of nozzles alone (for a given size), and what is obtained by increasing their length. Attempts to lower losses of thrust due to lack of balance by making highly elongated nozzles are, from the practical point of view, of little value for the following reasons: on the one hand, even a considerable in-

* Other aspects of nozzle optimization (for example, obtaining a uniform flow for a minimum length, etc.) which require that the two-dimensional character of the flow be considered, are not discussed here.

crease in the dimensions of the nozzle does not have a substantial effect on the magnitude of the frozen energy (in typical cases, for example, an increase of the dimensions of the nozzle by a factor of 10 results in a reduction of the frozen energy by approximately a factor of 1.5 [55]). On the other hand, when the length of the nozzle is increased, the losses due to friction become significantly greater, so that the question of the optimum length of the nozzle must be solved considering all factors. Such an analysis was made in [111]. General questions involving the construction of optimum contours for nonequilibrium flows were considered in [112,113] as well as [115].

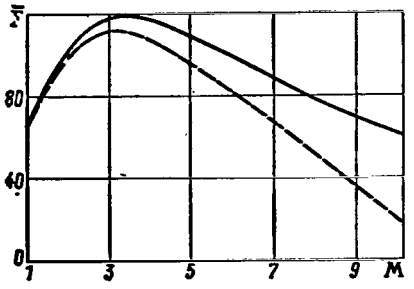

Figure 3.42. Thrust of a typical air-feed jet engine (dashed line — nonequilibrium flows, solid line — equilibrium flow):
F — net thrust per kilogram of air

In view of the difficulty of solving the boundary-value problem to which the problem of optimum profiling in its exact formulation can be reduced, the numerical results were obtained only in the one-dimensional approximation. In the case of the flow of oxygen through an axisymmetric nozzle for the following initial data in the entrance section: $M_1 = 1.1$; $r_1 = 2$ cm, $T_1 = 5000$ K, $p_1 = 100$ kG/cm^2, $z = 1$ m (length of the nozzle) and $p_\infty = 0$ it turned out, for example, that for optimum, conical, and parabolic contours, 38, 25, and 20%, respectively, of the thrust difference for the equilibrium and frozen flows is realized [114] (see also [116]). / 148

These results of course may be viewed only as estimates of the possible gain in thrust; to obtain more accurate data, it is necessary to consider the two-dimensional character of the flow. / 149

REFERENCES

1. Wray, K. L. and T. S. Freeman. Shock Front Structure in O_2 at High Mach Numbers, J. Chem. Physl, Vol. 40, No. 10 1964.

2. Zel'dovich, Ya. B., and Yu. P. Rayzer. Fizika udarnykh voln i vysokotemperaturnykh gazodinamicheskikh yavleniy (Physics of Shock Waves and High-Temperature Gas-Dynamic Phenomena), Moscow, Physics and Mathematics Press (Fizmatgiz), 1963.

3. Lun'kin, Yu. P. Structure of Shock Waves, Zhurnal Teoreticheskoy Fiziki (ZhTF), Vol. 27, No. 6, 1957.

4. Lun'kin, Yu. P. Parameters of a Gas Behind a Shock Wave, ZhTF, Vol. 29, No. 2, 1959.

5. D'yakov, S. P. Shock Waves in a Relaxing Medium, Zhurnal Eksperimental'noy i Teoreticheskoy Fiziki (ZhETF), Vol. 27, No. 6, 1954.

6. Gladkov, A. A. Variation of Density in Strong Shock Waves. Trudy TsAGI, No. 1007, 1966.

7. Clarke, J., and M. MacChesny. Dynamics of Real Gases, 1967.

8. Predvotitelev, A. S., Ye. V. Stupochenko, A. S. Pleshanov, Ye. V. Samuylov and I. B. Rozhdestvenskiy. Tablitsy termodinamicheskikh funktsiy vozdukha (dlya temperatur ot 200 do 6000°K i davleniy ot 0.001 do 1000 atmosfer). [Tables of Thermodynamic Functions of the Air (for the Temperatures from 200 to 6000°K and Pressures from 0.001 to 1000 atm)]. Izdatel'stvo AN SSSR, 1961.

9. Predvoditelev, A. S., Ye. V. Stupochenko, Ye. V. Samuylov, I. P. Stakhanov, A. S. Pleshanov and I. B. Rozhdestvenskiy. Tablitsy termodinamicheskikh funktsiy vozdukha (dlya temperatur ot 6000 do 12,000°K i davleniy ot 0.001 do 1000 atmosfer). [Tables of Thermodynamic Functions of the Air (for Temperatures from 6000 to 12,000°K and Pressures from 0.001 to 1000 atm)]. Izdatel'stvo AN SSSR, 1957.

10. Predvoditelev, A. S., Ye. V. Stupochenko, A. S. Pleshanov, Ye. V. Samuylov, and I. B. Rozhdestvenskiy. Tablitsy termodinamicheskikh funktsiy vozdukha (dlya temperatur ot 12,000 do 20,000°K i davleniy ot 0.001 do 1000 atmosfer). [Tables of Thermodynamic Functions of the Air (for Temperatures from 12,000 to 20,000°K and Pressures from 0.001 to 1000 atm)]. Izdatel'stvo AN SSSR, 1959.

11. Predvoditelev, A. S., et al. Tablitsy gazodinamicheskikh i termodinamicheskikh velichin potoka vozdikha za pryamym skachkom uplotneniya. (Tables of Gas-Dynamic and Thermodynamic Variables for the Air Flow Behind a Normal Shock Wave). Izdatel'stvo AN SSSR, 1959.

12. Kuznetsov, N. M. Termodinamicheskiye funktsii i udarnyye adiabaty vozdukha pri vysokikh temperaturakh. (Thermodynamic Functions and Shock Adiabates of High-Temperature Air). Moscow, Machine Building Press (Mashinostroyenie), 1965.

13. Kuznetsov, S. I. Diagrammy i tablitsy techeniya dissotsiiruyushchego vozdukha okolo klina, konusa i vypukloy poverkhnosti (Diagrams and Tables of Flow Over Dissociating Air Around a Wedge, Cone, and a Convex Surface). Moscow, Defense Press (Oborongiz), 1962.

14. Kuznetsov, N.M. Structure of a Shock Wave in the Air Considering the Kinetics of Chemical Reactions. Inzhenerno-Fizicheskiy Zhurnal, Vol. 3, No. 9, 1960.

15. Stupochenko, Ye. V., S. A. Losev, and A. I. Osipov. Relaksatsionnyye protsessy v udarnykh volnakh (Relaxation Processes in Shock Waves), Moscow, Fizmatgiz, 1965.

16. Anisimov, S. I., N. M. Kuznetsov, and Ye. F. Nogotov. Structure of Shock Waves in the Air Considering Kinetics of Chemical Reactions and Excitation of Molecular Vibrations of Nitrogen. "Teplofizika vysokikh temperatur", Vol. 2, No. 3, 1964.

17. Duff, R. E. and N. Davidson. Calculation of Reaction Profiles Behind Steady State Shock Waves. P. II. The Dissociation of Air. J. Shem. Phys., X, Vol. 31, No. 4, 1959.

18. Lin, S. Ch. and J. D. Teare. Rate of Ionization behind Shock Waves in Air. P. II Theoretical Interpretations. Phys. of Fluids, III, Vol. 6, No. 3, 1963.

19. Ray, K. L. Chemical Kinetics of High-temperature Air. In the Collection: Investigation of Hypersonic Flows, Moscow, "Mir" Press, 1964.

20. Lin, S. Ch., R. A. Neal and W. I. Fyfe. Rate of Ionization behind Shock Waves in Air. P. 1. Experimental Results. Phys. of Fluids, Vol. 5, No. 12, 1962.

21. Biberman, L. N. and I. G. Yakubov. State of a Gas Behind the Front of a Strong Shock Wave, "Teplofizika vysokikh temperatur", Vol. 3, No. 3, 1965.

22. Wilson, J. Ionization Rate of Air behind High-Speed Shock Waves. Phys. of Fluids, X, Vol. 9, No. 10, 1966.

23. Zheleznyak, M. B., and A. Kh. Mnatsakanyan. Ionization Relaxation behind Shock Waves in Air. "Teplofizika vysokikh temperatur", Vol. 6, No. 3, 1968.

24. Losev, S. A. and V. A. Polyanskiy. Nonequilibrium Ionization of Air behind the Front of a Shock Wave at the Speed 5-10 km/sec. Izvestiya AN SSSR, MZhG, No. 1, 1968.

25. Treanor, C. E. and P. V. Marrone. Effect of Dissociation on the Rate of Vibrational Relaxation. Phys of Fluids, IX, Vol. 5, No. 9, 1962.

26. Marrone, P. V. and C. E. Treanor. Vibration and Dissociation Coupling behind Strong Shock Waves. Symp. on Dynamics of Manned Lifting Planetary Entry, N.Y. London, 1963.

27. Camac, M. and A. Vaughan. O_2 Dissociation Rates in O_2- Ar Mixtures. J. Chem. Phys. II, Vol. 34, No. 2, 1961.

28. Losev, S. A. and V. A. Polyanskiy. Effect of Vibrational Relaxation of Molecules on the Characteristics of Dissociating Air behind the Front of a Strong Shock Wave. Izvestiya, AN SSSR, MZhG, No. 4, 1969.

29. Zhurin, V. V. and O. K. Kostko. Calculation of Thermodynamic Gas Parameters behind a Strong Shock Wave in Argon, "Teplofizika vysokikh temperatur", No. 6, 1967.

30. Bortner, M. H. Chemical Kinetics of Planetary Entry. Symposium on Dynamics of Manned Lifting Planetary Entry. N. Y. - London, 1963.

31. McKenzie, R. L. The Qualitative Behavior and Effects of Nonequilibrium Chemistry behind Strong Shock Waves in Gas Mixtures of CO_2 and N_2. AIAA Technical Papers. Stepping Stones to Mars. Meeting Baltimore, Maryland, 1966.

32. Zel'dovich, Ya. B. Propagation of a Shock Wave in a Gas with Reversible Chemical Reactions, ZhETF, Vol. 16, No. 4 1946.

33. Polyanskiy, O. Yu. Instability of Certain Stationary Flows of a Relaxing Gas, Izvestiya AN SSSR, "Mekhanika", No. 3. 1965.

34. Vincenti, V. G. and Ch. H. Kruger. Introduction to Physical Gas Dynamics, New York, Wiley, 1965.

35. Becker, E. One Dimensional Steady Compression Flows in a Gas with Relaxation. ZAMM, IX, Vol. 46, No. 6, 1966.

36. Clarke, J. F. and J. B. Rodgers. Shock Waves in a Gas with Several Relaxing Internal Energy Modes. J. Fluid Mech. Vol. 21, No. 4, 1965.

37. Stupochenko, Ye. V. and I. P. Stakhanov. Theory of Non-stationary Discontinuities in Relaxing Media, Doklady AN SSSR, Vol. 117, No. 1, 1957.

38. Sarychev, V. M. Flows of a Dissociating Gas in the Absence of a Local Thermodynamic Equilibrium, Doklady AN SSSR, Vol. 185, No. 5, 1969.

39. Katskova, O. N. and A. N. Krayko. Calculation of Two-Dimensional and Axisymmetric Supersonic Flows in the Presence of Irreversible Processes, Trudy VTs AN SSR, No. 4, 1963.

40. Katskova, O. N., and A. P. Krayko. Raschet ploskikh i osesimmetrichnykh techeniy pri nalichii neobratimykh protsessov (Calculation of Planar and Axisymmetric Flows in the Presence of Irreversible Processes). Trudy Vychislitelnogo Tsentra (VTs), 1964.

41. Zupnik, T. F., E. N. Nilson and others. Application of the Method of Characteristics Including Reaction Kinetics to Nozzle Flow. AIAA Paper N 64-97, 1964.

42. Migdal, D. and A. Goldford. Chemical Nonequilibrium Studies in Supersonic Nozzle Flows. AIAAJ, IX Vol. 3, No. 9, 1965.

43. Wood, A. D., J. F. Sprinfield and A. I. Pallone. Determination of the Effects of Chemical and Vibrational Relaxation on an Inviscid Hypersonic Flow Field. AIAA J., Vol. 2, No. 10, 1964.

44. Katskova, O. N. and P. I. Chushkin. Three-dimensional Supersonic Flows of a Gas with Nonequilibrium Processes. Zhurnal vychislitel'noy matematiki i matematicheskoy fiziki, Vol. 9, No. 5, 1968.

45. Penner, S. S. Introduction to the Study of Flow Systems, Butterworths, London, 1955.

46. Yel'yashevich, M. A. and S. I. Anisimov. Relation Phenomena in a High-Speed Flow of a Gas. Doklady AN BSSR, Vol. 5, No. 8, 1961.

47. Bray, K. N. C. Atomic Recombination in a Hypersonic Wind Tunnel Nozzle. J. Fluid Mechanics, VII, Vol. 6, No. 1, 1959. See also the Collection: Gas Dynamics and Heat Exchange in the Case of Chemical Reactions. Moscow, IL, 1962.

48. Lordi, J. A. Comparison of Exact and Approximate Solutions for Nonequilibrium Nozzle Flows. ARS J., VIII Vol. 32 No. 8, 1962.

49. Stollery, J. L. and J. E. Smith. A Note on the Variation of Vibrational Temperature along a Nozzle. J. Fluid Mechanics, VI, Vol. 13, No. 2, 1962.

50. Stollery, J. L., J. E. Smith and C. Park. The Effects of Vibrational Relaxation on Hypersonic Nozzle Flows - Co. "The High Temperature Aspects of Hypersonic Flow. Proc. of the AGARD-NATO Specialists. Meeting Rhode - Saint - Genese, Belgium, 3-6 April 1962". Oxford and others, 1964, (AGARDograph N 68).

51. Stollery, J. L. and C. Park. Computer Solutions to the Problem of Vibrational Relaxation in Hypersonic Nozzle Flows. J. Fluid Mechanics, V, Vol. 19, No. 1, 1964.

52. Kamzolov, V. N. and Yu. G. Pirumov. Calculation of Non-equilibrium Flows in Nozzles, Izvestiya AN SSSR, NZhG, No. 6, 1966.

53. Glowacki, W. J. Effect of Finite Oxygen Recombination Rate on the Flow Conditions in Hypersonic Nozzles. In Coll.: "Advances in Hypervelocity Techniques, Pros. of the Second Symposium on Hypervelocity Techniques". New York, 1962, pp. 523-563. See also collection: Sovremennaya tekhnika aerodinamicheskikh issledovaniy pri giperzvukovykh skorost'yakh (Modern Techniques of Aerodynamic Studies at Hypersonic Velocities), Moscow, Mashinostroyeniye, 1965. See also: Voprosy raketnoy tekhniki, 1963, No. 2.

54. Eschenroeder, A. Q., D. W. Boyer and J. G. Hall. Nonequilibrium Expansions of Air with Coupled Chemical Reactions - Phys. of Fluids, V, Vol. 5, No. 5, 1962. See also: Voprosy raketnoy tekhniki, No. 2, 1963.

55. Lordi, J. A. and R. E. Mates. Nonequilibrium Effects on High-Enthalpy Expansions of Air. AIAA J., Vol. 3, No. 10, 1965. "Third Hypervelocity Techniques Symposium. Advanced Experimental Techniques for Study of Hypervelocity Flight. Denver, March, 1964". Part 2, Denver, 1964.

56. Eschenroeder, A. Q. Entropy Changes in Nonequilibrium Flows. Phys. of Fluids, X, Vol. 6, No. 10, 1963. See also: Mekhanika, Collection of Foreign Translated Articles, No. 5, 1964.

57. Phinney, R. Criterion for Vibrational Freezing in a Nozzle Expansion. AIAA J., Vol. 1, No. 2, 1963.

58. Phinney, R. Nondimensional Solutions of Flows with Vibrational Relaxation. AIAA J., Vol. 2, No. 2, 1964.

59. Sebacher, D. I. A Correlation of N_2 Vibrational-Translational Relaxation Times. AIAA J., Vol. 5, No. 4, 1967.

60. Hurle, J. R., A. L. Russo and T. Gordon. Experimental Studies of Vibrational and Dissociative Nonequilibrium in Expanded Gas Flows. AIAA Paper N 63 - 439, 1963.

61. Wilde, K. A Complex Kinetics in Adiabatic Flow: C-H-O-(N) Systems. AIAA J., Vol. 3, No. 10, 1965.

62. Franciscus, L. C. and A. Lezberg. Effects of Exhaust Nozzle Recombination on Hypersonic Ramjet Performance: 11. Analytical Investigation. AIAA J., Vol. 1, No. 9, 1963.

63. Migdal, D. and A. Goldford. Exact Kinetic and Approximate Nozzle Recombination Losses. AIAA J., Vol. 2, No. 8, 1964.

64. Stulov, V. P., and V. P. Shkadova. One-dimensional Nonequilibrium Flow of Air, Izvestiya AN SSSR, MZhG, No. 2, 1968.

65. Anisimov, S. I. and G. S. Romanov. Nonequilibrium Flow of Air through Nozzles. Prikladnaya matematika i teoreticheskaya fizika (PMTF), No. 1, 1962.

66. Der, J. J. Theoretical Studies of Supersonic Two-Dimensional and Axisymmetric Nonequilibrium Flow, Including Calculations of Flow through a Nozzle. NASA TR-164, 1963.

67. Zonars, D., T. M. Weeks and T. E. Miller. Non-Equilibrium Nozzle Calculation Techniques. AIAA Paper, No. 66-635, 1966.

68. Tirumalesa, D. Nozzle Flows with Coupled Vibrational and Dissociational Nonequilibrium. AIAA J., Vol. 5, No. 2, 1967.

69. Zonars, D. Nonequilibrium Regime at Airflow in Countered Nozzles: Theory and Experiment. AIAA J., Vol. 5, No. 1, 1967.

70. Tirumalesa, D. Rotational Relaxation in Hypersonic Low-Density Flows. AIAA J., Vol. 6, No. 4, 1968.

71. Nagamatsu, H. T. and R. E. Sheer. Vibrational Relaxation and Recombination of Nitrogen and Air in Hypersonic Nozzle Flows. AIAA J., Vol. 3, No. 8, 1965.

72. Duffy, R. E. Experimental Study of Nonequilibrium Expanding Flows. AIAA J., Vol. 3, No. 2, 1965.

73. Hurle, I. R. and A. L. Russo. Spectrum-Line Reversal Measurements of Free Electron and Coupled N_2 Vibrational Temperatures in Expansion Flows. Journal of Chem. Phys Vol. 43, 1965.

74. Lezberg, E. A. and L. O. Franciscus. Effect of Exhaust Nozzle Recombination on Hypersonic Ramjet Performance. I. Experimental Measurements. AIAA, Vol. 1, No. 9, 1963.

75. Chen Che Jen. Experimental Investigation of Atomic Recombination in a Supersonic Nozzle. J. Fluid Mechanics, Vol. 17, No. 3, 1963.

76. Boynton, F. P. Chemical Kinetic Analysis of Rocket Exhaust Temperature Measurements. AIAA J., Vol. 2, No. 3, 1964.

77. Zauderer, B. Experimental Study of Nonequilibrium Ionization in a Linear MHD - Generator. AIAA J., Vol. 6, No. 4, 1968.

78. Koppenwallner, G., K. Bütefisch and K. Kienappel. Experimental Investigations on Hypersonic Nozzle Flow for Very Low Density Gas Density with Oscillation Relaxation. Deutsche Luft - and Raumfahrt, DRL FB 67-69, 1967.

79. Just, Th. and H. Pipport. Measurements of Relaxation Effects in Nozzle Flows of Hot combustion Gases using a Shock Tube Arrangement. "Ztschr. für Flugwissenschaften, II, Vol. 14, No. 2, 1966.

80. Eschenroeder, A. Q. and I. W. Daiber. Ionization Nonequilibrium in Expanding Flows. ARS J. Vol. 32, No. 2, 1962.

81. Bray, K. N. C. Electron-Ion Recombination in Argon Flowing Through a Supersonic Nozzle. In Coll.: "The High Temperature Aspects of Hypersonic Flow. Proc. of the AGARD-NATO Specialists' Meeting. Rhode-Saint-Genese, Belgium, 3 - 6 April 1962". Oxford and others, 1964.

82. Blythe, P. A. Nonequilibrium Flow Through a Nozzle. In Coll.: "High Temperature in Aeronautics. Proc. of the Symposium Held in Turin 10-12 September, 1962." Oxford and others, 1964.

83. Blythe, P. A. Asymptotic Solutions in Nonequilibrium Nozzle Flow. J. Fluid Mechanics, X, Vol. 20, No. 2, 1964.

84. Cheng, H. K. and R. S. Lee. Freezing of Dissociation in Supersonic Nozzle Flows. AIAA Paper, No. 66-1, 1966.

85. Cheng, H. K. and R. S. Lee. Nonequilibrium Transition Patterns of a Quasi-One-Dimensional Dissociating Gas Flow. AIAA J., Vol. 5, No. 9, 1967.

86. Vasyl'yeva, A. V. and Yu. S. Sayasov. Theory of the Freezing of Non-Equilibrium Processes in Streams of Low-Temperature Plasma, PMTF, No. 1, 1968.

87. Bray, K. N. C. Simplified Sudden-Freezing Analysis for Non-Equilibrium Nozzle Flows. ARS J., Vol. 31, No. 6, 1961.

88. Harris, C. J. Comment on Nonequilibrium Effects on High-Enthalpy Expansion of Air. AIAA J., Vol. 4, No. 6, 1966.

89. Harney, D. J. Slender Body Aerodynamic Testing Potential of High Energy Wind Tunnels. AIAA Paper, No. 68-382, 1968.

90. Ring, L. E. and P. W. Johnson. Correlation and Prediction of Air Nonequilibrium in Nozzles. AIAA Paper, No. 68-378, 1968.

91. Williams, I. C. III Correlation of the Sudden Freezing Point in Nonequilibrium Nozzle Flows. AIAA J., Vol. 3, No. 6 1965.

92. Heis, Yu. D. and R. F. Probstin. Theory of Hypersonic Flows, 1962.

93. Johannesen, N. Analysis of Vibrational Relaxation Regions by Means of the Rayleigh-Line Method. J. Fluid Mechanics, Vol. 10, No. 1, 1961.

94. Pleshanov, A. S. Transition of a Non-equilibrium Gas Through the Critical Section of a Nozzle. Doklady AN SSSR, Vol. 158, No. 1, 1964.

95. Pleshanov, A. S. and P. A. Kon'kov. Nonisentropic Non-equilibrium Gas Flow through a Nozzle Considering Friction and Heat Exchange. In the Collection: Issledovaniye po fizicheskoy gazodinamike (Investigation in Physical Gas Dynamics). 1966.

96. Zhigulev, V. N. Problem of the Flow of a Nonequilibrium Gas. Doklady AN SSSR, Vol. 149, No. 6, 1963.

97. Polyanskiy, O. Yu. Certain Features of Nonequilibrium Gas Flows near the Critical Section of the Lavalle Nozzle. Trudy TsAGI, No. 1007, 1966.

98. Emanuel, G. A General Method for Numerical Integration through a Saddle. Point Singularity with Application to One-dimensional Nonequilibrium Nozzle Flow. AEDC, TDR, Rep. N 64-29 (Clearinghouse Feder. Scient. and Techn. Inform. N AD 428563). S. L. 1964.

99. Galyun, N.S. and A. N. Krayko. Calculation of Nonequilibrium Flows, Izvestiya AN SSSR, "Mekhanika i Mashinostroyeniye", No. 6, 1964.

100. Krayko, A. N. Numerical Integration of Equations with a Small Parameter in Front of the Highest Derivative. Zhurnal vychislitel'noy matematiki i matematicheskoy fiziki. Vol. 9, No. 2, 1960.

101. Dushin, V. K. Solution of a System of Relaxation Equations when Calculating the Flows of a Reacting Gas Mixture whose State is Close to Equilibrium. Zhurnal vychislitel'noy i matematicheskoy fiziki, Vol. 9, No. 5, 1969.

102. Curtiss, C. F. and J. O. Hirschfelder. Integration of Stiff Equations. Proc. Nat. Acad. Sci. of USA. I Vol. 38, No. 1, 1952.

103. Treanor, C. E. A Method for the Numerical Integration of Coupled First-Order Differential Equations with Greatly Different Time Constants. "Mathematics of Computation" Vol. 20, No. 93, 1966.

104. Pavlova, L. N. Nonequilibrium Flows of a Dissociating Air Close to Equilibrium. Izvestiya AN SSSR, OTN, "Mekhanika i mashinostroyeniye", No. 3, 1961.

105. Moretti, G. A New Technique for the Numerical Analysis of Non-equilibrium Flows. AIAA J., Vol. 3, No. 2, 1965.

106. De Groat, J. J. and M. J. Abbett. A Computation of One-Dimensional Combustion of Methane. AIAA J., II, Vol. 3 No. 2, 1965.

107. Kinslow, M. and J. T. Miller. Nonequilibrium Expansion of a Diatomic Gas through a Convergent - Divergent Nozzle. Phys. of Fluids. IX, Vol. 9, No. 9, 1966.

108. Olson, W. T. Recombination and Condensation Processes in High Area Ratio Nozzles - ARS J., Vol. 32, No. 5, 1962.

109. Dugger, G. L. Comparison of Hypersonic Ramjet Engines with Subsonic and Supersonic Combustion — Combustion and Propulsion, IV-th AGARD Colloquium, Pergamon Press, Oxford, 1961.

110. Smith, I. E. The Effects of Dissociation in Rockets, Ramjets and Wind Tunnel. Dissociating and Ionising Gases in Engineering, London, 1964.

111. Sarli, V. J., A. W. Blackman and D. Migdal. Exhaust Nozzle Recombination of Dissociated Hydrogen — Air Combustion Products. AIAA - ASME Hypersonic Ramjet Conference Paper N 63120, 1963, AIAA J. Vol. 3, No. 1, 1965.

112. Krayko, A. N. Variational Problems of Gas Dynamics of Nonequilibrium and Equilibrium Flows, PMM, Vol. 28, No. 2, 1964.

113. Hoffman, I. D. A General Method for Determining Optimum Thurst Nozzle Contours for Chemically Reacting Gas Flow. AIAA J. Vol. 5, No. 4, 1967.

114. Galyun, N.S. and A. N. Krayko. A Variational Problem in One-dimensional Nonequilibrium Gas Dynamics, Izvestiya AN SSSR, MZhG, No. 2, 1966.

115. Osipov, A. A. Solution of Variational Problems of Gas Dynamics of Supersonic Nonequilibrium Flows. Izv. AN SSSR, MZhG, No. 1, 1969.

116. Berns, R. R. and J. M. Bonyer. Determination of Optimum Hozzle Contours for the Expansion of Dissociated Gases by Method of the Variational Calculus. "Austronautica Acta", VIII, Vol. 13, No. 5-6, 1968.

117. Chirikhin, A. V. A Method of Calculating the Freezing Temperature for a Flow of Nitrogen through a Hypersonic Nozzle, Uchenyye zapiski TsAGI, No. 6, 1971.

118. Sayapin, G. N. Calculation of Nonequilibrium Flows of Nitrogen through Nozzles. Uchenyye zapiski TsAGI, No. 1, 1972.

119. Losev, S. A., O. P. Shatalov, and M. S. Yalovin. Effect of Anharmonicity on the Time of Relaxation in Adiabatic Excitation and De-activation of Molecular Vibrations. Doklady AN SSSR, Vol. 195, No. 3, 1970.

120. Bray, K.N.C. Vibrational Relaxation of Anharmonic Oscillator Molecules: Relaxation under Isothermal Conditions. J. Phys. B, Ser. 2, Vol. 1, No. 4, 1968

121. Rosenberg, C. W., R. L. Taylor and J. D. Teare. Vibrational Relaxation of CO in Nonequilibrium Nozzle Flow. Journal Chem. Pnys., Vol. 48, No. 12, 1968.

122. Basov, N.G., V. G. Mikhaylov, A. N. Orayevskiy and V. A. Shcheglov. Determination of the Inverted Population of Molecules in a Supersonic Flow of a Binary Gas through a Laval Nozzle, ZhTF, Vol. 38, No. 12, 1968.

123. Polyanskiy, O.Yu. Effect of Nonequilibrium Processes on the Gas Dynamic Parameters in Hypersonic Units and at the Critical Point of a Blunt Body, Uchenyye zapiski TsAGI, Vol. II, No. 5, 1971.

124. Vinocur, M. On Stagnation-Point Conditions in Nonequilibrium Inviscid Blunt Body Flows. J. Fluid Mech. Vol. 43, p. 1, 1970.

125. Polyanskiy, O. Yu. Peculiarities of the Structure of Weak Shock Waves in a Relaxing Gas. Uchenyye zapiski TsAGI, Vol. II, No. 6, 1971.

CHAPTER 4

NONEQUILIBRIUM FLOW AROUND BODIES

4.1 General properties and characteristics /155

During the flight of hypersonic aircraft in the atmosphere of the Earth at altitudes of 40—80 km at velocities of more than 3 km/sec, nonequilibrium becomes an important property of the flow, since in this range of velocities and altitudes the characteristic relaxation lengths in the shock layer are commensurate with the size of the body and the energy — related to the internal degrees of freedom — is great enough that the physical-chemical processes may greatly influence these gas dynamic parameters. Table 12 gives an idea of these values where the altitudes H are presented at which the characteristic width of the relaxation zone behind a direct shock wave is 1 cm and 1 m.* The table also gives the temperatures T_f and T_e in the frozen and equilibrium flows behind a shock wave.

The practical necessity of studying nonequilibrium flows around blunt bodies is determined by the fact that the braking trajectories in the atmosphere of the Earth of many types of hypersonic aircraft (artificial earth satellites, hypersonic orbital aircraft, aircraft returning from space, etc.) lie within the altitude and velocity region where the flow is greatly determined by nonequilibrium processes.

---

* The distance at which the temperature differs by 10% from its equilibrium values is used as the relaxation length d.

Figure 4.1 shows typical flight trajectories of hypersonic aircraft and the boundaries of different flow regions in the region $d/\Delta \ll 0.1$ (d is the characteristic relaxation length behind a normal shock wave, Δ — distance of the shock wave from the body), the flow is close to equilibrium flow, and in the region $d/\Delta > 10$ — close to frozen flow. Close to and above the boundary $d/\Delta = 0.1$, the nonequilibrium processes have a great influence on the flow dynamics.

This chapter will investigate inviscid adiabatic flows of gas mixtures, whose components represent reacting gases which are thermally perfect. The equation of state

TABLE 12*

TEMPERATURE BEHIND A NORMAL SHOCK WAVE AND ALTITUDE ABOVE THE SURFACE OF THE EARTH, WHERE THE CHARACTERISTIC RELAXATION LENGTHS BEHIND THE NORMAL SHOCK WAVE ARE 1 CM AND 1 M

V_∞ км/sec		3	5	7	10
M_∞		10,1	16,8	23,5	33,6
T_f K		$4,5 \cdot 10^3$	$12 \cdot 10^3$	$24 \cdot 10^3$	$49 \cdot 10^3$
T_e K		$2,7 \cdot 10^3$	$4,9 \cdot 10^3$	$5,9 \cdot 10^3$	$9,5 \cdot 10^3$
H км	$d = 1$ см	35	45	55	60
	$d = 1$ м	65	75	85	90

* Translator's Note: Commas represent decimal points.

Note. The M_∞ number and temperature T_e were calculated for H = 70 km.

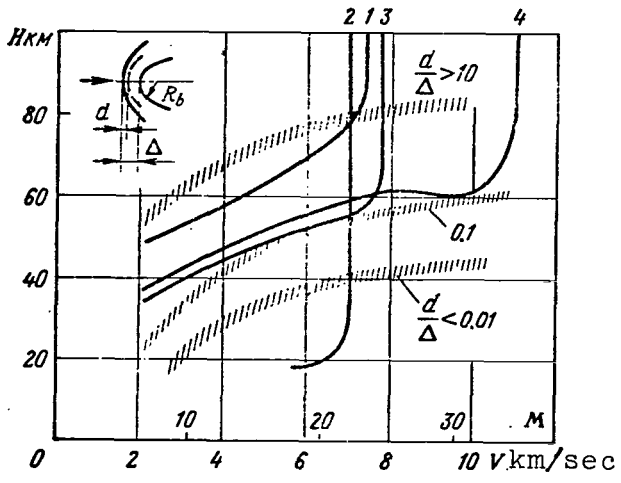

Figure 4.1. Boundaries of different flow regions around a blunt body (for $R_b = 1$ m), and typical flight trajectories of hypersonic aircraft: 1 - glider; 2 - intercontinental ballistic rockets; 3 - artificial earth satellite; 4 - Lunnik (glider)

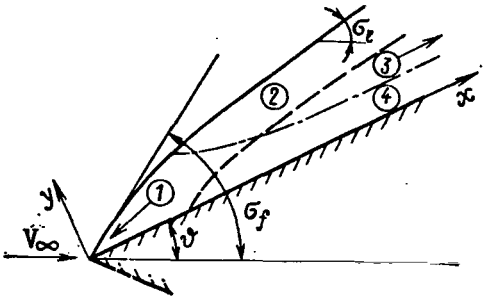

Figure 4.2. Diagram of non-equilibrium flow around a wedge [dashed line - boundary of relaxation zone behind shock waves (arbitrary), (dot-dash line - boundary of the relaxation entropy layer close to the wedge surface (arbitrary)].

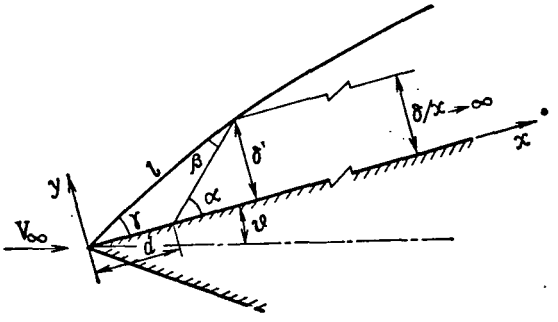

Figure 4.3. Determination of the relaxation layer thickness.

for these mixtures has the form

/157

$$p=\frac{\rho RT}{\overline{M}};\quad \left(\overline{M}=\sum_i \alpha_i M_i=1\Big/\sum_i \frac{\alpha_i}{M_i}\right). \tag{4.1}$$

We shall assume that the energy equation (caloric equation of state) may be given in the form

$$h=h(p,\ \rho,\ \langle q_i\rangle)\ \text{ or }\ h=h(T,\ \langle q_i\rangle)^*. \tag{4.2}$$

The notation and more detailed expressions for h and p are given in Section 2.1.

The system of differential equations describing the flow of inviscid non-heat conducting, relaxing gas consists of the continuity equation, momentum equations, energy equation, and kinetic equations (relaxation equations)

$$\frac{d\rho}{dt}+\rho\,\mathrm{div}\,\vec{V}=0; \tag{4.3}$$

$$\frac{d\vec{V}}{dt}+\frac{\mathrm{grad}\,p}{\rho}=0; \tag{4.4}$$

$$\frac{dh}{dt}-\frac{dp}{\rho dt}=0; \tag{4.5}$$

$$\frac{dq_i}{dt}=F_i(T,\ \rho,\ \langle q_j\rangle)\quad (i,\ j=1,\ 2,\ldots,\ n). \tag{4.6}$$

Here d/dt designates the total time derivative

$$\frac{d}{dt}=\frac{\partial}{\partial t}+u\frac{\partial}{\partial x}+v\frac{\partial}{\partial y}+w\frac{\partial}{\partial z}. \tag{4.7}$$

---

* The form h = h (T, $\langle q_i \rangle$) is only valid for mixtures of thermally ideal gases.

To close system (4.3) — (4.6), we must add to it equations (4.1) and (4.2). Specific expressions for F_i for certain processes and notes on selecting the parameters q_i are given in Chapter 1, and Sections 3.2 and 2.1.

In practice, instead of certain equations of kinetics (4.6), the following equations are frequently used.

$$\sum_i \alpha_i = 1 \quad \text{or} \quad \sum_i \xi_i = 1 \tag{4.8}$$

as well as the equations expressing the conservation of atoms of a certain type (see Chapter 1). The energy equation (4.5) may sometimes be more conveniently written in the form

$$\frac{d}{dt}\left(h + \frac{V^2}{2}\right) - \frac{\partial p}{\rho \partial t} = 0, \tag{4.9}$$

from which the Bernoulli equation follows for stationary flows

$$h + V^2/2 = \text{const.} \tag{4.10}$$

/158

The boundary and initial conditions for nonequilibrium flows have the same form as for ideal gas flows in the absence of viscosity and thermal conductivity: non-flow conditions on the body surface, and dynamic compatibility conditions at the shock wave front, which supplement the conditions of the continuous change in the parameters q_i when passing through a shock wave. For steady flows these conditions assume the following form.

$$\left.\begin{aligned} &\rho_\infty V_{n\infty} = \rho_1 V_{n1}; \\ &p_\infty + \rho_\infty V_{n\infty}^2 = p_1 + \rho_1 V_{n1}^2; \\ &h_\infty + V_\infty^2/2 = h_1 + V_1^2/2; \\ &V_{\tau\infty} = V_{\tau 1}; \\ &q_{i\infty} = q_{i1} \quad (i = 1, 2, \ldots, n), \end{aligned}\right\} \tag{4.11}$$

where

$$h_1 = h_1(T_1,\ q_{1\infty},\ q_{2\infty}, \ldots,\ q_{n\infty}).$$

If certain degrees of freedom are excited in a uniform manner, the expression for the enthalpy h_1 assumes the form

$$h_1 = h(T,\ q_{1e},\ q_{2e}, \ldots,\ q_{ke},\ q_{k+1\,\infty}, \ldots,\ q_{n\infty}), \tag{4.12}$$

where q_{1e}, $q_{2e}\ldots$, q_{ke} are the parameters which describe the degrees of freedom which are in equilibrium; $q_{ie} = q_{ie}(T_1, \rho_1)$

When a nonequilibrium flow passes around a body, an important role is played by the relaxation parameter $\bar{\tau}$ which equals the ratio of the characteristic relaxation time to the characteristic gas dynamic time t_c ;

$$\bar{\tau} = \tau / t_c. \tag{4.13}$$

This parameter characterizes the relative rate at which the equilibrium is established in the flow. If we have the following in the entire flow region being examined

$$\bar{\tau} \sim 1, \tag{4.14}$$

we shall call this flow essentially nonequilibrium flow. If

$$\bar{\tau} \gg 1, \tag{4.15}$$

then it is close to frozen flow, and if

$$\bar{\tau} \ll 1, \tag{4.16}$$

it will be close to equilibrium flow.

However, as a rule, in the problems of flow around bodies striving to the corresponding limiting states ($\bar{\tau} = 0$ and $\bar{\tau} = \infty$) is non-uniform, i.e., there are different types of layers,

regions ("lines" "surfaces", " points ") where the flow parameters greatly differ from their values in frozen and equilibrium flows. /159 These are typical examples of flows with singular perturbations. Some of these layers, which are usually called relaxation, entropy or vortex layers, have a great deal in common with a viscous boundary layer.

In the cases of $\bar{\tau} \ll 1$ or $\bar{\tau} \gg 1$ the primary influence of nonequilibrium is, as a rule, localized in these singular regions. The parameters of these regions are the relaxation layer behind the shock wave, in which the flow parameters asymptotically strive to their equilibrium values, the relaxation entropy layers close to the surface of a blunt and pointed body, etc. These layers will be described in greater detail in an examination of flows around a wedge, a cone, a blunt body, etc.

In many cases, in the case of flow around bodies, the region $\bar{\tau} \sim 1$ will comprise a comparatively small portion of the entire shock layer region, and thus in a large portion of it the flow will be either close to equilibrium flow or close to frozen flow. Those flows which are frozen in certain regions (usually they are called simply "frozen", although it is more correct to call them "freezing") represent a special example of flows which differ greatly from similar equilibrium flows and flows of an ideal gas.

The influence of nonequilibrium processes on the flow dynamics is determined by many factors which characterize the thermodynamics and kinetic properties of a medium, the flow regimes, geometry of the body, etc. If we attempt to find all of the dimensionless parameters which determine the flow, then for complex gas mixtures a more cumbersome system is obtained for these parameters than in the case examined above

of one-dimensional flows (see Section 3.2). Therefore, in problems of flow around bodies, methods are of great importance which are based on utilizing certain parameters (characteristic values) which play the role of parameters of approximate, particular similarity and which synthesize in themselves the basic relationships which reveal the influence of physico-chemical processes on the gas dynamic characteristics. These parameters may include universal parameters which are common for many classes of flows — for example, the energy parameter W, the compressibility factor Z, and the parameter $\varkappa_s=\left(\frac{\partial \ln p}{\partial \ln \rho}\right)_s$ (for more details, see Section 3.2) — and particular parameters which pertain to individual types of flows, for example, the parameter of the effective compression in a shock layer around blunt bodies, etc. (See Section 4.6). In the flow field of an ideal gas, these parameters are constant ($W=0, Z=1, \varkappa_s=\text{const}=c_p/c_v$). In an equilibrium flow, they are functions of the state. In a nonequilibrium flow, they are determined to a significant extent by the kinetic properties of the medium and the flow configuration, and they greatly differ from the values of these parameters in equilibrium and frozen flows.

/160

It is sometimes assumed, when determining the influence of nonequilibrium processes on flow dynamics, that the values of the gas dynamic parameters in a real nonequilibrium flow will lie in the region between their values in equilibrium and frozen flows. In some cases, this assumption makes it possible to establish the boundaries between which the parameters of nonequilibrium flows are located. However, this is not always the case. One example may be the flow around blunt cylinders and plates, when thermodynamic equilibrium is rapidly established close to the front of the front shock wave (in the region where the wave is close to a normal wave), and then there is a sharp freezing of the physico-chemical processes as the flow expands.

The necessity of taking into account nonequilibrium processes greatly complicates the mathematical description of the flows. The simple formulas which are frequently encountered in classical gas dynamics are almost completely lacking here. Even in those rare cases where analytical solutions can be obtained, it is difficult to analyze them, as a rule, due to the cumbersome nature of the expressions. Therefore, a knowledge of the basic characteristics of nonequilibrium flows should be obtained with the simplest models of nonequilibrium media, resorting to a qualitative analysis and approximate estimates in order to avoid cumbersome formulas and algorithms. Only the final results will be given for flows with complex kinetics. The interesting details of the calculations may be found in the original articles and special handbooks. We should now stress the fact that in the majority of cases, reliable quantitative results may only be obtained on the basis of precise numerical methods, with adequate allowance for the kinetic properties of the medium.

4.2 Laws of similarity in the case of hypersonic flow around slender bodies.

Let us examine hypersonic flow around slender bodies, when the perturbations introduced by the bodies into the flow are small (small as compared with the velocity head — for pressure, and the velocity of unperturbed flow — for velocity). In this case, the method of small perturbations is an effective method for solving the problems of gas dynamics for flows of an ideal gas and a gas in a state of thermodynamic equilibrium. The results obtained by this method, particularly the law of plane cross-sections (the principle of equivalence with unsteady flow considering a small number of measurements) and the law of similarity represent a very powerful method for an

experimental and theoretical investigation of hypersonic flows (for more details, see [1, 2, 3]).

The question then arises as to the extent to which these results may be applied to nonequilibrium flows. /161

The law of plane cross sections, and its generalization to the case of slender bodies at large angles of attack, given by the V. V. Sychev [4], and also the law of similarity which follows from this, remain in force for nonequilibrium flows. Physically, this is apparent, since the decisive characteristic which lies at the basis of the law of plane cross sections, is the approximate constancy of the gas velocity component along the body axis (which makes it possible to examine the flow in transverse cross sections). This characteristic is satisfied for slender bodies which move at hypersonic velocities, independently of the specific form of equation of state and the velocities of the physico-chemical processes.

It follows from a rigorous mathematical proof, which we shall not give here, that the error of the law of plane cross sections for nonequilibrium flows, just as in the classical case, will be on the order of ϑ^2 (ϑ — is a small parameter which characterizes the maximum angle of deviation of the velocity vector; the relative body thickness may be used as ϑ for steady flows).

Thus, in the case of nonequilibrium flows, if we disregard terms on the order of ϑ^2 as compared with unity, we arrive at the equations of the small perturbation method, which represent the exact equations for the corresponding unsteady flow in a plane. In essence, these equations are just as complex as the initial equations of stationary flows, and there are still no examples of their solutions obtained without any additional

simplifying assumptions. One assumption which simplifies the problem, in particular, may be the condition $\varepsilon \ll 1$, where ε is the ratio of the density in the unperturbed flow ρ_∞ to the density behind the shock wave (for an ideal gas $\varepsilon=\frac{\varkappa-1}{\varkappa+1}$). The methods for calculating such flows and the bibliographic references may be found, for example, in [1 and 2].

By means of the combined method based on the concurrent application of the law of plane cross sections and the method of the "thin shock layer" in [5], for example, a solution is given for the problems of the flow of gas with relaxation of vibrational degrees of freedom around a thin wedge and cone.

The solution is given in a form which is customary for this method, for example

$$p = p_1 + \varepsilon p_2 + \varepsilon^2 p_3 + \dots;$$
$$\rho = \rho_1/\varepsilon + \rho_2 + \varepsilon\rho_3 + \dots$$

etc. In the first approximation, the solution does not depend on the vibrational energy and is the same as for an ideal gas. A term caused by the nonequilibrium is not included in the solution of the second approximation for the pressure p_2 and the axial velocity component u_2. This means that p and u in this case are least sensitive to the influence of relaxation processes. One feature of the expression p_3 for a wedge and a cone lies in the fact that the pressure — in contrast, for example, to the density — changes in a non-monotonic manner in the relaxation process from a frozen state to an equilibrium state.

/162

Let us now turn to the law of similarity for hypersonic flow around slender bodies. This law follows from the equations of the small perturbation method, and it may be regarded as a direct result of the law of plane cross sections. The functional

dependence of gas dynamic parameters for steady flow around bodies, whose surface may be described by the following equation in a Cartesian (x, y, z) coordinate system connected with the body

$$f(\vartheta x,\ y,\ z)=0 \tag{4.17}$$

(a family of affinely similar bodies) has the form

$$p=p(\vartheta x,\ y,\ z;\ V_\infty\vartheta,\ \alpha/\vartheta,\ \rho_\infty,\ T_\infty), \tag{4.18}$$

where α is the angle of attack.

Similar expressions exist for the remaining gas dynamic functions and the aerodynamic coefficients, for example

$$c_y=\vartheta^2F(V_\infty\vartheta,\ L\vartheta,\ \alpha/\vartheta,\ \rho_\infty,\ T_\infty)^*. \tag{4.19}$$

For slender, three-dimensional bodies located in a flow at a large angle of attack, the parameters $V_\infty\vartheta$ and α/ϑ may be replaced by their generalized form $V_\infty\sin\alpha$ and ϑ ctg α [4]. When there is slight blunting, one similarity parameter appears

$$\lambda=c_x'(d/L)^{1+j}/\vartheta^{3+j}, \tag{4.20}$$

where c_x' is the effective bluntness drag coefficient**; d — characteristic bluntness dimension (thickness); j = 0 in the plane case and j = 1 in the axisymmetric case. (For more details see [1], Chapter V, or [2], Chapter II).

---

* Here, in the calculation of c_y, the force pertains to the body area.

** For calculation of c_x' see, for example, [3, 6, 7].

Relationship (4.18) represents a very general form following from the law of plane cross sections, and is only valid to the same extent that the law of plane cross sections is valid. Therefore, it may be applied both for an ideal gas and for a real gas in the case of equilibrium and nonequilibrium physico-chemical processes.

Attention should be called to the following two factors:

I. Formula (4.18) is only valid for one and the same medium with its individual thermochemical and kinetic properties. In the case of an ideal gas with constant heat capacity, the individual nature of the medium is characterized by a single parameter κ. The possibility of simulation in this case is extended not only to dimensions, form of the bodies, and velocity V_∞, but also to the medium.

In the general case, the possibility of simulating the media is excluded. The possibility only arises for gases, whose equation of state and equation of kinetics have certain special (self-modeling) properties which allow similarity. For example, /163 an ideal dissociating gas has such properties. The right to simulate a medium must be "paid for" by a large number of new similarity parameters (in the general case not only physical processes, but also the state of the unperturbed flow must be simulated. For more details, see, for example, [6]).

For certain simple gas models, the law of similarity may assume a simple form in the case of nonequilibrium flows. For example, for the model of vibrational relaxation which is characterized by the condition

$$c_{vk} = \text{const} \quad \text{and} \quad \tau = \text{const},$$

relationship (4.18) assumes the form

$$p=p\left(\vartheta x,\ y,\ z;\ \varkappa,\ c_{vk}/c_p,\ M_\infty\vartheta,\ \frac{V_\infty\tau}{L};\ \frac{a}{\vartheta}\right).$$

As compared with the case of an ideal gas, only two new similarity parameters occur here c_{vk}/c_p and $V_\infty\tau/L$. (In this example, the similarity is extended to the medium, i.e. the requirements that it is necessary to have one and the same gas in order to observe the similarity is eliminated here.)

II. The second comment pertains to the invariance of the equations when the linear scales are changed, i.e., the possibility of a geometrically similar transformation of the models with a change in their dimensions.

The equations of motion for ideal or equilibrium gases assume such a transformation in the absence of viscosity. This transformation is not possible in the case of dissipative processes, for example, caused by viscosity or nonequilibrium. This is due to the appearance of new dimensional quantities in the equations of gas dynamics and kinetics (in the case of nonequilibrium flows, the characteristic relaxation times are such quantities), from which we may form the dimensionless combinations $\frac{\tau_{i0}V_\infty}{L}$

i.e.

$$\frac{\tau_{i0}V_\infty}{L}\ (i=1.2,\ldots)\ \text{-similarity parameters} \quad (4.21)$$

In the general case, for similar flows the quantities τ_{i0} must be the same, since they are determined by the density, temperature and initial values of the parameters q_i. Therefore the ratio V_∞/L must be identical for such flows, and since $V_\infty\vartheta$ is the similarity parameter, this means that in the general case of nonequilibrium flows, which obey the functional law (4.18), the value of $L\vartheta$ must also be identical, i.e., / 164

$L\vartheta$ - similarity parameter (4.22)

Condition (4.22) means that in the general case of arbitrary nonequilibrium flows the affine similarity transformation must be accompanied by the necessary condition of conservation of transverse body dimensions ($L\vartheta$ characterizes the transverse dimension of the body).

Thus, in the general case of an arbitrary medium with nonequilibrium processes, the requirements of the hypersonic similarity law are not very exacting for varying certain parameters in model experiments or in comparing different flows.

Much greater practical advantages may be obtained from the similarity law in certain special cases or in the case of its approximate application. Thus, the number of similarity parameters is reduced, and, in the place of old parameters, certain new similarity parameters appear which make it possible to expand the simulation possibilities. For example, for pure two-atomic gases which dissociate according to the scheme $A_2 + B_2 \rightleftarrows 2\,AB$, i.e., when the forward and inverse reactions are binary (see Section 1.3), the gas equilibrium composition does not depend on pressure (density), and is always determined by temperature. Therefore, the density ρ_∞ may be excluded from the number of decisive parameters.

The relaxation time τ in gases in the case of such binary processes is inversely proportional to the density $\tau = \frac{f(T)}{\rho}$. Taking this relationship into account and utilizing the basic condition (4.21) of the constancy of the parameter $\tau V_\infty/L$, for binary processes, instead of two similarity parameters $L\vartheta$ and ρ_∞, we obtain one similarity parameter $\rho_\infty L\vartheta$ or $\frac{\rho_\infty L}{V_\infty}$, i.e.

$$\rho L\vartheta\left(\text{or } \frac{\rho L}{V_\infty}\right) - \text{similarity parameter for binary processes.} \qquad (4.23)$$

Similarly, for three-molecular reactions (reactions of the third order), the combination $\rho^2 L\vartheta$ could be the similarity parameter, etc.

In practice, gases are most frequently encountered which dissociate according to the scheme $AB + M \rightleftarrows A + B + M$, i. e., the forward reaction (dissociation) is of the second order and the inverse reaction (recombination) is of the third order. If recombination reactions can be disregarded in flows of these gases, the law of binary similarity $\rho_\infty L = \text{const}$ will be satisfied in these cases, although it is only approximately true. (The degree to which this law is approximated is usually verified by computations or experimentally). These gases include nitrogen, oxygen and air when the flow is far from an equilibrium flow. The applications of the binary similarity law will be discussed in greater detail in Section 4.6. /165

In conclusion, Table 13 shows the use of similarity laws in the case of flows around slender affinely similar bodies at small angles of attack. (See Table 13 on Page 214).

4.3 Nonequilibrium flows around a wedge and cone

Let us now turn to specific examples of flows, when the influence of nonequilibrium processes is apparent in the " purest " form. Let us examine supersonic flow around a wedge with an attached shock wave. The unperturbed flow may be both an equilibrium flow ($q_\infty = q_{e\infty}$) and a nonequilibrium flow ($q_\infty \neq q_{e\infty}$). (The latter is typical for experiments in hypersonic

TABLE 13

Characteristics of medium	Ideal gas	Arbitrary gas in equilibrium state	Arbitrary nonequilibrium gas	Nonequilibrium gas, obeying condition of binary similarity
Similarity parameters	$\varkappa$, $M_\infty\vartheta$, $\frac{\alpha}{\vartheta}$, λ $\left(\lambda=\frac{c_x'(d/L)^{j+1}}{\vartheta^{j+3}}\right)$	$V_\infty\vartheta$, $\frac{\alpha}{\vartheta}$, λ, T_∞, ϱ_∞	$V_\infty\vartheta$, $L\vartheta$, $\frac{\alpha}{\vartheta}$, λ, T_∞, ϱ_∞	$V_\infty\vartheta$, $\frac{\varrho_\infty L}{V_\infty}$, $\frac{\alpha}{\vartheta}$, λ, T_∞
Possibility of medium simulation	Possible	Impossible (only possible in certain cases, for example, for an ideal dissociating gas, and also in the case of partial simulation)		
Possibility of changing linear scales of models retaining geometric similarity	Possible	Possible	Impossible	Only possible when condition $\varrho_\infty L\vartheta=\text{const}$ is satisfied
Similarity parameters in limiting case of flow with very strong impact waves ($M\vartheta \gg 1$	$\varkappa$, $\frac{\alpha}{\vartheta}$, λ	$V_\infty\vartheta$, $\frac{\alpha}{\vartheta}$, λ, ϱ_∞	$V_\infty\vartheta$, $L\vartheta$, $\frac{\alpha}{\vartheta}$, λ, ϱ_∞	$V_\infty\vartheta$, $\frac{\varrho_\infty L}{V_\infty}$, $\frac{\alpha}{\vartheta}$, λ

/ 165

wind tunnels).

Let us select the characteristic relaxation length behind the shock wave $u_f\tau_f$ as the basic length scale (u is the velocity component along the wedge surface and the index "f" corresponds to frozen flow $\tau_f=\tau(p_v, T_f)$.

At distances $r \ll u_f\tau_f$ from the wedge apex (Region 1 in Figure 4.2), the flow will be close to frozen flow; in particular, /166 the shock wave inclination σ will equal σ_f — the angle of shock wave inclination in frozen flow.

It is apparent that far from the wedge apex (in the scale $u_f\tau_f$), independent of the local flow structure in Region 1 and in regions adjacent to it with the characteristic transverse dimension $u_v\tau_v$, the angle of the shock wave inclination will be similar to, and in the limit, equal σ_e — the angle of the shock wave inclination in equilibrium flow. Region 2 of nonequilibrium flow (relaxation layer) is adjacent to the shock wave. The width of this region will be on the order of $u_f\tau_f \sin(\sigma_e - \vartheta)$. In Region 3, which is far from both the shock wave and the wedge surface, the flow will be close to equilibrium flow, just as behind an oblique shock with the angle of inclination σ_e.

In Region 4, which is adjacent to the wedge surface, the pressure far from its apex must be the same as in Region 3, but it is not necessary that all the remaining flow parameters equal their values in Region 3 since, in the first place, the initial conditions in Regions 3 and 4 are different (different inclinations of the shock wave) and, in the second place, the entropy increases along the streamlines in these regions will also be different, since, for example, the laws governing the change in the transverse cross section of the streamtubes will be different.

The existence of these regions (layers) was first noted by V. N. Zhigulev [8], and later by several other authors [9, 10]. These layers are usually called relaxation entropy layers, although the term "entropy" may possibly not be felicitous, since it is usually associated with flows with very large relative changes in entropy, and in such layers the relative entropy change is small, as will be seen later. Therefore, it has been proposed [3] that these layers be called weak vorticity layers.

Let us establish the relative changes in temperature T, density ρ, velocity u, and entropy S in a relaxation entropy layer for flows, which are characterized by relatively small energy parameters W. The index "3" designates that the term belongs to Region 3, and the index w characterizes the parameters on the wedge surface far from its apex (both states are equilibrium states). Since the jet stream adjacent to the wedge surface passes through the shock wave at the angle of inclination σ_f, S_w equals $S_e(\sigma_f)$ — entropy in an equilibrium flow during the transition through an oblique shock wave at the angle σ_f plus a certain addition related to the fact that the law governing the change in the jet stream transverse cross section close to the wedge surface differs from the law governing the change in the jet stream in a flow with an infinite oblique shock wave with the angle of inclination σ_f. However, calculations show that if the relative change in the jet stream F is small (this is related to the small value of the parameter W), then in the first approximation such small variations in the area are not apparent in the entropy increase and $S_w \approx S_e(\sigma_f)$. Thus

$$\delta S = S_w - S_3 = S_e(\sigma_f) - S_e(\sigma_e),$$

where σS is the entropy change along the layer.

The quantities δT, $\delta \rho$ and δu are expressed by δS. Let us determine these values for the case of a slender wedge in a hypersonic gas stream with nonequilibrium excitation of the vibrational degrees of freedom. We shall assume that

$$\vartheta \ll 1; \quad K = \vartheta M_\infty \gg 1. \tag{4.24}$$

In this case, the internal gas energy is a function only of the temperature and since $p_w = p_3$, a $T_w - T_3 \ll T_3$ (due to the smallness

of W), we have

$$\delta S = c_V \ln \frac{p_w/p_3}{(\rho_w/\rho_3)^{\varkappa}} + \int_{T_3}^{T_w} c_{Vk} \frac{dT}{T} \approx -\varkappa c_V \frac{\rho_w - \rho_3}{\rho_3}. \qquad (4.25)$$

Carrying out the calculations within an accuracy of terms of the order ΔW, where

$$\Delta W = \frac{e_k(T_3) - e_{k\infty}}{c_p T_3}, \qquad (4.26)$$

/168

we obtain

$$\left.\begin{aligned}
\delta\bar{S} &= (S_w - S_3)/c_V = \frac{2(\varkappa-1)\varkappa}{(\varkappa+1)}\Delta W;\\
\delta\bar{\rho} &= \frac{\rho_w - \rho_3}{\rho_3} = -\frac{2(\varkappa-1)}{(\varkappa+1)}\Delta W;\\
\delta\bar{T} &= \frac{T_w - T_3}{T_3} = -\delta\bar{\rho} = \frac{2(\varkappa-1)}{\varkappa+1}\Delta W;\\
\delta\bar{u} &= \frac{u_w - u_3}{u_3} = -\frac{\varkappa(\varkappa-1)\vartheta^2}{\varkappa+1}\Delta W.
\end{aligned}\right\} \qquad (4.27)$$

If the unperturbed flow is in a state of equilibrium, then $0 < \Delta W < \frac{R}{c_p} = \frac{\varkappa-1}{\varkappa}$. Therefore, for flows with vibratory relaxation, the relative drops in density, temperature, and velocity in the relaxation entropy layer are small. The density and velocity decrease across the relaxation entropy layer in the direction of the wall, and the temperature increases.

Let us establish the characteristic width of this layer, i.e., the distance in the direction perpendicular to the wedge surface, at which the quantity $\rho_3 - \rho_w$ will be on the order of $\rho - \rho_w$. We shall use the fact that the characteristic relaxation length is on the order of $d = u_f \tau_f$. It follows from this that the characteristic distance l along the shock wave from the wedge apex, at which there is a change in the angle of inclination for the shock wave from σ_f to σ_e, is determined by the

intersection with the shock wave of characteristics drawn from the region on the wedge surface, located at a distance on the order of d from its apex. Knowing the angles σ_f, σ_e and the number M_f behind the shock wave (when $M_\infty \gg 1$ the value $M_f \approx \frac{1}{\vartheta}\sqrt{\frac{2}{\varkappa(\varkappa-1)}}$), we may determine the characteristic thickness of the relaxation layer σ (Figure 4.3).

We have $\gamma \approx \frac{\varkappa-1}{2}\vartheta$, $\alpha = \frac{1}{M_f} = \vartheta\sqrt{\frac{\varkappa(\varkappa-1)}{2}}$,

$$\beta = \alpha - \gamma \approx \vartheta\left(\sqrt{\frac{\varkappa(\varkappa-1)}{2}} - \frac{\varkappa-1}{2}\right);\ l \approx \frac{d\gamma}{\beta};\ \delta' = l\alpha \approx \frac{d\gamma\alpha}{\beta}$$

(the notation is given in Figure 4.3), and thus

$$\delta \approx \delta' \approx u_f \tau_f \vartheta\varepsilon \frac{1}{1-\sqrt{\varepsilon}},$$

where

$$\varepsilon = \frac{\varkappa-1}{\varkappa+1}. \qquad (4.28)$$

It may be approximately assumed that the law governing the change in the flow parameters across the layer is exponential, namely /169

$$\rho = \rho_3 + (\rho_w - \rho_3)e^{-y/\delta} = \rho_3(1 + \bar{\delta}\rho e^{-y/\delta}). \qquad (4.29)$$

The basic characteristics described above will be repeated in other nonequilibrium flows. Naturally, these determinations give only a very general representation of the characteristics of nonequilibrium flows around pointed bodies.

The flow characteristics of a relaxing gas around pointed bodies are greatly clarified by a solution of the problem regarding the flow of gas around a wedge with nonequilibrium excitation of the vibrational degrees of freedom, which was obtained by V. N. Zhigulev [8] by linearization according to the small parameter*

$$W_1 = e_k(T_f)/c_p T_f. \tag{4.30}$$

The basic solution with which the linearization was carried out was the solution for the flow of an ideal gas around a wedge in the case of frozen vibrational degrees of freedom (the index "f"). This solution, which changes into an exact solution when $W_1 \to 0$, in the (x, y) Cartesian coordinate system (see Figure 4.2, $\bar{x}=x/u_f\tau_f$, $\bar{y}=y/u_f\tau_f$) may be written in the form

/170

$$\left.\begin{aligned}
\bar{p} &= \frac{p-p_f}{W_1\rho_f u_f^2} = A\left\{\operatorname{tg}\gamma\left(1-e^{-\bar{x}+\bar{y}\operatorname{ctg}\gamma}\right)-\nu+\right.\\
&\left.+\frac{1}{\mu}\left[e^{-\bar{x}+\mu\bar{y}}+2\sum_{l=1}^{\infty}(-s)^l e^{-\bar{x}m^l}\operatorname{ch}(\mu\bar{y}m^l)\right]\right\};\\
\bar{v} &= v/W_1 u_f = -A\left[e^{-\bar{x}+\bar{y}\operatorname{ctg}\gamma}+e^{-\bar{x}-\mu\bar{y}}-\right.\\
&\left.-2\sum_{l=1}^{\infty}(-s)^l e^{-\bar{x}m^l}\operatorname{sh}(\mu\bar{y}m^l)\right];
\end{aligned}\right| \tag{4.31}$$

*If the advancing flow is nonequilibrium flow, i.e., $e_{k\infty}\neq 0$ then the method and the solution are the same as before. In this case, the small parameter will not be W_1, but $\Delta W = W_1 - W_\infty$, where $W_\infty = e_{k\infty}/c_p T_f$. An analysis of this case is given by A. V. Chirikhin [11].

$$
\left.
\begin{aligned}
&\bar{u}=\frac{u-u_f}{W_1 u_f}=F(\bar{y})-\bar{p};\\
&F(\bar{y})=\frac{1+k\,\mathrm{tg}\,\gamma}{k}\,\frac{1}{\mu}\,\frac{1}{(1-\mu^2\,\mathrm{tg}^2\,\gamma}\times\\
&\times\left[-\mu\nu+e^{-\bar{y}(\mathrm{ctg}\,\gamma-\mu)}+2\sum_{l=1}^{\infty}(-s)^l\,e^{-\bar{y}(\mathrm{ctg}\gamma m^l}\right];\\
&\bar{T}=\frac{T-T_f}{W_1 T_f}=(\varkappa-1)M_f^2(\bar{p}-F(\bar{y}))-\bar{e}_k;\\
&\bar{\rho}=\frac{\rho-\rho_f}{W_1\rho_f}=\varkappa M_f^2\bar{p}-\bar{T};\\
&\bar{e}_k=\frac{e_k}{W_1 c_p T_f}=1-e^{-\bar{x}+\bar{y}\,\mathrm{ctg}\,\gamma}.
\end{aligned}
\right\}
\qquad (4.31)
$$

Here

$$
\left.
\begin{aligned}
&A=\frac{\mathrm{tg}\,\gamma}{1-\mathrm{tg}^2\,\gamma\mu^2};\quad s=\frac{1-\mu\nu}{1+\mu\nu};\quad m=\frac{1-\mu\,\mathrm{tg}\,\gamma}{1+\mu\,\mathrm{tg}\,\gamma};\\
&\nu=\frac{2\varepsilon\,\mathrm{ctg}\,\gamma-(1-\varepsilon)(\varkappa-1)M_f^2\sin\gamma\cos\gamma}{\varkappa M_f^2(\sin^2\gamma+\varepsilon\cos^2\gamma)-1+\varepsilon\,\mathrm{ctg}^2\,\gamma-(\varkappa-1)M_f^2};\\
&k=\frac{2\varepsilon-(1-\varepsilon)(\varkappa-1)M_f^2\sin^2\gamma}{\varkappa M_f^2(1-\varepsilon)\sin^2\gamma-1-\varepsilon};\quad \varepsilon=\rho_\infty/\rho_f.
\end{aligned}
\right\}
\qquad (4.32)
$$

It may be readily established that when $\bar{x}\to\infty$ and for finite $\bar{y}$, the quantity $\bar{p}$ strives to a constant limit

$$
\bar{p}_{x\to\infty}=\frac{\mathrm{tg}^2\,\gamma-\nu\,\mathrm{tg}\,\gamma}{1-\mu^2\,\mathrm{tg}^2\,\gamma}. \qquad (4.33)
$$

The expression for $F(\bar{y})$ shows that there is a vortex layer close to the wedge surface whose thickness is on the order of the characteristic relaxation length $u_f\tau_f$. With an increase in /171 the M_∞ number, the layer thickness decreases. An analysis of expressions (4.31) confirms the flow picture which was described at the beginning of the section (Figure 4.4).

The pressure only changes in the relaxation layer zone behind the shock wave. In the case of large $\bar{x}$, the remaining values remain functions only of $\bar{y}$, and outside of the relaxation, boundary entropy layer the flow is practically uniform.

Figure 4.5 gives graphs of the normalized pressure increase $(p - p_f)/W_1 p_f$ along the wedge surface for $\kappa = 1.4$. We should note that the dependence of $p - p_f$, $u - u_f$ and $\sigma - \sigma_f$ (which is close to a linear dependence) on the parameter W will only hold for very small values of W. With an increase in W (here we have in mind the more energetic processes: dissociation, etc.), there is a very rapid slow down of the increase and of stabilization $p - p_f$, $u - u_f$, as well as the angle of inclination of the shock wave σ. Thus, p, u, and σ greatly differ from T and ρ, for which there is no such stabilization.

In order to obtain precise quantitative results, even in the simplest cases of a wedge and a cone, we must turn to numerical computational methods. The results obtained by the method of characteristics for nitrogen with vibrational relaxation, an ideally dissociating gas, and air, as well as a discussion of certain methods of calculating supersonic nonequilibrium flows may be found in [9 — 25].

The distribution of the gasdynamic parameters in the flow /172
field around a cone is just the same as around a wedge, with the exception of a decrease of the thickness of the relaxation entropy layer with an increase in x, and the effect of "re-expansion" of the flow, close to which the pressure strives to its asymptotic value nonmonotonically (Figure 4.6) [13] (compare with the distribution of p in the case of flow around a wedge for small angles ϑ, Figure 4.5a). The change in T and ρ along the surface of the wedge and the cone in air is shown in Figure 4.7 [15].

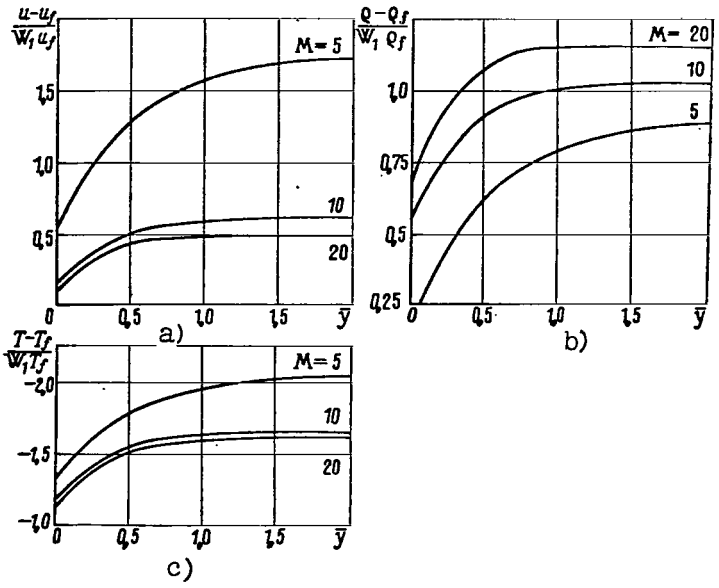

Figure 4.4. Characteristics of entropy relaxation layer when x = ∞.
a - velocity profile;
b - density profile;
c - temperature profile.

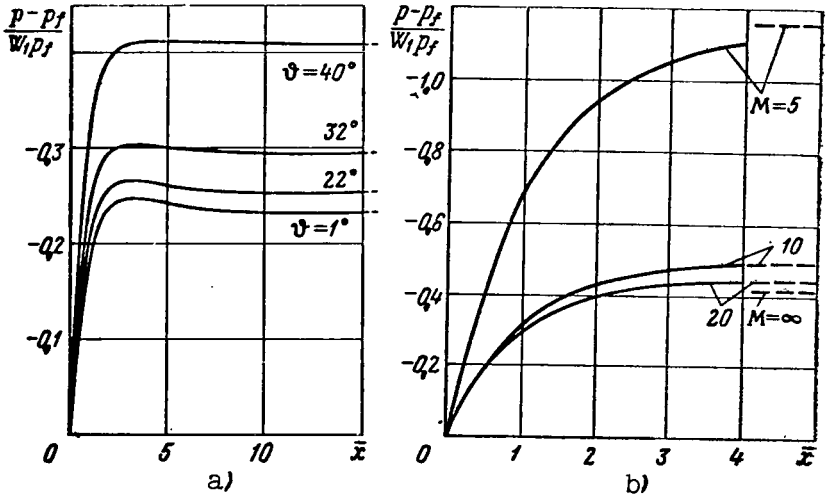

Figure 4.5 Change in pressure coefficient along the wedge surface (dashed line asymptotic values when $\bar{x} \to \infty$):
a — when M = ∞; b — when ϑ = 40°.

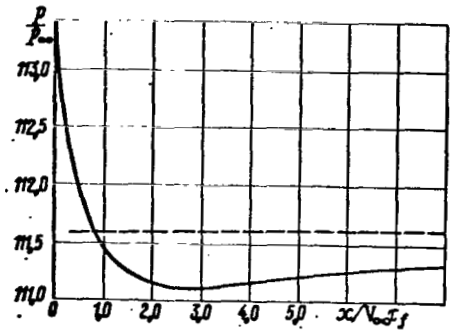

Figure 4.6. Pressure distribution along cone surface in a stream of nitrogen with vibratory nonequilibrium when ϑ = 46.4°; M_∞= 12; T_∞ = 300K (dashed line — equilibrium flow)

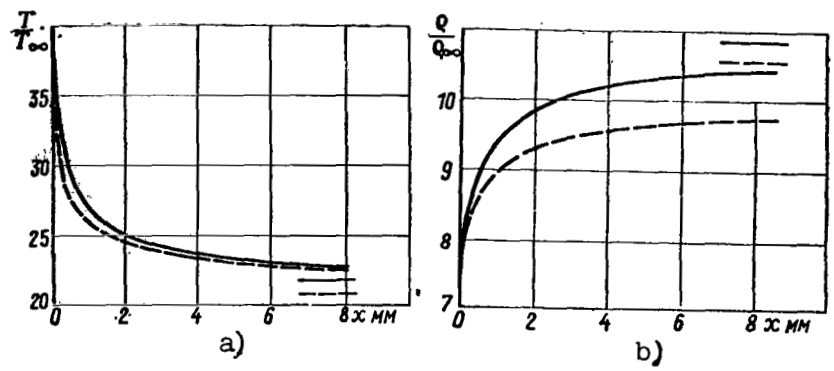

Figure 4.7. Temperature change (a) and density change (b) along wedge surface (dashed line, ϑ = 41.04°) and along a cone (solid line ϑ = 45.43°) in air (vibrations are balanced) when V_∞ = 6638 m/sec: the dotted lines designate the asymptotic values when $x \to \infty$.

Figure 4.8 [15] gives data which show that, when an air stream passes around a wedge, the binary law of similarity is valid in the major portion of the flow field. In spite of the fact that the pressure on the wedge and the cone depends slightly on nonequilibrium processes, in certain cases their influence may be considerable. For example, the aerodynamic characteristics of the wedge c_y^α and m_z^α, and the position of the pressure center X_p, may fall outside of the limits within which they change in equilibrium and frozen flows [26, 27]. The displacement of X_p is connected exclusively with the influence of nonequilibrium, and in certain cases may be on the order of one percent of the wedge length. /173

4.4. Characteristics of the propagation of small perturbations in a relaxing medium. Notes on methods of calculating nonequilibrium flows around slender pointed bodies /174

In addition to the method of characteristics and other similar computational methods, other methods, which were developed for ideal gas flows, are widely used in the gas dynamics of nonequilibrium flows. In particular, this pertains to the linearization method based on the smallness of perturbations of the basic homogeneous flow. The problem of the propagation of sound is a classical example [28 — 33].

Let us consider a plane, monochromatic sonic wave propagated in a fixed medium, which is characterized by a single relaxation parameter q. Let us represent p, ρ, etc., in the wave in the form of a constant term corresponding to the state of the unperturbed medium, and a small perturbation: $p = p_0 + p'$,

$\rho = \rho_0 + \rho'$, $q = q_0 + q'$, and $u = u_0 + u' = u'$.

Taking the fact into account that $h(p, \rho, q) = h_0 + h_p p' + h_\rho \rho' + h_q q'$ and $q_e = q_0 + q_{e\rho}\rho' + q_{ep}p'$, from Equations (4.1) — (4.6) we obtain a system of linear homogeneous equations with respect to the small quantities u', p', ρ', and q' [Equation (4.6) is taken in the form of (3.59)]. The time t and the coordinate x are the independent variables. If we search for the solution in the form $p' = p_0' e^{i(\omega t + kx)}$, $q' = q_0' e^{i(\omega t + kx)}$, etc., where p_0', q_0', etc., are constants, as a result of substituting these expressions in the system of linear equations obtained, we obtain a system of linear homogeneous algebraic equations with respect to the amplitudes p_0', q_0', etc., which has a nontrivial solution only if its determinant Δ equals zero.

Equating Δ to zero, we obtain the following relationship, which connects ω and k

$$\frac{\omega^2}{k^2} = \frac{-h_\rho(1 + i\omega\tau) - h_q q_{ep}}{\left(h_p - \frac{1}{\rho}\right)(1 + i\omega\tau) + h_q q_{ep}}. \qquad (4.35)$$

All the terms in the right side of this equation are calculated by definition in an unperturbed state, for example, $h_\rho = \frac{\partial h(p_0, \rho_0, q_0)}{\partial \rho}$, etc. It may be seen from (4.35) that when $\tau \neq 0$ and $\tau \neq \infty$, the ratio ω^2/k^2 represents a complex quantity, and since ω is a real quantity, the wave number k must be a complex number.

Representing k in the form $k = k_1 - k_2$ (k_1, $k_2 > 0$) and setting $\omega/k_1 = a$, we obtain

$$p' = p_0' e^{i\omega\left(t - \frac{x}{a}\right)} e^{-k_2 x}, \quad u' = u_0' e^{i\omega\left(t - \frac{x}{a}\right)} e^{-k_2 x}$$

etc. It may be seen from these expressions that the quantity a, which equals ω/k_1, is the phase velocity of sound in terms of its physical meaning, and k_2 is the absorbtion coefficient. In the limiting cases of high frequency ($\omega\tau \to \infty$) and low frequency ($\omega\tau \to 0$) sonic vibrations, the expressions for the speed of sound assume the form (2.52) and (2.53).

If the state of the gas depends on several parameters q_i, then

$$a_f^2 = -\frac{h_\rho}{h_p - 1/\rho}; \quad a_e^2 = \frac{-h_\rho - \sum_i h_{q_i} \frac{\partial q_{ei}}{\partial \rho}}{h_p - \sum_i h_{q_i} \frac{\partial q_{ei}}{\partial p} - \frac{1}{\rho}} = \frac{-\bar{h}_\rho}{\bar{h}_p - \frac{1}{\rho}}, \qquad (4.36)$$

where

$$\bar{h}(p, \rho) = h(p, \rho, \langle q_{ei}(p, \rho) \rangle).$$

It may be shown that these expressions are identical to the /175 relations

$$a_f^2 = \left(\frac{\partial p}{\partial \rho}\right)_{s,q} \quad \text{and} \quad a_e^2 = \left(\frac{\partial p}{\partial \rho}\right)_{s, q=q_e}$$

In the general case, when the parameter $\omega\tau$ is a finite quantity and does not equal zero, the phase velocity of sound a and the absorbtion coefficient k_2 depend on the frequency ω.

When $\omega\tau \gg 1$, we obtain the following from Expressions (4.35) and (4.36)

$$a = a_f[1 + O(\varepsilon)^2)]; \quad k_2 = \frac{a_f^2 - a_e^2}{a_f^2} \frac{1}{2a_f\tau +} [1 + O(\varepsilon^2)], \qquad (4.37)$$

where

$$\varepsilon = (\omega\tau)^{-1};\quad \tau^{+} = \tau\frac{a_e^2}{a_f^2}\frac{h_\rho}{h_\rho + h_q q_{e\rho}} \sim \tau. \tag{4.38}$$

Thus, the rate at which sonic perturbations of the frequency ω are propagated when $\omega\tau \gg 1$ in the first approximation equals the frozen speed of sound a_f, and the absorbtion coefficient k_2 is inversely proportional to τ and does not depend on the frequency.

When $\omega\tau \ll 1$,

$$a = a_e(1 + O[(\omega\tau)^2]);\ k_2 = \frac{a_f^2 - a_e^2}{a_e^2}\frac{\omega^2\tau^{+}}{2a_e}(1 + O[(\omega\tau)^2]), \tag{4.39}$$

i.e., $a \approx a_e$, and the coefficient k_2 is proportional to $\omega^2\tau$. It follows from these relationships that at a distance which equals the characteristic relaxation length $d = a_f\tau$, the nature of the sound absorbtion varies, depending on the value of $\omega\tau$.

High frequency perturbations ($\omega\tau \to \infty$) are absorbed most rapidly: $k_2 d \approx \frac{a_f^2 - a_e^2}{2a_f^2}$; low frequency perturbations ($\omega\tau \to 0$) are propagated practically without damping.* This is a very important result. It enables us to understand the law governing the propagation of small perturbations in the supersonic flow of a relaxing gas. If the perturbation may be represented in the form of a Fourier series (integral), then the high-frequency harmonics

*Sometimes, instead of $k_2 d$, use is made of the parameter $k_2\lambda$ — the absorbtion coefficient at a distance equal to the wavelength λ: $k_2\lambda = \pi\alpha\omega\tau^{+}[1 + (\omega\tau^{+})^2]^{-1}(1 + O(\alpha))$, $\alpha = (a_f^2 - a_e^2)/a_f^2$. The quantity $k_2\lambda$ when $\omega\tau \to 0$ and $\omega\tau \to \infty$ strives to zero and has a maximum when $\omega\tau^{+} \approx 1$.

(a Mach cone with the largest angle opening corresponds to them) are damped most rapidly, and the low frequency harmonics, which are grouped around a cone with the angle arcsin (a_e/U_∞), are damped most slowly. Distortion of the signal thus occurs.

If it is assumed that the perturbation source (profile, etc.) lies on the y = 0 axis, then the perturbation passing from it to a certain point (x, y) is comprised of perturbations which arise at different points of the y = 0 axis, and thus the averaged value of the initial perturbation is transmitted to the point (x, y).

Interesting results in the study of the general properties of the linear equation

$$d_\infty \frac{\partial}{\partial x}\left[\left(M_{f\infty}^2-1\right)\frac{\partial^2\varphi}{\partial x^2}-\frac{\partial^2\varphi}{\partial y^2}-\frac{\partial^2\varphi}{\partial z^2}\right]+ \\ +\left(M_{e\infty}^2-1\right)\frac{\partial^2\varphi}{\partial x^2}-\frac{\partial^2\varphi}{\partial y^2}-\frac{\partial^2\varphi}{\partial z^2}=0, \qquad (4.40)$$

where /176

$$M_{f\infty}=U_\infty/a_{f\infty};\quad M_{e\infty}=U_\infty/a_{e\infty};\quad d_\infty=U_\infty\tau^+,$$

were obtained when solving several specific problems by Ye. V. Stupochenko and I. P. Stakhanov [34 — 37], and also Chu, Clarke, and Vincenti [32, 33, 38 — 40].

The Laplace transform is usually used to solve Equation (4.40), and the problem is essentially reduced to finding the inverse of the Laplace transform. As a rule, the solution has a rather cumbersome form, but the fact that it is represented in an analytical form makes it possible to study comparatively easily the flow characteristics, particularly its asymptotic behavior.

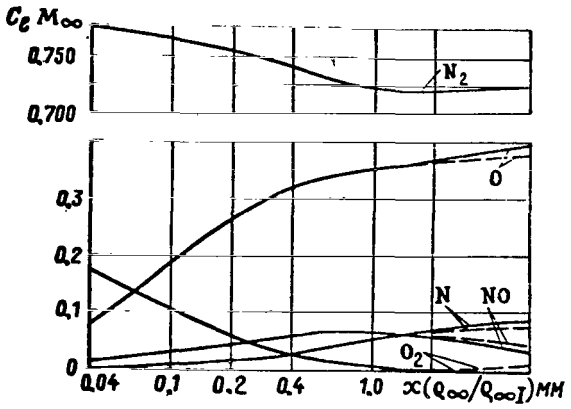

Figure 4.8. Change in concentration of components along wedge surface in air (vibrations are balanced) when M_∞ = 20; T_∞ - 273.16K; ϑ = 41.04° (solid lines designate coinciding values when $\rho_\infty = \rho_{\infty 1}$ = 0.01293 kg/M^3 and ρ_∞ = 0.5 $\rho_{\infty 1}$, and the dashed lines - when ρ_∞ = 10 $\rho_{\infty 1}$)

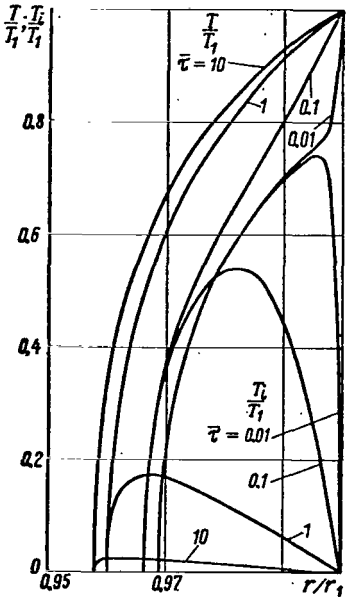

Figure 4.9. Change in temperature of active (T) and internal (T_i) degrees of freedom across shock layer for the two-dimensional problem (self-modeling solution).

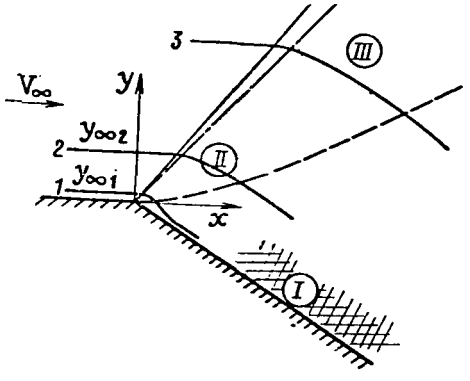

Figure 4.10. Diagram of flow around convex corner. (Solid line - first frozen line of perturbations; dot dash line - first equilibrium line of perturbations; dashed line - closed characteristic of the first family in a rarefaction fan):
1,2,3 - streamlines; I - region of slightly eddying flow; II - relaxation region; III - region of Prandtl-Meyer equilibrium flow.

The studies [41 — 53] were devoted to investigating different steady and unsteady flows in the case of one or several nonequilibrium processes. Attention should be called to the modification of the linear theory proposed by A. N. Krayko and R. A. Tkalenko [54]. The modification consists of changing to new dependent and independent variables, so that in these variables the coefficients in the precise equations subject to linearization become slowly changing functions of the unknown quantities. This greatly widens the possibilities of using the linear theory.

The solutions of different self-modeling problems occupy an important position in classicial gas dynamics. These problems represent a rare exception for nonequilibrium flows due to the appearance of several new dimensional constants. Let us discuss one class of one-dimensional unsteady motions of a relaxing gas which occurs when the energy equation and the relaxation equation have the form

$$e = c_V T + c_{Vi} T_i; \quad \frac{dT_i}{dt} = \frac{T - T_i}{\tau},$$

where c_v, c_{v_i} and τ are constants.

For such a gas model, the system of equations of gas dynamics and the conditions on the shock wave when $p_\infty = 0$ assume the following class of self-modeling motions, found by V. N. Zhigulev

$$\begin{gathered} \rho \sim e^{Ct} G(\xi); \quad p \sim e^{(C+2k)t} P(\xi); \\ u \sim e^{kt} V(\xi); \quad T \sim e^{2kt} H(\xi); \quad T_i \sim e^{2kt} H_i(\xi), \end{gathered} \tag{4.41}$$

where the self-modeling variable ξ is proportional to re^{-kt} (r — coordinate, C and k — constants). In particular, this class of

motions includes the motion of a gas expelled by a piston according to the exponential law $u_w = u_0 e^{kt}$, $-\infty < t < \infty$, $u_0 =$ const (in this case $C = 0$).

The study [55] investigated a system of ordinary differential equations, and gave the results of calculating u, p, ρ, T, and T_i for planar and axisymmetric motions. By way of an example, Figure 4.9 gives the temperature distribution across the shock layer for different values of the parameter $\bar{\tau} = k\tau$ (two-dimensional problem). According to the hypersonic law of plane cross sections, these results may be used to analyze the flow around certain planar and axisymmetric bodies. /177

4.5. Supersonic flow past a convex corner (Prandtl-Meyer Flow)

The influence of nonequilibrium is manifested in all flows where there is a rapid change in the gas state. These flows include steady, supersonic flow around a convex corner, and its unsteady analog — flow in a centered rarefaction wave. In the classical case, these solutions represent simple waves, i.e., flows in which the propagations are propagated only in one direction, and — in view of the self-modeling nature of these flows — their mathematical investigation is reduced to solving ordinary differential equations.

Simple waves cannot exist in a relaxing medium. Perturbations, which are initially propagated in one direction, passing through the vortex layers, are reflected backwards, which leads to a more complex flow structure.

Let us examine the general picture of flow around a blunt corner. Let us follow (Figure 4.10) the manner in which the flow parameters change along three streamlines. The first streamline is located close to the wall ($y_{\infty 1} \ll a_\infty \tau_\infty$); the second — at the distance $y_{\infty 2}$ from the wall ($y_2 \sim a_\infty \tau_\infty$); and the third — far from the wall $y_{\infty 3} \gg a_\infty \tau_\infty$.

Along the first streamline, the flow in the rarefaction fan will be close to frozen, and the relaxation zone with the characteristic dimension u'τ' is extended farther (the prime designates the values on the closing characteristic of the first family drawn from the apex of the corner), in which the flow parameters approximate their asymptotic values when $x \to \infty$. It is apparent that the pressure when $x \to \infty$ in the entire flow region is identical and equals the pressure p_e in the equilibrium flow.

Along the third streamline (the length of an arc along this streamline in the rarefaction fan is much greater than the characteristic relaxation length u_τ), the flow parameters will change in the same way as in equilibrium flow, i.e., in an "equilibrium" simple Prandtl-Meyer fan.

The second streamline lies in the region of nonequilibrium flow. The characteristics of nonequilibrium flows around a corner can be clearly seen (Figure 4.11a) when solving this problem in the linearization formulation [32]. (An analog of the results for ideal gas flows, which are given in Figure 4.11a, is the linearized solution, in which p, ρ, and other parameters change abruptly on the characteristic of the first family going from the corner apex, and not the precise solution, in which p, ρ, etc., change smoothly in the rarefaction fan.)

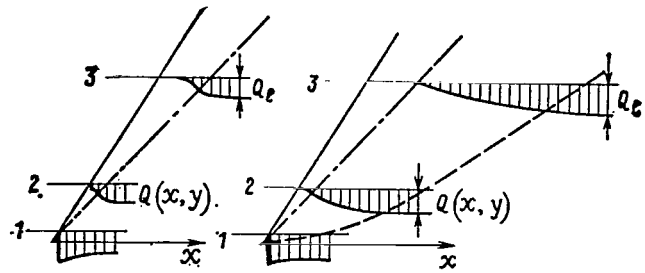

Figure 4.11. Schematic nature of the change in the gas dynamic parameters along three streamlines (solid lines — first frozen line of perturbations; dashed-dotted line — first equilibrium line of perturbations; dashed line — closing characteristic of the first family).

a — according to linear theory; b — according to an exact solution; Q — any gasdynamic parameter; 1, 2, 3 — streamlines.

Figure 4.11b shows schematically the change in the gas dynamic parameters along three typical streamlines, which follow from the precise solutions. There is a vortex layer close to the wall at a great distance from the corner apex. Calculations show that the change in T, ρ, S, and other parameters is small across this layer.

At the present time, there are a great many studies which have investigated the Prandtl-Meyer flow, a centered rarefaction fan, and other flows similar to it [38, 56 — 65]. Figures 4.12 — 4.14 show the distribution of pressure, temperature, and the degree of dissociation α along the wall for an ideal dissociating gas for the following initial data: M = 2, $p_\infty/R_{A_2}T_d\rho_d = 0.87\cdot10^{-8}$, $T_\infty/T_d = 0.06$ [56]. The dimensionless /179 coordinate $\bar{x} = xC\rho_d/\sqrt{R_{A_2}T_d}$ is given along the abscissa axis (C is the constant in the expression for the dissociation rate, and s is assumed to equal zero, see Chapter 2), and along the ordinate axis

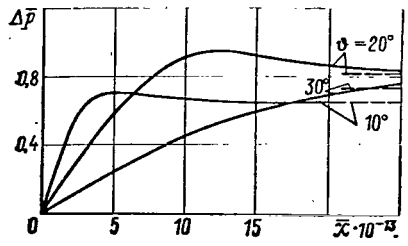

Figure 4.12. Pressure change along wall (dashed line — asymptotic values $\Delta\bar{p}(\infty) = \Delta\bar{p}_e$).

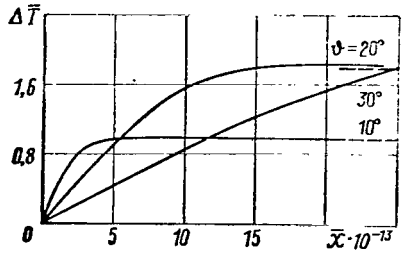

Figure 4.13. Temperature change along wall.

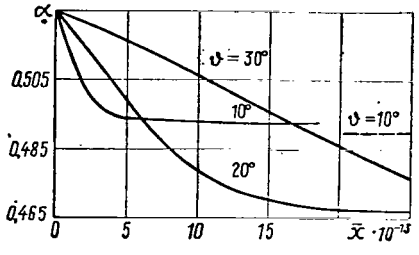

Figure 4.14. Change in degree of dissociation α along wall.

$$\Delta p = \{[p - p(0)]/R_A T_d \rho_d\}\, 10^9$$

and

$$\Delta\bar{T} = \{[T - T(0)]/T_d\}\, 10^2$$

p(0) and T(0) are the initial values at the wall.

In contrast to the relative difference [p - p(0)]/p(0), the absolute pressure difference p - p(0) changes nonmonotonically as a function of the angle ϑ, since when $\vartheta \to 0$ the difference (p - p(0)) → 0 due to the small influence of nonequilibrium processes, and at the corner ϑ, which is close to the limiting value, p and p(0) strive to zero due to the large flow expansion.

In several studies, analytical solutions of the problem of flow around a blunt corner are obtained under certain assumptions [38, 58, 63]. Thus, V. P. Stulov [58] for the model of an ideal dissociating gas obtained a solution in the region close to the corner apex without any limitations on ϑ. (The solution was found in the form of the series $\varphi = \varphi_f(1 + r\varphi_1 + r^2\varphi_2 + \ldots)$, where φ_f is the solution for frozen flow.)

An approximate solution in the region between the last characteristic of the rarefaction fan and a side of the corner was obtained in the same way. It was shown that in a relaxing gas the discontinuity of normal derivatives on the initial frozen characteristic is damped very rapidly with increasing distance from the apex (according to a law which is almost an exponential law).

When there is abrupt flow expansion, frequently it is rapidly frozen, and in the first approximation all of the flow may be assumed to be frozen, which is characterized by a constant adiabatic index κ_f. In this frozen flow, the gas dynamic parameters may differ greatly from their equilibrium values. /180

Typical results derived from comparing equilibrium and frozen air flows during flow around a corner are given in Figure 4.15 [33] ($\Delta\vartheta$ — flow angle of turn). It may be noted that the nonequilibrium processes have a great influence on the pressure and temperature just as in the case of flow in a nozzle.

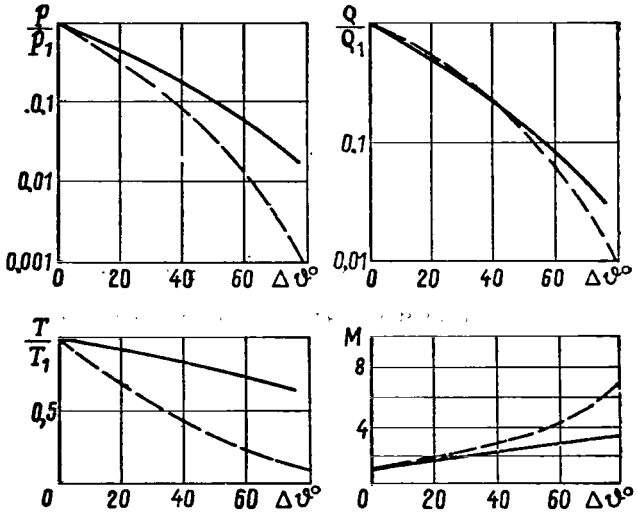

Figure 4.15. Comparison of parameters of equilibrium and frozen flows of air passing around a corner at $M_1 = 1$; $T_1 = 6140$ K; $p_1 = 1.2$ kG/cm^2.

4.6. Flow around blunt bodies

Typical characteristics

Nonequilibrium flow around blunt bodies has been studied in great detail both with the example of the simplest models of nonequilibrium media [67 — 69], and for gas mixtures with complex kinetics (air and others) [70 — 107]. The following typical characteristics of nonequilibrium flow around blunt bodies may be noted.

1. The great influence of nonequilibrium processes on temperature, density, concentration of components in the shock layer, and also on the shock wave stand-off distance from the body surface. /181

2. Nonequilibrium processes have a different influence on the pressure in different regions of the flow field: slight — close to the front body surface, and strong — in regions of considerable flow expansion.*

3. A large change in the state of the flow in the shock layer — from almost equilibrium flow to almost frozen flow.

4. Differing types of relaxation layers — regions with large gradients of gas dynamic parameters.

Let us discuss these characteristics in greater detail. For example, let us determine the influence of nonequilibrium processes on the pressure in the shock layer at the front

*We have in mind here bodies with a great change in the surface angles of inclination.

surface of a body. When $M \gg 1$, the pressure behind the shock wave p_1 and at the critical point p_0' will be determined by the following relationships:

In the flow of an ideal gas (index "f")

$$p_{1f} \approx \rho_\infty V_\infty^2 (1-\varepsilon_f); \quad p_{0f}' \approx \rho_\infty V_\infty^2 \left(1 - \frac{\varepsilon_f}{2}\right); \quad \varepsilon_f = \frac{\rho_\infty}{\rho_{1f}} \approx \frac{\varkappa - 1}{\varkappa + 1}; \qquad (4.42a)$$

In equilibrium flow (index "e")

$$p_{1e} \approx \rho_\infty V_\infty^2 (1-\varepsilon_e); \quad p_{0e} \approx \rho_\infty V_\infty^2 \left(1 - \frac{\varepsilon_e}{2}\right);$$
$$\varepsilon_e = \frac{\rho_\infty}{\rho_{1e}} \approx \frac{h_1 - e_1}{h_1 + e_1}; \qquad (4.42b)$$

In nonequilibrium flow

$$p_1 \approx \rho_\infty V_\infty^2 (1-\varepsilon_f); \quad \rho_\infty V_\infty^2 \left(1 - \frac{\varepsilon_f}{2}\right) < p_0' < \rho_\infty V_\infty^2 \left(1 - \frac{\varepsilon_e}{2}\right); \qquad (4.42c)$$

Thus, it may be assumed that the pressure in the shock layer in front of the body depends slightly on the state of the flow and

$$p \approx \rho_\infty V_\infty^2 \qquad (4.43)$$

(for more details see [120, 121]).

The picture will be different for temperature and density. In nonequilibrium flow, the temperature along the critical streamline changes from T_{1f} at the shock wave to $T_0' = T_e(H, p_0')$ at the critical point, where $H = h_\infty + V_\infty^2/2$ is the braking enthalpy.

For T_{1f}, we have /182

$$T_{1f}=\frac{h_1}{c_{p\infty}}\approx\frac{V_\infty^2(1-\varepsilon^2)}{R}M_\infty\frac{\varkappa-1}{\varkappa};\quad \varepsilon=\frac{\varkappa-1}{\varkappa+1};\quad \varkappa=\frac{c_{p\infty}}{c_{V\infty}}. \qquad (4.44)$$

We may determine T_0' by using the tables of thermodynamic functions or the graphs of $T = T(p, h)$ (for air, see Figure 2.2).

Similar calculations may be made for the density change across a nonequilibrium shock layer

$$\rho_1=\rho_{1f}\approx\rho_\infty\frac{\varkappa+1}{\varkappa-1};\quad \rho_0'=p_0M_{0e}/RT_0 \text{ or } \frac{\rho_0'}{\rho_1}\approx\frac{T_1}{T_{0e}Z_0}, \qquad (4.45)$$

where $Z_0 = M_\infty/M(T_{0e}', p_0')$. Figure 2.1 gives graphs showing the dependence of Z on T and p for air. Using the graphs of 2.1 and 2.2, we find, for example, that for flight in the atmosphere of the Earth at a velocity of V_∞ = 7 km/sec at an altitude of 70 km (thus $H \approx V_\infty^2/2$ = 24.5 km/sec^2 = 5850 cal/g; $p'_0 \approx \rho_\infty V_\infty^2$ = 0.024 kG/cm^2) temperature in the shock layer changes by approximately a factor of four from the shock wave to the critical point, and the density changes by a factor of 2.2

$$(T_1=2{,}4\cdot10^4\,\text{K};\ T_{0e}'=5{,}9\cdot10^3\,\text{K};\ Z(T_{0e}', p_0')=1{,}9).$$

We should note that nonequilibrium processes have a very slight influence on the temperature at the critical point [120, 121]. Thus, for air T_0' differs from T_{0e}' only by several tenths of a percent.

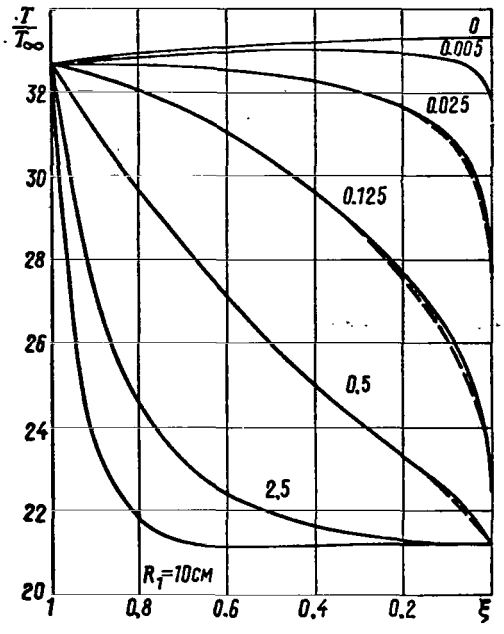

Figure 4.16. Temperature change along critical streamline for air when $M_\infty = 14$; $p_\infty = 0.0117$ kG/cm^2; $T_\infty = 230$ K.

The change in T and ρ in the shock layer depends basically on the dimensionless relaxation time $\bar{\tau}$ (4.13). Figure 4.16 shows typical results derived from calculating the temperature along the critical streamline from a shock wave to a body, obtained by "truncation" of series [97] (the dashed and solid curves pertain to the first and second truncations, respectively).

Throughout the entire shock layer from the front portion to the lateral portion, the value of $\bar{\tau}$ changes very greatly, by several orders of magnitude — a similar situation occurs in hypersonic nozzles.* For example, if the characteristic relaxation length $d \approx 0.1\Delta$ behind the shock wave on the axis of symmetry, then the flow at the front surface of the body will be close to equilibrium flow. However, in the adjacent region of the shock layer, where the temperature and pressure behind the oblique shock wave are approximately 1.5 — 2 times less than the temperature and pressure behind a normal shock wave, the relaxation time increases approximately by an order of magnitude, and the characteristic velocity increases by approximately a factor of $1/\varepsilon$, i.e., the value of $\bar{\tau}$ increases /183 approximately by two orders of magnitude. With further expansion

*Here and below we have in mind bodies with a great change in the surface angles of inclination, for example, a blunt cylinder, a blunt cone with a small angle of opening, etc.

of the gas, $\bar{\tau}$ will continue to increase, and conditions may occur under which the flow becomes frozen.

Therefore, in order to classify the flows in a shock layer it is advantageous to use two characteristic values of the parameter $\bar{\tau}$

$$\bar{\tau}_1 = \tau_1 / t_{c\ pl},$$

where τ_1 is the characteristic relaxation time behind a normal shock wave, and $t_{c1} = R_b/V_\infty$ is the characteristic time of a gas particle motion in the region of the shock layer before the body and $\bar{\tau}_2 = \tau_2/t_{c2}$, where τ_2 is the characteristic relaxation time in the region of the front body surface, and $t_{c2} = L/V_\infty$ (L is the length of the body) is the characteristic time of gas motion along the body.

Using the parameters $\bar{\tau}_1$ and $\bar{\tau}_2$, we may determine the following basic types of flows in a shock layer around blunt bodies:

1. $\bar{\tau}_1 \ll 1$, $\bar{\tau}_2 \ll 1$ — practically equilibrium flow (nonequilibrium processes are significant only in a very narrow relaxation layer behind the shock wave); /184

2. $\bar{\tau}_1 \ll 1$, $\bar{\tau}_2 \sim 1$ — flow with a developable nonequilibrium region;

3. $\bar{\tau}_1 \ll 1$, $\bar{\tau}_2 \gg 1$ — frozen flow (after an equilibrium state is reached behind the shock wave);

4. $\bar{\tau}_1 \sim 1$, $\bar{\tau}_2 \gg 1$ — frozen flow (an equilibrium state is not reached);

5. $\bar{\tau}_1 \gg 1$, $\bar{\tau}_2 \gg 1$ — practically frozen flow with a narrow near-equilibrium region close to the critical point and a region of large gradients of T and ρ in the relaxation entropy layer close to the body surface; see [66];

6. $\bar{\tau}_1 \gg 1$, $\bar{\tau}_2 < 1$ — flow which is frozen in the region of the nose, later changing to equilibrium flow — this may be realized for bodies such as slender needles; the case is of little interest for present day problems of aerodynamics.

Regime 5 is typical for flights of bodies at high altitudes, where the influence of viscosity must be taken into account. In actuality, in these regimes a relaxation entropy layer will occur within the viscous layer.

Regimes 3 and 4 are of the greatest practical interest (when nonequilibrium is significant). These regimes are typical for flights of hypersonic aircraft at velocities of 4 — 8 km per second at altitudes of 40 — 70 km. In these cases, the state of the flow changes from almost equilibrium flow in the

forward portion of the shock layer to almost frozen flow close to the lateral surface.

In the region of frozen flow, the temperature and pressure may differ greatly from the temperature and pressure in equilibrium flow. The studies [85, 86] (see below, Figure 4.26) give typical results derived from calculating the pressure distribution along the lateral surface of blunt bodies. In regimes 3 and 4, nonequilibrium processes may have a great influence on certain aerodynamic characteristics, such as m_z and c_y [88], and on the position of the forward shock wave (regime 4). The main reason for this is the increase in the adiabatic index: $\kappa_f > \kappa_\infty > \kappa_e$.

The stand-off distance of the shock wave Δ in flows of an ideal and equilibrium gas when $M \gg 1$ is determined primarily by the magnitude of compression in the normal shock wave ($\Delta \sim \rho_\infty/\rho_1$).

In nonequilibrium flow when $\bar{\tau}_1 \sim 1$, the density across the shock layer is variable, and Δ will depend on the effective compression ε_{ef}^{-1}, where /185

$$\varepsilon_{ef} = \frac{\rho_\infty}{\rho_{ef}}; \quad \rho_{ef} = \int_0^1 \rho d\xi^* \qquad \rho_f \leqslant \rho_{ef} \leqslant \rho_e. \tag{4.46}$$

The value of Δ may be determined by using the formula given by V. P. Stulov [89]

$$\frac{\Delta}{R_1} = \frac{\varepsilon_{ef}}{1 + \sqrt{\frac{\delta}{3}\varepsilon_0}}. \tag{4.47}$$

---

* ξ is a dimensionless coordinate along the critical streamline. On the axis of symmetry $\xi = 0$; on the shock wave $\xi = 1$.

(The formula was obtained when processing the results of numerical calculations for bodies of various forms: spheres, ellipsoids, bodies of segmental form with rounding, etc., R_1 — radius of curvature of shock wave on the axis of symmetry; $\varepsilon_0 = \rho_\infty/\rho_0'$, ρ_0' — density at the critical point.) In the particular case of sphere when $0.04 < \varepsilon < 0.2$ we may use the formula [89]

$$\frac{\Delta}{R_b} = 0.82\varepsilon. \tag{4.48}$$

(See also [81, 108, 109] regarding the calculation of Δ.)

In some of the simplest cases, we obtain the explicit dependence of the influence of the parameter $\bar{\tau}$ on the shock wave stand-off distance. For the model of a gas with nonequilibrium excitation of vibrational degrees of freedom, Blythe obtained the following formula [69, 3]

$$\frac{\Delta - \Delta_f}{\Delta - \Delta_e} = e^{\bar{\tau}_1 - 1} \int_{\bar{\tau}_1}^{\infty} \frac{e^{-\xi}\, d\xi}{\xi^2}; \quad \bar{\tau}_1 = \frac{\tau V_\infty}{R_b} \tag{4.49}$$

(the concept of a thin shock layer was used; τ was assumed to be constant). A graph of this function is shown in Figure 4.17.

---

* This expression may be written in terms of the integral power function $E_1(x)$.

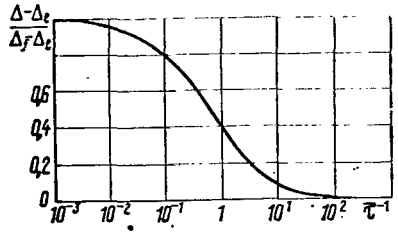

Figure 4.17. Dependence of shock wave stand-off distance on the parameter $\bar{\tau}$ (axisymmetric flow).

Methods of calculating nonequilibrium flows around blunt bodies

In studying nonequilibrium gas flow around blunt bodies, we found different methods developed for flows of an ideal gas, for example: the method of integral relationships (O. M. Belotserkovskiy, V. K. Dushin, Yu. P. Lun'kin, R. D. Popov, S. B. Koleshko, Shin, Baron, Springfield, Hermann, Theones, et al. [70 — 75, 90, 91, 101],) method of straight lines (G. F. Telenin, V. P. Stulov, V. B. Minostsev, G. N. Sayapin, L. I. Turchak, V. P. Shkadova, et al. [76 — 78, 81 — 84]), the inverse method (Lick, Hall, Eschenroeder, Marrone, Perini, Melnik, et al. [92, 93, 103]), the method of finite differences (Bogachevskiy, Rubin, Mates, A. L. Kosorukov [87, 94, 102]), the method of streamtubes (Bloom, Steiger, et al. [95]), the method of a thin shock layer (Murzinov, I. N. Freeman, Blythe, Ellington, et al. [67 — 69, 86, 110]), the method of series truncation (S. I. Anisimov, Yu. V. Khodyko, Conti, Van Dyke [79, 97, 98, 100, 105]). /186

To analyze the flow near the critical point, the method of local asymptotic expansions is used [100]. The supersonic flow regions are usually determined by the method of characteristics [13, 15 — 17, 23, 24], etc.

Approximate methods have also been proposed, which were particularly developed to calculate nonequilibrium flows around blunt bodies, for example, a method based on the flow behind a normal shock wave and in the shock layer around the frontal surface of bodies (Gibson and Marrone [111, 112]), or a method

using the model of instantaneous freezing [88, 99].

In the latter method, all flow fields are divided into two regions, in one of which the flow is assumed to be an equilibrium flow (or an ideal gas flow with the corresponding value of κ), and in the other — frozen flow. The selection of the freezing surface is to a certain extent arbitrary. This surface may be calculated by using, for example, the Bray freezing criteria (3.74) and determining the geometric location of freezing points for different streamlines.

An even simpler procedure may be followed, by assuming, for example, that the flow is frozen immediately behind the characteristic of the second family, passing through the sonic point on the body surface. Thus, on the section of the shock wave intersected by this characteristic, the flow may be assumed to be either frozen or equilibrium, freezing immediately behind the shock wave [99]. In a certain range of V_∞, ρ_∞, T_∞ such a simple model gives fairly good results.

The method of the agreement of flows behind a shock wave and in a shock layer, in the case of flow around blunt bodies, is based on the following property of the flows: the gas enthalpy remains almost constant behind the shock wave and in the shock layer close to the blunt region when $\rho_\infty/\rho_1 \ll 1$.

We shall show that, if the reaction kinetics is determined /187
by binary processes, this agreement is exact under the condition h = const. Actually, in the case of binary kinetics the relaxation equations assume the form

$$\frac{dq_j}{dt}=f_j(T,\ p,\ \langle q_l\rangle)=pf_j(T,\langle q_l\rangle)(i,\ j=1,\ 2,\ldots,\ n). \qquad (4.50)$$

However, if the gas is a mixture of reacting ideal gases, then the expression for the enthalpy may be written in the form

$$h=h(T,\ \langle q_i\rangle)\quad \text{or}\quad T=T(h,\ \langle q_i\rangle). \tag{4.51}$$

Then

$$\frac{dq_j}{dt}=pf_2(h,\ \langle q_i\rangle). \tag{4.52}$$

We shall assume that p is the known function of t. Let us introduce the new correlation variable

$$d\chi=Cpdt, \tag{4.53}$$

where C is a certain constant. In addition, it is advantageous to assume that χ is a dimensionless quantity. Therefore, the dimensionality C equals $[p]^{-1}[t]^{-1}$ (for example, $C = p_1\tau_1)^{-1}$).

Equation (4.52) may now be written in the form

$$C\frac{dq_j}{d\chi}=f_j(h,\ \langle q_i\rangle). \tag{4.52a}$$

This equation has the same form for flow behind a shock wave, and for flow in a shock layer (here h is a parameter which is the same for both flows). If the initial conditions (conditions on the shock wave) for both flows are identical,* then the solutions $q_j = q_j(h, \chi)$ will be identical.

*For this to be the case, ρ_∞, T_∞, and $V_\infty \sin\sigma$ for both flows must be identical.

It follows from equations $h = h(T, \langle q_i \rangle)$ and $p = \rho RT/M(\langle q_i \rangle)$ that T and p/ρ for these flows for identical χ will also be the same. This comprises the agreement between such flows.

The purpose of further transformations is to express this agreement in analytical form, i.e., to write the expression in terms of the coordinates and parameters characterizing the streamline being considered. Let us use the fact that the pressure and velocity distribution along the streamline in a shock layer in the first approximation may be determined from the Newton theory:

$$p(\sigma, s) = p_1(\rho_\infty, V_\infty \sin\sigma)\varphi(\sigma, s), \quad u = u(\sigma),$$

where σ is the angle of inclination of the shock wave to the direction $\vec{V}_\infty$ at the point where the given streamline intersects the shock wave; $s = \xi/R_1$, ξ — distance along the streamline from the point where it intersects the shock wave to the point being considered; R_1 — shock wave radius of curvature on the axis of symmetry. /189

The results of comparing the flows of different gases (ideal, equilibrium, and gases with differing kinetics in a nonequilibrium state) show that the function $\varphi(s, \sigma)$, which equals p/p_1, does not depend on the state of the gas, its composition, kinetics, or conditions in unperturbed flow. Therefore, we may assume that the function $\varphi(s, \sigma)$ has a universal nature, and it may be assumed to be known beforehand from precise calculations or — approximately — from Newton's theory.

Taking this fact into account, from Formula (4.53) we obtain the expression for χ in the shock layer

$$\chi(s, \sigma) = \frac{C p_1 R_1}{u(\sigma)} \int_0^s \varphi(s, \sigma)\, ds. \qquad (4.54)$$

For a normal shock wave

$$\chi = C_1 \int_0^x \frac{p\, dx}{u}, \qquad (4.55)$$

where x is the coordinate directed along the normal to the shock wave. These relationships solve the problem.

It is true that one problem remains unanswered — the agreement of the flows would appear to be inapplicable to a critical streamline, since close to the critical point the gas is always in an equilibrium state, and it is impossible to disregard the recombination processes which are not binary. However, along the critical streamline close to the critical point, just as behind a normal shock wave $p \approx \text{const} = p_1$ (i.e., $\Psi = \text{const}$), and the flows will always agree independently of the reaction kinetics.

Along the critical streamline, we have

$$\chi = C p_1 R_1 \int_0^s \frac{ds}{u(s)}. \qquad (4.56)$$

For flows which are far from equilibrium flows (this method can only be applied to such flows), the velocity u on the axis of symmetry may be assumed to depend linearly on s

$$u(s) = \frac{V_\infty \rho_\infty}{\rho_1}\left(1 - \frac{s}{\Delta}\right). \qquad (4.57)$$

Thus, if the initial conditions in both flows are identical, i.e., if when $\chi = s = x = 0$ the quantities $q_i = q_{i\infty}$; $h = h_1(V_\infty, \sigma)$ and $p = p_1(V_\infty, \sigma)$ are identical on the streamlines being considered behind a normal shock wave and in the shock layer around a blunt body, then for equal χ in both flows the functions

$$T(\chi);\ q_i(\chi);\ \frac{\rho(\chi)}{\rho(\chi)}$$

are identical. We thus have

$$\rho(\chi)_{\substack{\text{in shock}\\ \text{layer}}} = \frac{\rho(\chi)_{\text{behind shock}}\, p(\chi)_{\substack{\text{in shock}\\ \text{layer}}}}{p(\chi)_{\text{behind shock}}} \approx \approx \rho(\chi)_{\text{behind shock}}(s, \sigma). \tag{4.58}$$

Figure 4.18 [112] gives graphs illustrating the accuracy /189 of the method of flow agreement for two streamlines A and B, which intersect the shock wave at points corresponding to the polar angle $\vartheta = 9$ and 35°. The difference in the precise and approximate results for streamlines B when $V_\infty = 4.6$ km/sec is due primarily to the enthalpy change along the streamline.

We shall not describe other methods of calculating the flows around blunt bodies, which were developed for flows of an ideal and equilibrium gas, and which are described in detail in several monographs and articles. Usually, modifications are given of these methods, related to the specific nature of non-equilibrium flows. Thus, in the method of integral relationships the approximation of gas dynamic parameters (or their complexes) is usually given in a direction not across, but along the shock layer, in which these complexes change to a lesser degree (scheme II). The relaxation equation is usually not approximated, but

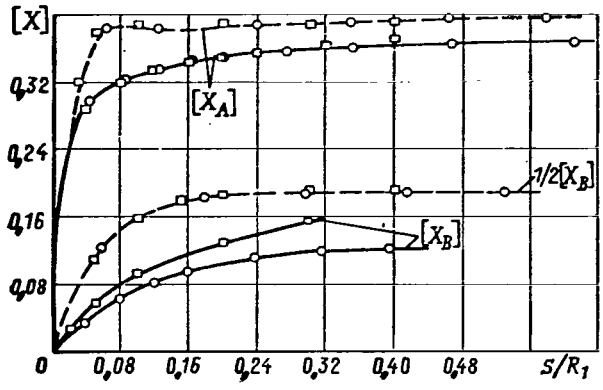

Figure 4.18. Comparison of precise and approximate solutions for concentrations of oxygen atoms in a shock layer along the streamlines A and B for air (MCA) at H = 61 km (solid lines — at V_∞ = 4.6 km/sec; dashed line — at V_∞ = 7.0 km/sec. The computational data are designated as follows: stars — precise solution; squares — approximate solution).

s — distance along streamline; [X] — mole/initial mole.

is written along the streamline, etc. See, for example, [70].

Results of numerical calculations

The studies listed above contain numerous results derived from calculating nonequilibrium flows around blunt bodies. Figures 4.19 — 4.31 give some of these results, primarily for air. Since previous authors, as a rule, used differing data on the kinetics and reaction velocity constants, we shall make several general comments.

The following kinetic model is usually used for air:

/190

$$\left.\begin{array}{ll} (1)\ O_2+M\rightleftarrows 2O+M; & (6)\ N_2+O_2\rightleftarrows 2NO; \\ (2)\ N_2+M\rightleftarrows 2N+M; & (7)\ N+O\rightleftarrows NO^++e; \\ (3)\ NO+M\rightleftarrows N+O+M; & (8)\ N+N\rightleftarrows N_2^++e; \\ (4)\ N+O_2\rightleftarrows NO+O; & (9)\ O+O\rightleftarrows O_2^++e. \\ (5)\ N_2+O\rightleftarrows NO+N; & \end{array}\right\} \qquad (4.59)$$

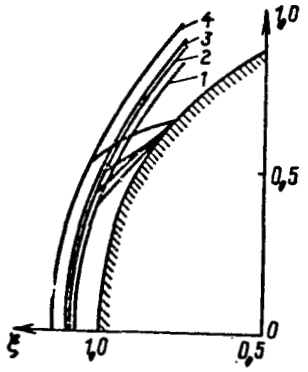

Figure 4.19. Position and form of shock wave and sonic line in the case of an oxygen flow around a sphere: $M = 10$; $T_\infty = 290$ K; $p_\infty = 10^{-2}$ kG/cm^2; $R_b = 1$ cm.

1 — equilibrium flow; 2 — flow in the case of equilibrium excitation of vibrations; 3 — vibrations and dissociation are not in equilibrium; 4 — frozen flow ($\kappa = 1.4$).

At $T < 7000$ — 8000 K, it is usually assumed that the vibrational degrees of freedom are excited uniformly. At $T > 8000$ K, the vibrational relaxation is calculated on the basis of a certain kinetic model (see Chapter 1, and also [75, 76, 77]). The influence of the simultaneous occurrence of vibrational and dissociation relaxation on the shock wave stand-off distance is illustrated in Figure 4.19 [75].

When $M_\infty \lesssim 30$, ionization is small, and its influence on the flow field is insignificant. Therefore, the electron concentration in these cases is frequently determined on the basis of the known flow field, which is found without taking into account the ionization processes.

A simplified model is usually used in the range of numbers /191 $M_\infty = 10$ — 15: the air is assumed to be a mixture of N_2, O_2, and O, in which there is a single reaction (4.59) (1), and vibrational degrees of freedom of N_2 and O_2 are assumed to be excited uniformly.

The reaction velocity constants are usually taken from the data of Wray, Lin, and Teare, or Bortner (see Chapter 1), or data similar to this.

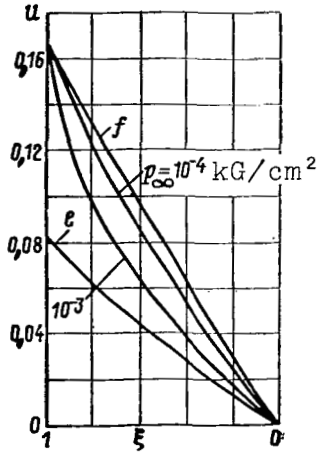

Figure 4.20. Velocity change along critical streamlines: M_∞ = 18 (nonequilibrium vibration); p_∞ = 10^{-4} and 10^{-3} kG/cm^2; T_∞ = 250 K; R_b = 1.5 cm; f — in frozen flow; e — in equilibrium flow.

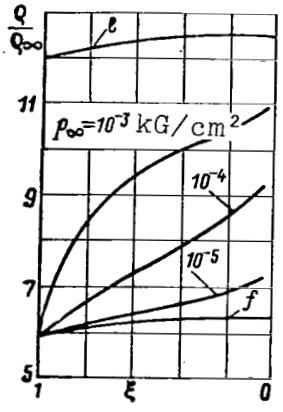

Figure 4.21. Density change along critical streamlines (conditions are the same as for Figure 4.20).

As a rule, we can disregard small variations in the velocity constants within the framework of a single kinetic model. Therefore, in order to avoid a cumbersome description of the figures with insignificant details, data on the reaction rates in each specific case will not be specifically given.

Thus, in order to completely establish the design case, in addition to the gas composition, the figures will give V_∞, T_∞, ρ_∞, and R_b (or R_1) or M_∞, T_∞, p_∞, and R_b. Figures 4.20 — 4.23 give data illustrating the change in the gas dynamic parameters on the axis of symmetry and the shock wave stand-off distance for a sphere in an air flow. (The results were obtained by the method of straight lines [76, 77]. Here and below, ξ is the dimensionless coordinate along the symmetry axis. On the body ξ = 0; on the shock wave, ξ = 1.)

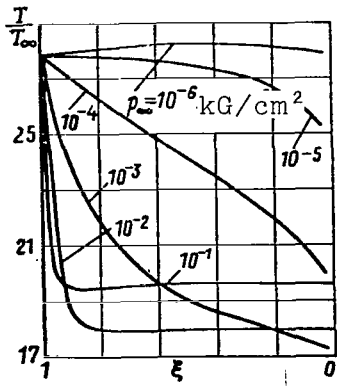

Figure 4.22. Temperature change along critical streamline (conditions are the same as for Figure 4.20).

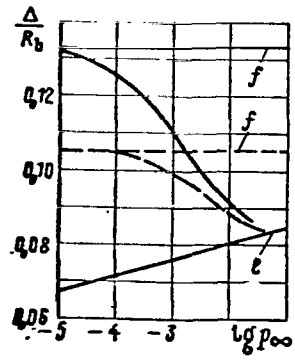

Figure 4.23. Dependence of shock wave stand-off distance Δ on pressure in an unperturbed flow when M_∞ = 13; T = 250 K; R_b = 1.5 cm; $[p_\infty]$ = kG/cm² (solid lines — with allowance for relaxation of vibrational degrees of freedom; dashed lines — with equilibrium excitation of vibrational degrees of freedom).

We should note that the dependence of the velocity u on ξ in a nonequilibrium flow (especially when $\bar{\tau} \ll 1$) may greatly differ from a linear dependence which is typical for equilibrium and frozen flows. In Figures 4.21 and 4.22, the curves of ρ and T for the cases $\bar{\tau} \gg 1$ and $\bar{\tau} \sim 1$ are not drawn up to the critical point, close /192 to which they change sharply (see Figure 4.16).

The NO concentration, and also the concentrations of other components, greatly depend on the kinetic model of the air (4.24). At the same time, the influence of individual reactions, as well as the rates at which they take place, on the gas dynamic parameters is small (Figure 4.25) [74]. Attention should be called to the fact that the concentration maximum of NO greatly exceeds its equilibrium concentration.

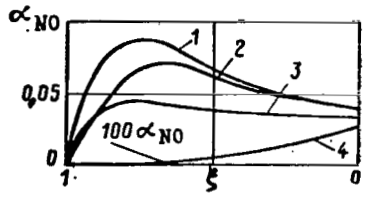

Figure 4.24. Dependence of nitric oxide concentration along critical streamline on the number of reactions considered [see Formula (4.59)] for a sphere when R_b = 1 cm; M_∞ = 15; p_∞ = 0.01165 kG/cm²; T_∞ = 231 K. 1 — all six reactions; 2 — without reaction (4); 3 — without reaction (5); 4 — without reactions (4), (5), and (6).

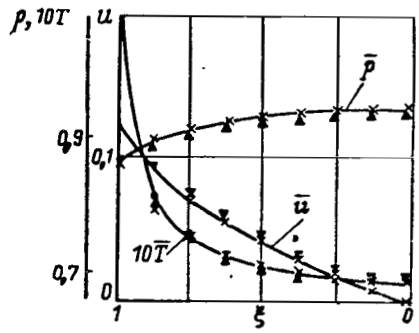

Figure 4.25. Dependence of $\bar{p}$, $\bar{u}$, and $\bar{T}$ along critical streamline on number of reactions considered for a sphere when R_b = 1 cm; M_∞ = 15; p_∞ = 0.01165 kG/cm²; T_∞ = 231 K [solid lines — all six reactions; crosses — without reaction (4); dots — without reaction (5); triangles — without reactions (4), (5), and (6)].

$$\bar{u} = \frac{u}{V_{max}}; \quad \bar{p} = \frac{p}{\rho_\infty V_{max}^2};$$

$$\bar{T} = T \Big| \frac{V_{max}^2 M_\infty}{R}$$

As was already noted, the pressure on the lateral surface of a blunt plate and cylinder in a nonequilibrium flow may differ greatly from the pressure in flows of an ideal and equilibrium gas. The data given in Figure 4.26 substantiate this [86].

Use of the binary similarity law in the case of flow around blunt bodies

The binary similarity law has been widely used in the study of nonequilibrium flows. In those cases when the recombination processes can be disregarded in the entire flow region, there is no question regarding the use of the binary similarity law. However, in the case of flow around the blunt bodies close to the critical point there is always an equilibrium zone, in which the recombination is great and consequently the binary similarity law cannot be applied. (We can only hope that, with sufficiently /193

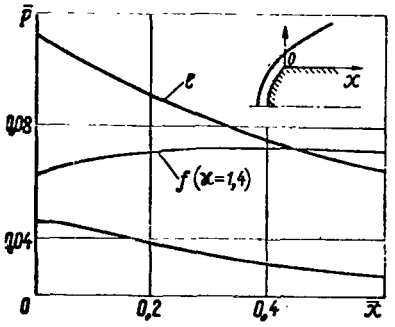

Figure 4.26. Pressure distribution along cylinder lateral surface with spherical bluntness for air when M = 25; T_∞ = 250 K; $p_\infty = 2.5 \times 10^{-4}$ kG/cm^2; R_b = 2 m.

$\bar{x} = x/R_b$; e — in equilibrium flow; f — in frozen flow.

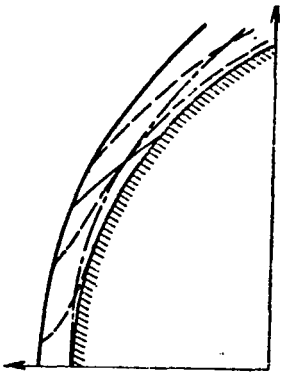

Figure 4.27. Position of shock wave, streamline, sonic line, and local equilibrium line when M_∞ = 10; p_∞ = 0.01 kG/cm^2; T_∞ = 290 K; R_b = 0.1 m (cross-hatched curves — streamlines; dashed-dotted line — local equilibrium line).

small values of the parameter $\rho_\infty R_b$, to which flow which is close to frozen flow corresponds, the influence of this zone on the remaining field will be small.) In addition, close to the surface of the body there is a zone in which the recombination processes predominate over the dissociation processes. By way of an example, Figure 4.27 [70] shows a picture of a flow of nonequilibrium-dissociating oxygen around a sphere. This figure shows a line of local equilibrium $\alpha = \alpha_e$. Downstream from this line, the recombination processes predominate over the dissociation processes.

Thus, it is necessary to perform a special analysis in order to establish the boundary of applicability of the binary similarity law in the case of flow around blunt bodies. This analysis was performed by Gibson and Marrone [112] for an ideal

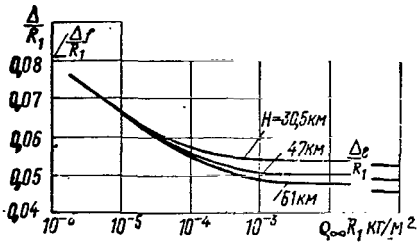

Figure 4.28. Illustration of the use of the binary similarity law for the stand-off distance of a shock wave [112] when V_∞ = 7 kg/sec.

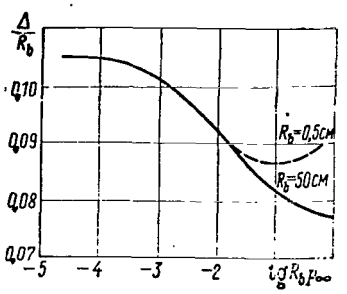

Figure 4.29. Illustration of the use of the binary similarity law for determining the stand-off distance of a shock wave [77] when M_∞ = 13 (the quantity $R_b p_\infty$ is given in kG/cm).

dissociating gas and for air. Individual results derived from checking the binary similarity law are also contained in [70, 76, 77, 93, 113, 114, etc.].

Figures 4.28 and 4.29 show graphs of the stand-off distance of the shock wave Δ from the sphere surface for air. An increase in Δ with an increase in p_∞ for the upper curve in Figure 4.29 occurs in the region where there is practically equilibrium flow, i.e., this shows the influence of p_∞ on Δ for equilibrium flow.

Figure 4.30 shows the distribution of density and concentration of electrons across the shock layer [81]. Naturally, along the critical streamline for these values the binary similarity law is satisfied much less exactly than for the shock wave stand-off distance. It was shown in [112] that for V_∞ = 7 km/sec the shock wave stand-off distance and the concentration of atomic components are satisfactorily correlated in agreement with the binary similarity law when $\rho_\infty R < 10^{-4}$ kg/m^2 and $\rho < 1.8 \cdot 10^{-2}$ kg/m^3, and for V_∞ = 4.5 km/sec — when $\rho_\infty R$ 10^{-3} kg/m^2.

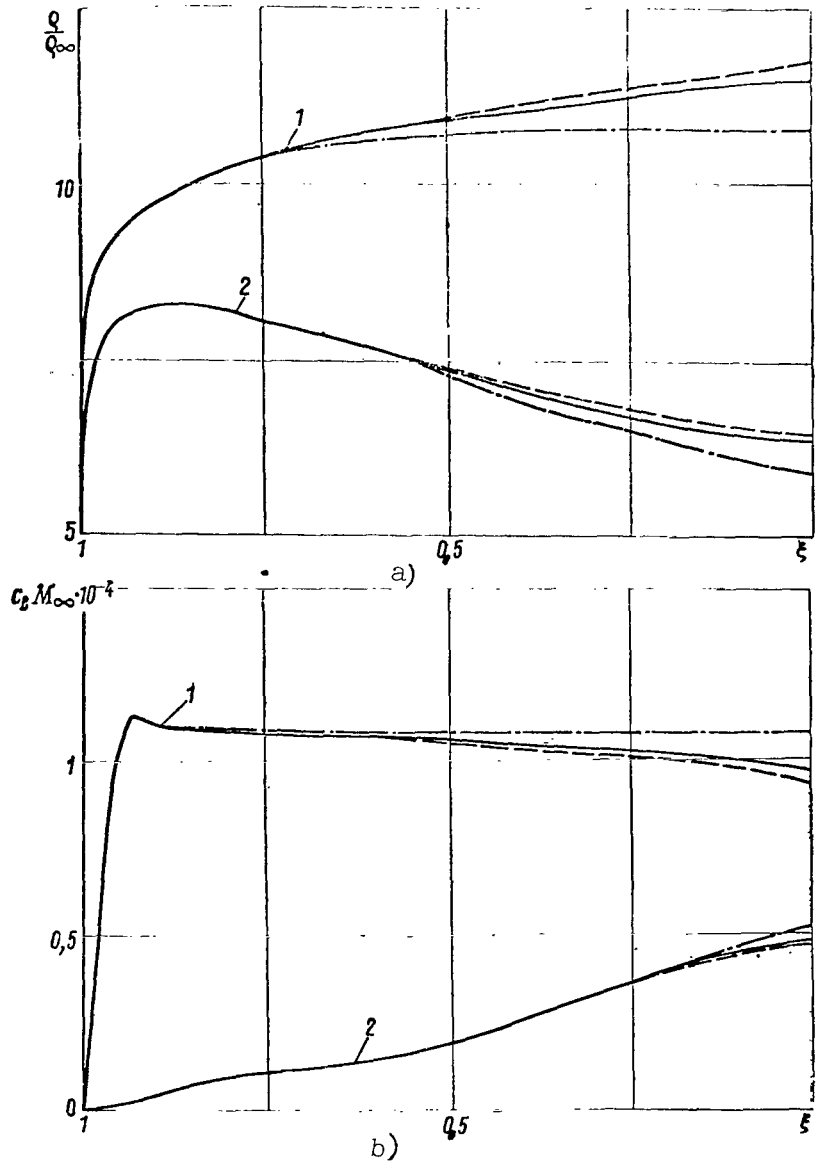

Figure 4.30. Illustration of the use of the binary similarity law for the density distribution ρ and electron concentration $\bar{c}_e = c_e M_\infty$ across a shock layer around a sphere along two lines when $M_\infty = 15$; $R_b p_\infty = 0.15$ kG/cm (dashed lines when $R_b = 15$ cm; $p_\infty = 10^{-2}$ kG/cm^2; solid lines — when $R_b = 150$ cm; $p_\infty = 10^{-3}$ kG/cm^2; and dashed-dotted lines when $R_b = 1500$ cm; $p_\infty = 10^{-4}$ kG/cm^2): 1 — for $\vartheta = 0$ (critical streamline); 2 — for $\vartheta = 43°$.

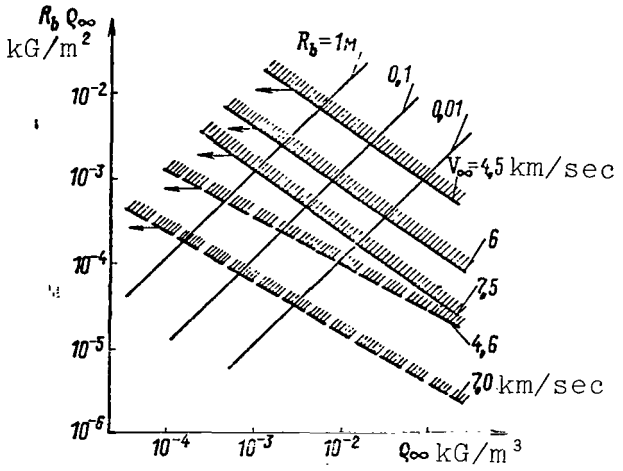

Figure 4.31. Region of applicability of binary similarity law (solid lines — according to data from [114]; cross-hatched lines — according to data from [112]).

Figure 4.31 gives graphs showing the regions of applicability of the binary similarity law based on results from [112 and [114]. To the left of the boundaries in the direction of the arrow there is a region where the binary similarity law is satisfied. Since the selection of the criterion for determining these boundaries is arbitrary, and the computational method is approximate, there is a great divergence in the recommendations of the authors [112 and 114]. As a criterion for determining the boundary, the study [112] selected the condition $r_F/r_R = 0.3$ for the reaction $N_2 + M = 2N + M$, where r_F and r_R are the velocities of the forward and inverse reactions. The study [114] gives the relative error in calculating the concentrations $\varepsilon = 0.01$ in the cross section $\vartheta_2 = 0.9$ on a streamline, whose point of intersection with the shockwave corresponds to the angle $\vartheta_1 = 0.2$ (ϑ_1, ϑ_2 — polar angles in radians). /196

The graphs given in Figure 4.31 make it possible, in particular, to determine the minimum dimensions of the model which are permissible when simulating natural conditions in wind tunnels. The influence of viscosity must be taken into account when determining the boundaries of applicability of the binary similarity law under conditions corresponding to the altitudes $H \gtrsim 80$ km.

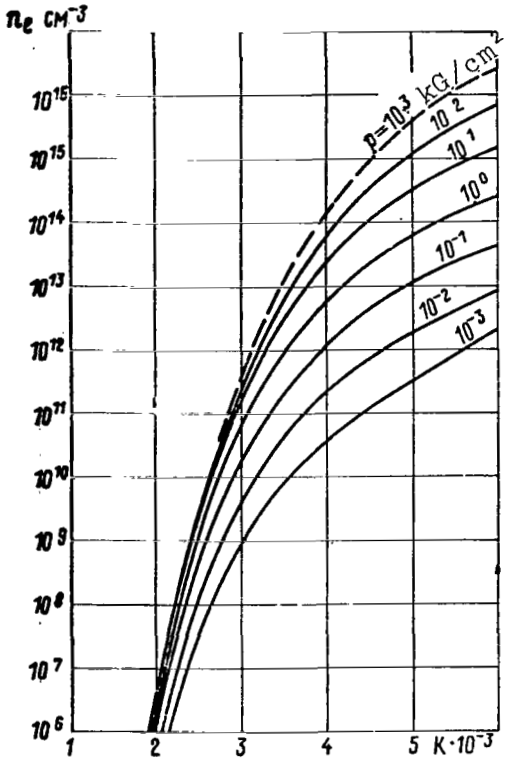

Figure 4.32. Equilibrium electron concentration in air.

Electron concentration in the shock layer

One of the important problems related to the flight of hypersonic aircraft in the atmosphere is the problem of radio communication. The propagation of radio waves in a gas greatly depends on the presence of charged particles in these waves, particularly electrons. When the electron concentration n_e exceeds a certain value n_{e*}, radio communication /197 with the aircraft is disturbed. This critical value is a function of the radio signal frequency.

Thus, for waves in the centimeter range radio communication is disrupted at concentrations of $n_{e*} \sim 10^{13}$ particles/cm^3; for waves in the meter range, this occurs at $n_{e*} \sim 10^{9}$ particles/cm^3 [115]. The degree of ionization must thus be insignificant, for example, less than 10^{-8}. Thus, ionization is important even if it is insignificant in terms of energy.

As a rule, to calculate equilibrium and nonequilibrium electron concentrations, the results of precise calculations must be used. Approximate relations, which are well satisfied for simple gases, produce a large error when applied to multi-component gases such as air. For example, equilibrium concentration of /198

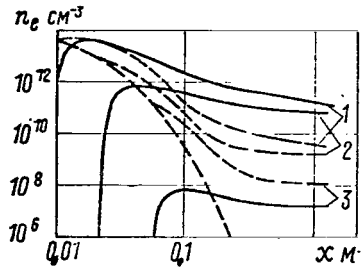

Figure 4.33. Influence of nonequilibrium on electron concentration change along three streamlines (see Figure 4.34). In a shock layer around a blunt cone when V_∞ = 5.5 km/sec; H = 50 km (solid lines — in nonequilibrium flow; dashed lines — in equilibrium flow).

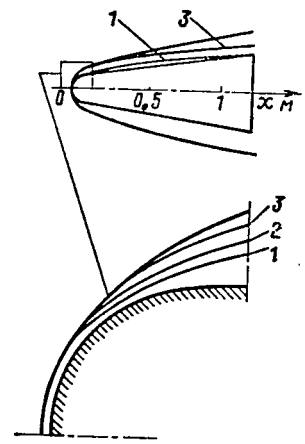

Figure 4.34. Position of streamlines (for Figure 4.33).

electrons in air corresponds very poorly to the approximate relation $n_e \sim V\bar{\rho}f(T)$ even for very low temperatures, when the degree of ionization is low.

Figure 4.32 gives graphs of the equilibrium concentration of electrons as a function of T and p [116]. At flight velocities of 4 — 6.5 km/sec in the atmosphere of the Earth, the main charged particles in the shock layer will be NO^+ and e. The main reaction which must be taken into account when calculating the nonequilibrium electron concentration under conditions of comparatively low temperatures (for flight velocities less than 7 km/sec), will be the reaction $N + O \rightleftarrows NO^+ + e$. As the velocity increases, the positively charged particle N^+ becomes predominant; see Figure 2.3. Thus, other ionization reactions begin to play a significant (and sometimes the main) role, and different ionization reactions may be decisive in different regions of the shock layer. The studies [110, 116 — 118] give certain results derived from calculating the electron concentration field during the motion of blunt bodies in the air.

Figure 4.33 [110] gives graphs showing the change in n_e along three streamlines in the flow field around a blunt cone with the length L = 1.3 m with the angle of opening 9°, and a radius of spherical blunting of 10 cm (x is the coordinate along the cone axis which equals zero, and corresponds to the position of the shock wave; the streamlines are shown in Figure 4.34). As a rule, the method of streamtubes is used for an approximate calculation of n_e in a shock layer. The pressure along the streamtubes and their relative position is determined from calculations of equilibrium or completely frozen (ideal gas) flows. Certain recommendations on formulating the streamlines and finding the pressure along them are given in [119]. /199

REFERENCES

1. Chernyy, G. G. Techeniya gaza s bol'shoy sverkhzvukovoy skorost'yu (Gas Flow at a High Supersonic Velocity), Moscow, Fizmatgiz, 1959.

2. Hayes, W. D. and R. F. Probstein. Hypersonic Flow Theory. Moscow, Foreign Literature Press (IL), 1962.

3. Hayes, W. D. and R. F. Probstein. Hypersonic Flow Theory. Second Edition, Inviscid Flow, Vol. 1, Academic Press, N. Y., London, 1966.

4. Sychev. V. V. Three-Dimensional Hypersonic Gas Flows around Slender Bodies at Large Angles of Attack. Prikladnaya matematika i mekhanika (PMM), Vol. 24, No. 2, 1960.

5. Lee, R. S. Hypersonic Nonequilibrium Flow over Slender Bodies. J. Fluid Mech, VII, Vol. 23, Part 3, 1965.

6. Inger, G. R. Similitude of Hypersonic Flows over Slender Bodies in Nonequilibrium Dissociated Gases. AIAA J., Vol. 1, No. 1, 1963.

7. Voronkin, V. G. Pressure Distribution on Blunt Cones in the Case of Nonequilibrium Flow. Izvestiya AN SSSR, MAhG, No. 1, 1970.

8. Zhigulev, V. N. Effect of a Relaxation Boundary Layer, Doklady akedemii nauk (DAN) SSSR, Vol. 144, No. 6, 1962.

9. Sedney, R., J. C. South, and N. Gerber. Characteristic Calculation of Nonequilibrium Flows. In the collection The High Temperature Aspects of Hypersonic Flow. Proc. of the AGARD-NATO Specialists' Meeting, Rhode-Saint-Genese, Belgium, 3 — 6 April 1962, Oxford and others, 1964.

10. Lee, R. S. Unified Analysis of Supersonic Nonequilibrium Flow over a Wedge. Part 1. Vibrational Nonequilibrium. AIAA J., Vol. 2, No. 4, 1964.

11. Chirikhin, A. V. Influence of Nonequilibrium in an Advancing Flow around a Wedge. Izvestiya AN SSSR, MZhG, No. 6, 1969.

12. Capiaux R. and M. Washington. Nonequilibrium Flow Past a Wedge, AIAA J., Vol. 1, No. 3, 1963.

13. Sedney, R. and N. Gerber. Nonequilibrium Flow over a Cone. AIAA J., Vol. 1, No. 11, 1963.

14. Arkhipov, V. N. and K. S. Khoroshko. Method of Calculating Relaxation in the Problem of Flow Around a Cone. PMTF, No. 6, 1962.

15. Spurk, I. H., N. Gerber, and R. Sedney. Characteristic Calculation of Flow Fields with Chemical Reactions. AIAA J., Vol. 4, No. 1, 1966.

16. Dushin, V. K. Use of the Method of Characteristics to Calculate Supersonic External Gas Flows in the Case of Nonequilibrium Processes. In the collection: Chislennyye metody resheniya zadach matematicheskoy fiziki (Numerical Methods of Solving Problems of Mathematical Physics). Moscow, Nauka Press, 1966.

17. Sedney, R. A. Survey of the Method of Characteristics for Nonequilibrium Internal Flows. AIAA Paper No. 69 — 6, 1969.

18. Theones, J. Nonequilibrium Flow Past a Circular Cone Including Freestream Dissociation. AIAA J., Vol. 4, No. 8, 1966.

19. DeJarnette, F. R. Application of Lax's Finite-Difference Method to Nonequilibrium Hypersonic Flow Problems. NASA TR R-234, 1966.

20. Sauerwein, H. A. General Numerical Method of Characteristics. AIAA Paper No. 65 — 25. 1965.

21. South, J. C. Application of the Method of Integral Relations to Supersonic Nonequilibrium Flow Past Wedges and Cones. NASA TR R-205, 1964.

22. South, J. C. and P. A. Newman. Application of the Method of Integral Relations to Real Gas Flows Past Pointed Bodies. AIAA J., Vol. 3, No. 9, 1965.

23. Katskova, O. N. and P. I. Chushkin. Three-Dimensional Supersonic Gas Flows with Nonequilibrium Processes. Zhurnal Vychislit matem. i matem. fiz., Vol. 8, No. 5, 1968.

24. Chushkin, P. I. Metod kharakteristik dlya prostranstvennykh sverkhzvukovykh techeniy (Method of Characteristics for Three-Dimensional Supersonic Flows). Moscow, VTs, AN SSSR, 1968. /200

25. Sedney, R. and N. Gerber. Shock Curvature and Gradients at the Tip of Pointed Axisymmetric Bodies in Nonequilibrium Flow. J. Fluid Mech., Vol. 29, No. 4, 1967.

26. Polyanskiy, O. Yu. Aerodynamic Characteristics of a Slender Wedge in a Hypersonic Nonequilibrium Flow. Izvestiya AN SSSR, MZhG, No. 6, 1967.

27. Sayapin, G. N. Aerodynamic Characteristics of a Wedge in Hypersonic Nonequilibrium Flow. Trudy TsAGI, No. 1139, 1969.

28. Landau, L. D. and Ye. M. Lifshits. Mekhanika sploshnykh sred (Mechanics of Continuous Media), GITTL, 1964.

29. Mandel'shtam, L. I. and M. A. Leontovich. Theory of Sound Absorption in a Fluid. ZhETF, Vol. 7, No. 3, 1937.

30. Broer, L. J. F. Characteristics of the Equations of Motion of a Reacting Gas. J. Fluid Mech., VII, Vol. 4, No. 3, 1958.

31. Zel'dovich, Ya. B. and Yu. P. Rayzer. Fizika udarnykh voln i vysokotemperaturnykh gidrodinamicheskikh yavleniy (Physics of Shock Waves and High Temperature Hydrodynamic Phenomena), Moscow, Fizmatgiz, 1966.

32. Clark, J. and M. Makchesni. Dynamics of Real Gases. Moscow, Mir Press, 1967.

33. Vincenti, W. G. and Ch. Ha. Kruger. Introduction to Physical Gas Dynamics, New York, Wiley, 1965.

34. Stupochenko, Ye. V. and I. P. Stakhanov. Theory of Nonstationary Discontinuities in Relaxing Media. DAN SSR, Vol. 117, No. 1, 1957.

35. Stupochenko, Ye. V. and I. P. Stakhanov. Equations of Relaxation Hydrodynamics. DAN SSSR, Vol. 134, No. 4, 1960.

36. Stakhanov, I. P. and Ye. V. Stupochenko. Structure of the Mach Line in Relaxing Media. DAN SSSR, Vol. 134, No. 5, 1960.

37. Stakhanov, I. P. and Ye. V. Stupochenko. Problems of the Hydrodynamics of Relaxing Media. PMTF, No. 2, 1963.

38. Clarke, I. F. The Linearized Flow of a Dissociating Gas. J. Fluid Mech., Vol. 7, 1960, p. 4.

39. Clarke, I. F. Relaxation Effects on the Flow over Slender Bodies. J. Fluid Mech., Vol. 11, 1961, p. 4.

40. Vincenti, W. G. Nonequilibrium Flow over a Wavy Wall. J. Fluid Mech., Vol. 6, 1959, p. 4.

41. Moore, F. K. and W. E. Gibson. Propagation of Weak Disturbances in Gas Subject to Relaxation Effects. JASS, Vol. 27, No. 2, 1960.

42. Der, I. I. Linearized Supersonic Nonequilibrium Flow Past an Arbitrary Boundary. NASA TR R-119, 1961.

43. Ryhming, I. L. On Slender Airfoil Theory for Nonequilibrium Flow, JASS, Vol. 29, No. 9, 1962.

44. Tkalenko, R. A. Supersonic Nonequilibrium Gas Flow around Slender Bodies of Revolution. PMTF, No. 2, 1964.

45. Khodyko, Yu. V. Flow around a Slender Cone of Revolution by a Relaxating Gas. DAN SSSR, Vol. 8, No. 8, 1964.

46. Napolitano, L. G. Generalized Velocity Potential Equation for Plurireacting Mixtures. Arch. Mech. Stosowanej, Vol. 16, No. 2, 1964.

47. Wang, K. C. Unsteady Linearized Relaxing Flow Past Slender Bodies. Phys. of Fluids, I, Vol. 7, No. 1, 1964.

48. Sislyan, Zh. S. Linearized Steady State Equilibrium Flows of a Compressible Gas. Izvestiya AN SSSR, MZhG, No. 2, 1966.

49. Krayko, A. N. Study of Slightly Perturbed Supersonic Flows for an Arbitrary Number of Nonequilibrium Processes. PMM, Vol. 30, No. 4, 1966.

50. Krayko, A. N. and R. A. Tkalenko. Slender Plane Bodies of Minimum Wave Impedance in Nonequilibrium Supersonic Flow. Izvestiya AN SSSR, MZhG, No. 4, 1967.

51. Morioka, S. Supersonic Jet of an Ideal Dissociating Gas with Finite Reaction Rate. J. Phys. Soc. of Japan, Vol. 18, No. 2, 1963.

52. Murasaki, T. and S. Morioka. Linearized Nonequilibrium Flow of a Partially Ionized Gas with a Radiative Loss. J. Phys. Soc. Japan, Vol. 20, No. 8, 1965. /201

53. Tkalenko, R. A. Slender Bodies of Revolution Having the Least Wave Impedance in Nonequilibrium Supersonic Flow. Izvestiya AN SSSR, MZhG, No. 6, 1969.

54. Krayko, A. N. and R. A. Tkalenko. Formulation of the Linear Theory of Nonequilibrium and Equilibrium Flows. Izvestiya AN SSSR, MZhG, No. 6, 1968.

55. Polyanskiy, O. Yu. and N. G. Lebedeva. One Class of Self-Modeling Motion of a Relaxing Gas. Zhurnal vychislit. matem. i matem. fiz., Vol. 6, No. 6, 1966.

56. Appleton, I. P. Structure of a Prandtl-Meyer Expansion in an Ideal Dissociating Gas. Phys. Fluids, Vol. 6, No. 8, 1963.

57. Clever, I. W. The Two-Dimensional Flow of an Ideal Dissociating Gas. Granfield College of Aeronautics, Report No. 123, 1959.

58. Stulov, V. P. Flow of an Ideally-Dissociating Gas around a Convex Body with Allowance for Nonequilibrium. Izvestiya AN SSSR, Otdeleniye tekhnicheskikh nauk (OTN), Mekhanika i mashiny, No. 3, 1962.

59. Wood, W. W. and F. R. Parker. Structure of a Centered Rarefaction Wave in a Relaxing Gas. Phys. of Fluids, Vol. 1, No. 3, 1958.

60. Arkhipov, V. N. Rarefaction Waves in a Relaxing Gas Mixture. PMTF, No. 4, 1962.

61. Arkhipov, V. N. and L. I. Severinov. Rotational Relaxation in a Plane-Parallel Rarefaction Wave. PMTF, No. 5, 1963.

62. Dubinskaya, N. V., R. A. Gzhelyak, and I. V. Igonina. Calculation of Prandtl-Meyer Flow with Allowance for Nonequilibrium Dissociation of Air. Numerical Methods in Gas Dynamics. Collection of Reports, VTs MGU, No. IV, 1965.

63. Blythe, P. A. Prandtl-Meyer Flow in a Relaxing Gas. ARC CP No. 727, 1964.

64. Glass, I. I. and A. Takano. Nonequilibrium Expansion Flows of Dissociated Oxygen and Ionized Argon around a Corner. In the Collection Progress in Aeronautical Sciences, Vol. 6, Pergamon Press, 1965.

65. Sundaram, T. R. Relaxation Entropy Layer for a Convex Corner in a Linearized Supersonic Flow, AIAA J., Vol. 6, No. 5, 1968.

66. Gladkov, A. A. Effect of a Relaxation Entropy Layer. PMTF, No. 1, 1964.

67. Freeman, N. C. Nonequilibrium Flow of an Ideal Dissociating Gas. J. Fluid Mech., Vol. 4, No. 4, 1958. See also the collection: Mekhanika, Vol. 55, No. 3, 1959.

68. Murzinov, I. N. Gas Flow in the Vicinity of the Critical Point of a Blunt Body at a Finite Excitation Rate of Vibrational Degrees of Freedom. Izvestiya AN SSSR, OTN, Mekhanika i mashiny, No. 6, 1961.

69. Blythe, P. A. The Effect of Vibrational Relaxation on Hypersonic Flow Past Blunt Bodies. Aeron. Quart., Vol. 14, 1963.

70. Belotserkovskiy, O. M., et al. Obtekaniye zatuplennykh tel sverkhzvukovym potokom gaza (Flow Around Blunt Bodies by a Supersonic Gas Stream), Second Edition, VTs AN SSSR, 1967.

71. Belotserkovskiy, O. M. and V. K. Dushin. Supersonic Gas Flow around Blunt Bodies. Zhurnal vychisl. matem. i matem. fiz., Vol. 4, No. 1, 1964.

72. Lun'kin, Yu. P. and F. D. Popov. Influence of Nonequilibrium Dissociation on Supersonic Flow Around Blunt Bodies. Zhurnal vychisl. mat. i mat. fiz., Vol. 4, No. 5, 1964.

73. Dushin, V. K. and Yu. P. Lun'kin. Supersonic Flow of Nonequilibrium-Dissociating Air around Blunt Bodies. ZhTF, Vol. 35, No. 8, 1965.

74. Lun'kin, Yu. P. and F. D. Popov. Influence of Vibrational-Dissociation Relaxation on Supersonic Flow around Blunt Bodies. ZhTF, Vol. 36, 1966, p. 4.

75. Koleshko, S. B., Yu. P. Lun'kin, and F. D. Popov. Influence /202 of Simultaneous Vibrational and Dissociative Relaxation on Supersonic Flow around Blunt Bodies. In the collection: Aerodinamicheskiye issledovaniya sverkhzvukovykh techeniy (Aerodynamic Study of Supersonic Flows). Moscow-Leningrad, Nauka Press, 1967.

76. Stulov, V. P. and G. F. Telenin. Nonequilibrium Supersonic Air Flow around a Sphere. Izvestiya AN SSSR, Mekhanika, No. 1, 1965.

77. Stulov, V. P. and L. I. Turchak. Supersonic Air Flow around a Sphere Considering Vibrational Relaxation. Izvestiya AN SSSR, MZhG, No. 5, 1966.

78. Sayapin, G. N. Study of Characteristics of Hypersonic Nonequilibrium Gas Flow around Blunt Bodies. Izvestiya AN SSSR, MZhG, No. 6, 1966.

79. Anisimov, S. I. and Yu. V. Khodyko. Flow of Gas around Leading Critical Point of a Blunt Body with Slow Excitation of Vibrations. ZhTF, Vol. 33, No. 11, 1963.

80. Stulov, V. P. and V. P. Shkadova. One-Dimensional Nonequilibrium Air Flow. Izvestiya AN SSSR, MZhG, No. 2, 1968.

81. Shkadova, V. P. Near-Equilibrium Air Flow around Bodies of Revolution. Izvestiya AN SSSR, MZhG, No. 1, 1969.

82. Stulov, V. P. and L. I. Turchak. Supersonic Flow around a Sphere of a Detonating Mixture. Izvestiya AN SSSR, MZhG, No. 6, 1968.

83. Stulov, V. P. and L. I. Turchak. Nonequilibrium Chemical Reactions in a Shock Layer during the Flow around a Sphere of a Mixture of Carbon Dioxide, Nitrogen, and Argon. Izvestiya AN SSSR, MZhG, No. 5, 1969.

84. Stulov, V. P. and L. I. Turchak. Supersonic Flow around Blunt Bodies in the Presence of Rapid Nonequilibrium Processes. Izvestiya AN SSSR, MZhG, No. 5, 1967.

85. Severinov, L. I. Calculation of the Supersonic Portion of a Perturbed Region in a Blunt Body in the Case of Supersonic Nonequilibrium Flow. Zhurnal vychisl. matem. i matem. fiz., Vol. 8, No. 3, 1968.

86. Dushin, V. K. Solution of a System of Relaxation Equations in the Calculation of a Reacting Gas Mixture Which Is Close to Equilibrium. Zhurnal vychisl, matem. i matem. fiz., Vol. 9, No. 5, 1969.

87. Kosorukov, A. L. Flow Around the Forward Part of a Blunt Body Considering Nonequilibrium Excitation of Vibrational Degrees of Freedom. Izvestiya AN SSSR, MZhG, No. 1, 1970.

88. Lebedev, M. G., V. B. Minostsev, G. F. Telenin and G. P. Tinyakov. Approximate Method of Determining the Influence of a Gas during Hypersonic Flow around Segmental Bodies. Izvestiya AN SSSR, MZhG, No. 2, 1969.

89. Stulov, V. P. Similarity Law in the Case of Supersonic Flow around Blunt Bodies. Izvestiya AN SSSR, MZhG, No. 4, 1969.

90. Shin, W. C. L. and J. B. Baron. Nonequilibrium Blunt Body Flow Using the Method of Integral Relations. AIAA J., Vol. 2, No. 6, 1964.

91. Springfield, J. F. Steady, Inviscid Flow of a Relaxing Gas about a Blunt Body with Supersonic Velocity. In the collection: Proceedings of the 1964 Heat Transfer and Fluid Mech. Inst., University of California Berkeley, Stanford, 1964.

92. Lick, W. Inviscid Flow of a Reacting Mixture of Gases around Blunt Body. J. Fluid Mech., Vol. 7, No. 1, 1960.

93. Hall, I. G., A. Q. Eschenroeder, and P. V. Marrone. Blunt Nose Inviscid Airflows with Coupled Nonequilibrium Processes, JASS, Vol. 29, No. 9, 1962.

94. Bohachevsky, I. O. and E. L. Rubin. A Direct Method for Computation of Nonequilibrium Flows with Detached Shock Waves. AIAA J., Vol. 4, No. 4, 1966.

95. Bloom, M. and M. Steiger. Inviscid Flows with Nonequilibrium Molecular Dissociation for Pressure Distributions Encountered in Hypersonic Flight. JASS, Vol. 24, No. 11, 1960.

96. Ellington, D. Approximate Method for Hypersonic Nonequilibrium Body Airflow. AIAA J., Vol. 1, No. 8, 1963.

97. Conti, R. J. Stagnation Equilibrium Layer in Nonequilibrium Blunt Body Flows. AIAA J., Vol. 2, No. 11, 1964. /203

98. Conti, R. J. A Theoretical Study of Nonequilibrium Blunt Body Flows. J. Fluid Mech., Vol. 24, Part 1, 1966.

99. Vaglio-Laurin, R. and M. H. Bloom. Chemical Effects in External Hypersonic Flows. In the Collection: Hypersonic Flow Research. New York and London, 1962, pp. 205 - 254. See also: Study of Hypersonic Flows, Moscow, IL, 1964.

100. Conti, R. and M. Van Dyke. Inviscid Reacting Flow Near a Stagnation Point. J. Fluid Mech., Vol. 35, 1969, p. 4.

101. Hermann, R. and J. Theones. Hypersonic Flow of Air past Circular Cylinder with Nonequilibrium Oxygen Dissociation Including Dissociation of the Free Stream. In the collection: Jahrbuch 1965 der WGIR (1965 Yearbook of the WGIR), Braunschweig, 1966.

102. Bohachevsky, I. O., E. L. Rubin, and R. E. Mates. A Direct Method for Computation of Nonequilibrium Flows with Detached Shock Waves. I. Two-Dimensional Flows. II. Axisymmetric Blunt Body at an Angle of Attack. AIAA J., Vol. 4, No. 4, 1966.

103. Perini, L. L. and W. L. Melnik. Nonequilibrium Hypersonic Flow past Smooth Symmetric Bodies. J. Spacecraft and Rockets, Vol. 5, No. 3, 1968.

104. Katzen, E. D. and G. E. Kaattary. Flow around Blunt Bodies Including Effects of Angles of Attack, Nonequilibrium Flow and Vapor Injection. In the Collection: Amer. Inst. Aeronaut. and Astronaut. Entry Technology Conference, October 12 - 14, 1964. AIAA Publ. CP-9, 1964.

105. Van Dyke, M. The Blunt Body Problem Revisited. In the collection: Fundamental Phenomena in Hypersonic Flow. Proc. of the Internat. Symposium Sponsored by Cornell Aeronautical Laboratory, New York, 1966.

106. Sussman, M. B. and J. R. Baron. Approximate Analysis of Linearized Inviscid Relaxing Gas Flow. Phys. of Fluids, X, Vol. 10, No. 10, 1967.

107. Nanda, K. D. Nonequilibrium Flow Past an Infinite Corrugated Cylinder. AIAA J., Vol. 4, No. 8, 1966.

108. Maslennikov, V. G. Study of Outgoing Shock Wave in the Case of Supersonic Motion of Ellipsoids of Revolution in Gases with Differing Intramolecular Structure. In the collection: Aerodinamicheskiye issledovaniya sverkhzvukovykh techeniy (Aerodynamic Study of Supersonic Flows). Moscow-Leningrad, 1967.

109. Inouye, Mamoru. Shock Standoff Distance for Equilibrium Flow Around Hemispheres Obtained from Numerical Calculations. AIAA J., Vol. 3, No. 1, 1965.

110. Ball, W. H. and F. J. Lyon. Nonequilibrium Chemistry Effects in Hypersonic Shock Layers. AIAA Paper No. 66-420, 1966.

111. Gibson, W. E. and P. V. Marrone. Correspondence between Normal Shock and Blunt Body Flows. Phys. of Fluids, Vol. 5, No. 12, 1962.

112. Gibson, W. E. and P. V. Marrone. A Similitude for Nonequilibrium Phenomena in Hypersonic Flight. In the collection: The High Temperature Aspects of Hypersonic Flow. Oxford and others, 1964.

113. Gibson, W. E. Dissociation Scaling for Nonequilibrium Blunt Nose Flows. ARS J., Vol. 32, No. 2, 1962.

114. Ellington, D. Binary Scaling Limits for Hypersonic Flight. AIAA J., Vol. 5, No. 9, 1967.

115. Sisco, W. B. and J. M. Fiskin. Basic Hypersonic Plasma Data of Equilibrium Air for Electromagnetic and other Requirements. Planetary and Space Science, Vol. 6, 1961.

116. Martin, J. Atmospheric Entry. Moscow, Mir Press, 1969.

117. Campard, D. and M. Faucheux. Determination of Dissociated and Ionized Particle Densities in Nitrogen Plasma in Nonequilibrium Flow, Recherche aerospatiale, Vol. I - II, No. 110, 1966.

118. Hermann, R. Hypersonic Aerodynamic Problems at Re-Entry of Space Vehicles. Univ. of Alabama Research Institute, Rep., No. 29, 1965.

119. McKenzie, R. L. A Correspondence of Blunt Body Nonequilibrium Shock Layers. AIAA J., Vol. 5, 1968.

120. Polyanskiy, O. Yu. Influence of Nonequilibrium Processes on Gasdynamic Parameters in Hypersonic Equipment and at the Critical Point of a Blunt Body. Uchenyye zapiski TsAGI, No. 5, 1971.

121. Vinocur, M. On Stagnation Point Conditions in Nonequilibrium Inviscid Blunt Body Flows. J. Fluid Mech., Vol. 43, 1970, p. 1.

CHAPTER 5

NONEQUILIBRIUM PROCESSES IN A BOUNDARY LAYER

Heat transmission in rocket nozzles and on the surface of /205
hypersonic aircraft, fuel combustion, chemically reacting flows in the wakes behind bodies, and other important problems related to the development of hypersonic engines and aircraft designed for entry into the atmosphere may be studied within the framework of boundary layer theory.

At the present time, there are several monographs [1 — 4] (not to speak of numerous articles), which examine chemical reactions in a boundary layer. However, the research is frequently limited to an infinitely large reaction rate in a gas or on a surface (i.e., the case of equilibrium), which excludes chemical kinetics from the analysis.

This chapter (with exception of Section 5.5) only discusses the laminary boundary layer with chemical reactions; however, the basic conclusions obtained may be applied to a turbulent boundary layer. Combustion processes in jets, surface sublimation, and gas blowout are not examined; each of these questions represents an independent problem. Some of them have been discussed in the monographs indicated above.

5.1. Boundary layer equations in the case of nonequilibrium physico-chemical processes

Initial equations and boundary conditions

Let us first give the basic equations of a laminar boundary layer for a multi-component mixture of gases in the case of chemical reactions. In accordance with the Prandtl method [1, 5], we assume that $\delta \ll R_b$ (δ — boundary layer thickness, and R_b — radius of curvature of the generatrix or characteristic length of a body). From the general equations (2.32), (2.34), (2.35), and (2.39) in the case of planar (j = 0) or axisymmetric (j = 1) /206 steady motion of a mixture of gases, we obtain the following expressions:

Equation of continuity

$$\frac{\partial (\rho u r^j)}{\partial x} + \frac{\partial (\rho v r^j)}{\partial y} = 0; \tag{5.1}$$

Equation of momentum

$$\rho\left(u \frac{\partial u}{\partial x} + v \frac{\partial u}{\partial y}\right) = -\frac{dp}{dx} + \frac{\partial}{\partial y}\left(\mu \frac{\partial u}{\partial y}\right); \tag{5.2}$$

Equation of energy

$$\rho\left(u \frac{\partial h}{\partial x} + v \frac{\partial h}{\partial y}\right) - u \frac{dp}{dx} = -\frac{\partial (q)}{\partial y} + \mu \left(\frac{\partial u}{\partial y}\right)^2; \tag{5.3}$$

Equation of conservation of mass concentration of the i-th component

$$\rho\left(u\frac{\partial\alpha_i}{\partial x}+v\frac{\partial\alpha_i}{\partial y}\right)=-\frac{\partial}{\partial y}(\rho\alpha_i\hat{v}_i)+M_iJ_i; \qquad (5.4)$$

Equation of state

$$p=\left(\sum_i\frac{\alpha_i}{M_i}\right)\rho RT, \qquad (5.5)$$

where the enthalpy h is determined with allowance for the chemical energy for forming the i-th component as

$$h=\sum_i\alpha_ih_i; \qquad (5.6)$$

$$h_i=\int_0^T c_{pi}dT+h_i^\circ. \qquad (5.7)$$

In Formulas (5.1) — (5.7) the coordinates x, y, and r, and also the corresponding velocity components u and v are determined as is shown in Figure 5.1 [the half-angle aperture of a wedge ν = 0 (r = 0) corresponds to a flat plate]. The quantities ρ, μ, and p, respectively, designate the density, viscosity coefficient, and pressure of a mixture of gases; M_i designates the molecular weight of the i-th component; α_i — its mass concentration; $\hat{v}_i$ — diffusion rate; c_{pi} — specific heat of uniformly excited degrees of freedom at a constant pressure;* J_i — rate at which the i-th component of a gas is formed per unit volume, and h_i° is the heat of formation (for molecules h_i° = 0).

*The vibration energy e_k is added to the right side of Equation (5.7) in the case of relaxation of vibrational degrees of freedom. This energy is determined from a relaxation equation such as (1.75). An example is examined in Section 5.3.

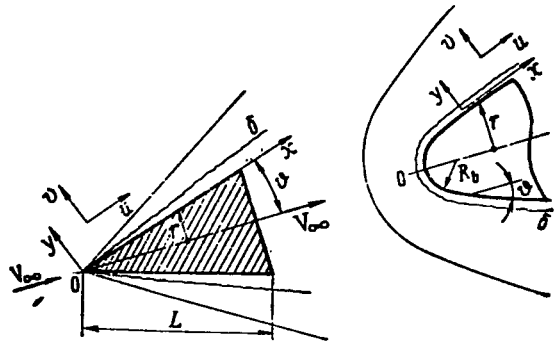

Figure 5.1. Coordinate system.

The conservation equations obtained differ from the corresponding equations of classical boundary layer by the heat flux q, and also by the quantities $\hat{v}_i$ and J_i. /207

For the n-th component boundary layer (under the condition $\partial p/\partial y = 0$), the diffusion rate is determined from the following equation in agreement with the kinetic theory [6]

$$\sum_{k=1}^{n} \frac{\alpha_k}{M_k D_{ik}} (\hat{v}_i - \hat{v}_k) = \sum_{k=1}^{n} \frac{\alpha_k}{M_k} \left(\frac{\nabla \alpha_k}{\alpha_k} - \frac{\nabla \alpha_i}{\alpha_i} \right) + \nabla \ln T \sum_{k=1}^{n} \frac{\alpha_k}{\rho M_k D_{ik}} \left(\frac{D_k^T}{\alpha_k} - \frac{D_i^T}{\alpha_i} \right), \tag{5.8}$$

where $i \neq k$ and $i = 1, 2, \ldots, n$; D_{ik} — binary diffusion coefficient between the components i and k; D_i^T — thermal diffusion coefficient.

It is rather complex to calculate a nonequilibrium boundary layer. Therefore, it is desirable to write the expression for the diffusion rate. In comparison with diffusion caused by the concentration gradients, the contribution made by thermal diffusion is usually small [6]. For binary mixture components, Equation (5.8) may then be reduced to the well-known Fick relationship

$$\alpha_i \hat{v}_i = -D_{ik} \nabla \alpha_i. \tag{5.9}$$

A similar relationship may be used in the case of a multicomponent mixture, if M_k and D_{ik} do not greatly differ. This problem is examined in more detail, for example, in [7].

In accordance with (5.9), Equation (5.4) assumes the form /208

$$\rho\left(u\frac{\partial a_i}{\partial x}+v\frac{\partial a_i}{\partial y}\right)=\frac{\partial}{\partial y}\left(\rho D_i\frac{\partial a_i}{\partial y}\right)+M_iJ_i. \qquad (5.10)$$

Let us now turn to the expression J_i. For chemically frozen flows, we have

$$J_i=0. \qquad (5.11)$$

In the general case, we must use Expression (1.36) for J_i.

In the case of the dissociation-recombination of a diatomic gas, which is of the greatest interest, we may write

$$J\left(\frac{M}{\rho}\right)=-4k_r\left(\frac{p}{RT}\right)^2\left[\frac{\alpha^2}{1+\alpha}-\left(\frac{\alpha_e^2}{1-\alpha_e^2}\right)(1-\alpha)\right], \qquad (5.12)$$

where α designates the atomic mass concentration, and $\alpha_e^2/(1-\alpha_e^2)$, which corresponds to the equilibrium concentration, is determined by means of (2.15). The first term in the brackets gives the recombination rate, and the second gives the dissociation rate.

In an examination of the dissociation-recombination of air in a boundary layer, the model of a binary mixture of atoms and molecules is frequently used. Actually, the transport characteristics and the values of k_r are very similar for nitrogen and for oxygen. Therefore, when the predominant reaction is recombination, we may combine all the atoms and all the molecules, and

— using the corresponding average heat of formation — we obtain an acceptable solution. However, if the predominate reaction is dissociation, the error obtained by combining nitrogen and oxygen is very great. This is due to the fact that the expression for $\alpha_e^2/(1-\alpha_e^2)$ contains the exponential function of the reaction heat [see Equation (2.15)], which is very different for oxygen and nitrogen.

For a multi-component system, the thermal flux is caused by thermal conductivity and the transport of energy by diffusing components.* Therefore,

$$q = -\lambda\frac{\partial T}{\partial y} - \rho\sum_{i=1}^{n} h_i D_i \frac{\partial \alpha_i}{\partial y}, \qquad (5.13)$$

where λ is the thermal conductivity coefficient, and Relationship (5.9) is used for the diffusion rate.

Using the expression obtained for q, we may rewrite the energy equation (5.3) in the following form /209

$$\rho\left(u\frac{\partial h}{\partial x} + v\frac{\partial h}{\partial y}\right) - u\frac{\partial p}{dx} = \frac{\partial}{\partial y}\left(\lambda\frac{\partial T}{\partial y} + \rho\sum_i h_i D_i \frac{\partial \alpha_i}{\partial y}\right) + \mu\left(\frac{\partial u}{\partial y}\right)^2. \qquad (5.14)$$

Thus, for determining (5 + i) unknown quantities ρ, u, v, h, T, and α_i, we have the same number of equations (5.1), (5.2), (5.14), (5.10), (5.5), and (5.6). Instead of one of the equations (5.10), we may use the relationships

$$\sum_i \alpha_i = 1; \quad \sum_i \alpha_i \hat{v}_i = 0; \quad \sum_i M_i J_i = 0. \qquad (5.15)$$

*In the case of relaxation of vibrational degrees of freedom, the expression for the heat flux is found in Section 5.3.

Instead of (5.14), other forms of the energy equation may be used. For example, for total enthalpy

$$H=h+u^2/2, \tag{5.16}$$

combining Equation (5.14) with Equation (5.2), multiplied by u, and using the continuity equation, we obtain the energy equation in the following form

$$\rho\left(u\frac{\partial H}{\partial x}+v\frac{\partial H}{\partial y}\right)=\frac{\partial}{\partial y}\left\{\frac{\mu}{\mathrm{Pr}}\left[\frac{\partial H}{\partial y}+(\mathrm{Pr}-1)\frac{\partial (u^2/2)}{\partial y}+\right.\right.$$
$$\left.\left.+\sum_i(\mathrm{Le}_i-1)\,h_i\frac{\partial a_i}{\partial y}\right]\right\}, \tag{5.17}$$

where the Prandtl number Pr is determined by the relationships

$$\mathrm{Pr}=\frac{\mu c_p}{\lambda} \tag{5.18}$$

and

$$c_p=\sum_i a_i c_{pi}. \tag{5.19}$$

The Lewis-Semenov number Le_i for the component i is determined as follows

$$\mathrm{Le}_i=\frac{\rho D_i c_p}{\lambda}=\frac{\mathrm{Pr}}{\mathrm{Sc}_i}, \tag{5.20}$$

and the Schmidt number

$$\mathrm{Sc}_i=\frac{\mu}{\rho D_i}. \tag{5.21}$$

In another form, the energy equation may be written for the /210 temperature T. It may be obtained from (5.14) by means of (5.10) in the form

$$\rho c_p\left(u\frac{\partial T}{\partial x}+v\frac{\partial T}{\partial y}\right)-u\frac{dp}{dx}=\frac{\partial}{\partial y}\left(\lambda\frac{\partial T}{\partial y}\right)+$$
$$+\sum_i \rho D_i\left(\frac{\partial a_i}{\partial y}\right)\left(\frac{\partial h_i}{\partial y}\right)+\mu\left(\frac{\partial u}{\partial y}\right)^2-\sum_i h_i M_i J_i. \qquad (5.22)$$

It must be noted that in the case of frozen reactions in a gas, the role of total enthalpy H in (5.17) is played by the frozen total enthalpy

$$H_f=\sum_i a_i\int_0^T c_{pi}dT+\frac{u^2}{2}=H-\sum_i a_i h_i^\circ. \qquad (5.23)$$

Let us now examine the boundary conditions. In accordance with the general boundary layer theory, the variables on the outer boundary (in the case $y \to \infty$ or $y = \delta$) are assumed to be given, i.e.,

$$u=u_\delta; \qquad (5.24)$$

$$a_i=a_{i\delta}; \qquad (5.25)$$

$$T=T_\delta \qquad \text{etc.} \qquad (5.26)$$

The form of the boundary conditions on the surface (when $y = 0$) depends on the formulation of the problem. Since the processes of combustion, sublimation, and blowout of gas are not considered, it is assumed that the surface of the body is impermeable, and its form unchanged.*

*More general cases of boundary conditions on a surface are given, for example, in [2] or [4].

For the velocity components on a surface, we may use the attachment conditions

$$u=v=0. \tag{5.27}$$

The surface temperature is assumed to be known

$$T=T_w. \tag{5.28}$$

If a heat insulated surface is considered, then

$$q_w=0. \tag{5.29}$$

The boundary condition on the surface for Equation (5.10) is obtained from the equality of the mass flux $\left(\rho_i D_i \frac{\partial a_i}{\partial y}\right)_w$ of the component i, transported by diffusion from a gas, and the rate at which the ith component is formed as a result of the catalytic /211 action of the surface itself [see Chapter 1, Formula (1.54)]. Thus, we obtain

$$\rho D_i \frac{\partial a_i}{\partial y}=k_{wi}\left[(\rho a_i)^{n_i}-\frac{(\rho a_i)_e^{n_i}}{(\rho a_j)_e^{n_j}}(\rho a_j)^{n_j}\right]. \tag{5.30}$$

The indices "i" and "j" refer to the reagent and the reaction products. In the recombination of a dissociated diatomic gas (i — atoms; j — molecules) for a cold surface ($T_W \lesssim$ 2000 K for air), we may disregard the second term in the brackets in the Equation (5.30); in addition, the order of the reaction n_i = 1. The catalycity coefficient k_W, which is assumed to be a known function of the coordinate x on a surface, is directed connected with the so-called recombination efficiency γ_W, determined as the ratio of the number of recombining atoms to the total number

of atoms which fall on a unit surface per unit of time

$$\gamma_w = k_w \sqrt{\frac{2\pi M_i}{RT_w}} \quad \text{for} \quad n_i = 1). \tag{5.31}$$

Table 14 gives the characteristic values of k_w for different materials located in a stream of air or nitrogen.

The boundary conditions on the surface for Equations (5.17) and (5.14) may be written in the form

$$H_w = h_w = \sum_i \alpha_{iw} \int_0^{T_w} c_{pi} dT + \sum_i \alpha_{iw} h_i^\circ. \tag{5.32}$$

As a rule, since the values of α_{iw} are not known previously, the boundary conditions for enthalpy are determined from a solution of Equation (5.10) for the component concentration. Using the energy equation in the form (5.22) with the boundary condition (5.28) has no apparent advantages as compared with Equations (5.14) or (5.17), since the solution of Equation (5.22) greatly depends on the equation for the component concentration (5.10).

In conclusion, let us give the expression for the heat flux on a surface. Using Expression (5.13), we may write

$$q_w = q_c + q_d = -\lambda_w \left(\frac{\partial T}{\partial y}\right)_w - \rho_w \sum_i D_{iw} h_{iw} \left(\frac{\partial a_i}{\partial y}\right)_w, \tag{5.33}$$

where q_d is part of the heat flux caused by the transport of energy by the diffusing components, or in another form

/212

$$-q_w=\frac{\mu_w}{\mathrm{Pr}_w}\left[\left(\frac{\partial H}{\partial y}\right)_w+\sum_i(\mathrm{Le}_{iw}-1)h_{iw}\left(\frac{\partial a_i}{\partial y}\right)_w\right]. \qquad (5.34)$$

If no chemical reactions take place either in the gas or on the surface, the heat flux may be expressed in the form

$$-q_{wf}=\frac{\mu_w}{\mathrm{Pr}_w}\left(\frac{\partial H_f}{\partial y}\right)_w. \qquad (5.35)$$

We may determine the influence of chemical reactions on the heat flux, if we approximately assume $\mathrm{Pr} \approx \mathrm{Le}_i \approx 1$. Thus, for a boundary layer both with chemical reactions and in their absence, the energy equations and the expressions for the heat fluxes identically coincide, with the exception of the fact that in the first case, expression H is used, and in the second case — H_j.

Consequently, /213

$$\frac{q_w}{q_{wf}}\approx\frac{H_\delta-h_w}{H_{f\delta}-h_{fw}}=1+\frac{\sum_i a_{i\delta}h_i^\circ-\sum_i a_{iw}h_i^\circ}{H_{f\delta}-h_{fw}}. \qquad (5.36)$$

Equation (5.36) shows that the heat flux is increased by the quantity

$$\frac{\sum_i a_{i\delta}h_i^\circ-\sum_i a_{iw}h_i^\circ}{H_{f\delta}-h_{fw}}$$

due to the chemical reactions which take place either in the gas phase or on the surface. The maximum increase in the heat flux is characteristic for an equilibrium boundary layer close to a cold surface or for an arbitrary state of the boundary layer

TABLE 14

DATA FOR THE CATALYCITY COEFFICIENT OF A SURFACE k_w (WHEN T_w = 350 K)

Surface	Gas	k_w cm/sec
Copper	Nitrogen	1000
	Oxygen	2200
Cupric oxide	Nitrogen	400 — 1400
	Oxygen	250 — 2600
Nickel	Nitrogen	400
	Oxygen	360
Nickel oxide	Oxygen	20 — 800
Silver	Nitrogen	2400
	Oxygen	3100
	Air	1000 — 2600
Silver oxide	Nitrogen	130
	Oxygen	1600 — 2200
Gold	Oxygen	70 — 3100
Platinum	Nitrogen	1300
	Oxygen	1300
Platinum oxide	Oxygen	10 — 90
Tungsten	Nitrogen	26
Silicon monoxide	Oxygen	<1
	Air	1 — 130

close to an ideally catalytic cold surface (in both cases, $\alpha_{iw} = 0$).

Equation (5.36) gives only a qualitative representation, since the quantity $\Sigma\alpha_{iw}h_i^\circ$ was not known beforehand.

Transport coefficients

To solve the equations given above, it is necessary to have the appropriate expressions for the transport coefficients μ, λ, and D_{ij} of a gas mixture. The transport coefficients are determined in the kinetic theory of gases by solving the Boltzmann equation by means of the first two terms in the Chapman-Enskog expansion [6]. This theory gives the best results when applied to a monoatomic neutral gas. However, it has been shown a posteriori that the region in which these results may be applied is much wider than follows from the premises of the theory. Let us give the final expressions for the transport coefficients [2, 4].

The viscosity coefficient of the i-th component of a pure gas may be expressed by the formula

$$\mu_i \text{ g/cm·sec} = 2{,}67\cdot 10^{-5}\frac{\sqrt{M_i T}}{\sigma_i^2 \Omega_i^{(2,2)*}}, \qquad (5.37)$$

where M_i is the molecular weight; T — temperature in K; σ_i — collision diameter (in Å), and $\Omega_i^{(2/2)*}$ — "collision" integral, which will be discussed later. For a mixture of gases containing n components, an adequate approximation is given by the Wilke formula

/214

$$\mu = \sum_{i=1}^{n} \frac{\mu_i}{\left[1 + \sum\limits_{\substack{k=1 \\ k\neq i}}^{n} G_{ik}\frac{x_k}{x_i}\right]}, \qquad (5.38)$$

where μ_i is determined by Formula (5.37); x_i is the molar concentration of the i-th component

$$\left(x_i = \frac{a_i}{M_i}\Big/\sum_i a_i/M_i\right);$$

$$G_{ik}=\frac{[1+(\mu_i/\mu_k)^{1.2}(M_k/M_i)^{1/4}]^2}{(2\sqrt{2})\sqrt{1+(M_i/M_k)}}. \qquad (5.39)$$

The binary diffusion coefficients, which in the last analysis express the diffusion flows of a multi-component mixture, are determined by the formula

$$D_{ij}\ \mathrm{cm}^2/\mathrm{sec}=D_{ji}=2{,}63\cdot10^{-3}\frac{\sqrt{(M_i+M_j)/2M_iM_jT^3}}{p\sigma_{ij}^2\Omega^{(1,1)*}}, \qquad (5.40)$$

where p is the pressure in kG/cm^2, and $\sigma_{ij}=\frac{1}{2}(\sigma_i+\sigma_j)$ is the collision diameter in Å and $\Omega^{(1,1)*}$ — "collision" integral, which will be examined later.

In the case of a multi-atomic gas, the transport coefficients and even the form of the equations themselves depend on the nature of the flow and the relaxing degree of freedom [8, 9, 10, 11]. It is very difficult to calculate this type of nonequilibrium flows, since in the majority of cases the effective excitation cross sections of internal degrees of freedom are unknown. Only in a few particular cases is it possible to carry out the calculations up to the end. For example, this was done in the study by V. M. Kuznetsov [12] for vibrational relaxation.*

For practical calculations, it is necessary to simplify the problem, using the assumptions which lead to satisfactory accuracy. An approximate asymptotic method of obtaining the transport properties and equations of motion of multi-atomic nonequilibrium gases and their mixtures was developed, for example, in a study by V. S. Galkin and M. N. Kogan [13]. They found that the viscosity coefficient μ has the same value as for a monatomic

*This case was examined in greater detail in Section 5.3.

gas (or a mixture of monatomic gases). The internal degrees of freedom only influence the heat conductivity. Thus, if /215

$$\lambda_i \text{ cal/cm·sec·K)} = \frac{15}{4} R\mu_i/M_i, \qquad (5.41)$$

where λ_i is the thermal conductivity coefficient of a monatomic gas, calculated according to the Chapman-Enskog theory, then for a pure multi-atomic gas we may write

$$\lambda_i' = \lambda_i + \rho D c_{vi},$$

where D is the self-diffusion coefficient; c_{vi} is the specific heat coefficient of internal degrees of freedom which are in equilibrium with the translational degrees of freedom.

The second term represents the so-called modified Aiken correction [6], with which the expression for λ_i' in the form

$$\lambda'/\lambda = 0{,}115 + 0{,}354 c_{pi} M_i/R = 0{,}469 + 0{,}354 c_{vi} M_i/R \qquad (5.42)$$

gives a good agreement with experimental data for many gases in a wide temperature range. In the case of a mixture of multi-atomic gases, similar formulas have a very complex form. At the present time, the following simplified Mason and Sachsen formula is widely used

$$\lambda = \sum_{i=1}^{n} \frac{\lambda_i'}{\left[1 + 1{,}065 \sum_{k=1}^{n} G_{ik} x_k/x_i\right]}, \qquad (5.43)$$

where λ_i' is determined by Formula (5.42), and G_{ik} — by Formula (5.39).

In order to determine the transport coefficients, it is necessary to know σ and ε — parameters of the intramolecular interaction potential and $\Omega^{(l,s)*}$ — the value of the "collision" integrals.*

In particular, for the frequently used Lennard-Jones potential

$$\varphi = 4\varepsilon_i [(\sigma_i/r)^{12} - (\sigma_i/r)^6] \qquad (5.44)$$

(Figure 5.2), the values of ε_i and σ_i found empirically for certain gases are given in Table 15.**

The dependence of $\Omega^{(1,1)*}$ and $\Omega^{(2,2)*}$ on kT/ε for the Lennard-Jones potential is shown in Figure 5.3.

Using the formulas given above, we can calculate the air transport properties up to the temperatures at which there is great ionization of particles. These calculations have been performed by many authors (see, for example, [14 — 17]). It should be noted that the computational accuracy in each case does not exceed 25%. Figures 5.4 and 5.5 give certain results derived from calculating the viscosity coefficient μ and the thermal conductivity coefficient λ of air in the temperature range T = 2000 — 6000 K at a pressure of p = 1 kG/cm^2. Figure 5.6 shows the dependence of the parameters Pr, Le, and Sc [see (5.18), (5.20), and (5.21)] on the concentration of atoms α for the model of an ideally dissociating gas (oxygen). /216

*The integrals $\Omega^{(l,s)*}$ express the difference between the molecule model employed and the model of solid spheres. For solid spheres, all $\Omega^{(l,s)*} = 1$.

**In a calculation of the parameters of dissimilar molecular interactions, the "combinational rules" are used:

$$\sigma_{ij} = \frac{1}{2}(\sigma_i + \sigma_j); \quad \varepsilon_{ij} = \sqrt{\varepsilon_i \varepsilon_j}.$$

TABLE 15

EMPIRICAL VALUES OF FORCE CONSTANTS FOR THE LENNARD-JONES POTENTIAL

Gas	O_2	O	N_2	N	NO	CO_2
ε/k in K	128	~59000	79,8	~113200	119	190
σ in Å	3,54	1,07	3,75	0,97	3,47	4,00

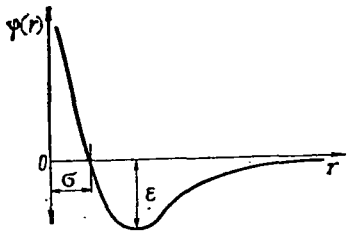

Figure 5.2. Form of Lennard-Jones potential.

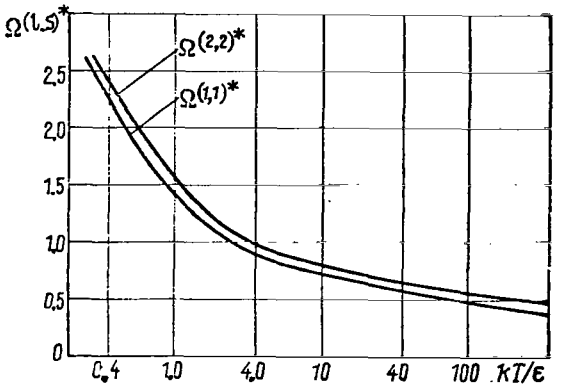

Figure 5.3. Value of reduced collision integrals for the Lennard-Jones potential.

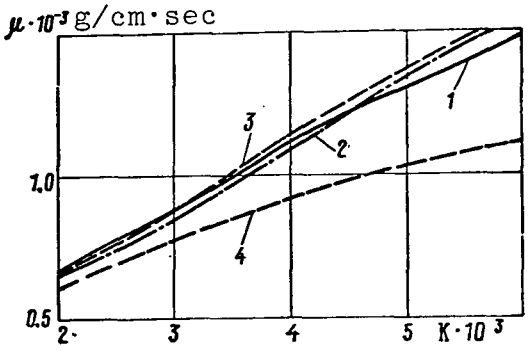

Figure 5.4. Viscosity coefficient for equilibrium air at a pressure of p = 1 kG/cm².

1 — computational results from [14]; 2 — from [15]; 3 — from [16]; 4 — calculation based on the Sutherland formula.

These values maintain the same relationship for air [2]. To simplify the calculations, it is sometimes assumed that these /217 parameters are constants (Pr ≈ 0.7; Le ≈ 1.4; Sc ≈ 0.5) or even equal unity.

At high temperatures, the characteristics of the air transport properties remain a constant source of unreliability in the

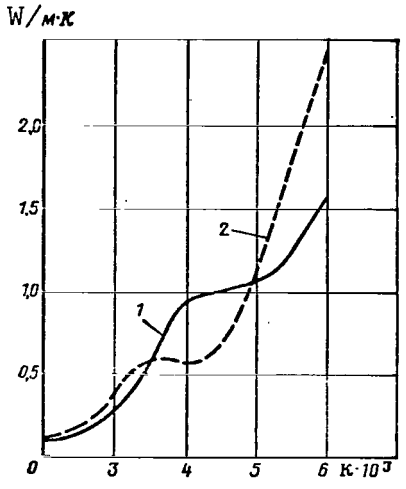

Figure 5.5. Thermal conductivity coefficient for equilibrium air at a pressure of p = 1 kG/cm^2.
1 — computational results from [14]; 2 — from [16].

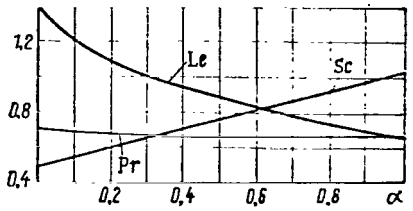

Figure 5.6. Dependence of the Prandtl number Pr, Lewis-Semenov number Le, and the Schmidt number Sc on the concentration of atoms α for ideally dissociating oxygen.

accuracy of calculating the heat transfer in reacting gas mixtures, due to the absence of a sufficient amount of reliable experimental data.

Reduction of boundary layer equations to standard form

In order to simplify the solution of the initial equations, it is advantageous to change to new variables (similarity coordinates). Using the Dorodnitsyn transformation in a form proposed by Lees [18] (see also [19]), we introduce

$$\eta = \frac{r^j u_\delta}{\sqrt{2\xi}} \int_0^y \rho dy; \tag{5.45}$$

$$\xi = \int_0^x \rho_\delta \mu_\delta u_\delta r^{2j} dx. \tag{5.46}$$

The continuity equation (5.1) is automatically satisfied by introducing the stream function ψ. Let us determine the dimensionless stream function f in the form $f(\eta, \xi)=\psi/\sqrt{2\xi}$. Then

$$f_\eta=\frac{\partial f}{\partial \eta}=\frac{u}{u_\delta}. \tag{5.47}$$

Let us also set

$$g=\frac{H}{H_\delta};\quad z_i=\frac{\alpha_i}{\alpha_{i\delta}};\quad l=\frac{\rho\mu}{\rho_\delta\mu_\delta}. \tag{5.48}$$

After transforming Equations (5.2), (5.10), and (5.14) to the variables η and ξ, we obtain the following equations:

Equation of momentum

$$(lf_{\eta\eta})_\eta+ff_{\eta\eta}+2\left(\frac{\xi}{u_\delta}\frac{du_\delta}{d\xi}\right)[\rho_\delta/\rho-f_\eta^2]=2\xi(f_\eta f_{\eta\xi}-f_\xi f_{\eta\eta}); \tag{5.49}$$

Energy equation

$$\left(\frac{l}{\mathrm{Pr}}g_\eta\right)_\eta+fg_\eta+\frac{u_\delta^2}{H_\delta}\left[l\left(1-\frac{1}{\mathrm{Pr}}\right)f_\eta f_{\eta\eta}\right]_\eta+ \\ +\left[\sum_i\frac{(\mathrm{Le}_i-1)}{\mathrm{Pr}}l\frac{\alpha_{i\delta}h_i}{H_\delta}(z_i)_\eta\right]_\eta=2\xi(f_\eta g_\xi-f_\xi g_\eta); \tag{5.50}$$

Equation for concentration

$$\left[\frac{l}{\mathrm{Sc}_i}(z_i)_\eta\right]_\eta+f(z_i)_\eta-2z_if_\eta\left(\frac{\xi}{\alpha_{i\delta}}\frac{d\alpha_{i\delta}}{d\xi}\right)+ \\ +\zeta_{gi}\frac{\dot{\omega}_i}{\alpha_{i\delta}}=2\xi[f_\eta(z_i)_\xi-f_\xi(z_i)_\eta], \tag{5.51}$$

where $\dot{\omega}_i = J_i\left(\frac{M_i}{\rho}\right)\tau_{gi}$ is the dimensionless formation rate of the i-th component; τ_{gi} — characteristic time of chemical reactions in the gas;* /219

$$\zeta_{gi} = 2\frac{L}{u_\infty}\frac{\rho_i\mu_\delta}{(\rho_i\mu_\delta)_0}\frac{1}{[F(x)]^2}\left(\frac{1}{\tau_{gi}}\right); \qquad (5.52)$$

$$F(x) = \frac{\dfrac{\rho_i\mu_\delta}{(\rho_i\mu_\delta)_0}\dfrac{u_\delta}{u_\infty}\left(\dfrac{r}{L}\right)^j}{\sqrt{\displaystyle\int_0^{\bar{x}}\frac{\rho_i\mu_\delta}{(\rho_\delta\mu_\delta)_0}\frac{u_\delta}{u_\infty}\left(\frac{r}{L}\right)^{2j}d\bar{x}}}, \qquad (5.53)$$

where $\bar{x} = x/L$; L (or R_b) is the characteristic size of the body** (see Figure 5.1).

The boundary conditions (5.25) — (5.32) assume the following form: when $\eta = 0$

$$f = f_\eta = 0; \qquad (5.54)$$

$$g = g_w(\xi) = \sum_i z_{iw}\frac{\alpha_{i\delta}\int_0^{T_w} c_{pi}dT}{H_\delta} + \sum_i z_{iw}\frac{\alpha_{i\delta}h_i^\circ}{H_\delta}; \qquad (5.55)$$

---

*For example, for J(M/ρ) determined by Expression (5.12), we have:

$$1/\tau_{gi} \sim k_r(p/RT)^2.$$

**The expression for ζ_{gi}, in the case of flow around the critical point of a body, wedge, and cone, is (5.73) and (5.125).

$$(z_i)_\eta = \zeta_{wi}(\xi)\left[(z_i)^{n_l} - \frac{1}{(\rho)^{n_i}}\frac{(\rho z_i)_e^{n_l}}{(\rho z_j)_e^{n_j}}(\rho z_j)^{n_j}\right], \tag{5.56}$$

where

$$\zeta_{wi}(\xi) = \frac{(\rho_w a_{i\delta})^{n_i} k_w}{\frac{l_w}{\mathrm{Sc}_w} a_{i\delta}\sqrt{\frac{(\rho_\delta \mu_\delta)_0 u_\infty}{2L}}}\frac{1}{F(x)}, \tag{5.57}$$

and when $\eta \to \infty$

$$f_\eta = g = z_i = 1. \tag{5.58}$$

The energy equation in the form (5.22) may be transformed to the form /220

$$\begin{aligned}&\left[\frac{c_p}{c_{p\delta}}\frac{l}{\mathrm{Pr}}\theta_{\gamma_i}\right]_{\gamma_i} + \frac{c_p}{c_{p\delta}} f\theta_{\gamma_i} - \sum\left[\frac{h_i}{c_{p\delta}T_\delta}\zeta_{gi}\dot{\omega}_i\right] + \\ &+ l\left(\frac{u_\xi^2}{c_{p\delta}T_\delta}\right)(f_{\gamma_i\gamma_i})^2 + \sum\left(\frac{c_{pl}}{c_{p\delta}}\right)\alpha_{i\delta}\frac{l}{\mathrm{Pr}}\mathrm{Le}_i(z_i)_{\gamma_i}\theta_{\gamma_i} = \\ &= f_{\gamma_i}\left[2\left(\frac{c_p}{c_{p\delta}}\right)\theta\frac{d\ln T_\delta}{d\ln\xi} + 2\left(\frac{u_\delta^2}{c_{p\delta}T_\delta}\right)\frac{\rho_\delta}{\rho}\left(\frac{d\ln u_\delta}{d\ln\xi}\right)\right] + \\ &+ 2\left(\frac{c_p}{c_{p\delta}}\right)\xi(f_{\gamma_i}\theta_\xi - f_\xi\theta_\eta),\end{aligned} \tag{5.59}$$

where $\theta = T/T^*_\delta$.

In the case of the given surface temperature, the boundary conditions for Equation (5.59) will be:

---

*When $M_\delta \gg 1$, in the expression for θ we must use the braking temperature T_0, instead of T_δ, since when $M_\delta \to \infty$ $T_\delta \to 0$. Correspondingly, $c_{p\delta}$ is replaced by c_{p0}.

for $\eta = 0$, $\theta = \theta_w = T_w/T_\delta$;

for $\eta \to \infty$, $\theta = 1$. (5.60

Reactions in a gas and on the surface (catalytic surface). Damkeler number

Let us clarify the physical meaning of parameters ζ_{wi} and ζ_{gi} determined by Equations (5.57) and (5.52) [3]. In the case of the linear law governing the concentration change across the boundary layer, the diffusion flow of the i-th component to the surface may be expressed in the form

$$\rho_w D_{iw}\left(\frac{\partial a_i}{\partial y}\right)_w = (z_i)_\eta\left[\frac{l_w}{\mathrm{Sc}_w} a_{i\delta}\sqrt{\frac{(\rho_\delta\mu_\delta)_0 u_\infty}{2L}} F(x)\right], \qquad (5.61)$$

where $(z_i)_\eta$ = const.

Consequently, the term in the brackets expresses the rate of formation of the i-th component per unit area of the surface with a single concentration difference across the boundary layer. Let us call this quantity the characteristic diffusion rate.

Turning to Equation (5.57), we may note that the denominator of the expression, which determines ζ_{wi}, precisely equals the characteristic diffusion rate. At the same time, the numerator of Equation (5.57) represents the characteristic rate of formation of the i-th component by means of a reaction on the surface (per unit area). The function ζ_{wi} therefore expresses /221 the ratio of the characteristic reaction rate on the surface to the characteristic diffusion rate for the i-th component. Taking the inverse values of the characteristic velocities and multiplying each of them by the density and the thickness of the boundary

layer, we may express ζ_{wi} by the ratio of the characteristic diffusion time (τ_{dif}) to the characteristic reaction time on the surface (τ_{sur}).

Thus,

$$\zeta_{wi}(\xi) = \left(\frac{\tau_{dif}}{\tau_{sur}}\right)i. \qquad (5.62)$$

This ratio of the characteristic times is called the Damkeler number of the surface for the i-th component.

Let us first consider the case when $\zeta_{wi} \to 0$. The right side of Equation (5.56) vanishes. Therefore, the reaction on the surface has almost no influence on the particle concentration in the boundary layer:

$$\left(\frac{\partial a_l}{\partial \eta}\right)_{\tau_i=0} = 0. \qquad (5.63)$$

This is the so-called flow with "frozen" reactions on the surface (or noncatalytic surface). It must be noted that freezing reactions on the surface do not necessarily mean that $k_w \to 0$. It simply means that the reaction rate is much less than the diffusion rate, although the absolute value of the reaction rate may be much greater.

Let us now consider another limiting case: $\zeta_{wi} \to \infty$. Since the value of the terms in the right side of Equation (5.56) is limited, this means that the value in the parentheses in the right side of the equation must approximate zero, as $\zeta_{wi} \to \infty$. It follows from this that

$$(z_l)_w \to (z_{le})_w. \qquad (5.64)$$

The limiting case, when the particle concentration on the surface approaches a value corresponding to the equilibrium state, is called flow with "equilibrium" reactions on the surface (or an ideally catalytic surface). It must again be pointed out that the equilibrium limit does not mean that we must have $k_w \to \infty$. It simply means that the reaction rate is much greater than the diffusion rate.

In the general case of the finite values of ζ_{wi}, the gas on the surface is in a nonequilibrium state, and the boundary condition (5.56) must be used in a general form.

Let us now consider Expression (5.52). Since the thickness of the boundary layer [see Equation (5.45)]

$$\delta \sim \sqrt{\frac{2(\rho_\delta \mu_\delta)_0 L}{u_\infty}} \frac{1}{F(x)} \frac{\rho_\delta \mu_\delta}{(\rho_\delta \mu_\delta)_0} \frac{1}{\rho}, \qquad (5.65)$$

it may be readily seen from Relationships (5.65) and (5.61) that /222 the coefficient when $1/\tau_{gi}$ in (5.52) is none other than the characteristic diffusion time (τ_{dif}) of the i-th component. It thus follows that

$$\zeta_{gi} = \left(\frac{\tau_{dif}}{\tau_g}\right)_i. \qquad (5.66)$$

By analogy with (5.62), let us call ζ_{gi} the Damkeler number of the gas phase.

Just as in the case of reactions on the surface, the condition $\zeta_{gi} \to 0$ means that the influence of reactions in the gas upon the boundary layer is negligibly small, and the boundary layer is called chemically "frozen." This does not mean that we must have $1/\tau_{gi} = 0$. It is only necessary that $\tau_{gi} \gg \tau_{dif}$.

In another limiting case $\zeta_{gi} \to \infty$, the quantity in the brackets in (5.12) must strive to zero, because each of the terms in (5.51) and (5.59) remains finite. This means that the rates of the forward and inverse reactions must be equal at each point of the boundary layer. Therefore, a state of local chemical equilibrium must exist in the boundary layer. Such a boundary layer is called an "equilibrium" layer. For an equilibrium boundary layer, the differential equation (5.51) may be replaced by an algebraic equation* (see Chapter 1).

Method of solving the equations

The system of equations and boundary conditions obtained for a boundary layer with nonequilibrium chemical reactions in the gas and on the surface is essentially a nonlinear system, and is difficult to study. Therefore, attempts were first made to obtain the solution with certain simplifying assumptions. First of all, nonequilibrium reactions in the gas and on the surface are examined separately.

---

*In the case of an equilibrium boundary layer and a noncatalytic surface, close to it there is a thin, nonequilibrium sublayer, in which there is a transition from equilibrium conditions in the gas to the condition $(\partial\alpha_i/\partial_y)_w = 0$ on the surface (the discontinuity $\partial\alpha_i/\partial y)_{y\to 0}$). However, if the surface is cold, the concentration of atoms is vanishingly small in a thick layer of gas, where $T \lesssim 2000$ K for air, and there is no reaction on the surface (due to the absence of a reagent), and the boundary condition becomes trivial ($\alpha_{iw} = 0$).

If it is assumed that the flow in the boundary layer is frozen ($\zeta_{gi} \to 0$, $M \cdot J_i \to 0$), then the basic reactions and the boundary conditions [with the exception of (5.56)] will be the same as in the classical boundary layer theory. In addition, the equations of momentum and energy in all cases which are important in practice are assumed to be independent of the equations for conservation of concentration, and their form coincides with the corresponding boundary layer equations, without allowing for chemical reactions. The only problem then remaining is to find a solution of the concentration equation (5.56) with the boundary condition (5.57), which would make it possible to determine the thermal flux q_d due to the reactions on the body surface. /223

In an analytical study of this problem, flows are usually examined for which the momentum equation has a self-modeling solution, which depends only on the coordinate η — a solution of the Blasius type or a solution for the critical point of a blunt body. In addition, as a rule, it is assumed that the numbers Sc_i and l are constant across the boundary layer.

Under these conditions, solutions were obtained for a flat plate, wedge, cone, and also in the vicinity of the critical point. The influence of the surface catalytic properties on the thermal flow to the body was clarified, including the case of a continuous or abrupt change in the catalycity along the surface.

On the other hand, in an investigation of nonequilibrium chemical reactions within the boundary layer, it is assumed that the reactions on the body surface are either frozen ($\zeta_{wi} \to 0$) or occur at such a rate that the gas on the surface is in a state of chemical equilibrium ($\zeta_{wi} \to \infty$). However, in this case the

presence of the term $M_i J_i/\rho$ in the equations, which is a complex function of the variables T and α_i, makes it difficult to perform any complete analytical investigation. The methods of the numerical solution of such a problem are still being finalized, and at the present time only a few cases have been calculated.

Nevertheless, by using the corresponding approximations and different methods (expansion in series, local similarity, integral method, etc.), it is possible to reach a fairly good understanding of the problem of a nonequilibrium boundary layer. In particular, the numerical methods have made it possible to determine the influence of the variation in the values of Le_i, Pr and ζ on the concentration profile and the distribution of the thermal flow along the body surface. In addition, several studies have recently appeared, in which an attempt was made to examine the concurrent influence of chemical reactions within the boundary layer and on the body surface.

Unfortunately, there is still very little experimental verification of the theoretical results obtained at the present time.

The basic methods of the solution and the results obtained will be examined in the following sections.

5.2. Vicinity of critical point. Flow around blunt bodies

/224

The simplest case for studying a nonequilibrium boundary layer is the vicinity of the critical point on a blunt body, where — in view of the flow symmetry — the characteristics only depend on the coordinates y (or η). Thus, all terms in

the right sides of Equations (5.49) — (5.51), (5.59) vanish, and a system of ordinary differential equations is obtained. At the same time, this case is of great practical importance, since one of the maximum values of the thermal flux corresponds to the critical point region.

Within the framework of the theory of an infinitely thin boundary layer, the conditions on the external boundary in the vicinity of the critical point may be assumed to be equilibrium conditions and to correspond to an adiabatic freezing of gas in the critical jet stream passing through a normal shock wave.* Thus, at hypersonic flight velocities, the longitudinal velocity gradient at the critical point may be determined, for example, from the modified Newton law for pressure distribution:

$$\beta_i = \left(\frac{du_\delta}{dx}\right)_{x=0} = \frac{1}{R_b}\sqrt{\frac{2(p_\delta - p_\infty)}{\rho_\delta}}, \qquad (5.67)$$

where R_b is the radius of the body bluntness; $p_\delta = p_0'$.

The body surface is usually a little colder than the gas at the external boundary of the boundary layer in the vicinity of the critical point. Therefore, the atoms will diffuse to the surface, recombining close to it. The state of the boundary layer (equilibrium, nonequilibrium, frozen) is determined by the relative velocity of the recombination and diffusion processes, i.e., the Damkeler number of the gas phase (5.52).

As an illustration, Figure 5.7 shows the flow regimes in the boundary layer as a function of altitude and flight velocity for a body with R_b = 1 m (noncatalytic surface, T_w = 1000 K). /225

*The flow influence in the viscous region upon the characteristics of inviscid flow will be examined in Section 5.4 for flights at high altitudes.

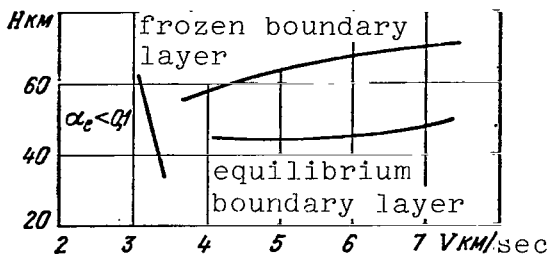

Figure 5.7. Flow regimes in boundary layer (in vicinity of critical point) for a body with R_b = 1 m (non-catalytic surface).

In calculating the boundaries, it was assumed that the concentration of atoms on the body surface differed by more than 10% from the corresponding values for frozen and equilibrium flow.

Let us examine in succession the different flow regimes in the boundary layer.

Equilibrium boundary layer

In determining the thermal flux through a body in the case of thermodynamic equilibrium within the boundary layer, the catalytic nature of the surface is of no importance, since $(\alpha_e)_{y\to 0} \approx 0$ for a cold surface.

In addition, it was found that in the case of an ideally catalytic surface, for which the boundary condition (5.64) has the same form ($\alpha_w \approx 0$), the values of the thermal flux both for equilibrium and for frozen flows in the boundary layer are very similar,* in spite of the differing distribution of atoms across the boundary layer. This means that the thermal flux in this case is primarily determined by the difference in the total flow enthalpies at the external boundary of the boundary layer and on the body surface, and differs very little from the specific mechanism of heat transfer.

Fay and Riddell [20] approximated the results of their calculations for an ideally catalytic surface with different

*For a Le number, which is very close to unity, see Formula (5.44).

values of $\rho\mu$, Le, and Pr by the following formula

$$(h_w = c_p T_w \ll H_\delta;\ j = 1):$$
$$-q_w \approx 0{,}763\,(\mathrm{Pr})^{-0{,}6}\left(\frac{\rho_w \mu_w}{\rho_\delta \mu_\delta}\right)^{0{,}1}\sqrt{\beta_i \rho_\delta \mu_\delta}\,[H_\delta - c_p T_w]\times \qquad (5.68)$$
$$\times\left\{1+(\mathrm{Le}^m-1)\,\frac{\Delta h^\circ \alpha_\delta}{H_\delta}\right\},$$

where $m = \begin{cases} 0.52 & \text{— for an equilibrium boundary layer;} \\ 0.63 & \text{— for a frozen boundary layer;} \end{cases}$

Δh° — the average value of recombination energy per unit mass of oxygen and nitrogen atoms.

Within the scatter of the data, experimental results [21, 22] obtained in a wind tunnel coincide with the dependence determined by Formula (5.68). An expression which is similar to (5.68) was obtained previously by Lees [18].

For practical calculations of the thermal flux at the critical point in the case of equilibrium flow (T_0 < 12000 K, $p_\infty = 10^{-3}$ — 10 kG/cm^2, a formula given in [23] is also used, which within an accuracy of ±7% corresponds with Formula (5.68): /226

$$-q_w\left[\frac{\text{kcal}}{\text{m}^2\cdot\text{sec}}\right] = 0{,}137\cdot 10^{-7}\sqrt{\frac{(1+j)\,\rho_\infty\left[\frac{\text{kG}\cdot\text{sec}^2}{\text{m}^4}\right]}{R_b\,[\text{m}]}}\times$$
$$\times\left(V_\infty\left[\frac{\text{m}}{\text{sec}}\right]\right)^{3{,}25}\left\{1-0{,}834\cdot 10^4\,\frac{c_p T_w\left[\frac{\text{kcal}}{\text{kg}}\right]}{\left(V_\infty\left[\frac{\text{m}}{\text{sec}}\right]\right)^2}\right\}, \qquad (5.69)$$

where R_b is the average contour radius of curvature at the critical point.

Utilizing the hypothesis of "local similarity" (i.e., considering ordinary differential equations with respect to the variable η with ξ as a parameter), Lees [18] proposed a formula

for calculating the equilibrium thermal flux along a cold surface /227 of blunt bodies, which was refined by Kemp, Rose, and Detra [24] and was represented in the following form

$$\frac{q(x)}{q(0)}=F(x)\frac{\left[1+0{,}096\sqrt{\frac{2x}{u_\delta}\frac{du_\delta}{dx}}\right]}{[1+0{,}096(1+f)^{-1/2}]}, \qquad (5.70)$$

where q(0) is the thermal flux at the critical point determined by Formula (5.68).

Expression (5.70) closely coincides with the results of precise numerical calculations [25, 26, 27], and also with the results of measurements in a wind tunnel of the thermal flux at the surface of blunt cones [28], a hemisphere, and a flat plane [24] (Figure 5.8).

Nonequilibrium boundary layer

The influence of nonequilibrium processes within a boundary layer upon the heat transfer characteristics may be most simply studied for a binary mixture first. In this case, Equations (5.49) — (5.51) assume the form

$$\left.\begin{aligned}
&(lf'')'+ff''+\frac{1}{(1+f)}[\rho_\delta/\rho-(f')^2]=0;\\
&\left(\frac{l}{\mathrm{Sc}}z'\right)'+fz'-\zeta_g\frac{1}{\theta^{\omega+2}}\left[\frac{a_\delta z^2}{1+a_\delta z}-\right.\\
&\qquad\left.-\frac{1}{a_\delta}\left(\frac{a_e^2}{1-a_e^2}\right)(1-a_\delta z)\right]=0;\\
&\left[\frac{c_p}{c_{p\delta}}\frac{l}{\mathrm{Pr}}\theta'\right]'+\frac{c_p}{c_{p\delta}}f\theta'+\frac{l}{\mathrm{Pr}}\cdot\mathrm{Le}\,a_\delta\frac{(c_{pA}-c_{pM})}{c_{p\delta}}\theta'z'+\\
&+\zeta_g\frac{\Delta h^\circ}{c_{p\delta}T_\delta}\frac{1}{\theta^{2+\omega}}\left[\frac{a_\delta^2z^2}{1+a_\delta z}-\left(\frac{a_e^2}{1-a_e^2}\right)(1-a_\delta z)\right]=0
\end{aligned}\right\} \qquad (5.71)$$

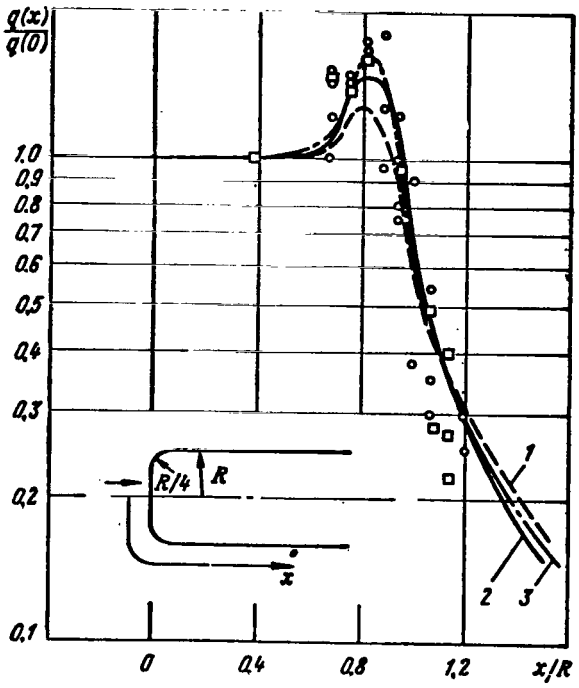

Figure 5.8. Distribution of thermal fluxes along blunt body surface (calculation was performed for p = 10 mm Hg).

1 — calculation performed by method of local similarity [24]; 2 — calculation by the method of finite differences [27] (equilibrium flow); 3 — calculation by the method of finite differences [27] (nonequilibrium flow); small circles designate experimental data when M_∞ = 8.6 to 9.6; p = 10 mm Hg; squares — when M_∞ = 7.4 to 7.9; p = 100 mm Hg.

with the following boundary conditions:

$$\left.\begin{array}{l} \text{at } \eta = 0,\ f = f' = 0,\ \theta = \theta_w; \\ \quad z' = 0 \\ \qquad \text{(noncatalytic surface)} \\ \quad z = 0 \\ \qquad \text{(ideally catalytic surface)} \end{array}\right\} \quad (5.72)$$

$$\text{at } \eta \to \infty\ f' = z = \theta = 1.$$

Here $z = \alpha/\alpha_\delta$, and the superscript "'" designates the derivative with respect to the coordinate η (5.45). The Damkeler number of the gas phase (5.52) will be:

$$\zeta_g = \frac{4}{(1+j)\beta_i}\frac{k_r'}{T_\delta^{\omega+2}}\left(\frac{p_\delta}{R}\right)^2, \quad (5.73)$$

/228

where k_r' is the constant part of the recombination velocity coefficient $2k_r = k_r'/T^w$ (w = 3/2), see Formula (1.49).

Fay and Riddell [20] numerically integrated Equations (5.71) to (5.72) when j = 1; Pr = 0.71; Le = 1.4; T_w = 300 K; H_δ = 5850 kcal/kg; α_δ = 0.536 and different Damkeler numbers. It was assumed that

$$c_{pA} = \frac{5}{2}\frac{R}{M/2};\ c_{pM} = \frac{R}{M}[{}^7/_2 + \exp(-800/T)];$$

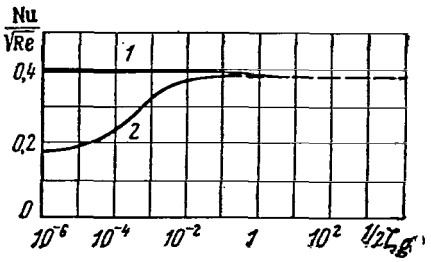

Figure 5.9. Nonequilibrium heat transport in the vicinity of the critical point.

1 —ideally catalytic surface; 2 — noncatalytic surface.

The equilibrium concentration of atoms was approximated by the formula $\alpha_e = \alpha_i \exp\left[\text{const}\left(1-\frac{1}{\theta}\right)\right]$, and the Sutherland formula was used for the viscosity coefficient.

Figure 5.9 gives results of calculating the heat transfer parameter $\mathrm{Nu}/\sqrt{\mathrm{Re}}$, which is directly related to the thermal flux:

$$-q_w = \left[\frac{\mathrm{Nu}}{\sqrt{\mathrm{Re}}}\right]\sqrt{\beta_i \rho_w \mu_w}\,\frac{[H_\delta - c_p T_w]}{\mathrm{Pr}}. \qquad (5.74)$$

In the region of the critical point at Le = 1 and for an arbitrary Pr number, the equation for conservation of total energy (5.50) coincides with the energy equation for a gas in which there are no chemical reactions. Consequently, at Le = 1, it is valid for all values of ζ_g. Since h_w is fixed for an ideally catalytic surface, the thermal flux depends on ζ_g only in terms of the influence of Le ≠ 1 and the change in the transport characteristics. It follows from Figure 5.9 that the thermal flux is actually constant throughout the entire range in which /229 ζ_g changes, even at Le = 1.4.

The curve in Figure 5.9 for a noncatalytic surface indicates that the heat transfer is greatly reduced, if the recombination rate in the gas is low (the flow is frozen in the boundary layer), and the surface material prevents the recombination of atoms (for example, glass-like materials). In this case, the thermal

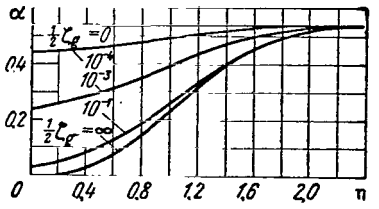

Figure 5.10. Atomic concentration profiles in the vicinity of the critical point (noncatalytic surface).

flux may be approximately expressed by the Formula (5.68) at Le = 0, i.e., Relationship (5.44) is valid under the computation conditions assumed in [20]. The atom concentration profiles (in the case of a noncatalytic surface) are given in Figure 5.10.

As follows from the solutions given above, many simplifying assumptions must be made in a study of the complex equations of the nonequilibrium boundary layer. However, due to the great nonlinearity of these equations, it is impossible to reach a definite conclusion regarding the accuracy of the quantitative results, without concurrently allowing for the action of all the factors. In this connection, it is of great value to formulate precise numerical methods of solving these equations, which make it possible to examine the flow around bodies of an arbitrary form and to use a complete chemical model of air. At the present time, either different methods are /230 used [29, 30], or the method of generalized integral relationships of Dorodnitsyn [31, 32].

For example, the study of B. G. Gromov [26] examines nonequilibrium flow in the boundary layer around blunt bodies, and a mixture of N, O, NO, O_2 and N_2 was used as the air model, considering fixed reactions in the gas phase. To obtain a solution, a nine-point three-layer difference scheme was used [33], which made it possible — without changing the grid parameters — to perform the calculations in the entire range from equilibrium to frozen flow regimes.

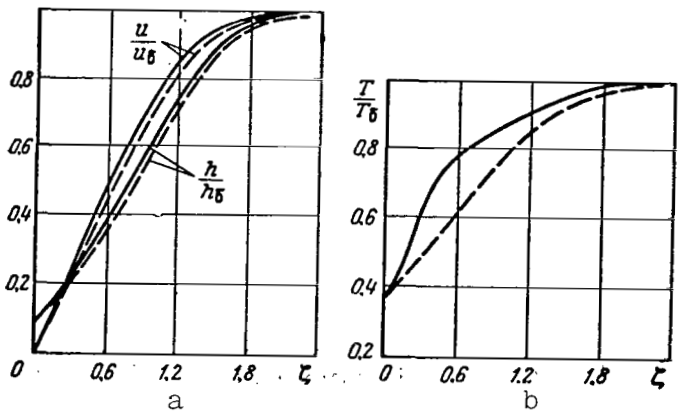

Figure 5.11. Results of calculating characteristics of boundary layer in vicinity of critical point (ideally catalytic surface) at p_δ = 0.1 kG/cm^2; T_δ = 7000 K; T_w = 2500 K (solid lines — equilibrium values; dashed lines — frozen values).
a — enthalpy profiles h/h_δ and velocity profiles u/u_δ; b — temperature profile T/T_δ.

Figures 5.11 — 5.13 present certain results of using the B. G. Gromov method to calculate the boundary layer characteristics at the critical point when p_δ = 0.1 kG/cm^2; T_δ = 7000 K; T_w = 2500 K and different values of $\zeta=\sqrt{\frac{\beta_1}{\rho_w\mu_w}}\int_0^y \rho dy$. For an ideally catalytic surface, the enthalpy and velocity profiles /231 (see Figure 5.11a) change very little when passing from frozen flow to an equilibrium flow, in spite of the great change in the temperature distribution (see Figure 5.11b) and the chemical composition of the gas (see Figure 5.12). The heat transfer parameter $Nu/\sqrt{Re}$ (solid line in Figure 5.13), just as in the case of a binary mixture [20], does not depend on the nonequilibrium nature of the flow, although the mechanism by which heat is transferred is different (the dashed line in Figure 5.13 corresponds to part of the thermal flux caused only by heat conductivity).

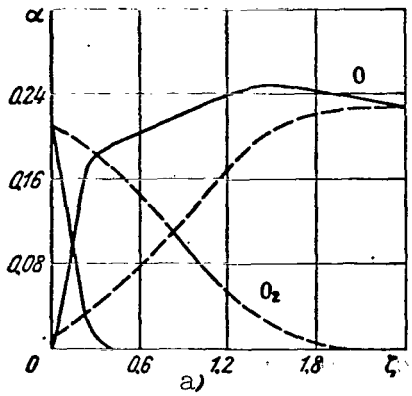

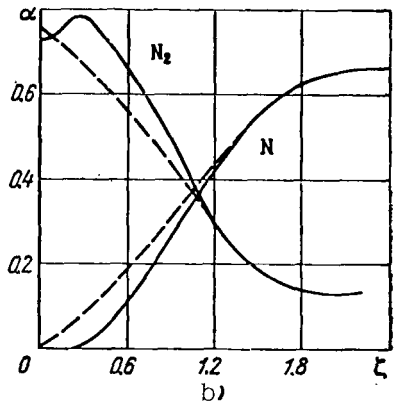

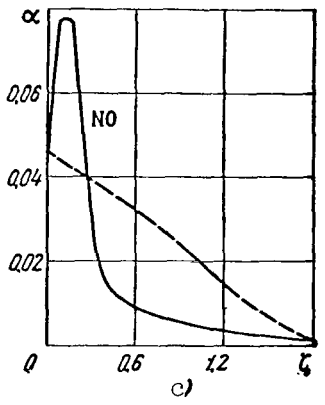

Figure 5.12. Profiles of chemical component concentrations under the same conditions as in Figure 5.11.

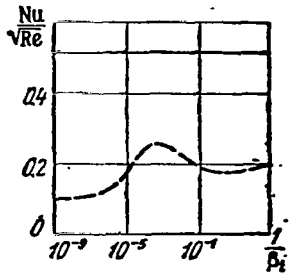

Figure 5.13. Nonequilibrium heat transport in the vicinity of the critical point (catalytic surface) at p_δ = 0.1 kG/cm^2; T_δ = 7000 K; T_w = 2500 K (solid line — total thermal flux; dashed line — part of thermal flux caused by heat conductivity).

As compared with the case of a binary mixture, one unusual characteristic of the solution obtained is a change (due to chemical reactions) in the separation by diffusion of the mixture across the boundary layer. Thus, for example, the difference in the oxygen mass concentrations $\left(\alpha_{[O]}+\frac{M_{[O]}}{M_{[NO]}}\alpha_{[NO]}+\alpha_{[O_2]}\right)$ on a body surface and on the external boundary of the boundary layer, under the conditions given above at the critical point, corresponds to 0.0028 at $\beta_i^{-1} = 10^{-9}$ seconds, and 0.0164 at $\beta_i^{-1} = 10^{3}$ seconds.

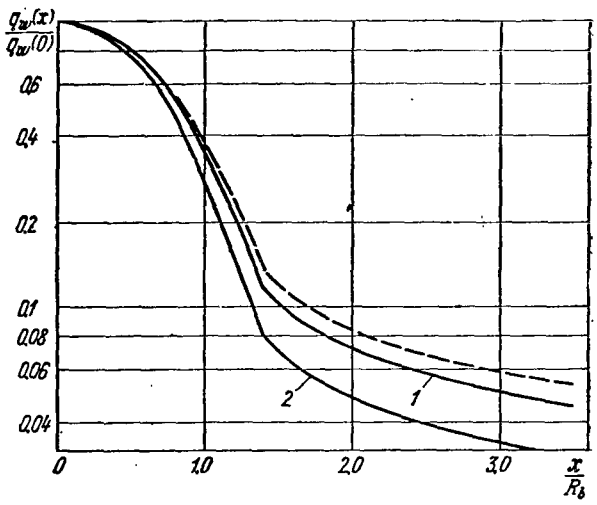

Figure 5.14. Thermal flux distribution along cone surface $\vartheta=10°$ with spherical blunting (noncatalytic surface) at M = 25; $p = 10^{-2}$ kG/cm^2; T_w = 1000 K for air (dashed line — equilibrium flow; solid line — nonequilibrium flow).
1 — at R_b = 1.7 m; 2 — at 0.017 m.

Calculations of the nonequilibrium boundary layer across the surface of a blunt cone [26] have confirmed the fact that, for an ideally catalytic surface and in the case of a multi-component gas mixture, the thermal flux distribution across the surface is practically identical for all flow regimes (the difference does not exceed 2%), and is similar to that given by the "local similarity" theory, particularly Formula (5.70). The distribution of the flow parameter $c_f\sqrt{\mathrm{Re}}_x$ along the surface for all flow regimes does not differ by more than 12%.

At the same time, calculations of B. G. Gromov have shown that chemical reactions in the boundary layer around a noncatalytic surface are rapidly frozen in the case of flow around a spherical blunt body, and this has a great influence on the thermal flux distribution, particularly in the region of great expansion (Figure 5.14).

Frozen boundary layer with chemical reactions on the surface

In this case, the magnitude of the thermal flux at the critical point depends on the catalytic nature of the surface. It is therefore of interest to study the influence of nonequilibrium processes on the body surface in the case of frozen /232

reactions in a gas phase, i.e., under the condition that $\zeta_g \to 0$ in Equations (5.51) and (5.59).

For purposes of simplicity, let us examine a binary mixture and assume that Le = const, Pr = const, and l = const. As Lees has shown [18], for a cold body surface $\rho_\delta/\rho_w \ll 1$, and we may disregard the third term in the equation of momentum. In addition, since $\int_0^T (c_{pA} - c_{pM})\,dT \ll h^\circ$ and $u_\delta^2 \ll H_\delta$ only the first two terms remain in the energy equation (5.50) written for frozen retardation enthalpy $g_f = H_f/H_{f\delta}$. Thus, in the vicinity of the critical point for a frozen flow, Equations (5.49) and (5.50) assume the form

$$\tilde{f}''' + \tilde{f}\tilde{f}'' = 0; \tag{5.75}$$

$$g_f' + \mathrm{Pr}\,\tilde{f} g_f' = 0 \tag{5.76}$$

with the following boundary conditions /233

$$\text{for } \tilde{\eta} \to \infty \quad \tilde{f}' = g_f = 1; \tag{5.77}$$

$$\text{for } \tilde{\eta} = 0 \quad \tilde{f} = \tilde{f}' = 0; \tag{5.78}$$

$$(g_f)_w = \frac{c_{pw} T_w}{H_\delta - a_\delta h^\circ}. \tag{5.79}$$

Here the superscript "'" designates the derivative with respect to the variable $\tilde{\eta} = \eta/\sqrt{l}$ and $\tilde{f} = f/\sqrt{l}$.

Equations (5.75) and (5.76) with the boundary conditions (5.77) — (5.79) are not related to the equation of concentration conservation (5.51), and their solutions are well known from the classical theory of the boundary layer [1]. Thus, on the body surface

$$\tilde{f}''(0)=\frac{0{,}664}{\sqrt{2}}\approx 0{,}47;\ g_f(0)\approx 0{,}47\,(\mathrm{Pr})^{1/3}[1-g_f(0)]. \qquad (5.80)$$

This makes it possible to determine the part of the thermal flux q_c caused by the heat conductivity

$$-q_c=\frac{\mu_w}{\mathrm{Pr}}\left(\frac{\partial h_f}{\partial y}\right)_w\approx 0{,}47\,(\mathrm{Pr})^{-2/3}\sqrt{(1+j)\,\rho_\delta\mu_\delta\beta_i l}\times \qquad (5.81)$$
$$\times[(H_\delta-\alpha_\delta h^\circ)-c_{pw}T_w].$$

Thus, the problem reduces to solving the concentration equation

$$z''+\mathrm{Sc}\,\tilde{f}\cdot z'=0\quad (z=\alpha/\alpha_\delta). \qquad (5.82)$$

with the boundary condition $z(\infty) = 1$ and condition (5.56), which may be written in the following form for a cold body surface $(z_w)_e \approx 0$)

$$z'(0)=\zeta_0[z(0)]^n. \qquad (5.83)$$

Here

$$\zeta_0=\frac{\mathrm{Sc}\,\rho_w^n k_w \alpha_\delta^{n-1}}{\sqrt{(1+j)\,(\rho_\delta\mu_\delta)_0\beta_i l}}=\frac{\mathrm{Sc}\,k_w}{\mu_w}\sqrt{\frac{(\rho_\delta\mu_\delta)_0 l}{(1+j)\beta_i}}(\alpha_\delta\rho_w)^{n-1} \qquad (5.84)$$

is the Damkeler number (5.57) for gas recombination on the body surface (it is assumed that ρ_w is known).

Integrating Equation (5.82) twice and using the boundary conditions, we obtain

$$z(\tilde{\eta})-z(0)=z'(0)\bar{I}_z(\tilde{\eta}), \qquad (5.85)$$

where

$$I_z(\tilde{\eta}) = \int_0^{\tilde{\eta}} \exp\left[- \mathrm{Sc} \int_0^{\tilde{\eta}} \tilde{f} d\tilde{\eta} \right] d\tilde{\eta} \qquad (5.86)$$

or

$$1 - z(0) = \zeta_0 I_z(\infty) z^n(0). \qquad (5.87)$$

If $\tilde{f}$ is a Blasius function [Equation (5.75)], then /234

$$I_z(\infty) \approx \frac{1}{0{,}47\,\mathrm{Sc}^{1/3}}. \qquad (5.88)$$

The majority of catalytic reactions pertain to first order reactions, or the order of the reactions ranges between 1/2 and 1. In this case, solution of Equation (5.87) has the following form: when n = 1

$$z_w = z(0) = \frac{1}{1 + \zeta_0 I_z(\infty)} \qquad (5.89)$$

(this solution was obtained by Goulard [34]); at n = 1/2

$$z_w^{1/2} = \sqrt{z(0)} = -\frac{1}{2}\zeta_0 I_z(\infty) + \sqrt{1 + \left[\frac{1}{2}\zeta_0 I_z(\infty)\right]^2}. \qquad (5.90)$$

The corresponding curves for the change in $z_w = \varphi(\zeta_0)$ are shown in Figure 5.15. When $\zeta_0 \to \infty$, all z_w strive to an equilibrium limit equal to zero in the assumed approximation, and the surface represents a sink of infinite intensity for atoms, and when $\zeta_0 \to 0$, the diffusion flow disappears ($z_w' = 0$) leading to homogeneous distribution of the atoms ($z \to 1$) in the boundary layer. The transition from the frozen limit ($\zeta_0 \to 0$) to the equilibrium limit ($\zeta_0 \to \infty$) occurs more rapidly as the index n decreases.

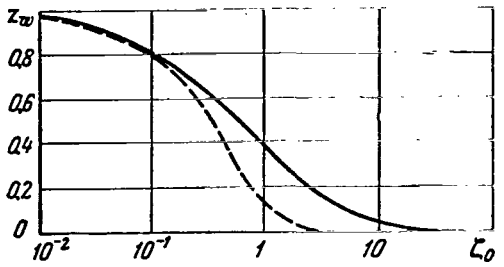

Figure 5.15. Concentration of atoms on body surface in vicinity of critical point (solid line — heterogeneous reactions have the order n = 1; dashed line — heterogeneous reactions with n = 1/2).

Let us calculate the portion of the thermal flux q_d caused by catalytic reactions on the surface. In agreement with expressions (5.32) and (5.41), for a binary mixture

$$-q_d = k_w (\rho_w a_w)^n h^\circ = \frac{1}{Sc} \sqrt{(1+j)\,\rho_\delta \mu_\delta \beta_i l}\,(a_i h^\circ)\, z'(0). \qquad (5.91)$$

Combining Equations (5.81) and (5.91), we obtain the following expression for the total thermal flux

$$-q_w = -(q_c + q_d) = 0{,}47\,(\mathrm{Pr})^{-2/3} \sqrt{(1+j)\,\rho_\delta \mu_\delta \beta_i l} \times \times (H_\delta - c_{pw} T_w) \left\{ 1 + [(\mathrm{Le})^{2/3} \Phi - 1] \frac{a_i h^\circ}{(H_\delta - c_{pw} T_w)} \right\}. \qquad (5.92)$$

Here the factor $\Phi = 1 - z(0)$ takes into account the influence of /235 catalytic reactions upon the thermal flux on the body in the frozen boundary layer. It follows from Equation (5.87) that when $\zeta_0 \to 0$ $\Phi = 0$, and when $\zeta_0 \to \infty$ $\Phi = 1$. In these limiting cases, Expression (5.92) accurately corresponds to Lees' results [18], and is very similar to the Fay and Riddell formula (5.68).*

Expression (5.92) makes it possible to establish the possible decrease in the thermal flux caused by a finite recombination rate of the gas on the body surface

*We must assume $l = 1{,}32\,(\rho_w \mu_w / \rho_\delta \mu_\delta)^{0.2}$ for the best agreement with Formula (5.68).

$$\frac{q_w}{q_{w\max}} = 1 - \frac{(\mathrm{Le})^{2/3}\frac{\alpha_\delta h^\circ}{\Delta H_f}}{\left[1 + [(\mathrm{Le})^{2/3} - 1]\frac{\alpha_\delta h^\circ}{\Delta H_f}\right]}(1 - \Phi), \qquad (5.93)$$

where $(q_w)_{max}$ corresponds to the maximum thermal flux q_w under equilibrium conditions on the surface; $(\zeta_0 \to \infty, \Phi = 1)$, and $\Delta H_f = (H_\delta - \alpha_\delta h^\circ) - c_{pw}T_w$ is the difference in the values of the frozen enthalpy on the outer boundary of the boundary layer and on the body surface. /236

Figure 5.16, taken from [34], gives the results derived from calculating with Formula (5.93) (when Le = 1.4; Pr = 0.71, and l = 1) the ratio $q_w/(q_w)_{max}$ at the critical point of the body with R_b = 50 cm, T_w = 700 K at an altitude of H $\cong$ 61 km with a differing flight velocity V_∞. The abscissa axis gives the corresponding values of k_w for the surface materials. The effect of decreasing the thermal flux is very apparent (in the case of frozen reactions in the gas phase) with the transition from metallic to oxide and glass fiber coverings.

It follows from the structure of the formula for z(0) [see, for example, Equations (5.89), (5.90)] and ζ_0 (5.84) that a decrease in the bluntness radius (increasing β_1) or a density decrease has a similar influence on the decrease in the thermal flux on the body surface.*

*When there is a great decrease in density in the surrounding space, the influence of a boundary layer with inviscid flow must be taken into account. As a result of this, the use of non-catalytic surfaces becomes less effective (see Section 5.4).

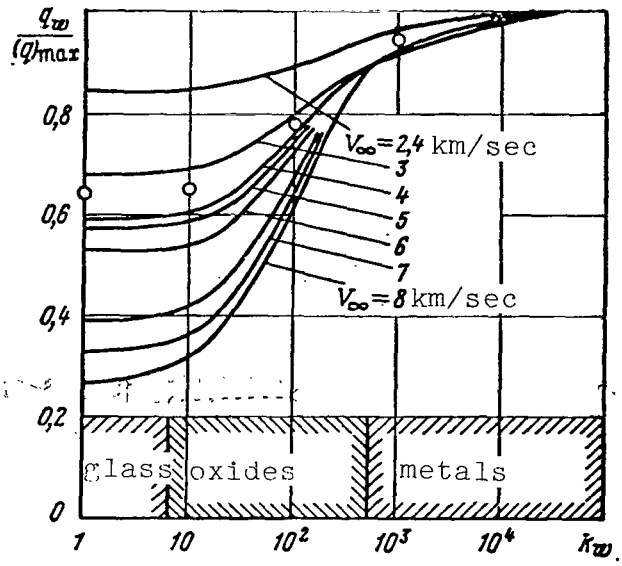

Figure 5.16. Influence of surface catalycity on thermal flux at the critical point when H_∞ = 61 km; R_b = 0.5 m; T_w = 700 K (dots indicate computational results from [45] for non-equilibrium boundary layer at V_∞ = 8 km/sec).

The catalytic recombination of atoms of a binary mixture, in the case of hypersonic flow around blunt bodies (in particular, a cone with spherical bluntness), may be studied by means of the local similarity method [3], if the characteristic reaction rate along the body surface and the characteristic diffusion rate change simultaneously, so that their ratio (Damkeler number) changes very little. The method of local similarity for studying frozen boundary layers was first used in [35].

The influence of the variability of k_w upon the chemical reactions on the surface may be illustrated in the particular case of the continuous change in k_w along the surface of a blunt body [36]. If

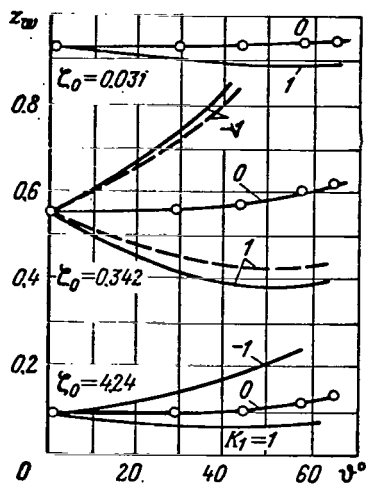

Figure 5.17. Distribution of atom concentrations along hemisphere surface at α_δ = 0.5; Sc = 0.72; k_w/μ_w = $1 + K_1\nu$ (solid lines — solution by expansion method in power series; dashed lines — calculation by method of local similarity; points designate calculation by integral method).

z_w = 0 at $\zeta_0 \to \infty$ and z_w = 1 at ζ_0 = 0 for all K_1.

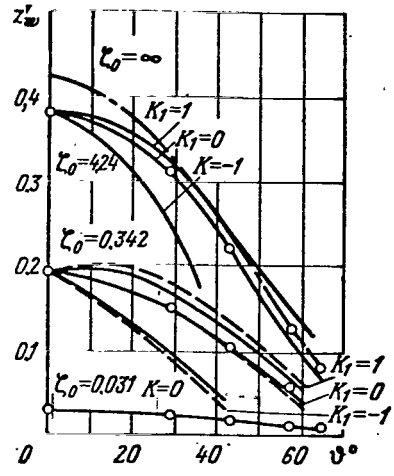

Figure 5.18. Function $z_w'(\nu)$ proportional to the component of the thermal flux q_d under the same conditions as Figure 5.17 (z_w' = 0 at ζ_0 = 0 for all K_1).

$$\frac{k_w}{\mu_w}=(1+K_1\vartheta)\left(\frac{k_w}{\mu_w}\right)_0, \quad (5.94)$$

where ν is the angle determined from the axis of symmetry, and then

$$z_w(\vartheta)=z_w(0)\left\{1-\frac{\zeta_0}{[\zeta_0-Y_1'(0)]}K_1\vartheta+\ldots\right\}; \quad (5.95)$$

$$-q_d(\vartheta)=q_d(0)\left\{1-\frac{Y_1'(0)}{[\zeta_0-Y_1'(0)]}K_1\vartheta-\ldots\right\}, \quad (5.96)$$

where the values at the critical point $z_w(0)$, $q_d(0)$ and the Damkeler number ζ_0 are determined by Expressions (5.89), (5.91), /237

and (5.84), and the values of $Y'(0)=\varphi(Sc)$ are determined from the graph in Figure 5.34 when n/k = 1. Figures 5.17 and 5.18 give the computational results for $z_w(\vartheta)$ and $z_w'(\vartheta)\sim q_d(\vartheta)$ for Sc = 0.7, α_δ = 0.5 and several values of K_1 and ζ_0, as well as a comparison with the results obtained by the method of local similarity and the integral method.

When $K_1 \leq 0$, the flow expansion decreases the local catalytic surface for all $0 \leq \zeta_0 < \infty$ as compared with the corresponding value at the critical point. In other words, the Damkeler number decreases monotonically as the result of an increase in the recombination time on the surface when $K_1 < 0$, and a decrease in the diffusion time in the boundary layer (due to a pressure drop and a velocity increase). For $K_1 < -1$, the first factor may greatly decrease the local catalytic nature of the surface, even when $\zeta_0 \gg 1$.

On the other hand, at $K_1 > 0$, the concentration of atoms and the thermal flux change nonmonotonically. In this case, the /238 effect of inviscid expansion opposes the recombination velocity increase on the surface, and at first the effective catalytic nature of the surface increases. At a certain ϑ, which rapidly increases with an increase in K_1, the value of $z_w(\vartheta)$ reaches a minimum, and the value of $q_d(\vartheta)$ — a maximum. This occurs when the flow expansion becomes greater than the increase in k_w/μ_w. In the general case, $(k_w/\mu_w)\sim 1+K_1\vartheta^a$. At a = 2, there is a $K_1 > 0$ at which the quantities $z_w(\vartheta)$ and $q_d(\vartheta)$ will remain approximately constant in the greater portion of the flow region. If $a \geq 3$ and $K_1 > 0$, outside of the critical point $z_w(\vartheta)$ will assume its maximum value, and $q_d(\vartheta)$ will assume its minimum value.

One of the important consequences of the theory of catalytic reactions is the determination of atom concentration in an advancing flow in high temperature experimental equipment, by measuring the thermal flux on the surfaces with differing catalytic properties. The most precise determination of the atom concentration is possible when the recombination is frozen in the gas phase. By measuring the thermal flux on one of the two surfaces which is noncatalytic, we obtain q_c, whereas measurements on the catalytic surface give $q_w = q_c + q_d$. The difference between the two thermal fluxes determines the value of q_d, from which we may obtain α_δ by means of the theory given above. The studies [37 — 40] give a more detailed discussion of the methods and results of the measurements, for example.

Concurrent influence of nonequilibrium processes in a boundary layer and on a body surface

From the practical viewpoint, the most important problem is determining the thermal flux with simultaneous consideration of nonequilibrium processes both in the gas and on the body surface.

In the vicinity of the critical point of a blunt body, the main zone of reactions in the gas — namely the recombination reactions — is close to the cold body surface. A very simple way to obtain an analytical solution is to pass to the limit, replacing the reaction in the gas by an equivalent reaction (second order) on the surface itself. In this case, the concentration of atoms on the body surface is determined from the boundary condition (5.32), which assumes the following form for a binary mixture

$$\rho_w D_w \left(\frac{\partial z}{\partial y}\right)_w = k_g \frac{1}{\alpha_\delta} \frac{z_w^2}{(1+z_w)} + \rho_w k_w z_w \qquad (5.97)$$

Such a rough approach was followed, for example, in [41], where the unknown quantity k_g was determined by performing a comparison with the results of numerical calculations for a noncatalytic surface. /239

However, it is possible to obtain an approximate solution [42]* in closed form, retaining the essential nonlinear characteristics of the dissociation-recombination process in the gas. This solution was extended to the case of small gas density in surrounding space (see Section 5.4).

For constant values of Pr, Sc, and l (n = 1) and the conditions $c_{pA} = c_{pM}$, for a binary mixture of gases Equations (5.71) in the vicinity of the critical point may be transformed to the form

$$\mathrm{Sc}\,\tilde{f} z' + z'' = \frac{\alpha_\delta}{(1+\alpha_\delta)} \Gamma \mathfrak{N}(z, \theta); \qquad (5.98)$$

$$\mathrm{Pr}\,\tilde{f} \theta' + \theta'' = -\frac{\alpha_\delta}{(1+\alpha_\delta)} H_d \Gamma R(z, \theta). \qquad (5.99)$$

with the following boundary conditions

$$z(\infty) = \theta(\infty) = 1; \quad \theta(0) = \theta_w; \quad z'(0) = \zeta_w z(0). \qquad (5.100)$$

*Similar considerations were also used in [43].

The superscript "'" designates the derivative with respect to the variable $\tilde{\eta}=\eta/\sqrt{\bar{l}}$; $\tilde{f}=f/\sqrt{\bar{l}}$ is the Blausius function, which approximately satisfies the equation of momentum in the case of a cold body surface;

$$\Gamma=\frac{4k_r'\cdot \mathrm{Sc}}{(1+j)\,\beta_l}\frac{1}{T_\delta^{2+\omega}}\left(\frac{p_\delta}{R}\right)^2 \qquad (5.101)$$

is the Damkeler number for recombination in a gas;*

$$H_d=\frac{\mathrm{Lc}}{c_{pM}T_\delta}(a_i h^\circ); \qquad (5.102)$$

$$\zeta_w=\frac{\mathrm{Sc}\,k_w}{\mu_w}\sqrt{\frac{l\rho_\delta\mu_\delta}{(1+j)\,\beta_l}} \qquad (5.103)$$

Damkeler number for reactions on the surface, which coincides with the expression for ζ_0 (5.84), and the function

$$R\left(z,\,\theta\right)=\frac{1}{\theta^{2+\omega}}\frac{(1+\alpha_\delta)}{(1+\alpha_\delta z)}\left\{z^2-\frac{(1-\alpha_\delta^2 z^2)}{(1-\alpha_\delta^2)}\exp\left[-\frac{\theta_d}{\theta}(1-\theta)\right]\right\} \qquad (5.104)$$

$$(\theta_d=h^\circ M/RT_\delta)$$

characterizes the local rate at which atoms are formed as a result of the dissociation and recombination reactions. The functon R(z, θ) identically equals zero in the case of the /240

*The quantity Γ differs only by the factor Sc from ζ_g (5.73).

equilibrium state of the gas in the boundary layer ($\Gamma \to \infty$).*

Integrating Equations (5.98) — (5.99) twice, as linear nonhomogeneous equations, and using the boundary conditions (5.100), we may obtain the formal expressions for $z(\tilde{\eta})$ and $\theta(\tilde{\eta})$ in terms of the integrals of the functions $\tilde{f}$ and R. In particular, on the body surface (when $\tilde{\eta} = 0$), we have

$$z(0)=\frac{1}{\zeta_w} z'(0)=z_f(0)\left[1-\frac{\alpha_\delta}{(1+\alpha_\delta)}\Gamma J_z(\infty)\right]; \qquad (5.105)$$

$$\theta'(0)=0{,}47\,(\mathrm{Pr})^{1/3}\left\{[1-\theta_w]+H_d\frac{J_\delta(\infty)}{J_z(\infty)}\left[1-\frac{z(0)}{z_f(0)}\right]\right\}, \qquad (5.106)$$

where $z_f(0)$ is the well-known Goulard solution [34] for frozen flow ($\Gamma = 0$) [see Formula (5.85)];

$$J_z(\infty)=\int_0^\infty \exp\left(-\mathrm{Sc}\int_0^\infty \tilde{f}\,d\tilde{\eta}\right)\int_0^\infty \exp\left(\mathrm{Sc}\int_0^\infty \tilde{f}\,d\tilde{\eta}\right) R\,d\tilde{\eta}; \qquad (5.107)$$

and $J_\theta(\infty)$ is obtained from Equation (5.107) by replacing Sc by Pr in the integrands.

The value of the thermal flux on the body surface in dimensionless form will be

---

*The equilibrium concentration of the atoms is implicitly approximated by the formula

$$\frac{\alpha_e^2}{1-\alpha_e^2}=\frac{\alpha_\delta^2}{(1-\alpha_\delta^2)}\exp\left[\theta_d\,(1-T_\delta/T_e)\right].$$

$$+Q_w = -\frac{\mathrm{Pr}}{c_{pM}T_\delta}\frac{q_w}{\sqrt{(1+j)\,\rho_\delta\mu_\delta\beta l}} = \theta'(0) + H_d z'(0) =$$
$$= 0{,}47\,(\mathrm{Pr})^{1/3}\left\{[1-\theta_w] + H_d\frac{J_\theta(\infty)}{J_z(\infty)}[1-z(0)]\right\} + \qquad (5.108)$$
$$+ H_d\zeta_w z(0)\left[1-(\mathrm{Le})^{1/3}\frac{J_\theta(\infty)}{J_z(\infty)}\right].$$

The results of the calculations [42] show that for a cold surface the relationship

$$J_\theta(\infty)/J_z(\infty) \approx (\mathrm{Le})^{-0{,}48} - (\mathrm{Le})^{-0{,}45}$$

(for the Le numbers which do not differ from one) does not depend on Γ and ζ_w. Consequently, the quantity in the last brackets in Expression (5.108) identically equals zero when Le = 1, and is negligibly small in the entire range in which Le changes. Taking the fact into account that in equilibrium flow $z_e(0) \approx 0$, we may readily obtain the following simple relationship:

$$\frac{Q_w - Q_{wf}}{Q_{we} - Q_{wf}} = 1 - \frac{z(0)}{z_f(0)}. \qquad (5.109)$$

Thus, to determine the thermal flux on the surface, it is sufficient to know the value of z(0). The equilibrium Q_{we} and frozen Q_{wf} values of the thermal flux may be calculated by means of Formulas (5.68) and (5.92). For this purpose, it is first necessary to determine the value of the integral $J_z(\infty)$ determined by (5.107).

Analyzing the numerical results of Fay and Riddell [20], Enger showed that the value of the integral $J_z(\infty)$ depends primarily on the values of the function R in the recombination portion of the boundary layer close to a cold surface. Based on this, the function R was approximated as follows:

$$R \approx \left[\frac{1+\alpha_\delta}{1+\alpha_\delta z(0)}\right]\frac{1}{\theta_f^{2+\omega}} z^2\left\{1-\exp\left[-\frac{\theta_d}{\theta_f}(1-\theta_f)\right]\right\}. \qquad (5.110)$$

Here

$$\theta_f(\tilde{\eta}) = \theta_w + (1-\theta_w) g_f(\tilde{\eta}); \qquad (5.111)$$

$$z(\tilde{\eta}) \simeq z(0) + \frac{z'(0)}{0{,}47\,\mathrm{Sc}^{1/3}} g_f(\eta), \qquad (5.112)$$

where

$$g_f(\eta) = 0{,}47\,(\mathrm{Pr})^{1/3} \int_0^{\tilde{\eta}} \exp\left[-\mathrm{Pr}\int_0^{\eta} \tilde{f} d\tilde{\eta}\right] d\tilde{\eta}$$

is the Goulard solution [34] for frozen flow ($g_f(\infty) = 1$.

Expression (5.112) is exact for small values of $\tilde{\eta}$ for all Γ, and also for all $\tilde{\eta}$ for $\Gamma \ll 1$. As was shown in [42], the function $1/\theta^{2+\omega}$ closely correlates the influence of temperature upon the nonequilibrium thermal flux to a noncatalytic surface. Since $z_e(0) \approx z_e'(0) \approx 0$, it may be expected that Expression (5.110) will give the acceptable solutions for characteristics on the body surface when $\Gamma \gg 1$.

Using the assumed approximation of R, we may express $J_z(\infty)$ in terms of z(0) and the corresponding characteristics of frozen flow. Substituting the expression obtained $J_z(\infty)$ in

(5.105), we obtain the quadratic equation, whose solution has the form

$$(z(0) = z_f(0)\frac{\sqrt{[1+\alpha_\delta z_f(0)]^2+4\Gamma^*}-[1-\alpha_\delta z_f(0)]}{2[\alpha_\delta z_f(0)+\Gamma^*]}, \qquad (5.113)$$

where /242

$$\Gamma^* = \alpha_\delta \Gamma \left\{ \frac{J_{z,F_1}+2\left(\frac{\zeta_w}{0{,}47\,Sc^{1/3}}\right)J_{z,F_2}+\left(\frac{\zeta_w}{0{,}47\,Sc^{1/3}}\right)^2 J_{z,F_3}}{\left[1+\left(\frac{\zeta_w}{0{,}47\,Sc^{1/3}}\right)\right]^2} \right\}_- \qquad (5.114)$$

is the generalized Damkeler number which simultaneously takes into account the influence of reactions in the gas and on the body surface.

The values $\alpha z_f(0) > 1$ in Figure 5.19 pertain to the generalization of the given solution to the case of vortex interaction with the boundary layer (see Section 5.4).

The values of the function $J_{z,\ F_i}$ $(i = 1, 2, 3)$ were published in [44], and some of them are given in Figure 5.20 (the curves for $u_\delta^2/2c_pT_\delta=0$) correspond to the solution at the critical point). The strong dependence of the function $J_{z,\ F_i}$ on θ_d when $\theta_w \gtrsim 0.3$ indicates the increasing influence of the dissociation process in a gas (as compared with the recombination process), which leads to a decrease in the accuracy of the

*The unique dependence of Q_w on $z(0)$ is naturally caused by the simplifying assumptions made, although the results of numerical calculations confirm the slight influence of other flow characteristics on this dependence.

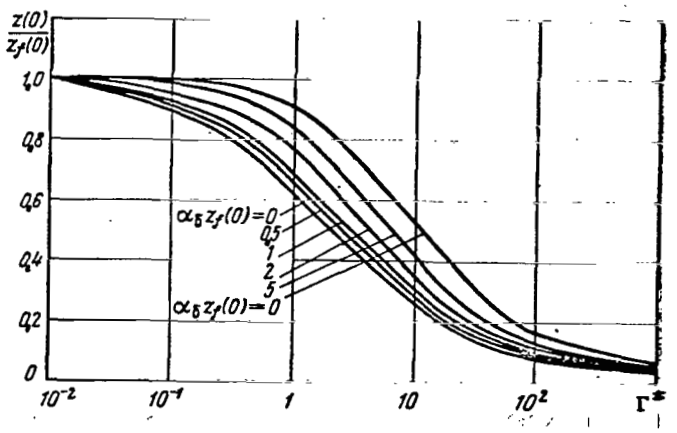

Figure 5.19. General solution in the region of the critical point during the concurrent influence of nonequilibrium processes in the boundary layer and on the body surface.

approximation R assumed (5.110) for catalytic surfaces ($\zeta_w > 1$).

Figure 5.21* shows typical calculation results, which characterize the relative influence of homogeneous and heterogeneous reactions upon the thermal flux at the critical point when $\delta = 0.536$; $\theta_d = 10$; $\theta_w = 0.04$; Le = 1.4; Pr = 0.7 and w = +3/2. This figure gives a comparison with the results of the calculations by Fay and Riddell [20] for the limiting cases $\zeta_w = 0$ and $\zeta_w \to \infty$. Taking the fact into account that several simplifying assumptions were made when formulating the solution, the agreement of the results is considered to be satisfactory (for atom concentrations on the surface, the agreement of the results is even better). /243

As may be seen from the graph in Figure 5.21a, the relative value of the thermal flux is entirely determined by the

*In Figure 5.21b, the quantity $Q^* = (Q_{we} - Q_w) c_{pM} T_\delta / 0{,}47\ \mathrm{Pr}^{1/3} \alpha_\delta h^\circ$, which is plotted along the ordinate axis, corresponds to the difference between equilibrium and nonequilibrium thermal fluxes.

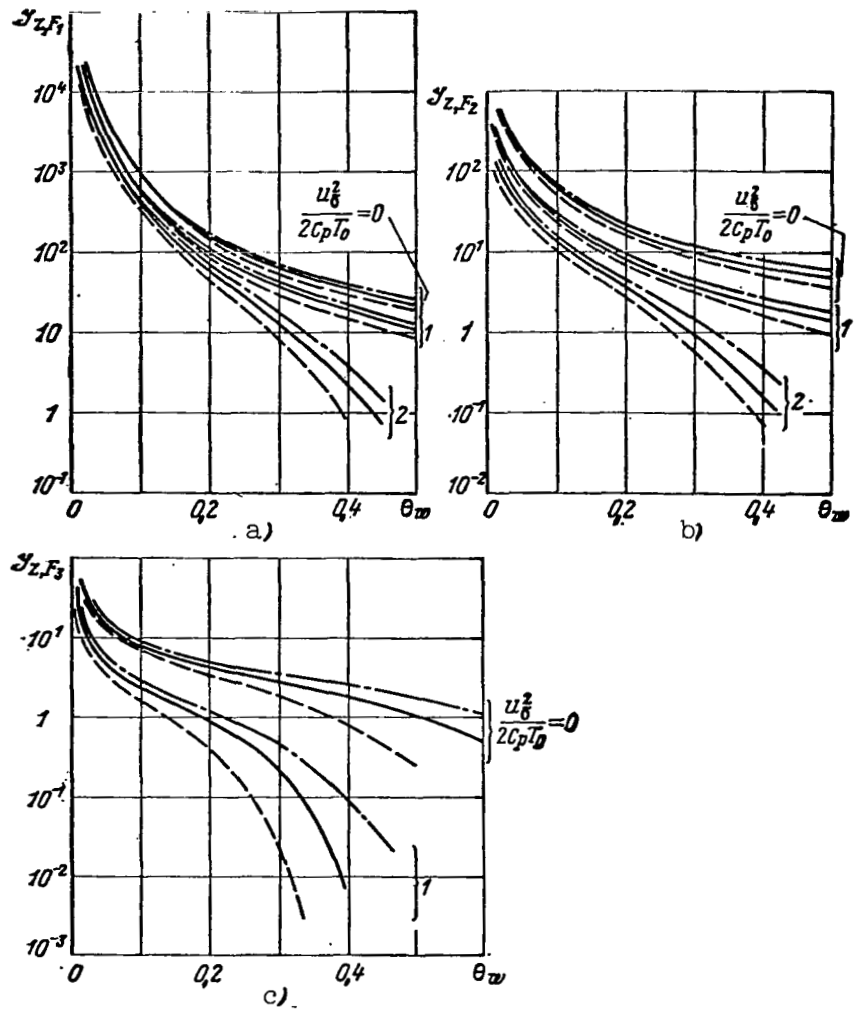

Figure 5.20. Functions $J_{z,\ F_i}{}^{1}{}_{Ei}$ (i = 1, 2, 3) when Pr = 0.70; Sc = 0.5; w = +1.5 (dotted-dashed lines — for θ_d = 25; solid lines — for θ_d = 15; and dashed lines — for θ_d = 5).

---

dissociation-recombination rate in a gas, when the catalytic nature of the surface is either very small (ζ_w < 0.1) or is very great (ζ_w > 20). However, when ζ_w ~ 0(1), the reaction rate on the surface has a very great influence (if only the

/244

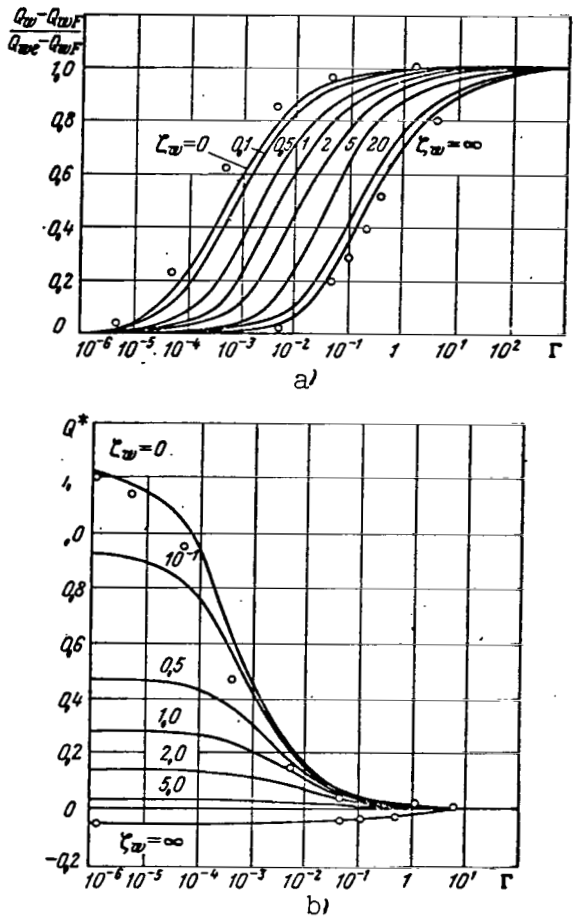

Figure 5.21. Relative influence of reactions in a gas and on the body surface upon the thermal flux at the critical point when θ_w = 0.04; θ_d = 10; ω = +1.5; Pr = 0.7; Le = 1.4; α_δ = 0.536 (the dots indicate the numerical solution of Fay and Riddell [20]).

boundary layer is not in a state close to equilibrium). This is related to the fact that the state of the gas close to the surface is controlled by the boundary condition (5.100). An increase in the catalytic characteristics decreases the atom concentration close to the surface and, consequently, the recombination rate in the gas. Thus, the moment at which equilibrium is reached is shifted to higher values of Γ.

Figure 5.21b shows the similar influence of the rate of homogeneous and heterogeneous reactions upon $Q^* \sim Q_{we} - Q_w$. The value of the thermal flux is very sensitive to the rate of heterogeneous reactions on the surface when $\zeta_w \sim 0(1)$, as well as to the rate of homogeneous reactions in a gas when $\zeta_w \ll 1$. However, at $\zeta_w \gg 1$, the influence of the reaction rate in a gas becomes negligibly small, since $Q_{wf} - Q_{we} \sim (Le)^{0.63} - (Le)^{0.52}$ (5.68).

The general conclusion may be reached that, when one of the two parameters (Γ or ζ_w), which determine the reaction rate in the gas and on the body surface, becomes very large, the thermal flux ceases to depend on another parameter (although the influence of reactions on the surface is greater).

The solution (5.113) by means of the local similarity method may be extended [44] to the flow around blunt bodies (when $u_i^2/b_p T_i \ll 1$), if we replace β_i by

$$\frac{\rho_\delta \mu_\delta r^{2j} u_\delta^2}{2(1+j)\int_0^x \rho_\delta \mu_\delta r^{2j} u_\delta dx}$$

in Formulas (5.101) and (5.103).

Results are available of precise numerical calculations of the concurrent influence of nonequilibrium processes in a boundary layer and on a body surface for a multi-component mixture of gases. For example, in the work of V. G. Vorokin and L. K. Geraskina [45] there is a numerical calculation of nonequilibrium air flow in the vicinity of the critical point and along the generatrix of blunt cones and cylinders. A mixture of N, O, NO, O_2 and N_2 is used as the chemical model, taking into account six reactions in the gas phase. Either the concentration of components or the surface catalytic coefficient are given on the body surface:

$$k_w[O] = k_w[N] = k_w; \quad k_w[NO] = 0.$$

An implicit two-layer, six-point difference scheme was used to obtain a solution [45].

The calculations made by authors of [45] made it possible to determine the thermal flux on a body with a given surface catalycity, with allowance for nonequilibrium air flow within the boundary layer. Figure 5.16 illustrates the increase in the thermal flux at the critical point of a body, caused by nonequilibrium processes in the air, as compared with the thermal flux for a frozen boundary layer, for which the data in [45] closely coincide with the data Goulard [34] calculated for a binary mixture. An analysis of the calculation results [45], in particular, the thermal flux distribution, confirms the fact that the influence of the flow regime and the boundary conditions is approximately the same at the critical point and along a spherical blunt body, but differs noticeably along the lateral surface of a blunt cone and cylinder (Figure 5.22). /245 /246

The numerical calculation of flow around a graphite sphere by dissociating oxygen, with allowance for the finite heterogeneous reaction rates on the surface and also in the body pores, was performed in the study already mentioned [4]. In view of the specific nature of this problem, those readers interested in the characteristics of the results obtained are referred directly to the study itself [4].

5.3. Flat plate, wedge, and cone

The flow in the boundary layer of a plate (wedge) and cone* represents another wide area of research on nonequilibrium flows. Just like flow in the vicinity of the critical point of a blunt body, these flows have direct practical applications ("lifting" surface of aircraft) and are amenable to certain mathematical simplifications. /247

*The interaction of the boundary layer with inviscid flow behind the shock wave is not considered.

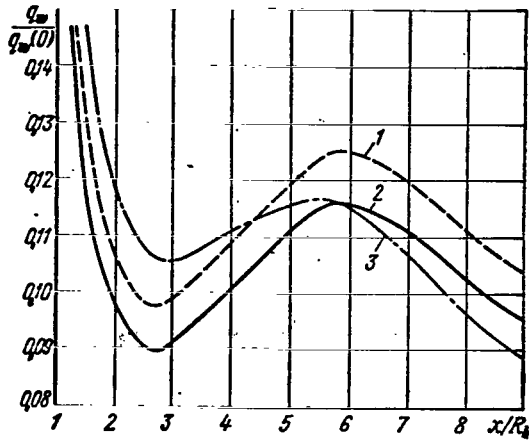

Figure 5.22. Thermal flux distribution along the surface of a blunt cone when $\nu = 20°$; $R_b = 0.5$ m; $T_w = 700$ K; $p_0 = 0.216$ kG/cm^2; $T_0 = 6900$ K for air.
1 — frozen boundary layer ($k_w = 10^2$ cm/sec); 2 — nonequilibrium boundary layer ($k_w = 10^2$ cm/sec); 3 — frozen boundary layer ($k_w = 0$).

Let us assume that the body being considered (plate, wedge, or cone) has the characteristic dimension L. Depending on the ratio between the characteristic reaction time in the gas and the characteristic diffusion time, which are determined in the last analysis by the velocity and altitude of the body, and also by the half-angle of opening ν for the wedge or the cone, the flow may be equilibrium, nonequilibrium, or frozen. If L is such that the flow at the distance x = L may be assumed to be equilibrium flow, as the gas moves along the body surface from x = 0 to x = L, all the flow regimes are implemented in sequence, beginning with frozen flow (at x = 0, $\delta = 0$ — consequently $\tau_{dif} = 0$).

In addition, in contrast to the region of the critical point, in the case of flow around a plate (wedge) or cone, the self-modeling (which does not depend on the coordinate ξ) solution of equations (5.49) — (5.51) holds only in the limiting cases of frozen ($\zeta_{gi} \to 0$) or equilibrium ($\zeta_{gi} \to \infty$) flows. Since $\zeta_{wi} \sim \sqrt{x}$ (see Equation (5.57)), the body surface must be either noncatalytic, or ideally catalytic and sufficiently cold ($\alpha_w \approx 0$).

We shall first examine the results of calculating equilibrium flow.

Equilibrium boundary layer

Numerous results derived from calculating the equilibrium boundary layer have shown that the corresponding characteristics of flow and heat transfer in dissociating air may be calculated with an accuracy which is sufficient for practical purposes by the so-called method of determining (or conditional) enthalpy [19]. According to this method, all of the characteristics of the air which depend on temperature are calculated for a certain enthalpy which is appropriately selected and which lies between the maximum values in the boundary layer.

For example, the determining enthalpy is found by the method of successive approximations according to a formula proposed by V. A. Bashkin:

$$h^* = \frac{0{,}563\,\mathrm{Pr}}{0{,}123+\mathrm{Pr}}\,h_\delta + \frac{0{,}126+0{,}437\,\mathrm{Pr}}{0{,}126+\mathrm{Pr}}\,h_w + \frac{0{,}211\,\mathrm{Pr}}{1{,}53+\mathrm{Pr}}\,u_\delta^2 \qquad (5.115)$$

(in many cases, we may confine ourselves to the first approximation, i.e., we may assume $\mathrm{Pr} \approx \mathrm{Pr}_w$).

The value of the parameter $l^* = \rho^*\mu^*/\rho_\delta\mu_\delta$ (see, for example, Figure 5.23) is determined from the determining enthalpy h* by means of existing tables or graphs. After this, the characteristics of flow and heat transfer are calculated according to the following formulas

$$c_f = \frac{2\tau_w}{\rho_\delta u_\delta^2} = 0{,}665\sqrt{\frac{(1+2j)\,l}{\mathrm{Re}_x}}; \qquad (5.116)$$

$$c_h=\frac{-q_w}{\rho_\delta u_\delta (h_r-h_w)}=0{,}1446\,\frac{(1{,}3+\mathrm{Pr})}{\mathrm{Pr}}\sqrt{\frac{(1+2j)\,l^*}{\mathrm{Re}_x}}, \qquad (5.117)$$

where $h_r=h_\delta+\frac{0{,}91\,\mathrm{Pr}}{0{,}82+\mathrm{Pr}}u_\delta^2$ is the enthalpy of a thermally insulated surface. The Reynolds number Re_x is calculated from the flow parameters at the external boundary of the boundary layer.

Nonequilibrium boundary layer

Let us determine the characteristics of flow with the example of vibrational relaxation. In this case, the continuity equation (5.1), the momentum equation (5.2), and the energy equation (in the form of (5.3)) are the same as before, except that the thermal flux has the following form [6]

$$q=q_c+q_k=-\lambda\frac{\partial T}{\partial y}-\lambda_k\frac{\partial T_k}{\partial y}, \qquad (5.118)$$

where T_k is the vibrational temperature; $\lambda_k(T, T_k)$ is the coefficient of the internal heat conductivity,* and the enthalpy h will be

$$h=\int_0^T c_p dT=(7/2)\frac{R}{M}T+e_k. \qquad (5.119)$$

Here the vibrational energy e_k (for the model of a harmonic oscillator) will be

/249

$$e_k(T_k)=\frac{RT_v/M}{[\exp(T_v/T_k)-1]}, \qquad (5.120)$$

*It is assumed that the translational and rotational degrees of freedom are excited uniformly.

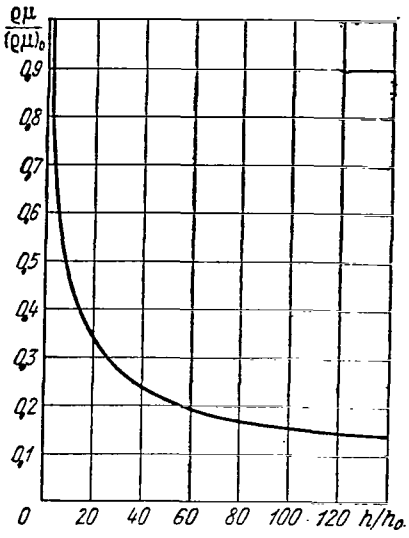

Figure 5.23. Dependence of the parameter $\rho\mu$ on the enthalpy h when $h_0 = 65.55$ cal/g; $\mu_0 = 1.724 \cdot 10^{-4}$ g/cm·sec; $\rho_0 = p_\delta/RT_0$; $T_0 = 273$ K.

where T_ν is the characteristic vibrational temperature (for example, for oxygen $T_\nu = 2239$ K, for nitrogen $T_\nu = 3395$ K).

Instead of the equation for conservation of concentration, the system is closed by the relaxation equation for the quantity e_k, which has the following form in the case of a boundary layer [46]

$$\rho\left(u\frac{\partial e_k}{\partial x}+v\frac{\partial e_k}{\partial y}\right)=\rho\frac{e_k(T)-e_k(T_k)}{\tau_k(\rho,T)}+\frac{\partial}{\partial y}\left(\lambda_k\frac{\partial T_k}{\partial y}\right). \qquad (5.121)$$

Here τ_k is the relaxation time (analog of the characteristic relaxation time τ_g).

It must be noted that Equation (5.121) is valid when $(T - T_k)/T \sim 0(1)$, i.e., in the case of a two-temperature relaxation [8], when the time for establishing equilibrium within the external (translational and vibrational) and within the vibrational degrees of freedom is a little less than the time τ_k for establishing equilibrium between these degrees of freedom (total thermodynamic equilibrium).

The study by V. M. Kuznetsov and S. N. Seliverstov [46] gives the most complete and accurate solution of the problem of flow around a flat plate in this formulation.* The authors examined both a completely noncatalytic plate $(\partial T/\partial y)_w = (\partial T_k/\partial y)_w = 0$ and a plate with a given degree of catalytic characteristics ($T = T_w$; $T_k = (T_k)_w$).**

The mathematical model assumed makes it possible to rigorously investigate a nonequilibrium boundary layer for all values of $(\zeta_k = x/u_\delta(\tau_k)_\delta$ from frozen flow $(\zeta_k \ll 1)$ to equilibrium flow $(\zeta_k \to \infty)$, and to establish the characteristic flow features.

If the gas is in equilibrium at the outer boundary of the boundary layer, then the equilibrium is disturbed and the gas is heated within the boundary layer (due to viscous energy dissipation) and when the gas is cooled close to the cold body surface, which influences its catalytic properties. The development of nonequilibrium processes during flow around a flat plate is illustrated by the characteristic profiles of nondimensional temperatures $\theta = T/T_\delta$ and $\theta_k = T_k/T_\delta$ in the case of nitrogen N_2 flow along the surface of a thermally insulated plate (Figure 5.24a) and for a surface with a given

---

*A similar problem was solved approximately in [47, 48] with several simplifying assumptions.

**It is assumed that $T = T_k = T_\delta$ on the outer boundary of the boundary layer, although this is not necessary and may be taken into account by the method used in this study.

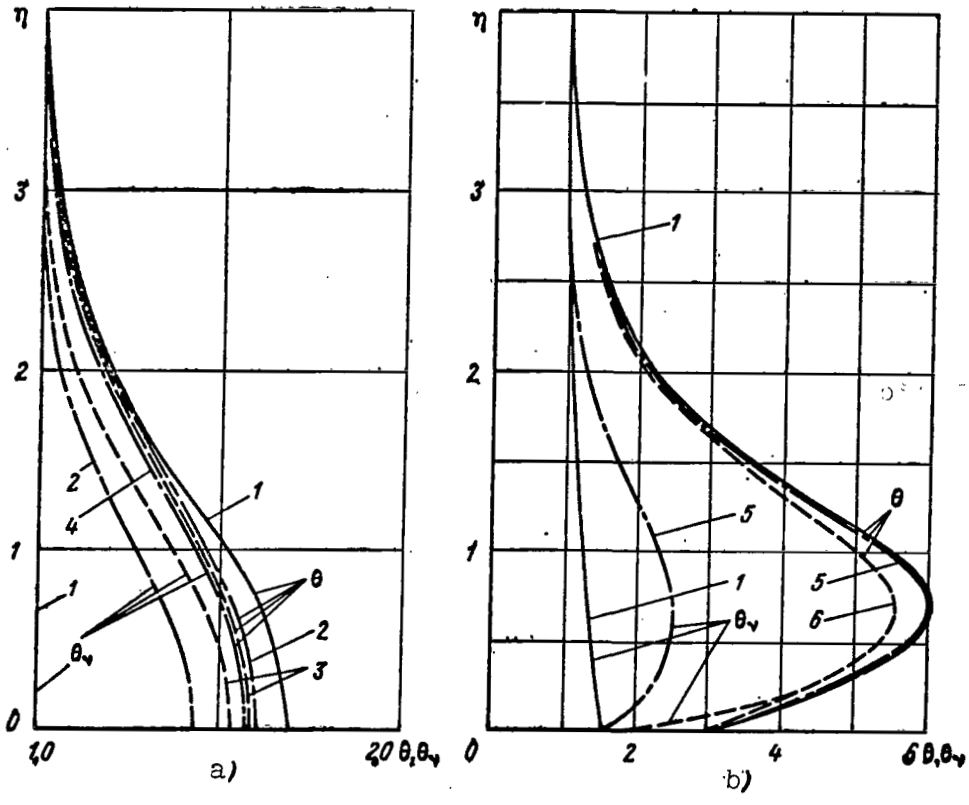

Figure 5.24. Temperature profiles $\theta = T/T_\delta$ and $\theta_k = T_k/T_\delta$ during the flow of relaxing nitrogen along the surface of a flat plate.

a — thermally insulated surface ($\theta'_w = (\theta'_k)_w = 0$; $M_\delta = 2$; $T_\delta = 3336$ K); b — surface with a given catalycity ($M_\delta = 8$; $T_\delta = 330$ K; $T_w = 1000$ K; $(T_k)_w = 550$ K); 1 — at $\zeta_k = x/u_\delta(\tau_k)_w = 0$; 2 — at $\zeta_k = 0.06$; 3 — at $\zeta_k = 0.2$; 4 — at $\zeta_k \to \infty$; 5 — at $\zeta_k = 0.2 \cdot 10^3$; 6 — at $\zeta_k = 0.19 \cdot 10^5$.

catalytic nature* (Figure 5.24b). In the latter case, the profiles of T and T_k when $\zeta_k \to \infty$ coincide in a large portion of the boundary layer, and only differ in the region of the plate /251

*To increase the influence of nonequilibrium in this case, a hypothetical model of nitrogen N_2 was studied, in which the rotational degrees of freedom were replaced by the vibrational degrees of freedom.

directly adjacent to the surface.

Calculations performed in [46] also showed that the dimensionless value of the surface flow $c_\tau = \frac{\tau_w \sqrt{\mathrm{Re}_x}}{\rho_\delta u_\delta^2}$* and the total thermal flux ($\sim c_h \sqrt{\mathrm{Re}_x}$) for a catalytic surface are constant throughout the entire nonequilibrium region, whereas the change along the plate surface of the components of the thermal flux from the outer (q_c) and vibrational (q_k) degrees of freedom greatly depends on the values of T_w and $(T_k)_w$, as well as on the energy capacity of the relaxing degrees of freedom. This conclusion is also valid in examination of nonequilibrium dissociation. Figure 5.25 presents values of

$$c_\tau;\ Q_c = \frac{-q_c \sqrt{\mathrm{Re}_x}}{\rho_\delta u_\delta (c_V)_\delta T_\delta};\quad Q_k = \frac{-q_k \sqrt{\mathrm{Re}_x}}{\rho_\delta u_\delta (c_V)_\delta T_\delta} \text{ and } Q_w = Q_c + Q_k$$

by way of an example, along a plate surface for nitrogen flow (hypothetical model).

The solution obtained in [46] may be extended to the case /252 of supersonic flow around a wedge, and also a cone, if conditions at the outer boundary of the boundary layer are known. Estimates made in [52] showed that at $\mathrm{Re}_x \ll 10^8$ for air it is first possible to solve the problem of inviscid flow (with allowance for relaxation effects), and then the solution obtained may be used for the outer boundary conditions in the case of a boundary layer. If $\zeta_k = \frac{x}{u_\delta (\tau_k)_\delta} \gtrsim 1$, then the field of inviscid flow is completely a nonequilibrium field (at $\zeta_k \ll 1$ there is a frozen flow of an ideal gas with $\kappa = 7/5$). When $\zeta_k \gg 1$, the

*The Reynolds number Re_x is determined from the flow parameters on the outer boundary of the boundary layer and by the distance x from the nose.

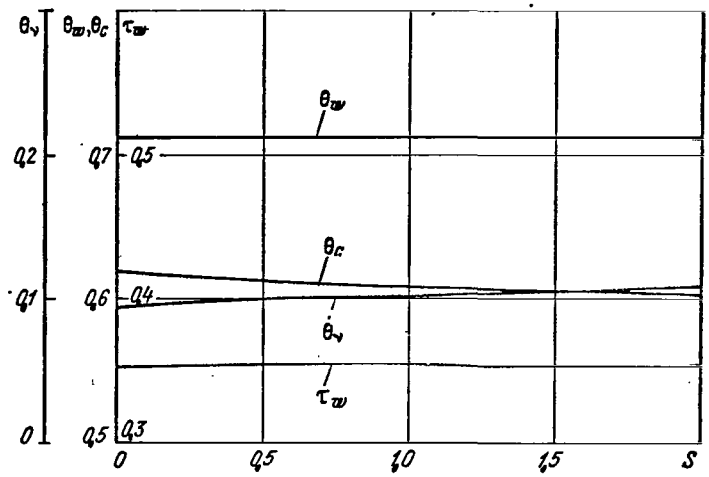

Figure 5.25. Characteristics of flow and heat transfer along the surface of a flat plate during the flow of relaxing nitrogen (hypothetical model) at $M_\delta = 8$; $T = 330$ K; $T_w = 1000$ K; $(T_k)_w = 550$ K.

characteristics of inviscid flow correspond to equilibrium flow around a wedge. Thus, close to the body surface there is a relaxation entropy layer* (see Section 4.3), in which the flow characteristics change only along the normal to the body.

Consequently, in this case it is necessary to use the condition on the lower boundary of the relaxation entropy layer (when $y = 0$, $x \to \infty$ [51]) as the external boundary conditions in the problem of equilibrium viscous flow. The cross hatched region in Figure 5.26 is the region of flight regimes where the presence of a relaxation entropy layer ($0.1L > u_\delta \tau_k > 10\delta$) must be taken into account for a wedge with a half-angle of opening $\vartheta = 40°$ and the characteristic length $L = 1$ m and $L = 10$ m. At

*A relaxation entropy layer on a wedge exists in the case of flow of gas with dissociation; on a cone, this layer is diffused due to the three-dimensional effect.

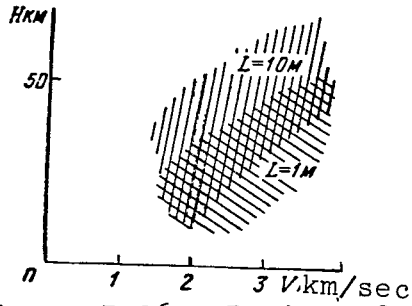

Figure 5.26. Region of relaxation entropy layer during the flow of air along a wedge surface at $\vartheta = 40°$; L = 1 m, and L = 10 m.

$Re_x > 10^9$ — 10^{11}, the relaxation layer is absorbed by the viscous boundary layer, on whose outer boundary equilibrium conditions of flow around a wedge exist.

Let us now consider non-equilibrium chemical reactions within a boundary layer, assuming that the surface is either an ideally catalytic surface ($\zeta_w \to \infty$), or a completely noncatalytic surface ($\zeta_w \to 0$). It is natural to begin with the method of expansion in series, which — although it is valid only in the vicinity of the leading edge — nevertheless makes it possible to reach important qualitative conclusions regarding the behavior of the boundary layer as a whole.

We will perform the investigation on the basis of [3] and [52] for the model of a dissociating diatomic gas, assuming that Pr, Sc and l are constants, and c_{pi} are also constants and equal each other. /253

In this case, changing to the variable $\tilde{\eta} = \eta/\sqrt{l}$, for the function $\tilde{f} = f/\sqrt{l}$ from (5.49) we obtain the well-known Blasius equation, and Equations (5.51) and (5.59) assume the form

$$\frac{1}{Sc} z'' + \tilde{f} z' = 2\zeta_g \tilde{f}' \frac{\partial z}{\partial \zeta_g} + \zeta_g \Phi(z, \theta); \qquad (5.122)$$

$$\frac{1}{Pr} \theta'' + \tilde{f}\theta' + \left(\frac{u_\delta^2}{c_p T_\delta}\right)(\tilde{f}'')^2 = 2\zeta_g \tilde{f}' \frac{\partial \theta}{\partial \zeta_g} - \zeta_g \left(\frac{a_\delta h^\circ}{c_p T_\delta}\right) \Phi(z, \theta) \qquad (5.123)$$

with the following boundary conditions

$$\left.\begin{aligned}
&\text{for } \tilde{\eta}\to\infty \quad z=\theta=1;\\
&\text{for } \tilde{\eta}=0 \quad \theta(0)=\theta_w;\\
&\qquad z(0)=z_w=0 \quad (\text{for } \zeta_w\to\infty);\\
&\qquad z'(0)=z'_w=0 \quad (\text{for } \zeta_w=0),
\end{aligned}\right\} \tag{5.124}$$

where $z = \alpha/\alpha_\delta$; $\theta = T/T_\delta$; "'" designates the derivative with respect to the coordinate $\tilde{\eta}$:

$$\zeta_g=\frac{4}{(1+2j)}\frac{k'_r}{T_\delta^{\omega+2}}\left(\frac{p}{R}\right)^2\frac{x}{u_\delta} \tag{5.125}$$

is the Damkeler number for recommendation in a gas (j = 0 corresponds to a plate or a supersonic wedge, j = 1 — to a cone);

$$\Phi(z,\ \theta)=\frac{1}{\theta^{\omega+2}}\left\{\frac{\alpha_\delta z^2}{(1+\alpha_\delta z)}-\frac{K_p}{4p}\frac{(1-\alpha_\delta z)}{\alpha_\delta}\exp[-T_d/T]\right\}^*. \tag{5.126}$$

We shall search for the solution in the form

$$\left.\begin{aligned}
z(\tilde{\eta},\ \zeta_g)&=z_0(\tilde{\eta})+\zeta_g z_1(\tilde{\eta})+\zeta_g^2 z_2(\tilde{\eta})+\ldots;\\
\theta(\tilde{\eta},\ \zeta_g)&=\theta_0(\tilde{\eta})+\zeta_g\theta_1(\tilde{\eta})+\zeta_g^2\theta_2(\tilde{\eta})+\ldots.
\end{aligned}\right\} \tag{5.127}$$

Substituting Expression (5.127) in Equations (5.122) — (5.123), in the zero approximation ($\zeta_g = 0$), we obtain the equations for a frozen boundary layer, which may be reduced to linear equations of the first order, whose solutions are well

*Compare with Expression (5.104).

known (see [1]).

In particular, /254

$$\left.\begin{aligned}(z_0')_x &\simeq 0{,}47\,\mathrm{Sc}^{1/3} \quad (\text{for } \zeta_w \to \infty);\\ (\theta_0')_x &\simeq 0{,}47\,\mathrm{Pr}^{1/3}\left[1-\theta_w+\frac{u_\delta^2}{2c_pT_\delta}\sqrt{\mathrm{Pr}}\right].\end{aligned}\right\} \qquad (5.128)$$

In the first approximation, collecting terms for ζ_g in the first power, we obtain the following system of equations

$$\left.\begin{aligned}&\frac{1}{\mathrm{Sc}}\,z_1'+\tilde{f}z_1'-2\tilde{f}'z_1=\Phi_0;\\ &\frac{1}{\mathrm{Pr}}\,\theta_1'+\tilde{f}\theta_1'-2f'\theta_1=-\left(\frac{a_\delta h^\circ}{c_pT_\delta}\right)\Phi_0\end{aligned}\right\} \qquad (5.129)$$

with the boundary conditions

$$\left.\begin{aligned}&\theta_1(0)=\theta_1(\infty)=0;\\ &z_1(0)=z_1(\infty)=0 \quad (\text{for } \zeta_w\to\infty);\\ &z_1'(0)=z_1(\infty)=0 \quad (\text{for } \zeta_w=0),\end{aligned}\right\} \qquad (5.130)$$

where $\Phi_0 = \Phi(z_0;\ \theta_0)$.

Since Equations (5.129) are linear, their general solution may be written in the form

$$\theta_1(\tilde{\eta})=-\left(\frac{a_\delta h^\circ}{c_pT_\delta}\right)\Upsilon_1(\mathrm{Pr},\ \tilde{\eta})\left\{Y_1(\mathrm{Pr},\ \tilde{\eta})-Y_1(\mathrm{Pr},\ \infty)\frac{Y_2(\mathrm{Pr},\ \tilde{\eta})}{Y_2(\mathrm{Pr},\ \infty)}\right\}; \qquad (5.131)$$

for $\zeta_w \to \infty$

$$z_1(\tilde{\eta})=\Upsilon_1(\mathrm{Sc},\ \tilde{\eta})\left\{Y_1(\mathrm{Sc},\ \tilde{\eta})-Y_1(\mathrm{Sc},\ \infty)\frac{Y_2(\mathrm{Sc},\ \tilde{\eta})}{Y_2(\mathrm{Sc},\ \infty)}\right\}; \qquad (5.132)$$

for $\zeta_w=0$

$$z_1(\tau_i)=\Upsilon_1(\mathrm{Sc},\ \tilde{\eta})\{Y_1(\mathrm{Sc},\ \tilde{\eta})-Y_1(\mathrm{Sc},\ \infty)\}, \tag{5.133}$$

where $\Upsilon_1(\mathrm{Pr},\ \tilde{\eta})$ designates a solution of the homogeneous equation (Figure 5.27)

$$\frac{1}{\mathrm{Pr}}\Upsilon_1''+\tilde{f}\Upsilon_1'-2\tilde{f}_1'\Upsilon_1=0 \tag{5.134}$$

with the following initial conditions: $\Upsilon_1(\mathrm{Pr},\ 0)=1;\ \Upsilon_1'(\mathrm{Pr},\ 0)=0;$

/255

$$Y_1(\mathrm{Pr},\ \tilde{\eta})=\int_0^{\tilde{\eta}}\frac{\exp\left[-\mathrm{Pr}\int_0^{u_1}\tilde{f}du_1\right]}{[\Upsilon_1(\mathrm{Pr},\ u_1)]^2}\times \tag{5.135}$$

$$\times\left\{\int_0^{u_1}\Upsilon_1(\mathrm{Pr},\ u_2)\exp\left[\mathrm{Pr}\int_0^{u_2}\tilde{f}du_3\right]\Phi_0(u_2)\,du_2\right\}du_1;$$

$$Y_2(\mathrm{Pr},\ \tilde{\eta})=\int_0^{\tilde{\eta}}\frac{\exp\left[-\mathrm{Pr}\int_0^{u_1}\tilde{f}du_2\right]}{[\Upsilon_1(\mathrm{Pr},\ u_1)]^2}du_1. \tag{5.136}$$

The integrals $\Upsilon_1(\mathrm{Sc},\ \tilde{\eta})$, $Y_1(\mathrm{Sc},\ \tilde{\eta})$ and $Y_2(\mathrm{Sc},\ \tilde{\eta})$ have the same form as in Formulas (5.134), (5.135), and (5.136) only the Pr number is replaced by Sc.

The thermal flux determined by Expression (5.13) may be represented according to (5.41) in the following form

$$-q_w=\rho_\delta u_\delta\frac{(c_pT_\delta)}{\mathrm{Pr}}\sqrt{\frac{(1+2j)\,l}{2\mathrm{Re}_x}}\left\{\left[(\theta_0')_w+\mathrm{Le}\left(\frac{a_\delta h^\circ}{c_pT_\delta}\right)(z_0')_w\right]+\right. \tag{5.137}$$

$$\left.+\zeta_g\left[(\theta_1')_w+\mathrm{Le}\left(\frac{a_\delta h^\circ}{c_pT_\delta}\right)(z_1')_w\right]+\ldots\right\}.$$

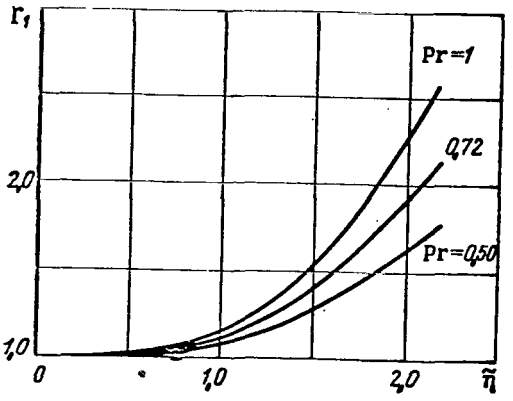

Figure 5.27. Function $\gamma_1=\varphi(\tilde{\eta}, \mathrm{Pr})$

In the first approximation, the thermal flux q_1 caused by reactions in the gas will be /256

$$q_1=\zeta_g\left[(\theta_1')_w+\mathrm{Le}\left(\frac{a_\delta h^\circ}{c_p T_\delta}\right)(z_1')_w\right]=$$

$$=\zeta_g\left(\frac{a_\delta h^\circ}{c_p T_\delta}\right)\left[\frac{Y_1(\mathrm{Pr},\infty)}{Y_2(\mathrm{Pr},\infty)}-(\mathrm{Le})\frac{Y_1(\mathrm{Sc},\infty)}{Y_2(\mathrm{Sc},\infty)}\right]\ (\text{for } \zeta_w\to\infty);$$

$$\text{and } q_1=\zeta_g\left(\frac{a_\delta h^\circ}{c_p T_\delta}\right)\frac{Y_1(\mathrm{Pr},\infty)}{Y_2(\mathrm{Pr},\infty)}\ (\text{for } \zeta_w=0).$$

It may be again be seen that when Le = 1 for a catalytic surface ($\zeta_w \to \infty$), the magnitude of the thermal flux does not depend on the degree of flow nonequilibrium within the boundary layer.

Expansion in series in powers of $1/\zeta_g$ was used previously in studies of V. P. Stulov [53, 54] to obtain the solution in the case when the flow is close to equilibrium flow.

Similar methods of the small parameter were successfully used in [55, 56, etc.]. In the last of these studies, the influence of vibratory relaxation on dissociation was taken into account.

Before turning to the results of numerical calculations, let us give certain general rules for nonequilibrium boundary layers, which may be obtained by analyzing the solution obtained above.

It follows from the expression for Φ that the first term in the brackets in Equation (5.126) indicates the recombination process in the boundary layer, and the second — the dissociation process. It is possible to obtain the criteria establishing which of the reactions is the predominant reaction for the given flow conditions. These criteria are valid not only close to the leading edge, but also in the remaining part of the boundary layer. The dissociation process will be predominant in the boundary layer, if the condition $(z_1')_w > 0$ is satisfied close to the surface (for $\zeta_w \to \infty$) or $(z_1)_w > 0$ (for $\zeta_w = 0$). Since

$$(z_1')_w = -\frac{Y_1(\mathrm{Sc}, \infty)}{Y_2(\mathrm{Sc}, \infty)} \quad (\text{for } \zeta_w \to \infty);$$
$$(z_1)_w = -Y_1(\mathrm{Sc}, \infty) \quad (\text{for } \zeta_w = 0),$$

and the integral $Y_2(\mathrm{Sc}, \infty)$ is positive, the magnitude and sign of $(z_1')_w$ and $(z_1)_w$ directly depend on the value of $-Y_1(\mathrm{Sc}, \infty)$. Inger [3, page 224] obtained the values of the function

$$\left[\frac{1+\alpha_\delta}{\alpha_\delta}\right] Y_1(\mathrm{Sc}, \infty)$$

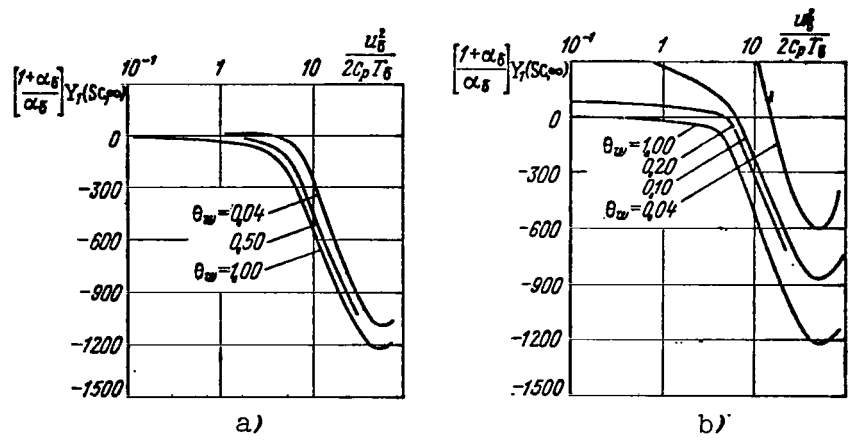

Figure 5.28. Function $\left[\frac{1+\alpha_\delta}{\alpha_\delta}\right]Y_1(\mathrm{Sc}, \infty) = \varphi(u_\delta^2/2\overline{c}_pT_\delta)$:

a — ideally catalytic surface; b — noncatalytic surface.

which barely changes with a change in α_δ. The results of his calculations are reproduced in Figure 5.28.

Let us first consider the case of an ideally catalytic surface. According to the results shown in Figure 5.28a, when $\zeta_w \to \infty$ recombination is never the predominant reaction in the gas phase. /257

At $u_\delta^2/2c_pT_\delta \ll 1$, the temperature monotonically decreases in the direction of the outer boundary of the boundary layer toward the body surface. However, the predominance of recombination within the boundary layer is not due to infinitely rapid recombination on the surface itself, or to removal of the atoms from the flow due to diffusion. In this case, in general no reaction predominates. When $u_\delta^2/2c_pT_\delta$ is large, $(M_\delta^2 \gg 1)$, the temperature profile within the boundary layer has a maximum ($T_{max} \gg T_\delta$), and

there the dissociation reaction predominates (at $u_\delta^2/2c_pT_\delta \lesssim 5$). Since dissociation in a gas occurs far from the surface, the surface temperature has only a small influence on the value of $Y_1(Sc, \infty)$ (see Figure 5.28a).

Let us now consider the boundary layer around a noncatalytic surface. In this case, the surface does not serve as more than a sink for the atoms, and close to a cold surface, when $u_\delta^2/2c_pT_\delta$ is small and T_δ is large, there is intense recombination in the gas. As may be seen from the expression for (5.126), the recombination rate is proportional to $1/(T)^{\omega+2} \simeq 1/(T)^{3,5}$. Therefore, the recombination primarily occurs close to the surface, where the temperature is at a minimum, and the value of $Y_1(Sc, \infty)$ depends strongly on the surface temperature (see Figure 5.28b). Due to /258 the rapid recombination, dissociation in the gas phase predominates only when $u_\delta^2/2c_pT \gtrsim 10$ and $\theta_w \lesssim 0,1$, and even in this region $Y_1(Sc, \infty)$ depends on the surface temperature.

Rae [52], examining the case when the predominate reaction in the boundary layer on a flat plate is dissociation and when it occurs (due to the exponential dependence of the dissociation rate on temperature) in the region of the maximum frozen temperature, used the method of steepest descents to analytically calculate the integral $Y_1(Sc, \infty)$ and represented the solution for the concentration α_w on the surface of a plate in a closed form. His form has a simple physical interpretation: if the atoms are produced only at the point θ_{0max}, then

$$\frac{d\alpha}{dt}\Big|_{\zeta_g=0} \approx \left(\frac{MJ}{\rho}\right)_{\theta_{0max}} \quad \text{or} \quad \alpha \sim \frac{x}{u_\infty}\left(\frac{MJ}{\rho}\right)_{\theta_{0max}}.$$

In the final form, the formula includes a numerical factor which takes into account the diffusion of atoms toward the surface. Although the solution obtained is only valid at $\zeta_g \ll 1$, Rae [52] extended his solution to arbitrary values of ζ_g, replacing the maximum value of θ_0 by the maximum local value of θ at the point under consideration x (method of local similarity). He retained the previous dependence between θ_{max} and α_w, and took recombination into account. In the case of an adiabatic flat plate, the maximum temperature is reached on the surface of the plate, and the Rae solution (at Pr = 1) assumes the form

$$\alpha_w = \frac{2x}{u_\delta}\left(\frac{MJ}{\rho}\right)_w \frac{\theta_w Y_2(\mathrm{Sc}, \infty)}{(f''_w)^{1+\mathrm{Sc}}}\sqrt{\frac{2\pi}{(u_\delta^2/c_pT_\delta)\theta_d}}. \qquad (5.138)$$

At Pr = Sc = 1, the values θ_w and α_w are related by the following formula

$$\theta_w = 1 + \frac{u_\delta^2}{2c_pT_\delta} - \frac{\alpha_w h^\circ}{c_pT_\delta}. \qquad (5.139)$$

Defining the values of α_w, Equations (5.138) and (5.139) may be solved with respect to x, i.e., we may find the dependence $\alpha_w = \varphi(x)$. Calculations using these formulas for an adiabatic flat plate provide a good agreement with calculations using the integral method of Pol'gauzen [3],* and also according to the

*The same satisfactory results must be obtained in the case of a cold surface at $\zeta_w \to \infty$. If a surface is cold, and $\zeta_w = 0$, the solution is inapplicable, since in this case — in addition to a dissociation zone in the region of maximum temperature — there is a recombination zone close to the cold surface, which is not completely considered in the calculation method proposed by Rae.

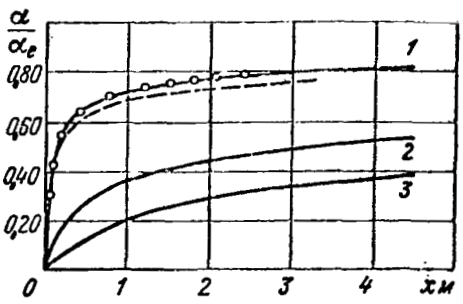

Figure 5.29. Oxygen relaxation along the adiabatic surface of a flat plate (solid lines — integral method [3]; dashed lines — method of local similarity [52]; points — method of finite differences [57]).

1 — at M_δ = 15; H = 30.5 km; $(\alpha_w)_e$ - 0.527; 2 — at M_δ = 10; H = 30.5 km; $(\alpha_w)_e$ = 0.146; 3 — M_δ = 10; H = 61 km; $(\alpha_w)_e$ = 0.366.

method of finite differences [57] (Figure 5.29). The results presented in Figure 5.29 for oxygen /259 show that at an altitude of H = 30 — 60 km when M $\lesssim$ 20, the boundary layer even at about three meters still remains a nonequilibrium layer. For nitrogen, relaxation will occur at greater lengths, since T_d for nitrogen is a little greater than for oxygen. Similarly, relaxation will be a little slower when the boundary layer is cooled at the surface.

It follows from an analysis of the equations of a nonequilibrium boundary layer around a plate, wedge, or cone (5.122) — (5.125) that, when dissociation is the predominant reaction, the chemical state of the boundary layer is determined by the parameters T_δ, T_w and by the product $\zeta g/p$ for the given gas* and for the given surface catalycity. If it is assumed that T_δ and T_w are approximately constant, the chemical condition of the boundary layer will be the same where the values of ζ_g/p coincide, which are determined by the expression

$$\zeta_g/p \sim \frac{1}{u_\delta} \frac{k_r'}{(T_\delta)^{\omega+2}} (px).$$

*In the case $M_\delta \gg 1$ the braking temperature T_0 is used, instead of T_δ.

If we also establish the value of u_i, then ζ_g/p will be proportional to px. In other words, the binary similarity law is satisfied (see Section 4.2).

The results of numerical calculations [58] confirm the fact /260 that the binary similarity law fairly well correlates the values of the component concentrations in the presence of diffusion, if the dissociation process predominates in the boundary layer.

By way of an illustration, Figure 5.30 gives the maximum electron concentrations for air in the boundary layer for a cone, which were obtained in [59] by means of the binary similarity law. If we use the maximum "frozen" value of the temperature T_{max}, the equations for concentration conservation of individual air components may be as follows

$$\frac{l}{\mathrm{Sc}}\alpha_i^{\cdot}+f\alpha_i^{\prime}+\frac{2}{3}\frac{x}{u_\delta}\left(\frac{M_i}{\rho}J_i\right)=0;$$

When $l \cong$ const, $\mathrm{Sc}_i \cong$ const, they may be regarded as ordinary linear differential equations for determining the concentration α_i. An approximate calculation of $(M_i/\rho)J_i = \varphi(T_{max})$ was made in [59].

The final result is obtained in the form

$$\frac{n_e}{p_\delta}\sim\frac{\exp\left[-185\,000/T_{\max}\right]}{(T_{\max})^{6,5}}\left[\frac{p_\delta x}{u_\delta}\right]^3. \qquad (5.140)$$

As a whole, this dependence coincides fairly well with the results of numerical calculations [58 and 60]; however, the absolute values diverge by almost one order of magnitude. Therefore, it is advantageous to use it only for estimates, and also for parametric calculations.

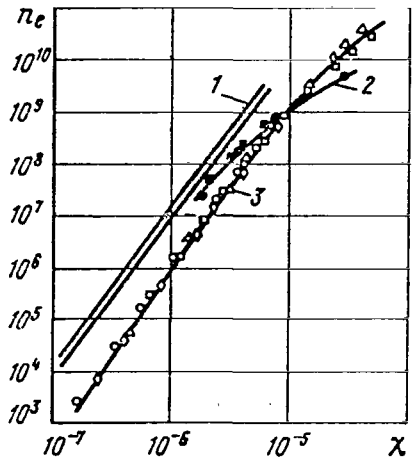

Figure 5.30. Maximum electron density in a boundary layer on a cone

$$\chi=\left(\frac{\rho_\delta x}{u_\delta}\right)\left\{\frac{\exp[37-185000/T_{max}]}{(T_{max}/5000)^{6.5}}\right\}^{1/2}\left(\frac{kG\cdot sec}{cm^2}\right)$$

1 — approximate theory [69]; 2 — calculation by integral relationships; 3 — calculated by method of finite differences [60].

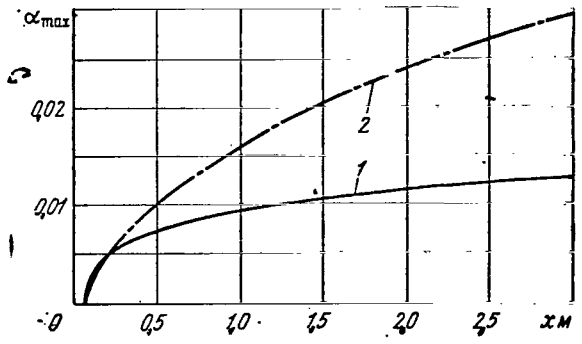

Figure 5.31. Change in maximum atom concentration in a boundary layer during the flow of relaxing oxygen along a cone surface (catalytic surface) at ϑ = 10°; V_∞ = 6.7 km/sec; H = 46 km; T_w = 1200 K:

1 — calculation by method of integral relationship [60] with allowance for variation of thermodynamic properties and transport characteristics; 2 — calculation by method of finite differences [59] (Pr = 0.7; Le - 1.4); u and H profiles are fixed).

Numerical methods for the solution, which make it possible to depart from the simplifying assumptions and to consider the complete chemical model of air, have been developed [27, 45, 57, 58, 60]. However, the majority of the examples of numerical calculations which have been published have been limited to a /261 comparison with existing results (see, for example, Figure 5.29).

For identical values of the thermodynamic properties, and the transport characteristics in the case of relaxing oxygen flow around a cone, the results derived from calculations using the method of finite differences [57] and the method of integral relationships [58] closely coincide. However, the study [58] took into account the influence of the physical gas properties

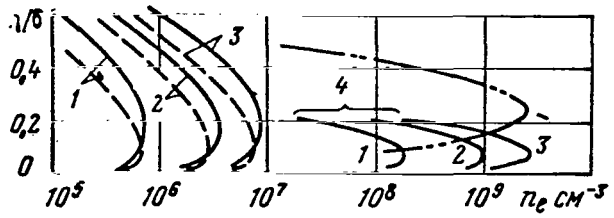

Figure 5.32. Electron density profiles in nonequilibrium boundary layer on a cone at $\vartheta = 8°$; $V_\infty = 6.7$ km/sec (catalytic surface); $T_w = 1000$ K. Influence of diffusion law when H = 46 km (solid lines — multi-component diffusion; dashed lines — binary diffusion-Fick law; dotted-dashed lines — equilibrium state).
1 — when x = 1.5 m; 2 — when x = 3.1 m; 3 — when x = 4.6 m; 4 — without considering diffusion.

upon the velocity and enthalpy profiles, and discovered rather important differences, particularly in the value of the maximum concentration of atoms (Figure 5.31). A study was also made [58] of the influence of different factors upon the characteristics of a nonequilibrium boundary layer in air (taking into account seven reactions) in the case of flow around a cone.

By way of an example, Figure 5.32 gives profiles of the electron concentrations n_e which correspond to flights at an altitude of H = 46 km. The decisive influence of diffusion on the profile n_e may be clearly seen in a comparison with computational results using the method of streamtubes, in which diffusion is not taken into account. The use of the customary Fick law, instead of the law of multicomponent diffusion, for air changes the results very little. It may be noted that the electron concentration is primarily determined by the concentrations of N and O, and the diffusion of the electron-ion pair produces a secondary effect. At a distance of $x \cong 4.6$ m from the cone apex, the value of n_e is approximately two orders of magnitude smaller than the equilibrium values. The velocity constants taken from the study by Lin and Teere* were used in the calculation; when the values of /262

*See Section 1.4.

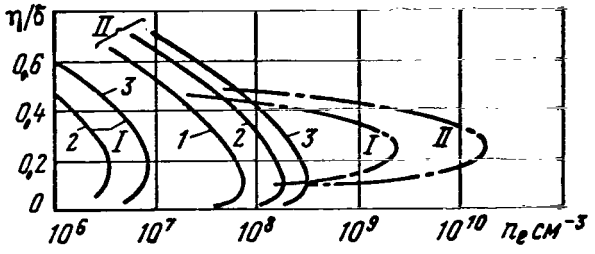

Figure 5.33. Influence of flight velocity for the same conditions as shown in Figure 5.32 (solid lines — nonequilibrium state; dotted-dashed lines — equilibrium state).

I — when H = 46 km; II — when H = 35 km; 1 — when x = 1.5 m; 2 — when x = 3.1 m; 3 — when x = 4.6 m.

the constants taken from the study by Rae* were used, the electron concentration decreased by approximately a factor of two. The influence of flight velocity on the value of n_e is shown in Figure 5.33.

Experimental studies of heat transfer in a nonequilibrium boundary layer on a flat plate, carried out in a wind tunnel [61], showed that in dissociating air the experimental data closely coincide, for example, with results of calculations in [24], whereas the experimental data were approximately 30% lower than the calculated values in an ionized stream of air or nitrogen. The study [61] has pointed out the great necessity of further research on the flow of a multi-component ionized gas. /263

Frozen boundary layer with chemical reactions on the surface

Just as in the solution of a similar problem for the critical point, we shall limit ourselves to investigating the flow of a binary mixture when $c_{pA} \simeq c_{pM} \simeq \bar{c}_p$ and constant values of l, Pr, and Sc. In this case, for frozen flow in the boundary layer ($\zeta_g = 0$) the equation of momentum (5.49) and the energy equation (5.50) for the total frozen enthalpy, having the

*See Section 1.4.

form*

$$\tilde{f}'''+\tilde{f}\tilde{f}''=0;$$

$$\frac{1}{\mathrm{Pr}}g_f'+\tilde{f}g_f'=\frac{u_\delta^2}{2(H_f)_\delta}\left(1-\frac{1}{\mathrm{Pr}}\right)[(\tilde{f}')^2]'$$

with the boundary conditions (5.77), do not depend on the concentration conservation equation, and their solutions are well known from the classical boundary layer theory (see, for example, [1]).

In particular, the solution of the energy equation determines the magnitude of the convective flux q_c

$$-q_c=0{,}47\rho_\delta u_\delta(\mathrm{Pr})^{-2/3}\sqrt{\frac{l(1+2f)}{2\mathrm{Re}_x}}\left[\bar{c}_p T_\delta+\frac{1}{2}\sqrt{\mathrm{Pr}}\,u_\delta^2-c_p T_w\right]. \qquad (5.141)$$

Thus, the problem reduces to solving the concentration equation, which in this case has the form**

$$\frac{1}{\mathrm{Sc}}z''+\tilde{f}z'=2s\tilde{f}'\frac{\partial z}{\partial s} \qquad (5.142)$$

with the following boundary conditions for a cold surface, if the order of the reaction n = 1

$$\left.\begin{array}{l}\text{for } \tilde{\eta}\to\infty \quad z=1;\\ \text{for } \tilde{\eta}=0 \quad z'(0,\,s)=\zeta_w z(0,\,s).\end{array}\right\} \qquad (5.143)$$

Here $Z = \alpha/\alpha_\delta$, and the dimensionless coordinate s is determined by the following relationship

*The superscript "'" designates the derivative with respect to the variable $\tilde{\eta} = \eta/\sqrt{l}$, and $\tilde{f} = f/\sqrt{l}$ is the Blasius function.

**In particular, an analogy with the problem of heat transfer for a nonisothermal flat plate thus follows [1].

$$s=\frac{\xi}{(\rho_\delta\mu_\delta)_0 u_\infty (L)^{1+2j}}=\frac{u_\delta (\lg\vartheta)^{2j}}{u_\infty}\frac{(x/L)^{1+2j}}{(1+2j)}; \qquad (5.144)$$

$$\zeta_w=\frac{\mathrm{Sc}\,\rho_w k_w}{\sqrt{\frac{(1+2j)}{2L}(\rho_\delta\mu_\delta)u_\delta l}}\sqrt{x/L} \qquad (5.145)$$

is the Damkeler number for reactions on the surface (it is assumed that the value of ρ_w is known).

The expression for the thermal flux q_d caused by chemical reactions on the surface has the form

$$-q_d=\rho_\delta u_\delta\frac{1}{\mathrm{Sc}}\sqrt{\frac{(1+2j)\,l}{2\,\mathrm{Re}_x}}(\alpha_\delta h^\circ)z'_w(0,\ s)=\rho_w k_w(\alpha_\delta h^\circ)z_w(0,\ s). \qquad (5.146)$$

The total thermal flux on the body will be

$$q_w=q_c+q_d.$$

The precise solution of the problem in the form of power series will be given below based on the results of [62] and [36]. It is valid in the case of a continuous change in k_w along the body surface.

Let us represent the Damkeler number ζ_w in the form

$$\zeta_w(s)=\sum_{n=0}^{\infty}b_n s^{n/k}, \qquad (5.147)$$

where k is an arbitrary constant.

Since Equation (5.142) is linear, its general solution which satisfies the boundary conditions (5.143) may be written as follows using the method of separation of variables

$$z(\tilde{\eta},\ s)=1+\sum_{n=0}^{\infty} a_n \Upsilon_n(\tilde{\eta})\, s^{n/k}, \tag{5.148}$$

where the constants a_n are expressed in terms of the coefficients b_n

$$\left.\begin{aligned} a_0&=\frac{b_0}{\Upsilon_0'(0)-b_0};\\ a_1&=\frac{(1+a_0)\,b_1}{\Upsilon_1'(0)-b_0};\\ &\cdots\cdots\cdots\cdots\\ a_n&=\frac{(1+a_0)\,b_n+\sum_{l=1}^{n-1} b_l a_{n-l}}{\Upsilon_n'(0)-b_0}, \end{aligned}\right\} \tag{5.149}$$

and $\Upsilon_n(\tilde{\eta})$ is the solution of the differential equation /265

$$\frac{1}{Sc}\Upsilon_n''+\tilde{f}\Upsilon_n'-2\left(\frac{n}{k}\right)\tilde{f}'\Upsilon_n=0 \tag{5.150}$$

with the boundary conditions

$$\Upsilon_n(0)=1;\quad \Upsilon_n(\infty)=0.$$

For a plate (wedge) and a cone, the Damkeler number is represented by one term, i.e., all b_n, except, for example, b_1 may be set equal to zero ($\zeta_w=b_1 s^{1/k}$). Then

$$\begin{aligned} a_0&=0,\\ a_1&=b_1/\Upsilon_1'(0);\\ &\cdots\cdots\cdots\\ a_n&=b_1^n\Big/\prod_{l=1}^{l=n}\Upsilon_l'(0), \end{aligned}$$

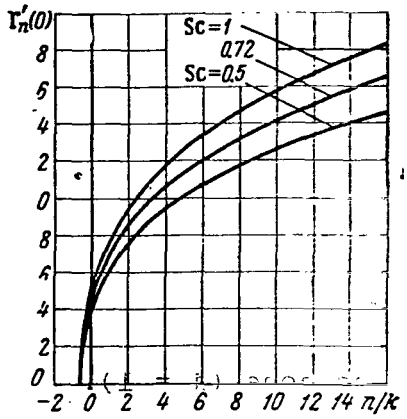

Figure 5.34. Function $\Upsilon_n'(0) = \varphi(n/k, Sc)$

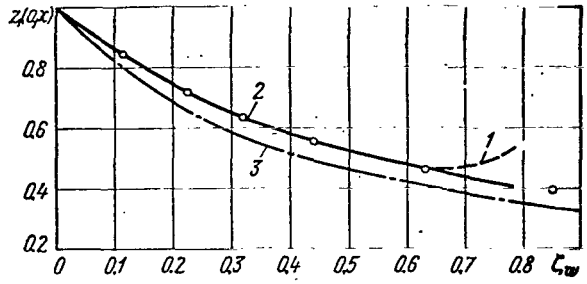

Figure 5.35. Change in atom concentration z(0, x) along flat plate surface for a linear law of surface catalycity distribution ($k_w \sim x$).

1 — solution by expansion in power series (10 terms in the series); 2 — the same (15 terms in the series); 3 — solution by local similarity; the dots designate the results obtained by the Lighthill-Volterra method [65].

and from (5.148), we obtain

$$z(0, s) = z(0, \zeta_w) = 1 + \sum_{n=1}^{\infty} \frac{(\zeta_w)^n}{\prod_{i=1}^{n} \Upsilon_i'(0)}, \qquad (5.151)$$

where ζ_w is determined by (5.145), and the values of $\Upsilon_n'(0)$ are found by solving Equation (5.150) when k = 2(1 + 2j), i.e., k = 2 — for a plate and a wedge, k = 6 — for a cone (the values $\Upsilon_n'(0) = \varphi(n/k, Sc)$ for k = 2 are given in Figure 5.34).

As follows from an analysis of the solutions (5.150) (for k = 2), when $n \to \infty$ the function $\Upsilon_n'(0) \sim n^{1/2}$, i.e., the series determined by Expression (5.151), converges uniformly for all values of x/L, although calculations show that the convergence is rather slow when $\zeta_w \geq 1$.

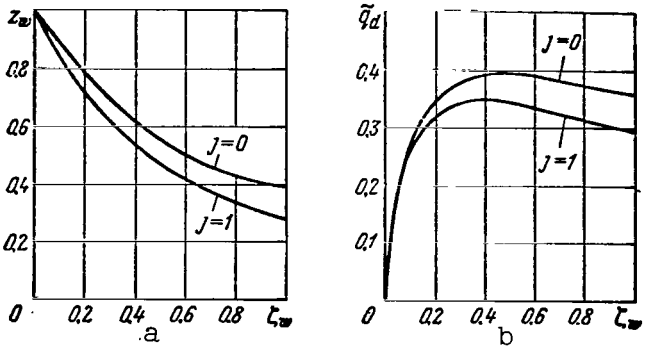

Figure 5.36. Solutions for flat plate (j = 0) and cone (j = 1).

Figure 5.35 shows the distribution of atom concentrations along the surface of a flat plate (or wedge), calculated by means of Equation (5.151) when Sc = 0.72 with allowance for 10 and 15 terms in the series. With an increase in $\zeta_w \sim \sqrt{x}$, the atom concentration strives to its equilibrium value (zero). The method of local similarity (i.e., the solution (5.89), when the /266 local value of $\zeta_w(x)$ is used as ζ_0) reduces the value of z(0, x), due to the rapid change in the flow characteristics near the leading edge.

A solution in the form of (5.151) is applicable when $k_w \sim x^d$. In this case, the Damkeler number assumes the form

$$\tilde{\zeta}_w = \zeta_w x^d \sim (s)^{\frac{1+2d}{2(1+2j)}}, \qquad (5.152)$$

i.e., in order to determine $\Upsilon_n'(0)$ it is necessary to use the solution of Equation (5.150) when k = 2 (1 + 2j)/(1 + 2d). By way of an example, Figure 5.36 gives the values of $z_w(0, \tilde{\zeta}_w)$ and $q_d = x^d z_w(0, \tilde{\zeta}_w)$ for a plate and a cone when d = 1/2 and $\tilde{\zeta}_w \sim x$.

In more recent studies, for example [63], the solution for a flat plate when $\zeta_w \sim s^{1/k}$ was obtained in closed form, utilizing the asymptotic expansions of the solutions of the boundary layer equations.

It is useful to write the following simple approximate expression for determining the concentration of atoms along the plate (wedge) surface, obtained in [3] when using the integral method of Pol'gauzen:

$$z_w = \frac{1-\left[1+0{,}458\left(\frac{\zeta_w}{0{,}48\,\mathrm{Sc}^{1/3}}\right)\right]^{-2{,}3}}{1{,}053\left(\frac{\zeta_w}{0{,}48\,\mathrm{Sc}^{1/3}}\right)}. \qquad (5.153)$$

Calculations using this formula also provide good agreement with /267 the results of calculations using other methods.

Experimental verification of the accuracy of existing computational methods was proposed in [64] by measuring the heat transfer in a wind tunnel on a flat plate with a catalytic and noncatalytic surface. The measurements showed that, in order to have an agreement with experimental data, it is very important to take into account the change of $\rho\mu$ close to the surface and the influence of a change in the Prandtl number.

In a study of the problem of nonequilibrium reactions on a surface, one method which is widely used is the transformation of the concentration equation to an integral equation of the Volterra type. A solution of this equation was obtained in [65] for a majority of the body forms which are of interest, and, in particular, for a continuous and abrupt change in k_w along the surface.

In the Dorodnitsyn variables ξ and

$$\eta = u_\delta (r)^j \int_0^y \rho/\rho_\delta dy \qquad (5.154)$$

the concentration equation (5.10) assumes the form

$$U\frac{\partial z}{\partial \xi} + V\frac{\partial z}{\partial \eta} = \frac{\mu_\delta}{\mathrm{Sc}\,\rho_\delta}\frac{\partial^2 z}{\partial \eta^2}, \qquad (5.155)$$

where

$$U = \frac{\partial \psi}{\partial \eta} = u/u_\delta; \quad V = -\frac{\partial \psi}{\partial \xi}.$$

The boundary conditions (5.143) for a cooled surface (when n = 1) /268 may be written in the form

$$\left.\begin{aligned} &\text{for } \eta \to \infty \quad z = 1; \\ &\text{for } \eta = 0 \quad \left(\frac{\partial z}{\partial \eta}\right)_w = \frac{\mathrm{Sc}\,(\rho_w k_w)}{(\mu_\delta u_\delta)\, l\,(r)^j}\, z(0, \xi). \end{aligned}\right\} \qquad (5.156)$$

The form of Equation (5.155) coincides with the energy equation studied by Lighthill [66]. Following the procedure of Lighthill, we replace the real velocity distribution in the boundary layer by its asymptotic value close to the body surface:

$$U = \left(\frac{\partial u}{\partial y}\right)_w y.$$

Then, using the method given in [66], we can transform Equation (5.155) to the following form:

$$\left(\frac{\partial z}{\partial \eta}\right)_w = (\mathrm{Sc})^{1/3}(1 - z_{w,0})\left(\frac{\partial U}{\partial \eta}\right)_w - \frac{(\mathrm{Sc})^{1/3}}{(3)^{2/3}\,\Gamma(4/3)\,(\mu_\delta/\rho_\delta)^{1/3}} \sqrt{\left(\frac{\partial U}{\partial \eta}\right)_w} \int_0^\xi \frac{dz/d\varphi}{\left[\int_\varphi^\xi \sqrt{(\partial U/\partial \eta)_w}\, d\varphi\right]^{1/3}} d\varphi, \quad (5.157)$$

where Γ (4/3) is the value of the gamma function.

In the case of a flat plate (wedge) and a cone, the concentration of atoms in the nose $z_{w0} = 1$ ($\zeta_{w0} = 0$). Since the equation of momentum in the coordinates (ξ, η) coincides with the corresponding equation for an incompressible boundary layer around a flat plate, we have

$$\left(\frac{\partial U}{\partial \eta}\right)_w = \frac{0{,}332}{\sqrt{\xi \mu_\delta/\rho_\delta}}.$$

Also using the boundary condition (5.156), we finally obtain the following nonlinear integral Volterra equation:*

$$z_w = -\left[\frac{0{,}48\,\mathrm{Sc}^{1/3}}{\zeta_w(s)}\right](s)^{1/4} \int_0^s \frac{dz_w/d\varphi}{[s^{3/4} - \varphi^{3/4}]^{1/3}} d\varphi. \quad (5.158)$$

Let us use Equation (5.157) to solve the problem in the case of an abrupt change in k_w on a plate or a wedge, when the surface consists of individual segments of different materials with differing catalycity. /269

*In principle, in a similar way we may obtain from Equation (5.157) the concentration distribution along the surface for all body forms and a continuous change in k_w, if we use the corresponding expression for $(\partial U/\partial t)_w$, with allowance for the pressure gradient along the surface and the corresponding initial value of z_{w0} for blunt bodies.

Let us assume k_w changes abruptly at the point ξ_1 up to a certain arbitrary finite value. Equation (5.157) when $\xi > \xi_1$ assumes the form

$$z_w(\Phi)=\frac{1}{\zeta_d(x)}\left\{0{,}98\left[1-z_w(x_1)\right]\Phi^{-1/2}-\Phi^{-1/4}\int_1^{\Phi}\frac{dz_w/d\varphi}{[\Phi^{3.4}-\varphi^{3/4}]^{1/3}}\,d\varphi\right\}, \qquad (5.159)$$

where

$$\Phi=\xi/\xi_1=x/x_1;$$
$$\zeta_d(x_1)=\frac{Sc^{2/3}\rho_w k_w}{0{,}339\sqrt{\rho_\delta \mu_\delta u_\delta l}}\sqrt{x_1}. \qquad (5.160)$$

The method of solving Equation (5.159) consists of dividing the integration interval into small segments and approximating $z_w(\varphi)$ by a function such that Equation (5.159) can be integrated analytically for each segment. The solutions obtained numerically may be summed, beginning with $\Phi = 1$, and we can thus obtain the continuous solution $z_w(\Phi)$.

In [65] on the kth segment of $\Phi_{k-1}\leqslant\varphi\leqslant\Phi_k$, the solution for $z_w(\varphi)$ was represented in the form $z_{w,k}=a_k-b_k\varphi^{3/4}$, where the coefficients a_k and b_k were found from Equation (5.159) and the continuity equation z_w. The use of this method for the calculations in the case of constant k_w provided an agreement with data given in [36] within an accuracy of 3%, when $\Phi_k-\Phi_{k-1}=0{,}1$.

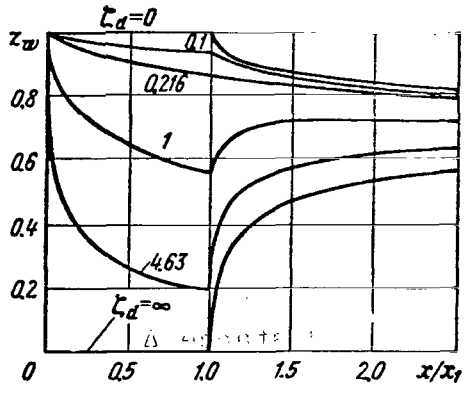

Figure 5.37. Abrupt change in catalycity along flat plate.

Figure 5.37 gives the results of calculating the atom concentrations along a flat plate (wedge) for several combinations of values k_w when $0 \leq x \leq x_1$ [when $x > x_1$ the value $\zeta_d(x/x_1) = 0.216$]. In the case of an abrupt change in k_w, the process by which the atom concentration on the surface approaches the value corresponding to a constant value of k_w occurs very slowly. This has a direct /270 effect on the value of the thermal flux q_d caused by reactions on the body surface.

In particular, it may greatly increase the sensitivity (i.e., the ratio q_d/q_w) of a catalytic sensor for measuring the atom concentration in an advancing flow, if the noncatalytic surface is located before the catalytic surface. The results of experimental studies performed in [67] confirmed this.

5.4. Nonequilibrium processes with a small density of the surrounding gas (critical point)

Up to this time, nonequilibrium processes in the inviscid region and in the boundary layer have been investigated independently. However, with a decrease in the surrounding gas density (increase in the flight altitude) the thickness of the boundary layer increases, and interaction of the boundary layer with inviscid flow must be taken into account. For slender pointed bodies, the influence of nonequilibrium processes under the

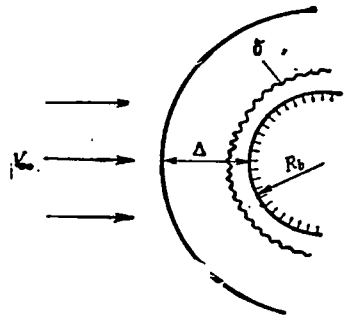

Figure 5.38. Diagram of flow in vicinity of critical point.

interaction conditions is small [68]. Therefore, we shall examine the case of spherical blunting, which is of great practical value.

Classical boundary layer theory may be applied when the boundary layer thickness δ is small as compared with the distance Δ from the shock wave to the body (Figure 5.38). As the Reynolds number decreases, there is an increase in the influence of the vortex interaction of the boundary layer with inviscid flow, i.e., vorticity in the layer of an inviscid gas (caused by a curvilinear shock wave) becomes comparable to the transverse velocity gradient due to shearing stresses in the boundary layer.

With a further decrease in the gas density in the surrounding space, viscous flow occupies an ever increasing portion of the region of the shock layer beween the shock wave and the body (viscous layer regime). In addition, the thickness of the shock wave itself ceases to be negligibly small as compared with the value of Δ ("diffused" layer). According to estimates, for a body with a closed surface and a bluntness radius of $R_b \approx 0.3$ m, the viscous layer regime in the case of hypersonic flight velocities begins approximately at an altitude of $H \approx 75$ km.

Theory of slender shock layer

Remaining within the framework of Navier-Stokes equations, /271 we shall study the flow up to the "diffused" layer regime. In the (x, y) coordinates of the boundary layer, the Navier-Stokes equations in the plane (j = 0) or the axisymmetric (j = 1) case

have the following form:

$$\frac{\partial (r^j \rho u)}{\partial x} + \frac{\partial (K r^j \rho v)}{\partial y} = 0;$$

$$\rho \left[u \frac{\partial u}{\partial x} + Kv \frac{\partial u}{\partial y} + \frac{uv}{R_b} \right] = -\frac{\partial p}{\partial x} + \frac{\partial \tau_{xx}}{\partial x} + \frac{\partial (K\tau_{xy})}{\partial y} + \frac{\tau_{xy}}{R_b} + j \left[\frac{(\tau_{xx} - \tau_{\Phi\Phi})}{r} \frac{\partial r}{\partial x} + K \frac{\tau_{xy}}{r} \frac{\partial r}{\partial y} \right];$$

$$\rho \left[u \frac{\partial v}{\partial x} + Kv \frac{\partial v}{\partial y} - \frac{u^2}{R_b} \right] = -K \frac{\partial p}{\partial y} + K \frac{\partial \tau_{yy}}{\partial y} + \frac{\partial \tau_{xy}}{\partial x} + \frac{1}{R_b} [\tau_{yy} - \tau_{xx}] + j \left[\frac{\tau_{xy}}{r} \frac{\partial r}{\partial x} + \frac{K(\tau_{yy} - \tau_{xx})}{r} \frac{\partial r}{\partial y} \right];$$

$$\rho \left[u \frac{\partial H}{\partial x} + Kv \frac{\partial H}{\partial y} \right] = \frac{\partial}{\partial x} \left(\frac{\lambda}{K} \frac{\partial T}{\partial x} \right) + \frac{\partial}{\partial y} \left(K\lambda \frac{\partial T}{\partial y} \right) + \frac{\partial}{\partial x} \left(u\tau_{xx} + v\tau_{xy} \right) + \frac{\partial}{\partial y} [K(u\tau_{xy} + v\tau_{yy})] + j \frac{1}{r} \left\{ \left[\frac{\lambda}{K} \left(\frac{\partial T}{\partial x} \right) \frac{\partial r}{\partial x} + K\lambda \left(\frac{\partial T}{\partial y} \right) \frac{\partial r}{\partial y} \right] + \left[(u\tau_{xx} + v\tau_{xy}) \frac{\partial r}{\partial x} + K(u\tau_{xy} + v\tau_{yy}) \frac{\partial r}{\partial y} \right] \right\};$$

$$\tau_{xx} = \frac{2\mu}{K} \left(\frac{\partial u}{\partial x} + \frac{v}{R_b} \right) + \left(\mu' - \frac{2}{3}\mu \right) \left[\frac{1}{K} \frac{\partial u}{\partial x} + \frac{\partial v}{\partial y} + \frac{v}{KR_b} + j \left(\frac{u}{Kr} \frac{\partial r}{\partial x} + \frac{v}{r} \frac{\partial r}{\partial y} \right) \right];$$

$$\tau_{yy} = 2\mu \frac{\partial v}{\partial y} + \left(\mu' - \frac{2}{3}\mu \right) \left[\frac{1}{K} \frac{\partial u}{\partial x} + \frac{\partial v}{\partial y} + \frac{v}{KR_b} + j \left(\frac{u}{Kr} \frac{\partial r}{\partial x} + \frac{v}{r} \frac{\partial r}{\partial y} \right) \right];$$

$$\tau_{\Phi\Phi} = j \left\{ \frac{2\mu}{r} \left(\frac{u}{K} \frac{\partial r}{\partial x} + v \frac{\partial r}{\partial y} \right) + \left(\mu' - \frac{2}{3}\mu \right) \left[\frac{1}{K} \frac{\partial u}{\partial x} + \frac{\partial v}{\partial y} + \frac{v}{KR_b} + \frac{u}{Kr} \frac{\partial r}{\partial x} + \frac{v}{r} \frac{\partial r}{\partial y} \right] \right\};$$

$$\tau_{xy} = \mu \left[\frac{1}{K} \frac{\partial v}{\partial x} + \frac{\partial u}{\partial y} - \frac{u}{KR_b} \right],$$

where Φ is the azimuthal angle; $R_b(x)$ — body radius of curvature; /272 $K = 1 + \frac{y}{R_b(x)}$; μ' — second viscosity coefficient (volumetric viscosity).

In view of the elliptical nature of these equations, generally speaking it is impossible to perform a local study of flow even in the vicinity of the critical point.

Using the assumption of a large degree of compression behind the shock wave ($\rho_\infty/\rho_1 \to 0$), Cheng [69] divided the entire flow field around a blunt body into two regions: the transitional region through the shock wave (thickness of this region δ_s is on the order of the mean free path in the advancing flow, and the density $\rho \sim O(\rho_\infty)$, and the region of the shock layer with a thickness of $\Delta \approx (\rho_\infty/\rho_1)R_b$ with a density of $\rho_1 \gg \rho_\infty$. It is assumed that both of these regions are slender as compared with the characteristic size of the body (for example, R_b). Then, discarding terms of the order (Δ/R_b) and higher in the Navier-Stokes equations, we obtain the following form of equations in the shock layer region [69] (see also [70]):*

$$\left.\begin{aligned}
&\frac{\partial(\rho u r^j)}{\partial x}+\frac{\partial(\rho v r^j)}{\partial y}=0;\\
&\frac{\partial p}{\partial x}+\rho u\frac{\partial u}{\partial x}+\rho v\frac{\partial u}{\partial y}=\frac{\partial}{\partial y}\left(\mu\frac{\partial u}{\partial y}\right);\\
&\frac{\partial p}{\partial y}=\frac{1}{R_b}\rho u^2;\\
&\rho u\frac{\partial H}{\partial x}+\rho v\frac{\partial H}{\partial y}=\frac{\partial}{\partial y}\left\{\frac{\mu}{\mathrm{Pr}}\frac{\partial}{\partial y}\left[H-(1-\mathrm{Pr})\frac{u^2}{2}\right]\right\}.
\end{aligned}\right\} \qquad (5.161)$$

These are ordinary parabolic boundary layer equations with an additional equation for dp/dy (at the critical streamline $p \approx \text{const} \approx \rho_\infty V_\infty^2$). The shock layer region may be studied independently of the transitional region through the shock wave, if the

*The term $\partial p/\partial x$ is retained for better agreement with solutions using large Reynolds numbers.

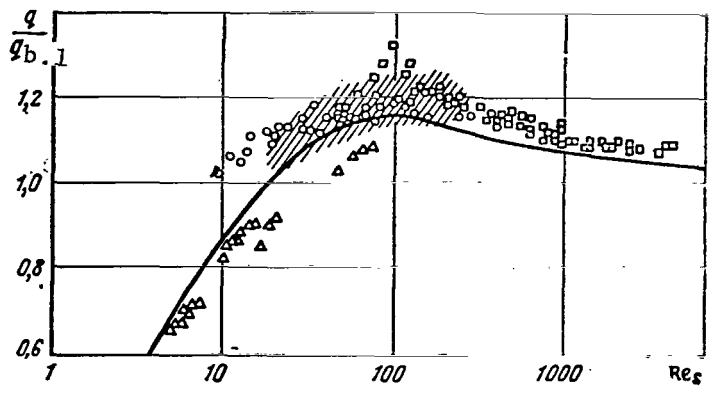

Figure 5.39. Comparison of theoretical and experimental data on thermal flux q at the critical point (solid line — calculation of Cheng [69]; dots designate experimental data; squares — from [72] at T_0 = 1230 K; circles from [73] at T_0 = 1170 K; triangles from [74] at T_0 = 3000 K; cross-hatched region — experiment from [75] at γ_w = 1).

ordinary Hugoniot equations for a viscous layer regime are used as the outer boundary conditions for Equation (5.161) and if we use for the "diffused" layer expressions taking into account viscous stresses and thermal fluxes behind the shock wave ("slip" conditions at the shock wave) [71, 69]:

$$\left.\begin{aligned} &\rho_1 v_1 = -\rho_\infty V_\infty \sin\sigma;\\ &p_1 = \rho_\infty V_\infty^2 \sin^2\sigma;\\ &\rho_\infty V_\infty \sin\sigma\,[V_\infty\cos\sigma - u_1] = \mu_1 \frac{\partial u_1}{\partial y};\\ &\rho_\infty V_\infty \sin\sigma\,[H_\infty - H_1] = \frac{\mu_1}{\mathrm{Pr}}\left[\frac{\partial H_1}{\partial y} - (1-\mathrm{Pr})\,u_1\frac{\partial u_1}{\partial y}\right]; \end{aligned}\right\} \qquad (5.162)$$

where σ is the angle of inclination for the shock wave, and the subscript "1" pertains to conditions behind the shock wave. /273

Customary attachment conditions are used as the boundary conditions on the surface, since for the cold surface being considered boundary shock waves of velocity and temperature are small in the region of applicability for this theory.

To illustrate the influence of a decrease in the gas density, Figure 5.39 shows the change in the critical flux q at the critical point as compared with its value $q_{b.l}$, calculated according to classical boundary layer theory. The calculation was performed for gas with excited vibrational degrees of freedom $\left(\frac{\varkappa-1}{2\varkappa}=0{,}13\right)$* at Pr = 0.71, $T_w/T_0 \to 0$, $M_\infty \to \infty$ as a function of the Reynolds number $\mathrm{Re}_s=\frac{\rho_\infty V_\infty R_b}{\mu_1}$ (μ_1 was determined according to the small parameters behind the normal shock wave). Experimental data in [72, 73, 74, and 75] confirm the theoretical dependence calculated by Cheng [69] on the basis of the flow model examined above. It is interesting to note that when $\mathrm{Re}_s \to 0$ the values /274 of the thermal flux calculated by Cheng coincide with the corresponding values for freely-molecular flow when the accommodation coefficient equals unity

$$q_{\mathrm{Re}\to 0}=\frac{1}{2}\rho_\infty V_\infty^3.$$

Basic equations and boundary conditions

Nonequilibrium flow in the vicinity of the critical point of a blunt body, in the case of a low density of the surrounding gas, may also be studied on the basis of the model of a slender shock layer. Thus, for a binary mixture of atoms (with the mass

*It was assumed that the chemical reactions are frozen, and the expression $\beta_i \sim \sqrt{\frac{8}{3}\rho_\infty/\rho_1}$ was used for the velocity gradient [compare with Expression (5.67)].

concentration α) and molecules* the basic equations in the case of a low gas density have the following form

$$ff''+(lf'')'=\frac{1}{(1+j)}[(f')^2-\rho_{\delta e}/\rho]; \qquad (5.163)$$

$$f\alpha'+\left(\frac{l}{\mathrm{Sc}}\alpha'\right)'=\frac{1}{(1+j)\beta_i}\frac{M}{\rho}J; \qquad (5.164)$$

$$fH'+\left(\frac{l}{\mathrm{Pr}}H'\right)'+\left[\frac{(\mathrm{Le}-1)}{\mathrm{Pr}}lh^\circ\alpha'\right]'=0. \qquad (5.165)$$

Here the superscript "'" designates the derivative with respect to the similarity variable

$$\eta=\sqrt{\frac{(1+j)\beta_i}{l\rho_1\mu_1}}\int_0^y\rho dy;$$

and the stream function is determined by the relationship

$$\psi=\sqrt{\frac{(1+j)\beta_i}{l\rho_1\mu_1}}(x)^{1+j}f(\eta);$$

The quantity β_i is the velocity gradient at the critical point in inviscid flow (see 5.67), assuming that $\frac{dp_\delta}{dx}=-\rho_{ie}\beta_i^2x)$ (the Newton law).

The following expression is used to determine the rate at which atoms are formed

*A binary mixture of atoms and molecules is usually used as the simplest model of the dissociation and recombination processes in air (see Section 5.1).

$$\left(\frac{M}{\rho}\right)J=-4k_r'(T)^{-\omega}\left(\frac{p}{RT}\right)^2\left[\frac{\alpha^2}{1+\alpha^2}-\frac{K_p(T)}{4p}(1-\alpha)\right]. \qquad (5.166)$$

The vibrational degrees of freedom are assumed to be completely excited. Instead of Equation (5.165), we may write the corresponding equation for temperature, using the following equation /275

$$H=\bar{c}_pT+\alpha h^\circ. \qquad (5.167)$$

The boundary conditions on the surface ($\eta = 0$):

$$\left.\begin{aligned} &f(0)=f'(0)=0;\\ &H(0)=\bar{c}_{pw}T_w+\alpha(0)h^\circ;\\ &(\text{or } T(0)=T_w);\\ &\alpha'(0)=\zeta_w\alpha(0), \end{aligned}\right\} \qquad (5.168)$$

where

$$\zeta_w=\frac{\mathrm{Sc}\,k_w}{\mu_w}\sqrt{\frac{\rho_1\mu_1 l}{(1+j)\beta_i}} \qquad (5.169)$$

is the Damkeler number for reactions on the surface.

The "slip" boundary conditions on the shock wave ($\eta = \eta_1$) are

$$\left.\begin{aligned} &f'(\eta_1)=\frac{V_\infty}{\beta_i R_b}-\frac{1}{l}\frac{f''(\eta_1)}{f(\eta_1)};\\ &\alpha_1=\alpha_\infty-\frac{1}{l}\frac{\alpha_1'}{\mathrm{Sc}\,f_1(\eta_1)};\\ &H_1=H_\infty-\frac{1}{l}\left[\frac{H_1'+(\mathrm{Le}-1)h^\circ\alpha_1'}{\mathrm{Pr}\,f_1}\right];\\ &f_1=\left[\frac{1}{l}\left(\frac{\rho_\infty/\rho_1}{1+j}\right)\frac{V_\infty}{\beta_i R_b}\right]^{1/2}\sqrt{\mathrm{Re}_s}=\frac{\rho_\infty V_\infty}{\sqrt{(1+j)\beta_i l\rho_1\mu_1}}. \end{aligned}\right\} \qquad (5.170)$$

The last boundary condition serves for determining the unknown coordinate of the shock η_1. The desired value of the thermal flux q_w on the body surface may be expressed by solving the system of equations (5.163) — (5.165) as follows

$$-q_w = \frac{\mu_w \rho_w}{\mathrm{Pr}} \sqrt{\frac{(1+j)\beta_i}{\rho_1 \mu_1 l}} [H'(0) + (\mathrm{Le} - 1) h^c \zeta_w \alpha(0)]. \qquad (5.171)$$

Results of numerical calculations

One of the first calculations of the thermal flux for the viscous layer regime was performed by Chung [76]. Figure 5.40 gives some of his calculation results in the form of the ratio of the thermal flux q to the equilibrium value q_e as a function of the flight altitude H. The calculation was performed for a noncatalytic surface ($\zeta_w = 0$). /276

One characteristic of the solution obtained is the minimum value of the thermal flux as compared to the equilibrium value at H ≈ 64 km (for R_b = 0.3 m) and H ≈ 73 km (for R_b ≈ 1.52 m). This corresponds to the moment when the degree of dissociation on the outer boundary of the viscous layer retains its equilibrium (maximum) value, and recombination within the viscous layer is almost entirely frozen. With a decrease in the flight altitude, the recombination process is accelerated in the viscous layer, energy of dissociation is liberated, and the thermal flux increases. With an increase in the altitude, the degree of dissociation decreases in the shock layer (relaxation time increases), and the ratio of the thermal fluxes again increases, since a small part of the total energy is spent on dissociation, and is frozen in the viscous layer.

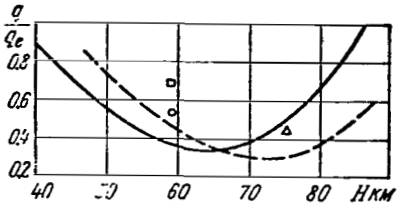

Figure 5.40. Influence of chemical reactions on the thermal flux upon non-catalytic surface (solid line at R_b = 0.3 m; V_∞ = 7.92 km/sec; T_w = 1500 K; dashed line at R_b = 1.52 m; V_∞ = 7.92 km/sec; T_w = 1500 K; the points designate: circles at R_b = 0.3 m; V_∞ = 7.92 km/sec; T_w = 1000 K; squares at R_b = 1.52 m; V_∞ = 7.92 km/sec; T_w = 1000 K; triangles at R_b = 0.3 m; V_∞ = 9.1 km/sec; T_w = 1500 K.

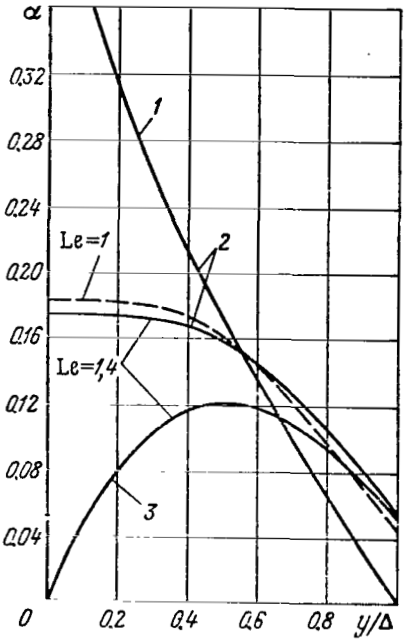

Figure 5.41. Profiles of atom concentration in the vicinity of the critical point at V_∞ = 7.92 km/sec; T_w = 1500 K; R_b = 0.3 m; H ≈ 85 km.

1 — inviscid solution; 2 — noncatalytic surface; 3 — ideally catalytic surface; dashed lines — noncatalytic surface.

Nonequilibrium flows in a viscious shock layer were also examined in [77, 78, 79].

Cheng [69] studied the problem of nonequilibrium dissociation in the vicinity of the critical point in the viscous and "diffused" layer regime. He showed (Figure 5.41) that the concentration shock behind the shock wave is not negligibly small, as Chung experienced [76], as well as others, even when we may disregard changes in the tangential velocity and enthalpy behind the shock wave. The solution obtained in [76] coincides with /277

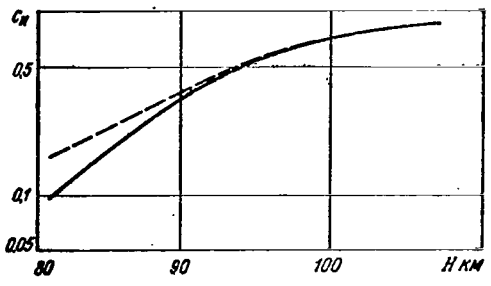

Figure 5.42. Heat transfer coefficient

$$c_h = \frac{q_w}{\rho_\infty V_\infty (H_\infty - h_{we})}$$

at the critical point when V_∞ = 7.92 km/sec; R_b = 0.3 m; T_w = 1500 K (solid line — noncatalytic surface; dashed line — ideally catalytic surface).

the inviscid profile close to the shock wave and is comparable to the solution [69] close to the surface. With a small decrease in the density in the surrounding medium, as a result of a decrease in the enthalpy in the shock wave (due to "slip") and the interaction of the cooled surface, the temperature in the shock layer decreases so much that the dissociation process becomes insignificant. Since the difference in the characteristics of noncatalytic and catalytic surfaces depends on the number of participating atoms, as the density decreases in the surrounding medium the effectiveness of using a noncatalytic surface to reduce the heat transfer decreases, and at H $\gtrsim$ 95 km (for a body with R_b = 0.3 m) the difference in the heat transfer disappears completely (Figure 5.42). Using the law of binary similarity $\rho_\infty R_b$ = const (which is valid in the region where dissociation is the predominant reaction), we may convert the results of Cheng [69] to other values of R_b.

Studying the results of numerical calculations [80, 81, 76, 69] of equilibrium and nonequilibrium flows in the case of low gas density in the surrounding space, we may reach the following conclusion (Figure 5.43): the dimensionless value of the shock wave stand-off distance $\frac{\Delta}{R_b}\frac{\rho_{he}}{\rho_\infty}$ (ρ_{he} — gas density in inviscid flow at the critical point) is almost independent of the Reynolds number Re_s. /278

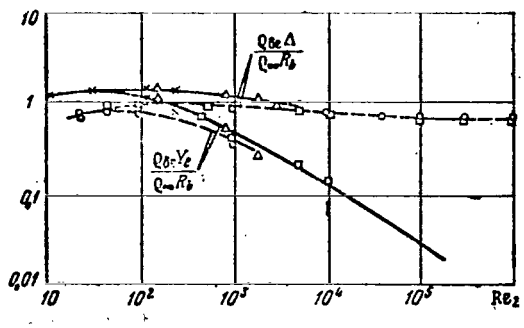

Figure 5.43. Thickness of shock layer and adiabatic flow region (solid lines — nonequilibrium flow; dashed lines — equilibrium flow). The squares designate data from [80]; the circles — from [81]; the triangles — from [76]; and the crosses — from [69].

Another dimensionless quantity $(\gamma_\delta/R_b)(\rho_{\delta e}/\rho_\infty)$ shown in Figure 5.43 characterizes the thickness of the shock layer close to the surface, where 99% of the entire change in enthalpy takes place in the layer behind the shock wave (outside of this region, the flow behind the shock wave is assumed to be adiabatic flow). This thickness changes in proportion to $1/\sqrt{Re_s}$, and at $Re_s \approx 10^2$ the shock layer becomes viscous. However (at least for bodies with a bluntness radius of $R_b \leq 1$ m and for a velocity of $V_\infty \leq 7.6$ km/sec) the gas in the entire shock layer is practically frozen.

Approximate analytical determination of the thermal flux

Using the data given above, on the basis of a model of a slender shock layer, Inger [82] obtained an approximate solution in closed form in the most important (in terms of studying nonequilibrium processes in the gas) flow regimes. This regime encompasses both large Reynolds numbers, when the usual theory of a slender boundary layer with a uniformly dissociated inviscid shock layer is valid, and for small Reynolds numbers up to $Re_s \approx 10^2$, when there is an outer region of inviscid frozen nonequilibrium shock layer which surrounds the inner (not necessarily slender as compared with Δ) viscous layer.

To obtain an analytical solution, Inger used the following simplifying assumptions: a binary mixture of atoms and molecules /279 was being examined, the values of Pr, Sc, c_p, and the product $\rho\mu$ were constant, and the following expression was used for $K_p(T)$ in Equation (5.166)

$$K_p(T)=AT^s[1-\exp(-T_\nu/T)]\exp(-T_d/T)^*. \qquad (5.172)$$

Inger was able to generalize his previous solution [42]** for a nonequilibrium boundary layer in the vicinity of the critical point in the case of arbitrary surface catalycity to the case of a low density of the surrounding gas. In spite of the assumptions made, the analytical expression obtained for the nonequilibrium thermal flux may be used for tentative estimates, since existing results of numerical estimates are extremely limited. In this connection, it is useful to describe the procedure for calculating the nonequilibrium thermal flux (in the axisymmetric case, i.e., at j = 1).

1. First, the equilibrium characteristics of inviscid flow at the critical point (β_i, $\rho_{\delta e}$, etc.) are determined in the usual way, and the ratio of the characteristic time of the flow to the dissociation time in inviscid flow is calculated

$$\Gamma_i=\frac{k_f' A (T_d)^{\omega+s-2}}{2\beta_i}\frac{p}{(R)^2}, \qquad (5.173)$$

The Damkeler number for reactions on the surface is ζ_w (5.169), and the first approximation is calculated for conditions behind

*When considering excitation of only the basic electron level and s = 3/2, the following are assumed for oxygen: A ≈ 66; T_ν = 2239 K; T_d = 61000 K; for nitrogen — A ≈ 44; T_ν = 3395 K; T_d = 121,000 K.

**See Section 5.2.

the shock wave [including f_1 and Re_s, see (5.170)], assuming the reactions are frozen and disregarding the "slip" conditions behind the shock wave. The first approximation for α_1, obtained according to the following formula

$$\alpha_1=\alpha_\infty+\frac{\Gamma_i}{l\,\mathrm{Sc}\,(f_1)^2}R_i(\alpha_1), \tag{5.174}$$

where

$$R_i(\alpha)=(1-\alpha)\left(\frac{T_i}{T_d}\right)^{-\omega+s-2}\frac{[1-\exp(-T_*/T)]}{\exp(T_d/T)}- \\ -\frac{4p}{A\,(T_d)^s}\left(\frac{T_d}{T}\right)^{\omega+2}\frac{\alpha^2}{(1+\alpha)}, \tag{5.175}$$

is sufficient, as a rule.

2. In the approximation of vortex interaction, the parameters of inviscid flow are joined with the solution on the boundary of the viscous region for the following values of the stream function f_δ, which correspond to values of f(Pr) for /280 H_δ/H_∞ = 0.99 in boundary layer theory:

Pr	0,5	0,7	1
f_δ	4,48	3,38	2,19

For the selected value of f_δ, the function $\chi(\alpha)$ is calculated from the equation

$$\chi(\alpha_\delta)=\chi(\alpha_1)+\Gamma_i F(f_\delta), \tag{5.176}$$

where

$$F(f_\delta)\approx\sqrt{\rho_1/\rho_{\delta e}}\ln\frac{[\sqrt{1+C(f_\delta/f_1)}+1][\sqrt{1+C}-1]}{[\sqrt{1+C(f_\delta/f_1)}-1][\sqrt{1+C}+1]}; \qquad (5.177)$$

$$C\approx(\rho_1/\rho_{\delta e})l^{-1}\frac{[(V_\infty/\beta_i R_b)^2-\rho_{\delta e}/\rho_1]}{[1+2(lf_1)^{-2}(V_\infty/\beta_i R_b)]}[1+O(1/l^3 f_1^3)];$$
$$\chi(\alpha_i)\approx-\chi_d(\alpha_{\delta e})\ln\left[1-\frac{\chi_d(\alpha_i)}{\chi_d(\alpha_{\delta e})}\right]\sim\chi_d(\alpha_i). \qquad (5.178)$$

Using the graph (Figure 5.44), we can determine the value of α_δ — the concentration of atoms on the outer boundary of the viscous region. After this, Equation (5.167) can be used to find the value of T_δ and, consequently, $R_i(\alpha_\delta)$, and the Damkeler number for the recombination of gas in the viscous region:

$$\Gamma=\frac{2\,\mathrm{Sc}}{\beta_i}k_r'(T_\delta)^{-\omega-2}\left(\frac{p_\delta}{R}\right)^2. \qquad (5.179)$$

3. The ratio $z(0) = \alpha(0)/\alpha_\delta$ on the body surface is found from the following equation (see Figure 5.19)

$$\frac{z(0)}{z_f(0)}=\frac{\sqrt{[1+\alpha_\delta z_f(0)]^2+4\Gamma^*}-[1-\alpha_\delta z_f(0)]}{2[\alpha_\delta z_f(0)+\Gamma^*]}, \qquad (5.180)$$

where

$$z_f(0)=\frac{(1+r_d)}{[1+\zeta_w I_z(f_\delta)]} \qquad (5.181)$$

is the Goulard solution [34] for frozen flow, generalized to the case of vortex interaction, and

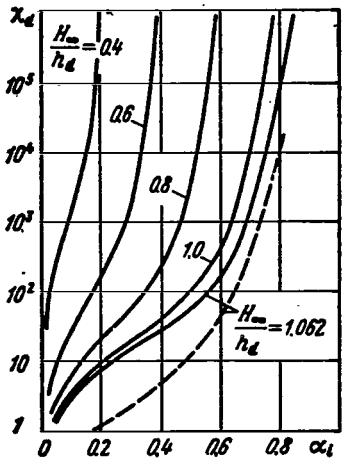

Figure 5.44. Values of the function at $\chi_d(\alpha_i)$ when $+\omega + s = 0$; $\bar{c}_p/R_m = 9/2$ (solid lines for $T_\nu/T_d = 0.031$; dashed lines for $T_\nu/T_d \to \infty$).

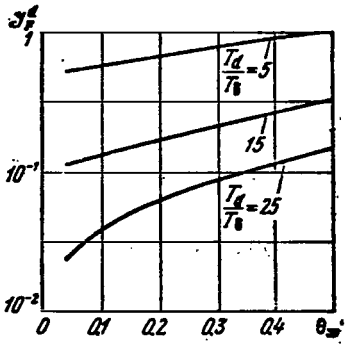

Figure 5.45. Value of the function J_F^d for $+\omega + s = 0$.

$$\Gamma^*=(1+r_d)\alpha_\delta\Gamma\frac{[J_{F_1}+2\zeta_w I_z(f_\delta)J_{F_2}+\zeta_w^2 I_z^2(f_\delta)J_{F_3}]}{[1+\zeta_w I_z(f_\delta)]^2} \qquad (5.182)$$

is the generalized Damkeler number, which simultaneously takes into account the influence of reactions in the gas and on the body surface. The function

$$r_d=\frac{\mathrm{Sc}\,\Gamma_l}{\alpha_\delta}R_i(\alpha J_\delta)_F^d \qquad (5.183)$$

characterizes the influence of nonequilibrium dissociation in inviscid flow upon the flow characteristics in the viscous region. The numerical values of the function J_F^d are given in Figure 5.45. /281

The functions $I_z(f_\delta)$ and $(J_F)_i$ when $\theta_w \leq 0.3$ and $|\Omega_\delta < 1|$ are related to the functions $I_z(\infty)$ and $J_{z,\,F_i}$, which are given in [36] (see Figure 5.20), as follows:

$$(J_F)_i = \frac{J_{z,F_i}}{\left[1 + 0{,}5\Omega_\delta - 0{,}11\Omega_\delta^2\right]^{N_i}} \quad (i = 1,\ 2,\ 3);$$

$$(N_1 = 1{,}35;\quad N_2 = 0{,}36;\quad N_3 = -0{,}66)$$

$$I_z(f_\delta) \approx \frac{1}{0{,}47\,\mathrm{Sc}^{1/3}\left[1 + 0{,}5\Omega_\delta - 0{,}11\Omega_\delta^2\right]},$$

where

$$\Omega_\delta = \frac{\left[(V_\infty/\beta_i R_b)^2 - \rho_{te}/\rho_1\right]\left[1 - 2\,(\rho_1/\rho_\infty)\,\dfrac{l}{\mathrm{Re}_s}\right]}{\sqrt{\mathrm{Re}_s \dfrac{2}{l}\,(\rho_\infty/\rho_1)\,(V_\infty/\beta_i R_b)}} \qquad (5.184)$$

is the parameter of the vortex interaction of Cheng [69], which is generalized with allowance for nonequilibrium dissociation in inviscid flow and the "slip" conditions behind the shock wave.

4. The unknown ratio of the thermal flux q_w to its equil- /282 ibrium value is determined by the expression*

$$\frac{I_\theta(f_\delta)\,q_w}{[I_\theta(f_\delta)\,q_w]_e} = \frac{1 - \theta_w + H_d\,\dfrac{J_\theta(f_\delta)}{J_z(f_\delta)}\,[1 - z(0)]}{1 - \theta_w + H_d\left\{\dfrac{1}{\mathrm{Le}} + \dfrac{\alpha_e}{\alpha_\delta}\left[\dfrac{J_\theta(f_\delta)}{J_z(f_\delta)} - \dfrac{1}{\mathrm{Le}}\right]\right.}, \qquad (5.185)$$

where the subscript "e" corresponds to the total equilibrium flow

*There was a misprint in the denominator of the corresponding formula (44) in [82].

$$H_d = \alpha_\delta \mathrm{Le}\, h^\circ / c_p T_\delta;\quad \frac{J_\theta(f_\delta)}{J_z(f_\delta)} \approx (\mathrm{Le})^{-0,45};\quad \theta_w = \frac{T_w}{T_\delta},$$

and $I_\theta(f_\delta)$ is obtained from $I_z(f_\delta)$ by replacing Sc by Pr. At Le = 1 the right side of Equation (5.185) is reduced to the well-known expression

$$\frac{H_\infty - H(0)}{H_\infty - c_p T_w}.$$

It must be noted that the equilibrium state of the gas on the outer boundary of the viscous layer is taken into account in this solution. Within the framework of boundary layer theory $\alpha_\delta = \alpha_e$ and close to a cooled surface, the gas characteristics are completely determined by the new recombination rate in the boundary layer (see Section 5.2).

However, for a low gas density in the surrounding space, the state of the gas in the inviscid flow region is far from an equilibrium state. Since there is rapid freezing of recombination close to a cooled surface, the degree of gas dissociation in the inviscid region becomes the decisive factor when calculating the characteristics on a body surface. When the reactions within the viscous region are frozen [$\Gamma^* \ll 1$, $r_d \gtrsim 0(1)$], then $z(0) \approx z_f(0) \sim 1 + r_d$. At a constant flight velocity $r_d \sim p/\beta_i \sim \rho_\infty R_b$ the previous relationship expresses the binary similarity law (see Section 4.2).

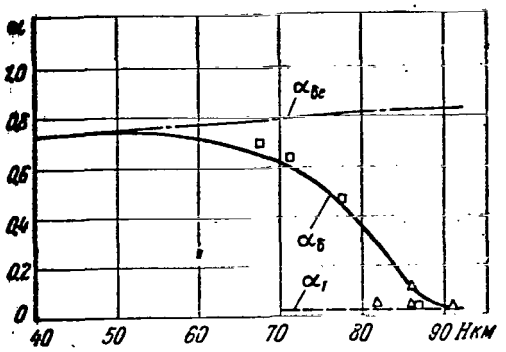

Figure 5.46. Concentration of atoms in the shock layer at V_∞ = 7.92 km/sec; R_b = 0.3 m; Le = 1 (noncatalytic surface): squares designate data from [76]; triangles — from [69].

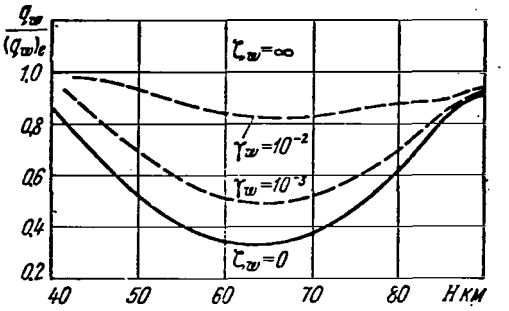

Figure 5.47. Value of nonequilibrium thermal flux at the critical point at V_∞ = 7.92 km/sec; R_b = 0.3 m; Le = 1.

Figure 5.46 gives the results of performing calculations with the method described above of the atom concentration α_δ on the outer boundary of the viscous layer for a body with R_b = 0.3 m at a velocity of $V_\infty \approx 7.92$ km/sec as a function of the flight altitude (Le = 1, noncatalytic surface). It gives the values of $\alpha_{\delta e}$ — the equilibrium concentration of atoms in inviscid flow in the vicinity of the critical point, and α_1 — the concentration of atoms behind the shock wave. The good agreement with the results of numerical calculations of Chung [76] and Cheng [69] must be noted.

Calculations of the thermal flux performed in [82] also closely coincide with the data of Chung [76].

This calculation method makes it possible to study the /283
influence of a catalytic surface (parameter ζ_w) upon the thermal flux with a change in the flight altitude. Figure 5.47 plots the dashed lines corresponding to the recombination efficiency coefficients $\gamma_w = 10^{-2}$ (typical value for metal oxides [34]) and $\gamma_w = 10^{-3}$ (Pyrex [34]). The use of materials such as glass for the coverings greatly reduces the thermal flux at the critical point in the altitude range of 45 — 80 km (for $R_b = 0.3$ m), which may be particularly important for hypersonic aircraft designed for prolonged flights at high altitudes.

A decrease in the thermal flux with the use of noncatalytic /284
coverings (H_3PO_4 and SiO) is also confirmed by experimental studies at $M = 4.7$ — 6.5 and $Re_s = 20$ — 250 [75].

In conclusion, we should note that results have recently been published from numerical calculations of nonequilibrium processes at a low gas density for a complete chemical model of air (see, for example [83]).

5.5. Characteristics of nonequilibrium flows in the wake behind a body

The problem of communicating with objects entering the atmosphere at hypersonic velocities has become of particular interest recently with respect to studying nonequilibrium flows in a wake.

The selection of the wavelength necessary for communication depends, in particular, on the critical frequency of electromagnetic vibration propagation (radio waves, light), which in

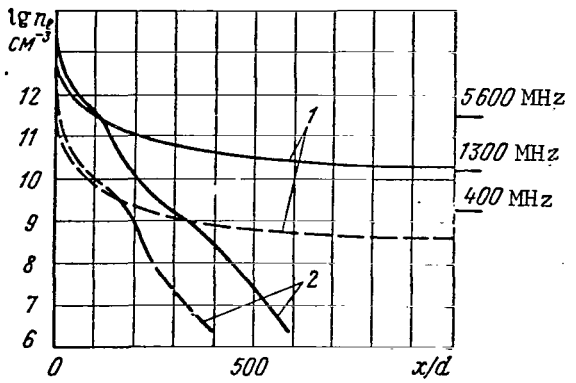

Figure 5.48. Electron density distribution along axis of wake behind blunt body at M = 32 (solid lines at H = 30 km; dashed lines at H = 61 km).

1 — frozen flow; 2 — equilibrium flow.

turn is directly determined by the electron concentration in the medium through which the waves pass. It is apparent that electrons, produced as a result of gas heating behind the shock wave and also in the viscous boundary layer around the body, enter the wake behind the body. Figure 5.48 [84] shows the characteristic change in the electron concentration n_e (particle/cm^3) along the wake axis (x — distance from the body, d — target diameter) when M = 22 at an altitude of 30 and 61 km. The curves refer to the limiting cases of frozen and equilibrium flows. The critical frequencies corresponding to different ranges of radio waves and ultrashort waves are also given. Due to the nonequilibrium processes, the wake may be observed at distances which are hundreds and even thousands of times greater than the characteristic body dimensions.

General picture of the flow

Let us briefly recall the picture of the flow in a wake /285
(Figure 5.49). Behind the rear part of the body, the separated boundary layer in the form of a free jet stream 4 defines the bottom region (near wake) where there is returning circulating flow. The size of this region is on the order of the characteristic diameter of the body. Behind the joining region 8 of the free boundary layer in the contraction region — the "throat" of the wake 9 where the gas is slowed down and heated — there is a short region in which the gas expands up to the pressure of the

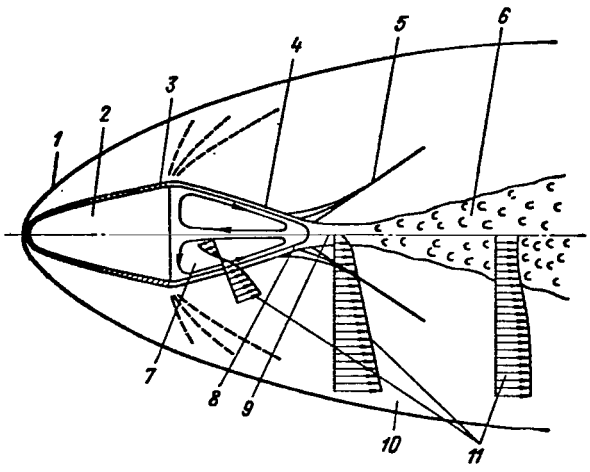

Figure 5.49. Picture of flow in wake behind body flying at hypersonic velocity.

1 — forward shock wave; 2 — body; 3 — boundary layer; 4 — free jet stream; 5 — rear shock wave; 6 — viscous internal wake; 7 — region of returning circulating flow; 8 — rear critical point; 9 — "throat" of wake; 10 — vortex outer wake; 11 — velocity profiles.

surrounding space, which continues as the region of the viscous inner wake 6. In the outer portion of the wake 10 (or in the entropy wake), the vorticity is determined by the inclination of the forward and, partially, by the final shock waves, through which the corresponding gas particles pass. The inner wake characteristics are determined by intense mixing (diffusion) of the gas and possible transition to turbulent flow. The rate of turbulent diffusion is much greater than that of laminar diffusion, and the turbulent front, which expands, encompasses part of the flow which initially is located in the outer part of the inviscid vortex wake.

The problem of the flow in the wake behind a body is one of the most important problems, and includes the majority of contemporary problems of the mechanics of liquids and gases.

In the investigation of the near wake region, on the basis of works by Chapman [85], Lees [86], and others, including Soviet studies [87 — 89], at the present time methods have been developed which make it possible to accurately determine the flow parameters up to the rear critical point ("throat" region). However, this was done primarily for the simplest forms of bodies under the assumption of equilibrium and laminar flow. On the

other hand, it is known that the initial thickness of the boundary layer, the form of the body, the M number, and the interaction between viscous and inviscid flows (see [90 — 92]) influence the velocity along the dividing streamline, which defines the region of circulating flow. This influences the ratio of the /286
enthalpy at the rear critical point to the total enthalpy in inviscid flow (according to the Chapman theory, it approximately equals 0.58). This enthalpy ratio is ~0.3 in the wake behind a slender body [90 — 93].

The lack of precise information on the nature of the flow field close to the "throat" creates great difficulties in calculating nonequilibrium processes in a wake, since the rate of the chemical reactions (ionization) is very sensitive to the /287
temperature in the "throat" region. Together with the adjacent portion of the laminar wake, this region is the "source" of electrons and atoms in contrast to the turbulent section of the wake, where the gas is cooled.

As the analysis of numerous experimental data shows [94 — 98], obtained in wind tunnels and on ballistic equipment, the transition to the turbulent flow first occurs in the far wake with a certain critical Reynolds number. As the density of the surrounding medium increases, the transition point x_T moves upstream to the "throat," and the critical Reynolds number remains approximately constant and depends primarily on the local number M at the transition point or the M_r number in the rear portion of the body.

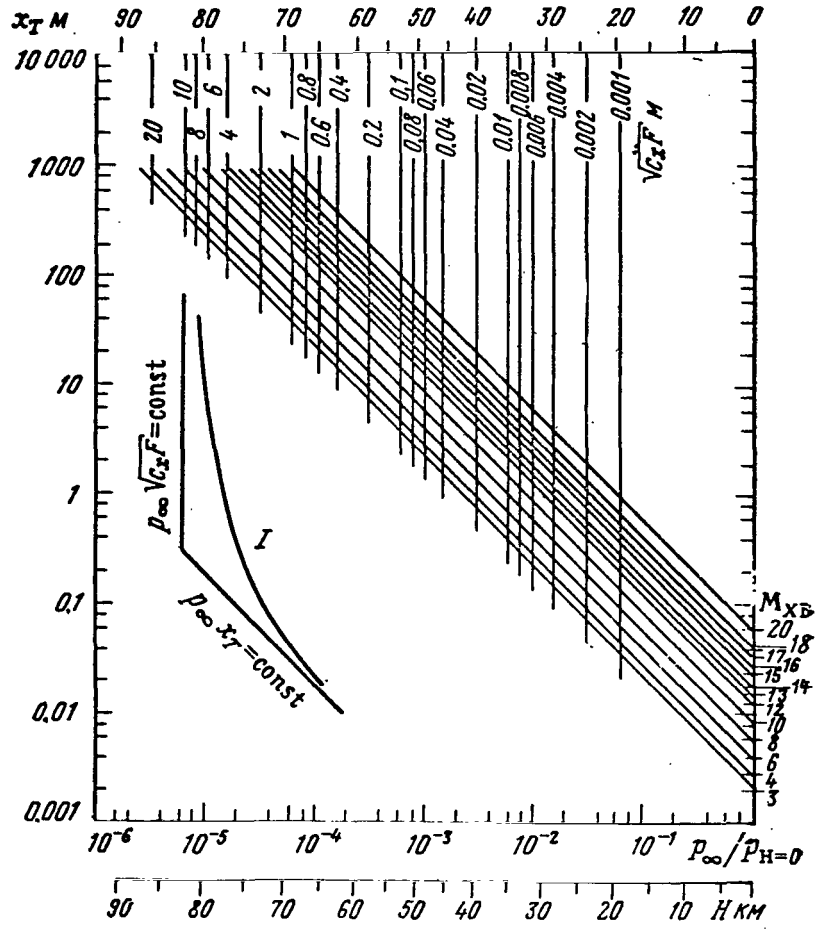

Figure 5.50. Graph for determining transition to turbulent flow in the wake.

I — interporlation curve between limiting dependencies.

Correlation (within an accuracy of the factor 2) of the results of experimental studies in the transition region in a wake* may be obtained by the interpolation curve in Figure 5.50

*The protraction of the transition in the wake, observed in the studies of Wilson [98], at hypersonic velocities may be explained by the fact that in the high-entropy region of the wake at $M_\infty \geq 20$ the density is very low, and it is very difficult to determine the transition by means of optical devices. The transition becomes significant when the turbulent front breaks through into the cold outer region of the wake.

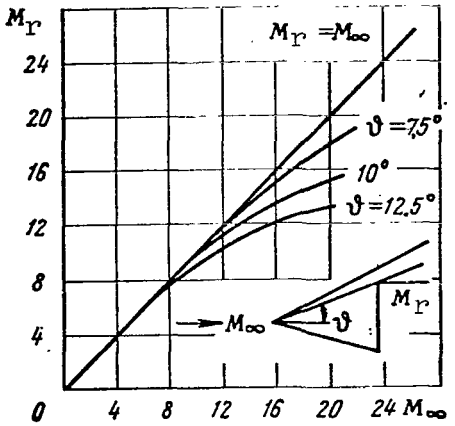

Figure 5.51. Dependence of M_r on M_∞ for cones.

[99]. The vertical lines in this figure correspond to the limiting dependence for the far wake:

$$\frac{p_\infty}{p_{H=0}}\sqrt{c_x F} = 0{,}67\cdot 10^{-4}\ \text{м}$$

where $p_{H=0}$ is the pressure on the surface of the Earth. The inclined lines

$$\lg\left[\frac{p_\infty}{p_{H=0}}x_T(\text{м})\right] = -2{,}882 + 0{,}082M_r$$

correspond to the limiting dependence for the near wake. The function $M_r = f(M_\infty)$ for sharp cones is shown in Figure 5.51, for spheres $M_r \approx 3$ at all $M_\infty > 5$.

At the present time, only a semiempirical calculation of the turbulent wake is possible. Different models have been proposed* to calculate the influence of contraction upon the turbulent viscosity coefficient ε (or the diffusion coefficient, since it is usually assumed that $Pr_T = Le_T = 1$). The proposed turbulent models** provide a better prediction of the change in the parameters along the body axis than their radial distribution [102].

*See footnote on page 383.

**For example, $\varepsilon = 0{,}02\delta\rho_0(u_\delta - u_0)\ldots$ [100]; $\varepsilon = 0{,}04\delta\rho_\delta(u_\delta - u_0)\ldots$ [84]; $\varepsilon = 0{,}02\delta(u_\delta - u_0)(\rho_\delta^2/\rho_0)(y/\eta)^2\ldots$ [101], where δ is the local radius of the turbulent nucleus; the subscript "δ" refers to the outer boundary of the nucleus; the subscript "0" — to the axis.

The development of turbulent flow in the near wake, and particularly the rate at which the wake is cooled, depend greatly on the form of the body, since it influences the form of the forward shock wave and the distribution of the momentum loss in the outer wake [103]. However, at $x/\sqrt{c_x F} > 10^3$ practically all of the body drag equals the loss of momentum in the turbulent viscous wake, and the width of the wake (in Dorodnitsyn variables) behind this region is very well determined (for bodies of revolution) by the relation

$$\eta_\delta = \sqrt{2\int_0^\delta \rho/\rho_\delta y dy} \sim (c_x F x)^{1/3}.$$

This coincides with the similar dependence for the self-modeling /288 solution in an incompressible liquid [104]. In the case of thermodynamic equilibrium, there is naturally a rapid decrease in temperature $T \sim (x)^{-2/3}$ along the wake axis.

The mixing processes of the turbulent nucleus with the outer inviscid wake play an important role in the investigation of nonequilibrium flows in a wake. Two limiting mixing models are possible: the so-called inviscid disordered convection and homogeneous mixing [105]. In the first case, the gas particles entering the nucleus are "split up" and are mixed without the participation of molecular diffusion and viscous dissipation, so that the parameters of the incoming gas do not change (model of the "layer cake"). In the second case, the gas particles entering the wake are simultaneously mixed with gas particles in the nucleus, which corresponds to an infinitely rapid dissipation. A modified model of turbulent diffusion in the following form was proposed in [106]

$$\varepsilon = K\delta(\rho_\delta u_\delta - \rho_0 u_0), \qquad (5.186)$$

where

$$K(x) = K_i + (K_T - K_i)\frac{(x - x_i)^2}{(x_T - x_i)^3}(3x_T - x_i - 2x)$$

The quantity K_i corresponds to the average value of the laminar diffusion coefficient; K_T — the experimental value of the turbulent diffusion coefficient ($K_T \approx 0.02$); x_i — origin of laminar flow instability and x_T — origin of developed turbulent flow, determined on the basis of experimental data, for example [98].

Basic equations and calculation methods

Taking nonequilibrium processes into account greatly complicates the study of the characteristics in each region of the flow. In this connection, the integral methods of solutions [84, 100, 105, 107, 108] have been used most extensively in calculating nonequilibrium flows. These methods make it possible to give the correct picture of the change in a certain flow characteristic as a function of the distance to the body.

According to the integral method, Equations (5.2) — (5.4)* are satisfied exactly on the axis (at r = 0):

$$\left.\begin{aligned}
&u_0\frac{du_0}{dx} = 2\frac{\mu_0}{\rho_\infty}\frac{1}{\delta_m^2}\frac{\partial^2 u_0}{\partial n^2};\\
&u_0\frac{dH_0}{dx} = 2\frac{\mu_0}{\rho_\infty}\frac{1}{\delta_m^2}\frac{1}{\mathrm{Pr}_0}\left[\frac{\partial^2 H_0}{\partial n^2} + \right.\\
&\left. + (\mathrm{Pr}_0 - 1)\,u_0\frac{\partial^2 u_0}{\partial n^2} + \sum_i (\mathrm{Le}_{i0} - 1)\,h_i^\circ\frac{\partial a_{i0}}{\partial n}\right];\\
&u_0\frac{da_{i0}}{dx} = 2\frac{\mu_0}{\rho_\infty}\frac{1}{\delta_m^2}\frac{1}{\mathrm{Sc}_{i0}}\frac{\partial^2 a_{i0}}{\partial n^2} + M_{i0}I_i;
\end{aligned}\right\} \qquad (5.187)$$

*These equations, where μ is replaced by the corresponding value of the turbulent viscosity coefficient ε, are used to determine the values of $\bar{u}$, $\bar{\rho}$, $\bar{T}$ averaged over time in turbulent motion.

On the average, these equations are satisfied in the remaining portion of the viscous wake: /289

$$\left.\begin{aligned}
&\frac{d}{dx}\left[\delta_m^2\int_0^1 u\,(u_\delta-u)\,ndn\right]=\left(\frac{du_\delta}{dx}\right)\delta_m^2\int_0^1 u\,dn-\frac{\mu_\delta r\dfrac{\partial u_\delta}{\partial r}}{\rho_\infty};\\
&\frac{d}{dx}\left[\delta_m^2\int_0^1 u\,(H_\delta-H)\,ndn\right]=-\frac{1}{\rho_\infty}\frac{\mu_\delta r}{\mathrm{Pr}_\delta}\left\{\frac{\partial H_\delta}{\partial r}+\right.\\
&\qquad\left.+(\mathrm{Pr}_\delta-1)\,u_\delta\frac{\partial u_\delta}{\partial r}+\sum_i(\mathrm{Le}_{i\delta}-1)\,h_i^\circ\frac{\partial a_{i\delta}}{\partial r}\right\};\\
&\frac{d}{dx}\left[\delta_m^2\int_0^1 u\,(a_{i\delta}-a_i)\,ndn\right]=\left(\frac{da_{i\delta}}{dx}\right)\delta_m^2\int_0^1 u\,dn-\\
&-\frac{1}{\rho_\infty}\frac{1}{\mathrm{Sc}_{i\delta}}\mu_\delta r\frac{\partial a_{i\delta}}{\partial r}-\delta_m^2\int_0^1 M_iJ_i\,ndn;
\end{aligned}\right\}\qquad(5.188)$$

for which the appropriate number of arbitrary parameters are used, depending on the form of the profile selected, for example,

$$\left.\begin{aligned}
&\frac{u-u_0}{u_\delta-u_0}=f_1(n);\quad\frac{a_i-a_{i0}}{a_{i\delta}-a_{i0}}=f_2(n);\\
&\frac{H-H}{H_\delta-H_0}=f_3(n)+\frac{\partial^2H_0/\partial n^2}{(H_\delta-H_0)}f_3(n),
\end{aligned}\right\}\qquad(5.189)$$

where $f_i(n)$ are selected based on the condition that the initial data are satisfied.

In the equations given above, it is assumed that

$$\left.\begin{aligned}
&p\approx\mathrm{const}\approx p_\infty;\\
&\rho_\infty\delta_m^2 hdn=\rho rdr\quad(r\to\delta,\ n\to1),
\end{aligned}\right\}\qquad(5.190)$$

where the subscript "0" refers to the values of the parameters on the axis, and the subscript "δ" refers to the outer boundary of the viscous wake, which are assumed to be known. Since, at velocities which are less than approximately the first cosmic

velocity (~7.8 km/sec),* the chemical processes have a slight /290
influence on the equation of momentum, we may determine the law governing wake expansion $\delta_m(x)$, assuming there is thermodynamic equilibrium in the gas.

The method of integral relationships [109] or the finite difference method [110, 111] are used in several studies to calculate nonequilibrium flows in a wake. However, one disadvantage of all these studies is the unsatisfactory value of the "initial conditions," i.e., the characteristics of the flow field in the region of the "throat," which were discussed previously. As a rule, it is assumed that in the region of the "throat" the gas is frozen with a composition corresponding to the composition in the rear part of the body, and then the gas expands isentropically up to the pressure in the surrounding space. The ratio of the enthalpy in the "throat" to the total enthalpy in the advancing flow for blunt bodies is assumed to equal 0.5 — 0.6 for slender pointed bodies ~0.3. In the best case, the characteristics of inviscid flow are calculated by the method of streamtubes with a known (from calculations of equilibrium flow) pressure distribution.

Concentration of electrons in the wake behind pointed and blunt bodies

In a study of nonequilibrium flows in a wake, the greatest attention is given to determining the electron concentration. The use of microwave technology (open resonator and horn-lens antenna) in tests on ballistic equipment [106, 112, 113, 114] has made it possible in recent years to obtain a large amount

* Translator's note: The first cosmic velocity designates the minimum initial velocity that a body must acquire to become an Earth satellite.

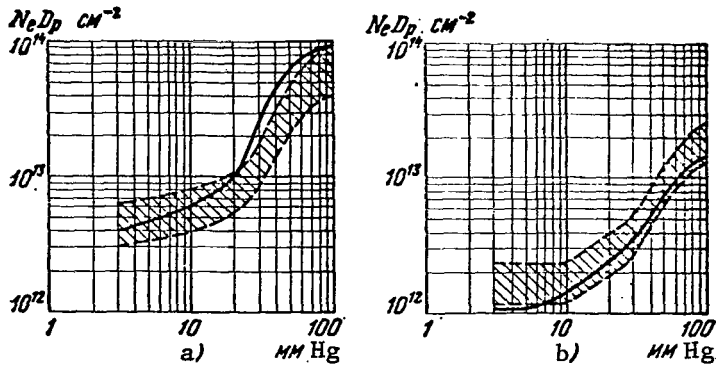

Figure 5.52. Change in total electron density in wake behind sphere with a diameter of 15 mm at a flight velocity of 6.6 km per second (solid lines — data from theoretical calculation; cross-hatched region — experimental data).

a — for x/d = 3; b — for x/d = 10.

of experimental data and to improve existing calculation methods.

At flight velocities up to ~7 km/sec, the nonequilibrium concentration of electrons in the wake is determined by the following basic reactions:

(recombination) $NO^+ + e \rightleftarrows N + O$;

(electron capture, or attachment) $O_2 + e + O_2 \rightleftarrows O_2^- + O_2$;

(charge transfer) $O_2^- + O \rightleftarrows O_2 + O^-$.

The most complete summary of reactions and the corresponding constants may be found in [115, 116].

Existing computational methods are more suitable for calculating flows behind blunt bodies, since in this case the electron concentration is caused primarily by the large temperature values behind the forward shock wave (i.e., in the inviscid

region of the wake with a width on the order of the body diameter). The influence of the composite nature of the flow in the inner (viscous) portion of the wake begins to play an important role only at great distances ($x/d \geq 10^3$) as the mixing process develops, particularly when the turbulent front breaks through into the cold inviscid portion of the wake.

Figure 5.52 gives data characterizing the development of the methods for calculating the electron concentration in the wake behind a sphere. The change in the total electron density $N_e D_p = \int_{-\infty}^{\infty} n_e dr$ (D_p — diameter of ionized portion of the wake) in the near wake is insensitive [114] to the mixing model used, and may be satisfactorily described by the comparatively simple theoretical scheme: by the integral method, taking into account only the recombination reaction [105]. Experimental proof of the binary similarity ($\sim p_\infty d$) for ionization in the wake behind a sphere up to $x/d \approx 2 \cdot 10^3$, when the value of $N_e D_p$ changes by four orders of magnitude, is given in [112].

A comparison of the results from calculating ionization in the turbulent far wake with experimental data [112, 113] has shown that in this case, in addition to the complex kinetics of chemical processes, an important role in the electron concentration change is played by the mechanism of the turbulent nucleus mixing with the inviscid flow and the model assumed for turbulent viscosity [114]. In particular, the experimental data greatly differ from the theoretical values calculated for the limiting cases of the model of inviscid, disordered convection and the model of homogeneous mixing. The use of the modified model according to Formula (5.186) (Figure 5.53) provides better agreement where "8 × 10" and "13 × 39" designate the different schemes for the chemical reactions used in air (the first term

/292

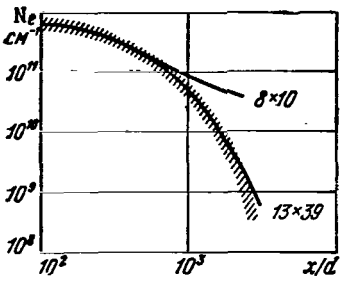

Figure 5.53. Linear electron density in wake behind sphere with a diameter of 5 mm at a pressure in the surrounding medium of p = 75 mm Hg (solid lines — data from theoretical calculation at a velocity of 6.25 km/sec; cross-hatched region — experimental data at a velocity from 5.89 to 6.6 km/sec).

is the amount of reacting particles, and the second term is the amount of reactions considered in agreement with data in [115]).

Other theoretical approaches, based on the studies [117 — 119] are still in the stage of development.

The wake behind slender bodies is much less intense and shorter, since in this case the region of high temperatures is concentrated in the boundary layer, and the internal (laminar or turbulent) region of the wake is surrounded by the cold flow of an inviscid gas, where recombination of electrons may be disregarded. It is thus particularly important to determine the initial conditions in the "throat" of the wake, taking into account the influence of the body bluntness and nonequilibrium ionization in the region of the returning circulating flow. With identical initial conditions, the results of calculating the nonequilibrium electron concentration along the axis of the wake behind a pointed cone, which were obtained independently of other methods, lead to the scatter shown in Figure 5.54 [108]. /293 It may also be seen here that the mechanism of electron attachment to oxygen begins to take place at $x/d \approx 10^2$, when the temperature decreases approximately below 800 K.

In the case of a blunt cone, the high electron concentration is retained up to absorption by the viscous nucleus of the streamlines passing through the point on the shock wave with low intensity. The use of a modified turbulent viscosity model (5.186) makes the

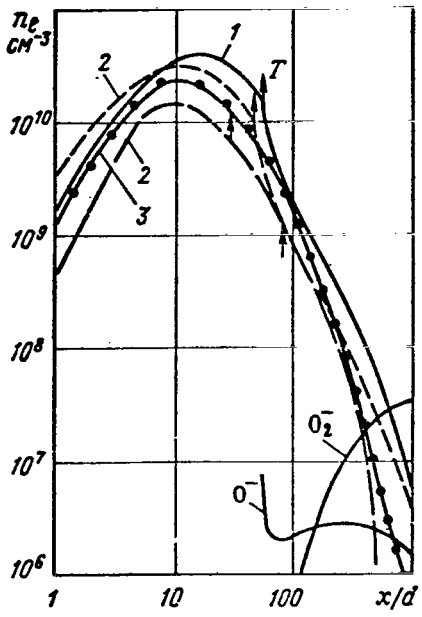

Figure 5.54. Electron density distribution along the wake axis behind a pointed cone at ν = 8°; d = 0.85 m; flight velocity V_∞ = 6.7 km/sec at an altitude of H = 46 km.

1 — integral method; 2 — finite difference method; 3 — method of integral relationships; T — transition point.

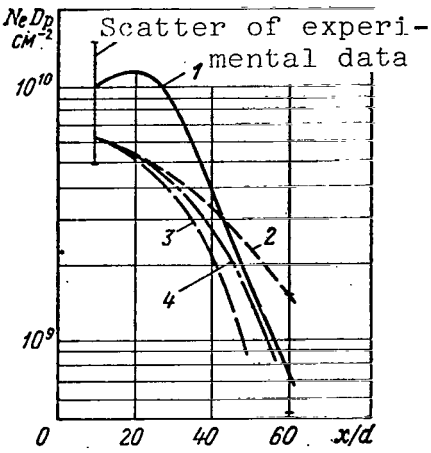

Figure 5.55. Change in total electron density in wake behind blunt cone at ν = 12.5°, d_n = 0.38 mm; d = 6.35 mm; flight velocity 7 km/second and pressure of p_∞ = 75 mm Hg.

1 — experimental data; 2 — data from theoretical calculation taking into consideration seven components (N_2, O_2, N, O, NO, NO^+, e^-); 3 — the same, with the addition of components O^- and O_2^-; 4 — same with the addition of components O^-, O_2^-, NO_2, and NO_2^-.

computational data approximate the experimental relations, particularly when the kinetics of the chemical processes are refined (Figure 5.55 [114]).

The presence of even small admixtures which have a low ionization potential (for example, sodium, see Figure 5.56 [108]), has a great influence on the rate at which the electron concentration decreases along the wake. The slower (due to triple

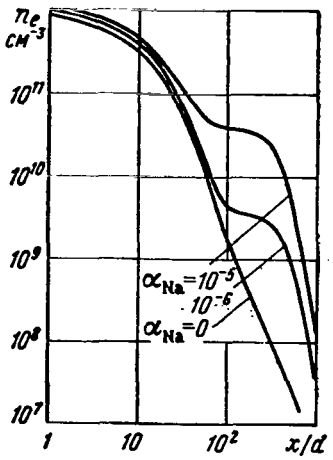

Figure 5.56. Influence of Na admixture on electron density distribution along wake axis behind blunt cone at ϑ = 12°; d_n = 1.14 m; d = 2.28 m; flight velocity 7 km/sec at an altitude of H ≈ 38 km.

collisions) recombination of sodium electrons does not have an influence until the process by which electrons are attached to oxygen becomes significant.

Research problems and difficulties

In the general case, admixtures in the flow, which are produced, for example, when the material of the body surface is disturbed, greatly complicate the kinetics of processes in the wake behind the body. Even in pure air, a lack of equilibrium between different degrees of freedom and quanta levels may greatly change the reaction rate. Finally, an important problem is the influence of the density pulsations of electrons and other particles on the average reaction rates [114, 120].

It must be emphasized that the scattering by the turbulent wake of electromagnetic waves incident to it depends exactly on the mean square electron density pulsations, which are related to the scale and intensity of turbulent pulsations [116, 120]. To calculate the electron density pulsations, there are several approximations [117 — 119, 121], whose suitability, however, may only be shown by direct measurements of electron concentrations in turbulent regions.

Thus, the flow parameter distribution (including the electron concentration) in wakes behind bodies entering the atmosphere at a hypersonic velocity is a result of the complex mutual influence of the form of the body, the chemical kinetics, and the process of transition from the laminar to the turbulent flow regime. Although at the present time the basic characteristics have been studied, including the characteristics of non-equilibrium flows, as a whole, as Lees writes in his summary article [103], "... a satisfactory, comprehensive description of the hypersonic wake cannot be obtained until the gaps are filled in our present knowledge about the mechanics of liquids, kinetic processes, and the mechanics of radiation."

REFERENCES

1. Loytsyanskiy, L. G. Laminarnyy pogranichnyy sloy (Laminar Boundary Layer). Moscow, Fizmatgiz, 1962.

2. Dorrens, U. Kh. Giperzvukovyye techeniya vyazkogo gaza (Viscous Gas Hypersonic Flows), Moscow, Mir Press, 1966.

3. Chung, P. M. Chemically Reacting Nonequilibrium Boundary Layers. In: Advances in Heat Transfer, 1965, Vol. 2, pp. 109-270.

4. Alekseyev, B. V. Pogranichnyy sloy s khimicheskimi reaktsiyami (Boundary Layer with Chemical Reactions), Moscow, VTs, AN SSSR, 1967.

5. Ginzburg, I. P. Aerogazodinamika (Aerogasdynamics), Moscow, "Vysshaya shkola," 1966.

6. Hirshfelder, J., C. Curtis, and R. Bird. Molecular Theory of Gases and Liquids. Moscow, Foreign Literature Publishing House (IL), 1961.

7. Tirskiy, G. A. Calculation of Effective Diffusion Coefficients in Laminar Dissociating Multi-Component Boundary Layer. Prikladnaya matematika i mekhanika (PMM), No. 1, 1969.

8. Samuylov, Ye. V. Influence of Internal Degrees of Freedom /294
of Particles upon the Transport Coefficients of a Multi-Component Mixture of Gases. In the collection: Fizicheskaya gazodinamika (Physical Gas Dynamics), Moscow, Izdatel'stov AN SSSR, 1959.

9. Zhigulev, V. N. Equations of Motion of a Nonequilibrium Medium with Allowance for Radiation. Inzh. zhurnal, Vol. IV, No. 2, 3, 1964.

10. Kogan, M. N. Dinamika razrezhennogo gaza (Dynamics of a Rarefied Gas), Moscow, Nauka Press, 1967.

11. Vallander, S. V., I. A. Yegorova, and M. A. Rydalevskaya. Extending the Chapman-Enskog Method to a Mixture of Gases with Internal Degrees of Freedom and Chemical Reactions. In the collection: Aerodinamika razrezhennykh gazov (Aerodyanmics of Rarefied Gases), II, Izdatel'stov LGU, 1965.

12. Kuznetsov, V. M. Dissipative Coefficients in Strongly Nonequilibrium Gas Mixtures with Binary Collisions. Inzh. zhurnal, Vol. V, No. 5, 1965.

13. Galkin, V. S. and M. N. Kogan. Equations of Nonequilibrium Flows of Multi-Atomic Gases in the Aitken Approximation. In the collection: Problemy gidrodinamiki i mekhaniki sploshnoy sredy (Problems of Hydrodynamics and Mechanics of a Continuous Medium), Moscow, Nauka Press, 1969.

14. Stupochenko, Ye. V., B. B. Dotsenko, I. P. Stakhanov, and Ye. V. Samuylov. Methods of Calculating the Kinetic Coefficients of Air at High Temperatures. In the collection: Fizicheskaya gazodinamika (Physical Gas-dynamics), Edited by A. S. Predvoditelev, Moscow, Izdatel'stvo AN SSSR, 1959.

15. Bade, W. L., E. A. Mason, and K. S. Yun. Transport Properties of Dissociated Air. ARS Journal, No. 8, 1961.

16. Peng, T. C. and A. L. Pindroh. An Improved Calculation of Gas Properties at High Temperatures — Air. ARS Preprint, No. 1995-61, 1961.

17. Sevast'yanov, R. M. and M. D. Zdunkevich. Thermodynamic Functions of Gas Mixtures for High Air Temperatures, Inzh. zhurnal, Vol. IV, No. 4, 1964.

18. Lees, L. Laminar Heat Transfer over Blunt-Nosed Bodies at Hypersonic Flight Speeds. Jet Propulsion, No. 4, 1956; see also, the Collection: Scientific Problems of Artificial Satellites, 1959.

19. Hayes, J. E. and R. F. Probstin. Theory of Hypersonic Flow, Moscow, IL, 1962.

20. Fay, J. A. and F. Riddell. Theory of Stagnation Point Heat Transfer in Dissociated Air. JAS, No. 2, 1958. See also, the collection: Gazodinamika i teploobmen pri nalichii khimicheskikh reaktsiy (Gasdynamics and Heat Exchange in the Presence of Chemical Reactions). Moscow, IL, 1962.

21. Rose, P. and W. Stark. Stagnation Point Heat Transfer Measurements in Dissociated Air. JAS, No. 2, 1958.

22. Vitale, A., E. Kaegi, N. Diaconis and W. Warren. Results from Aerodynamic Studies of Blunt Bodies in Hypersonic Flows of Partially Dissociated Air. Heat Transfer and Fluid Mech., Inst. Prepr. of Papers, Stanford, 1958.

23. Detra, R. W., N. H. Kemp, and F. R. Riddell. Addendum to Heat Transfer to Satellite Vehicles Re-Entering the Atmosphere. Jet Propulsion, No. 12, 1957.

24. Kemp, N. H., P. H. Rose, and R. W. Detra. Laminar Heat Transfer around Blunt Bodies in Dissociated Air. JASS, No. 6, 1959.

25. Murzinov, I. N. Laminar Boundary Layer on a Sphere in Hypersonic Flow of Uniformly Dissociating Air. Izvestiya AN SSSR, NZhG, No. 2, 1966.

26. Gromov, V. G. Chemically Nonequilibrium Laminary Boundary Layer in Dissociating Air. Izvestiya AN SSSR, MZhG, No. 2, 1966.

27. Smith, A. M. O. and N. Jaffe. General Method for Solving the Nonequilibrium Boundary Layer Equations of a Dissociating Gas. AIAA Pap., 65-129, 1965.

28. Zakkay, V. Laminar Heat Transfer and Pressure Measurements over Blunt-Nosed Cones at Large of Attack. JAS, No. 12, 1958.

29. Petukhov, I. V. Numerical Integration of Laminary Boundary Layer Equations. DAN SSSR, Vol. 132, No. 2, 1960.

30. Brailovskaya, I. Yu. and L. A. Chudov. Solving Boundary Layer Equations by the Difference Method. Collection of articles by the TTs MGU: Vyschislitel'nyye metody i programmirovaniye (Computational Methods and Programming), Izdatel'stvo MGU, No. 1, 1962. /295

31. Dorodnitsyn, A. A. One Method of Solving Laminar Boundary Layer Equations. Prikladnaya mekhanika i tekhnicheskaya fizika (PMTF), No. 3, 1960.

32. Pavlovskiy, Yu. N. Numerical Calculation of the Boundary Layer in a Compressed Gas. Zhurnal vychisl. matem. i matem. fiz., Vol. 2, No. 5, 1962.

33. Gromov, V. G. Use of a Three-Layer Difference Scheme to Solve Boundary Layer Equations. Izvestiya AN SSSR, OTN, Mekhanika i mashina, No. 5, 1963.

34. Goulard, R. On Catalytic Recombination Rates in Hypersonic Stagnation on Heat Transfer. Jet propulsion, Vol. 28, No. 11, 1958.

35. Frank-Kamenetskiy, D. A. Diffusion Theory of Heterogeneous Reactions. Zhurnal fizicheskoy khimii, Vol. 13, No. 6, 1939.

36. Inger, G. R. Dissociated Laminary Boundary Layer Flows over Surfaces with Arbitrary Continuous Distributions of Catalycity. Internat. J. Heat and Mass Transfer, No. 9, 1963.

37. Rosner, D. E. Catalytic Probes for the Determination of Atom Concentrations in High Speed Gas Streams. ARS J., No. 7, 1962.

38. Hartunian, R. A. and W. P. Thompson. Nonequilibrium Stagnation Point Heat Transfer Including Surface Catalysis. AIAA Paper, No. 63-464, 1963.

39. Starner, K. E. and W. P. Thompson. Arc Tunnel Studies of Nonequilibrium Stagnation Point Heat Transfer. Proceedings of the 1966 Heat Transfer and Fluid Mechanics Institute, June 22-24, 1966.

40. Reddy, N. M. Use of Self-Calibrating Catalytic Probes to Measure Free Stream Atom Concentration. Phys. of Fluids, Vol. 10, No. 9, 1967.

41. Chung, P. M. and S. W. Liu. Simultaneous Gas Phase and Surface Atom Recombination for Stagnation Boundary Layer. AIAA J., Vol. 1, No. 4, 1963.

42. Inger, G. R. Nonequilibrium Stagnation Point Boundary Layers with Arbitrary Surface Catalycity. AIAA J., Vol. 1, No. 8, 1963.

43. Ladnova, L. A. Approximate Method of Calculating Nonequilibrium Laminar Boundary Layer for a Wall with Arbitrary Catalytic Activity. Vestnik LGU, Seriya "Matematika, mekhanika, astronomiya," Vol. 1, No. 1, 1967.

44. Inger, G. R. Analytical Prediction of Nonequilibrium Heat Transfer around Blunt-Nosed Bodies. J. of Spacecraft and Rockets, No. 3, 1966.

45. Voronkin, V. G. and L. K. Geraskina. Nonequilibrium Laminar Boundary Layer of Dissociating Air on Axisymmetric Bodies. Izvestiya AN SSSR, MZhG, No. 3, 1969.

46. Kuznetsov, V. M. and S. N. Seliverstov. Flow around a Plate by a Viscous Flow of Nonequilibrium Gas. Izvestiya AN SSSR, MZhG, No. 1, 1967.

47. Lun'kin, Yu, P. and Si-Tsin Yan. Influence of Rotational and Vibrational Relaxation on the Laminar Boundary Layer of a Plate. PMTF, No. 1, 1963.

48. Ladnova, L. A. Laminar Nonequilibrium Boudary Layer on a Flat Plate. Vestnik, LGU, Seriya Matematika, mekhanika, i astronomiya, No. 19, 1964, p. 4.

49. Yegorov, B. V. Relaxation Equation for Vibrational Degrees of Freedom of a Diatomic Gas. Izvestiya AN SSSR, Mekhanika, No. 3, 1965.

50. Agafonov, V. P. Determination of the Influence of a Relaxation Boundary Layer upon the Characteristics of Viscous Flow around a Wedge. Inzhenernyy zhurnal, Vol. 5, No. 1, 1965.

51. Zhigulev, V. N. Effect of a Relaxation Boundary Layer, DAN SSSR, Vol. 144, No. 6, 1962.

52. Rae, W. J. A Solution for the Nonequilibrium Flat Plate Boundary Layer. AIAA J., Vol. 1, No. 10, 1963.

53. Stulov, V. P. Boundary Layer on a Plate with Allowance for Nonequilibrium Dissociation. Izvestiya AN SSSR, Mekhanika i mashina, No. 3, 1961.

54. Stulov, V. P. Heat Transfer in a Laminar Boundary Layer on a Plate with Allowance for Chemical Nonequilibrium. Izvestiya AN SSSR, Mekhanika i mashina, No. 5, 1961.

55. Ladnova, L. A. Small Parameter Method for Calculating Chemically Nonequilibrium Laminar Boundary Layer of a Plate. Vestnik LGU, Matematika, mekhanika, astronomiya No. 1, 1966, p. 1. /296

56. Lun'kin, Yu. P., and S. B. Koleshko. Laminary Boundary Layer on a Plate in the Case of Vibrational and Dissociating Relaxation. In the collection: Gidrogazodinamika (Hydrogasdynamics). Moscow-Leningrad, Mashinostroyeniye, 1966.

57. Blottner, F. G. Chemical Nonequilibrium Boundary Layer. AIAA J., Vol. 2, No. 2, 1964.

58. Pallone, A. J., J. A. Moore, and J. I. Erdos. Nonequilibrium Nonsimilar Solutions of the Laminar Boundary Layer Equations. AIAA J., Vol. 2, No. 10, 1964.

59. Levinsky, E. S. and F. L. Fernandez. Approximate Nonequilibrium Air Ionization in Hypersonic Flows over Sharp Cones. AIAA J., Vol. 2, No. 3, 1964.

60. Blottner, F. G. Nonequilibrium Laminar Boundary Layer Flow of Ionized Air. AIAA J., Vol. 2, No. 11, 1964.

61. Nerem, R. M. Laminary Boundary Layer Heat Transfer Measurements on Flat Plate in Dissociated and Partially Ionized Air. Proceeding of the 1966 Heat Transfer and Fluid Mechanics Institute, June 22-24, 1966.

62. Chambre, P. L. and A. Acrivos. On Chemical Surface Reactions in Laminar Boundary Layer Flows. J. Applied Phys., No. 11, 1956.

63. Li, T. Y. and P. S. Kirk. Asymptotic Method of Solution of the Frozen Dissociated Laminar Boundary Layer Flow Over a Flat Plate Surface with Arbitrarily Distributed Catalycity. Internat. J. Heat and Mass Transfer, Vol. 10, No. 3, 1967.

64. Vidal, R. J. and T. C. Golian. Heat Transfer Measurements with a Catalytic Flat Plate in Dissociated Oxygen. AIAA Paper, No. 67-163, 1967.

65. Chung, P. M., S. W. Liu, and H. Mirels. Effect of Discontinuity of Surface Catalycity on Boundary Layer Flow of Dissociated Gas. Internat. J. of Heat and Mass Transfer, No. 3, 1963.

66. Lighthill, M. J. Contributions to the Theory of Heat Transfer through a Laminar Boundary Layer. Proc. Royal Soc., Ser. A., No. 1070, 1950.

67. Lassau, G. and B. Le Fur. Concentration Profiles in a Frozen Laminar Boundary Layer with Continuous and Discontinuous Catalyzer Distribution on the Wall, Internat. J. Heat and Mass Transfer, Vol. 10, No. 7, 1967.

68. Provotorov, V. P. Viscous Interation on a Plate in Hypersonic Flow of a Nonequilibrium Dissociating Gas. Uchenyye zapiski Tsentral'nogo aerogidrodinamicheskogo instituta im. N. Ye. Zhukovskogo (TsAGI), Vol. II, No. 1, 1971.

69. Cheng, H. K. The Blunt Body Problem in Hypersonic Flow at Low Reynolds Number. IAS Paper, No. 63-92, 1963.

70. Shidlovskiy, V. P. Vvedeniye v dinamiku razrezhennogo gaza (Introduction to Dynamics of a Rarefied Gas), Moscow, Nauka Press, 1966.

71. Sedov, L. I., M. P. Mikhaylova, and G. G. Chernyy. Influence of Viscosity and Thermal Conductivity on Gas Flow Behind a Strongly Curved Shock Wave. Vestnik MGU, Seriya "Fiz. -mat. i yestestv. nauk.", Vol. 2, No. 3, 1953.

72. Ferri, A., V. Zakkay, and L. Ting. On Blunt Body Heat Transfer at Hypersonic Speed and Low Reynolds Numbers. JASS, No. 7, 1962.

73. Ferri, A. and V. Zakkay. Measurements of Stagnation Point Heat Transfer at Low Reynolds Numbers. JASS, No. 7, 1962.

74. Potter, J. L. and J. T. Miller. Total Heating Load on Blunt Axisymmetric Bodies in Low Density Flow. AIAA J., Vol. 1, No. 2, 1963.

75. Carden, W. A. Experimental Heat Transfer to Hemispheres in Nonequilibrium Dissociated Hypersonic Flow with Surface Catalysis and Second Order Effects. AIAA J., Vol. 4, No. 10, 1966.

76. Chung, P. M. Hypersonic Viscous Shock Layer of Nonequilibrium Dissociating Gas. NASA TR-R109, 1961.

77. Shin, W. C. L. and R. S. Krupp. Viscous Nonequilibrium Blunt Body Flow. AIAA J., Vol. 5, No. 1, 1967.

78. Ladnova, L. A. Dissociation Relaxation in a Viscous Hypersonic Layer. Vestnik LGU, Matematika, mekhanika, astronomiya, Vol. 3, No. 13, 1967. /297

79. Ladnova, L. A. Nonequilibrium Viscous Shock Layer on a Body with Arbitrary Catalytic Surface Activity. Vestnik LGU, Matematika, mekhanika, astronomiya, Vol. 3, No. 13, 1969.

80. Hoshizaki, H., S. Neice, K. K. Chen. Stagnation Point Heat Transfer Rates at Low Reynolds Numbers. IAS Paper, No. 60-68, 1960.

81. Goldberg, L. and S. Scala. Mass Transfer in the Hypersonic Low Reynolds Number Viscous Layer. IAS Paper, No. 62-80, 1962.

82. Inger, G. R. Nonequilibrium Hypersonic Stagnation Flow with Arbitrary Surface Catalycity including Low Reynolds Number Effects. Intern. J. Heat and Mass Transfer, No. 8, 1966.

83. Blottner, F. G. Viscous Shock Layer at the Stagnation Point with Nonequilibrium Air Chemistry. AIAA J., Vol. 7, No. 12, 1969.

84. Lees, L. and L. Hromas. Turbulent Diffusion in the Wake of a Blunt Nosed Body at Hypersonic Speeds. JASS, No. 8, 1962.

85. Chapman, D. R. Laminar Mixing of a Compressible Fluid. NACA Rep. 1950, No. 958.

86. Crocco, L. and L. A. Lees. Mixing Theory for the Interaction Between Dissipative Flows and Nearly Isentropic Streams. JAS, No. 10, 1952.

87. Yel'kin, Yu. G., V. Ya. Neyland, and L. A. Sokolov. Base Pressure Behind a Wedge in Supersonic Flow. Inzhernyy zhurnal, III, 1963, p. 2.

88. Tagirov, R. K. Influence of Initial Boundary Layer on Base Pressure. Izvestiya AN SSSR, MZhG, No. 2, 1966.

89. Bondarev, Ye. N. Approximate Calculation of Interaction of Supersonic Flow with Laminar Layer in Region of Separated Flow. Izvestiya AN SSSR, MZhG, No. 5, 1966.

90. Denison, M. R. and E. Baum. Compressible Free Shear Layer with Finite Initial Thickness. AIAA J., Vol. 1, No. 2, 1963.

91. Kubota, T. and C. F. Dewey Jr. Momentum Integral Methods for the Laminar Free Shear Layer. AIAA J., Vol. 2, No. 4, 1964.

92. Lees, L. and B. L. Reeves. Supersonic Separated and Reattaching Laminar Flows. I General Theory and Application to Adiabatic Boundary Layer — Shock Wave Interactions. AIAA J., Vol. 2, No. 11, 1964.

93. Zempel, R. E. and E. P. Muntz. Slender Body Near Wake Density Measurements at Mach Numbers 13 and 18. AIAA Preprint, No. 63-271, 1963.

94. Slattery, R. E. and W. G. Clay. Experimental Measurements of Turbulent Transition, Motion, Statistics, and Gross Radial Growth Behind Hypervelocity Objects. Physics of Fluids, Vol. 5, No. 7, 1962.

95. Fay, J. and A. Goldburg. The Unsteady Hypersonic Wake Behind Spheres. AIAA J., Vol. 1, No. 10, 1963.

96. Levensteins, Z. J. Hypersonic Wake Characteristics Behind Spheres and Cones. AIAA J., Vol. 1, No. 12, 1963.

97. Pallone, A. J., J. I. Erdos, J. Eckerman, and W. McKay. Hypersonic Laminar Wakes and Transition Studies. AIAA J., Vol. 2, No. 5, 1964.

98. Wilson, L. N. The Far Wake Behavior of Hypersonic Spheres. AIAA J., Vol. 5, No. 7, 1967; Far Wake Behavior of Hypersonic Blunted Cones. AIAA J., Vol. 5, No. 8, 1967.

99. Goldburg, A. A. Summary Analysis of Laboratory Hypersonic Wake Fluid Mechanics Transition Experiments. AIAA Paper, No. 67-33, 1967.

100. Bloom, M. H. and M. H. Steiger. Diffusion and Chemical Relaxation in Free Mixing. IAS Paper, No. 63-67, 1963.

101. Ting, L. and P. A. Libby. Remarks on the Eddy Viscosity in Compressible Mixing Flows. JASS, Vol. 27, No. 10, 1960.

102. Fox, H., V. Zakkay, and R. A. Sinhe. A Review of Problems in the Nonreacting Turbulent Far Wake. Astronautica Acta, Vol. 14, No. 3, 1969.

103. Lees, L. Hypersonic Wakes and Trails. AIAA J., Vol. 2, No. 3, 1964.

104. Landau, L. D. and Ye. M. Lifshits. Mekhanika sploshnykh sred (Mechanics of Continuous Media), Moscow, GITTL, 1953.

105. Lin, S. C. and J. E. Hayes. A Quasi One-Dimensional Model for Chemically Reacting Turbulent Wakes of Hypersonic Objects. AIAA J., Vol. 2, No. 7, 1964. /298

106. Wen, K. S., T. Chen, and R. A. Hayami. An Eddy Diffusion Model for Predicting Rapid Wake Ionization Decay behind Hypersonic Cones. AIAA Paper, No. 67-21, 1967.

107. Val'o-Laurin, R. and M. Blum. Chemical Phenomena in External Hypersonic Flows. In the collection: Issledovaniya giperzvukovykh techeniy (Study of Hypersonic Flows), Moscow, Mir Press, 1964.

108. Webb, W. H. and L. A. Hromas. Turbulent Diffusion of a Reacting Wake. AIAA J., Vol. 3, No. 5, 1965.

109. Lien, H., J. I. Erdos, and A. J. Pallone. Nonequilibrium Wakes with Laminar and Turbulent Transport. AIAA Paper, No. 63-447, 1963.

110. Zeiberg, S. L. and G. D. Bleich. Finite Difference Calculation of Hypersonic Wakes. AIAA J., Vol. 2, No. 8, 1964.

111. Khoroshko, K. S. Hypersonic Wake Behind Blunt Bodies. Izvestiya AN SSSR, MZhG, No. 2, 1969.

112. Hayami, R. A. and R. I. Primich. Wake Electron Density Measurements behind Hypersonic Spheres and Cones. Fluid Physics of Hypersonic Wakes, Vol. 2, 1967.

113. Kornegay, W. M. Electron Density Decay in Wakes. AIAA J., Vol. 3, No. 10, 1965.

114. Eschenroeder, A. Q. Kinetic Processes in Hypersonic Wakes. Fluid Physics of Hypersonic Wakes, Vol. 1, 1967.

115. Wen, K. S., T. Chen, and B. A. Lieu. Theoretical Study of Hypersonic Sphere Wakes in Air and Comparisons with Experiments. Part I. Turbulent Diffusion. Part II. Chemical Kinetics. AIAA Paper, No. 68-703. 1968.

116. Martin, J. Atmospheric Entry. Moscow, Mir Press, 1969.

117. Proudlon, A. P. and S. A. Feldman. New Model for Mixing and Fluctuation in Turbulent Wake. AIAA J., Vol. 3, No. 4, 1965.

118. Lin, S. C. A Bimodel Approximation for Reacting Turbulent Flows. Part II. AIAA J., Vol. 4, No. 2, 1966.

119. Gibson, W. E. Stockhastic Model for Turbulent Reacting Wakes. AIAA J., Vol. 4, No. 11, 1966.

120. Lykoudis, P. S. A Review of Hypersonic Wake. AIAA J., Vol. 4, No. 4, 1966.

121. Schapker, R. L. Electron Density Fluctuations in Hypersonic Wakes with Dissociative Neutralization Chemistry. AIAA Paper, No. 68-688, 1968.

CHAPTER 6

RADIATION IN HYPERSONIC GASDYNAMICS

6.1. Basic concepts and definitions

In shock layers which are produced when hypersonic aircraft /299 move in the atmosphere, energy is transported by radiation, which is new for classical aerodynamics, and which may have an influence on the heating of the aircraft and the gas parameters in the shock layer. Within the framework of the continuous media model, this chapter examines the problems of the flow of radiating air, without studying the detailed quantum-mechanical picture of the interaction of the radiation field with matter. The analysis is confined to only the macroscopic characteristics of interaction.

The radiation is characterized by the oscillation frequency of the electromagnetic field ν or the wavelength λ connected with the frequency by the relationship $\lambda = c/\nu$, where c is the speed of light. From the quantum point of view, radiation is a group of photons, or light quanta, whose energy ε is directly proportional to the frequency of electromagnetic oscillations $\varepsilon = h\nu$, where h is the Planck constant.

The absorbtion and radiation of light quanta in a gas occurs when the energy state of the gas particles changes. The form of the transitions, and consequently the energy and frequency of the quanta, depend on the nature of the gas, its temperature, and pressure. Bound-bound transitions in monatomic gases occur

between electron states of atoms, and in a multi-atomic gas — between the vibrational, rotational, and electron levels of molecules. These transitions give a line spectrum, which has the form of a system of lines in the case of molecular transitions.

A neutral atom is produced in the recombination of an ion and a free electron, and an excess of energy is given off in the form of radiation. This transition, and the photoionization process which is opposite to it, pertain to free-bound transitions. Free-free transitions are transitions which occur when the energy /300 of the free electrons changes in the field of positive ions and neutral particles. The radiation produced in the case of free-free transitions is called bremsstrahlung. Free-bound and free-free transitions give a continuous radiation spectrum.

In order to study each of these transitions in detail, we shall try to solve the problem of the flow of a radiating gas, using the integral characteristics of the interaction of the radiation electromagnetic field and matter. Since the flow velocities of the gas are a little less than the speed of light, we shall assume that the radiation is propagated in a fixed gas. We shall give certain definitions which are necessary in order to describe the radiation field and its interaction with matter. More detailed information may be found in the references on radiative transport [1 — 5].

The basic factor which is used to obtain all quantities characterizing the radiation field is the spectral radiation intensity, which is introduced as follows. Let us assume $d\varepsilon_\nu$ is the radiation energy which, in the frequency interval from ν to $\nu + d\nu$ in the time dt, is transported over an arbitrarily oriented element of the area dA (Figure 6.1) surrounding point P, in an element of the solid angle $d\Omega$ in the direction $\vec{s}$. Then the

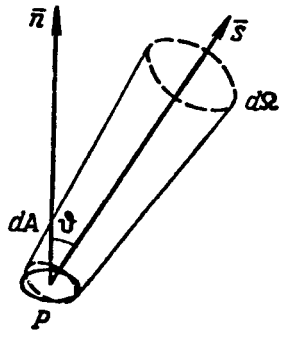

Figure 6.1. Determination of specific radiation intensity.

spectral radiation intensity I_ν at the point P in the direction $\vec{s}$ with the frequency ν will be determined by the relationship

$$dE_\nu = I_\nu \cos\vartheta \, dA \, d\Omega \, d\nu \, dt. \quad (6.1)$$

Here ϑ is the angle between the direction $\vec{s}$ and the normal to dA.

According to this definition, the spectral radiation intensity is a function of time, frequency, and also coordinate and direction in space, and equals the amount of energy passing per unit time in unit solid angle and unit frequency interval through a unit surface located perpendicularly to $\vec{s}$.

The radiation spectral flux is determined as the energy of radiation per unit interval of frequency passing per unit time through a unit area in all directions

$$F_\nu = \int I_\nu \cos\vartheta \, d\Omega. \quad (6.2)$$

"Complete," or integral quantities, just like the total radiation intensity I and the total radiant energy flux F, are obtained by integrating the spectral terms over the entire frequency spectrum. /301

For example,

$$I = \int_0^\infty I_\nu \, d\nu. \quad (6.3)$$

The coefficients of absorption and radiation are macroscopic characteristics for the interaction of the radiation field with matter. They are usually determined as follows. Let us consider the elementary volume dV of the radiative gas. The amount of energy radiated by this volume in the time dt in the frequency interval from ν to $\nu + d\nu$ in all directions is

$$d\varepsilon_\nu = j_\nu dV d\nu dt. \qquad (6.4)$$

Here $j\nu$ is the volumetric radiation coefficient of the material at the frequency ν. In order to obtain the mass radiation coefficient, we must divide the volumetric coefficient by the density of the material.

We shall follow the change in the intensity of radiation falling at a right angle on the layer of nonradiative gas. As has been shown experimentally and theoretically, this change will be proportional to the intensity of the incident radiation I_ν and the path traversed:

$$dI_\nu = -k_\nu I_\nu dx, \qquad (6.5)$$

where k_ν is determined as the volumetric radiation absorption coefficient at the frequency ν. The inverse value of the volumetric absorption coefficient $1/k_\nu$ represents the radiation mean free path of the frequency ν.

There is one form of interaction between the radiation field and matter — radiation scattering. However, in gas dynamic problems the scattering is very insignificant as compared with the absorption and it can be disregarded [5, 6].

The main equation for the radiation theory — the equation of radiation transport — may be written by examining the balance of radiant energy per unit of volume of a radiative and absorbing gas. For the steady case, the radiation transport equation has the form

$$\frac{dI_\nu}{ds} = j_\nu - k_\nu I_\nu. \qquad (6.6)$$

The derivative of I_ν in this equation is calculated along the fixed direction $\vec{s}$, in which the radiation of intensity I_ν is propagated.

In the case of complete thermodynamic equilibrium in a medium, the radiation intensity in any direction is constant and equals the radiation intensity of an absolutely black body. /302 From Equation (6.6), in the case of complete thermodynamic equilibrium, we have

$$j_\nu = k_\nu B_\nu, \qquad (6.7)$$

where B_ν is the distribution of the equilibrium radiation intensity determined by the Planck law

$$B_\nu = \frac{2h\nu^3}{c^2}[\exp(h\nu/kT) - 1]^{-1}, \qquad (6.8)$$

and k is the Boltsmann constant. The total intensity of the equilibrium radiation is

$$B = \frac{\sigma}{\pi}T^4, \qquad (6.9)$$

where σ is the Stefan-Boltsmann constant. Formula (6.7) represents an example of the Kirchoff law, according to which the ratio between the radiation coefficients and absorption

coefficients for any body in a state of thermodynamic equilibrium does not depend on the nature of the body, but only on its temperature, and equals the radiation intensity of a black body.

For the flow of real gases, it is impossible to speak of the existence of complete thermodynamic equilibrium in these gases. However, if the concept of a continuous medium is valid, within the framework of which the present examination is conducted, it is possible to introduce the well-known assumption of the occurrence of local thermodynamic equilibrium in the gas. This assumption is based on the fact that collisions between gas particles occur much more frequently than absorption and radiation. As a result, the energy of excitation between gas particles is redistributed, and the emission of photons is characterized by the local thermal state of the medium. Therefore, the radiation coefficient of gas particles in the volume dV at a temperature of T in an arbitrary temperature field may equal the coefficient which would be valid in the case of complete thermodynamic equilibrium with the same temperature. For this volume, the formula of Planck and the law of Kirchoff would be valid.

In the case of local thermodynamic equilibrium, the transport equation (6.6) has the form

$$\frac{dI_\nu}{ds} = k'_\nu (B_\nu - I_\nu). \qquad (6.10)$$

Here the term $k'_\nu = k_\nu[1-\exp(-h\nu/kT)]$ is called the absorption coefficient with allowance for forced radiation, and is a basic characteristic of the radiating medium. Below the prime ("'") for the absorption coefficient will be everywhere omitted.

Let us find the formal solution of the radiation transport equation in a gas (6.10), assuming $B_\nu(T)$ and $k_\nu(\rho, T)$ are known functions of the coordinates. The radiation intensity I_ν at the point s on a ray with the direction $\vec{s}$ has the form /303

$$I_\nu = \exp\left(-\int_0^s k_\nu dr\right)\left[C + \int_0^s k_\nu B_\nu \exp\left(\int_0^r k_\nu d\xi\right) dr\right], \qquad (6.11)$$

where C represents the integration constant determined from the condition s = 0 on the boundary of the medium. Thus, for known distributions of temperature and gas density and the dependence of the absorption coefficient on temperature, density, and frequency, finding the radiation intensity at any point of a body simply reduces to a quadrature — integration over the ray. Approximate methods of solving the radiation transport equation are given in the literature on astrophysics [1 — 4].

6.2. Gas equations of motion with allowance for radiation

Radiant heat exchange in a gas influences its motion and its condition. This influence is related to the fact that, in the case of emission and absorption of light, a gas loses or acquires energy. Therefore, the state of the moving gas with radiation is described by the equations of gasdynamics, which, in the case of radiation exchange, must be generalized with allowance for the interaction of radiation with a gas. Since radiant heat exchange depends on the gas temperature and density, the radiation transport equation must be added to the equations of gasdynamics which are generalized to the case of radiation transport.

Let us write the equations of motion for an inviscid gas with allowance for radiation [6 — 8]. We shall disregard the radiation pressure and density of the radiation energy in these equations, since, for nonastrophysical assumptions, they are small as compared with the pressure and density of the internal gas energy [5, 6]. Therefore, the equations of continuity and momentum will apparently be the same as those which do not take radiation into account:

$$\frac{\partial \rho}{\partial t} + \operatorname{div} \rho \vec{v} = 0; \tag{6.12}$$

$$\rho \frac{d\vec{v}}{dt} + \operatorname{grad} p = 0. \tag{6.13}$$

Here ρ and p are the density and pressure of the gas, and $\vec{v}$ is the velocity vector of the gas particles.

When writing the energy equation, we must take the fact into account that a gas particle emits and absorbs energy. Therefore, we must add the vector divergence of the radiant flux to the energy equation. We then have

$$\rho \frac{d}{dt}\left(\frac{v^2}{2} + e\right) + \operatorname{div} p\vec{v} + \operatorname{div} \vec{F} = 0, \tag{6.14}$$

where e is the internal energy per unit of gas mass and /304

$$\operatorname{div} \vec{F} = 4\pi \int_0^\infty k_\nu B_\nu d\nu - \int_0^\infty \int_{4\pi} k_\nu I_\nu d\Omega d\nu. \tag{6.15}$$

We must add the equation of state for the gas to the system of equations (6.12), (6.13), and (6.14)

$$p=f(\rho, T) \tag{6.16}$$

as well as the radiant energy transport equation

$$\frac{dI_\nu}{ds}=k_\nu(B_\nu-I_\nu). \tag{6.17}$$

In the case of the gas flow of emitting, absorbing, and reflecting surfaces, this must be taken into account in the boundary conditions to solve the transport equation of radiant energy.

In the general case, the equations of gasdynamics, with allowance for radiation, represent a system of nonlinear integral differential equations with given boundary and initial conditions. This system is made more complex by the fact that the radiation flux depends on the geometric configuration of the flow field. Therefore, in the study of the flow of radiative gas different assumptions are used which simplify the problem and make it possible to provide a qualitative determination of the influence of the radiant heat transfer. These assumptions may be all of the approximations and limiting cases of the flows of ordinary gasdynamics, for example, the inviscid flow of gas behind a shock wave, or the flow in the boundary layer. Different approximations related to the nature of the radiation may be used. This may be either the frequently used hypothesis of a grey gas, according to which the radiation absorption coefficient is used which does not depend on the radiation frequency, or the limiting cases of a strongly absorbing or transparent, nonabsorbing gas. The method of small perturbations may also be used, when radiation has a small influence on the gas flow. Finally,

wide use is made of the assumption of the radiation field dependence only on one three-dimensional variable. The validity of certain functions which are frequently used at the same time may be studied by means of the characteristic flow parameters.

Chapter 2 examines the characteristic gasdynamic flow parameters (similarity parameters) which make it possible to establish the influence of different forces and transport processes on the gas flow. We shall give below the parameters which take into account the influence of radiation on the gas flow. Let us use L to designate the characteristic length of the gas volume, and k* to designate the characteristic value of the radiation absorption coefficient. The product $k^*L = \omega$ is called the characteristic optical thickness of the gas volume. Since $1/k^* = L^*$ is the mean free path of radiation in the volume, /305 $\omega = L/L^*$ represents the ratio of the characteristic dimension of the radiating region to the mean free path of light quanta. The value of the parameter ω characterizes the interaction of radiation with the gas volume being considered. If the parameter $\omega \ll 1$, then the radiation freely leaves the gas volume, without being absorbed in it, and at $\omega \gg 1$ there is repeated absorption and emission of quanta in the volume or, as it is called, the radiation "is suppressed." The parameter ω is usually designated by τ, and in certain studies it is called the Bouguer Bu number. Sometimes, instead of ω, the radiation Knudsen number is introduced $Kn_r = L^*/L$, which represents a value which is inverse that of the parameter ω.

Let us examine the energy equation (6.14). The order of magnitude of the vector divergence of radiant flux from Equation (6.15) will be $\operatorname{div} \vec{F} \sim 4\pi B k^*$ (B and k* designate the order of magnitude of B_ν and k_ν, and, for purposes of definition,

it is assumed that the radiation absorption coefficient does not depend on frequency). Then the ratio of the characteristic value of the term, which takes radiation into account in the energy equation, to the characteristic value of the inertia terms will be

$$W=\frac{8\pi Bk^{*}t}{\rho v^{2}}=\frac{8\pi Bk^{*}L}{\rho v^{3}}, \qquad (6.18)$$

where t is the characteristic time of occurrence of a gas particle in a radiating zone; v — its characteristic velocity, and ρ — the gas characteristic density. This parameter characterizes the energy influence of radiation on the gas flow. If the parameter W is small, then the influence of radiation on the flow is small. When the value of the parameter $W \gtrsim 1$, then the radiation will have a great influence on the parameters and flow of the gas. In the literature, this parameter is designated by different symbols, but most frequently of all by the letter Γ.

Let us obtain the limiting forms of the gas equations of motion with allowance for radiation for different values of the characteristic optical thickness of the gas volume.

We shall assume that the gas is optically thick ($\omega \gg 1$). Substituting the values of k_ν and $k_\nu B_\nu$, which are expanded in Taylor series in the vicinity of the point s, into the expression for the radiation intensity (6.11), we obtain

$$I_\nu(s)=B_\nu(s)-\frac{\partial B_\nu}{\partial s}\frac{1}{k_\nu(s)}+0\left(\frac{B_\nu}{\omega^{2}}\right). \qquad (6.19)$$

Using this solution, we find the expression for the vector divergence of the radiant flux

$$\operatorname{div}\vec{F}=\operatorname{div}\left(\frac{1}{3k_R}\operatorname{grad}B\right), \tag{6.20}$$

where k_R is the average radiation absorption coefficient, introduced by Rosseland, which is determined by the expression

/306

$$\frac{1}{k_R}\int_0^\infty\frac{\partial B_\nu}{\partial T}d\nu=\int_0^\infty\frac{1}{k_\nu}\frac{\partial B_\nu}{\partial T}d\nu, \tag{6.21}$$

and B is the total intensity of equilibrium radiation (6.9).

Thus, for the case of almost grey radiation ($\omega \gg 1$), the integral, differential system of equations of gasdynamics, with allowance for radiation, may be transformed into a system of differential equations:

$$\left.\begin{aligned}&\frac{\partial\rho}{\partial t}+\operatorname{div}\rho\vec{v}=0;\\&\rho\frac{d\vec{v}}{dt}+\operatorname{grad}p=0;\\&\rho\frac{d}{dt}\left(\frac{v^2}{2}+e\right)+\operatorname{div}p\vec{v}+\operatorname{div}\left(\frac{1}{3k_R}\operatorname{grad}B\right)=0;\\&p=f(\rho,T).\end{aligned}\right\} \tag{6.22}$$

As follows from (6.20), the transfer of radiant energy from particle to particle in the case $\omega \gg 1$ is formally similar to ordinary heat conductivity. In this case, the heat conductivity coefficient is the well-known function of gas temperature and density. The strongly heated gas region thus loses its energy only from the thin surface layer, which encompasses the region where the radiation is blocked. In the case of $\omega \gg 1$, the approximation is called the approximation of radiant heat conductivity.

Let us now turn to the opposite case of an optically thin gas, when the characteristic optical thickness of the gas is small, i.e., $\omega \ll 1$. Since in this case the quantity I_ν (6.11) has the order of $B_\nu\omega$, the expression for the vector divergence of the radiant flux (6.15) assumes the form

$$\operatorname{div} F_r \cong 4\pi \int_0^\infty k_\nu B_\nu d\nu. \tag{6.23}$$

In other words, if $\omega \ll 1$, we may disregard the radiation absorption in the gas volume, i.e., in the $\omega \ll 1$ approximation, the gas particles only emit spontaneously, without absorbing radiant energy.

For the case of an optically thin gas, the equations of gasdynamics assume the form

$$\left.\begin{aligned} &\frac{\partial \rho}{\partial t} + \operatorname{div} \rho \vec{v} = 0; \\ &\rho \frac{d\vec{v}}{dt} + \operatorname{grad} p = 0; \\ &\rho \frac{d}{dt}\left(\frac{v^2}{2} + e\right) + \operatorname{div} p\vec{v} + 4\pi \int_0^\infty k_\nu B_\nu d\nu = 0; \\ &p = f(\rho, T). \end{aligned}\right\} \tag{6.24}$$

The term taking into account the influence of radiation when $\omega \ll 1$ may be formally regarded as the sink of heat distributed over the heated gas volume. The strength of this sink is the well-known function of the gas temperature and density. In the case of an optically thin gas, the Planck average absorption coefficient k_P is used, which is determined as /307

$$k_P B = \int_0^\infty k_\nu B_\nu d\nu. \tag{6.25}$$

In many problems of gasdynamics, for example in the case of hypersonic flow of air around bodies, both the analyzed cases $\omega \ll 1$ and $\omega \gg 1$, as well as the intermediate case $\omega \sim 1$, may be encountered.

6.3. Nonequilibrium radiation

It has been found [9 — 14] in experiments in wind tunnels that the radiation from the chemically nonequilibrium zone behind a shock wave exceeds by several factors the level of radiation from the equilibrium region. This phenomenon of excess radiation from the nonequilibrium zone is called "nonequilibrium radiation." Although the processes leading to nonequilibrium radiation are very complex and have been studied inadequately at the present, we shall attempt to give a suitable model for this phenomenon.

When a gas passes through a shock wave of great intensity, translational and rotational degrees of freedom of the molecules are completely excited by the gas. This leads to a very high translational temperature for the gas. As the gas moves further downstream, the gas translational temperature will decrease since the energy of the particle translational motion will be spent on the excitation of vibrational and electron molecular degrees of freedom, and also on dissociation of molecules and on ionization, until thermochemical equilibrium is established in the gas. (The picture of relaxation behind a shock wave is described in detail in Section 3.1.) If the probability is very great that the radiative states of the molecules are excited and the probability that the corresponding lifetime in the excited state in τ_e is small, and the dissociation of the radiative molecules takes place in the characteristic time τ_d, when $\tau_d \gg \tau_e$, then the population of the radiative excited levels of the molecules

may greatly exceed the equilibrium value. In other words, in view of the delay in the dissociation process there is a region directly behind the shock wave front where the concentration of excited molecules greatly exceeds the equilibrium concentration, and this leads to a peak of the excess radiation.

For shock wave velocities which exceed 10 km/sec, the relaxation picture is different — the molecules dissociate very rapidly. In this case, nonequilibrium radiation is caused by molecular ions which are produced during associative ionization /308 [reactions like (1.105)]. The concentration of these ions may be much greater than the equilibrium concentration, since the opposite processes (dissociative recombination and recharging) are less effective and take place at slower rates than does associative ionization.

In order that the radiation intensity reaches a maximum value of E_{max}, a determined time is necessary — the time of excitation τ_{max} and a certain relaxation time. This makes it possible to decrease the radiation intensity to an equilibrium level. The width of the nonequilibrium relaxation zone $d_{0.1}$ is assumed to be the distance from the front of a normal shock wave (Figure 6.2), at which the radiation intensity differs from the equilibrium value by 10%, and $d_{max} = \tau_{max} u_s$ (u_s is the shock wave velocity) is the distance corresponding to the maximum intensity. Since the excitation processes and chemical reactions behind the shock wave are primarily binary, as was already noted in Section 3.1, the width of the relaxation zone $d_{0.1}$ will be inversely proportional to the gas density. In its turn, the nonequilibrium radiation intensity is proportional to the density. Therefore, the integral radiation flux from the nonequilibrium zone will

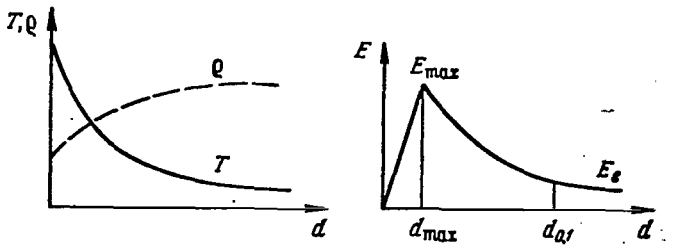

Figure 6.2. Model of nonequilibrium radiation.

not depend on the gas density, but only on the shock wave velocity. This phenomenon was observed in [10] and was called "the plateau of the radiative front" and was confirmed experimentally [10 — 12].

In actuality, the nonequilibrium radiation may not be completely independent of the advancing flux density, since, even under the assumption of binary conditions behind the shock wave, there are factors which distort the independence of the total radiation (from the equilibrium zone) from density. Let us examine these processes.

Nonequilibrium radiation will depend on density in the case of strong, radiation cooling of the shock layer, when the energy removed by the radiation comprises a significant portion of the total flow energy, and the escape of radiation leads to the uncompensated loss of excited particles. This independence /309 is absent, when the shock layer is not thin, and it is necessary to take into account absorption in the shock layer.

Let us examine nonequilibrium radiation behind the shock wave around the spherical forward part of a body moving at hypersonic velocity. It may be assumed that along each streamline of the shock layer there is approximately the same distribution of nonequilibrium radiation as behind a normal shock wave

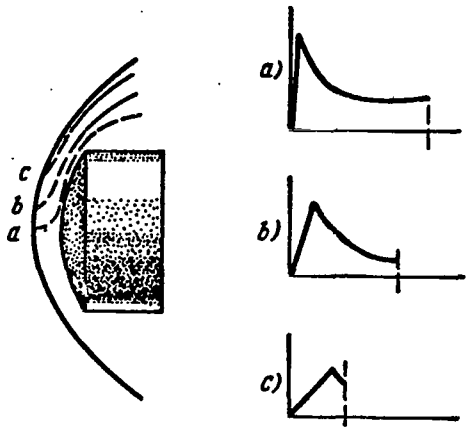

Figure 6.3. Diagram of flow around blunt body and radiation intensity distribution along the streamline.

of the corresponding intensity. Figure 6.3 shows the case when the nonequilibrium zone occupies the entire shock layer, and the intensity distribution of nonequilibrium radiation on three streamlines is given. If the time required for the gas particles to move along the streamline is less than the radiation relaxation time, the integral radiation from this streamline will be less than the radiation from the nonequilibrium zone behind the normal shock wave. This phenomenon is called "truncation of the radiation profile." Since the radiation relaxation time or the width of the nonequilibrium zone is inversely proportional to the gas density, at first, with a decrease in the gas density, the radiation will be reduced from a constant value until the width of the nonequilibrium zone is comparable with the wave stand-off distance. With a further decrease in density, the radiation from the nonequilibrium zone will sharply drop due to the truncation of the radiation profile.

There is a process, which is called the "collision limit," when, due to the small concentration of gas particles, the number of collisions is small and the concentration of excited particles decreases due to radiation much more rapidly than it increases due to collisions. Therefore, the population of the excited /310 molecular levels is less than is necessary at a given temperature, and the integral radiation from the nonequilibrium zone will be proportional to the density [15]. The critical gas density ρ^*, below which the collision limit has an effect, was estimated in

TABLE 16

CRITICAL DENSITY FOR "COLLISION LIMIT"*

Band system	ϱ^*/ϱ_0	H^* км for $\varrho^* = 10\varrho_\infty$
NO(β)	1,3·10−3	65
NO(γ)	0,9·10−4	82
O_2(III.—P.)	5,5·10−2	53
N_2^+(1−)	3,6·10−2	39
N_2(1+)	0,1·10−2	66
N_2(2+)	3,1·10−2	40

*The commas represent decimal points.

[15] for different systems of molecular bands, and is shown in Table 16 (ρ_0 is the gas density under normal conditions; H* — critical altitude.

Based on results derived from measuring radiation from the shock layer, a graph is compiled (Figure 6.4) in [10] which applies to the problem of heat transfer by radiation upon entry into the atmosphere. The solid line in the graph shows the radiant thermal flux at a critical point of a spherical body with a radius of one meter, flying at a velocity of 7.6 km/sec as a function of the flight altitude. At low altitudes, the equilibrium radiation reaches a maximum determined by the black body radiation. At an altitude of about 50 km, nonequilibrium becomes important, and the curve strives to assume the form of a plateau. With a further increase in the altitude, the radiant flux begins to decrease, since factors disturbing the independence of the nonequilibrium radiation from the gas density have a considerable influence. At an altitude of about 90 km, the shock layer becomes completely viscous, and this leads to a sharp decrease in the radiation. At higher altitudes, a shock wave is

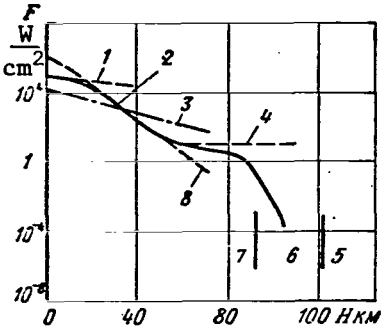

Figure 6.4. Dependence of radiation flux at the critical point of a sphere R = 1 m on altitude at V_∞ = 7.6 km/sec.

1 — black body; 2 — equilibrium radiation; 3 — convective thermal flux; 4 — plateau of radiative front; 5 — free-molecular flow; 6 — formation of shock; 7 — inviscid flow; 8 — nonequilibrium radiation.

not formed in front of the body, and the flow becomes free-molecular flow.

To calculate the intensity of radiation from the nonequilibrium zone behind a normal shock wave, it is necessary to note the kinetics of the chemical reactions in the gas, i.e., to determine the concentration of the gas components, its density, and temperature. Generally speaking, when calculating the kinetics in the energy conservation equations the energy losses due to radiation must be taken into account, and the system of chemical reactions used must include reactions occurring with radiation. However, as estimates made in [14] have shown, during the flow around a sphere with a radius of 60 cm moving at a velocity of about 11 km/sec at an altitude of 60 km, the energy removed by radiation will be on the order of one percent of the total flux of energy. Therefore, when calculating the kinetics, as a rule, the energy removed by radiation and reactions occurring with radiation are not taken into account, and the usual system for calculating parameters behind a normal shock wave is used, which is discussed in Section 3.1.

Nonequilibrium radiation of air, which is observed in experiments, may be primarily attributed to nitrogen molecules N_2 (the first and second positive band system), a molecular ion of nitrogen N_2^+ (the first negative band system), the band system

Schuman-Runge (Sc-R) of oxygen molecules, O_2, and molecules of nitric oxide NO (β and γ band system). The role of the radiation of atomic lines in the integral nonequilibrium radiation flux has also been noted in [14]. As the shock wave velocity increases, the role of molecules in nonequilibrium radiation will decrease, since the rate of molecular dissociation increases, and for shock wave velocities greater than 10 km/sec, the main contribution to nonequilibrium radiation will be made by molecular ions (N_2^+, O_2^+, NO^+) which are produced in the process of associative ionization, and by the spectral lines of atoms [16 — 18]. /311

The contribution of the basic molecular systems to radiation from the nonequilibrium zone may be calculated by means of the following simple relationships:

$$E[N_2(1+)]=2{,}5\cdot 10^{-13} n_{N_2}\exp(-90\,000/T_e); \qquad (6.26)$$

$$E[N_2(2+)]=3{,}4\cdot 10^{-11} n_{N_2}\exp(-129\,500/T_e); \qquad (6.27)$$

$$E[N_2^+(1-)]=1{,}6\cdot 10^{-12} n_{N_2^+}\exp(-36\,000/T_e); \qquad (6.28)$$

$$E[O_2(\text{Ш.}-\text{Р.})]=9{,}4\cdot 10^{-12} n_{O_2}\exp(-70\,000/T_e); \qquad (6.29)$$

$$E[NO(\beta)]=4{,}84\cdot 10^{-12} n_{NO}\exp(-65\,000/T_e); \qquad (6.30)$$

$$E[NO(\gamma)]=3{,}53\cdot 10^{-13} n_{NO}\exp(-63\,250/T_e), \qquad (6.31)$$

where n_{N_2}, n_{O_2}, n_{NO}, $n_{N_2^+}$ is the number of molecules of nitrogen, oxygen, nitric oxide, and the molecular ions of nitrogen per 1 cm^3, respectively; T_e — excitation temperature of electron levels of molecules in K; E — radiation intensity in $W/cm^3 \cdot cp$. Formulas (6.26) — (6.28) were taken from [14], and Formulas (6.29) — (6.31) were obtained by A. D. Nadezhin who used the results from [19].

The main problem in calculating nonequilibrium radiation is to determine the excitation temperature of molecular electron levels. A hypothesis exists, which has been confirmed by certain experiments (see [20, 21]), that the molecular electron degrees of freedom are closely related to the vibrational energy, and it may therefore be assumed that the population of the excited levels corresponds to the gas vibrational temperature. Other experiments [13] have shown that this relationship does not exist for air. Since the mechanism for the excitation of molecular levels is not clear and since many important collision processes are not known, it may be presently assumed that during the time in which equilibrium is approached behind a strong shock wave, only the chemical composition of the gas changes, and all other degrees of freedom, including the electron degrees of freedom, will be in local thermodynamic equilibrium with translational degrees of freedom, and their temperature will equal the translational temperature.

Therefore, radiation from the nonequilibrium zone behind a normal shock wave is calculated as follows. The concentration of the gas components and the translational temperature are determined according to the scheme discussed in Section 3.1, /312 and then the radiation intensity is calculated according to Formulas (6.26.) — (6.31).

The use of the translational temperature as the excitation temperature of molecular levels makes the calculated radiation level exceed the actual intensity of radiation from the nonequilibrium zone, particularly close to the shock wave front. Therefore, the nonequilibrium radiation intensity distribution obtained as a result of the calculation must be assumed to be too high. By way of an example, Figure 6.5 gives the results of calculating the radiation intensity in the relaxation zone

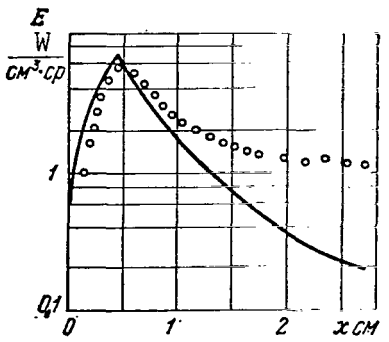

Figure 6.5. Comparison of calculated (solid lines) and measured (experimental points) intensity of nonequilibrium radiation in the spectral interval 0.55 — 1.0 microns at V_s = 9.6 km/sec and p = 0.1 mm Hg.

behind a normal shock wave, moving at a velocity of 9.6 km/sec in air with a pressure before the front of 0.1 mm Hg, and also the measured intensity in the 0.55 to 1.0 μ spectral interval [14]. The difference between the theoretical curve and the experimental points is not surprising, since in this spectral interval there are other sources of radiation which are not taken into account in the calculation (recombination radiation and nitrogen atomic lines), and the temperature, density and concentration in the relaxation zone are only known approximately due to the inaccurate reaction constants. In spite of this, the radiation intensity distribution obtained behind the shock wave front corresponds to the observed distribution. Thus, we may use this method to calculate the intensity of nonequilibrium radiation behind the front of a normal shock wave.

There is another way to calculate the intensity of radiation from the nonequilibrium zone behind a normal shock wave [22], which is used in a study of the chemical relaxation of air behind a normal shock wave with allowance for radiation in [23]. In this study, the energy conservation equation takes into account the loss of energy due to radiation, and three reactions of electron excitation and three reactions of the radiation of the first and second positive band systems of nitrogen molecules and the first negative band system of the molecular ion of nitrogen were added to the system of reactions. In order to calculate the intensity of radiation from the solutions of the equations

of kinetics, the concentration of excited molecules was selected, and the average spectral characteristics of the molecules were given in [22]. The value of the integral nonequilibrium radiative /313 flux which was obtained coincided with the experimental value. Calculations confirmed that allowance for de-excitation lead to the dependence of the total flux of radiation from the nonequilibrium zone on the altitude. This method of calculating the intensity of nonequilibrium radiation has no particular advantages over the former method, since even when the radiation is accurately averaged within the limits of one band according to the method given in [22], the mechanism and the cross sections of the molecular electron excitation remain unexplained. For reliable determinations of nonequilibrium radiation, the first method was preferable due to its simplicity. However, the second method gives even more precise results, if the optical characteristics of the molecules are completely known.

The mechanism of excitation for the first negative band of the molecular ion of nitrogen N_2^+ was studied in [24]. The excitation cross section of N_2^+ by electron impact and by the vibrationally excited molecule of nitrogen was obtained, and it was shown that for flight velocities of $V_\infty \leq 6$ km/sec the second excitation mechanism plays the primary role, and for $V_\infty \geq 8$ km/sec, the first mechanism plays the primary role.

The three-dimensional distribution of the radiant flux falling on a sphere with a radius of 60 cm, which moves at an altitude of 60 km at a velocity of 10.7 km/sec, was calculated in [14] as follows. The modified Newton theory was used to calculate the pressure distribution behind the shock wave and on the sphere surface. Under the assumption that the gas flow behind the shock wave is equilibrium flow, the position of the streamtubes was determined. In addition, using the calculations

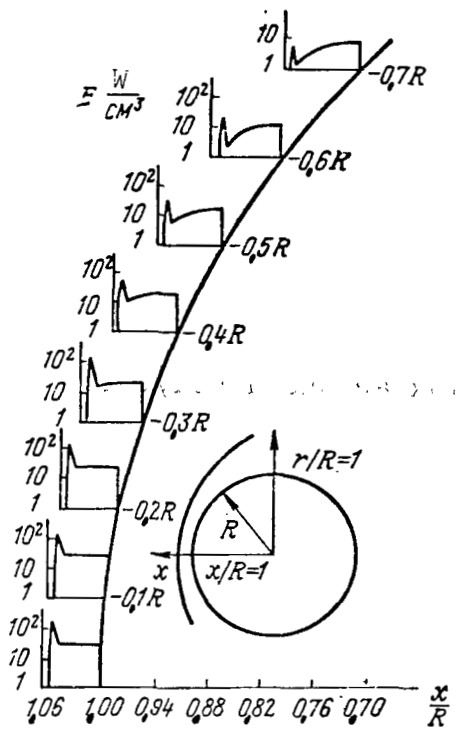

Figure 6.6. Radiation intensity distribution in shock layer.

R — sphere radius; x — distance from center of sphere; r — radius of circular cylinder.

of thermodynamic properties and the gas composition behind the normal shock wave, the parameters were examined along each streamtube. Then the new position of the streamtube was determined, and the iteration process was repeated until the position of the streamtubes did not change. The distribution of the gas concentration and parameters along the streamtubes, just as behind a normal shock wave, was used to calculate the radiation field according to Formulas (6.26) — (6.28) with allowance for radiation in the equilibrium zone. The assumption was implicitly introduced that the width of the relaxation zone and the distance from the shock wave up to the location of maximum radiation intensity in the streamtube were the same as behind a normal shock wave. Figure 6.6 gives the results of this calculation in the form of the radiation intensity distribution in cross sections produced by the intersection of the shock layer with circular cylinders having different radii r, whose axis coincides with the flow axis of symmetry. Although the intensity of radiation emitted by the nonequilibrium zone is much greater than the intensity of the radiation in the equilibrium zone, the proportion of nonequilibrium radiation in the radiation integral flux is small. Figure 6.7 shows the distribution of the radiation integral flux on the surface of the body in the flow, calculated from the radiation

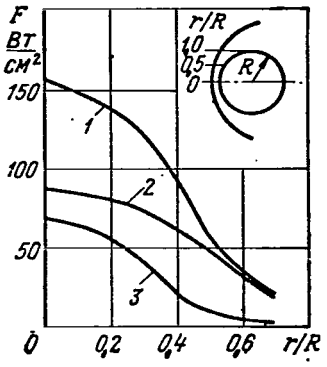

Figure 6.7. Distribution of radiant flux over sphere surface: 1 - total radiation; 2 - equilibrium radiation; 3 - nonequilibrium radiation.

intensity distribution shown in Figure 6.6, without allowance for absorption, and also the distribution of nonequilibrium and equilibrium radiant thermal fluxes.

For an estimate of the radiant flux around a body, a calculation similar to that given in above will be satisfactory, but it cannot be confirmed a priori that the distribution of the parameters in the stream-tube will be identical to the distribution behind the normal shock wave. Therefore, it will be more accurate to make a detailed calculation of flow around the body, with allowance for chemical reactions and radiation, having in mind the removal of energy by radiation and allowance for absorption in the shock layer. However, unreliable values /314 of the velocity constants of the chemical reactions and the ionization rates at high temperatures prevent this type of complex calculations. In addition, the excitation mechanism has not been studied, and there are no data on the transverse cross sections for different systems of molecular bands. The behavior of the vibrational temperature and the temperature of the molecular electron excitation, as well as their interconnection with the translational temperature of the gas, have not been clarified. Generally speaking, it would be most valid to study a nonequilibrium gas and its radiation [25, 26]. However, such an analysis is extremely complex and very little success has been reached in this area.

6.4. Radiation thermal fluxes and the flow of a radiant inviscid gas around blunt bodies

The first problem to appear historically in radiation gas dynamics was the problem of determining the radiation thermal fluxes which fall on the surface of a body entering the atmosphere. For entry velocities on the order of the first cosmic velocity, the temperatures in the equilibrium shock layer are moderate and the influence of radiation on the gas flow will be insignificant. Therefore, the radiation thermal flux may be represented in the form of an addition to the convective flux, and it may be calculated from the flow field which is unperturbed by the radiation. /315

However, at atmospheric entry velocities on the order of the second cosmic velocity, it was shown above that the radiation may have a great influence on the gas flow in the shock layer, and the radiation thermal fluxes will be comparable with the convective fluxes, and may even exceed them. A qualitative diagram (Figure 6.8) [27] gives the regions of altitudes and flight velocities for which the parameters behind the shock wave make it possible to use certain approximations to calculate the flows of a radiant gas. We may distinguish between four cases of flows of an equilibrium radiant gas. In the first place, when the radiation has very little influence on the gas flow ($W \ll 1$), the shock layer remains approximately isothermal. On the other hand, at $W \gtrsim 1$ the removal of energy by radiation from the shock layer leads to the fact that the gas particle temperature decreases as the braking point is approached. These two cases without absorption of the radiation in the shock layer must be supplemented by two cases with absorption.

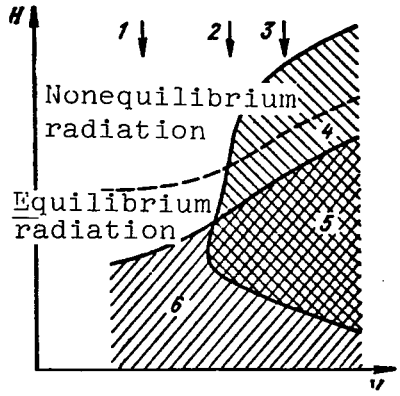

Figure 6.8. Diagram of altitude-velocity (dashed line — boundary of equilibrium and nonequilibrium flows).

1 — satellite velocity; 2 — return velocity from the Moon; 3 — return velocity from Mars; 4 — removal of radiation energy; 5 — radiation absorption and energy removal by radiation 6 — radiation absorption.

The equilibrium radiant flux at the braking point is obtained by adding the contributions to radiation from all the elementary volumes of the shock layer

$$F=\frac{1}{4\pi}\int\frac{E(\rho, T)}{r^2}dV, \qquad (6.32)$$

where r is the distance from the braking point to an element of the volume dV. Since the distance from a detached shock wave up to a body with the bluntness radius R approximately equals $R\rho_\infty/\rho$, where ρ_∞ and ρ are the gas density before and after the shock, then the distance from the shock wave to the body is small as compared with the bluntness radius. Therefore, we may regard the radiation at the critical point of a blunt body in the same way as if it had originated from an infinitely flat layer of gas with a thickness equal to the shock wave stand-off distance Δ. For a nonabsorbing, isothermal shock layer ($W \ll 1$; $\omega \ll 1$), the expression for the flux of radiation falling on the body at the critical point will be /316

$$F=\frac{1}{2}E(\rho, T)\Delta, \qquad (6.33)$$

or

$$F=\frac{1}{2}E(\rho, T)R\frac{\rho_\infty}{\rho}. \qquad (6.34)$$

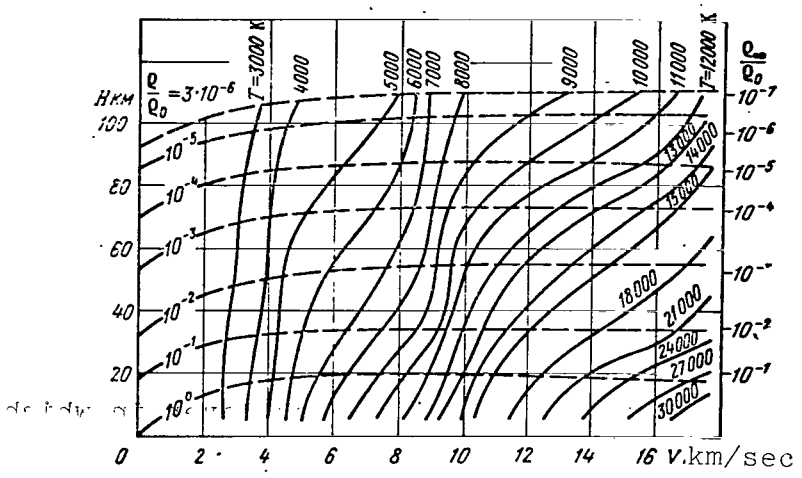

Figure 6.9. Temperature and velocity directly behind shock wave in standard atmosphere.

The coefficient 1/2 is introduced in these expressions, since the energy is emitted to both sides of an infinitely flat layer. The radiant thermal flux for an isothermal boundary layer is proportional to the radius of the forward part R, whereas the convective flux will be inversely proportional to $\sqrt{R}$. Using the graphs in Figure 6.9 [28] and Figure 6.10 [27], with Formulas (6.33) and (6.34) we may rapidly establish the radiant thermal flux at the critical point of a blunt body with a given radius of bluntness.

Unfortunately, this simple method of determining the equilibrium radiant flux falling on a body entering the atmosphere gives satisfactory results only in a limited range of altitudes and flight velocities, when we may disregard the influence of radiation on the gas flow in the shock layer and the gas may be assumed to be optically transparent, i.e., it does not absorb radiation. Allowance for these factors decreases the radiant thermal flux on the body, and this method of

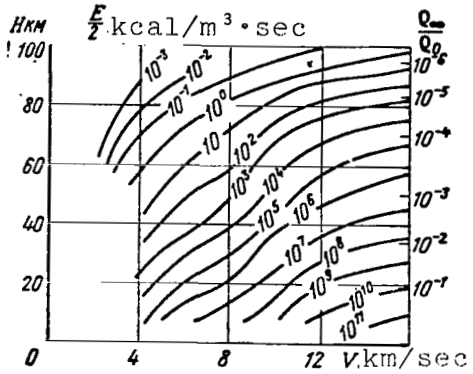

Figure 6.10. Equilibrium radiation intensity.

determining the radiant flux may give results which are too high. Therefore, for these cases of gas flow in a shock layer, which is assumed to be a plane parallel layer, the radiant thermal flux may be calculated according to other formulas. /317

For a shock layer in which radiation absorption is not taken into account, but only removal of energy by radiation, the radiant thermal flux at the critical point is

$$F=\frac{1}{2}\int_0^{\Delta} E(\rho, T)\,dx. \tag{6.35}$$

In the case of a nonisothermal layer with allowance for absorption, we have

$$F=2\pi\int_0^{\infty}\int_0^{\omega_\nu^0} B_\nu(t)\,E_2(\omega_\nu^\circ - t)\,dt\,d\nu. \tag{6.36}$$

Here

$$\omega_\nu=\int_0^{x} k_\nu dx;\quad \omega_\nu^\circ=\int_0^{\Delta} k_\nu dx;\quad E_2(t)$$

is the integral exponential function, determined by the formula

$$E_n(t)=\int_0^1 u^{n-2}\exp(-t/u)\,du. \tag{6.37}$$

For an isothermal absorbing layer, the radiant thermal flux at the critical point will be

$$F=2\pi\int_0^\infty B_\nu\left[\frac{1}{2}-E_3(\omega_\nu^\circ)\right]d\nu. \qquad (6.38)$$

As may be seen from these formulas, to calculate the radiant thermal fluxes at the critical point it is necessary to know the dependence of the volumetric coefficient of radiation absorption k_ν on the temperature and pressure of air, and the radiation frequency. A great many studies have been devoted to calculating the radiation absorption coefficients for air and to verifying them experimentally. The final results of these calculations are given in [29 and 30], which contain an extensive bibliography on this problem.

In [29] when calculating the absorption coefficient, the /318
vibrational-rotational structure of molecular spectra was taken into account, and the photoionization spectra were obtained according to the quantum defect method with individual allowance for all levels of the atoms of oxygen, nitrogen, and their ions. The line radiation of atoms and ions was calculated with allowance for the multiplet structure of the lines having a mixed dispersion-Doppler contour with a linear and quadratic Stark mechanism of expansion. The results of this calculation from [29] are given by way of an example in Figure 6.11 at an air pressure of p = 1 kG/cm^2 and different temperatures. The com- /319
plexity of the real absorption coefficient spectrum presented here shows how cumbersome detailed calculations will be of radiant thermal fluxes using formulas (6.36) and (6.38).

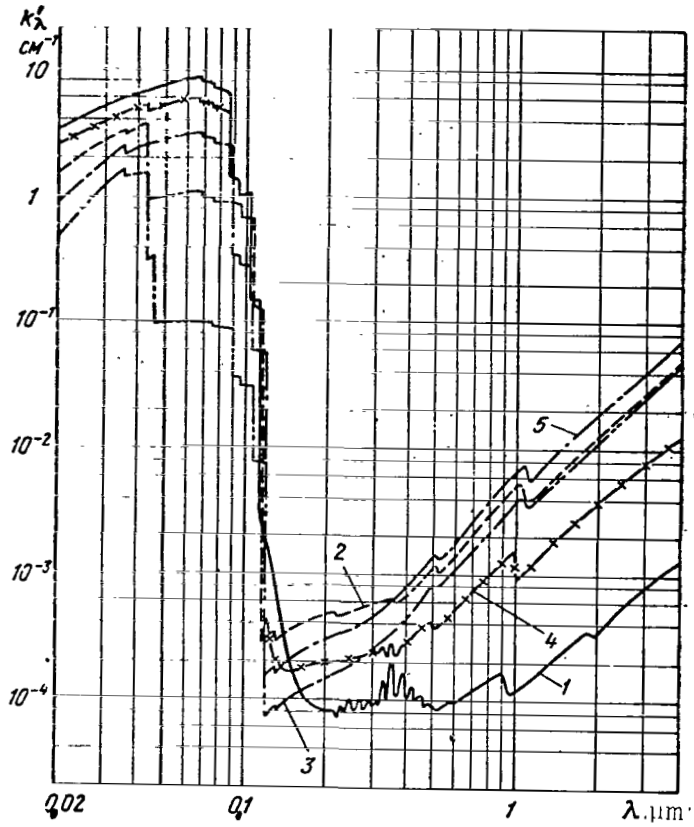

Figure 6.11. Radiation absorption coefficient in air at a pressure of p = 1 kG/cm^2.

1 — at T = 10,000 K; 2 — at T = 14,000 K; 3 — at T = 20,000 K; 4 — at T = 12,000 K; 5 — at T = 16,000 K.

To calculate the radiant thermal flux from an isothermal absorbing layer, the following expression is sometimes used instead of Formula (6.38)

$$F = \varepsilon \frac{\sigma}{\pi} T^4, \qquad (6.39)$$

where T is the gas layer temperature; $\sigma = 5.6694 \cdot 10^{-12}$ W·cm^{-2}·deg^{-4} — Stefan-Boltsmann constant; and ε — degree of blackness of the isothermal absorbing layer of gas. The calculated values

of the degree of blackness of the air layer are given in [31], and in [32] which includes the most recent achievements in the study of elementary radiation processes.

In the general case, to calculate the radiant thermal flux falling on the body entering the atmosphere, it is necessary to know the parameter distribution in the shock layer, which must be determined with allowance for radiation. Problems of the flow of an optically transparent gas around bodies ($\omega \ll 1$) have been studied most extensively, in which the radiation absorption is disregarded. In this case, as was already noted in Section 6.2, the equations of gasdynamics with allowance for radiation are greatly simplified and become purely differential equations. The difference between the problem of inviscid flow of a nonabsorbing gas around bodies and flow without radiation may be reduced to an additional term in the energy equation which designates the heat sink (distributed over the gas volume) with a strength which depends on the local conditions. Such an insignificant complication in formulating the problem of the flow of a nonabsorbing gas around bodies makes it possible to use the regular methods to solve them which are applied to problems without radiation.

In formulating the problems of inviscid flow of a radiant gas around blunt bodies, the following assumptions are commonly made: the gas in the shock layer is in local, thermodynamic and chemical equilibrium; none of the vapors from the body enter the shock layer; the thickness both of the shock wave and the boundary layer is small as compared with the distance of the shock wave to the body, and the gas viscosity and thermal conductivity in the entire shock layer are not taken into account.

The flow of an optically transparent gas at the critical point of a blunt body was examined in [33, 34, 35] under the assumption that the radiation had a small influence on the gas flow ($\omega \ll 1$, $W \ll 1$). Assuming that the flow in the vicinity of the critical point is one-dimensional in the case of hypersonic flow, by disregarding the influence of radiation on the gas pressure and velocity profile in the shock layer, we may reduce the system of gasdynamic equations to one energy equation. This formulation makes it possible to determine the temperature profile or the enthalpy profile across the shock layer, its thickness, and the value of the radiant thermal flux at the critical point. The study [36] used the method of truncation /320
of series according to a given form of the shock wave to obtain the flow parameters and the contour of a body in the flow in the vicinity of the critical point for several values of the parameter W. The qualitative nature of the influence of radiation on flow around a blunt body was also studied.

The reports [37, 38, and 39] studied an inviscid, optically transparent gas around blunt bodies. The most comprehensive study was the solution of the flow around a sphere given in [38, 39], which obtained the distribution of parameters in the subsonic region behind a curved shock wave. These studies used different methods of solving a differential system of gas dynamic equations with volumetric de-excitation (the method of straight lines was used in [38], and the method of integral relationships was used in [39]). The qualitative nature of these results in both studies is the same.

By way of an example, let us give the formulation of the problem and the results obtained in [38]. In a spherical coordinate system (r, ν, φ), the equations of gasdynamics were solved which describe the flow of a nonabsorbing, ideal gas behind a

detached shock wave before a sphere. The expression for the vector divergence of the radiant flux in the case of volumetric de-excitation (6.23) was given in the form of a power function of enthalpy and gas density. The real nature of the air properties behind a hypersonic shock wave were taken into account by means of the effective ratio of the heat capacities. The method of straight lines was used for the calculation [40], according to which, in the region where the solution is found, n rays are drawn from the center of a sphere, and, using the values of the functions, the intermediate values of the desired functions are approximated on the rays. This makes it possible to express the derivatives with respect to ν in the equations of gasdynamics in terms of the functions on the rays, and to obtain a system of ordinary differential equations which may be integrated over the rays. The well-known relationships for a shock are used on /321 on the surface of a shock wave, whose equation is also given in the form of the approximate polynomial $\Delta = \sum_{i=1}^{n} \Delta_i \vartheta^{2i}$. The solution of the problem may be reduced to selecting those stand-off distances Δ_i on the rays at which the velocity component u = 0 is normal to the sphere. On the zero ray, the transverse velocity component v vanishes, and v'_0 is introduced — the derivative of the transverse velocity component with respect to ν on the zero ray, referred to the velocity of the advancing flow.

Figures 6.12 — 6.16 give the results of calculating the flow of air around a sphere with the radius R = 1 m at a velocity of V_∞ = 11.4 km/sec at an altitude of 60 km [38]. The velocity component u which is normal to the body and the transverse velocity component v, which are presented in the graphs, refer to V_∞, the density ρ refers to the density of the advancing flow, and the enthalpy h refers to the square of the advancing flow velocity. The radiation thermal flux on the surface of the sphere

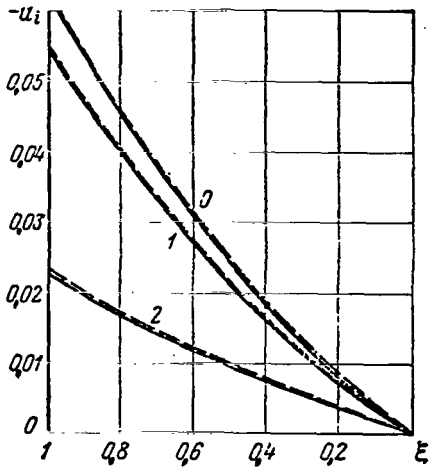

Figure 6.12. Distribution of normal velocity component of gas in a shock layer (solid lines — with allowance for radiation; dashed lines — without radiation). 0 — at $\nu = 0$; 1 — at $\nu = 0.3125$; 2 — at $\nu = 0.625$.

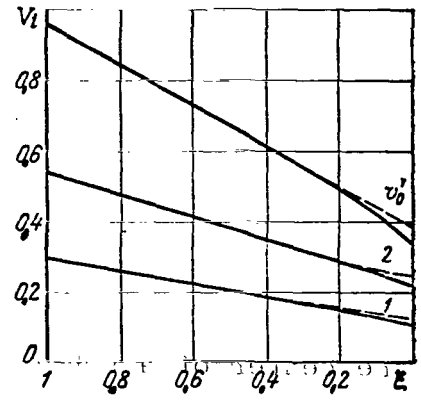

Figure 6.13. Distribution of tangential velocity component of gas in a shock layer (notation is the same as in Figure 6.12).

F refers to its value at the critical point. The values of these quantities are given in the rays which are located at the angles $\vartheta_0=0$; $\vartheta_1=0{,}3125$; $\vartheta_2=0{,}625$. The coordinate across the shock layer is $\xi=(r-R_b)/\Delta$. The value $\xi = 1$ corresponds to the wave; $\xi = 0$ — to the body. The boundary condition on the body ($u = 0$) is satisfied within an accuracy of no less than 0.1%. The shock wave stand-off distance along the rays is $\Delta_0 = 0.04601$, $\Delta_1 = 0.04869$, and $\Delta_2 = 0.05992$ for a flow with radiation and $\Delta_0 = 0.04798$, $\Delta_1 = 0.05066$, and $\Delta_2 = 0.06181$ — without radiation.

This example illustrates the general properties of inviscid /322 flows of a nonabsorbing gas around blunt bodies. The parameters of the shock layer undergo the greatest change, as compared with flows without radiation, in the vicinity of the braking point, since the gas particles remain here longer due to their lower velocity and undergo greater de-excitation. The radiation has

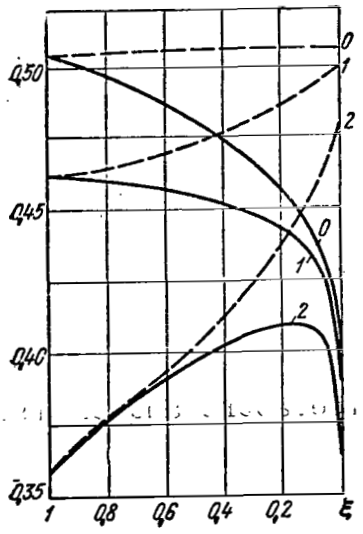

Figure 6.14. Distribution of gas enthalpy in shock layer (notation the same as in Figure 6.12).

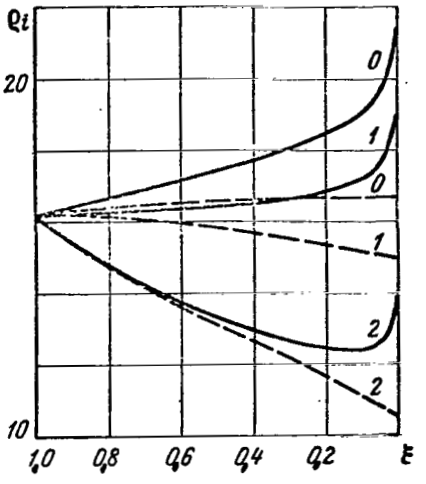

Figure 6.15. Distribution of gas density in shock layer (notation the same as in Figure 6.12).

the greatest influence on the distribution of enthalpy and density of the radiant gas; the influence on the velocity distribution of the flow geometry is much less.

De-excitation of the energy by the gas decreases its enthalpy and temperature, which is particularly great near the body surface. Therefore, the gas pressure across the shock layer is almost constant. This leads to additional condensation of the gas behind the shock wave, which is located close to the body surface. The sharp decrease in enthalpy and increase in the gas density close to the body surface points to the presence of a thin boundary layer, which is usually called the radiation entropy layer [36, 38, 41], which has an influence on the boundary layer parameters and on the processes of gas heat exchange with the body.

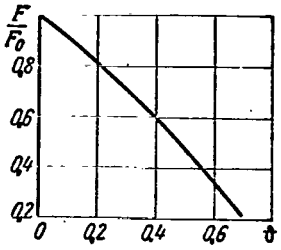

Figure 6.16. Radiant thermal flux distribution on sphere surface. $F_0=1.2 \times 10^3$ kcal·m^{-2}·sec^{-1}.

A decrease in the gas temperature and thickness of the shock layer leads to a decrease of the radiation thermal flux on the body surface. However, it is not possible to obtain the value of the temperature of an optically transparent gas on the body surface, since the temperature and enthalpy of the gas vanish on a body surface in the inviscid case. This occurs because an element of the gas on the zero streamline will radiate until it does not liberate any energy, and then the static enthalpy and temperature of the gas vanish on the body surface. This characteristic of flow without allowance for radiation was first noted in [42, 33], and later in [43, 44]. The sharp decrease in the temperature occurs in a very close vicinity to the body surface, and therefore, this characteristic has no great influence on the distribution of quantities in the inviscid shock layer or on the radiation thermal flux on the body. Attempts have been made to eliminate this characteristic [34, 45, 46]. It was established in [46] that for a very small, but finite absorption coefficient, the gas temperature on the body surface equals the body temperature.

As was already noted, in [34] the problem of the flow of a radiant gas around the critical point of a blunt body, under the condition that the radiation is absorbed in the contracted layer, was reduced to solving one integral — differential equation of energy:

$$\rho u \frac{\partial h}{\partial z} = -\pi k \left[4B - 2\int_0^{\omega} BE_1(\omega-\xi)d\xi - 2\int_{\omega}^{\omega_0} BE_1(\xi-\omega)d\xi \right]. \qquad (6.40)$$

Here ρ, h, and u are the density, enthalpy, and gas velocity, respectively, across the shock layer at the critical point; $\omega = kz$ — optical thickness of the gas; k — average absorption coefficient of the gas; z — coordinate (z = 0 corresponds to the wave; $z = z_0$ — to the body); $B = (\sigma/\pi)T^4$ — Planck function averaged over frequency; E_1 — integral, exponential function determined by (6.38). /323

The right side of Equation (6.40) represents the precise expression for the vector divergence of the radiant flux for a plane-parallel layer of gas with an arbitrary optical thickness. In the case of an optically transparent gas ($\omega \ll 1$), only the first term remains in this expression. To allow for absorption, the studies [34 and 45] used the method of "approximation based on the local temperature," which consists of the fact that the quantity B under the integration sign is expanded in Taylor series in the vicinity of its local value ($\omega = \xi$). However, neither retaining the first term of the expansion [34] nor the first two terms [45] make it possible to obtain the correct temperature on the boundary between the gas and the body surface, because there the expansion has no meaning. This characteristic is eliminated by allowing for the viscosity and thermal conductivity in the boundary layer. However, it is of interest to establish the real (in physical terms) behavior of the temperature in the case of inviscid radiant gas.

The nature of the characteristics occurring in the case of flow of an inviscid gas with an extremely small optical thickness around a critical point was discovered in [47]. This study obtained the asymptotic (in the sense of $\omega \to 0$) solution of Equation (6.40), which has the form

$$B(\omega)=\frac{\omega_0|\ln\omega_0|}{2}\left[1-\left(1-\frac{\omega_0|\ln\omega_0|}{2}\right)\left(\frac{\omega_0-\omega}{\omega_0}\right)^2\right]^{-1}. \qquad (6.41)$$

Here

$$\Omega=\frac{1}{2}W\omega_0^2|\ln\omega_0|$$

The quantity B refers to its value at the wave, and W is the parameter arising during the dimensional analysis of Equation (6.40) and characterizing the influence of radiation on the gas flow.

Let us consider the solution. On the wave (ω = 0) the function B(0) = 1 and on the body ($\omega = \omega_0$) the value

$$B(\omega_0)=\frac{1}{2}\omega_0|\ln\omega_0|.$$

When ω_0 strives to zero, the function B strives to unity everywhere, except the point $\omega = \omega_0$, where B strives to zero. Figure 6.17 shows the asymptotic solution (6.41) for W = 1 and different values of ω_0. A comparison of the numerical solution of the integral — differential equation (6.40) with the asymptotic solution showed [47] that they practically coincide for optical thicknesses of the shock layer $\omega_0 < 0.01$.

The asymptotic solution (6.41) shows that allowance for radiation absorption in the shock layer leads to a finite gas temperature at the wall at the critical point $T\sim(\omega_0|\ln\omega_0|)^{1/4}$. It strives to zero with a decrease in the shock layer optical thickness. The particular nature of the energy equilibrium of /324
a particle of radiant and absorbing gas at the critical point on the zero streamline thus becomes apparent. In this case, the

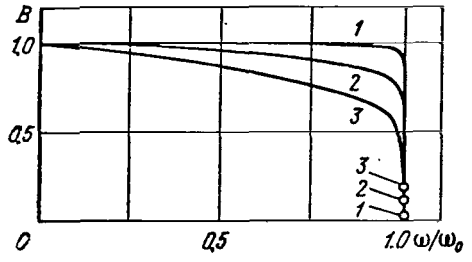

Figure 6.17. Behavior of asymptotic solution (6.41) for differing values of the optical thickness of the shock layer.
1 — at $\omega_0 = 0.01$; 2 — at $\omega_0 = 0.1$; 3 — at $\omega_0 = 0.3$.

particle emits as much energy as it absorbs from the entire volume of the radiant gas. Therefore, with an arbitrarily small, but finite optical thickness of the shock layer, the gas temperature on the surface of the body in the flow will be finite.

The authors of [47] call this type of equilibrium equilibrium "on the average," in contrast to complete thermodynamic equilibrium, which occurs at the critical point under other physical conditions — for example, in the case of nonequilibrium gas flow. This type of equilibrium is common for radiation, and occurs not only for grey gas, but also in the case of an arbitrary dependence of the absorption coefficient on frequency. The use of equilibrium "on the average" makes it possible to obtain a simple, general condition for determining the gas temperature at the critical point. For this purpose, it is necessary to set the vector divergence of the radiant flux equal to zero.

For any point on the body surface, the condition for determining the gas temperature may be expressed as follows

$$\rho v \frac{\partial H}{\partial s} = \operatorname{div} \vec{F}, \qquad (6.42)$$

where v is the velocity of the gas tangent to the body surface; H — total enthalpy, and d/ds — derivative along the surface.

The conclusion regarding the non-zero value of the gas temperature at the critical point of a blunt body in the case of radiation absorption was later confirmed in [48, 49].

Let us give other examples of solving the problem of flow of an inviscid, radiant and absorbing gas around blunt bodies. Absorption of radiation by an optically grey gas was taken into account in [50] by means of the so-called "differential approximation," within the framework of which the multi-dimensionality of the problem and radiation absorption in a shock layer may be considered. In this approximation, the exact differential equation of radiation transport is replaced by an approximating system of moment equations as follows. The moments are introduced for the radiation intensity of an optically grey gas:

/325

$$\left.\begin{aligned} I_1 &= \frac{1}{4\pi}\int I(\vartheta)\,d\Omega; \\ I_2 &= \frac{1}{4\pi}\int I(\vartheta)\cos\vartheta\,d\Omega; \\ I_3 &= \frac{1}{4\pi}\int I(\vartheta)\cos^2\vartheta\,d\Omega; \\ &\cdots\cdots\cdots\cdots \end{aligned}\right\} \qquad (6.43)$$

Here integration is performed over all solid angles. The first moment represents the average radiation intensity; the second moment represents the radiation energy flux; the third moment represents the radiation pressure. Multiplying the radiation transport equation

$$\cos\vartheta_i\frac{dI}{dx_i} = k(B-I), \qquad (6.44)$$

written for a grey gas on the ray $\vec{s}$, which makes the angle ϑ_i with the axis x_i, by the power $\cos\vartheta_i$ and integrating the relations obtained over all solid angles, we obtain an infinite system of equations for the moments. This system approximates the transport equation. The system is truncated in this case by a method

advanced by Eddington (Milne-Eddington [1 – 4] approximation). This method assumes that at the third moment the radiation intensity is absorbed which does not depend on direction. Then $I_3 = \frac{1}{3} I_1$, and the approximating transport equation of the system assumes the form

$$\frac{dF_i}{dx_i} = k(\pi B - I_1); \tag{6.45}$$

$$\frac{dI_1}{dx_i} = 3kF_i. \tag{6.46}$$

Since (6.45) represents the i-th component of the vector divergence of the radiant flux, the system of equations for the gasdynamics of a radiant gas becomes a purely differential system. This system was solved in [50] for different values of the shock layer optical thickness by truncation of the series, and the flow field and radiation around a blunt body, whose form was determined from the given form of the shock wave, were obtained. The authors of [50] emphasized that the solution they obtained was approximately accurate in the entire flow field and for all optical thicknesses. For large optical thicknesses of the shock layer, no singularities should exist on the boundary between the gas and the body, since a singularity arises only in the approximation of an optically transparent gas. However, since the temperature and other gas parameters on the body surface are determined from solving the system of differential equations within an accuracy which depends on the accuracy with which the condition of no flow on the body is satisfied, the results on the body have a certain degree of indeterminancy. Particularly apparent indeterminancy must appear in the case of flows with small values of the optical thickness of the shock layer ω and

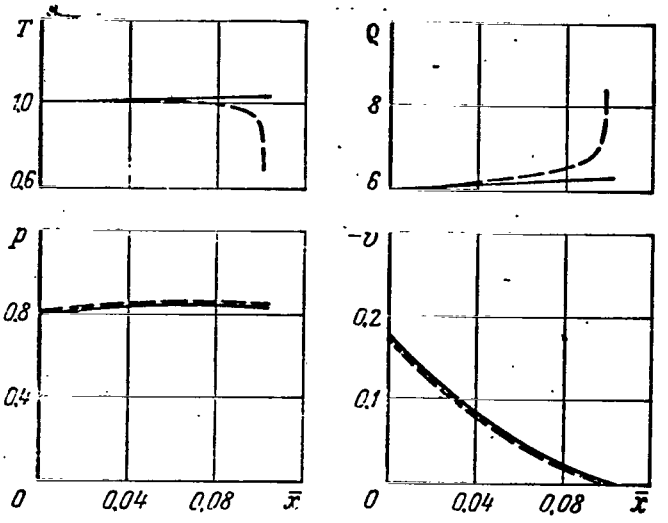

Figure 6.18. Distribution of relative values of temperature, density, pressure, and normal velocity component of gas in a shock layer (solid lines — without radiation; dashed lines — with allowance for radiation).

the parameter W (these parameters are designated by Bu and Γ, respectively, in [50]).

Figure 6.18, which was taken from [50], shows the relative values of temperature T, density ρ, pressure p, and the normal velocity component v along the braking line for Γ = 0.04 and Bu = 0.08. It may be seen from the graphs that the gas temperature close to the body surface decreases so sharply that small errors in determining the coordinate of the body surface may lead to very inaccurate values of the temperature. Therefore, in solutions of this type we must determine the gas temperature /326 on the body boundary from the condition of equilibrium "on the average."

Recently, calculations have been performed of the flow of an inviscid radiant and absorbing gas around blunt bodies, taking into account selectivity of radiation along the wavelengths [51 — 55]. In addition to the general assumptions given above, the studies [51 — 55] used the method of straight lines [40] to calculate flow around a sphere. To take into account the multidimensionality of the radiation field, it was assumed that the radiant shock layer in each cross section may be approximated by a plane-parallel layer of gas with the same distribution of parameters as in the cross section being considered. The calculations in these studies were performed by the method of successive approximations. In a calculation of the vector divergence of the radiant flux, it was assumed that the distribution of the gasdynamic parameters was known. The model of the radiant air in [51] was taken from [29], and in [52], it was taken from [30]. The distribution of $\mathrm{div}\vec{F}$ within the layer was used to solve the system of gasdynamic equations, and this procedure was repeated until the subsequent approximation coincided with the previous one.

These calculations have confirmed all of the qualitative /327
results on the influence of radiation obtained above. The solid line in Figure 6.19 designates the distribution of the radiation thermal flux along the front surface of a sphere with a radius of one meter, taken from [51], for a velocity of 10.5 km/sec at an altitude of 65 km; the dashed line, taken from [52], is for a velocity of 10 km/sec.

The flow around a sphere was also calculated in [53] by the method of integral relationships. To allow for the multidimensionality of the radiation field, the method of spherical harmonics was used, which made it possible to obtain a differential system of equations approximating the transport equation.

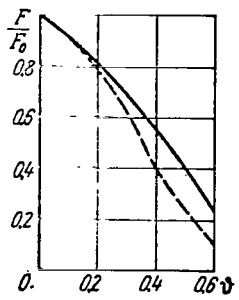

Figure 6.19. Distribution of radiant thermal flux over sphere surface (solid line at V_∞ = 10.5 km/sec, H = 65 km [51]; dashed line at V_∞ = 10 km/sec [52].

The first approximation of the method of spherical harmonics, used in this study, leads to the same differential equations as the Milne-Eddington approximation which is known in astrophysics.

In order to decrease the number of calculations necessary to solve the transport equation for each radiation wavelength, some authors [54, 55] have used simple stepped models for the absorption coefficient. The study [55] is interesting in that the method of adjustment is used to solve an integral — differential system of equations describing the flow of a radiant gas. In the opinion of the author of [55], the method of adjustment requires much less machine time and is particularly suitable for solving three-dimensional problems.

The qualitative agreement of the results of all studies mentioned in this section must be noted. However, a quantitative comparison of these results is difficult, just like the comparison of the machine time required for the calculations.

6.5. Flow of radiant viscous gas

As has already been repeatedly pointed out, when spacecraft enter the atmosphere of the Earth at velocities on the order of the second cosmic velocity and higher, radiation begins to have a great influence on the gas flow in the shock layer, and the radiant thermal fluxes on the surface of the spacecraft may

exceed the convective fluxes. The picture of the flow of gas in the shock layer under the influence of radiation changes, and the profiles of gas enthalpy and density sharply change. The shock wave is located closer to the spacecraft surface. In this case, it is impossible to calculate the convective thermal fluxes, without taking into account the interaction between radiation and the flow field.

This section is devoted to flows of a viscous radiant gas around blunt bodies entering the atmosphere of the Earth at hypersonic velocities. Viscous shear flows (Couette flow), flows in tubes and channels, and also flows around a wedge, cone, and plate will not be considered, since the influence of radiation in the boundary layer on the front surface on a landing spacecraft will be insignificant.

In aerodynamics, the flow field in the vicinity of the critical point of a blunt body is usually divided into inviscid flow in the shock layer and into a viscous boundary layer. The solution for the boundary layer gives the convective thermal flux on the body surface, and the conditions on the outer boundary of the boundary layer are determined by solving the problem of inviscid flow. The interaction of radiation with the flow field /328 is apparent, in the first place, in the fact that the gas enthalpy in the shock layer changes due to energy transport by radiation. In the second place, the gas velocity gradient changes along the outer boundary of the boundary layer. In the third place, it is necessary to consider additional boundary conditions to solve the equation of radiation transport in the boundary layer. Consequently, the conditions on the outer boundary of the boundary layer change as compared with the flow of a nonradiant gas, and it becomes complicated to determine these conditions [56, 57]. Therefore, in the first studies which were performed on the

concurrent influence of radiation and convection in the flow around blunt bodies, it was assumed [58, 59], and is still being assumed [60], that, due to the gradient (which is produced when radiation is considered) of the gas enthalpy across the shock layer, it is necessary to consider the molecular transport processes in the entire shock layer.

The concept of a completely viscous shock layer was used by many authors for a concurrent calculation of convective and radiant thermal fluxes at the critical point of a blunt body. However, this concept for shock layers, in which the Reynolds number Re_s calculated for conditions behind the shock wave exceeds 10^4, leads to an invalid complication of the calculation. This makes it necessary to use simplifying assumptions which decrease the reliability of the results obtained, and make it impossible to calculate three-dimensional flows. Therefore, for large Reynolds numbers for a shock wave, it is desirable to divide the shock layer into inviscid and viscous regions, especially since the methods of calculating the inviscid flow of a radiant gas around blunt bodies have been developed (see Section 6.4).

Studies performed in [61, 52] showed that the temperature gradients in a shock layer, caused by the outflow of radiation, are much less than the temperature changes in the boundary layer close to the body, and the influence of the boundary layer radiation on the flow in the shock layer is small. The magnitude of this influence does not exceed the magnitude of ordinary viscous interaction. Therefore, at Reynolds numbers $Re_s > 10^4$, it is possible to divide the flow in the shock layer into an inviscid region and a boundary layer, while the conditions on the body for inviscid flow are the precise (in the asymptotic sense

[at $Re_s \to \infty$]) conditions on the outer boundary of the boundary layer [61]. Even in the case when the boundary layer radiation has a great influence on flow in the shock layer, the flow may be divided into viscous and inviscid regions, taking into account the influence of the boundary layer radiation. In this case, flow in the shock layer may be calculated in the same way as intense viscous interaction is calculated, i.e., by the iteration method.

The viscous flow of a radiant gas may be described by a system of Navier-Stokes equations (see Section 5.1), adding to /329
the equation the energy term $\mathrm{div}\vec{F}$ (6.15), which takes into account the transport of radiant energy in the gas. In the general case, to calculate $\mathrm{div}\vec{F}$ it is necessary to solve the equation of radiant energy transport with the corresponding boundary conditions. The characteristic parameters making it possible to establish the influence of radiation on viscous gas flow will be the same: the characteristic optical thickness of the gas layer ω and the energy parameter W. The occurrence of the integral term $\mathrm{div}\vec{F}$ in the Navier-Stokes equation further complicates an extremely complex system of equations for viscous flows. Relatively simple solutions are only obtained in the approximation of radiant thermal conductivity, when the optical thickness of a viscous boundary layer with allowance for radiation is great ($\omega \gg 1$). In this case, the regular and radiant thermal conductivity may be combined [8, 42], and the boundary layer equations obtained from the Navier-Stokes equations assume self-modeling solutions [62]. In the case $\omega \lesssim 1$, which is more interesting for practical applications, we must solve a complex integral — differential system of equations for viscous flows, considering radiation. An optically transparent boundary layer ($\omega \ll 1$) is described by purely differential equations, but there are no self-modelling solutions, since in this case there are

two characteristic lengths of different order in the layer: the width of the boundary layer is proportional to the number $(\mathrm{Re})^{-1/2}$, and the characteristic mean free path of radiation is proportional to $\sim(k)^{-1}$.

It was noted at the beginning of this section that the influence of radiation upon heat exchage in the vicinity of a critical point of a blunt body is studied on the basis of an integral — differential system of equations, which takes into account molecular transport in the entire shock layer. One of the first such studies was [58]. The equations describing the flow of a radiant viscous gas in the vicinity of the critical point were obtained under the assumption that the shock layer thickness at the critical point is much less than the radius of a blunt body ($\Delta R_b \ll 1$, the hypothesis of a thin shock layer, see Section 5.4) and the pressure of the gas across the shock layer is constant (dp/dy = 0). It is assumed that radiation is transported only across the shock layer, and its expression for a plane-parallel gas layer, with allowance for radiation of the body surface, is used for the vector divergence of the radiant flux. The radiation absorption coefficient depends on the frequency, and there are no limitations on the optical thickness of the shock layer. The system of equations obtained may be rewritten by means of regular transformations of the boundary layer (see Section 5.1) under the assumption that all the variables depend only on η. The boundary conditions on the wave and the body surface are regular:

$$\left.\begin{array}{llll} f=f'=0, & h=h_w & \text{for} & \eta=0; \\ f=f_1, & h=1 & \text{for} & \eta=\eta_1. \end{array}\right\} \qquad (6.47)$$

We may integrate the system obtained by the method of successive approximations, assuming that $\operatorname{div}\vec{F} = 0$ in the zero approximation. /330

The gasdynamic formulation of the problem is similar for studying the interaction of radiation with the flow field in the vicinity of the critical point of a blunt body in all earlier studies [59, 63, 67], in which the concept of a completely viscous shock layer was used.* The authors of these studies assume that air in the shock layer is in local thermodynamic equilibrium, the shock wave and the gas in front of it are transparent for radiation from the shock layer, and the radiation is transported only across the shock layer. In principle, these studies differ in the specific form of $\operatorname{div}\vec{F}$ and by the assumptions with respect to the radiation absorption coefficient in the shock layer and the body surface radiation. We shall give expressions for $\operatorname{div}\vec{F}$ below, as well as the basic results of numerical calculations obtained in the studies above.

The expression for $\operatorname{div}\vec{F}$ is described in [59] for a plane-parallel layer of grey gas with the absorption coefficient k which depends only on the local conditions, and the body surface is assumed to be absolutely black:

$$\operatorname{div}\vec{F} = \frac{\partial F}{\partial y} = 2\sigma k\left[\int_0^{\omega_1} T^4 E_1(|\omega - \xi|)\,d\xi - 2T^4 - T_w^4 E_2(\omega)\right]. \qquad (6.48)$$

Here

$$\omega = \int_0^y k\,dy'; \quad \omega_1 = \int_0^\Delta k\,dy';$$

*In some of these studies, the influence of a blast of material from the body surface, which will not be examined here, was studied in addition to radiation.

E_n — is determined by Formula (6.38); T_w — temperature of the body surface.

The study [59] gives the results of numerical calculations (the air absorption coefficients are taken from [68]) of the flow field and convective heat transfer at the critical point for different values of the body bluntness radius and flight regimes. By way of an example, Figures 6.20 and 6.21 [59] give the distribution of parameters in the shock layer and the dependence of the convective heat transfer parameter at the critical point $Nu/\sqrt{Re}$ (5.74) on the entry velocity for several values of the bluntness radius. It may be seen in Figure 6.21 that the convective thermal flux, calculated with allowance for radiation, decreases and strongly depends on the bluntness radius. It is emphasized in [59] that the influence of radiation upon the convective heat transfer cannot only be related to a decrease in the gas enthalpy in the shock layer. Changes in the gas enthalpy and the convective thermal flux due to radiation are not proportional. For example, at R_b = 30.5 cm for flights at a velocity of 15 km/sec at an altitude of 58 km the difference in enthalpy $(h_\delta - h_w)$ due to radiation decreases by approximately 8%, and the convective thermal flux — by 15%. This indicates that, due to radiation, not only the gas enthalpy is changed, but also other parameters on the outer boundary of the boundary layer.

A study is made in [63] of the hypothesis of an optically transparent gas, and therefore $\mathrm{div}\vec{F}$ represents the energy emitted by a unit volume of shock layer per unit time, whose numerical values were taken from [69]. It was assumed in [64] that the air absorption coefficient k_ν depends on frequency, and a body with a constant surface temperature does not emit or reflect radiation. In this case, the expression for $\mathrm{div}\vec{F}$ has the form /331

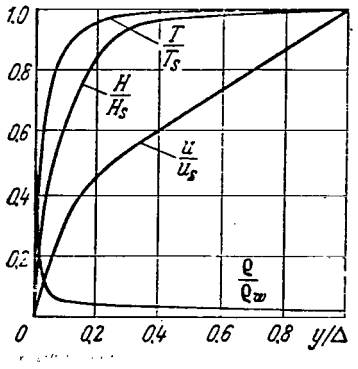

Figure 6.20. Flow field in shock layer at V_∞ = 15.2 km/sec; altitude — 75.6 km; R_b = 1.5 m; H — total enthalpy.

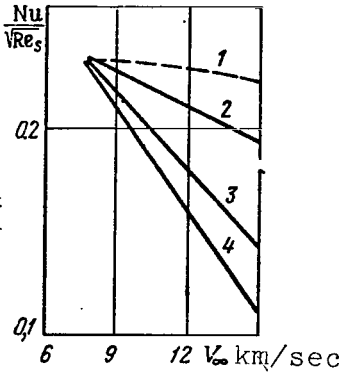

Figure 6.21. Parameter of convective heat transfer with allowance for the influence of radiation at T_w = 1500 K; p_s = 1 kG/cm^2.

1 — without allowance for radiation; 2 — with radiation at R_b = 0.305 m; 3 — at R_b = 0.915 m; 4 — at R_b = 1.525 m.

$$\operatorname{div}\vec{F}=2\pi\int_0^\infty k_\nu\left[\int_0^{\omega_{\nu_1}}B_\nu E_1(|\omega_\nu-\xi_\nu|)\,d\xi_\nu-2B_\nu\right]d\nu. \qquad (6.49)$$

In a calculation of the absorption coefficient, consideration is given to the free-free and free-bound transitions using the formulas from [70], and also the molecular continuum of oxygen (the Schuman-Runge band system with a diffused rotational structure) with the absorption coefficient according to the approximate formula of Zul'tser-Viland

$$k_\nu=1{,}49\cdot10^{-17}\cdot n_{O_2}\left[th\left(\frac{0{,}0975}{kT}\right)\right]^{1/2}\exp\left[-th\left(\frac{0{,}0975}{kT}\right)\times\left(\frac{h\nu-8{,}56}{0{,}805}\right)^2\right] \qquad (6.50)$$

and of nitrogen (Berdzh-Khopfil'd band)

$$k_\nu = 1{,}2 \cdot 10^{-17} n_{N_2} \exp\left[- \left| h\nu - 13{,}6 + \left(1 - \frac{0{,}603}{kT}\right) \right|^{1/3} \right]. \qquad (6.51)$$

In Formulas (6.50) and (6.51), n is the number of particles per cm^3; k_ν — in inverse centimeters; hv and kT in electron volts. On a frequency scale, twenty points were selected, between which the absorption coefficient was described by a linear function. Other radiation processes were not considered. The numerical calculations by the Karman-Pol'gauzen method in [63 and 64] showed that cooling by radiation and self-absorption has a slight influence on convective heating, whereas the radiant flux is greatly reduced. To sum up, the total thermal flux on the body surface /332 for flow with absorption of radiation is decreased as compared with the flow of an optically transparent gas. Figure 6.22 [64] gives the results of calculating thermal fluxes for an optically transparent and non-grey gas, which correspond to conditions for entry into the atmosphere of the Earth by a spacecraft returning from Mars, for different values of the nose bluntness radius. It may be seen from this graph that for a non-grey gas the bluntness radius, for which the total thermal flux is at a minimum, approximately equals 1.2 m, whereas for an optically transparent gas the minimum radius is less than 0.3 m.

We must approach with caution the results obtained by the Karman-Pol'gauzen method, since the representation of quantities in the shock layer by polynomials cannot correspond to the real behavior of a change in these quantities. Thus, in [63], the authors noted that the value of the gas enthalpy, which is represented by a polynomial, at certain points of the shock layer may exceed its value for the wave.

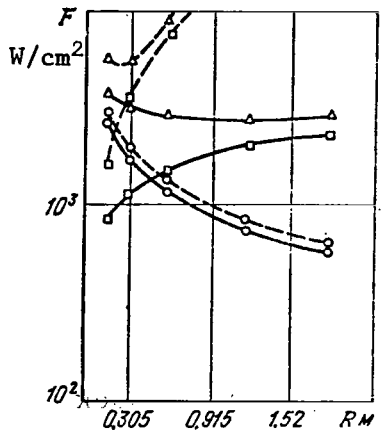

Figure 6.22. Dependence of thermal flux on bluntness radius at V_∞ = 15.25 km/sec at an altitude of 61 km (dashed lines — optical thickness of gas; solid lines — allowing for self-absorption; the dots designate: circles — convective thermal flux; squares — radiant flux; triangles — total thermal flux).

In a calculation of the radiation transport, the study [65] considered (in order of importance) the atomic lines, photoionization, bremsstrahlung, and molecular transitions in real air. The spectral absorption coefficient of air contained five hundred points with respect to frequency. To calculate the absorption coefficient in the atomic lines, including the transitions from the basic states, the Elesasser method was used [71], taking into consideration Stark expansion combined with a dispersion contour. The absorption coefficients for free-free and free-bound transitions were calculated from formulas given in [72, 73].

In the energy equation, radiation was taken into account in [65] by means of an approximate expression for $\operatorname{div}\vec{F}$ taken from [74]:

$$\operatorname{div}\vec{F}=\frac{\partial F}{\partial y}=-\frac{1}{\partial y}\left(\frac{\omega^*\lambda_R}{\omega_R+\omega^*}\cdot\frac{\partial T}{\partial y}\right)+\frac{4\delta T^4\omega_p k_p}{\omega_p+\omega_l}. \qquad (6.52)$$

Here k_p is the average Planck absorption coefficient (6.25);

$\lambda_R=1/k_R$ — inverse value of the Rosseland average absorption coefficient (6.21)

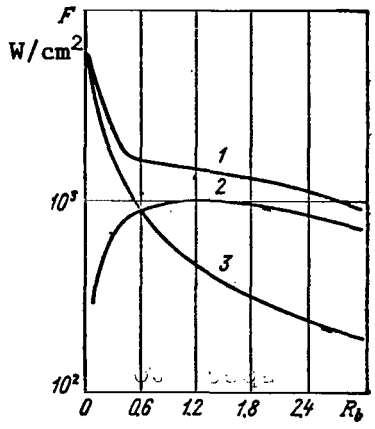

Figure 6.23. Dependence of thermal flux on bluntness radius at V_∞ = 11.8 km/sec at an altitude of 53 km.
1 — total thermal flux;
2 — radiant thermal flux;
3 — convective thermal flux.

$$\omega = \int_0^\infty \int_0^y k_\nu dy' d\nu; \quad \omega_p = \int_0^\Delta k_p dy';$$
$$\omega_R = \int_0^\Delta k_R dy'; \quad \omega_0 = \int_0^\infty \int_0^\Delta k_\nu dy' d\nu$$

is the optical thickness of the shock layer; $\omega' = T_{max}/(\partial T/\partial \omega)$; T_{max} — maximum temperature in the shock layer; $\omega^* = \omega_i[(1/\omega_0) + (1/\omega')]$, where $\omega_i = \omega$ at $\omega < \omega_0/2$, $\omega_i = \omega_0 - \omega$ at $\omega > \omega_0/2$.

Expression (6.52) represents /333 a combination of the expressions $\operatorname{div}\vec{F}$ for an optically thick and optically thin case, which is adequate for arbitrary optical thicknesses, with the exception of the immediate vicinity of the shock layer boundary. The graph given in Figure 6.23 [65] shows that, with allowance for radiation absorption in the lines and in the continuous spectrum, with simultaneous consideration of the interaction between the radiation and the flow field, convective and radiant heat transfer decreases to a greater extent than is indicated by the results of the previous studies, and the bluntness radius, at which the total heat transfer is at a minimum, will be much greater than was assumed previously.

The study [66], to calculate the flow of a viscous, selectively radiating gas in the vicinity of a critical point, used the iteration scheme of the method of linear descent, and the influence of viscosity was disregarded in the outer portion of the shock layer. In a calculation of the radiation heat exchange

at each point of the shock layer, the equations of radiation transport, which were written in the form of finite difference relationships, were integrated for different wavelengths and directions, and then the radiant thermal flux and $\mathrm{div}\vec{F}$ were determined by summation. The absorption coefficients for radiation by air were taken from [29].

The flow of a selectively radiating viscous gas around a critical point was also studied in [67], which used tables of the radiation absorption coefficient [30], and the method of successive approximations to solve a system of gasdynamic equations. As a result of calculations in [66 and 67], the authors obtained the profiles of values in the compressed layer, shock wave stand-off distance, as well as the radiant and convective thermal fluxes for several variations of flow around a sphere.

All of the studies given above confirmed the general qualitative results that the convective and radiation fluxes are reduced, as compared with calculations which do not consider the interaction of radiation with the flow field.

The interaction of the viscous and inviscid region of the flow of a radiant gas in the vicinity of the critical point of a blunt body was studied in [75] on the basis of model equations obtained for large Reynolds numbers in the approximation of a thin shock layer and in the approximation of similarity in the vicinity of the critical point. A study of the characteristic values of terms in the model equations indicated that, if the thickness of the viscous shock layer exceeds the optical thickness of the shock layer, then radiation absorption in the entire shock layer may be disregarded, since the layer in which absorption is insignificant is entirely submerged in the viscous boundary layer. It was shown also in [75], using the method of outer and

inner expansions, that for small, but finite optical thicknesses /334 of the shock layer the gas enthalpy on the boundary of the viscous boundary layer assumes a finite, non-zero value.

The asymptotic boundary layer at the critical point of a blunt body was examined in [61]. For this purpose, the equations of a chemically reactive, equilibrium boundary layer were solved (see Section 5.2) with the addition of $\mathrm{div}\vec{F}$, as well as the equations of radiation transport in real air, with the Lewis-Semenov number Le = 1. The transport and thermodynamic properties of real air were examined with the approximate formulas given in [76]. The conditions on the outer boundary of the boundary layer and the dependence of the radiation absorption coefficient for air were taken from [51], and on the body — the customary attachment conditions. As a result of the numerical solution by the method of successive approximations, it was found that the convective heat transport, with allowance for the radiant energy transport in the shock layer, is approximately twice as low as without allowance for radiation transport in the shock layer. Allowance for radiation transport in the boundary layer has a slight influence on the convective thermal flux.

6.6. Advancing radiation and precursor phenomena before strong shock waves

Up to the present, it has been assumed that the radiation emanating from a shock layer which is formed before spacecraft entering the dense layers of the atmosphere does not interact with the advancing flow of cold air, and the energy which is transported by radiation passes to infinity, without disturbing the advancing flow. However, in experiments in wind tunnels [77] and in radar observations of satellites entering the atmosphere of the Earth [78], it was found there is considerable

concentration of electrons in the cold gas in front of the strong shock waves at a great distance from the front of the shock waves. This type of phenomenon, which leads to deviation of the gas before the shock wave from the initial state, is usually called the precursor phenomenon. As recent experiments have shown [77], the precursor phenomena are caused primarily by intense radiation of a high temperature gas behind the shock wave (advancing radiation), which is absorbed by the unperturbed cold gas in front of the shock wave front. An understanding of the precursor phenomena is important both for interpreting the results of experiments on shock waves, and for a precise formulation of the problem of the flow around a blunt body under conditions corresponding to the entry of spacecraft into the atmosphere. No less important is the problem of identifying bodies entering the atmosphere, since precursor phenomena — in particular, pre-ionization — may greatly change the scattering surface of the radar signal.

Absorption of the advancing radiation in cold air in front of the shock wave front may lead to excitation, dissociation, and ionization of air molecules before the front [79 — 81]. Actually, the shock wave will move along the gas with a changed state and composition, which leads to a change in the relaxation processes and the equilibrium state of the gas behind the shock /335 waves. Due to this, it leads to a change in the values of the radiation and convective thermal fluxes on the surface of the body in the flow.

The problems of precursor phenomena, within the framework of the shock wave structure, have been extensively investigated in the monograph of Ya. B. Zel'dovich and Yu. P. Rayzer [5] for very intense shock waves with air temperatures behind the wave on the order of 10^5 — 10^6 K. For these shock waves, the very intense radiant energy flux is absorbed immediately in front of

the shock wave front (the radiation mean free path is very small), and thus greatly heats the cold air. In the case of shock waves which are formed before spacecraft entering the atmosphere of the Earth, the energy transported by the advancing radiation will be much less, and the gas temperature increase in front of the shock wave will be insignificant. The energy of the advancing radiation which is absorbed by the cold gas changes the composition and static enthalpy of the gas. Therefore, it is necessary to study the elementary processes leading to a change in the state and composition of the gas before the shock wave front.

Let us examine the characteristic parameters which make it possible to establish the influence of the absorption of the advancing radiation upon the gas flow behind the shock wave [82]. The basic parameter will be the optical thickness of the cold air layer $\omega^* = R_b k^*$, where R_b is the characteristic dimension of the body in the flow, and k^* is the characteristic value of the absorption coefficient of the advancing radiation in the cold air before the wave. The parameter ω^* shows how rapidly the advancing radiation is absorbed. If $\omega^* \gg 1$, then the mean free path of radiation in the cold air is small. The energy is absorbed immediately before the front, and the emitted energy is returned back to the shock layer. If $\omega^* \ll 1$, the radiation emanates to greater (with respect to the body size) distances from the shock wave, without undergoing absorption in the cold air and, in other words, the energy emitted from the shock front is scattered in space before the body in the flow. The energy parameter W^* represents the ratio of the advancing radiation flux to the flux of the kinetic energy of the air flowing over the shock wave

$$W^* = \frac{2F}{\rho_\infty V_\infty^3}. \qquad (6.53)$$

If $\omega^* \gtrsim 1$, then the parameter W^* characterizes the relative amount of energy removed by the advancing radiation from the shock layer and returned back to the layer. If $\omega^* \ll 1$, then the estimate of the energy returned to the shock layer assumes the form $W^*(\omega^*)^2$, since the energy of the advancing radiation is scattered in space before the body in the flow. The role of the absorption of the advancing radiation before the shock wave front is particularly imporant when $W^* \sim 1$ and $\omega^* \gtrsim 1$.

Let us establish the possible values of the parameter ω^* when a blunt body moves in the dense layers of the atmosphere of the Earth. It is known that cold air is transparent for radiation in the visible portion of the spectrum, and absorbs radiation in the ultraviolet and far-ultraviolet regions. Figure 6.24 [83] gives the dependence of the absorption cross section of cold atmospheric air components on the energy of quanta or the radiation wavelength. /336

The radiation absorption coefficient in cold air has the form

$$k_\lambda^* = \sum_i n_i \sigma_{\lambda i}, \qquad (6.54)$$

where $\sigma_{\lambda i}$ is the absorption cross section of the i-th component of air at the wavelength λ; n_i — concentration of the i-th component.

Figure 6.25 gives the dependence of the effective radiation mean free path in the atmospheric air $l^* = 1/\bar{k}^*$ on the altitude averaged over the range of absorbed wavelengths. We may use this graph to determine the value of ω^* for specific bluntness radii. Thus, for example, for a sphere with the radius $R_b = 1$ m

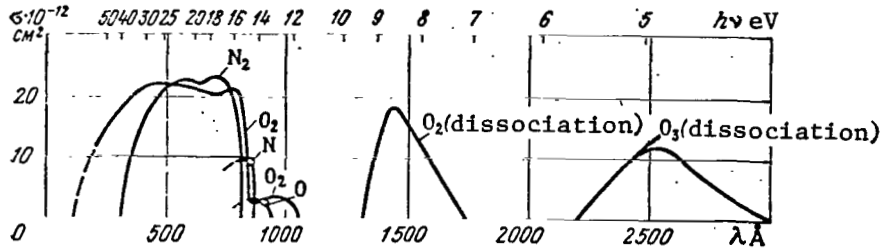

Figure 6.24. Cross section of continuous absorption in cold amospheric air.

the effective mean free path of the radiation at an altitude of approximately 70 km is comparable with the radius of a sphere, and at an altitude of 50 km, is comparable with the shock layer thickness.

The main portion of the emission of the shock layer, which is formed before a body entering the atmosphere of the Earth at a velocity on the order of or greater than the second cosmic velocity, is given by recombination in the basic state of nitrogen and oxygen atoms and by radiation in the spectral lines of these atoms. Thus a significant portion of the recombination radiation and several of the strong spectral lines belong to those wavelengths which are intensively absorbed in cold air [8]. Since radiation of the shock layer is blocked in the region of photoionization absorption, the magnitude of the flux of radiation from the shock layer may be estimated from /337 the formula

$$F=\frac{2\pi}{c^2h^3}(kT)^4\int\limits_{\frac{h\nu}{kT}}^{\infty}x^3\exp(-x)\,dx, \qquad (6.55)$$

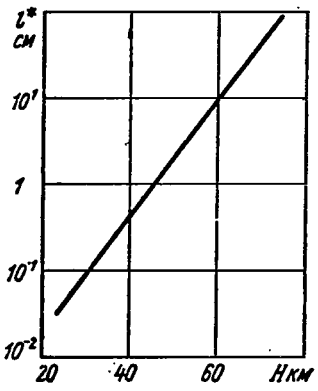

Figure 6.25. Average mean free path of radiation in cold air.

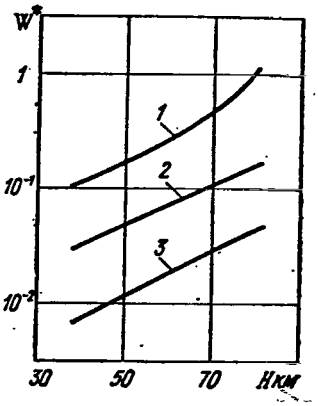

Figure 6.26. Results of calculating the parameter W* for different flight regimes (R_b = 1 m).

1 — at V_∞ = 18 km/sec; 2 — at V_∞ = 15 km/sec; 3 — at V_∞ = 12 km/sec.

where the lower integration limit corresponds to the wavelength boundary of oxygen molecule photoionization. Figure 6.26 gives the results of calculating the parameter W* according to (6.53) with this estimate of the absorbed flux of radiation. These results show that regimes for the entry of bodies into the dense layers of the atmosphere of the Earth exist, when a large part of the energy emitted from the shock layer is absorbed in front of the body and leads to the use of the incoming flow parameters.

Studies of the change in the composition and parameters before a strong shock wave in argon, caused by absorption of the advancing radiation, were performed in [84]. A solution of a similar problem for air is much more complex, since it is necessary to consider the reactions of the dissociative recombination type (1.106) which have a very large transverse cross section, in addition to photoionization reactions.

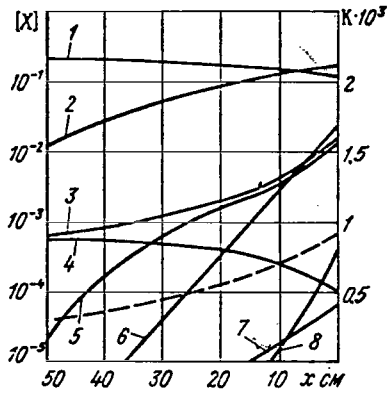

Figure 6.27. Distribution of relative number of particles (solid lines) and temperature (dashed line) before the shock wave front in air (V_∞ = 15 km/sec).

1 — $[O_2]$; 2 — [O]; 3 — [e]; 4 — $[O_2^+]$; 5 — $[O^+]$; 6 — [N]; 7 — $[N^+]$; 8 — $[N_2^+]$

Such a study was made in [82] for a shock wave in nitrogen, and the distributions were obtained of the concentrations of molecular and atomic nitrogen, their ions and the electrons, and also the distribution of the gas velocity, density, and temperature ahead of the shock wave. /338

It is of interest to calculate nonequilibrium air flow ahead of a strong shock wave with consideration of photoionization of nitrogen and oxygen molecules, photodissociation of oxygen molecules, photoionization of nitrogen and oxygen atoms, and also the reaction of dissociative recombination.

When the shock wave velocity and conditions at infinity are given, the flux of the advancing radiation in a continuous spectrum is determined according to Formula (6.55) and in the lines according to the results given in [30]. Then the method of successive approximations is used to give a concurrent solution of the equation of conservation and chemical kinetics ahead of the shock wave. Figure 6.27 gives the values of the relative number of particles $[O_2]$, [O], [e], $[O_2^+]$, $[O^+]$, [N], $[N_2^+]$, $[N^+]$ as a function of the distance to the shock wave front, and the change in the air temperature ahead of the shock wave at a velocity of V_∞ = 15 km/sec and with conditions at infinity corresponding to an altitude of 57 km.

The calculation results show a great change in the air composition before the shock wave, a certain increase in its temperature, and an insignificant change in the air density and velocity ahead of the front. All of these precursor effects, which are greatly intensified with an increase in the parameter W*, must be taken into account when calculating the parameters and composition of the air behind a shock wave.

REFERENCES

1. Sobolev, V. V. Kurs teoreticheskoy astrofiziki (Course on Theoretical Astrophysics). Moscow, Nauka Press, 1967.

2. Aller, L. Astrophysics, IL, 1955.

3. Chandrasekar, S. Transport of Radiant Energy. Moscow, IL, 1953.

4. Rosseland, S. Astrofizika na osnove teorii atoma (Astrophysics on the Basis of Atomic Theory). ONTI, 1936.

5. Zel'dovich, Ya. B. and Yu. P. Rayzer. Fizika udarnykh voln i vysokotemperaturnykh gazodinamicheskikh yavleniy (Physics of Shock Waves and High Temperature Gasdynamic Phenomena). Moscow, Fizmatgiz, 1963.

6. Vincenti, W. G. and C. H. Kruger. Introduction to Physical Gasdynamics. J. Willey and Sons, 1965.

7. Kuznetsov, Ye. S. Radiant Heat Exchange in a Moving Fluid Medium. Izvestiya AN SSSR, Seriya geografich. i geofizich., No. 1, 1941. /339

8. Zhigulev, V. N., Ye. A. Romishevskiy, and V. K. Vertushkin. Role of Radiation in Contemporary Problems of Gasdynamics. Inzhenernyy zhurnal, Vol. 1, No. 1, 1961.

9. Stupochenko, Ye. V., S. A. Losev, and A. I. Ospiov. Relaksatsionnyye protsessy v udarnykh volnakh (Relaxation Processes in Shock Waves). Moscow, Nauka Press, 1965.

10. Camm, J. C., B. Kivel, R. L. Taylor, and J. D. Teare. Absolute Intensity of Nonequilibrium Radiation in Air and Stagnation Heating at High Altitudes. JQSRT, Vol. 1, No. 1, 1961, p. 53.

11. Teare, J. D., S. Georgiev, and R. A. Allen. Radiation from the Nonequilibrium Shock Front. Hypersonic Flow Research, Acad. Press, 1962, pp. 281-317.

12. Allen, R. A., J. C. Keck, and J. C. Camm. Nonequilibrium Radiation in the Recombination Rate of Shock Heated Nitrogen. Phys. Fluids., Vol. 5, No. 3, 1962, p. 284.

13. Allen, R. A. Nonequilibrium Shock Front Rotational, Vibrational, and Electronic Temperature Measurements. JQSRT, Vol. 5, No. 3, 1965, p. 511.

14. Allen, R. A., P. Rose, and J. C. Camm. Nonequilibrium and Equilibrium Radiation at Supersatellite Re-Entry Velocities. IAS Paper, No. 63-77, 1963.

15. Martin, J. Atmospheric Entry, Mir Press, 1969.

16. Vorob'yev, V. S. and I. T. Yakubov. Reasons for the Formation of a Radiation Peak for Nonequilibrium Gas Behind a Shock Wave. Pis'ma ZhETF, Vol. IV, No. 2, 1966.

17. Vorob'yev, V. S. and I. T. Yakubov. Reasons for the Formation of a Radiation Peak for Nonequilibrium Gas behind a Shock Wave, TBT, Vol. 5, No. 3, 1967.

18. Yakubov, I. T. Radiation Maximum of Nonequilibrium Gas behind Strong Shock Waves. TVT, Vol. 5, No. 3, 1967.

19. Soshnikov, V. N. Cross Section of Optical Absorption in Electron Bands of Two-Atomic Molecules at High Temperatures. Optika i spektr., Vol. 17, No. 3, 1964.

20. Fayzulov, V. S., N. N. Sobolev, and Ye. M. Kudryavtsev. Spectroscopic Research on the State of a Gas behind a Shock Wave. Optika i spektr., Vol. 8, 1960.

21. Clouston, J. G., A. C. Caydon, and I. R. Hurle. Temperature Measurement of Shock Waves by Spectrum Line Reversal. II. Proc. Roy. Soc., A-252, 1959, p. 143.

22. Hansen, C. F. A Radiation Model for Nonequilibrium Molecular Gases. AIAA J., Vol. 2, No. 4, 1964, p. 611.

23. Artamonov, A. K., V. N. Arkhipov, and G. Ye. Starchenko. Relaxation and Radiation behind Normal Shock Waves. Izvestiya AN SSSR, MZhG, No. 3, 1966.

24. Nadezhin, A. D. and Ye. A. Romishevskiy. Nonequilibrium Radiation of a Strong Shock Wave. PMTF, No. 1, 1969.

25. Zhigulev, V. N. Equations of Motion of a Nonequilibrium Medium with Allowance for Radiation. Inzhenernyy zhur., Vol. IV, No. 2, p. 231; No. 3, 1964, p. 431.

26. Biberman, L. M., V. S. Vorob'yev, et al. Air Flow behind a Strong Shock Wave Front Considering Nonequilibrium Ionization and Radiation. Izvestiya AN SSSR, MZhG, No. 6, 1967.

27. Wick, B. H. Radiative Heating of Vehicles Entering the Earth's Atmosphere. High Temperature Aspects Hypersonical Flow. Pergamon Press, 1964, p. 607.

28. Bay Shi, I. Radiatsionnaya gazovaya dinamika (Radiation Gasdynamics). Mir Press, 1968.

29. Kamenshchikov, V. A., Yu. A. Plastinin, V. M. Nikolayev, and L. A. Novitskiy. Radiatsionnyye svoystva vysokotemperaturnykh gazov (Radiation Properties of High Temperature Gases). Moscow, Mashinostroyeniye, 1970.

30. Avilova, I. V., L. M. Biberman, et al. Optical Properties /340 of Hot Air, Vol. 9, No. 1, 1969.

31. Biberman, L. M., V. S. Vorob'yev, G. E. Norman, and I. T. Yakubov. Radiation Heating in the Case of Hypersonic Flow. Kosmicheskiye issledovaniya, Vol. 2, No. 3, 1964.

32. Kon'kov, A. A., V. Ya. Neyland, V. M. Nikolayev, and Yu. A. Plastin. Problems of Radiant Heat Exchange in Hypersonic Aerodynamics, Vol. 7, No. 1, 1969.

33. Lunev, V. V. and N. N. Murzinov. Influence of Radiation on the Flow in the Vicinity of the Critical Point of a Blunt Body. PMTF, No. 2, 1961.

34. Goulard, R. Preliminary Estimates of Radiative Transfer Effects on Detached Shock Layers. AIAA J., Vol. 2, No. 3, 1964, p. 494.

35. Chisnell, R. F. Radiation Effects in the Stagnation Point. AIAA J., Vol. 4, No. 10, 1966, p. 1818.

36. Romishevskiy, Ye. A. Calculation of Flow Close to the Critical Point of a Blunt Body with Allowance for Radiation. Inzhenernyy zhurnal, Vol. 5, No. 3, 1965.

37. Wilson, K. H. and H. Hoshizaki. Inviscid Nonadiabatic Flow about Blunt Bodies. AIAA J., Vol. 3, No. 1, 1965, p. 67.

38. Vertushkin, V. K. Flow of a Supersonic Air Flow around a Sphere with Allowance for Equilibrium Radiation. Kosmicheskiye issledovaniya, Vol. 4, No. 1, 1966.

39. Fomin, V. N. Hypersonic Gas Flow around Blunt Bodies with Allowance for Radiation. Zhurnal vych. matem, i matem. fiz., Vol. 6, No. 4, 1966.

40. Gilinskiy, S. M., G. F. Telenin, and G. P. Tinyakov. Method of Calculating Supersonic Flow around Blunt Bodies with a Detached Shock Wave. Izvestiya AN SSSR. Mekhanika i mashinostro., Vol. 9, No. 4, 1964.

41. Romishevskiy, Ye. A. Effect of a Radiation Entropy Layer. Izvestiya AN SSSR, MZhG, No. 2, 1966.

42. Nemchinov, I. V. and L. P. Topekha. Boundary Layer Close to Leading Critical Point in the Case of Heat Transmission by Radiation. PMTF, No. 4, 1960.

43. Goulard, R. A. Comment on Radiation from Hot Air and Its Effect on Stagnation Point Heating. J. Aero Space Sci., Vol. 28, No. 2, 1961, p. 158.

44. Kennet, H. Radiation Convection Interaction around a Sphere in Hypersonic Flow. ARS J., Vol. 32, No. 10, 1962, p. 1616.

45. Thomas, P. D. Transparency Assumption in Hypersonic Radiative Gasdynamics. AIAA J., Vol. 3, No. 8, 1965, p. 1401.

46. Olstad, W. B. Stagnation Point Solution on Inviscid Radiating Shock Layer. Proc. 1965 Heat Transfer Fluid Mech. Institute. Stanford Univer. Press, 1965, p. 138.

47. Vertushkin, V. K. and V. N. Zhigulev. Influence of Radiation on Flow in the Critical Point Region. Izvestiya AN SSSR, MZhG, No. 2, 1967.

48. Jischke, M. C. Optically Thin Stagnation Point Flow. AIAA J., Vol. 6, No. 11, 1968.

49. Stulov, V. P. and Ye. G. Shapiro. Influence of Radiation on Heat Exchange at the Critical Point of a Blunt Body. Izvestiya AN SSSR, MZhG, No. 2, 1969.

50. Cheng, P., and W. G. Vincenti. Inviscid Radiating Flow over a Blunt Body. J. Fluid Mech., Vol. 27, No. 4, 1967, p. 625. Mekhanika, No. 6, 1967, p. 106.

51. Bogolepov, V. V., Yu. G. Yel'kin, and V. Ya. Neyland. Calculation of Inviscid Radiation Gas Flow around a Blunt Body, Izvestiya AN SSSR, MZhG, No. 4, 1968.

52. Stulov, V. P. and Ye. G. Shapiro. Radiation of Shock Layer in the Case of Hypersonic Air Flow around Blunt Bodies. Izvestiya AN SSSR, MZhG, No. 1, 1970.

53. Lebedev, V. I., and V. N. Fomin. Hypersonic Gas Flow around Blunt Bodies with Allowance for Selective Radiation and Energy Absorption. Zhurnal vychisl. matem, i matem. fiz., Vol. 9, No. 3, 1969.

54. Chin, J. H. Effect of Non-Grey Self-Absorption and Energy Loss for Blunt Body Flows. JQSRT, Vol. 9, No. 1, 1969.

55. Callis, L. B. Time Asymptotic Solutions of Blunt-Body Stagnation Point Flows with Non-Grey Emission and Absorption of Radiation. AIAA Paper, No. 68-663, 1968.

56. Rumynskiy, A. N. Boundary Layer in Radiant and Absorbing Media. Izvestiya AN SSSR, Mekhanika i mashinostr., No. 2, 1960.

57. Lunev, V. V. and A. N. Rumynskiy. Interaction of Boundary Layer with External Flow Caused by Radiant Heat Exchange. PMTF, No. 6, 1961.

58. Rumynskiy, A. N. Heat Exchange at the Front Point Washed by a Radiant Medium. Izvestiya AN SSSR, Mekhanika i mashinostroy., No. 1, 1961.

59. Howe, J. T. and J. R. Viegas. Solution of the Ionized Radiationg Shock Layer, Including Re-absorption and Foreing Species Effects, and Stagnation Region Heat Transfer. Eksp.-Inf. Vsosoyuznyy institut nauchnoy i tekhnicheskoy informatsii (VINITI), Astronavtika i raketodinamika, Vol. 12, No. 52, 1964.

60. Belotserkovskiy, O. M., L. B. Biberman, et al. Hypersonic Gas Flow Around, and Heating of, Blunt Bodies Considering Radiation Transport. TVT, No. 3, 1969.

61. Yermank, Yu. N., and V. Ya. Neyland. Boundary Layer in a Radiant Gas. Uchenyye zapiski, TsAGI, Vol. 1, No. 6, 1970.

62. Romishevskiy, Ye. A. Boundary Layers and Stabilized Gas Discharge in the Case of Diffuse Radiation. Inzhenernyy zhurnal, Vol. 2, No. 1, 1962.

63. Hochizaki, H., and K. H. Wilson. Viscous, Radiating Shock Layer about a Blunt Body. AIAA J., Vol. 3, No. 9, 1965, p. 1614.

64. Hochizaki, H., and K. H. Wilson. Convective and Radiative Heat Transfer during Superorbital Entry. AIAA J., Vol. 1, 1967, p. 25.

65. Dirling, R. B.,W. S. Rigdon, and M. Thomas. Stagnation Point Heating Including Spectral Radiative Transfer. Proc. 1967 Heat Transfer Fluid Mech. Instit. Stanford Univers. Press, 1967, p. 141.

66. Anfimov, N. A. and V. P. Shari. Solution of a System of Equations of Motion of Selectively Radiant Gas in a Shock Layer. Izvestiya AN SSSR, MZhG, No. 3, 1968.

67. Biberman, L. M., and S. Ya. Bronin. Theory of Heating in the Case of Hypersonic Flow. DAN SSSR, Vol. 182, No. 3, 1968.

68. Goulard, R. and M. Gouldard. Energy Transfer in the Couette Flow of Radiant and Chemically Reacting Gas. Proc. 1959 Heat Transfer Fluid Mech. Institute, Stanford Univ. Press, 1959, p. 126.

69. Kivel, B. Radiation from Hot Air and Its Effect on Stagnation Point Heating. JASS, Vol. 28, No. 2, 1961, p. 96.

70. Biberman, L. M, and G. E. Norman. Recombination and Braking Radiation of a Plasma, Vol. 3, No. 3, 1963.

71. Elesasser, W. M. Heat Transfer by Infrared Radiation in the Atmosphere. Harvard Meteorol. Study, No. 6, 1942.

72. Rayzer, Yu. P. Simple Method of Calculating Average Level of Radiation in Ionized Bases at High Temperatures. ZhETF, Vol. 10, 1960.

73. Penner, S. S. and M. Thomas. Approximate Theoretical Calculation of Continuum Opacities. AIAA J., Vol. 2, No. 9, 1964, p. 1672.

74. Thomas, M. and W. S. Rigdon. A Simplified Formulation for Radiative Transfer. AIAA J., Vol. 2, No. 11, 1964, p. 2052.

75. Gogolepov, V.V., V.Ya. Neyland. Convective Heat Exchange in a Radiant Gas. Izvestiya AN SSSR, MZhG, No. 5, 1966.

76. Sevast'yanov, R. M. and M. D. Zdunkevich. Thermodynamic Functions of Gases at High Temperatures. Inzhenernyy zhurnal, Vol. 4, No. 4, 1964.

77. Lederman, S. and D. S. Wilson. Microwave Resonant Cavity Measurement of Shock Produced Electron Precursor. AIAA J., Vol. 5, No. 1, p. 70.

78. Lin, S. C. Radio Echoes from Manned Satellite during Re-Entry. J. Geophys. Res., Vol. 67, 1962, p. 3851. /342

79. Biberman, L. M. and B. A. Veklenko. Radiation Processes before a Shock Wave Front. ZhETF, Vol. 37, No. 1, 1959.

80. Lagar'kov, A. N. and I. T. Yakubov. Influence of Radiation on State of a Gas before a Shock Wave Front. Optika i spektr, Vol. 14, No. 2, 1963.

81. Biberman, L. M., V. G. Sevast'yanenko, and I. T. Yakubov. Oxygen Photodissociation before the Front of a Strong Shock Wave in Air. TVT, Vol. 2, No. 3, 1964.

82. Vertushkin, V. K. and Ye. A. Romishevskiy. Role of Radiation Absorption before a Shock Wave in the Case of Hypersonic Flow around a Blunt Body. Izvestiya AN SSSR, MZhG, No. 6, 1960.

83. Ditchburn, R. W. Absorption of Ultraviolet Radiation by the Atmospheric Gases. Proc. Royal Soc., Ser. A., Vol. 236, 1956, p. 216.

84. Nelson. H. F. and R. Goulard. Structure of Shock Waves with Nonequilibrium Radiation and Ionization. Phys. Fluids., Vol. 12, No. 8, 1969, p. 1605.

*U.S. GOVERNMENT PRINTING OFFICE: 1976 - 635-275/72

"The aeronautical and space activities of the United States shall be conducted so as to contribute . . . to the expansion of human knowledge of phenomena in the atmosphere and space. The Administration shall provide for the widest practicable and appropriate dissemination of information concerning its activities and the results thereof."

—NATIONAL AERONAUTICS AND SPACE ACT OF 1958

NASA SCIENTIFIC AND TECHNICAL PUBLICATIONS

TECHNICAL REPORTS: Scientific and technical information considered important, complete, and a lasting contribution to existing knowledge.

TECHNICAL NOTES: Information less broad in scope but nevertheless of importance as a contribution to existing knowledge.

TECHNICAL MEMORANDUMS: Information receiving limited distribution because of preliminary data, security classification, or other reasons. Also includes conference proceedings with either limited or unlimited distribution.

CONTRACTOR REPORTS: Scientific and technical information generated under a NASA contract or grant and considered an important contribution to existing knowledge.

TECHNICAL TRANSLATIONS: Information published in a foreign language considered to merit NASA distribution in English.

SPECIAL PUBLICATIONS: Information derived from or of value to NASA activities. Publications include final reports of major projects, monographs, data compilations, handbooks, sourcebooks, and special bibliographies.

TECHNOLOGY UTILIZATION PUBLICATIONS: Information on technology used by NASA that may be of particular interest in commercial and other non-aerospace applications. Publications include Tech Briefs, Technology Utilization Reports and Technology Surveys.

Details on the availability of these publications may be obtained from:

SCIENTIFIC AND TECHNICAL INFORMATION OFFICE

NATIONAL AERONAUTICS AND SPACE ADMINISTRATION

Washington, D.C. 20546